

**Proton Motion and Chirality Transfer in Model aza-Morita–  
Baylis–Hillman Reaction Systems**

A thesis submitted in partial fulfillment of the requirements for the degree of

**Doctor of Philosophy**

by

**Ryan Thomas Kenny**

MRes (Chemistry)

**Department of Molecular Sciences**

**Macquarie University**

**June 2019**

## Table of Contents

|  |       |
|--|-------|
| ABSTRACT .....   | VII   |
| DECLARATION .....  | VIII  |
| ACKNOWLEDGEMENTS .....   | IX    |
| PUBLICATIONS .....   | XI    |
| ABBREVIATIONS .....  | XII   |
| LIST OF FIGURES .....  | XIV   |
| LIST OF SCHEMES .....  | XIX   |
| LIST OF TABLES .....   | XXIII |
| NAMING CONVENTIONS .....   | XXIV  |
| CHAPTER 1 MODEL SYSTEMS FOR CHIRALITY TRANSFER BY ASYMMETRIC CATALYSIS .....   | 1     |
| 1. INTRODUCTION .....  | 2     |
| 1.1 Asymmetric Catalysis .....   | 2     |
| 1.2 Proton transfer as a fundamental process for coordinating reactive intermediates in catalysis .....                    | 7     |
| 1.3 The Morita–Baylis–Hillman Reaction: an organocatalytic model reaction for proton transfer .....                        | 10    |
| 1.4 From bifunctional to trifunctional organocatalysts for the MBH class .....   | 16    |
| 1.5 Chiral information propagation in a reaction network and the Soai reaction .....                                       | 21    |
| 1.5.1 Chiral information transfer in a network .....   | 22    |
| 1.5.2 The Soai reaction and chiral amplification .....   | 23    |
| 1.6 Project Aims .....   | 27    |
| 1.7 References .....   | 30    |
| CHAPTER 2 MECHANISTIC INVESTIGATIONS OF A PROTON SHUTTLE IN TRIFUNCTIONAL ORGANOCATALYSIS OF AN AZA-MBH MODEL SYSTEM ..... | 45    |
| 2.1 INTRODUCTION .....   | 46    |
| 2.1.1 Mechanistic understanding of organocatalytic modes of activation .....   | 46    |

|   |     |
|---|-----|
| 2.1.2 NMR techniques and analysis of organocatalytic intermediates .....                                    | 46  |
| 2.1.3 Existing NMR-based investigations of the MBH reaction .....   | 48  |
| 2.1.4 Specific aims .....   | 51  |
| 2.2. RESULTS AND DISCUSSION .....   | 52  |
| 2.2.1 Identification of a new reaction intermediate, the phosphonium benzoate ketone .....                  | 52  |
| 2.2.2 The PBK is a catalytically relevant intermediate in the trifunctional catalysis .....                 | 59  |
| 2.2.3 Solution structure analysis of trifunctional PBK .....  | 63  |
| 2.2.3.1 The overall phosphonium geometry promotes proton transfer .....                                     | 64  |
| 2.2.3.2 The conformation of the phosphonium butanone is primed for proton transfer .....                    | 67  |
| 2.2.3.3 Phenol Conformations .....  | 70  |
| 2.2.3.4 The PBK is an ion-pair with dynamic proton transfer .....   | 71  |
| 2.2.4 Computational analysis of the TF-1-PBK proton shuttle .....   | 75  |
| 2.2.5 Conclusion: Proton motion-based activation of the PBK for an expanded <i>aza</i> -MBH mechanism ..... | 78  |
| 2.3. EXPERIMENTAL .....   | 79  |
| 2.3.1 Materials and Methods .....   | 79  |
| 2.3.2 Proportion of PBK and structure elucidation .....   | 80  |
| 2.3.3 Initial Rates .....   | 90  |
| 2.3.4 Molecular Dynamics .....  | 91  |
| 2.3.5 Homonuclear J-Resolved Spectroscopy .....   | 91  |
| 2.3.6 2D Quantitative NOESY .....   | 94  |
| 2.3.7 1D Selective NOESY .....  | 95  |
| 2.3.8 3D HSQC-NOESY .....   | 96  |
| 2.3.9 Pulse Programs .....  | 98  |
| 2.4 REFERENCES .....  | 101 |
| CHAPTER 3 CONJUGATIVE CATALYSIS FROM AN AZA-MBH PROTON SHUTTLE .....  | 107 |
| 3.1 INTRODUCTION .....  | 108 |
| 3.1.1 Additives improve catalytic proficiency .....   | 108 |
| 3.1.2 Acid additives exhibit versatile roles in catalysis .....   | 108 |
| 3.1.3 Acid additive effects in the <i>aza</i> -MBH reaction .....   | 111 |

|  |     |
|--|-----|
| 3.1.4 Acid additives in acid switchable trifunctional organocatalysis .....  | 115 |
| 3.1.5 Specific aims.....   | 117 |
| 3.2 RESULTS AND DISCUSSION.....  | 117 |
| 3.2.1 Benzoic acid protonation state is critical for different stages of the reaction .....                            | 118 |
| 3.2.2 Proton abstraction: Establishing the proton transfer network .....   | 122 |
| 3.2.3 Conjugative catalysis is achieved with recognition of the cognate proton transfer pathway by the substrate ..... | 128 |
| 3.2.4 Conclusion.....  | 133 |
| 3.3 EXPERIMENTAL.....  | 135 |
| 3.3.1 Material and methods .....   | 135 |
| 3.3.1 Acid screen.....   | 136 |
| 3.3.2 Deuteration Studies.....   | 137 |
| 3.3.2.1 Preparation of <i>d</i> -Benzoic acid (BzOD).....  | 137 |
| 3.3.2.2 General Procedure for Deuteration of trifunctional organocatalysts.....  | 137 |
| 3.3.2.3 General Procedure for measuring rate of retro-Michael Elimination.....   | 138 |
| 3.3.3 Measuring secondary kinetic isotope effect.....  | 140 |
| 3.3.3.2 Measuring inverse secondary KIE .....  | 142 |
| 3.3.4 Preparation of imine substrates .....  | 144 |
| 3.3.4.1 General procedure for preparation of <i>N</i> -Ms protected imines ( <i>N</i> -Ms-Im-1) .....                  | 144 |
| 3.3.4.2 General procedure for <i>N</i> -Boc imine (NBoc-Im-1) .....  | 145 |
| 3.3.4.3 General procedure for aza-MBH reaction. ....   | 146 |
| 3.4 REFERENCES .....   | 148 |
| CHAPTER 4 SCOPE OF THE TRIFUNCTIONAL CONJUGATIVE CATALYSIS IN THE AZA-MBH MODEL SYSTEM.....                            | 154 |
| 4.1 INTRODUCTION .....   | 155 |
| 4.1.1 Nitrogen Heterocycles in organocatalysis .....   | 155 |
| 4.1.2 Pyridine carboxaldehyde as aza-MBH substrates. ....  | 156 |
| 4.1.2.1 2-carboxypyridine substrates .....   | 156 |
| 4.1.2.3 3-Pyridine carboxaldehyde .....  | 157 |
| 4.1.3 Proton motion specificity in conjugative catalysis.....  | 158 |
| 4.1.4 Specific aims.....   | 159 |
| 4.2 RESULTS AND DISCUSSION .....   | 159 |



|   |     |
|---|-----|
| 4.2.1 Synthesis of pyridine substrates .....  | 160 |
| 4.2.2 Profile of catalyst response to BzOH activation using a representative pyridinyl imine substrate..... | 161 |
| 4.2.3 Effect of the nitrogen (Brønsted base) position on deploying the proton shuttle .....                 | 164 |
| 4.2.4 Effect of the acid additive on catalytic proficiency for 3-pyridinyl imine substrates.....            | 167 |
| 4.2.5 Conclusion.....   | 172 |
| 4.3 EXPERIMENTAL.....   | 173 |
| 4.3.1 Materials and Methods .....   | 173 |
| 4.3.2 Synthesis of imine .....  | 174 |
| 4.3.2.1 General Procedure for NTs 3-pyridine carbaldimines (NTsPyr-Im-1–6) .....                            | 174 |
| 4.3.2.2 General Procedure for NTs 2-pyridine carbaldimines.....   | 177 |
| 4.3.2.3 General Procedure for NBoc pyridine carbaldimines .....   | 178 |
| 4.3.3 General procedures for catalysis.....   | 180 |
| 4.3.3.1 Pyridine aza-MBH .....  | 180 |
| 4.3.3.2 Acid screen.....  | 186 |
| 4.5 REFERENCES .....  | 187 |
| CHAPTER 5 PROPAGATION OF CHIRALITY VIA AN AZA-MBH–SOAI ASYMMETRIC RIPPLE .....                              | 192 |
| 5.1 INTRODUCTION .....  | 193 |
| 5.1.1 A suprareaction network by continuous chiral propagation .....  | 193 |
| 5.1.2 Chirality propagation by the Soai reaction .....  | 194 |
| 5.1.2.1 Known chiral initiators for the Soai reaction .....   | 194 |
| 5.1.2.1 Complexes in the Soai reaction for chirality amplification .....                                    | 197 |
| 5.1.3 Building an aza-MBH-Soai reaction system .....  | 199 |
| 5.1.4 Specific aims.....  | 200 |
| 5.2 RESULTS AND DISCUSSION.....   | 201 |
| 5.2.1 Development of a more robust synthesis of Soai Aldehydes .....  | 201 |
| 5.2.2 Enantioenriched aza-MBH adducts as chiral initiators for the Soai reaction .....                      | 203 |
| 5.2.3 A proton-shuttle driven aza-MBH reaction as a chiral initiator for the Soai reaction .....            | 208 |
| 5.2.4 A kinetically differentiated MBH reaction for engendering the Soai reaction .....                     | 210 |
| 5.3 Conclusion.....   | 213 |
| 5.4 EXPERIMENTAL.....   | 214 |
| 5.4.1 Materials and methods.....  | 214 |

|   |     |
|---|-----|
| 5.4.2 Synthesis of Soai Aldehydes via Lithium Halogen Exchange..... | 215 |
| 5.4.2.4 Data for compound 5.48 and 5.49.....                        | 218 |
| 5.4.3 Soai Reaction .....   | 220 |
| 5.5 REFERENCES .....  | 224 |
| CHAPTER 6 CONCLUSIONS AND FUTURE DIRECTIONS.....                    | 231 |
| 6.1 CONCLUSIONS .....   | 232 |
| 6.2 FUTURE DIRECTIONS .....   | 233 |
| APPENDIX.....   | 235 |

## Abstract

Proton transfer is a ubiquitous process in organic and biological chemistry, particularly prevalent in biological or designed asymmetric catalysis. Our initial work developed an acid-regulated, asymmetric organocatalysis of a model proton-transfer reaction known as the aza-Morita–Baylis–Hillman (aza-MBH) reaction, in which three catalytic motifs cooperate, within a BINAP chiral framework, to catalyse the aza-MBH reaction between methyl vinyl ketone and aryl *N*-tosyl imines only when activated by external benzoic acid (BzOH). New questions now focus on the exact nature of this switchable catalytic proficiency.

This thesis work will uncover mechanistic details that underpin this switchability. In Chapter 2, the origin of the acid-regulated catalytic proficiency in our trifunctional aza-MBH reaction was investigated by a combination of 2D NMR spectroscopy, molecular mechanics and DFT calculations. An ensemble solution structure of a new proton-shuttling ground state intermediate was identified and elucidated. In Chapter 3, the role of the acid additive in the C–C bond formation and proton transfer was investigated, and a new conjugative mode of catalysis was revealed after discovering a surprising role of the substrate in commanding the proton shuttle for the subsequent steps of C–C bond formation and proton transfer. In Chapter 4, new substrates for this conjugative mode of catalysis in the aza-MBH reaction were identified. Finally, in Chapter 5, kinetic differentiation of cognate substrates through this conjugative mode of catalysis in the aza-MBH reaction was propagated by the Soai reaction to create an asymmetric ripple for superior chiral amplification outcomes. It was then demonstrated that chemical diversity and chirality can both expand through chemical assemblies that undergo conjugative catalysis driven by coordinated proton transfer.

## **Declaration**

I certify that the work in this thesis entitled “Proton motion and chirality transfer in model aza-Morita–Baylis-Hillman reaction systems” has not previously been submitted for a degree nor has it been submitted as part of requirements for a degree to any other university or institution other than Macquarie University. I also certify that the thesis is an original piece of research and it has been written by me. Any help and assistance that I have received in my research work and the preparation of the thesis itself have been appropriately acknowledged. In addition, I certify that all information sources and literature used are indicated in the thesis.

Ryan Kenny

(SN: 42096642)

06/06/2019

## Acknowledgements

I would like to acknowledge the following people, without whom this thesis would not have been submitted.

My supervisor Dr Fei Liu for always providing guidance, feedback, encouragement and a good working environment. For developing my skills in communication, organisation and perseverance. Professor Peter Karuso who was always available to offer me advice and assistance, particularly regarding the NMR experiments presented herein. Dr Hans Senn for his help with DFT calculations.

Past and present members of the Liu group, Harry Spedding, Alex Moore, Sviatoslav Eliseenko and Ivan S. Estrada. Thank you for the time we got to spend in the lab together. Over the years we've experienced many unexpected set-backs but we have managed to keep pushing forward. You have all taught me so much about myself and different chemistry over the years and I am thankful to have worked alongside you all.

Past and present members of the Karuso group for training me in NMR spectroscopy and helping me to get started in the lab.

The academic and support staff at MolSci, in particular A/Prof Joanne Jamie, Dr Andrew Try, Dr Christopher McRae and Dr Damian Moran.

The laboratory technical staff Mark, Tony, Hong and Angela for their training on various instruments and the provision of emergency chemicals.

To the various members of Team Manganese— the dominant force. There are too many things to list here that I am thankful for. I am so grateful to have your support, and in turn support you, throughout our undergraduate, master and PhD.

My parents Bruce and Nicole Kenny and my brother Daniel and his wife Skye. Thank you for your understanding and encouragement over the past few years.

Lastly to my wife Stephanie. Thank you for your support, understanding and love over the course of my PhD. Your support and your drive in your own work has helped me immensely over the years and driven me to achieve my best.

## Publications

1. Kenny, R.; Liu, F., Trifunctional Organocatalysts: Catalytic Proficiency by Cooperative Activation. *Eur. J. Org. Chem.* **2015**, 2015 (24), 5304-5319.
2. Kenny, R.; Liu, F., Cooperative Trifunctional Organocatalysts for Proficient Proton Transfer Reactions. *Chem. Rec.* **2017**, 17 (5), 535-553.

## Abbreviations

|                      |   |
|----------------------|---|
| <b>3D HSQC-NOESY</b> | 3-Dimensional Heteronuclear Single Quantum Coherence Nuclear Overhauser Effect Spectroscopy |
| <b>aza-MBH</b>       | aza-Morita–Baylis–Hillman   |
| <b>BA</b>            | Brønsted Acid   |
| <b>BB</b>            | Brønsted Base   |
| <b>BF</b>            | Bifunctional  |
| <b>BzOH</b>          | Benzoic acid  |
| <b>COSY</b>          | Correlation Spectroscopy  |
| <b>DABCO</b>         | 1,4-diazabicyclo[2.2.2]octane   |
| <b>ee</b>            | Enantiomeric excess   |
| <b>er</b>            | Enantiomeric ratio  |
| <b>ESI-MS</b>        | Electrospray ionisation-mass spectrometry   |
| <b>GC</b>            | Gas chromatography  |
| <b>H2BC</b>          | Heteronuclear 2-Bond Correlation  |
| <b>HMBC</b>          | Heteronuclear Multiple Bond Correlation   |
| <b>HOMO</b>          | Highest occupied molecular orbital  |
| <b>HSQC</b>          | Heteronuclear Single Quantum Coherence  |
| <b>JRES</b>          | J-resolved  |
| <b>KIE</b>           | Kinetic Isotope effect  |
| <b>KSI</b>           | Ketosteroid isomerase   |
| <b>LA</b>            | Lewis Acid  |
| <b>LB</b>            | Lewis Base  |
| <b>LUMO</b>          | Lowest unoccupied molecular orbital   |
| <b>MBH</b>           | Morita–Baylis–Hillman   |
| <b>MAP</b>           | 2'-(diphenylphosphino)-[1,1'-binaphthalen]-2-amine  |
| <b>MOP</b>           | 2'-(diphenylphosphino)-[1,1'-binaphthalen]-2-ol   |
| <b>MVK</b>           | Methyl vinyl ketone (but-3-en-2-one)  |
| <b>NMR</b>           | Nuclear Magnetic Resonance  |
| <b>NOE</b>           | Nuclear Overhauser Effect   |
| <b>NOESY</b>         | Nuclear Overhauser Effect Spectroscopy  |
| <b>PBK</b>           | Phosphonium benzoate ketone   |
| <b>PDH</b>           | Pyruvate Dehydrogenase  |
| <b>Phe</b>           | Phenylalanine   |
| <b>PNP</b>           | <i>p</i> -nitrophenol   |
| <b>Pro</b>           | Proline   |
| <b>PTE</b>           | Proton-transfer-elimination   |
| <b>RDS</b>           | Rate-determining step   |
| <b>SET</b>           | Single electron transfer  |
| <b>TF</b>            | Trifunctional   |



|                                      |                           |
|--------------------------------------|---------------------------|
| <b>TIM</b>                           | Triosephosphate isomerase |
| <b>TPP</b>                           | Triphenylphosphine        |
| <b>TS</b>                            | Transition state          |
| <b>Zn<sup>i</sup>-Pr<sub>2</sub></b> | Diisopropylzinc           |

## List of Figures

|   |    |
|---|----|
| <b>Figure 1.1.</b> Generic mechanism for the MBH reaction and the proposed proton transfer pathways. ....   | 11 |
| <b>Figure 1.2.</b> Response to an acid additive for trifunctional organocatalyst <b>TF-1</b> . ....   | 20 |
| <b>Figure 1.3.</b> a) Asymmetric amplification by the Soai reaction of pyrimidine carboxaldehydes 1.28.b) Effect of catalyst <b>1.29</b> ee on product <b>1.29</b> ee. <sup>150</sup> .....   | 24 |
| <b>Figure 1.4.</b> The conceptual framework for the work covered in this a) Chapter 2–4 and b) Chapter 5 in this thesis. ....   | 29 |
| <b>Figure 2.1.</b> <sup>1</sup> H NMR spectra (600 MHz, CD <sub>2</sub> Cl <sub>2</sub> ) for a) <b>TF-1</b> b) <b>TF-1</b> and <b>MVK</b> c) <b>TF-1</b> , <b>MVK</b> and BzOH ( <b>TF-1-PBK</b> ) with an insert of the <sup>31</sup> P NMR spectrum.....   | 53 |
| <b>Figure 2.2.</b> a) Phase edited <sup>1</sup> H- <sup>13</sup> C HSQC (600 MHz, CD <sub>2</sub> Cl <sub>2</sub> ). b) <sup>1</sup> H- <sup>13</sup> C HMBC NMR spectrum (600 MHz, CD <sub>2</sub> Cl <sub>2</sub> ) expansion of <b>TF-1-PBK</b> at 278 K. c) Assignment map for <b>TF-1-PBK</b> , key structural HMBC correlations are shown in blue. The benzoate is not shown for clarity. d) <b>TF-2-PBK</b> as the model system for refinement of the butanone motif. .... | 56 |
| <b>Figure 2.3.</b> The proportion of the <b>PBK</b> relative to free phosphine at 10 °C and 20 °C. ....   | 58 |
| <b>Figure 2.4.</b> a) The initial rate for <b>TF-1</b> without (pathway 1) and BzOH (pathway 2). b) Shift in mechanism induced by key intermediates for Pathway 1 ( <b>TF-1-PE</b> ) and Pathway 2 ( <b>TF-1-PBK</b> ). ....  | 60 |
| <b>Figure 2.5.</b> a) Conversion and enantioselectivity determined for trifunctional organocatalysts through the <b>PBK</b> pathway, b) Conversion and enantioselectivity determined for bifunctional catalysts through the <b>PE</b> pathway. ....   | 61 |
| <b>Figure 2.6.</b> a) Structural model of the lowest energy structure from Cluster 3 with dihedral angle C-1–C-2–P–C(R)6. b) Dihedral angle plot highlighting identified clusters. c)   |    |

|  |    |
|--|----|
| Representative structures and distances for Cluster 1–4 with the key cluster 3 shown in more detail. ....  | 66 |
| <b>Figure 2.7.</b> a) Conformation of the phosphonium butanone and associated dihedral angles.<br>b) Staggered geometry of the phosphonium butanone favours hydrogen bonding.....  | 68 |
| <b>Figure 2.8.</b> a) Clustered structures identified from molecular dynamics. b) Representative structures for the identified structures. ....  | 71 |
| <b>Figure 2.9.</b> 3D HSQC-NOESY spectrum acquired displaying (a) aromatic and (b) aliphatic region for <b>TF-1-PBK</b> with $^{13}\text{C}_6\text{-BzOH}$ at 298 K. ....  | 72 |
| <b>Figure 2.10.</b> a) NOEs observed for <b>TF-1-PBK</b> at 298 K. b) The active position the benzoate adopts to initiate proton motion.....   | 73 |
| <b>Figure 2.11.</b> Activation of <b>TF-1-PBK</b> by proton transfer. ....   | 75 |
| <b>Figure 2.12.</b> a) The NMR observable tautomer <b>TF-1-PBK</b> is a gateway to different tautomeric forms of the <b>PBK</b> . b) Energies calculated for the <b>TF-1-PBK</b> tautomers c) <b>TF-1-PBK</b> as a KSI mimic. .... | 77 |
| <b>Figure 2E.1.</b> Model Spectra showing the proportion of <b>TF-1-PBK</b> at 10 °C. ....   | 81 |
| <b>Figure 2E.2.</b> Peak assignment map for <b>TF-1-PBK</b> . ....   | 82 |
| <b>Figure 2E.3.</b> $^1\text{H}$ NMR spectrum (600 MHz, $\text{CD}_2\text{Cl}_2$ ) for <b>TF-1-PBK</b> . a) Aromatic region and b) aliphatic region.....   | 83 |
| <b>Figure 2E.4.</b> $^{13}\text{C}$ NMR spectrum (150 MHz, $\text{CD}_2\text{Cl}_2$ ) for <b>TF-1-PBK</b> covering the spectral range a) 140–210 ppm, b) 126–138 ppm, c) 110–125 ppm, d) 18.80–50 ppm. ....                        | 84 |
| <b>Figure 2E.5.</b> HSQC spectrum of the aromatic region for <b>TF-1-PBK</b> in $\text{CD}_2\text{Cl}_2$ . ....  | 85 |
| <b>Figure 2E.6.</b> a) Complete COSY Spectrum (600 MHz, $\text{CD}_2\text{Cl}_2$ ) for <b>TF-1-PBK</b> . b) Expansion of the aromatic region (6.80–7.10 ppm) of <b>TF-1-PBK</b> .....  | 86 |

|   |     |
|---|-----|
| <b>Figure 2E.7.</b> a) Complete HMBC Spectrum (600 MHz, CD <sub>2</sub> Cl <sub>2</sub> ) for <b>TF-1-PBK</b> . b) Expansion of the aromatic region ( <sup>1</sup> H: 7.50–8.20 ppm; <sup>13</sup> C: 126–136 ppm) of <b>TF-1-PBK</b> . c) Expansion of the aromatic region ( <sup>1</sup> H: 6.80–7.50 ppm; <sup>13</sup> C: 126–136 ppm) of <b>TF-1-PBK</b> ..... | 87  |
| <b>Figure 2E.8.</b> 2D NOESY spectrum (400 ms mixing time, 600 MHz, CD <sub>2</sub> Cl <sub>2</sub> ) for <b>TF-1-PBK</b> covering a) the aromatic region and b) aliphatic region. ....   | 88  |
| <b>Figure 2E.9.</b> Key correlations for <b>TF-1-PBK</b> determined by 2D NMR spectroscopy, spin systems are shown in blue. ....  | 90  |
| <b>Figure 2E.10.</b> <sup>1</sup> H NMR spectrum (600 MHz, CDCl <sub>3</sub> ) for the phosphonium butanone of <b>TF-2-PBK</b> performed at (a) 278 K and (b) 298 K. The Rauhut-Currier side-product is annotated in (b). ....  | 92  |
| <b>Figure 2E.11.</b> a) Homonuclear <i>J</i> -Resolved experiment (600 MHz, CDCl <sub>3</sub> , 278 K) showing expansions for aliphatic protons b) H <sub>β3.43</sub> c) H <sub>α2.95</sub> d) H <sub>β2.82</sub> e) H <sub>α2.37</sub> .....   | 93  |
| <b>Figure 2E.12.</b> <b>TF-2-PBK</b> 2D NOESY spectrum (600 MHz, CDCl <sub>3</sub> , 278 K) with key NOEs annotated. ....   | 95  |
| <b>Figure 2E.13.</b> a) <b>TF-2-PBK</b> <sup>1</sup> H NMR spectrum (600 MHz, CD <sub>2</sub> Cl <sub>2</sub> ). b) 1D Selective NOESY spectrum from irradiation of H-β (3.34 ppm). c) 1D Selective NOESY spectrum from irradiation of H-β' (2.82 ppm) .....  | 96  |
| <b>Figure 2E.14.</b> Pulse program (hmbcgplpndqf) for 2D HMBC experiments.....  | 98  |
| <b>Figure 2E.15.</b> Pulse Program (hsqcedetgpsp.3) for phase-edited HSQC. <sup>44-46</sup> .....   | 98  |
| <b>Figure 2E.16.</b> Pulse Program (noesygpphzs) for quantitative 2D NOESY experiments. <sup>47-49</sup> ...  | 99  |
| <b>Figure 2E.17.</b> Pulse program (cosygpppqf) for 2D COSY experiments. ....   | 99  |
| <b>Figure 2E.18.</b> Pulse program (jresqf) for 2D homonuclear <i>J</i> -Resolved experiments.....  | 100 |
| <b>Figure 2E.19.</b> Pulse program (hsqcgpnwngx33d) for 3D HSQC-NOESY experiments. <sup>45, 50-52</sup>   | 100 |

|   |     |
|---|-----|
| <b>Figure 3.1.</b> Comparison of the acid additive on rate and <i>ee</i> of the <b>TF-1</b> catalysed <i>aza</i> -MBH reaction with a) substituted benzoic acids, b) hindered aromatic acids and 3) low $pK_a$ aromatic acids. ....   | 118 |
| <b>Figure 3.2.</b> a) Formation of <b><i>d</i>-MVK</b> and relative rate constants for deuterium incorporation for a panel of catalysts. b) Catalytic profiles for <i>aza</i> -MBH reaction .....   | 126 |
| <b>Figure 3.3.</b> Possible proton transfer pathways. a) Direct Protonation by benzoic acid. b) Cooperative protonation mediated by BzOH-catalyst complex. c) Formation of the <b>TF-1-Al</b> intermediate. d) The structural model for <b>TF-1-Al<sup>+</sup></b> show the conformation amenable to proton transfer.....   | 133 |
| <b>Figure 3E.1.</b> a) $^1\text{H}$ NMR spectrum (600 MHz, $\text{CD}_2\text{Cl}_2$ , 298 K) of the crude reaction mixture with <b>NTs-Im-1</b> and $\alpha$ - <b><i>d</i>-NTs-Im-1</b> catalysed by <b>TF-2</b> . b) $^1\text{H}$ NMR expansion (4.90-6.60 ppm) highlighting the key proton 5.21 ppm ( <b>NTs-MBH-1</b> ) and 6.10 ppm ( $\alpha$ - <b><i>d</i>-NTs-MBH-1</b> , <b>NTs-MBH-1</b> ). .... | 138 |
| <b>Figure 4.1.</b> 2-Pyridine <i>aza</i> -MBH adducts and catalysts used for the transformation.....  | 156 |
| <b>Figure 4.2.</b> 3-pyridine NTs <i>aza</i> -MBH adducts ( <b>NTsPyr-MBH-1</b> ) and the catalysts used for the transformation. ....   | 158 |
| <b>Figure 4.3.</b> Effect of the acid additive on rate and <i>ee</i> of the <b>TF-1</b> catalysed <i>aza</i> -MBH reaction with a) substituted BzOHs, b) hindered aromatic acids and 3) low $pK_a$ aromatic acids. ....   | 168 |
| <b>Figure 4.4.</b> Effect of BzOH loading on catalytic proficiency for model substrate <b>NTsPyr-Im-1</b> . ....  | 170 |
| <b>Figure 4.5.</b> Proton transfer network mediated by the cooperative action of chemical motifs. ....  | 171 |
| <b>Figure 5.1.</b> Enantioselectivity for control chiral initiators. ....   | 204 |

|   |     |
|---|-----|
| <b>Figure 5.2.</b> Comparison of methodology for the Soai reaction. ....  | 206 |
| <b>Figure 5.3.</b> Asymmetric amplification of <b>5.1</b> using alternate methodology with L-proline and<br>isolate <i>aza</i> -MBH adducts. ....           | 207 |
| <b>Figure 5.4.</b> Soai reactions initiated by various modes of the <i>aza</i> -MBH catalysis. ....   | 209 |
| <b>Figure 5.5.</b> a) Proton-transfer temporal sequenced <i>aza</i> -MBH–Soai reaction. b) Size of the<br>asymmetric ripple induced by proton transfer..... | 211 |

## List of Schemes

|  |    |
|--|----|
| <b>Scheme 1.1.</b> Common activation modes in organocatalysis. ....  | 4  |
| <b>Scheme 1.2.</b> Common organocatalytic motifs. ....   | 6  |
| <b>Scheme 1.3.</b> Proton transfer in the active sites of pyruvate dehydrogenase synchronises the reactions catalysed by each monomer. ....  | 7  |
| <b>Scheme 1.4.</b> Tautomerisation catalysed by KSI. ....  | 8  |
| <b>Scheme 1.5.</b> The isomerisation of dihydroxyacetone phosphate catalysed by TIM. ....  | 9  |
| <b>Scheme 1.6.</b> Aldol and MBH reactions as net proton transfer reactions. ....  | 10 |
| <b>Scheme 1.7.</b> The mechanism proposed by McQuade et al. <sup>113</sup> ....  | 13 |
| <b>Scheme 1.8.</b> Role of the protic product in the MBH autocatalysis. <sup>115, 122-123</sup> ....   | 14 |
| <b>Scheme 1.9.</b> Key Intermediates detected by ESI-MS from the MBH reaction mixture of methyl acrylate and benzaldehyde catalysed by <b>1.10</b> at t =10 with and without $\beta$ -naphthol. .... | 15 |
| <b>Scheme 1.10.</b> a) Examples of trifunctional organocatalysts. b) Liu group trifunctional organocatalysts. ....   | 17 |
| <b>Scheme 1.11.</b> a) The rationale behind the design of trifunctional organocatalysts for the aza-MBH. b) Bifunctional controls demonstrating the trifunctionality of the catalyst. ....           | 19 |
| <b>Scheme 1.12.</b> Tuning of the proficiency of trifunctional organocatalyst by changing the Brønsted acid. ....  | 21 |
| <b>Scheme 1.13.</b> Frank model for mutual inhibition. ....  | 25 |
| <b>Scheme 1.14.</b> Schematic for the Soai reaction. ....  | 25 |
| <b>Scheme 1.15.</b> The model substrate used to establish the limits of the Soai reaction. ....  | 26 |
| <b>Scheme 1.16.</b> Substrate scope for the Soai reaction. ....  | 26 |

|  |     |
|--|-----|
| <b>Scheme 2.1.</b> Studies reporting the formation of parasitic phosphonium butanone intermediates. <sup>33-36</sup> .....   | 49  |
| <b>Scheme 2.2.</b> Key question in this chapter concerns activation of <b>TF-1-PBK</b> . .....   | 52  |
| <b>Scheme 2.3.</b> Formation of <b>TF-1-PBK</b> via protonation of <b>TF-1-PE</b> . .....  | 54  |
| <b>Scheme 2.4.</b> Key structural features and methods of analysis.....  | 64  |
| <b>Scheme 3.1.</b> The povarov reaction catalysed by a chiral thiourea <b>3.8</b> . .....  | 110 |
| <b>Scheme 3.2.</b> Diastereodivergent Sulfa-Michael addition of thiols to $\alpha$ -branched enones. .   | 111 |
| <b>Scheme 3.3.</b> aza-MBH catalysed by $\beta$ -ICD-amide catalyst <b>3.14</b> . .....  | 112 |
| <b>Scheme 3.4.</b> The aza-MBH reaction catalysed by $\beta$ -ICD with improved enantioselectivity in the presence of ( <i>R</i> )-BINOL. ....   | 112 |
| <b>Scheme 3.5.</b> aza-MBH catalysed by <b>3.18</b> with different protic additives.....   | 113 |
| <b>Scheme 3.6.</b> acid-activated aza-MBH catalysed by <b>3.22</b> and benzoic acid. ....  | 113 |
| <b>Scheme 3.7.</b> Tautomeric forms of <b>TF-1-PBK</b> activate C–C bond formation. ....   | 117 |
| <b>Scheme 3.8.</b> a) Tautomers of <b>TF-1-PBK</b> highlighting the key tautomers for C-C bond formation. b) <b>TF-1-PE</b> and <b>TF-1-PBK</b> are in equilibrium in the presence of BzOH, but tautomerisation yields the nucleophilic enol <b>TF-1-PE.BzOH</b> . c) The trifunctional enol and enolate pathways are distinct. d) BzOH does not activate the enol pathway causing rate suppression for <b>MOP</b> ..... | 122 |
| <b>Scheme 3.9.</b> The phenol position and acidity influences proficiency. ....  | 123 |
| <b>Scheme 3.10.</b> Pathways accessible to <b>TF-1-PE.BzOH</b> . ....  | 124 |
| <b>Scheme 3.11.</b> a) Role of the protecting group in the stabilisation of the aldol adduct. b) Catalysis data for different protecting groups on the substrate. ....   | 130 |
| <b>Scheme 3.12.</b> Substrate-directed catalytic emergence for <b>TF-1-PE</b> and <b>TF-1-PE.BzOH</b> . .....  | 131 |



|  |     |
|--|-----|
| <b>Scheme 3.13.</b> BzOH activates a new mechanism for the trifunctional organocatalysed aza-MBH reaction.....   | 134 |
| <b>Scheme 3E.1.</b> Acid screen for model aza-MBH between <b>NTs-Im-1</b> and <b>MVK</b> by <b>TF-1</b> . ....   | 136 |
| <b>Scheme 3E.2.</b> Deuteration of benzoic acid by D <sub>2</sub> O.....   | 137 |
| <b>Scheme 3E.3.</b> Deuteration of trifunctional organocatalysts .....   | 137 |
| <b>Scheme 3E.4.</b> Deuteration and elimination of <b>d-MVK</b> . ....   | 139 |
| <b>Scheme 3E.5.</b> Synthesis of <b>α-d-NTs-Im-1</b> .....   | 140 |
| <b>Scheme 3E.6.</b> Reaction to perform 2° KIE analysis of the acid-regulated aza-MBH.....                       | 142 |
| <b>Scheme 3E.7.</b> TiCl <sub>4</sub> catalysed mesyl imine formation.....                                       | 144 |
| <b>Scheme 3E.8.</b> Preparation of N-Boc substrates via sulfones.....  | 145 |
| <b>Scheme 4.1.</b> Indirect synthesis of aza-MBH adducts by [1,3]-sigmatropic rearrangement. ....                | 157 |
| <b>Scheme 4.2.</b> Potential effects of the pyridine nitrogen base on proton-transfer catalysis..                | 159 |
| <b>Scheme 4.3.</b> Synthesis of substituted 3-pyridinecarboxaldehydes.....                                       | 160 |
| <b>Scheme 4.4.</b> Formation of the bis-sulfonamide product.....   | 161 |
| <b>Scheme 4.5.</b> Proton transfer catalysed by the pyridine nitrogen base a) with acid and b) without acid..... | 166 |
| <b>Scheme 4.6.</b> Effect of the substrate protecting group on reaction outcome for <b>TF-1</b> . ....           | 167 |
| <b>Scheme 4E.1.</b> Synthesis of 3-Pyridine substrates <b>NTsPyr-Im-1–6</b> .....                                | 174 |
| <b>Scheme 4E.2.</b> Synthesis of 2-Pyridine substrates ( <b>NTs-Pyr-Im-7–8</b> ). ....                           | 177 |
| <b>Scheme 4E.3.</b> Synthesis of NBoc protected imines. ....   | 178 |
| <b>Scheme 4E.4.</b> Acid screen for <b>NTsPyr-Im-1</b> with <b>TF-1</b> . ....                                   | 186 |
| <b>Scheme 5.1.</b> a) Conjoined reaction pathway yielding a single product. b) Sequential reactions cycles. .... | 193 |
| <b>Scheme 5.2.</b> Chiral Initiators for the Soai reaction with the configuration of <b>5.2</b> shown. ...       | 195 |

|   |     |
|---|-----|
| <b>Scheme 5.3.</b> Propagation of MBH reaction into the Soai space.....   | 199 |
| <b>Scheme 5.4.</b> a) Synthesis of substrates for the Soai Reaction via lithium-halogen exchange.<br>B) Side-product from the lithium-halogen exchange. c) Alternate synthesis by<br>desulfurative cross coupling.....        | 201 |
| <b>Scheme 5.5.</b> a) Reaction cycles connect the aza-MBH and Soai. b) The size of the asymmetric<br>ripple is a measure of the integrity of chirality transfer indicating the <i>er</i> outcome of the<br>Soai reaction..... | 208 |
| <b>Scheme 5E.1.</b> Preparation of <b>5.40</b> by Sonagoshira cross-coupling .....  | 215 |
| <b>Scheme 5E.2.</b> Preparation of <b>5.1</b> by Lithium-halogen exchange and formylation. ....   | 216 |
| <b>Scheme 5E.3.</b> Preparation of <b>5.1</b> by Barbier-type formylation. ....   | 217 |
| <b>Scheme 5E.4.</b> Preparation of <i>racemic</i> <b>5.2</b> . ....   | 220 |
| <b>Scheme 5E.5.</b> The Soai reaction using Method A.....   | 221 |
| <b>Scheme 5E.6.</b> The Soai reaction using Method B. ....  | 222 |

## List of Tables

|   |     |
|---|-----|
| <b>Table 1.1.</b> Compilation of mechanistic data for the MBH reaction.....   | 12  |
| <b>Table 2.1.</b> Selected NOEs and correlations .....  | 57  |
| <b>Table 2.2.</b> Coupling Constant and dihedral angle for the phosphonium butanone. ....   | 67  |
| <b>Table 2.3.</b> Quantitative NOE values for <b>TF-1-PBK</b> used for constrained molecular dynamics   | 89  |
| <b>Table 3.1.</b> Effect of the Brønsted Acid co-catalyst on the Dipolar Cycloaddition between<br>Crotonaldehyde ( <b>3.2</b> ) and Nitrones ( <b>3.3</b> ). .... | 109 |
| <b>Table 3.2.</b> Effect of various additives for the aza-MBH catalysed by <b>3.23</b> . ....   | 114 |
| <b>Table 3.3.</b> Effect of acid additives on trifunctional organocatalysis.....  | 115 |
| <b>Table 3.4.</b> Effect of the acid additive on catalytic proficiency.....   | 119 |
| <b>Table 3E.1.</b> Proportions of exchangeable protons deuterated. ....   | 138 |
| <b>Table 3E.2.</b> Summary of the second order rate constant for the elimination of <b>d-MVK</b> . ....   | 140 |
| <b>Table 4.1.</b> Effect of BzOH on catalysis for a series of catalysts.....  | 162 |
| <b>Table 4.2.</b> Conversion and enantioselectivity for pyridine substrates catalysed by <b>TF-2</b> . ...  | 164 |
| <b>Table 4.3.</b> Effect of the acid additive on catalytic proficiency for model pyridine substrates.<br>.....  | 168 |
| <b>Table 4.4.</b> Effect of BzOH loading on catalytic proficiency for model substrate <b>NTsPyr-Im-1</b> .<br>.....   | 170 |
| <b>Table 5.1.</b> Key mechanistic investigations of the asymmetric autocatalytic Soai reaction. .   | 198 |
| <b>Table 5.2.</b> Barbier-type formylation of pyrimidine <b>5.40</b> .....  | 203 |

## Naming conventions

The numbering system for all structures in this thesis follow one of two formats:

- For model systems present in multiple chapters, they are classified first by the class of compound and then sequential numbering: **Class.Compound#**. For example, all trifunctional organocatalysts following the convention TF-#.

| Compound Class               | Numbering Convention                 |
|------------------------------|--------------------------------------|
| Trifunctional organocatalyst | <b>TF-#</b>                          |
| Bifunctional organocatalyst  | <b>BF-#</b>                          |
| MBH Imine Substrate          | <b>PG-Im-#</b> (PG= Ts, Boc, Ms)     |
| MBH adduct                   | <b>PG-MBH-#</b> (PG= Ts, Boc, Ms)    |
| MBH pyridine Imine           | <b>PGPyr-Im-#</b> (PG= Ts, Boc, Ms)  |
| MBH Pyridine Imine           | <b>PGPyr-MBH-#</b> (PG= Ts, Boc, Ms) |

- Compounds that only appear in a single chapter or do not belong to a general class of compounds are numbered by: **Chapter#.Compound#**.

# **Chapter 1**

## **Model Systems for Chirality**

### **Transfer by Asymmetric**

### **Catalysis**

## 1. Introduction

The interest in the questions addressed in this thesis arose initially from understanding some mechanistic peculiarity in a model asymmetric catalytic reaction (the aza-Morita–Baylis–Hillman (aza-MBH) reaction). Asymmetric catalysis, in addition to its obvious technological utility for accessing chiral molecules and materials, has a special status in chemical reactivity, in that a transformation can be biased and accelerated by a pre-existing molecule. In the case of asymmetric autocatalysis, the product of the catalysis is also the catalyst, thus providing homologous chemical propagation that amplifies the initial bias (e.g. the Soai reaction or asymmetric autocatalysis). Here the investigations, starting with one asymmetric catalytic reaction, launch into understanding how some of the propagative nature of asymmetric catalysis can be introduced at the reaction level so that one asymmetric catalytic reaction (the aza-MBH) can differentiate, rather than cascade, into another (the Soai reaction).

The introductory chapter provides the background information for the following: 1) brief overview of asymmetric catalysis and modes of activation particularly relevant by organic catalysts; 2) proton transfer as a fundamental process for coordinating reactive intermediates in catalysis; 3) the MBH reaction as a model reaction for understanding proton transfer; 4) the Soai reaction (asymmetric autocatalysis) in chirality amplification in a reaction network; 5) project aims.

### 1.1 Asymmetric Catalysis

Asymmetric catalysis is an established approach for addressing the perpetual need for chiral compounds from achiral precursors. Development of asymmetric catalysts and syntheses underpin the economic viability of the pharmaceutical and materials industry,<sup>1-3</sup> a topic that

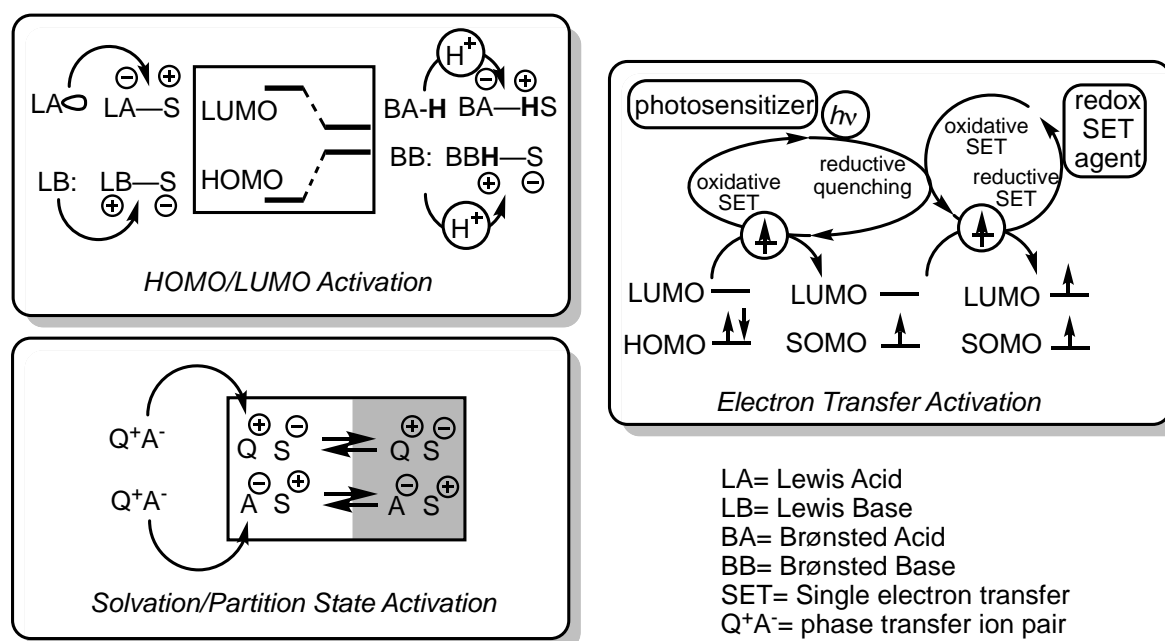
has been extensively investigated and reviewed.<sup>4-11</sup> Over the past century, catalysts have been prepared to meet the application demand from varieties of molecular compositions, including small organic molecules,<sup>12-22</sup> inorganic/metal complexes,<sup>23-25</sup> and enzymes.<sup>26-30</sup>

The three main classes of catalysts- enzymes, organometallics and organic catalysts- all have advantages and disadvantages in their effectiveness. The effectiveness of a catalyst can be assessed by the REAP factor: **R**ationale (activity based on mechanistic insight), **E**fficiency (low loading; ambient or green reaction conditions and facile catalyst recovery), **A**daptability (modular development for easy customisation) and **P**roficiency (high rate and enantioselectivity).<sup>31</sup> Enzymes satisfy the criteria for proficiency, efficiency and rationale but are more limited in adaptability, an issue that can be addressed by directed evolution in some cases.<sup>32-35</sup> Transition-metal catalysts can be highly proficient with low catalyst loading, easily adaptable by altering the ligand or metal centre, but mechanistically are less well understood.<sup>36-39</sup> In addition, the environmental impact and renewability issue reduces its long-term economic efficiency.<sup>40-41</sup> Organocatalysts are more easily adapted and mechanistically better understood. However, of the three catalyst domains, organocatalysts are the least proficient with only occasional examples of potency.<sup>42-43</sup>

Of the three domains of catalysts, the origin of catalytic power is investigated in depth for enzymes and their modes of activation. Much of the insight from understanding enzymatic catalysis has assisted in catalyst discovery in designed systems, yet our ability to mimic enzyme-like catalytic proficiency common to living systems remains very limited. In particular, a basic conceptual framework is lacking for understanding how enormous catalytic power can be initiated and evolved from a basal level with simple constituents. In other words,

asymmetric catalysis can be investigated, not from the perspective of technological utility, but as an entry into understanding chemical evolution that perhaps is predicated on a chemical system that has to first become propagative. In this sense, the organic catalytic paradigm may offer useful and tractable model systems for finding fundamental driving forces and principles behind evolvable chemical propagation.

Organocatalysts can be primarily characterised by the functional motifs that facilitate their activity. Many reviews have covered this topic extensively, from which a few primary modes of activation can be summarised (Scheme 1.1).<sup>44-52</sup>



**Scheme 1.1.** Common activation modes in organocatalysis.

These primary modes of activation (orbital activation, electron transfer activation, solvation state activation) promote electron exchange between molecules by altering the carriage, relay, and solvent environment in which the electron exchange occurs. From these primary modes of activation, basic operational strategies can be identified to facilitate distinct roles in authorising electron exchange: 1) HOMO/LUMO orbital activation by a Lewis acid/base (LA



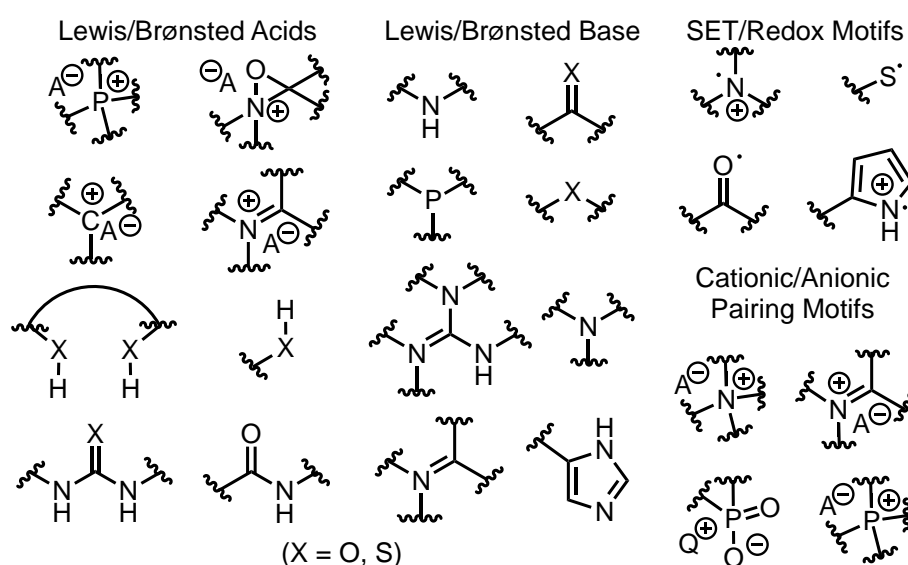
or LB) or Brønsted acid/base (BA or BB)(with a proton), 2) single electron transfer (SET) activation by a redox component in the ground state or excited state (with photon consumption), 3) solvation/partition state activation by either a cationic or anionic charge or dipole. Activation modes can overlap within a single reaction system, while the basic principles behind the mode of activation remain constant.<sup>53-56</sup>

Synergistic catalysts, in which HOMO and LUMO are simultaneously activated, is a potent approach for improved catalyst proficiency.<sup>57</sup> For example, iminium formation can lower the substrate LUMO and enamine formation can raise the substrate HOMO through Lewis and Brønsted acid/base interactions. In SET activation, a SET agent transfers an electron between substrates or reactants. In some cases, an additional photon is consumed to activate the catalyst to the excited state for the electron relay to occur. Alternatively, photonic energy can be transmitted by a catalyst to the substrate, without necessarily SET, such that subsequent SET processes can proceed in the excited state.<sup>58</sup> Overall, multiple SET/redox agents can be involved to catalyse a given reaction, with some of them consuming photons to complete their catalytic cycle. Powerful reaction cycles have been established by combining the selectivity of SET activation with HOMO/LUMO activation.<sup>59</sup>

In solvation/partition state activation, typically ionic catalysts bind to polar or charged intermediates and assists in stabilising transition structures of these high-energy species.<sup>60</sup> Additionally, the catalyst can polarise the starting substrates to activate the reaction. In phase-transfer catalysis, the catalyst–substrate complex also facilitates mass transfer to partition the substrate into the solution phase that contains the other reactants and is conducive to transition state (TS) stabilisation.<sup>61-62</sup> Ion pairing is a general phenomenon and

may occur concurrently with orbital activation or SET due to changing protonation state or charge electron transfer.<sup>49, 63</sup>

These primary modes of activation are typically performed by catalytic motifs, defined here as the chemical groups that present the catalytic functional components.<sup>43</sup> Some of the most prevalent chemical motifs employed in asymmetric organocatalysis as monofunctional activation motifs are shown in Scheme 1.2. Generally, one chemical motif can function in mechanistically distinct roles at different time points along a reaction pathway. Moreover, a motif is not restricted to a single mode of activation and can be involved in different types of catalysis. For example, a thiol group may act as a Brønsted acid in catalysis or as a SET agent.<sup>64-66</sup> Likewise, tertiary amines have wide-spread application as Lewis or Brønsted bases as well as SET agents.<sup>67-69</sup> When the chemical motifs for catalytic activation are compatible under the reaction conditions, catalysis by combining any of the three domains of activation modes has been a highly productive approach in finding novel reactions pathways.<sup>70-71</sup>

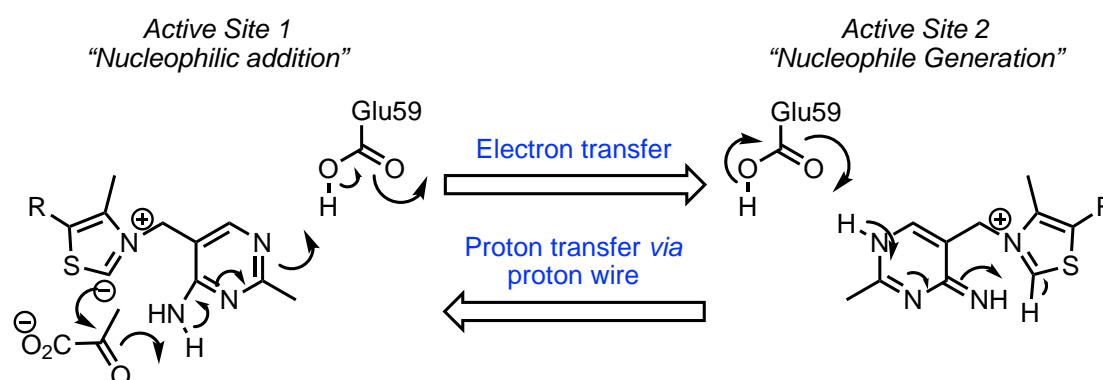


**Scheme 1.2.** Common organocatalytic motifs.

## 1.2 Proton transfer as a fundamental process for coordinating reactive intermediates in catalysis

Proton transfer is a fundamental process in organic and biological chemistry.<sup>72-75</sup> The hydrogen atom is the smallest of all elements and in the context of proton transfer reactions can be considered as an empty *s* orbital.<sup>76</sup> Proton motion not only provides chemical activation (orbital activation) but also simultaneously carries structural information.

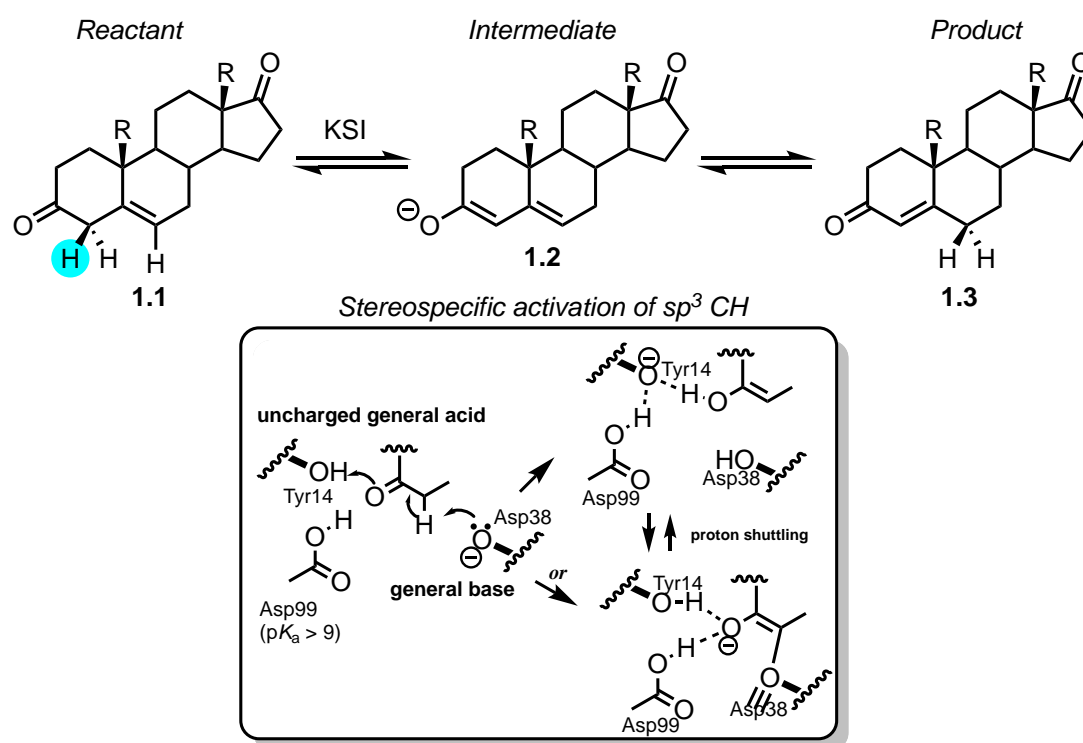
Enzymes have evolved to direct proton transfer with high temporal and spatial specificity. Pyruvate dehydrogenase (PDH) is a thiamine-dependent homodimer that displays classic "ping-pong" kinetics, and each monomer catalyses two half reactions. A proton wire synchronises the action of the two monomers; when one monomer requires a general acid, the other requires a general base ensuring coordination of protonation states between the two monomers (Scheme 1.3).<sup>77</sup> In this instance, coordinated proton motion provides temporal sequencing of the thiamine-dependent reaction.



**Scheme 1.3.** Proton transfer in the active sites of pyruvate dehydrogenase synchronises the reactions catalysed by each monomer.

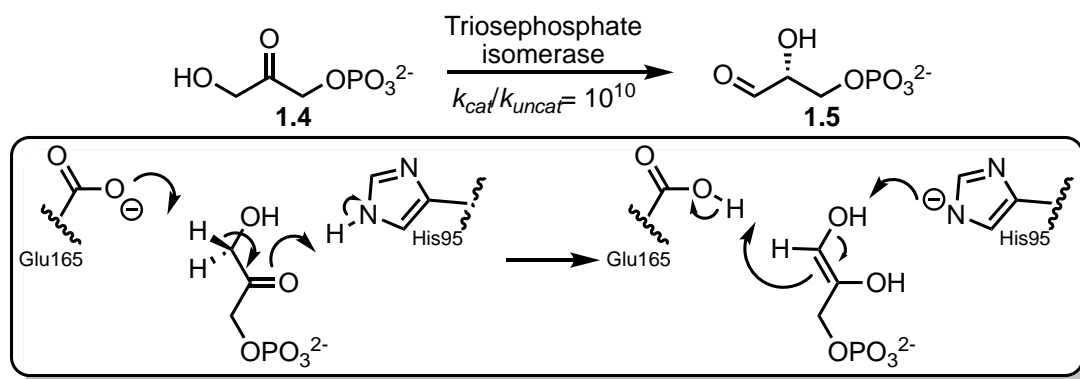
One of the most well-studied model systems to examine the origins of catalytic proficiency is the enzyme ketosteroid isomerase (KSI). KSI catalyses the isomerization of a variety of  $\Delta^5$ -3-

ketosteroids (**1.1**) to  $\Delta^4$ -3-ketosteroids (**1.3**) via activation and deprotonation of a  $sp^3$  C-H followed by proton transfer to isomerise the steroid through an intermediate dienolate (**1.2**) (Scheme 1.4).<sup>78-81</sup> Stereospecifically controlled proton transfer, coordinated by acid-base residues in the active site, is achieved with enormous rate enhancement over the uncatalysed reaction ( $k_{cat}/k_{uncat} = 10^{15}$ ).<sup>82</sup>



**Scheme 1.4.** Tautomerisation catalysed by KSI.

Temporal and spatial control of proton transfer is critical for the catalytic proficiency (i.e. large rate enhancement coupled to asymmetric induction) of enzymes.<sup>83-86</sup> The enzyme triosephosphate isomerase (TIM) controls proton transfer to enact stereospecific isomerisation of dihydroxyacetone phosphate (**1.4**) to D-glyceraldehyde phosphate (**1.5**) with the C-2 hydroxy in the (*R*) configuration (Scheme 1.5).<sup>87-91</sup> This reaction proceeds with  $10^{10}$  fold rate enhancement over the uncatalyzed reaction. This unprecedented rate elevation is achieved by the cooperation of mild chemical motifs (glutamic acid-165 and histidine-95) under ambient conditions.



**Scheme 1.5.** The isomerisation of dihydroxyacetone phosphate catalysed by TIM.

In organic reactions, proton transfer is frequently an essential process for ratifying electron exchange such as in the Direct Aldol and Strecker reaction.<sup>92-95</sup> Unlike enzymes that have evolved to perform catalysis in water, water is not a suitable solvent for many organocatalytic reactions.<sup>96</sup> Designing catalysts for proton transfer presents significant challenges for several reasons, including small energy barriers for proton exchange across various basic sites with diminished spatial control, undesired reactivity quenching of catalyst nucleophilic motifs, and the high tendency of protic initiation of undesirable pathways, especially in multistep organic reactions. Enzymes have evolved to tightly coordinate proton transfer with specific temporal and spatial control even in water, and such organised proton transfer in organocatalysis remains extremely difficult.

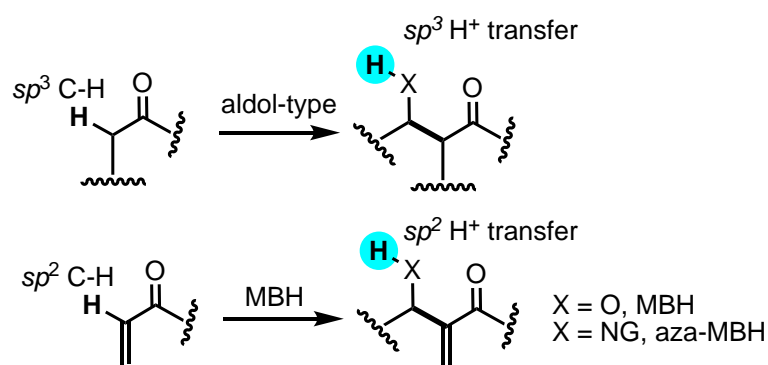
Biological systems have developed strategies to enable not just single reaction control but also sequences to organise transformations with a multitude of regulatory elements for constructing reaction networks that persist in time. In organic catalysis, very basic examples that mimic somewhat this “organised catalysis” exist, whereby multiple catalysts or catalytic modes of activation, from hybrid or uniform catalyst classes, cooperate to direct cascade or domino reaction pathways to achieve unprecedented chemical diversity and complexity.<sup>25, 71,</sup>

<sup>97-101</sup> One critical question in the long term is to extrapolate new organisational principles that

can allow basic, designed systems to potentially propagate and evolve, and processes such as proton transfer will likely be a key element in organising biomimetic reaction systems.

### 1.3 The Morita–Baylis–Hillman Reaction: an organocatalytic model reaction for proton transfer

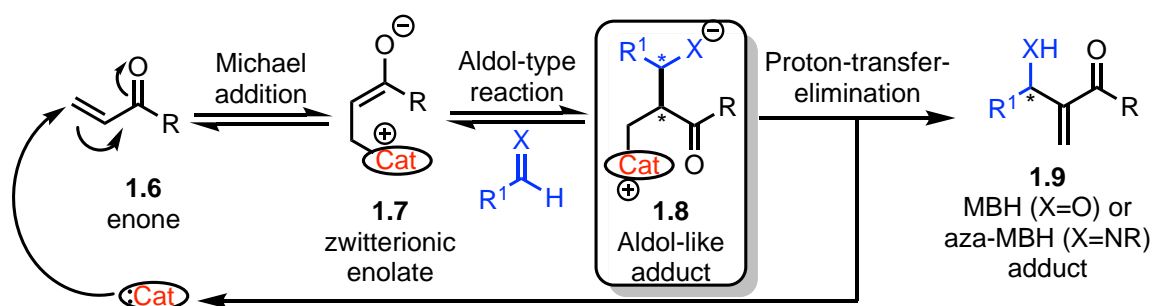
The Morita–Baylis–Hillman (MBH) reaction is the addition reaction between an aldehyde or an imine (in the case of the *aza*-MBH reaction) with an activated alkene catalysed by a nucleophilic catalyst.<sup>102-103</sup> It can be viewed as a net proton transfer reaction analogue of the aldol class of reactions (Scheme 1.6).



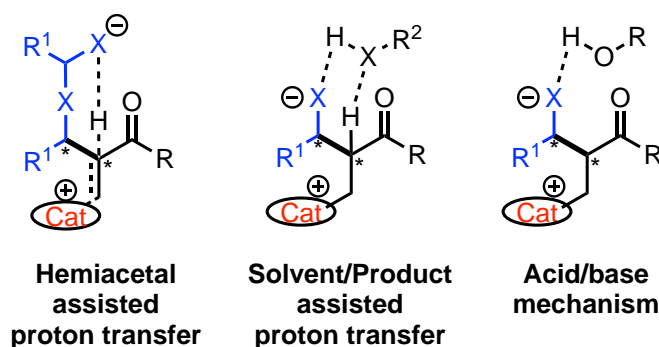
**Scheme 1.6.** Aldol and MBH reactions as net proton transfer reactions.

The synthetic utility of the MBH class of reaction is well established.<sup>104-107</sup> However, the asymmetric variant is underutilised in total synthesis or pharmaceutical synthesis in part due to the capricious substrate scope, low rates and difficulties in asymmetric induction. Developing proficient catalysts for the MBH reaction is attractive due to the wide variety of potential transformations that can be performed with the MBH adduct, in addition to its fundamental value as a model system for understanding coordinated proton transfer.

Extensive mechanistic investigation performed over the past two decades have deconvoluted the reaction mechanism and highlighted why developing proficient catalytic systems is a difficult challenge. The general mechanism has been accepted to consist of three distinct mechanistic steps (Figure 1.1).<sup>108-110</sup> Firstly, the activated alkene (**1.6**) undergoes a Michael addition in the presence of a phosphine or amine nucleophile to generate a zwitterionic intermediate (**1.7**). The incipient enolate then undergoes an Aldol or Mannich addition to generate second zwitterionic intermediate **1.8** (of which there are four diastereomers) and a new carbon-carbon bond. Finally, after a proton-transfer-elimination (PTE) step, an  $\alpha$ -methylene- $\beta$ -hydroxy-carbonyl or  $\beta$ -aminocarbonyl compound (**1.9**) is produced with the generation of a new chiral centre. A compilation of the mechanistic studies for the MBH reaction can be seen in Table 1.1.

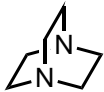
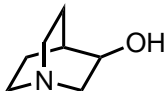
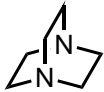

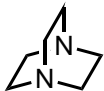

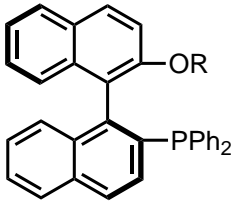
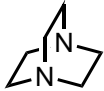


**Proton transfer mechanism for the MBH reaction**



**Figure 1.1.** Generic mechanism for the MBH reaction and the proposed proton transfer pathways.

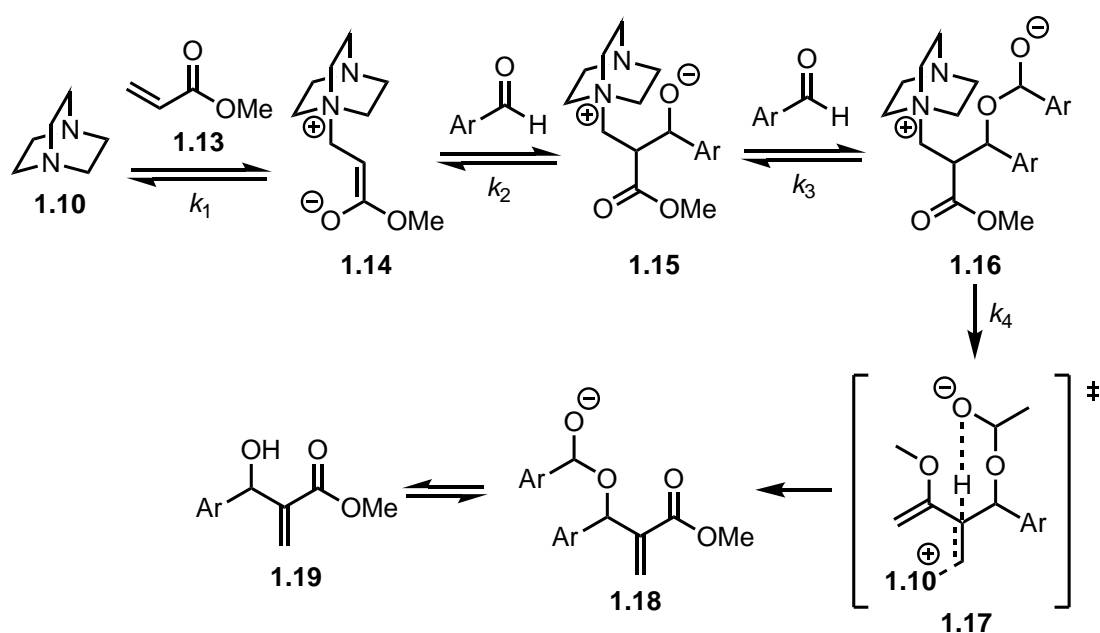
**Table 1.1.** Compilation of mechanistic data for the MBH reaction.

| Author                      | Year | Catalyst   | Conditions   | Methods   | Key findings   |
|-----------------------------|------|--|--|---|--|
| Hill, Isaacs <sup>111</sup> | 1990 | <br><b>1.10</b>   | Acrylonitrile, acetaldehyde, 25 °C, variable pressure                      | Gas-liquid chromatography   | MBH consists of a three-step mechanism: 1) Michael addition producing a zwitterionic enolate, 2) Aldol reaction, 3) PTE.                                     |
| Bode, Kaye <sup>112</sup>   | 1991 | <br><b>1.11</b>   | Acrylate esters, pyridine-carboxaldehydes CDCl <sub>3</sub> , 37 °C        | <sup>1</sup> H NMR spectroscopy                                   | Supported aldol reaction as RDS. Proposed hydrogen bond mediated stabilisation of enolate intermediate dictates the stereochemistry in the PTE.              |
| McQuade <sup>113-114</sup>  | 2005 | <br><b>1.10</b>   | Methyl acrylate, p-nitrobenzaldehyde, aprotic solvents                     | <sup>1</sup> H NMR spectroscopy, GC, kinetic isotope effect (KIE) | The reaction is second order in aldehyde and proceeds through a hemiacetal orchestrated proton transfer. PTE is RDS in aprotic solvents at early conversion. |
| Aggarwal <sup>115</sup>     | 2005 | <br><b>1.12</b>   | C(2)- <sup>2</sup> H and C(2)- <sup>1</sup> H ethyl acrylate, benzaldehyde | <sup>1</sup> H NMR spectroscopy                                   | Supported PTE as RDS, product autocatalysis and RDS shifting to the aldol step.  |
| Amarante <sup>116</sup>     | 2009 | <br><b>1.10</b>  | Methyl acrylate, benzaldehyde, β-naphthol                                  | ESI-MS  | McQuade's proposed pathway operates in the absence of an additional proton source. Aggarwal's dominates with an additional proton source.                    |
| Jacobsen <sup>117</sup>     | 2005 | <br><b>1.10</b> | Methyl acrylate, C(2)- <sup>2</sup> H methyl acrylate imines               | GC, <sup>2</sup> H KIE  | KIE showed that proton transfer elimination step was rate limiting during the initial stages of the reaction.  |
| Shi <sup>118</sup>          | 2005 | <br><b>AP-R</b> | Methyl vinyl ketone, tosylimine  | <sup>31</sup> P NMR, <sup>1</sup> H NMR spectroscopy              | Changes in <sup>31</sup> P chemical shift indicate the hydroxy group is important for the stability of the phosphonium enolate intermediate.                 |
| Leitner <sup>119</sup>      | 2005 | PPh <sub>3</sub><br><b>TPP</b>   | MVK, 4-fluorobenzylidene-tosylimine  | <sup>19</sup> F NMR spectroscopy                                  | Broken order of the imine indicated acid additive (phenol) accelerate proton transfer; aldol is rate limiting.   |
| Lindner <sup>120</sup>      | 2013 | PPh <sub>3</sub><br><b>TPP</b>   | Methyl vinyl ketone, tosylimine, p-nitrophenol                             | <sup>1</sup> H NMR, <sup>31</sup> P NMR, 2D-NMR spectroscopy      | Acid additives help to protonate the enolate to produce a phosphonium ketone that is unreactive. Presence of ketone is independent of solvent.               |
| Singleton <sup>121</sup>    | 2015 | <br><b>1.10</b> | Methyl acrylate, p-nitrobenzaldehyde, MeOD-d <sub>4</sub> , r. t.          | <sup>13</sup> C KIE, <sup>2</sup> H KIE, computational chemistry  | An acid-base mechanism after the aldol step is in operation in MeOH.   |



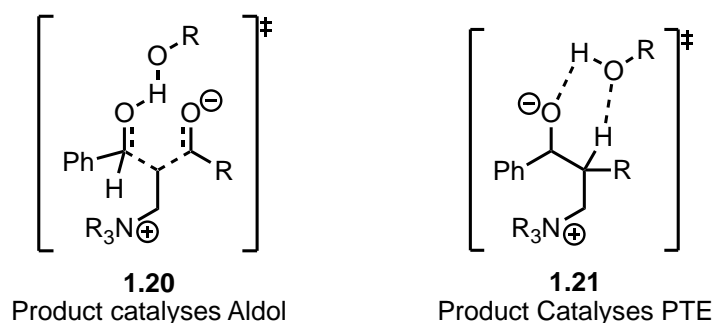
Hill and Isaacs demonstrated using a model MBH reaction catalysed by **1.10** that the MBH reaction consists of three key steps: 1) Michael addition, 2) Aldol addition and 3) proton-transfer-elimination.<sup>111</sup> Bode and Kaye later demonstrated using bifunctional catalyst **1.11** that the rate-determining step in the presence of an proton donor is the aldol addition.<sup>112</sup>

Three main mechanisms for the proton-transfer-elimination step have been proposed over the past two decades. McQuade et al.<sup>113-114</sup> demonstrated that for a model reaction between p-nitrobenzaldehyde and acrylate **1.13** catalysed by **1.10** in the absence of protic additive the rate determining step was not the Aldol reaction, rather it was the PTE, and the reaction was second order with respect to aldehyde. The author's proposed a mechanism that proceeds through a hemiacetal intermediate **1.16** (Scheme 1.7). This mechanism provides four-diastereomeric transition states (**1.17**), only one of which proceeds to the MBH acetal **1.18**, which can hydrolyse to yield the MBH adduct (**1.19**). They proposed this key TS was a factor for the slow rate of reaction as the other aldol adducts revert to substrate and **1.10** as PTE was slow.



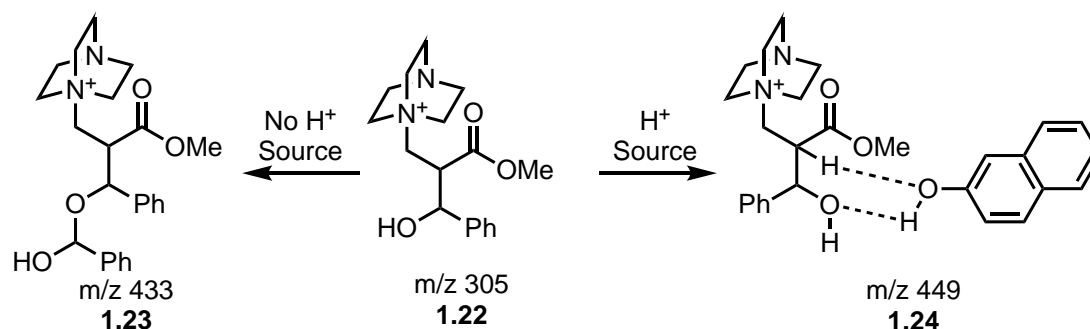
**Scheme 1.7.** The mechanism proposed by McQuade et al.<sup>113</sup>

Aggarwal et al. proposed a solvent or product catalyst PTE step.<sup>115, 122-123</sup> The initial rate for the MBH reaction between benzaldehyde and two Michael acceptors, C(2)-<sup>1</sup>H and C(2)-<sup>2</sup>H ethyl acrylate, catalysed by **1.12** was determined. The KIE induced by deuteration at the  $\alpha$ -position resulted in lower consumption of C(2)-<sup>2</sup>H ethyl acrylate at the early phases of the reaction, identifying PTE as rate limiting. At higher conversion autocatalysis was initiated by the MBH adduct, consequently, two different models were proposed, one where the product catalyses the formation of the aldol addition (**1.20**) and the second where the product catalyses the proton transfer elimination (**1.21**) (Scheme 1.8). Aggarwal proposed that in light of initial reports of successful catalysts that coordinated control of proton-transfer is critical for rate and *ee*.<sup>124-127</sup>



**Scheme 1.8.** Role of the protic product in the MBH autocatalysis.<sup>115, 122-123</sup>

Amarante et al.<sup>116</sup> attempted to differentiate the mechanisms proposed by Aggarwal and McQuade for the PTE step by ESI-MS/MS (Scheme 1.9). To test McQuade's proposal the reaction of benzaldehyde (3 equiv), methyl acrylate (1 equiv) and **1.10** (1 equiv) was monitored by removing an aliquot of the reaction mixture at the beginning of the reaction ( $t = 0$ ) and 10 minutes later ( $t = 10$ ), this was diluted with acidified acetonitrile and injected directly into the ESI source. Alongside the aldol adduct **1.22**, McQuade's proposed intermediate (**1.23**) was detected with  $m/z$  433. In the presence of  $\beta$ -naphthol, a loosely bound naphthol adduct (**1.24**) was observed.



**Scheme 1.9.** Key Intermediates detected by ESI-MS from the MBH reaction mixture of methyl acrylate and benzaldehyde catalysed by **1.10** at  $t = 10$  with and without  $\beta$ -naphthol.

Singleton and Plata performed an extensive investigation using a combination of DFT and kinetic analysis for the MBH reaction between methyl acrylate and benzaldehyde catalysed by **1.10** in methanol.<sup>121</sup> The thorough investigation concluded that in protic solvents proton transfer was an acid-base proton shuttle mechanism rather than a concerted process or a hemiacetal intermediate. This is not directly translatable to asymmetric systems since excess protic sources are generally detrimental to asymmetric induction.

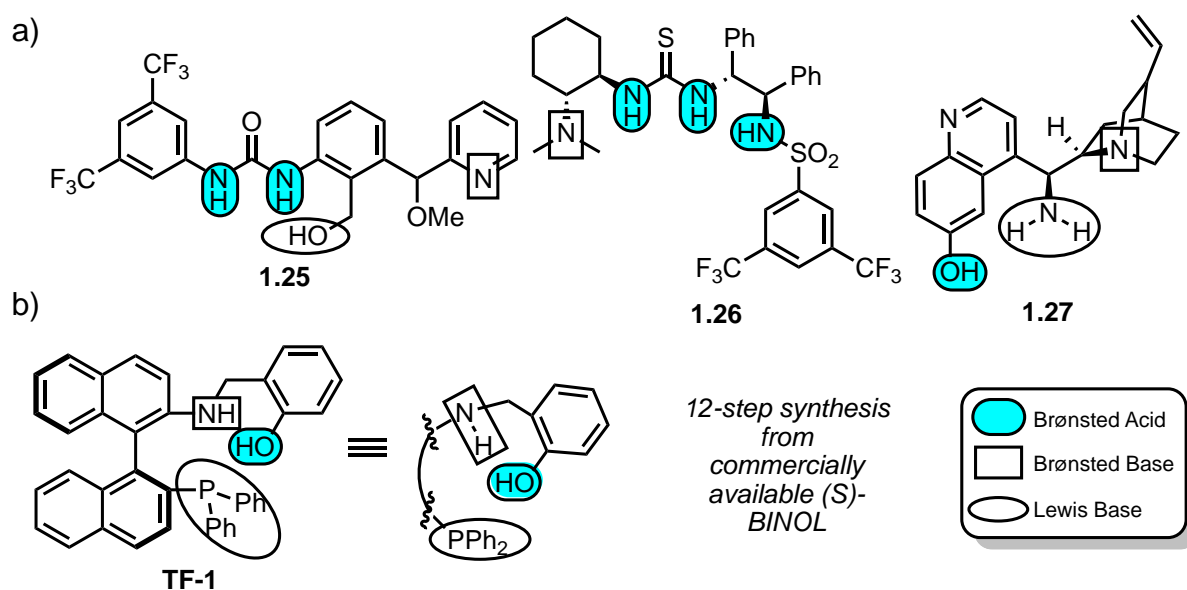
Catalyst design for the MBH reaction is a significant challenge due to the complexity of the reaction. Catalysts must be able to stabilise the two zwitterionic intermediates produced by the reversible Michael addition and Aldol addition steps to progress the reaction. The more serious issue is in the MBH reaction the rate determining step is condition dependent. Under aprotic conditions, the PTE step is rate-determining. However, as the protic MBH product accumulates, it is also capable of catalysing the proton transfer; as a result, the rate-determining step shifts to the Aldol-type addition. The capricious substrate scope and mechanistic complexity complicate the development of proficient and general catalysts for the MBH and aza-MBH reaction. The McQuade, Aggarwal and Singleton proposals for the PTE step are all condition dependent. In light of this a wide range of bifunctional catalysts for the

asymmetric *aza*-MBH tether a nucleophilic activating group (such as an amine or phosphine) to a hydrogen bond donor to stabilise the enolate and direct the proton transfer for only one diastereomer of the aldol adduct.

#### **1.4 From bifunctional to trifunctional organocatalysts for the MBH class**

While successful for the MBH class reactions in terms of enantioselectivity, bifunctional catalysts tend to suffer in catalytic proficiency with typically slow rates. The possibility of harnessing coordinated proton transfer to enhance the rate of reaction and asymmetric induction becomes a valid question. To this end, our group developed the first validated trifunctional organocatalysts to address the catalytic proficiency issues for this reaction with a view to understand how coordinated proton transfer may be elaborated in a model organic system.<sup>43</sup>

In some instances, in particular the *aza*-MBH reaction, the degree of rate acceleration and asymmetric induction by bifunctional organocatalysts can be limited due to substrate activation being coordinated by only two motifs. These limitations can be overcome by cooperativity between catalytic motifs of trifunctional organocatalysts. Trifunctional organocatalysts, compared to bifunctional organocatalysts, are less developed and represented in the literature. Currently, there are three reported trifunctional organocatalysts with complete validation for the functional assignment of each motif.



**Scheme 1.10.** a) Examples of trifunctional organocatalysts. b) Liu group trifunctional organocatalysts.

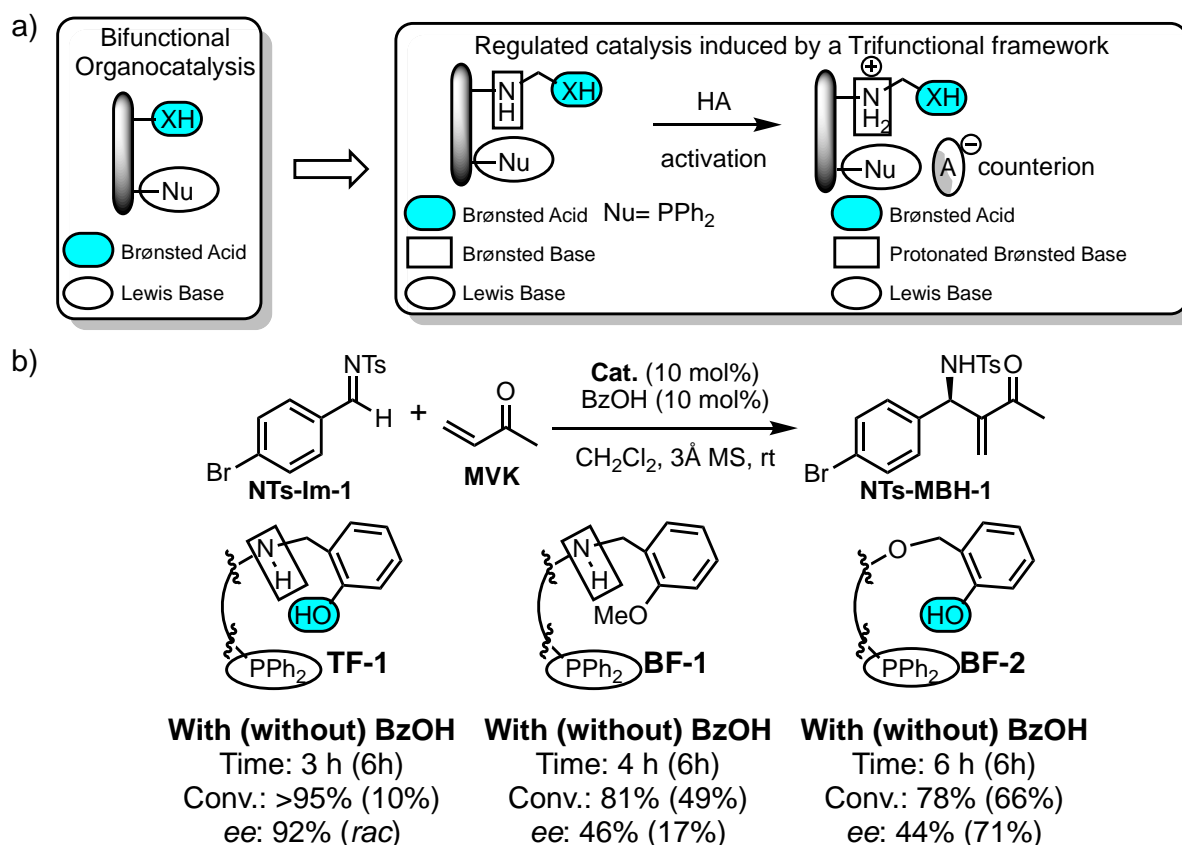
Sakai et al. constructed a biomimetic, trifunctional system **1.25** consisting of a sulfonamide (Brønsted acid), pyridine (Brønsted base) and alcohol (Lewis Base), mimicking the active site of serine hydrolase for transesterification between 2-propanol and vinyl trifluoroacetate (Scheme 1.10a).<sup>128</sup> Significant rate enhancement was observed over the uncatalyzed reaction ( $k_{cat}/k_{uncat} = 3.76 \times 10^6$ ). Removal of each catalytic motif significantly decreased the rate of reaction. This work was the very first demonstration of a validated trifunctional organocatalyst. However, there was no asymmetric induction.

Wang et al. developed a hydrogen bonding trifunctional catalyst **1.26** consisting of thiourea (Brønsted acid), sulfonamide (Brønsted acid) and tertiary amine (Lewis base) motifs for an asymmetric Michael addition between aryl and alkyl nitroolefins at low catalyst loading (1-5 mol%) with high *ee* (aryl up to 99%, alkyl up to 85%) and up to 97% yield (Scheme 1.10a).<sup>129</sup> Control catalysts demonstrated the importance of the second sulfonamide, with the removal

of this hydrogen bonding site coincided with a significant decrease in both yield and stereoselection (68% *ee*) for **1.26** catalysed reactions.

Chen et al. reported, a cinchona alkaloid derivative **1.27**, consisting of a primary amine (Lewis base), a tertiary amine (Brønsted base) and a phenol (Brønsted acid)(Scheme 1.10a) for an enantioselective 1,3-dipolar cycloaddition reaction between cyclic enones and azomethine imines in excellent yields (67–99%) and enantioselectivity (86–95% *ee*). Removal of the phenol Brønsted acid decreases the yield (56%) and enantioselectivity (51% *ee*) of the cycloaddition. The effect of cooperativity of the three motifs is unclear as the Brønsted base bifunctional control was not reported.

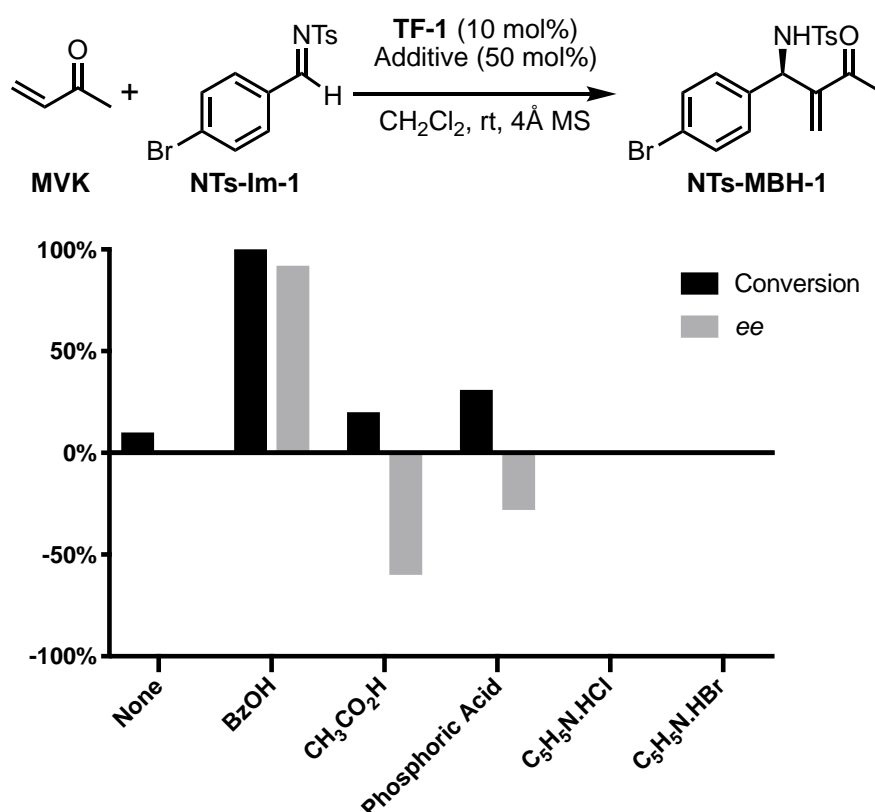
Our trifunctional framework (**TF-1**) was designed to explore cooperativity between different chemical motifs for promoting proton transfer that could deliver proficient catalysis (Scheme 1.10b).<sup>130</sup> These binaphthylene-based catalysts were prepared from a 12-step synthesis starting from commercially available (*S*)-BINOL. An additional acid-base pair was added to the typical Lewis base-Brønsted acid mode of bifunctional catalysts to develop a prototype trifunctional organocatalyst with external acid activation (Scheme 1.11a).<sup>131-134</sup> The prototype trifunctional organocatalyst **TF-1** contains a phosphine Lewis Base to act as a nucleophile for reaction initiation, a Brønsted acid (phenol) to stabilise the zwitterionic intermediate, an acid-activated Brønsted base (secondary amine) which may act as a switch to activate the catalytic pathway in the presence of a strong external Brønsted acid.



**Scheme 1.11.** a) The rationale behind the design of trifunctional organocatalysts for the aza-MBH. b) Bifunctional controls demonstrating the trifunctionality of the catalyst.

Catalysis requires all three motifs to achieve proficiency along with the addition of Benzoic acid (BzOH) (Scheme 1.11b). The trifunctional system was validated by demonstrating that each functional group has a distinct mechanistic role, and all three motifs cooperate to activate the proficient pathway. For example, the reaction rate from **BF-1** (no phenol Brønsted acid) is sluggish without acid, and the enantioselectivity of the reaction is decreased. Control catalyst **BF-2** (no amine Brønsted base) has a different response entirely to the addition of BzOH. Addition of BzOH decreases enantioselectivity of the reaction with slight rate acceleration. The prototype trifunctional organocatalyst **TF-1** by itself is a poor catalyst with a low rate and little asymmetric induction. However, the addition of BzOH switched on proficient catalysis with rate enhancement coupled to asymmetric induction.

Reactions performed with different acid additives demonstrates that the counterion has a clear role in catalysis (Figure 1.2). Other protic sources did not replicate the activating effects of BzOH. Reactions with acetic acid and phosphoric acid proceeded more slowly than BzOH yielding the aza-MBH adduct with the opposite sense of asymmetric induction. Moreover, pyridinium salts were ineffective as acid additives in the trifunctional aza-MBH reaction with no conversion observed after 24 hours.<sup>132</sup>

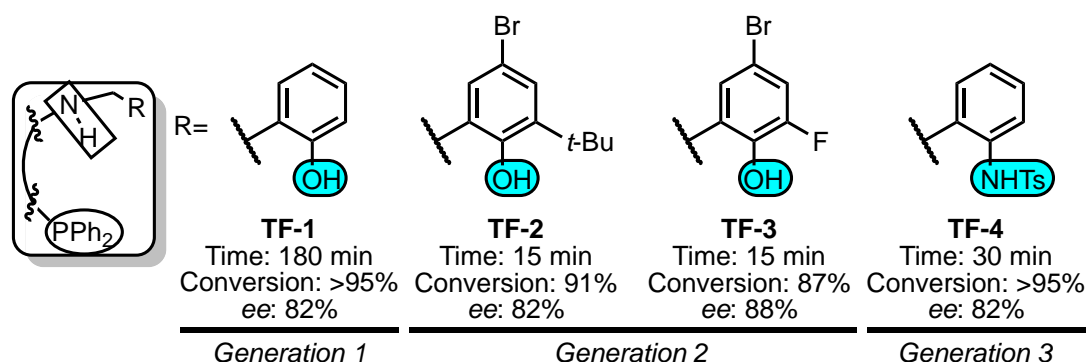


**Figure 1.2.** Response to an acid additive for trifunctional organocatalyst **TF-1**.

Further generations of trifunctional organocatalysts were prepared to investigate the roles of the motifs in catalytic proficiency. Increasing the acidity of the phenol increased the rate and level of enantioselectivity for the model aza-MBH reaction between **NTs-Im-1** and **MVK** to an extent. Catalysts **TF-2**, **TF-3** (Generation 2) and **TF-4** (Generation 3) all enhanced the rate of reaction and enantioselectivity compared to **TF-1** for the generic aza-MBH reaction between **MVK** and **NTs-Im-1** (Scheme 1.12). The second-generation catalysts **TF-2** and **TF-3** increased



the acidity of the phenol coinciding with a significant enhancement of rate and enantioselectivity.<sup>132</sup> The third generation catalysts, exemplified by the prototype **TF-4**, contain a sulfonamide in place of a phenol.<sup>134</sup> The third generation of catalyst exhibited comparable levels of reactivity to the second generation, and catalyst loading as low as 2 mol% could be achieved.



**Scheme 1.12.** Tuning of the proficiency of trifunctional organocatalyst by changing the Brønsted acid.

The multiple generations of catalysts demonstrate the essential and general role of BzOH activation in this regulated catalysis. In all generations the catalyst alone leads to the aza-MBH reaction being slow and without asymmetric induction. Across all generations of catalyst and in the presence of achiral BzOH, the previously sluggish trifunctional organocatalysts proceed with high rate and asymmetric induction. How BzOH activates this catalysis is unclear.

### 1.5 Chiral information propagation in a reaction network and the Soai reaction

Over the past decade, reaction systems have been developed to explore emergent properties that arise in complex systems.<sup>135</sup> Interest in developing reaction networks to observe emergent properties that may be conducive to life has risen over the past decade. While the field of systems chemistry is still in its infancy, emergent properties have been observed in

different model systems. Chiral systems are of particular interest as chiral molecules are ubiquitous in life.

#### **1.5.1 Chiral information transfer in a network**

Chirality is a way of specifying chemical information in chemical/biological systems. Biological systems rely on chiral building blocks (amino acids and sugars) for encoding genetic information and its subsequent functional expression. Chiral information within a chemical system, be it organic or biological, can be an indicator of organisational maturity enabling more complex functionality.<sup>136</sup> Initiation and propagation of chiral information is thought to be a prerequisite to chemical evolution that leads to life. "Symmetry breaking" events, the spontaneous generation of an imbalance between (*R*) and (*S*) enantiomers, have been proposed from a variety of- often intertwined- physical and chemical processes.<sup>137-144</sup> This symmetry breaking event is at the nexus for the generation of diversity and complexity.

Regardless of the initial symmetry breaking event, continuous induction of asymmetry and subsequent transfer of chirality from one chemical species to another are necessary to grow enantiomeric excess, and eventually homochirality, via autocatalytic pathways. Autocatalysis initiates self-amplification of the chiral product, enabling the chiral propagation event by dictating the configuration of a new product (homochirality transfer). Autocatalytic, homochirality transfer is one way of expanding the chiral chemical space by chiral amplification with one advantage of spontaneous or higher chirality propagation efficiency but another disadvantage of little chemical diversity growth. Heterochirality transfer (e.g. asymmetric catalysis that produces a chiral product distinct from the chiral catalyst) complements homochirality transfer by increasing chemical diversity during chiral

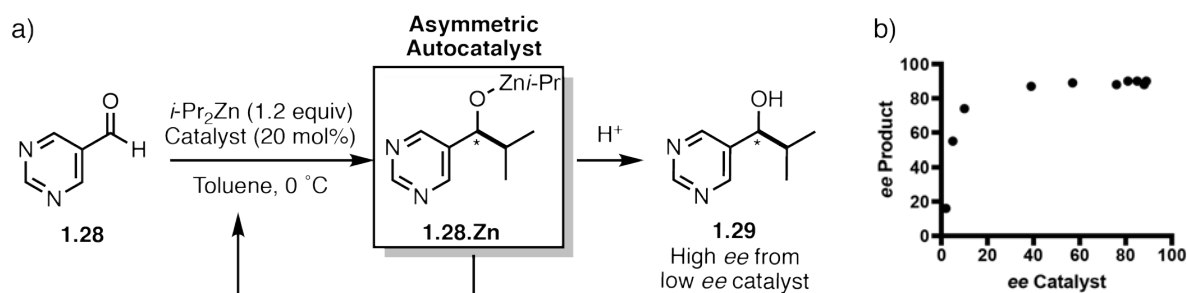
information propagation. One intriguing question is how these two modes of chiral information expansion can interact to expand both chiral information and chemical diversity for systems integration. Irrespective of the specific pathways taken, rate advantage is likely a primary selection criterion for the systems to continue and evolve.

Complex mixtures of chemical building blocks and enantioenriched products give rise to emergent properties. Emergent properties of homochirality have been observed in model systems comprised of amino acids. Homochiral products replicated significantly faster in a quaternary network of *racemic* amino acids demonstrating chiroselective replication of biopolymers.<sup>145</sup> In another instance, a complex network involving oligopeptides show behaviour where the presence or absence of substrates and templates would dictate the outcome of the system.<sup>146</sup> Recently, a system of co-existing replicators that compete for two common substrates diversified into two sets of replicators, one the descendant of the other.<sup>147</sup> Developing synthetic asymmetric autocatalytic reaction networks is a significant challenge, even more so by design.<sup>148-149</sup> One prototype system to investigate origins of homochirality is the asymmetric autocatalytic Soai reaction as discussed below.

### **1.5.2 The Soai reaction and chiral amplification**

The Soai reaction is a nucleophilic addition reaction between a 2-substituted pyrimidine carboxaldehyde and a diisopropylzinc generating substituted secondary alcohols with excellent enantioselectivity (Figure 1.3a).<sup>150</sup> The prototype reaction between pyrimidine

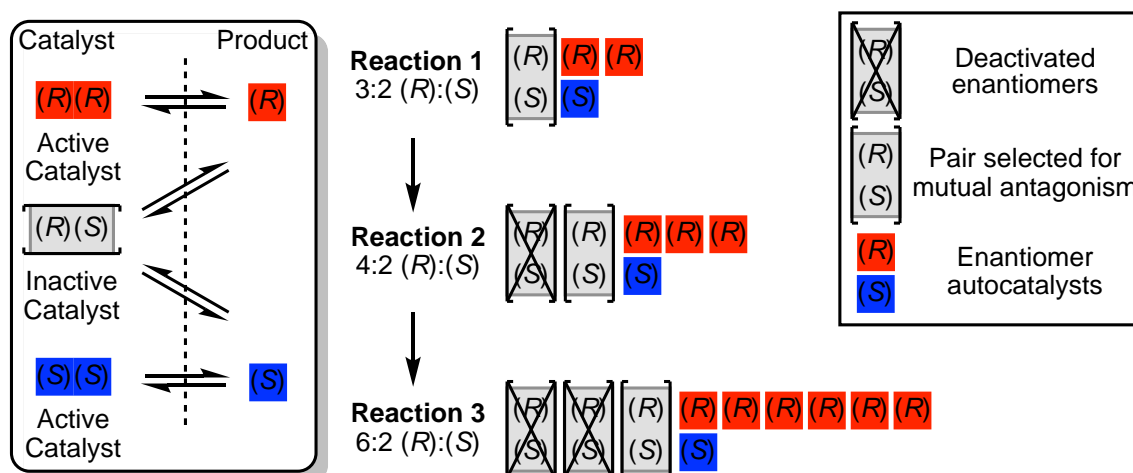
carboxaldehyde **1.28** and diisopropylzinc yielded **1.29** in high degrees of asymmetric induction over four rounds of asymmetric autocatalysis.<sup>150</sup>



**Figure 1.3.** a) Asymmetric amplification by the Soai reaction of pyrimidine carboxaldehydes **1.28**. b) Effect of catalyst **1.29** ee on product **1.29** ee.<sup>150</sup>

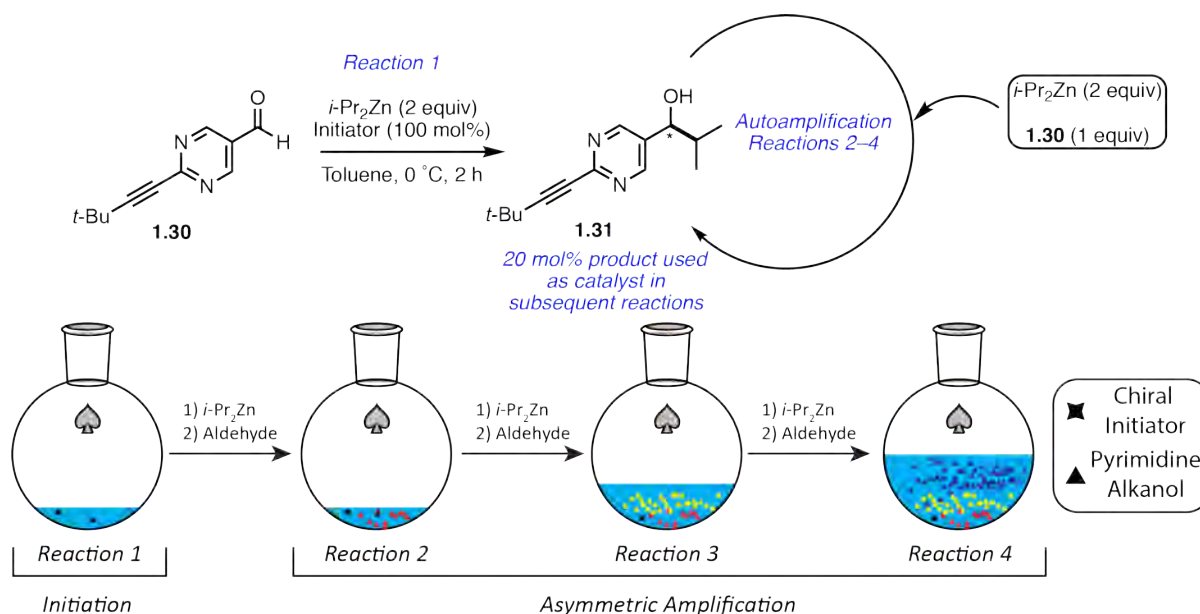
The Soai reaction is analogous to the MBH class reactions in that a protic species is produced from an aprotic starting material. The product formed, **1.28.Zn**, acts not only as the catalyst to activate the organozinc reagent but also as the template for chiral induction. The Soai reaction is the only known example of an autocatalytic chiral amplification reaction with the propensity to obtain high levels of asymmetric induction with or without the addition of a chiral additive. Moreover, high degrees of asymmetry can be achieved with low enantiopurity catalysts (Figure 1.3b). The Soai reaction can also be initiated with an external chiral additive (more details in Chapter 5).

The origins of chiral amplification in the Soai reaction are complex and extensively investigated since the initial observation of asymmetric autocatalysis by Soai et al.<sup>151-152</sup> The origin for the astounding amplification observed in the reaction is proposed to follow the Frank model of mutual inhibition (Scheme 1.13).<sup>153-154</sup> In this model, a molecule is capable of transferring chiral information to the nascent product if the homo- and heterochiral dimers differ in stability and/or reactivity. A small imbalance between the two enantiomers can then propagate this chiral information into near optical purity.



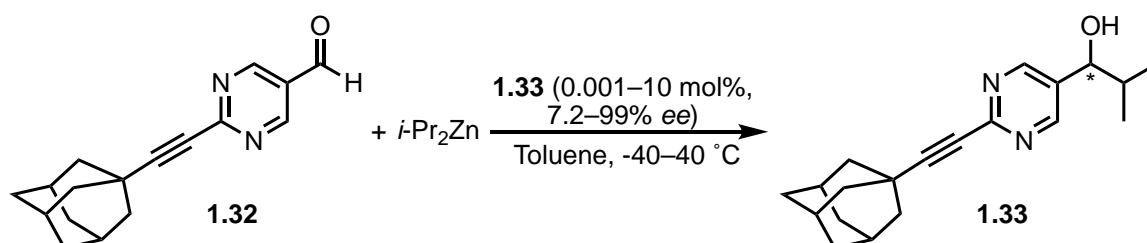
**Scheme 1.13.** Frank model for mutual inhibition.

The Soai reaction is a technically straight forward reaction to perform (Scheme 1.14).<sup>155</sup> The process can be broken down into a series of sub-reactions. In Reaction 1, the chiral initiator is mixed with aldehyde (**1.30**) and diisopropylzinc. Pyrimidine alkanol (**1.31**) generated in Reaction 1 is used without purification as the initiator for Reaction 2. For each subsequent reaction more aldehyde and diisopropylzinc is added to the reaction containing the product generated in the preceding reaction.



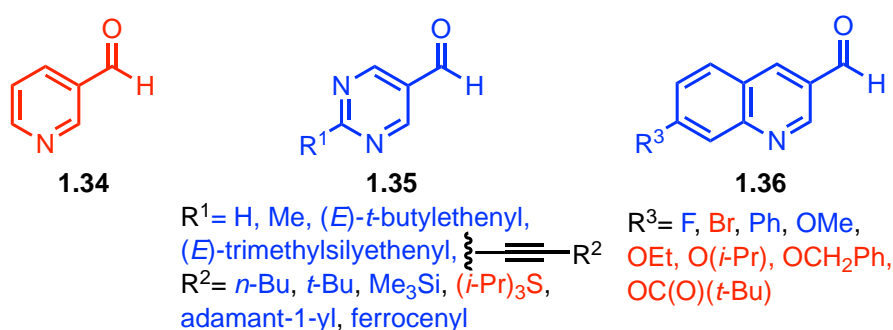
**Scheme 1.14.** Schematic for the Soai reaction.

Systematic studies of catalyst loading and enantiopurity, temperature, and *i*-Pr<sub>2</sub>Zn equivalence have established the limits of asymmetric amplification for the model substrate **1.32** (Scheme 1.15).<sup>156</sup> High degrees of asymmetric induction (93.1% *ee*) were achieved when catalysed by **1.33** with low *ee* (7.2%) and low loading (1.0 mol%). Higher loading of low *ee* catalyst decreased the efficiency of the chirality transfer. The most efficient temperature range for chiral amplification was observed between -15 °C–10 °C.



**Scheme 1.15.** The model substrate used to establish the limits of the Soai reaction.

The substrate scope of the asymmetric autocatalysis in the Soai reaction is limited to diisopropylzinc and aromatic aldehydes with at least one pyridinic nitrogen in the  $\gamma$ -position (Scheme 1.16).



*Blue substrates are successful candidates for asymmetric autocatalysis*  
*Red substrates are not successful candidates*

**Scheme 1.16.** Substrate scope for the Soai reaction.

Pyridine-3-carboxaldehyde (**1.34**) is ineffective as a substrate, whereas substituted pyrimidine-5-carboxaldehydes (**1.35**) are the most effective substrates. Within this class of

pyrimidine substrates, substitution at the 2-position is tolerated with the highest degrees of asymmetry recorded for alkyne substituents at this position. Bulky substituents on the alkyne, such as adamantly, *tert*-butyl and trimethylsilyl, are generally tolerated, and these are often the most efficient substrates for chiral amplification.<sup>157</sup> However, triisopropylsilyl-substituted alkynes are unresponsive to asymmetric autocatalysis potentially due to significant steric bulk. It is clear from the reactivity profile of **1.34** and **1.35** that the pyrimidine nitrogen is sensitive to the steric bulk of the alkyne and plays a pivotal role in the amplification of chirality. Monosubstituted quinoline (**1.36**) are sensitive to substitution at C-7. Fluoro-, phenyl and methoxy substituted quinolines are competent substrates, however bulkier ethers and bromo-substituted quinolines are inactive in the Soai reaction.

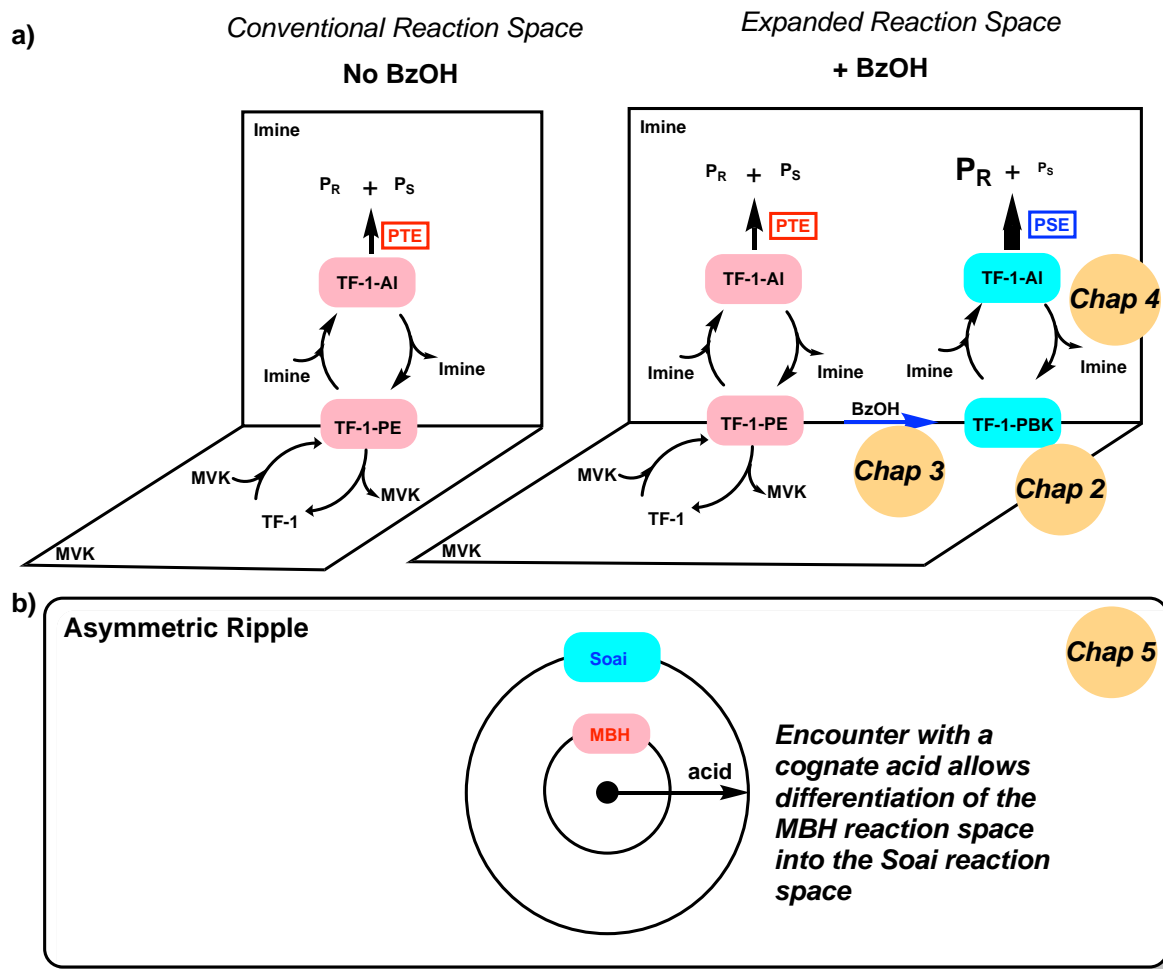
As outlined above, the Soai reaction demonstrates a powerful method by which a small initial imbalance of two enantiomers can rapidly propagate through a Frank-type mutual inhibition pathway. Chiral amplification is dependent upon the aldehyde substrate and the organozinc reagent. The integrity of the chirality transfer initiated by the Soai reaction provides the basis for constructing asymmetric reaction networks.

## 1.6 Project Aims

As outlined at the beginning of this chapter, the initial aims of this thesis were to investigate the mechanistic curiosity of the acid-regulated trifunctional organocatalysis of the aza-MBH reaction. Achiral BzOH differentiates between the proficient (rate coupled asymmetric induction) and *racemic* catalytic pathways. The nature of this activation is unclear.

This thesis will uncover mechanistic details that underpin the regulatory role of BzOH and the hidden role of the imine substrate in catalysis (Figure 1.4a). From this mechanistic insight, kinetic differentiation in the aza-MBH reaction system will be propagated by the Soai reaction (Figure 1.4b). In Chapter 2, the origin of catalytic proficiency in the acid-regulated trifunctional aza-MBH reaction was investigated by a combination of 2D NMR spectroscopy, molecular mechanics and DFT calculations. An ensemble solution structure of a new proton-shuttling ground state intermediate was elucidated. In Chapter 3, the role of the acid additive in C–C bond formation and proton transfer was investigated by deuterium incorporation kinetics. Additionally, the role of the substrate in the catalysis was investigated by preparing a series of imine substrates. In Chapter 4, new substrates for the aza-MBH reaction were identified that could proceed through the proton transfer mechanism. Finally, in Chapter 5, kinetic differentiation of cognate substrates by the capacity to recognise the proton shuttle mechanism in the MBH reaction was propagated in the asymmetric autocatalytic Soai reaction for superior chiral amplification outcomes.





**Figure 1.4.** The conceptual framework for the work covered in this a) Chapter 2–4 and b) Chapter 5 in this thesis.

## 1.7 References

1. Millership, J. S.; Fitzpatrick, A., Commonly used chiral drugs: A survey. *Chirality* **1993**, 5 (8), 573-576.
2. Nguyen, L. A.; He, H.; Pham-Huy, C., Chiral drugs: an overview. *Int. J. Biomed. Sci.* **2006**, 2 (2), 85-100.
3. Newman, D. J.; Cragg, G. M., Natural Products as Sources of New Drugs from 1981 to 2014. *J. Nat. Prod.* **2016**, 79 (3), 629-661.
4. Resnati, G., Synthesis of chiral and bioactive fluoroorganic compounds. *Tetrahedron* **1993**, 49 (42), 9385-9445.
5. Jacobsen, E. N.; Pfaltz, A.; Yamamoto, H., *Comprehensive Asymmetric Catalysis*. Springer: Berlin, 1999; Vol. 1-3.
6. Ojima, I., *Catalytic asymmetric synthesis*. John Wiley & Sons: New York, 2004.
7. Jacobsen, E. N.; Pfaltz, A.; Yamamoto, H., *Comprehensive Asymmetric Catalysis. Supplement 2*. Springer: Berlin, 2004; p v. <1-2 >.
8. Grabowski, E. J. J., Enantiopure drug synthesis: From methyldopa to imipenem to efavirenz. *Chirality* **2005**, 17 (S1), S249-S259.
9. Mikami, K.; Lautens, M., New Frontiers in Asymmetric Catalysis. In *New Frontiers in Asymmetric Catalysis*, Wiley: New York, 2007.
10. Ward, T. J.; Baker, B. A., Chiral Separations. *Anal. Chem.* **2008**, 80 (12), 4363-4372.
11. Blase, H. U.; Federsel, H.-J., *Asymmetric catalysis on industrial scale: challenges, approaches and solutions*. 2nd ed.; Wiley-VCH: Weinheim, 2010; p xxxvii, 542 p.
12. Dalko, P. I.; Moisan, L., In the Golden Age of Organocatalysis. *Angew. Chem., Int. Ed.* **2004**, 43 (39), 5138-5175.

13. A. Berkessel; Gröger, H., *Asymmetric Organocatalysis: From Biomimetic Concepts to Applications in Asymmetric Synthesis*. 1st ed.; Wiley-VCH: Weinheim, 2005.
14. Dalko, P. I., *Enantioselective Organocatalysis: Reactions and Experimental Procedures*. Wiley-VCH: Weinheim, 2007.
15. Dondoni, A.; Massi, A., *Asymmetric Organocatalysis: From Infancy to Adolescence*. *Angew. Chem., Int. Ed.* **2008**, 47 (25), 4638-4660.
16. List, B., *Asymmetric Organocatalysis*. Springer: Verlag Berlin Heidelberg, 2009; Vol. 291.
17. Pellissier, H., *Recent developments in asymmetric organocatalysis*. RSC Pub.: Cambridge, 2010; p xv, 241 p.
18. Waser, M., *Asymmetric Organocatalysis in Natural Product Syntheses*. Springer: Verlag Wien, 2012; p xi, 197 p.
19. List, B.; Maruoka, K., *Asymmetric Organocatalysis – Workbench Edition*. Thieme: Stuttgart, 2012.
20. List, B.; Maruoka, K., *Asymmetric Organocatalysis*. Thieme: Stuttgart, 2012.
21. Dalko, P. I., *Comprehensive Enantioselective Organocatalysis: Catalysts, Reactions, and Applications*, Vols 1-3. *Comprehensive Enantioselective Organocatalysis: Catalysts, Reactions, and Applications*, Vols 1-3 **2013**, 1-1438.
22. *Asian J. Org. Chem.* **2014**, 3 (4), 317-563.
23. Shibasaki, M.; Yamamoto, Y., *Multimetallic Catalysts in Organic Synthesis*. Wiley-VCH: Weinheim, 2004.
24. Bates, R., *Organic synthesis using transition metals*. 2nd ed.; Wiley: Chichester, West Sussex, 2012; p xi, 446 p.
25. Pellissier, H., Stereocontrolled domino reactions. *Chem. Rev.* **2013**, 113 (1), 442-524.

26. Wong, C. H.; Whitesides, G. M., *Enzymes in synthetic organic chemistry*. Pergamon: Oxford, 1994.
27. Drauz, K.; Waldmann, H., *Enzyme catalysis in organic synthesis : a comprehensive handbook*. 2nd ed.; Wiley-VCH: Weinheim, 2002.
28. Garcia-Junceda, E., *Multi-step enzyme catalysis : biotransformations and chemoenzymatic synthesis*. Wiley-VCH: Weinheim, 2008.
29. Gotor, V.; Alfonso, I.; García-Urdiales, E., *Asymmetric organic synthesis with enzymes*. Wiley-VCH: Weinheim, 2008.
30. Drauz, K.; Gröger, H.; May, O., *Enzyme catalysis in organic synthesis*. 3rd ed.; Wiley-VCH: Weinheim, 2012.
31. Wolfenden, R.; Snider, M. J., The Depth of Chemical Time and the Power of Enzymes as Catalysts. *Acc. Chem. Res.* **2001**, *34* (12), 938-945.
32. Kuchner, O.; Arnold, F. H., Directed evolution of enzyme catalysts. *Trends Biotechnol.* **1997**, *15* (12), 523-530.
33. Farinas, E. T.; Bulter, T.; Arnold, F. H., Directed enzyme evolution. *Curr. Opin. Biotechnol.* **2001**, *12* (6), 545-551.
34. Romero, P. A.; Arnold, F. H., Exploring protein fitness landscapes by directed evolution. *Nat. Rev. Mol. Cell Biol.* **2009**, *10* (12), 866-876.
35. Cheng, A. A.; Lu, T. K., Synthetic Biology: An Emerging Engineering Discipline. *Annu. Rev. Biomed. Eng.* **2012**, *14* (1), 155-178.
36. Brunner, H., Optically Active Organometallic Compounds of Transition Elements with Chiral Metal Atoms. *Angew. Chem., Int. Ed.* **1999**, *38* (9), 1194-1208.
37. Beller, M.; Bolm, C., *Transition Metals for Organic Synthesis*. Wiley VCH: Weinheim, Germany, 2008.

38. Crassous, J., Chiral transfer in coordination complexes: towards molecular materials. *Chem. Soc. Rev.* **2009**, *38* (3), 830-845.
39. Crassous, J., Transfer of chirality from ligands to metal centers: recent examples. *Chem. Commun.* **2012**, *48* (78), 9687-9695.
40. Sheldon, R. A.; Arends, I.; Hanefeld, U., *Green Chemistry and Catalysis*. Wiley VCH: Weinheim, Germany, 2007.
41. Zhou, Q.-L., Transition-Metal Catalysis and Organocatalysis: Where Can Progress Be Expected? *Angew. Chem., Int. Ed.* **2016**, *55* (18), 5352-5353.
42. Liu, F., The Upside of Downsizing: Asymmetric Trifunctional Organocatalysts as Small Enzyme Mimics for Cooperative Enhancement of Both Rate and Enantioselectivity With Regulation. *Chirality* **2013**, *25* (11), 675-683.
43. Kenny, R.; Liu, F., Trifunctional Organocatalysts: Catalytic Proficiency by Cooperative Activation. *Eur. J. Org. Chem.* **2015**, *2015* (24), 5304-5319.
44. Seayad, J.; List, B., Asymmetric organocatalysis. *Org. Biomol. Chem.* **2005**, *3* (5), 719-724.
45. MacMillan, D. W. C., The advent and development of organocatalysis. *Nature* **2008**, *455* (7211), 304-308.
46. Zeitler, K., Photoredox Catalysis with Visible Light. *Angew. Chem., Int. Ed.* **2009**, *48* (52), 9785-9789.
47. Brière, J.-F.; Oudeyer, S.; Dalla, V.; Levacher, V., Recent advances in cooperative ion pairing in asymmetric organocatalysis. *Chem. Soc. Rev.* **2012**, *41* (5), 1696-1707.
48. Brak, K.; Jacobsen, E. N., Asymmetric Ion-Pairing Catalysis. *Angew. Chem., Int. Ed.* **2013**, *52* (2), 534-561.

49. Shirakawa, S.; Maruoka, K., Recent Developments in Asymmetric Phase-Transfer Reactions. *Angew. Chem., Int. Ed.* **2013**, *52* (16), 4312-4348.
50. Volla, C. M. R.; Atodiresei, I.; Rueping, M., Catalytic C–C Bond-Forming Multi-Component Cascade or Domino Reactions: Pushing the Boundaries of Complexity in Asymmetric Organocatalysis. *Chem. Rev.* **2014**, *114* (4), 2390-2431.
51. Parmar, D.; Sugiono, E.; Raja, S.; Rueping, M., Complete Field Guide to Asymmetric BINOL-Phosphate Derived Brønsted Acid and Metal Catalysis: History and Classification by Mode of Activation; Brønsted Acidity, Hydrogen Bonding, Ion Pairing, and Metal Phosphates. *Chem. Rev.* **2014**, *114* (18), 9047-9153.
52. Qin, Y.; Zhu, L.; Luo, S., Organocatalysis in Inert C–H Bond Functionalization. *Chem. Rev.* **2017**, *117* (13), 9433-9520.
53. Schreiner, P. R., Metal-free organocatalysis through explicit hydrogen bonding interactions. *Chem. Soc. Rev.* **2003**, *32* (5), 289-296.
54. Knowles, R. R.; Jacobsen, E. N., Attractive noncovalent interactions in asymmetric catalysis: Links between enzymes and small molecule catalysts. *Proc. Natl. Acad. Sci.* **2010**, *107* (48), 20678-20685.
55. Yamada, S.; Fossey, J. S., Nitrogen cation-[small pi] interactions in asymmetric organocatalytic synthesis. *Org. Biomol. Chem.* **2011**, *9* (21), 7275-7281.
56. Zhao, Y.; Beuchat, C.; Domoto, Y.; Gajewy, J.; Wilson, A.; Mareda, J.; Sakai, N.; Matile, S., Anion– $\pi$  Catalysis. *J. Am. Chem. Soc.* **2014**, *136* (5), 2101-2111.
57. Allen, A. E.; MacMillan, D. W. C., Synergistic catalysis: A powerful synthetic strategy for new reaction development. *Chem. Sci.* **2012**, *3* (3), 633-658.
58. Arceo, E.; Montroni, E.; Melchiorre, P., Photo-Organocatalysis of Atom-Transfer Radical Additions to Alkenes. *Angew. Chem., Int. Ed.* **2014**, *53* (45), 12064-12068.

59. Hoffmann, N., Photochemical Reactions as Key Steps in Organic Synthesis. *Chem. Rev.* **2008**, *108* (3), 1052-1103.
60. Ooi, T.; Maruoka, K., Recent Advances in Asymmetric Phase-Transfer Catalysis. *Angew. Chem., Int. Ed.* **2007**, *46* (23), 4222-4266.
61. Mahlau, M.; List, B., Asymmetric Counteranion-Directed Catalysis: Concept, Definition, and Applications. *Angew. Chem., Int. Ed.* **2013**, *52* (2), 518-533.
62. Phipps, R. J.; Hamilton, G. L.; Toste, F. D., The progression of chiral anions from concepts to applications in asymmetric catalysis. *Nat. Chem.* **2012**, *4* (8), 603-614.
63. Tan, J.; Yasuda, N., Contemporary Asymmetric Phase Transfer Catalysis: Large-Scale Industrial Applications. *Org. Process Res. Dev.* **2015**, *19* (11), 1731-1746.
64. Qvortrup, K.; Rankic, D. A.; MacMillan, D. W. C., A General Strategy for Organocatalytic Activation of C–H Bonds via Photoredox Catalysis: Direct Arylation of Benzylic Ethers. *J. Am. Chem. Soc.* **2014**, *136* (2), 626-629.
65. Hager, D.; MacMillan, D. W. C., Activation of C–H Bonds via the Merger of Photoredox and Organocatalysis: A Coupling of Benzylic Ethers with Schiff Bases. *J. Am. Chem. Soc.* **2014**, *136* (49), 16986-16989.
66. Hashimoto, T.; Kawamata, Y.; Maruoka, K., An organic thiyl radical catalyst for enantioselective cyclization. *Nat. Chem.* **2014**, *6* (8), 702-705.
67. Nicewicz, D. A.; MacMillan, D. W. C., Merging Photoredox Catalysis with Organocatalysis: The Direct Asymmetric Alkylation of Aldehydes. *Science* **2008**, *322* (5898), 77-80.
68. Hu, J.; Wang, J.; Nguyen, T. H.; Zheng, N., The chemistry of amine radical cations produced by visible light photoredox catalysis. *Beilstein J. Org. Chem.* **2013**, *9*, 1977-2001.

69. Prier, C. K.; MacMillan, D. W. C., Amine  $\alpha$ -heteroarylation via photoredox catalysis: a homolytic aromatic substitution pathway. *Chem. Sci.* **2014**, 5 (11), 4173-4178.
70. Akiyama, T.; Itoh, J.; Fuchibe, K., Recent Progress in Chiral Brønsted Acid Catalysis. *Adv. Synth. Catal.* **2006**, 348 (9), 999-1010.
71. Wende, R. C.; Schreiner, P. R., Evolution of asymmetric organocatalysis: multi- and retrocatalysis. *Green Chem.* **2012**, 14 (7), 1821-1849.
72. Agmon, N., The Grotthuss mechanism. *Chem. Phys. Lett.* **1995**, 244 (5), 456-462.
73. Marx, D.; Tuckerman, M. E.; Hutter, J.; Parrinello, M., The nature of the hydrated excess proton in water. *Nature* **1999**, 397 (6720), 601-604.
74. Mohammed, O. F.; Pines, D.; Dreyer, J.; Pines, E.; Nibbering, E. T. J., Sequential Proton Transfer Through Water Bridges in Acid-Base Reactions. *Science* **2005**, 310 (5745), 83-86.
75. Marx, D., Proton Transfer 200 Years after von Grotthuss: Insights from Ab Initio Simulations. *ChemPhysChem* **2006**, 7 (9), 1848-1870.
76. Mohr, J. T.; Hong, A. Y.; Stoltz, B. M., Enantioselective protonation. *Nat. Chem.* **2009**, 1 (5), 359-369.
77. Frank, R. A. W.; Titman, C. M.; Pratap, J. V.; Luisi, B. F.; Perham, R. N., A Molecular Switch and Proton Wire Synchronize the Active Sites in Thiamine Enzymes. *Science* **2004**, 306 (5697), 872-876.
78. Kim, S. W.; Cha, S.-S.; Cho, H.-S.; Kim, J.-S.; Ha, N.-C.; Cho, M.-J.; Joo, S.; Kim, K. K.; Choi, K. Y.; Oh, B.-H., High-Resolution Crystal Structures of  $\Delta^5$ -3-Ketosteroid Isomerase with and without a Reaction Intermediate Analogue. *Biochemistry* **1997**, 36 (46), 14030-14036.
79. Kim, K. S.; Oh, K. S.; Lee, J. Y., Catalytic role of enzymes: Short strong H-bond-induced partial proton shuttles and charge redistributions. *Proc. Natl. Acad. Sci.* **2000**, 97 (12), 6373-6378.



80. Kamerlin, S. C. L.; Sharma, P. K.; Chu, Z. T.; Warshel, A., Ketosteroid isomerase provides further support for the idea that enzymes work by electrostatic preorganization. *Proc. Natl. Acad. Sci.* **2010**, *107* (9), 4075-4080.
81. Fried, S. D.; Bagchi, S.; Boxer, S. G., Extreme electric fields power catalysis in the active site of ketosteroid isomerase. *Science* **2014**, *346* (6216), 1510-1514.
82. Radzicka, A.; Wolfenden, R., A proficient enzyme. *Science* **1995**, *267* (5194), 90-93.
83. Eigen, M., Proton Transfer, Acid-Base Catalysis, and Enzymatic Hydrolysis. Part I: ELEMENTARY PROCESSES. *Angew. Chem., Int. Ed.* **1964**, *3* (1), 1-19.
84. Jencks, W. P., When is an intermediate not an intermediate? Enforced mechanisms of general acid-base, catalyzed, carbocation, carbanion, and ligand exchange reaction. *Acc. Chem. Res.* **1980**, *13* (6), 161-169.
85. Ciuffarin, E.; Loi, A.; Isola, M.; Lupetti, A.; Sagramora, L.; Senatore, L., Intramolecular hydrogen bonding catalysis of ester aminolysis in acetonitrile. *J. Org. Chem.* **1983**, *48* (7), 1047-1051.
86. Scheiner, S., Bent Hydrogen Bonds and Proton Transfers. *Acc. Chem. Res.* **1994**, *27* (12), 402-408.
87. Jencks, W. P., Requirements for general acid-base catalysis of complex reactions. *J. Am. Chem. Soc.* **1972**, *94* (13), 4731-4732.
88. Jencks, W. P., Enforced general acid-base catalysis of complex reactions and its limitations. *Acc. Chem. Res.* **1976**, *9* (12), 425-432.
89. Knowles, J. R.; Albery, W. J., Perfection in enzyme catalysis: the energetics of triosephosphate isomerase. *Acc. Chem. Res.* **1977**, *10* (4), 105-111.

90. Komives, E. A.; Chang, L. C.; Lolis, E.; Tilton, R. F.; Petsko, G. A.; Knowles, J. R., Electrophilic catalysis in triosephosphate isomerase: the role of histidine-95. *Biochemistry* **1991**, *30* (12), 3011-3019.
91. Richard, J. P., A Paradigm for Enzyme-Catalyzed Proton Transfer at Carbon: Triosephosphate Isomerase. *Biochemistry* **2012**, *51* (13), 2652-2661.
92. Kumagai, N.; Shibasaki, M., Recent Advances in Direct Catalytic Asymmetric Transformations under Proton-Transfer Conditions. *Angew. Chem., Int. Ed.* **2011**, *50* (21), 4760-4772.
93. Alcaide, B.; Almendros, P., The Direct Catalytic Asymmetric Aldol Reaction. *Eur. J. Org. Chem.* **2002**, *2002* (10), 1595-1601.
94. Wang, J.; Liu, X.; Feng, X., Asymmetric Strecker Reactions. *Chem. Rev.* **2011**, *111* (11), 6947-6983.
95. Trost, B. M.; Brindle, C. S., The direct catalytic asymmetric aldol reaction. *Chem. Soc. Rev.* **2010**, *39* (5), 1600-1632.
96. Raj, M.; Singh, V. K., Organocatalytic reactions in water. *Chem. Commun.* **2009**, (44), 6687-6703.
97. Enders, D.; Grondal, C.; Hüttl, M. R. M., Asymmetric Organocatalytic Domino Reactions. *Angew. Chem., Int. Ed.* **2007**, *46* (10), 1570-1581.
98. Davies, H. M. L.; Sorensen, E. J., Rapid complexity generation in natural product total synthesis. *Chem. Soc. Rev.* **2009**, *38* (11), 2981-2982.
99. Nicolaou, K. C.; Chen, J. S., The art of total synthesis through cascade reactions. *Chem. Soc. Rev.* **2009**, *38* (11), 2993-3009.
100. Nicolaou, K. C.; Edmonds, D. J.; Bulger, P. G., Cascade Reactions in Total Synthesis. *Angew. Chem., Int. Ed.* **2006**, *45* (43), 7134-7186.

101. Grondal, C.; Jeanty, M.; Enders, D., Organocatalytic cascade reactions as a new tool in total synthesis. *Nat. Chem.* **2010**, *2* (3), 167-178.
102. Morita, K.-i.; Suzuki, Z.; Hirose, H., A Tertiary Phosphine-catalyzed Reaction of Acrylic Compounds with Aldehydes. *Bull. Chem. Soc. Jpn.* **1968**, *41* (11), 2815-2815.
103. Baylis, A.; Hillman, M. In *German Patent 2155113*, 1972, Chem. Abs., 1972.
104. Masson, G.; Housseman, C.; Zhu, J., The Enantioselective Morita–Baylis–Hillman Reaction and Its Aza Counterpart. *Angew. Chem., Int. Ed.* **2007**, *46* (25), 4614-4628.
105. Declerck, V.; Martinez, J.; Lamaty, F., aza-Baylis–Hillman Reaction. *Chem. Rev.* **2009**, *109* (1), 1-48.
106. Basavaiah, D.; Reddy, B. S.; Badsara, S. S., Recent Contributions from the Baylis–Hillman Reaction to Organic Chemistry. *Chem. Rev.* **2010**, *110* (9), 5447-5674.
107. Wei, Y.; Shi, M., Recent Advances in Organocatalytic Asymmetric Morita–Baylis–Hillman/aza-Morita–Baylis–Hillman Reactions. *Chem. Rev.* **2013**, *113* (8), 6659-6690.
108. Basavaiah, D.; Rao, K. V.; Reddy, R. J., The Baylis-Hillman reaction: a novel source of attraction, opportunities, and challenges in synthetic chemistry. *Chem. Soc. Rev.* **2007**, *36* (10), 1581-1588.
109. Declerck, V.; Martinez, J.; Lamaty, F., aza-Baylis-Hillman reaction. *Chem. Rev.* **2009**, *109* (1), 1-48.
110. Basavaiah, D.; Veeraraghavaiah, G., The Baylis-Hillman reaction: a novel concept for creativity in chemistry. *Chem. Soc. Rev.* **2012**, *41* (1), 68-78.
111. Hill, J. S.; Isaacs, N. S., Mechanism of  $\alpha$ -substitution reactions of acrylic derivatives. *J. Phys. Org. Chem.* **1990**, *3* (5), 285-288.
112. Bode, M. L.; Kaye, P. T., A kinetic and mechanistic study of the Baylis-Hillman reaction. *Tetrahedron Lett.* **1991**, *32* (40), 5611-5614.

113. Price, K. E.; Broadwater, S. J.; Jung, H. M.; McQuade, D. T., Baylis–Hillman Mechanism: A New Interpretation in Aprotic Solvents. *Org. Lett.* **2005**, 7 (1), 147-150.
114. Price, K. E.; Broadwater, S. J.; Walker, B. J.; McQuade, D. T., A New Interpretation of the Baylis–Hillman Mechanism. *J. Org. Chem.* **2005**, 70 (10), 3980-3987.
115. Aggarwal, V. K.; Fulford, S. Y.; Lloyd-Jones, G. C., Reevaluation of the Mechanism of the Baylis–Hillman Reaction: Implications for Asymmetric Catalysis. *Angew. Chem., Int. Ed.* **2005**, 44 (11), 1706-1708.
116. Amarante, G. W.; Milagre, H. M. S.; Vaz, B. G.; Vilachã Ferreira, B. R.; Eberlin, M. N.; Coelho, F., Dualistic Nature of the Mechanism of the Morita–Baylis–Hillman Reaction Probed by Electrospray Ionization Mass Spectrometry. *J. Org. Chem.* **2009**, 74 (8), 3031-3037.
117. Raheem, I. T.; Jacobsen, E. N., Highly Enantioselective Aza-Baylis–Hillman Reactions Catalyzed by Chiral Thiourea Derivatives. *Adv. Synth. Catal.* **2005**, 347 (11-13), 1701-1708.
118. Shi, M.; Chen, L.-H.; Li, C.-Q., Chiral Phosphine Lewis Bases Catalyzed Asymmetric aza-Baylis–Hillman Reaction of N-Sulfonated Imines with Activated Olefins. *J. Am. Chem. Soc.* **2005**, 127 (11), 3790-3800.
119. Buskens, P.; Klankermayer, J.; Leitner, W., Bifunctional Activation and Racemization in the Catalytic Asymmetric Aza-Baylis–Hillman Reaction. *J. Am. Chem. Soc.* **2005**, 127 (48), 16762-16763.
120. Lindner, C.; Liu, Y.; Karaghiosoff, K.; Maryasin, B.; Zipse, H., The Aza-Morita–Baylis–Hillman Reaction: A Mechanistic and Kinetic Study. *Chemistry – A European Journal* **2013**, 19 (20), 6429-6434.
121. Plata, R. E.; Singleton, D. A., A Case Study of the Mechanism of Alcohol-Mediated Morita Baylis–Hillman Reactions. The Importance of Experimental Observations. *J. Am. Chem. Soc.* **2015**, 137 (11), 3811-3826.

122. Robiette, R.; Aggarwal, V. K.; Harvey, J. N., Mechanism of the Morita–Baylis–Hillman Reaction: A Computational Investigation. *J. Am. Chem. Soc.* **2007**, *129* (50), 15513-15525.
123. Aggarwal, V. K.; Emme, I.; Fulford, S. Y., Correlation between pKa and Reactivity of Quinuclidine-Based Catalysts in the Baylis–Hillman Reaction: Discovery of Quinuclidine as Optimum Catalyst Leading to Substantial Enhancement of Scope. *J. Org. Chem.* **2003**, *68* (3), 692-700.
124. Shi, M.; Chen, L.-H., Chiral phosphine Lewis base catalyzed asymmetric aza-Baylis–Hillman reaction of N-sulfonated imines with methyl vinyl ketone and phenyl acrylate. *Chem. Commun.* **2003**, (11), 1310-1311.
125. McDougal, N. T.; Schaus, S. E., Asymmetric Morita–Baylis–Hillman Reactions Catalyzed by Chiral Brønsted Acids. *J. Am. Chem. Soc.* **2003**, *125* (40), 12094-12095.
126. Imbriglio, J. E.; Vasbinder, M. M.; Miller, S. J., Dual Catalyst Control in the Amino Acid-Peptide-Catalyzed Enantioselective Baylis–Hillman Reaction. *Org. Lett.* **2003**, *5* (20), 3741-3743.
127. Yang, K.-S.; Lee, W.-D.; Pan, J.-F.; Chen, K., Chiral Lewis Acid-Catalyzed Asymmetric Baylis–Hillman Reactions. *J. Org. Chem.* **2003**, *68* (3), 915-919.
128. Ema, T.; Tanida, D.; Matsukawa, T.; Sakai, T., Biomimetic trifunctional organocatalyst showing a great acceleration for the transesterification between vinyl ester and alcohol. *Chem. Commun.* **2008**, (8), 957-959.
129. Wang, C.-J.; Zhang, Z.-H.; Dong, X.-Q.; Wu, X.-J., Chiral amine-thioureas bearing multiple hydrogen bonding donors: highly efficient organocatalysts for asymmetric Michael addition of acetylacetone to nitroolefins. *Chem. Commun.* **2008**, (12), 1431-1433.
130. Kenny, R.; Liu, F., Cooperative Trifunctional Organocatalysts for Proficient Proton Transfer Reactions. *Chem. Rec.* **2017**, *17* (5), 535-553.

131. Garnier, J.-M.; Liu, F., Trifunctional organocatalyst-promoted counterion catalysis for fast and enantioselective aza-Morita-Baylis-Hillman reactions at ambient temperature. *Org. Biomol. Chem.* **2009**, 7 (7), 1272-1275.
132. Garnier, J.-M.; Anstiss, C.; Liu, F., Enantioselective Trifunctional Organocatalysts for Rate- Enhanced Aza-Morita–Baylis–Hillman Reactions at Room Temperature. *Adv. Synth. Catal.* **2009**, 351 (3), 331-338.
133. Anstiss, C.; Garnier, J.-M.; Liu, F., Mechanistic investigations of multidentate organocatalyst-promoted counterion catalysis for fast and enantioselective aza-Morita-Baylis-Hillman reactions at ambient temperature. *Org. Biomol. Chem.* **2010**, 8 (19), 4400-4407.
134. Anstiss, C.; Liu, F., Cooperativity in the counterion catalysis of Morita/Baylis/Hillman reactions promoted by enantioselective trifunctional organocatalysts. *Tetrahedron* **2010**, 66 (29), 5486-5491.
135. Mattia, E.; Otto, S., Supramolecular systems chemistry. *Nat. Nanotechnol.* **2015**, 10 (2), 111-119.
136. Lehn, J.-M., Supramolecular chemistry — Molecular information and the design of supramolecular materials. *Makromolekulare Chemie. Macromolecular Symposia* **1993**, 69 (1), 1-17.
137. Brack, A., *The molecular origins of life: assembling pieces of the puzzle*. Cambridge University Press: 1998.
138. Lahav, N., *Biogenesis: theories of life's origin*. Oxford University Press on Demand: 1999.
139. Viedma, C., Chiral Symmetry Breaking During Crystallization: Complete Chiral Purity Induced by Nonlinear Autocatalysis and Recycling. *Phys. Rev. Lett.* **2005**, 94 (6), 065504.

140. Kuhn, H., Origin of life — Symmetry breaking in the universe: Emergence of homochirality. *Curr. Opin. Colloid Interface Sci.* **2008**, *13* (1), 3-11.
141. Mauksch, M.; Wei, S.; Freund, M.; Zamfir, A.; Tsogoeva, S. B., Spontaneous Mirror Symmetry Breaking in the Aldol Reaction and its Potential Relevance in Prebiotic Chemistry. *Origins Life Evol. Biospheres* **2010**, *40* (1), 79-91.
142. Steendam, R. R. E.; Verkade, J. M. M.; van Benthem, T. J. B.; Meekes, H.; van Enckevort, W. J. P.; Raap, J.; Rutjes, F. P. J. T.; Vlieg, E., Emergence of single-molecular chirality from achiral reactants. *Nat. Commun.* **2014**, *5*, 5543.
143. Ruiz-Mirazo, K.; Briones, C.; de la Escosura, A., Prebiotic Systems Chemistry: New Perspectives for the Origins of Life. *Chem. Rev.* **2014**, *114* (1), 285-366.
144. Sutherland, J. D., The Origin of Life—Out of the Blue. *Angew. Chem., Int. Ed.* **2016**, *55* (1), 104-121.
145. Saghatelian, A.; Yokobayashi, Y.; Soltani, K.; Ghadiri, M. R., A chiroselective peptide replicator. *Nature* **2001**, *409* (6822), 797-801.
146. Ashkenasy, G.; Jagasia, R.; Yadav, M.; Ghadiri, M. R., Design of a directed molecular network. *Proc. Natl. Acad. Sci.* **2004**, *101* (30), 10872-10877.
147. Sadownik, J. W.; Mattia, E.; Nowak, P.; Otto, S., Diversification of self-replicating molecules. *Nat. Chem.* **2016**, *8* (3), 264-269.
148. Dadon, Z.; Wagner, N.; Ashkenasy, G., The Road to Non-Enzymatic Molecular Networks. *Angew. Chem., Int. Ed.* **2008**, *47* (33), 6128-6136.
149. Ashkenasy, G.; Hermans, T. M.; Otto, S.; Taylor, A. F., Systems chemistry. *Chem. Soc. Rev.* **2017**, *46* (9), 2543-2554.
150. Soai, K.; Shibata, T.; Morioka, H.; Choji, K., Asymmetric autocatalysis and amplification of enantiomeric excess of a chiral molecule. *Nature* **1995**, *378* (6559), 767-768.

151. Buhse, T.; Noble-Terán, M. E.; Cruz, J.-M.; Micheau, J.-C.; Coudret, C., Chapter 4 - Kinetic and Structural Aspects of Mirror-Image Symmetry Breaking in the Soai Reaction. In *Advances in Asymmetric Autocatalysis and Related Topics*, Pályi, G.; Kurdi, R.; Zucchi, C., Eds. Academic Press: 2017; pp 71-110.
152. Soai, K.; Kawasaki, T.; Matsumoto, A., Asymmetric autocatalysis of pyrimidyl alkanol and related compounds. Self-replication, amplification of chirality and implication for the origin of biological enantioenriched chirality. *Tetrahedron* **2018**, *74* (16), 1973-1990.
153. Frank, F. C., On spontaneous asymmetric synthesis. *Biochim. Biophys. Acta* **1953**, *11* (4), 459-463.
154. Blackmond, D. G., Asymmetric autocatalysis and its implications for the origin of homochirality. *Proc. Natl. Acad. Sci.* **2004**, *101* (16), 5732-5736.
155. Sato, I.; Ohgo, Y.; Igarashi, H.; Nishiyama, D.; Kawasaki, T.; Soai, K., Determination of absolute configurations of amino acids by asymmetric autocatalysis of 2-alkynylpyrimidyl alkanol as a chiral sensor. *J. Organomet. Chem.* **2007**, *692* (9), 1783-1787.
156. Busch, M.; Schlageter, M.; Weingand, D.; Gehring, T., Systematic Studies using 2 - (1 - Adamantylethynyl)pyrimidine - 5 - carbaldehyde as a Starting Material in Soai's Asymmetric Autocatalysis. *Chemistry – A European Journal* **2009**, *15* (33), 8251-8258.
157. Gehring, T.; Busch, M.; Schlageter, M.; Weingand, D., A concise summary of experimental facts about the Soai reaction. *Chirality* **2010**, *22* (1E), E173-E182.



## **Chapter 2**

# **Mechanistic Investigations of a Proton Shuttle in Trifunctional Organocatalysis of an aza-MBH Model System**

## **2.1 Introduction**

### **2.1.1 Mechanistic understanding of organocatalytic modes of activation**

As introduced in Chapter 1, organocatalysts in many instances can be viewed as simple model systems with minimum motifs to achieve certain activation modes.<sup>1-2</sup> One classic example is the enamine-iminium mode of activation by proline.<sup>3-5</sup> Experimental evidence for the proposed enamine/iminium intermediate by NMR spectroscopy, DFT calculations and detailed mechanistic studies have determined how the geometry of the proline catalyst is critical for catalysis and highlighted the importance of the carboxylic acid in the 2-position.<sup>6</sup> The List–Houk model suggests that intramolecular addition of the enamine to an electrophile takes place via a cyclic transition state in which the carboxylic acid activates the electrophile while positioning the substrate for an intramolecular attack.<sup>6</sup> While computational analysis is often essential for understanding a mechanism, structural analysis in the solution phase is often critical to understand the catalytic nature of the reactive intermediates involved.

### **2.1.2 NMR techniques and analysis of organocatalytic intermediates**

NMR spectroscopy is a powerful tool for analysing the structure and conformational dynamics of organic molecules.<sup>7-9</sup> Dihedral angles extracted from the angular dependence of spin-spin coupling constants,<sup>10-11</sup> and distance-dependent intensity of NOEs can assist in relative stereochemical determination from ensemble averages<sup>12-13</sup> in addition to measuring dissociation constants in ligand and receptor interactions.<sup>14-16</sup> More recently, NMR analysis of complex organocatalytic reactions is frequently used to characterise reaction intermediates to understand the origins of stereoselectivity.<sup>17-21</sup> For example, <sup>1</sup>H NMR spectroscopy identified electron-rich dienamines as ground state intermediates formed between proline and  $\alpha,\beta$ -unsaturated aldehydes.<sup>22</sup> The proficiency of proline-based catalysts

has been rationalised by identifying isomeric oxazolidinones as a parasitic species formed from an enamine intermediate using NMR spectroscopy.<sup>23-24</sup> The enamine was shown to form the oxazolidinone by 2D exchange spectroscopy, and destabilisation of the oxazolidinone to promote enamine formation was correlated with higher catalyst activity.<sup>25</sup>

Structural insight from conformational analysis by characterising the active catalytic forms is often critical to understanding asymmetric induction. For example, analysis of the  $^3J_{\text{H}\alpha\text{H}\beta}$  scalar couplings, along with NOESY experiments, suggested that the “down” ring pucker of prolinol enamines was the preferred conformation for catalysis while the “up” ring pucker prevented the reaction because the  $\alpha$ -carbon substituents acted as a steric screen.<sup>26</sup> NOEs and residual dipolar coupling (RDC) were measured for peptide catalysts to identify the active conformers for a kinetic resolution of *trans*-cycloalkane-1,2-diols via monoacylation.<sup>27</sup> The ensemble identified was consistent with earlier DFT studies that the substrate and acylium cation are required to organise the catalysis via hydrogen bonding and dispersion interactions.<sup>28</sup> Also, dynamic changes in catalyst shape, as seen in the backbone conformation of a tripeptide for catalysing conjugate addition reactions of aldehydes to nitroalkenes to form  $\gamma$ -nitroaldehydes, have been observed by NOE analysis to identify a conformational shift upon enamine formation that accesses a more active catalytic conformer.<sup>21</sup>

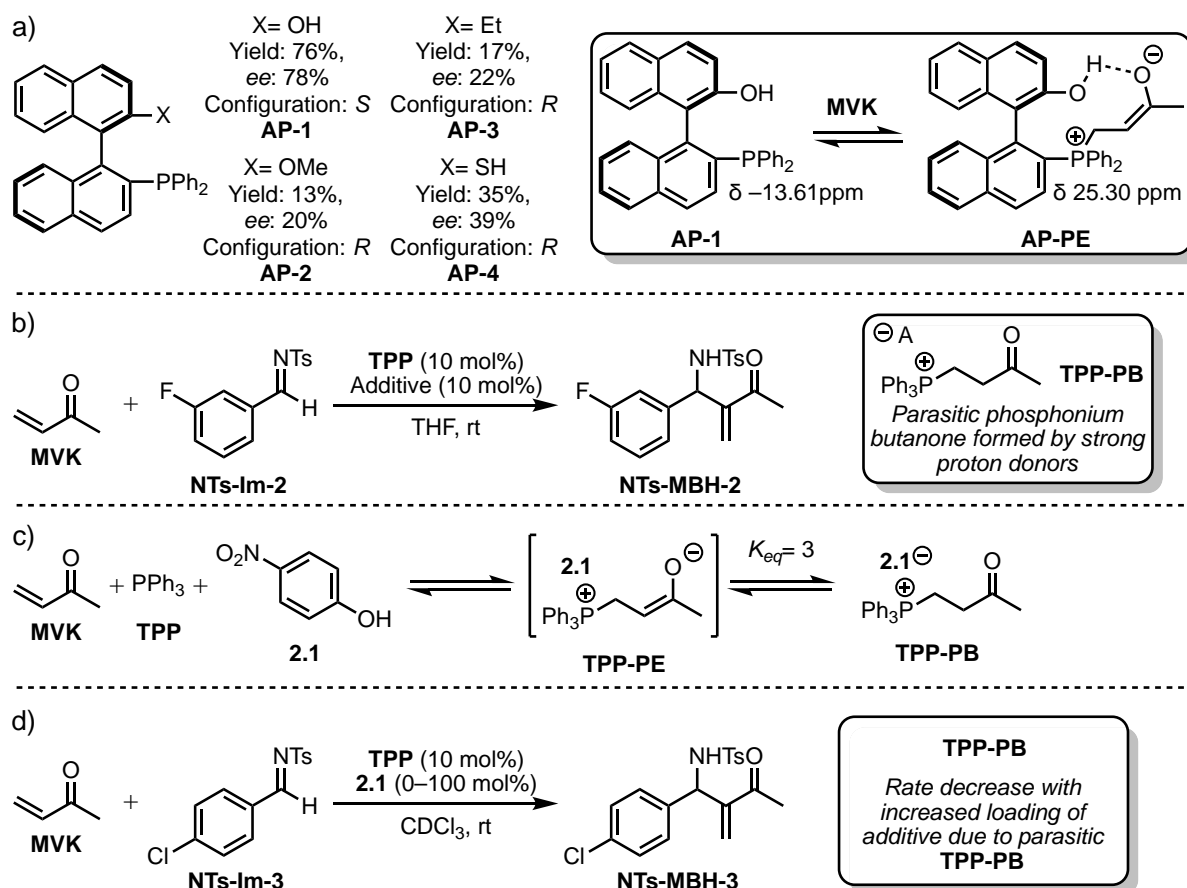
In addition to NOE analysis, coupling constant analysis is also a powerful tool for constructing structural models out of complex samples, such as mixtures of compounds with diastereotopic protons in an ABXY system. Techniques such as homonuclear *J*-resolved (JRES) spectroscopy enables the measurement of  $^xJ_{\text{HH}}$  coupling constants by separating chemical

shift and *J*-coupling,<sup>29-30</sup> often in a 2D JRES pulse sequence comprising of a relaxation delay– $90^\circ-(t_1/2)-180^\circ-(t_1/2)$ —acquisition.

Conformers identified by molecular mechanics and JRES spectroscopy can be refined to mechanistically relevant conforms using intermolecular distances extracted from quantitative NOE experiments. As will be discussed in Section 2.2.3 for our trifunctional catalysts with 28-30 proton environments, homonuclear JRES and quantitative NOEs were employed to extract structural understanding of the productive catalytic species for rationalising the proficiency (coupled rate and *ee* elevation) in our trifunctional organocatalytic system.

### **2.1.3 Existing NMR-based investigations of the MBH reaction**

While NMR-based investigations into the MBH or *aza*-MBH thus far have focused on measuring the kinetics of the reaction, there is a general lack of structural characterisation of any reactive species. It has been noted, in some instances, that no new species were identified by  $^1\text{H}$  NMR spectroscopy during kinetic analysis even at high field strength (600 MHz), which is consistent with the prototype MBH mechanism in which steps leading to high energy intermediates are reversible.<sup>31</sup>



**Scheme 2.1.** Studies reporting the formation of parasitic phosphonium butanone intermediates.<sup>32-35</sup>

Shi et al. reported the first  $^1\text{H}$  NMR evidence of an enolate intermediate for a binaphthylene bifunctional organocatalyst **AP-1** (Scheme 2.1a).<sup>32</sup> Upon addition of methyl vinyl ketone (**MVK**) to the bifunctional organocatalyst **AP-1**, the phenolic proton disappeared from the  $^1\text{H}$  NMR spectrum, while in the  $^{31}\text{P}$  NMR spectrum, a new peak (+25.30 ppm) emerged as the major signal along with the original peak at -13.61 ppm for the phosphine. This was proposed as evidence for a hydrogen-bond stabilised enolate (**AP-PE**) as a new major species in the reaction. However, no spectral analysis ( $^1\text{H}$  NMR,  $^{13}\text{C}$  NMR) of **AP-PE** was reported. At this point, it remains unresolved how an enolate such as **AP-PE**, a species presumably much higher in energy than the ground state (**AP-1** plus **MVK**), could be detected by NMR spectroscopy as the major species.

Leitner et al. reported ketone formation between triphenylphosphine (TPP) and MVK for the *racemic* aza-MBH reaction of **NTs-Im-2** in the presence of various Brønsted acid additives (Scheme 2.1b).<sup>33</sup> The reaction rate was monitored by <sup>1</sup>H NMR spectroscopy 3,5-bis(CF<sub>3</sub>)phenol ( $pK_a \sim 8$ ) was identified as the optimal additive. Stronger acid additives decreased the rate due to protonation of the phosphonium enolate to yield the phosphonium butanone **TPP-PB**. This report was the first <sup>1</sup>H NMR characterisation of a phosphonium butanone (**TPP-PB**) and demonstrated the need for balanced acidity of the protic additive for efficient catalysis. Strong acid additives protonate the enolate intermediate and can suppress the rate and weak acid additives are ineffective proton transfer catalysts.

Shi et al. expanded on their earlier mechanistic work using TPP and *p*-nitrophenol (**2.1**) (Scheme 2.1c).<sup>34</sup> They reported that the enolate intermediate was formed with TPP and MVK in the absence of phenol. Upon addition of **2.1**, the putative phosphonium butanone (**TPP-PB**) was formed in a 3:1 ratio with the free phosphine. The phosphonium aldol adduct prior to elimination was also observed in this report.

Zipse et al. demonstrated that a subcatalytic amount of a protic additive accelerated the rate, but superstoichiometric equivalents of the additive are suppressive (Scheme 2.1d).<sup>35</sup> Conversion of the model substrate (**NTs-Im-3**) to the aza-MBH adduct (**NTs-MBH-3**) was monitored by <sup>1</sup>H NMR spectroscopy to determine the effect on the reaction rate for different equivalents of **2.1**. In CDCl<sub>3</sub>, the acid additive enhanced the rate of reaction up to 10 mol%, while increasing the loading beyond 10 mol% resulted in a decrease in rate. Complete structure elucidation demonstrated that the parasitic intermediate (i.e. unproductive

intermediate) was the phosphonium butanone **TPP-PB**. At higher loadings of **2.1**, the equilibrium between the reactive enolate **TPP-PE** and inert ketone tautomer **TPP-PB** shifted towards the ketone suppressing reactivity. Under catalytic conditions, the enolate **TPP-PE** and ketone **TPP-PB** rapidly interconvert, but at a higher Brønsted acid loading, the equilibrium favours the formation of the stable phosphonium butanone ketone.

All of the literature precedents involving bifunctional or monofunctional phosphine catalysts demonstrate a strong acid additive such as benzoic acid (BzOH) quenches the reactive enolate and promotes ketone formation (Scheme 2.1).<sup>32-35</sup> This is in direct contrast to the switch-on effect of BzOH in our trifunctional system.<sup>36-39</sup> In this chapter, the role of BzOH in the trifunctional catalysis is investigated by taking a structural approach.

#### 2.1.4 Specific aims

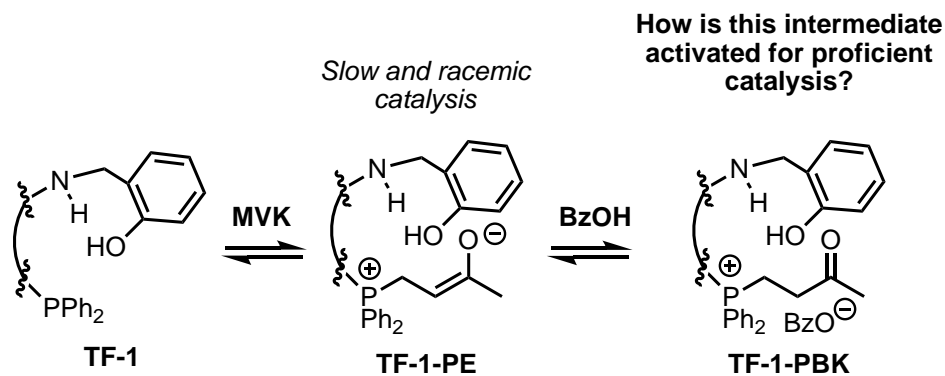
The nature and activation of the lowest energy intermediate in our trifunctional catalysis are currently undetermined. In this chapter, several aspects of the ground state intermediate, a phosphonium benzoate ketone identified by 2D NMR spectroscopy, are probed. The aims of this chapter are to:

- Characterise the ground state in our trifunctional organocatalysis by 2D NMR spectroscopy;
- Examine the role of the phosphonium benzoate ketone in the trifunctional catalysis;
- Construct an ensemble solution structure by conformational analysis using JRES spectroscopy and quantitative 2D NOESY experiments.

Addressing these aims will allow us, for the first time, to propose a mechanism by which the phosphonium benzoate ketone can be activated for catalysis.

## 2.2. Results and Discussion

In this section, the formation and structural analysis of a new ground state intermediate for the prototype trifunctional organocatalyst **TF-1**- a phosphonium benzoate ketone (**PBK**) **TF-1-PBK**, will be discussed (Scheme 2.2). After the initial identification (Section 2.2.1) and kinetic analysis for its catalytic relevance (Section 2.2.2), a solution structure model for **TF-1-PBK** was constructed (Section 2.2.3). Further NOE experiments revealed the constrained but dynamic nature of this ion-pair (Section 2.2.4), from which a proton-shuttling mechanism could be formulated. Computational analysis, in collaboration with the group of Dr Hans Senn (University of Glasgow), was performed to assess the relative stabilities of the tautomers of this proton-shuttling ion-pair (Section 2.2.5). In summary (Section 2.2.6), the intricate details of how proton transfer across different tautomeric form of **TF-1-PBK** are proposed to illustrate an expanded reactive network for the aza-MBH reaction.



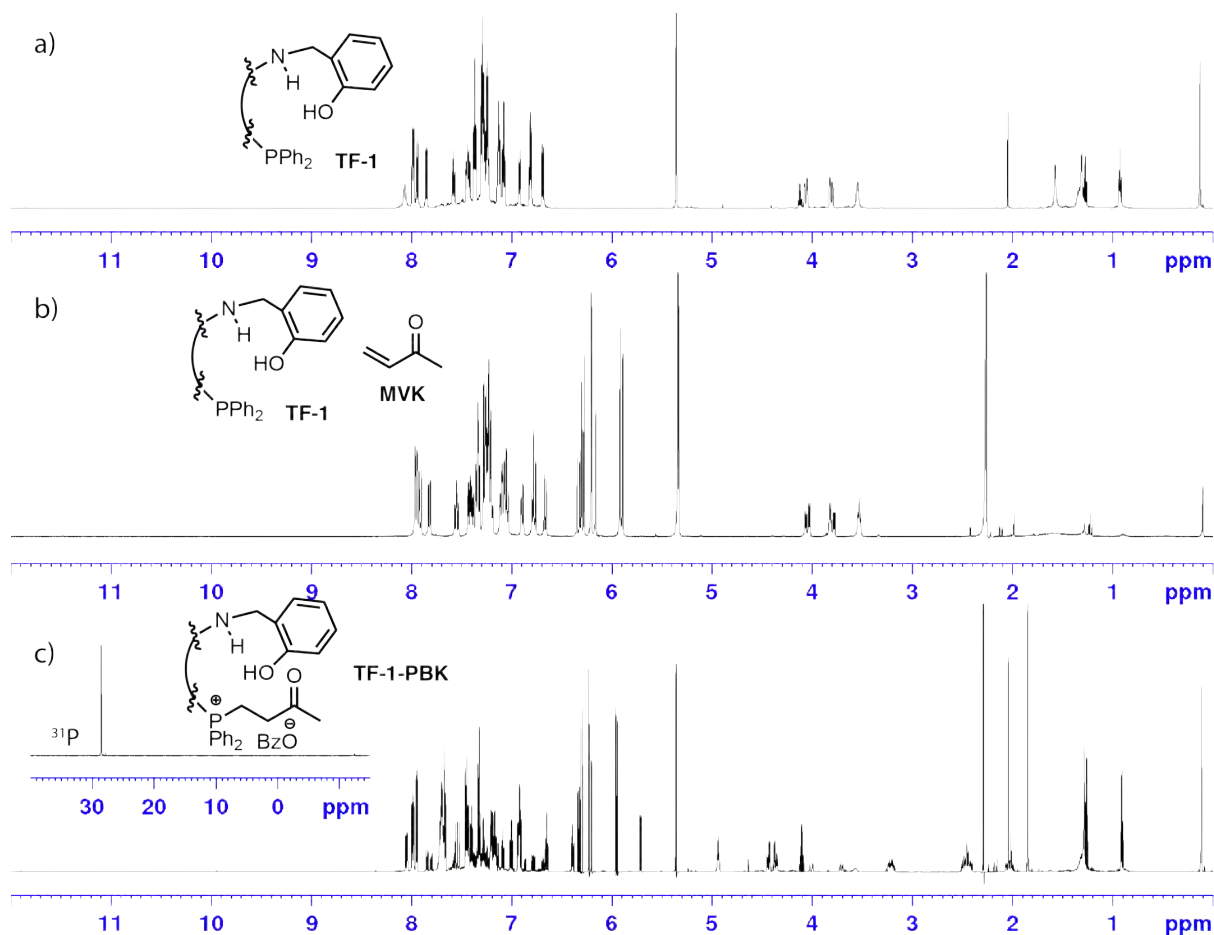
**Scheme 2.2.** Key question in this chapter concerns activation of **TF-1-PBK**.

### 2.2.1 Identification of a new reaction intermediate, the phosphonium benzoate ketone

A sample of **TF-1** dissolved in  $\text{CD}_2\text{Cl}_2$  (Figure 2.1a) was mixed with 2.0 equivalents of **MVK** and no new intermediates (i.e. a potential phosphonium enolate) were observed in the  $^1\text{H}$  NMR spectrum (Figure 2.1b). However, upon addition of 1.05 equivalents of **BzOH**, the colourless



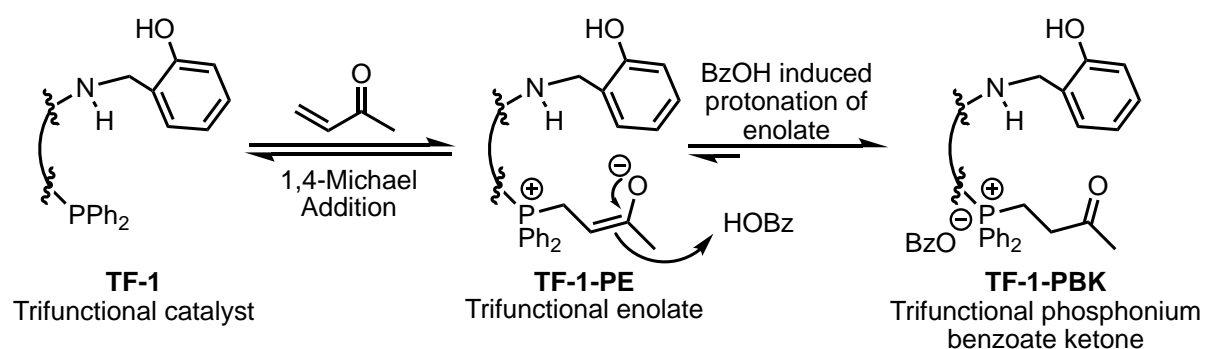
solution turned bright yellow and  $^1\text{H}$  and  $^{31}\text{P}$  NMR spectroscopy determined the conversion of **TF-1** to a new intermediate (Figure 2.1c)



**Figure 2.1.**  $^1\text{H}$  NMR spectra (600 MHz,  $\text{CD}_2\text{Cl}_2$ ) for a) **TF-1** b) **TF-1** and MVK c) **TF-1**, MVK and BzOH (**TF-1-PBK**) with an insert of the  $^{31}\text{P}$  NMR spectrum.

A new signal in the  $^{31}\text{P}$  NMR at 28.50 ppm, along with the diminished peak at -12.37 ppm for **TF-1** indicate the formation of a phosphonium centre (Figure 2.1c). Three new signals were observed in the aliphatic region between 2.0–3.3 ppm with a ratio of 1:2:1 of the  $^1\text{H}$  NMR spectrum is constituent with two overlapping AM systems of a phosphonium butanone. This is the protonated enolate that has tautomerized to its keto form and is consistent with prior reports of phosphonium ketones in the MBH reaction.<sup>32-35</sup> The proportion of **TF-1-PBK** to free catalyst (**TF-1**) was measured by integrating the two sets of methylene benzylic protons and

determined to be 4.12:1. This PBK is, therefore, a new ground state intermediate formed from **TF-1** with BzOH and MVK. Formation of the **PBK** proceeds via an initial Michael addition to generate the enolate **TF-1-PE**. The PBK **TF-1-PBK** is then generated by BzOH protonating the enolate and subsequent keto-enol tautomerisation (Scheme 2.3).



**Scheme 2.3.** Formation of **TF-1-PBK** via protonation of **TF-1-PE**.

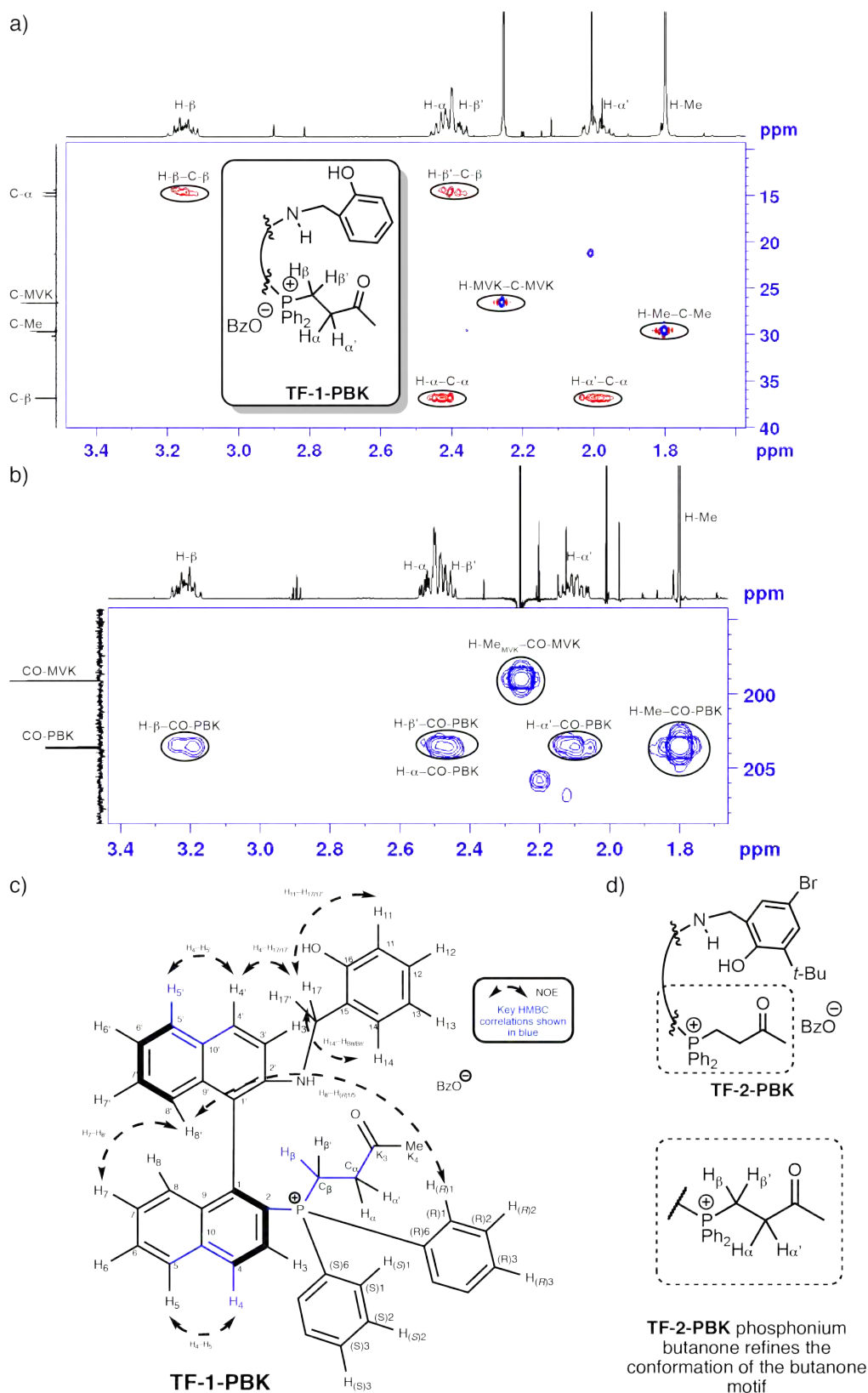
2D heteronuclear NMR spectroscopy provided further connectivity details for the phosphonium benzoate ketone (**TF-1-PBK**). The four diastereotopic methylene protons of the ABXY phosphonium butanone system were confirmed by  $^1\text{H}$ - $^{13}\text{C}$  phase-edited HSQC within the 2.0–3.3 ppm range (Figure 2.2a). The two sets of diastereotopic protons were correlated to two different carbon environments in the HSQC spectrum; 1)  $\text{C}_\beta$ : 15.2 ppm ( $d$ ,  $^1J_{\text{CP}} = 55$  Hz) and 2)  $\text{C}_\alpha$ : 36.9 ppm. The  $\alpha$ - and  $\beta$ -proton were assigned using the  $^1J_{\text{CP}}$  coupling constant observed for  $\text{C}_\beta$ . The through-bond relationship between  $\text{H}_\alpha$  and the **PBK** carbonyl were established by  $^1\text{H}$ - $^{13}\text{C}$  HMBC (Figure 2.2b). The carbonyl of the butanone displayed long-range C-P coupling constant at 203.6 ppm ( $^3J_{\text{CP}} = 12$  Hz). These structural details were utilised in the subsequent kinetic and mechanistic studies.

Complete structure elucidation was performed by 2D NMR spectroscopy. The **TF-PBK** structure is broken up into the following substructures: the two phenyl substituents (pro-*R*

and pro-*S*), *P*-naphthalene, *N*-naphthalene, the phosphonium butanone arm, and the phenol arm. Complete structural assignments for **TF-1-PBK** (Figure 2.2c) and second generation catalyst PBK **TF-2-PBK** (Figure 2.2d) were performed using a combination of 2D NMR experiments (HSQC, HMBC, H2BC, COSY and NOESY) at 5 °C. Key structural HMBC and NOE correlations can be seen in Table 2.1, complete structure elucidation and annotated spectra can be seen in the Experimental Section 2.3.2 Proportion of PBK and structure elucidation).

Complete annotation was performed by 2D NMR spectroscopy (HSQC, HMBC, COSY, NOESY). Furthermore, spin systems were consolidated using HMBC experiments to complete the annotation of **TF-1-PBK**. HMBC correlations to the heteroatom bound carbons (C-2' for *N*-naphthalene or C-2 for *P*-naphthalene) identified the two naphthalene units. For **TF-1-PBK** the spin systems for two prochiral phenyl substituents were identified, one upfield shifted (6.89 ppm (2H), 7.12 ppm (2H), 7.37 ppm (1H)) and one downfield shifted (7.58-7.70 ppm (5H)). NOEs from the upfield shifted spin system to the *N*-naphthalene indicated  $\pi$ - $\pi$  stacking between the phenyl and the *N*-naphthalene. No NOEs originated from the downfield shifted phenyl substituent to the *N*-naphthalene indicating that it is orientated "outward" into the solvent. The upfield shifted spin system was assigned to the Pro-*R* and the downfield system to Pro-*S* phenyl substituents. These assignments and NOEs are collected in Table 2.1.

The PBK is the ground state intermediate for the trifunctional organocatalyst with BzOH, which is consistent with the existing NMR studies (Section 2.1.3 Existing NMR-based investigations of the MBH reaction).<sup>32-35</sup> The next set of questions relates to the generality of the PBK as the general ground state for different catalysts and if the proportion of the PBK correlates with reactivity in the presence of BzOH for different catalysts.



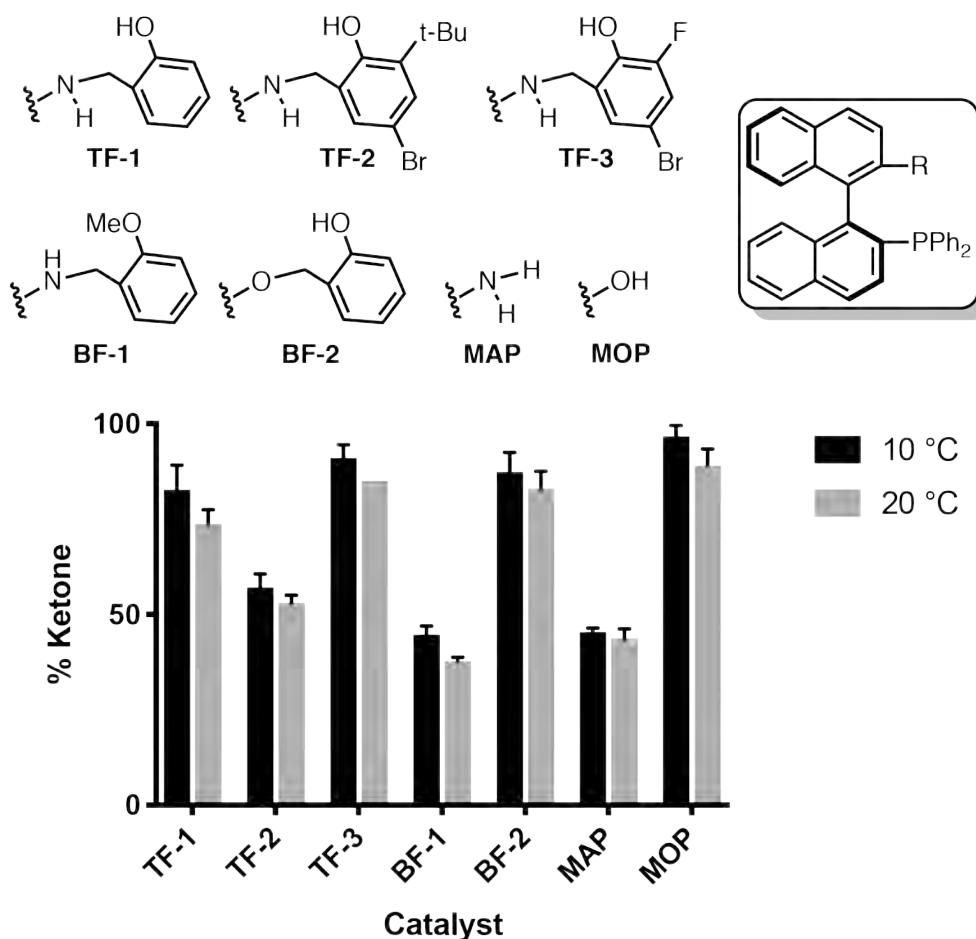
**Figure 2.2.** a) Phase edited  $^1\text{H}$ - $^{13}\text{C}$  HSQC (600 MHz,  $\text{CD}_2\text{Cl}_2$ ). b)  $^1\text{H}$ - $^{13}\text{C}$  HMBC NMR spectrum (600 MHz,  $\text{CD}_2\text{Cl}_2$ ) expansion of **TF-1-PBK** at 278 K. c) Assignment map for **TF-1-PBK**, key structural HMBC correlations are shown in blue. The benzoate is not shown for clarity. d) **TF-2-PBK** as the model system for refinement of the butanone motif.

**Table 2.1.** Selected NOEs and correlations.

| Proton |          | HMBC        |          | NOE         |                          |
|--------|----------|-------------|----------|-------------|--------------------------|
| -      | $\delta$ | -           | $\delta$ | -           | Distance /Å <sup>a</sup> |
| H-8'   | 5.77     | C-10'       | 126.6    | H-(R)1      | 3.28                     |
|        |          | C-6'        | 121.7    | H-7         | 3.41                     |
|        |          | C-1'        | 110.7    |             |                          |
| H-17   | 4.36     | C-15        | 124.7    | H-11/H-14   | 2.68                     |
|        |          | C-2'        | 146.0    | H-3         | 2.32                     |
|        |          |             |          | H- $\beta'$ | 4.49                     |
|        |          |             |          | NH          | 3.23                     |
| H-17'  | 4.25     | C-15        | 124.8    | H-11/H-14   | 2.56                     |
|        |          | C-2'        | 146.0    | H-3         | 2.63                     |
|        |          |             |          | N-H         | 3.05                     |
| H-3    | 7.53     | C-10        | 136.6    | H-(R)1      | 3.00                     |
|        |          | C-1         | 145.2    | H-(S)1      | 3.09                     |
| N-H    | 4.80     | -           | -        | H- $\beta'$ | 3.10                     |
|        |          |             |          | H-(R)1      | 3.53                     |
|        |          |             |          | H-3         | 3.62                     |
|        |          |             |          | H-(S)1      | 3.97                     |
| H-Me   | 1.78     | C- $\alpha$ | 36.9     | H-11/H-14   | 4.64                     |
|        |          |             |          | H-12        | 4.07                     |
|        |          |             |          | H-13        | 3.79                     |

a) Determined from quantitative 2D NOESY with the H-4'–H-5' NOE used as the calibrant (2.48 Å).

The equilibrium between the phosphine and PBK was measured for seven catalysts at two temperatures (10 °C and 20 °C) by <sup>1</sup>H NMR spectroscopy (600 MHz) to examine if the extent of the PBK formation may be relevant to catalysis. The PBK was formed for three trifunctional catalysts (**TF-1–3**), two bifunctional controls (**BF-1** and **BF-2**), **MAP** and **MOP** (Figure 2.3).



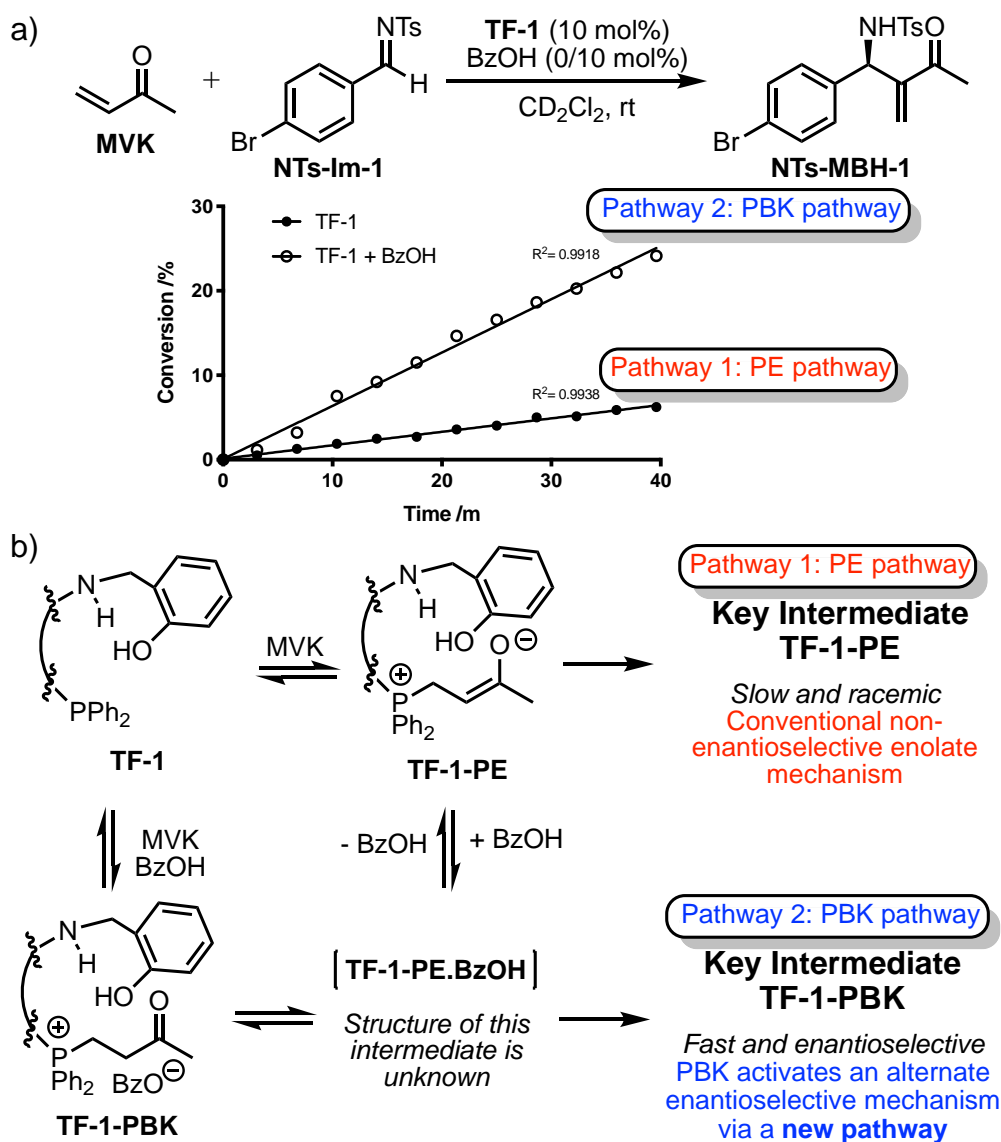
**Figure 2.3.** The proportion of the PBK relative to free phosphine at 10 °C and 20 °C.

The PBK was the ground state intermediate for all three trifunctional catalysts, **BF-2** and **MOP**. The proportion of PBK at 10 °C as measured by  $^1\text{H}$  NMR spectroscopy (600 MHz) ranged from  $45 \pm 3\%$  for **BF-1** to  $96 \pm 3\%$  for **MOP**. For all seven catalysts, the proportion of the thermodynamically more stable PBK was lower at 20 °C ( $38 \pm 1\%$  to  $89 \pm 4\%$ ). For trifunctional organocatalysts, **TF-1–3**, the proportion of the PBK was affected by the acidity of the phenol motif. More acidic phenol may form a stronger hydrogen bond that can transfer the proton to the developing enolate, stabilising the intermediate as the **PBK**. The highest proportion of PBK observed out of the three was for **TF-3**. The proportion of PBK for **TF-2** was lower than that for **TF-1**, which was somewhat unexpected for an acidic phenol. In this instance, the steric hindrance from the *ortho*- *t*-butyl substituent may diminish the stability of the PBK.

The bifunctional control **BF-2** without an amino group ( $87 \pm 5\%$ ) has a comparable proportion of ketone as **TF-1** ( $83 \pm 6\%$ ). However, the bifunctional control **BF-1** (without a phenol) has a significantly lower proportion of the PBK ( $45 \pm 3\%$ ). This is consistent with the role of the acidic phenol in stabilisation of the trifunctional PBK via H-bonding. **BF-1** and **MAP** both lack the phenolic proton and have near-identical proportions of the ketone supporting the phenol H-bonding role. In summary, the PBK is the ground state intermediate, and its proportion is increased by the presence of the phenol Brønsted acid. Activation of the PBK ground state to yield the nucleophilic enolate is the first critical step for trifunctional catalysts.

### 2.2.2 The PBK is a catalytically relevant intermediate in the trifunctional catalysis

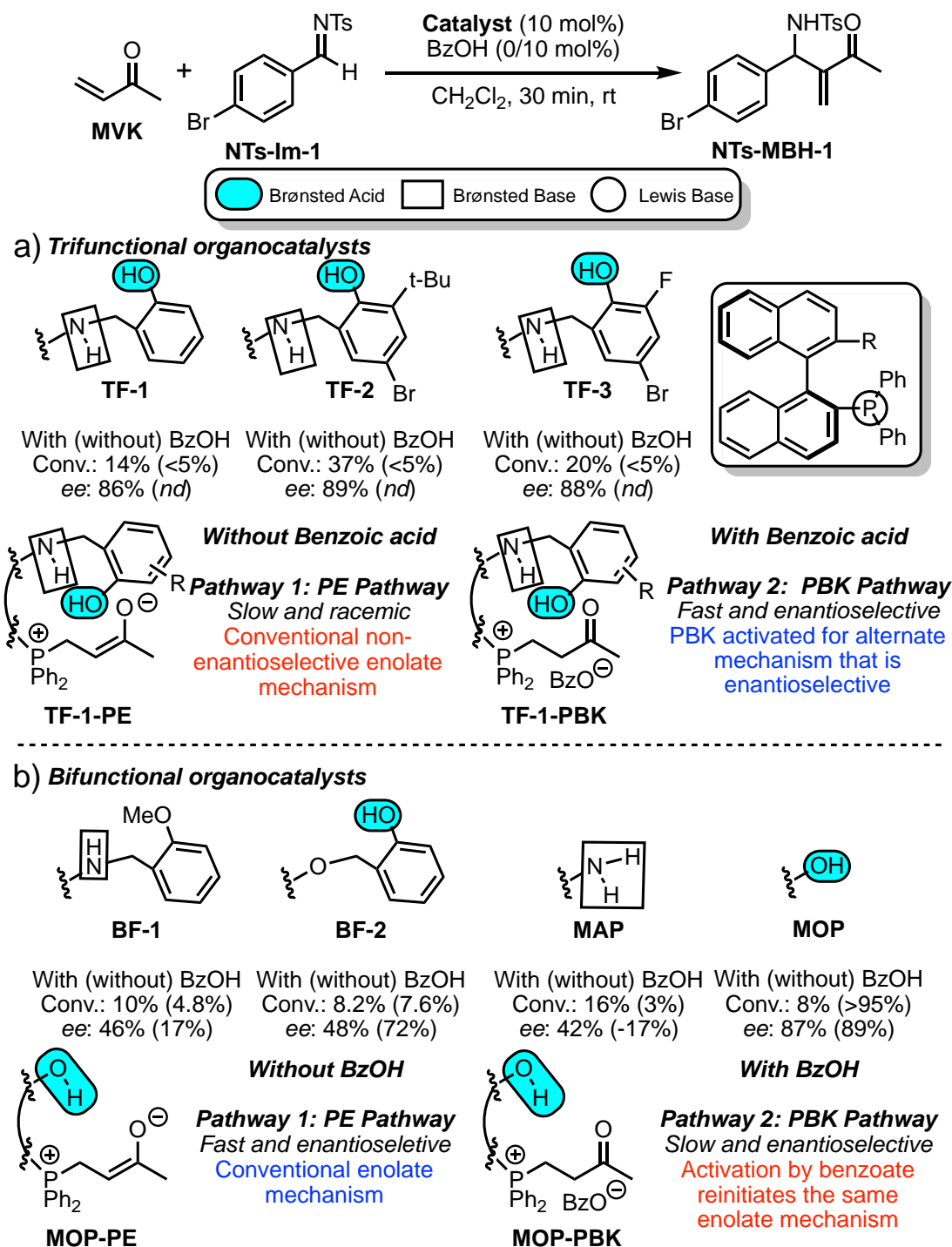
The initial rates (up to 30% conversion in 40 min) for the test reaction between (*E*)-*N*-(4-bromobenzylidene)-4-methylbenzenesulfonamide (**NTs-Im-1**) and **MVK** catalysed by **TF-1** at room temperature demonstrated a clear rate acceleration in the presence of BzOH (Figure 2.4a). The rate with BzOH was nearly 4-fold higher than without BzOHs moreover, the reaction shifts from a *racemic* variant to an enantioselective one (87% *ee*). A *different*, faster and enantioselective pathway emerges only in the presence of BzOH that outcompetes the background enolate pathway (Figure 2.4b). BzOH causes a mechanistic shift from a slow, *racemic* pathway through **TF-1-PE** (Pathway 1) to a fast and enantioselective mechanism through **TF-1-PBK** (Pathway 2).



**Figure 2.4.** a) The initial rate for **TF-1** without (pathway 1) and BzOH (pathway 2). b) Shift in mechanism induced by key intermediates for Pathway 1 (**TF-1-PE**) and Pathway 2 (**TF-1-PBK**).

The generality of this rate effect of BzOH was investigated further in bifunctional and trifunctional systems. A panel of seven catalysts, three trifunctional catalysts (**TF-1–3**) and four bifunctional controls (**BF-1**, **BF-2**, **MAP** and **MOP**), were first screened using the same test aza-MBH reaction (Figure 2.5) between **NTs-Im-1** and **MVK** at room temperature.





**Figure 2.5.** a) Conversion and enantioselectivity determined for trifunctional organocatalysts through the **PBK** pathway, b) Conversion and enantioselectivity determined for bifunctional catalysts through the **PE** pathway.

BzOH accelerates the rate of reaction for catalysts containing an amine motif (**TF-1-3**, **MAP**, **BF-1**). No conversion was observed for trifunctional catalysts without BzOH, but a concurrent elevation of rate and asymmetry was observed for all trifunctional catalysts with BzOH (Figure

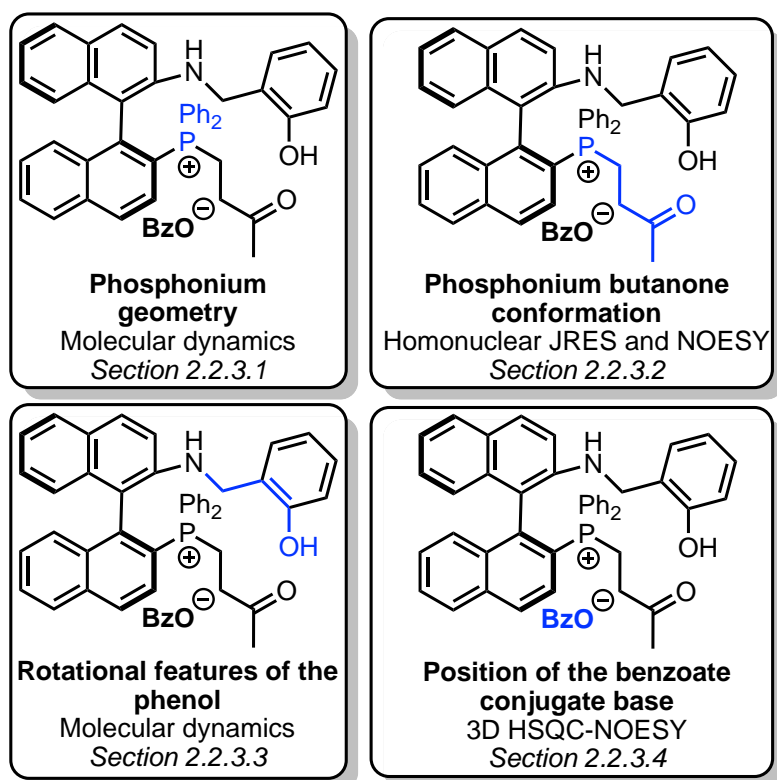
2.5a). The most proficient catalysis in the presence of BzOH was observed for **TF-2** (37% conversion in 30 min, 89% *ee*). BzOH has a more complex effect on catalysts without the amine motif (**BF-2** and **MOP**) affecting either rate or enantioselectivity independently. For **BF-2**, the enantioselectivity decreases from 72% to 48% with BzOH. The reaction rate is heavily suppressed (10-fold reduction) for the bifunctional catalyst **MOP** (Figure 2.5b). It is only the trifunctional system in which both rate and asymmetry are concurrently elevated. The ground state trifunctional PBK (i.e. **TF-1-PBK**), unlike **MOP-PBK**, is the gateway to fast and enantioselective catalysis via a distinctly different pathway accessible by **TF-1-PE**. There is one key question: *how is TF-1-PBK activated to access this new pathway?*

In summary, three distinct catalytic profiles are apparent; 1) concurrent asymmetric induction and rate elevation (trifunctional organocatalysts **TF-1-3**, **BF-1**); 2) suppression of rate and no change in *ee* (**MOP**); 3) slight suppression of rate and decrease in *ee* (**BF-2**). The extent of PBK formation is not correlated to the rate of the reaction, and a distinction is made between stabilisation and activation. **MOP** has the greatest degree of ketone formation with BzOH, and activation of the PBK to generate the nucleophile is sluggish. Thermodynamic stability of the **MOP-PBK** causes rate suppression with little change in enantioselectivity as the reaction still proceeds through the enolate mechanism (Figure 2.5b). **MOP-PBK** is, therefore, a parasitic intermediate. Contrast to this, there is no correlation between the proportion of ketone formation and the rate of the aza-MBH reaction for trifunctional catalysts. Activation of trifunctional **PBKs** is facile, and the reaction proceeds through a new pathway that is distinct from the conventional pathway driven by the *racemic* enolate.

While proton abstraction of the **PBK** intermediate is necessary in both the bifunctional (**MOP**) and trifunctional system to reclaim the nucleophilic enolate, the unusual rate elevation in the trifunctional case indicates new roles of the benzoate conjugate base that are inaccessible to the bifunctional system (Figure 2.5a). The benzoate conjugate base opens a new mechanism that is different from the non-enantioselective background enolate mechanism. How the benzoate counter-ion activates the trifunctional PBK became the next question.

### 2.2.3 Solution structure analysis of trifunctional PBK

A solution-phase model for the trifunctional PBK was developed using 2D NMR spectroscopy to address how the benzoate counter-ion may open an alternate mechanism that is unique to the trifunctional system but not bifunctional (i.e. **MOP**). In this case, characterisation by 2D NMR spectroscopy is advantageous to a crystal structure given the dynamic nature of PBK tautomerisation. Two catalysts, **TF-1** and **TF-2**, were used to form two PBKs, **TF-1-PBK** and **TF-2-PBK**. The **TF-2-PBK** aliphatic protons were baseline-resolved and so were amenable to refining the structural model of the phosphonium butanone motif. The structural model was constructed from the following investigations (Scheme 2.4): 1) phosphonium geometry by NOE-refined molecular dynamics, 2) conformational analysis of the butanone arm, 3) rotational features of the phenol motif by molecular dynamic; 4) the benzoate motion by  $^{13}\text{C}$  selective NOESY.



**Scheme 2.4.** Key structural features and methods of analysis.

Accessible conformations identified by unconstrained molecular dynamics were refined using quantitative NOEs (Section 2.2.3.1). The prochirality and conformation of the phosphonium butanone were determined by a conformational analysis combining homonuclear JRES and selective 1D and 2D NOESY experiments (Section 2.2.3.2). The dynamics of the phenol rotation were examined by molecular mechanics (Section 2.2.3). From the structural model, a detailed view of the PBK activation and the role of the benzoate conjugate base was then proposed (Section 2.2.3.4).

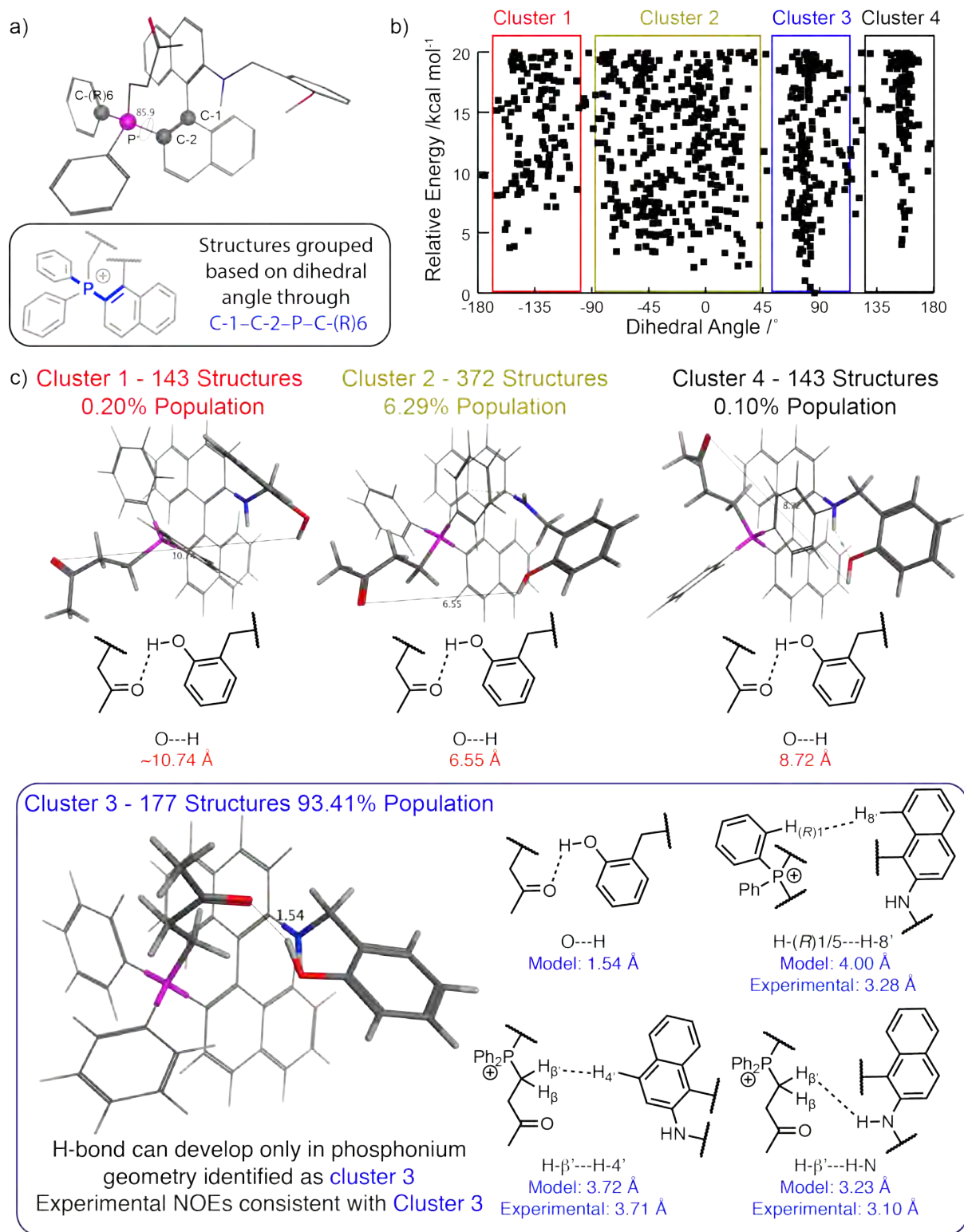
#### 2.2.3.1 The overall phosphonium geometry promotes proton transfer

Unconstrained molecular dynamics generated a library of structures for the global conformation of the **PBK**, which were grouped into four clusters based on the dihedral angle

C-1–C-2–P–C(*R*)6 as shown in Figure 2.6a. Further details regarding the molecular dynamics can be found in the experimental.

Four major clusters were identified with a preference for Cluster 3 identified by the Boltzmann distribution (Figure 2.6b,c). In this geometry, a hydrogen bond can develop between the carbonyl and phenol (Figure 2.6c). A secondary interaction between the pro-(*R*) phenyl substituent and *N*-naphthalene by  $\pi$ - $\pi$  stacking adds additional stabilisation to the geometry, making it the thermodynamically favoured geometry for the phosphonium. Cluster 1, 2 and 4 are higher in energy and lesser contributors to the dynamics of the system, but more importantly, hydrogen bonding is disfavoured.

Key structural distances were extracted from the lowest energy conformation in cluster 3 and compared to quantitative NOE values for **TF-1-PBK** (Figure 2.6c). Three key intramolecular distances were identified; H-8'–H-(*R*)1-5, NH–H- $\beta$ ', H-4'–H $\beta$ '. Details regarding optimisation of 2D NOESY parameters are the in experimental with intermolecular distances extracted in Table 2.1. The thermodynamically favourable geometry identified as cluster 3 was consistent with experimental NOEs and has two key aspects concerning stabilisation and activation of **TF-1-PBK**. Firstly, the geometry predisposes the development of a hydrogen bond from the phenol to the butanone carbonyl, which activates the LUMO of the **PBK** carbonyl initiating activation by tautomerisation. Hydrogen bonding from the phenol to the enolate in **TF-1-PE** is also critical for stabilisation prior to proton transfer to yield **TF-1-PBK**.



**Figure 2.6.** a) Structural model of the lowest energy structure from Cluster 3 with dihedral angle C-1-C-2-P-C(R)6. b) Dihedral angle plot highlighting identified clusters. c) Representative structures and distances for Cluster 1-4 with the key cluster 3 shown in more detail.

### 2.2.3.2 The conformation of the phosphonium butanone is primed for proton transfer

The conformational model for the phosphonium butanone arm was refined by extracting the  $^3J_{CP}$  and  $^3J_{HH}$  coupling constants, measured using 2D homonuclear J-Resolved experiments. All aliphatic protons were baseline resolved for **TF-2-PBK** in  $CDCl_3$ . The J-Resolved experiment was performed at 10 °C to suppress dimerisation of **MVK** via the Rauhut–Currier reaction and increase peak resolution (Figure 2E.10). The key coupling constants were extracted for  $\alpha$ -protons ( $H_{\alpha 2.37}$  and  $H_{\alpha 2.95}$ ) and  $\beta$ -protons ( $H_{\beta 2.82}$  and  $H_{\beta 3.43}$ ) and compared to models for the thermodynamically favoured staggered conformation of the phosphonium butanone (Table 2.2).

**Table 2.2.** Coupling Constant and dihedral angle for the phosphonium butanone.

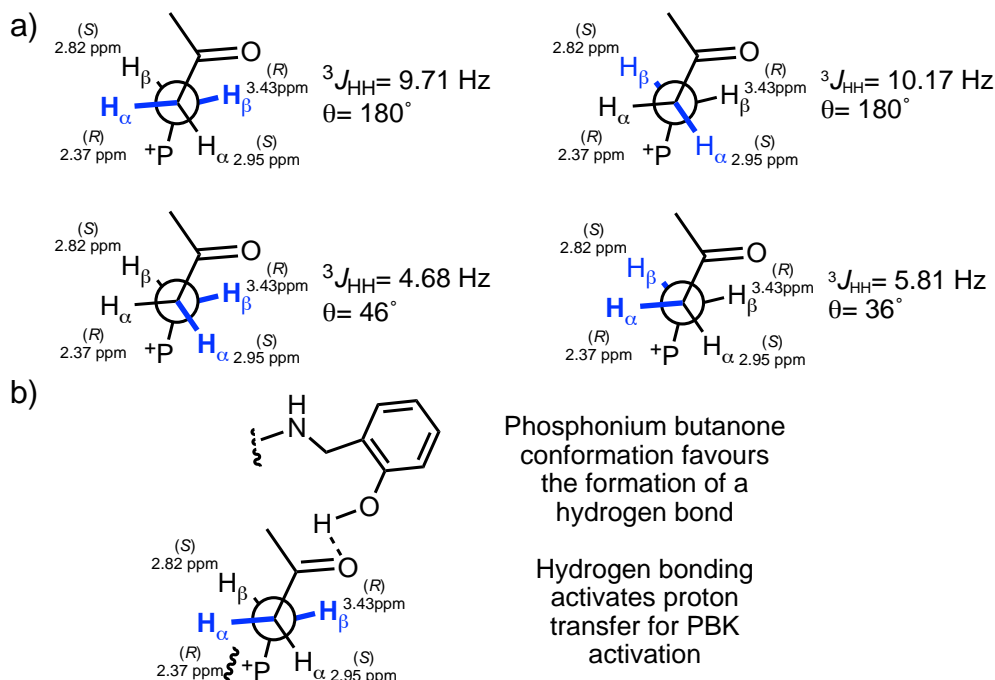
| Scalar Coupling                  | Expt. <sup>a</sup> | $^3J_{XX} / \text{Hz}$ |                      |                      |
|----------------------------------|--------------------|------------------------|----------------------|----------------------|
|                                  |                    | Model 1 <sup>b</sup>   | Model 2 <sup>b</sup> | Model 3 <sup>b</sup> |
| $H_{\alpha 2.37}-H_{\beta 2.82}$ | 4.68               | <b>2.3</b>             | 2.3                  | 10.26                |
| $H_{\alpha 2.37}-H_{\beta 3.43}$ | 10.17              | <b>10.16</b>           | 2.3                  | 2.3                  |
| $H_{\alpha 2.95}-H_{\beta 2.82}$ | 9.71               | <b>10.26</b>           | 2.3                  | 2.3                  |
| $H_{\alpha 2.95}-H_{\beta 3.43}$ | 5.81               | <b>2.3</b>             | 10.26                | 2.3                  |
| P–CO                             | 12.9               | <b>16.8</b>            | 3.6                  | 3.6                  |

a) Coupling constants extracted from homonuclear JRES experiments ( $^3J_{HH}$ ) and  $^{13}\text{C}$  NMR spectrum ( $^3J_{CP}$ ). b) The two protons  $H_{3.43}$  and  $H_{2.95}$  are highlighted in all models for clarity.

The phosphonium butanone was not freely rotating; instead, there was a bias towards a specific butanone conformation. Coupling constants suggests there is an *anti-periplanar* relationship between  $\text{C}=\text{O}-\text{P}$  and a *synclinal* relationship between  $H_{\alpha 2.37}$  and  $H_{\beta 2.82}$ . and either an *anti-periplanar*  $H_{\alpha 2.95}$  and  $H_{\beta 3.43}$ ;  $H_{\alpha 2.37}$  and  $H_{\beta 3.43}$  were either *anti-periplanar* ( $180^\circ$ ) or *periplanar* ( $0^\circ$ ). Both conformations satisfy the experimental coupling constants; however,

steric repulsions are minimised with an *anti-periplanar* conformation which enforces a staggered rather than eclipsed conformation (Table 2.2, Model 1).

Extraction of dihedral angles from the  $^3J_{\text{CP}}$  coupling constant between phosphorous and the carbonyl carbon is unreliable because the majority of  $^3J_{\text{CP}}$  coupling constants and Karplus equations reported are for phosphates or phosphonates.<sup>40-41</sup> The large size of the coupling constant ( $^3J_{\text{CP}} = 12 \text{ Hz}$ ) suggests that the phosphorous and carbon atoms have either a *periplanar* or *anti-periplanar* geometry. An *anti-periplanar* geometry enforces the thermodynamically favourable staggered geometry (Figure 2.7a). Proton assignments and absolute configuration of the butanone could not be determined by the coupling constants alone, NOE analysis was employed to determine the prochirality of the butanone alkyl protons (Section 2.3.6 and 2.3.7).



**Figure 2.7.** a) Conformation of the phosphonium butanone and associated dihedral angles. b) Staggered geometry of the phosphonium butanone favours hydrogen bonding.



Rotation is restricted for the phosphonium butanone and the Pro-(*R*) and Pro-(*S*)  $\beta$ -protons would give rise to different NOEs; therefore, NOE analysis can be used to assign the prochirality of the butanone protons. From the coupling constant analysis, the relationship between protons could be assigned, i.e. *anti-periplanar* or *synclinal*. The model developed from the coupling constant analysis predicts that pro-(*S*)  $\beta$  proton would show a larger NOE to the pro-*R* phenyl. The NOE between  $H_{\beta-2.82}$  and the Pro-*R* phenyl was larger than  $H_{\beta3.43}$  in the quantitative 2D NOESY for **TF-2-PBK** (Figure 2E.12). Consequently,  $H_{\beta-2.82}$  proton was assigned to the Pro-(*S*)  $\beta$  proton (Figure 2E.12). This was validated with a 1D selective NOESY demonstrating that a larger NOE was observed for  $H_{\beta-2.82}$  (1.6%, Figure 2E.13b) than  $H_{\beta3.43}$  (0.79%, Figure 2E.13a). The *anti-periplanar* relationship between  $H_{\beta-2.82}$  and  $H_{\alpha2.95}$  establishes the latter as the Pro-(*S*)  $\alpha$ -proton.

In summary, the complete conformational analysis determined the prochirality of the butanone protons and the overall conformation of the phosphonium butanone. Alternate staggered conformations do not satisfy the experimental coupling constants and NOEs and eclipsed conformations are thermodynamically unfavourable. The absolute configurations for the butanone protons of **TF-2-PBK** are:

|                                       |                                       |
|---------------------------------------|---------------------------------------|
| • $H_{\alpha2.37}$ – Pro-( <i>R</i> ) | • $H_{\alpha2.95}$ – Pro-( <i>S</i> ) |
| • $H_{\beta2.82}$ – Pro-( <i>S</i> )  | • $H_{\beta3.43}$ – Pro-( <i>R</i> )  |

Conformational bias towards a staggered ketone promotes the activation of the **PBK** ground state and hinders elimination of MVK via retro-Michael addition (Figure 2.7b). The carbonyl of a model ketone (2-butanone) favours eclipsed conformations with substituents (i.e. CO eclipsed with the C-3–C-4 bond).<sup>42</sup> In this instance, conformational preference of the C=O

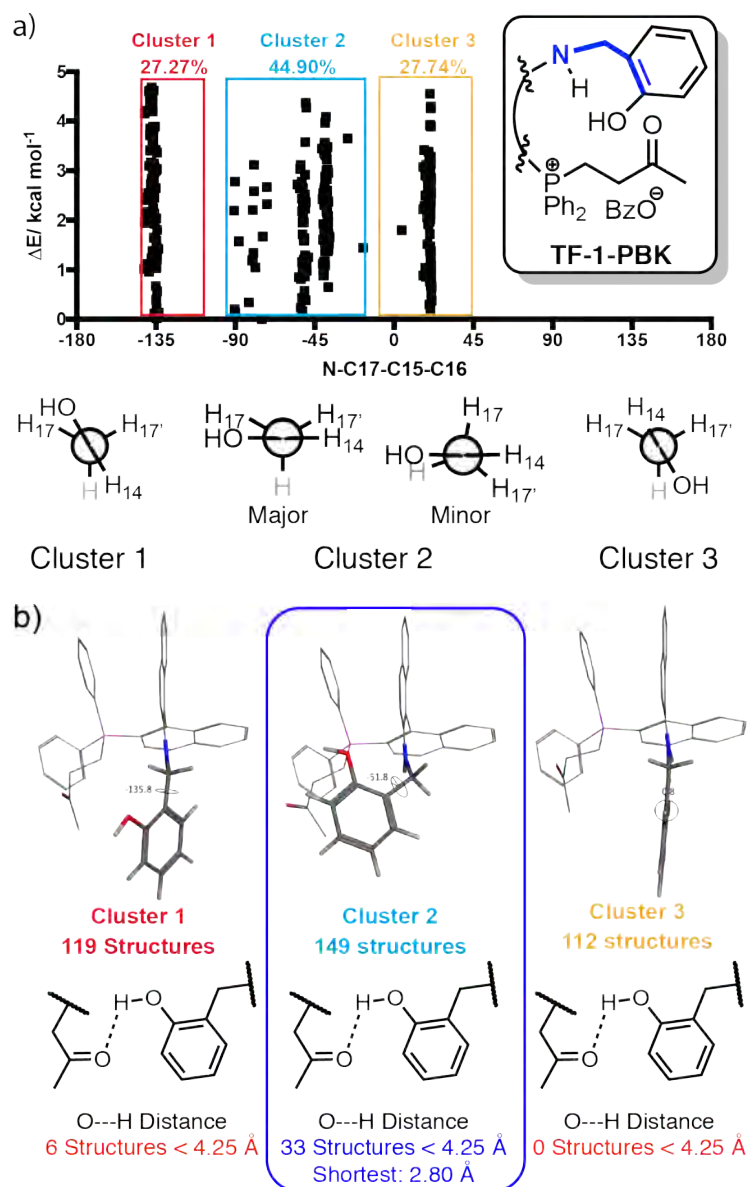
bond accelerates the tautomerisation of the **PBK** by the formation of a hydrogen bond between the carbonyl oxygen and the phenolic hydrogen which templates the proton transfer (Figure 2.7b). This component of the structural work contributes to understanding the atypical reaction profile of the trifunctional organocatalyst, and importantly, why the phenol motif is critical. The phenol hydrogen bond stabilises the observed conformation and is a precursor to proton transfer that activates the ground state intermediate for C–C bond formation.

Phenol acidity activates proficiency for trifunctional organocatalysis by increasing the rate of tautomerisation and proton transfer for the **PBK**. **TF-1-PBK**, as the general model for the trifunctional intermediate, is not a parasitic intermediate due to the conformational bias of butanone that accelerates proton transfer within the **PBK**. The next crucial question relates to the cooperativity between the phenol and the butanone motif for activating proton transfer in the **PBK** intermediate.

### 2.2.3.3 Phenol Conformations

The dynamic movements of the phenol arm were examined by molecular mechanics. The conformations identified were clustered based on the dihedral angle through N-C17-C15-C16 (Figure 2.8a). The phenol adopts one of three main conformations (Figure 2.8b); cluster 1 where the phenol was partially eclipsed with H-17 and H17', cluster 2 where the N–C-17 bond has rotated, cluster 3 where H-14 is eclipsed with H-17 and H17'. Cluster 2 was identified as the greatest contributor to the population (45%). Moreover, cluster 2 includes a structure with the shortest distance between the OH and carbonyl (2.80 Å) enables hydrogen bonding interactions to develop. Moreover, 33 structures in cluster 2 were identified with OH–O

distance less than 4.25 Å, while only six such structures were identified in Cluster 1 and none in Cluster 3. The dynamics of the phenol rotation suggest that Cluster 2 is the major contributor for activation of the **PBK** ground state.



**Figure 2.8.** a) Clustered structures identified from molecular dynamics. b) Representative structures for the identified structures.

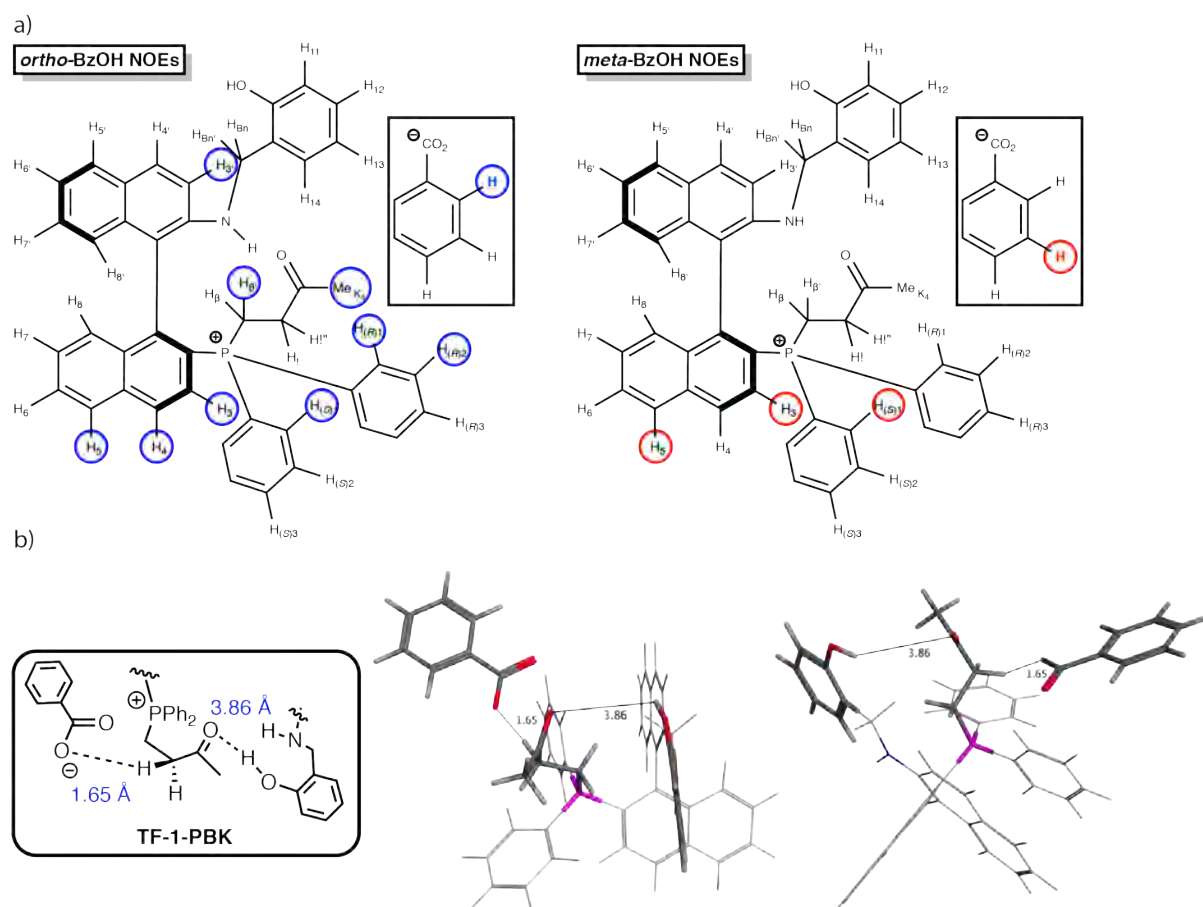
#### 2.2.3.4 The PBK is an ion-pair with dynamic proton transfer

The solution-phase model developed demonstrates the effect of the different motifs in activating the **PBK** via proton transfer. The remaining question relates to the position of the

a)



72



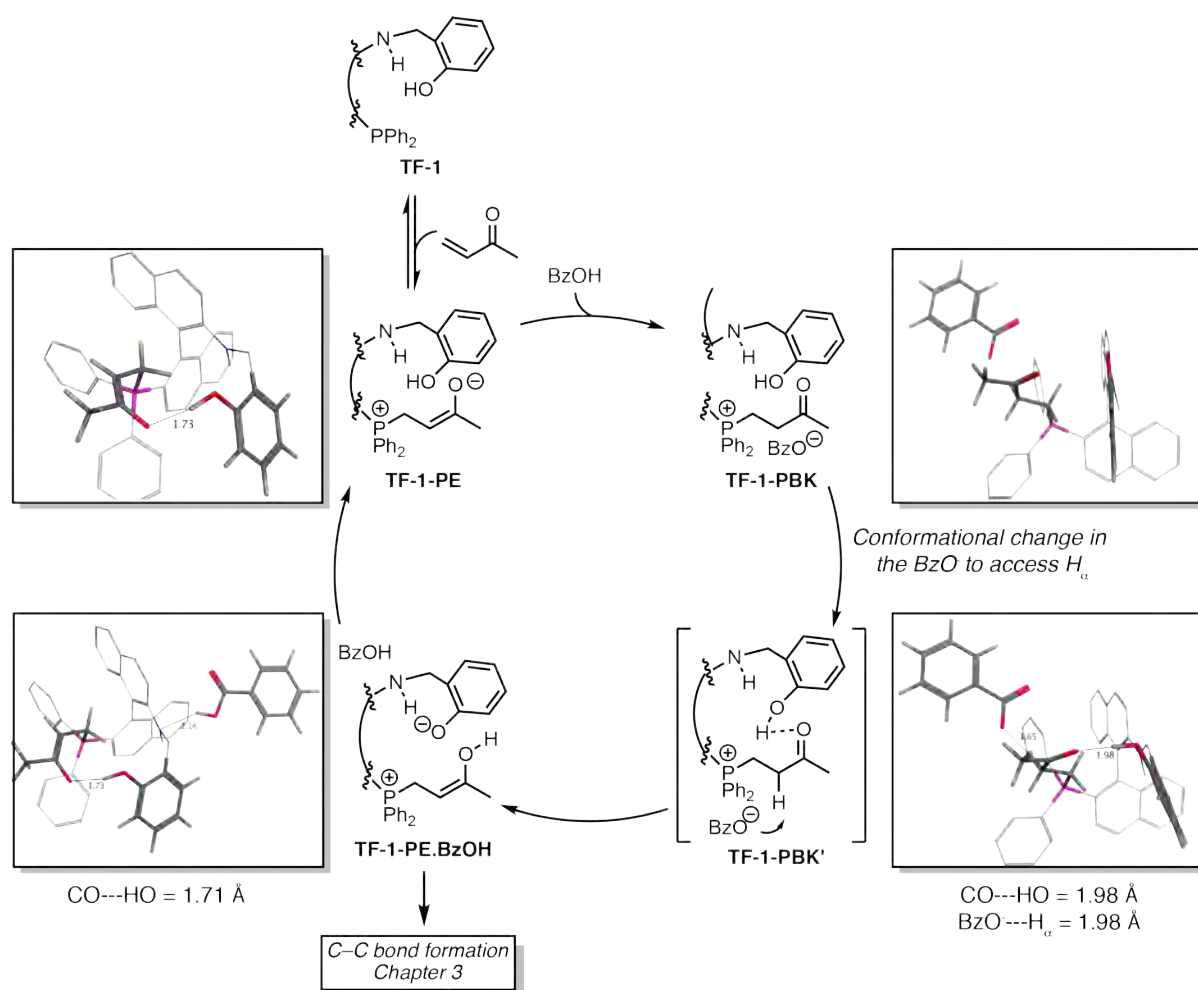
**Figure 2.10.** a) NOEs observed for **TF-1-PBK** at 298 K. b) The active position the benzoate adopts to initiate proton motion.

NOEs to the P naphthalene (H-3, H-4 and H-5) and the phenyl substituent (H-(R)1, H-(R)2, H-(S)1) suggest that the average position of the benzoate is close to the phosphonium and the butanone (Figure 2.10a). This is unsurprising as the coulombic attraction between the phosphonium and benzoate would be the determining factor for the benzoate global position in the ground state. No NOEs were observed from the *para*-position of the benzoate to the **PBK**, indicating that the carboxylate is oriented towards the butanone motif. The resting position of the benzoate is dynamic, and it is free to diffuse around the phosphonium. These dynamics are important as they provide the flexibility to position the benzoate close to the butanone to deprotonate  $H_{\alpha.Pro(R)}$  to yield **TF-1-PE.BzOH** (Figure 2.10b).

The conformational bias of the ketone and steric bulk of the Pro-(*S*) phenyl disfavours deprotonation of H<sub>α,Pro(*S*)</sub> over H<sub>α,Pro(*R*)</sub>. Following deprotonation, the coulombic attraction is diminished and the benzoate can migrate away from the phosphonium, likely guided by weak acid/base interaction between BzOH and the amine Brønsted base, such that the imine substrate can then approach the nucleophilic enolate.

These structural studies in Sections 2.2.3.1–2.2.3.4 demonstrate the critical features that contribute towards the activation and atypical reactivity of **TF-1-PBK**. The structural features of **TF-1-PBK** cooperate to activate the ground state intermediate and initiate proficient catalysis. Activation of the PBK is orchestrated by the cooperative action of the benzoate counter-ion and phenol motif. Hydrogen bonding by the phenol acts as a pre-proton transfer intermediate (**TF-1-PBK'**) to accelerate the rate of proton transfer from the α-position. From this data, a model for activation of the PBK by proton motion is shown in Figure 2.11.

Nucleophilic addition of **TF-1** to **MVK** yields **TF-1-PE**. Protonation and rapid tautomerisation yield the ground state **TF-1-PBK**. A hydrogen bond from the phenol to the ketone carbonyl coordinates the activation of **TF-1-PBK** and the concomitant proton abstraction. A distinction is made between **TF-1-PBK**, the ground state, and **TF-1-PBK'**, the pre-proton transfer intermediate. The latter is the activated form of the **PBK** with a proton network established between the benzoate, ketone and phenol. This intermediate then converts to **TF-1-PE.BzOH**, which is primed for C–C bond formation and proton transfer.



**Figure 2.11.** Activation of **TF-1-PBK** by proton transfer.

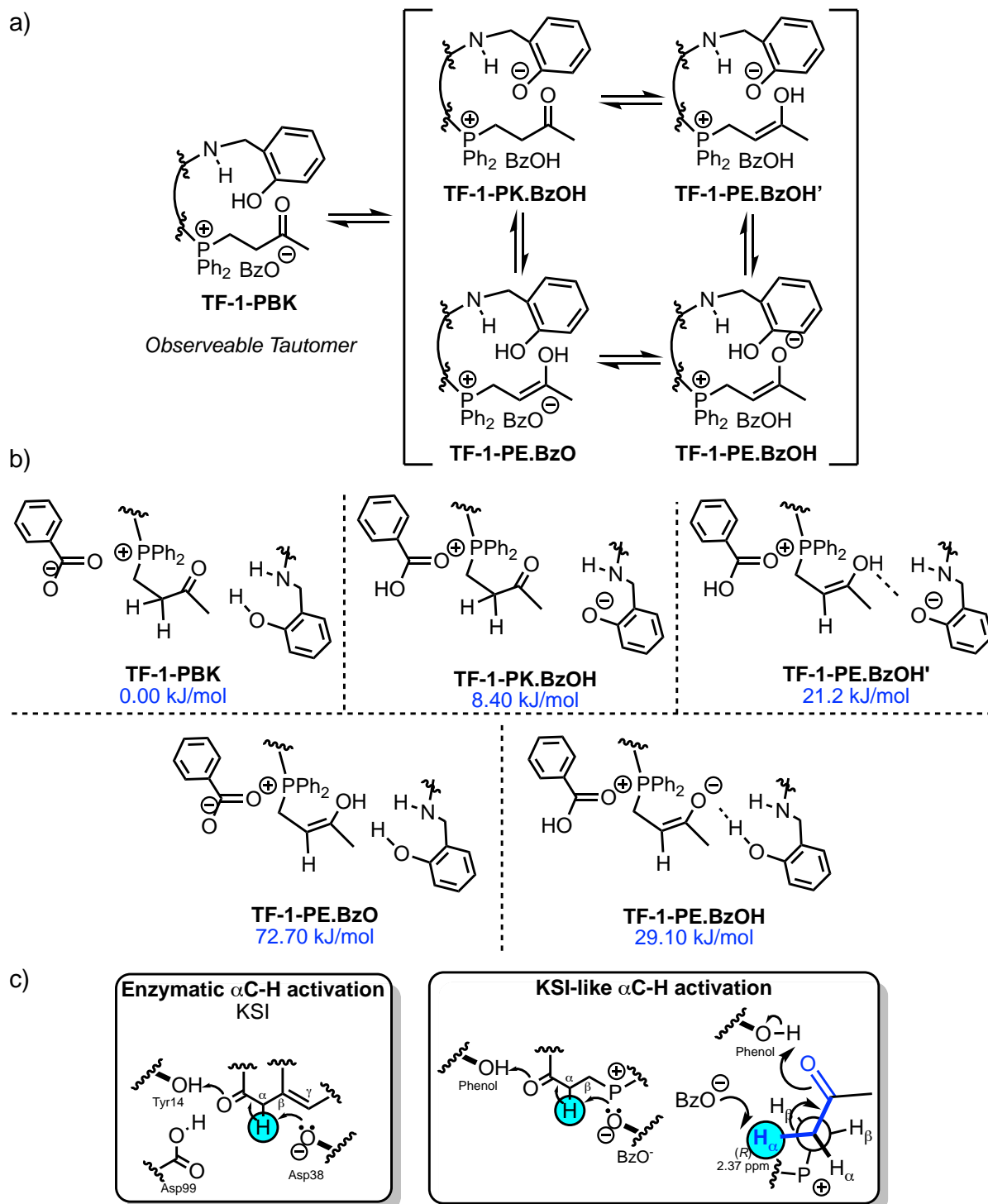
In summary, the **PBK** can be considered as an ion-pair with dynamic proton motion, rather than strictly a H-bonding activated intermediate. The benzoate counterion must be spatially organised to deprotonate an  $\alpha$ -proton of the phosphonium butanone to enable subsequent H-bonding assisted proton transfer for activating **PBK**. BzOH may then migrate towards the amine, enabling the approach of the imine substrate. The **PBK** is primed for proton transfer as a constrained ion-pair with a coulombic attraction between the benzoate and phosphonium. Most importantly, the constrained and coordinated motion of the benzoate conjugate base and phenol is essential to the activation of the PBK.

#### 2.2.4 Computational analysis of the TF-1-PBK proton shuttle

The experimental data suggest a continuous H-bonding assisted proton transfer within the PBK ion-pair. Four additional tautomeric forms are therefore possible for PBK after deprotonation: **TF-1-PBK.BzOH**, **TF-1-PE.BzOH'**, **TF-1-PE.BzO**, **TF-1-PE.BzOH** (Figure 2.12a). The intermediates **TF-1-PE.BzO**, **TF-1-PE.BzOH** and **TF-1-PE.BzOH'** are all possible nucleophiles for the C–C bond formation. The energy of these intermediates was calculated at the TPSS-D3(BJ)/def2-SVP/COSMO level of theory in collaboration with the group of Dr Hans Martin Senn at the University of Glasgow (Figure 2.12b).  $\alpha$ -CH activation of **TF-1-PBK** is analogous to the enzymatic  $\alpha$ -CH activation observed in KSI. In the case of **TF-1-PBK**, the benzoate counter-ion acts as the general base and the phenol acts as the general acid. Unlike KSI where the  $\alpha$ -CH activation enables the formation of a  $\beta$ -CH bond, for **TF-1-PBK** proton motion activates C–C bond formation (Figure 2.12c).

Following proton abstraction from **TF-1-PBK** phosphonium butanone, the intermediate rapidly interconverts between the various tautomers of the PBK. All tautomers are accessible at room temperatures except for **TF-1-PE.BzO** (72.7 kJ/mol). Proton transfer from the phenol to enolate is rapid with the enol form **TF-1-PE.BzOH'** (21.2 kJ/mol) lower in energy than the enolate **TF-1-PE.BzOH** (29.1 kJ/mol). Rapid interconversion of the tautomers enables the proton to move quickly around the stationary points (amine, phenol, carbonyl and benzoate). Unlike a standard enolate that is typically stabilised by H-bonding interactions, the proton motion embedded in the **PBK** expands a singular point of stabilisation into multiple protic forms in rapid equilibrium, which can be thought of as a proton bond dispersed into multiple donor-acceptor points.





**Figure 2.12.** a) The NMR observable tautomer **TF-1-PBK** is a gateway to different tautomeric forms of the PBK. b) Energies calculated for the **TF-1-PBK** tautomers c) TF-1-PBK as a KSI mimic.

Activation of the trifunctional PBK coincides with rate-coupled asymmetric catalysis due to the emergent properties of this proton motion. The dynamics of the system actively promote

geometries and conformations that are conducive to establishing the proton network. This network can then initiate an alternate mechanism that is not possible in the case of the standard enolate pathway without BzOH. Moreover, this motion is guided by the position of the stationary sites that cannot be replicated by simple bifunctional catalysts. As such, the **TF-1-PBK** is not a parasitic intermediate; *it enables the formation of the proton transfer network that in turn activates proficient catalysis*. How the proton transfer network enables proficient catalysis is the subject of Chapter 3 and 4.

#### **2.2.5 Conclusion: Proton motion-based activation of the PBK for an expanded *aza*-MBH mechanism**

In this chapter, the new ground state intermediate **PBK** in the trifunctional organocatalysed *aza*-MBH reaction was characterised using a combination of 2D NMR spectroscopy and computational methods. The activation of this intermediate was shown to depend upon the conformational preferences directed by the different motifs. Unlike bifunctional catalysts for the *aza*-MBH that proceed through an H-bond stabilised enolate intermediate as the reactive species for the C-C bond formation, the trifunctional system here, activated by BzOH, proceeds through a **PBK** intermediate with internally configured proton motion that allows the PBK to be activated as an enol for the C-C bond formation. The catalytic role of phosphine for nucleophilic activation, which is the case for the bifunctional, enolate-driven pathway, is relegated to nucleophilic initiation to form the new **PBK** ground state upon addition of BzOH. The catalytic pathway forward from the **PBK** is kinetically superior to that of the background enolate pathway. Thus, the role of BzOH in this trifunctional catalysis is expansionary, allowing the reaction space to enlarge laterally to include a new mode of activation for enhanced catalytic proficiency.

## 2.3. Experimental

### 2.3.1 Materials and Methods

Toluene and THF were distilled from sodium/benzophenone immediately before use. All other reagents were purchased from Sigma-Aldrich Castle Hill. Unless specified, all commercially available reagents were used without further purification. Dichloromethane was distilled from calcium hydride. All air and moisture sensitive reactions were performed under a nitrogen atmosphere. Reactions were magnetically stirred and monitored by thin-layer chromatography (TLC) using silica gel 60 F254 aluminium pre-coated plates from Merck (0.25 mm). Flash column chromatography was performed on silica gel (60 Å, 0.06–0.2 mm, 400 mesh from Scharlau).  $^{13}\text{C}_6$ -Benzoic acid was purchased from Sapphire Bioscience and recrystallised from distilled water before use.

All  $^1\text{H}$ ,  $^{13}\text{C}$  and 2D NMR experiments were performed on either a Bruker AVIIIHD 400 MHz NMR Spectrometer equipped with a BBFO SmartProbe (5mm) or DRX600 NMR spectrometer equipped with a TXI (5 mm) Cryoprobe. Chemical shifts were reported in ppm using residual  $\text{CHCl}_3$  ( $\delta_{\text{H}}$ ; 7.26 ppm,  $\delta_{\text{C}}$ ; 77.16 ppm) as an internal reference. All 2D NMR experiments were run with quadrature detection and a relaxation delay of 1–3 s. High power  $^1\text{H}$   $\pi/2$  pulses were determined to be ~9.5 ms, and  $^{13}\text{C}$  high power  $\pi/2$  pulse was 11.05 ms, and a low power pulse of 65 ms was used for GARP4 decoupling. Gradient pulses were delivered along the z-axis using a 100 step sine program. Heteronuclear single quantum coherence (HSQC) experiments were optimised for a  $^1J_{\text{CH}}$  coupling of 145 Hz and HMBC spectra for a coupling of 20 Hz, using 145 Hz to suppress  $^1J_{\text{CH}}$  couplings. HSQC experiments were performed using the hsqcetgpsi or hsqcedetgpsp.3 (phase-edited HSQC) pulse program, and HMBC experiments were performed using the hmbcgp1pndqf pulse program. HSQC spectra were processed ( $\pi/2$  shifted sine bell squared in both dimensions) phase sensitive and HMBC (sine squared in both

dimensions) with magnitude calculation in F1.  $^{13}\text{C}$  spectra were acquired using the UDEFT sequence. NOESY experiments were performed using the noesygpshz pulse program with a mixing time of 400 ms. All spectra were processed using Bruker TOPSPIN 3.5pl7. J-Resolved experiments were performed using the jresqf pulse program. Specific details regarding 2D NMR experiments will be outlined below. Trifunctional organocatalyst were prepared following the literature procedure.<sup>36-39</sup>

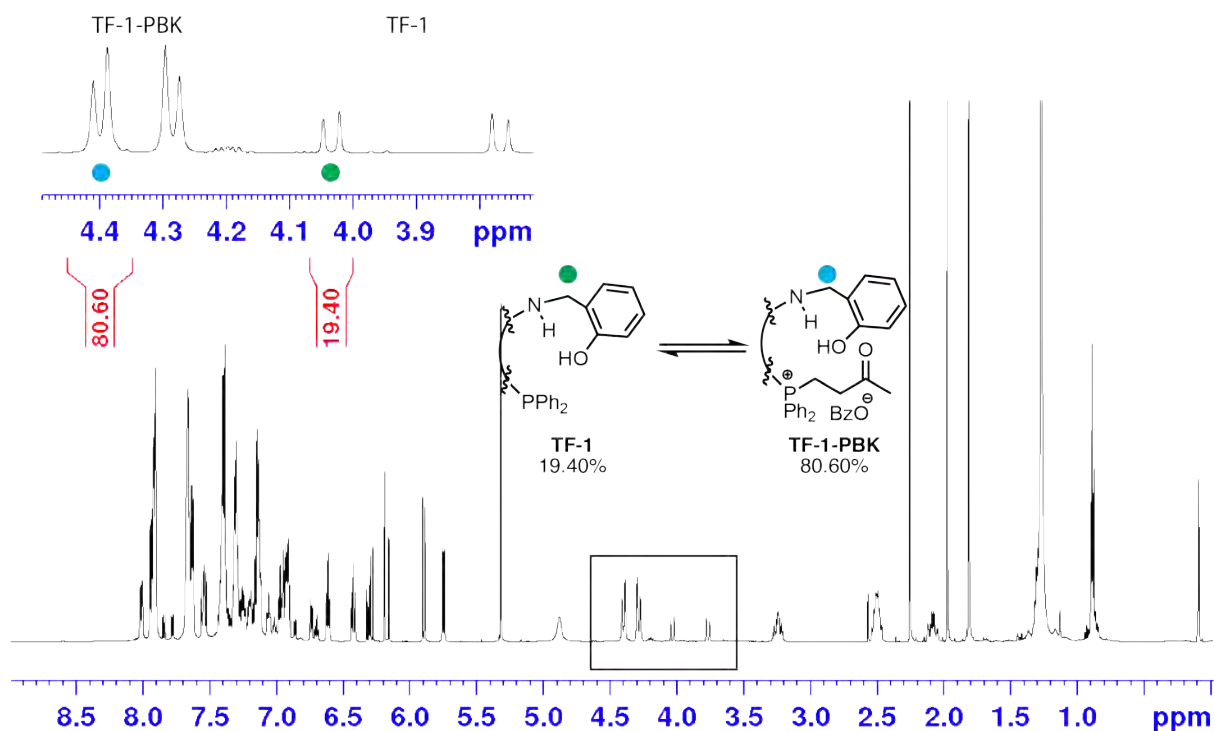
### **2.3.2 Proportion of PBK and structure elucidation**

Catalyst (10 mmol) was dissolved in  $\text{CD}_2\text{Cl}_2$  and a  $^1\text{H}$  NMR spectrum (600 MHz, core temperature 20 °C). MVK (20 mmol) was added and a spectrum collected before addition of BzOH (10 mmol). The NMR tube was inverted and mixed before injecting into the spectrometer, the sample shimmed and  $^1\text{H}$  NMR spectrum collected. The sample was left to reach equilibrium and the proportion of the PBK measured. The temperature was lowered to 10 °C and the proportion of the PBK was measured. The proportion of PBK can be seen in Supplementary Table 1. A model spectrum at 10 °C is shown in Figure 2E.1.

**Table 1E.1.** Proportion **PBK** for selected catalysts at 10 °C and 20 °C.

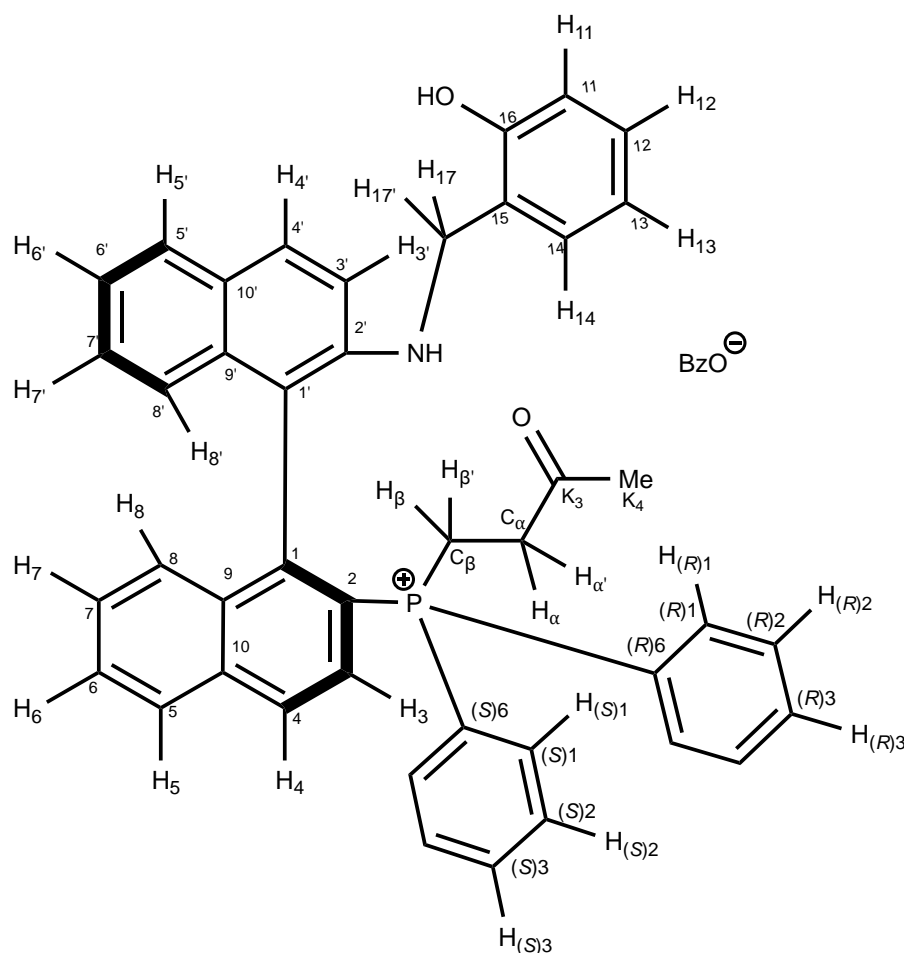
| <div style="display: flex; justify-content: space-around; align-items: center;"> <div style="text-align: center;"> <br/> <b>TF-1</b> </div> <div style="text-align: center;"> <br/> <b>TF-2</b> </div> <div style="text-align: center;"> <br/> <b>TF-3</b> </div> <div style="border: 1px solid black; padding: 5px;"> </div> </div> <div style="display: flex; justify-content: space-around; align-items: center; margin-top: 10px;"> <div style="text-align: center;"> <br/> <b>BF-1</b> </div> <div style="text-align: center;"> <br/> <b>BF-2</b> </div> <div style="text-align: center;"> <br/> <b>MAP</b> </div> <div style="text-align: center;"> <br/> <b>MOP</b> </div> </div> |                                       |    |     |         |       |    |    |         |
|--|---------------------------------------|----|-----|---------|-------|----|----|---------|
| Catalyst   | Proportion <b>PBK</b> <sup>a</sup> /% |    |     |         |       |    |    |         |
|  | 10 °C                                 |    |     |         | 20 °C |    |    |         |
|  | 1                                     | 2  | 3   | Average | 1     | 2  | 3  | Average |
| <b>TF-1</b>  | 80                                    | 78 | 90  | 83 ± 6  | 78    | 72 | 71 | 74 ± 3  |
| <b>TF-2</b>  | 61                                    | 56 | 54  | 57 ± 4  | 51    | 55 | 53 | 53 ± 2  |
| <b>TF-3</b>  | 93                                    | 87 | 93  | 91 ± 3  | 85    | 85 | 85 | 85 ± 1  |
| <b>BF-1</b>  | 42                                    | 46 | 46  | 45 ± 3  | 37    | 37 | 39 | 38 ± 1  |
| <b>BF-2</b>  | 93                                    | 86 | 83  | 87 ± 5  | 88    | 82 | 79 | 83 ± 5  |
| <b>MAP</b>   | 46                                    | 46 | 44  | 45 ± 1  | 44    | 46 | 41 | 44 ± 2  |
| <b>MOP</b>   | 95                                    | 95 | 100 | 96 ± 3  | 94    | 86 | 87 | 89 ± 4  |

a) Determined by <sup>1</sup>H NMR spectroscopy (600 MHz, CD<sub>2</sub>Cl<sub>2</sub>).



**Figure 2E.1.** Model Spectra showing the proportion of **TF-1-PBK** at 10 °C.

Complete structure elucidation by 2D NMR spectroscopy can be seen below for **TF-1-PBK**

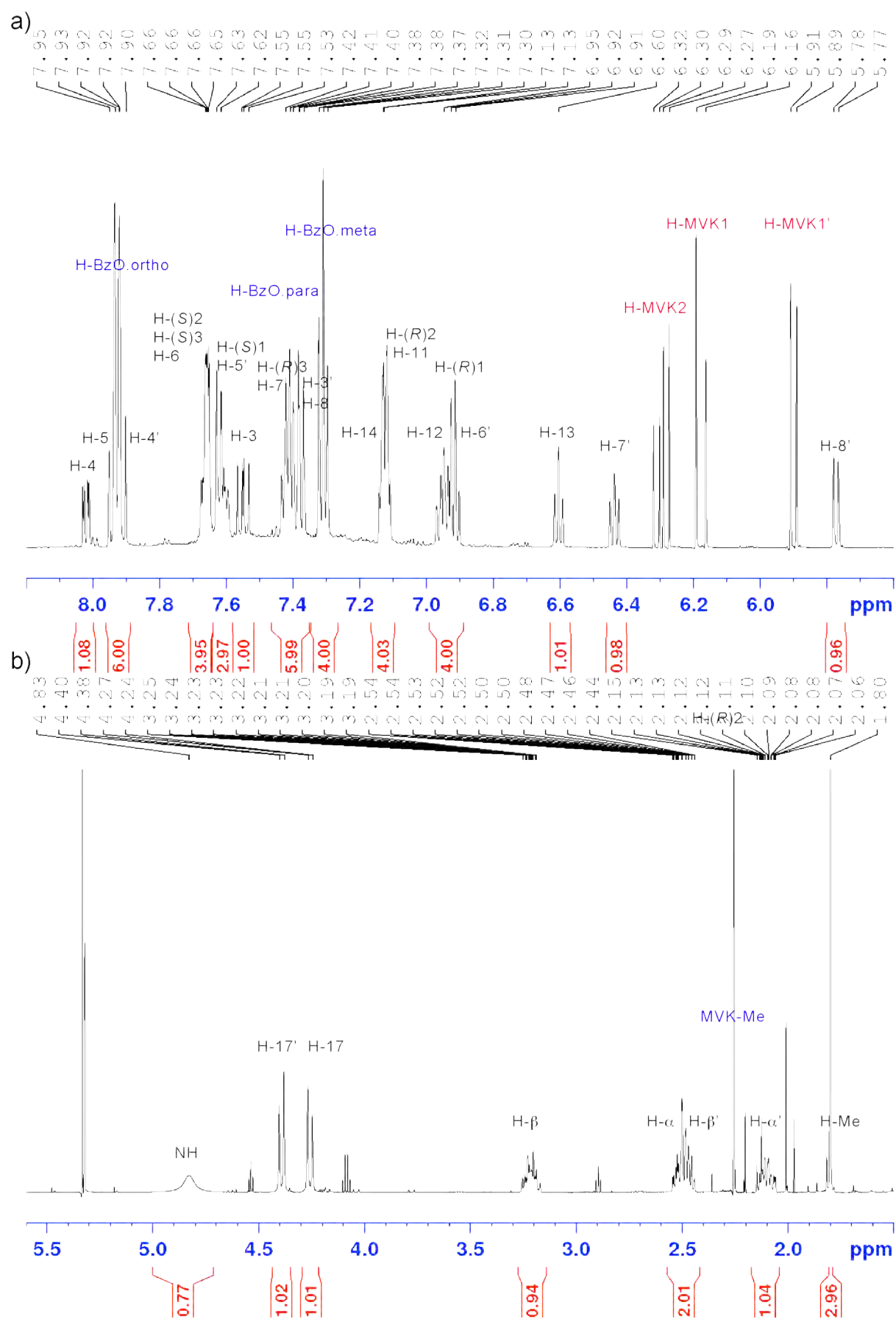


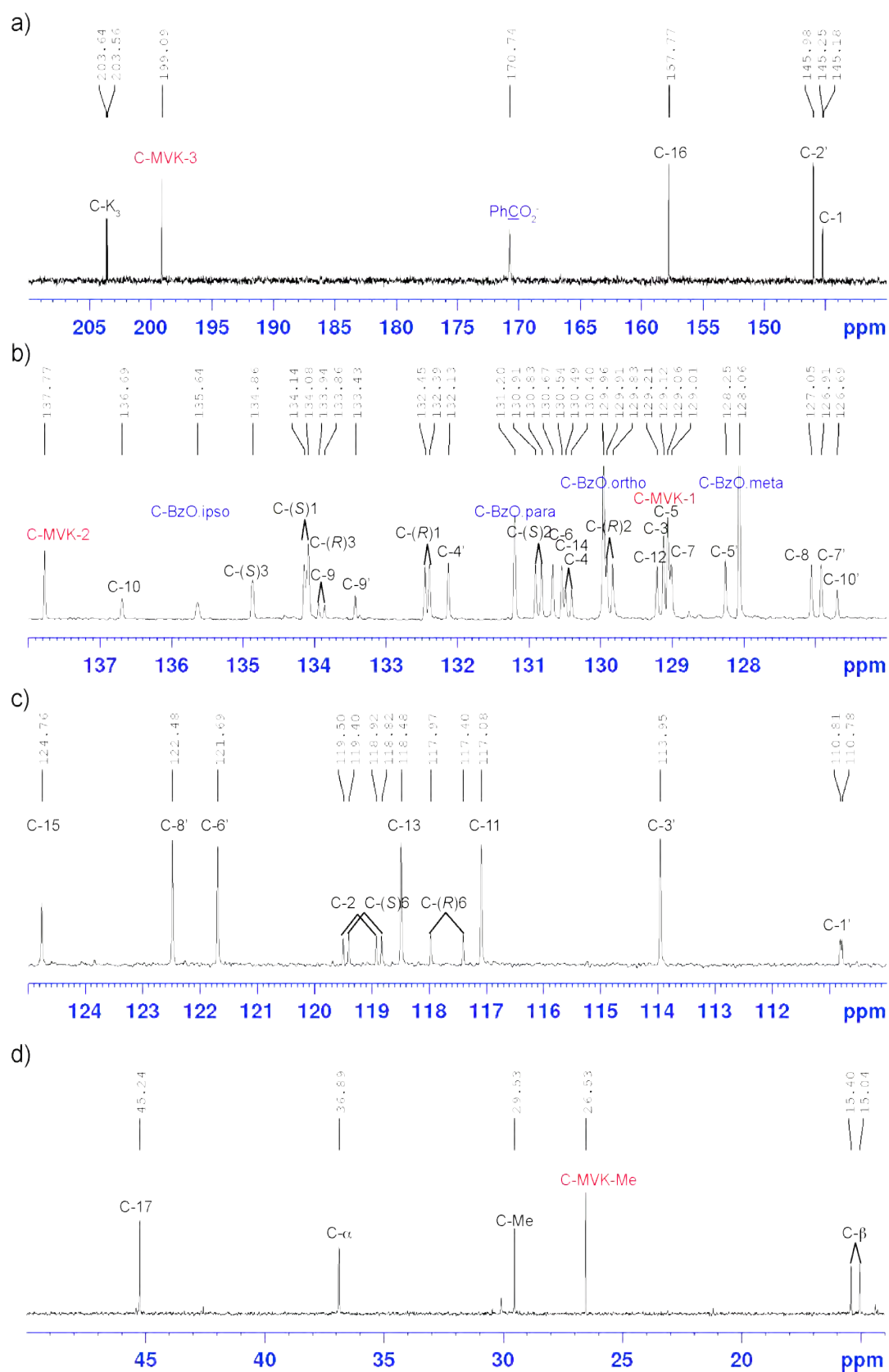
**Figure 2E.2.** Peak assignment map for **TF-1-PBK**.

**$^1\text{H}$  NMR** (600 MHz,  $\text{CD}_2\text{Cl}_2$ ,  $\delta$ ): 1.79 (s, 3H,  $\text{K}_4$ ), 2.10 (m, 1H,  $\text{H}-\alpha'$ ), 2.48 (m, 2H,  $\text{H}-\beta'$ ), 2.52 (m, 2H,  $\text{H}-\alpha$ ), 3.21 (m, 1H,  $\text{H}-\beta$ ), 4.23 (d, 1H,  $\text{H}-17'$ ,  $J = 13.5$  Hz), 4.39 (d, 1H,  $\text{H}-17$ ,  $J = 13.5$  Hz), 4.80 (b, 1H, NH), 5.77 (d, 1H,  $\text{H}-8'$ ,  $J = 8.5$  Hz), 6.44 (t, 1H,  $\text{H}-7'$ ,  $J = 8.5$  Hz), 6.61 (t, 1H,  $\text{H}_{13}$ ,  $J = 7.3$  Hz), 6.92 (m, 1H,  $\text{H}-6'$ ), 6.93 (m, 2H,  $\text{H}-(R)1$ ), 6.95 (m, 1H,  $\text{H}-12$ ), 7.11 (m, 4H,  $\text{H}-14$ ,  $\text{H}-11$ ,  $\text{H}-(R)2$ ), 7.37 (m, 2H,  $\text{H}-3'$ ,  $\text{H}-8$ ), 7.40 (m, 1H,  $\text{H}-(R)3$ ), 7.41 (m, 1H,  $\text{H}-7$ ), 7.55 (dd, 1H,  $\text{H}-3$ ,  $J = 8.8$ , 12.0 Hz), 7.61 (m, 2H,  $\text{H}-(S)1$ ), 7.62 (1H, d,  $\text{H}-5$ ), 7.66 (m, 4H,  $\text{H}-(S)2$ ,  $\text{H}-(S)3$ ,  $\text{H}-6$ ), 7.90 (d, 1H,  $\text{H}-4'$ ) 7.4 (d, 1H,  $\text{H}-5$ ,  $J = 8.2$  Hz), 8.02 (dd, 1H,  $\text{H}-4$ ,  $J = 8.8$ , 3.0 Hz).

**$^{13}\text{C}$  NMR** (125 MHz,  $\text{CD}_2\text{Cl}_2$ ,  $\delta$ ): 15.2 (d,  $^1J_{\text{CP}} = 54.9$  Hz,  $\text{C}-\alpha$ ), 29.5 ( $\text{C}-\text{K}_4$ ), 36.9 ( $\text{C}-\beta$ ), 45.2 ( $\text{C}-17$ ), 110.8 (d,  $^3J_{\text{CP}} = 5.1$  Hz,  $\text{C}-1'$ ), 113.9 ( $\text{C}-3'$ ), 117.1 ( $\text{C}-11$ ), 117.7 (d,  $^1J_{\text{CP}} = 85.2$  Hz,  $\text{C}-(R)6$ ), 118.5 ( $\text{C}-13$ ), 119.1 (d,  $^1J_{\text{CP}} = 87.5$  Hz,  $\text{C}-(S)6$ ), 119.2 (d,  $^1J_{\text{CP}} = 87.6$  Hz,  $\text{C}-2$ ), 121.7 ( $\text{C}-6'$ ), 122.5 ( $\text{C}-8'$ ), 124.8 ( $\text{C}-15$ ), 126.7 ( $\text{C}-10'$ ), 126.9 ( $\text{C}-7'$ ), 127.1 ( $\text{C}-8$ ), 128.3 ( $\text{C}-5'$ ), 129.0 ( $\text{C}-7$ ), 129.1 ( $\text{C}-5$ ) 129.1 ( $\text{C}-3$ ), 129.2 ( $\text{C}12$ ), 129.9 (d,  $^3J_{\text{CP}} = 12.6$  Hz,  $\text{C}-(R)2$ ), 130.5 (d,  $^3J_{\text{CP}} = 12.9$  Hz,  $\text{C}-4$ ), 130.5 ( $\text{C}-14$ ), 130.7 ( $\text{C}-6$ ), 130.9 (d,  $^3J_{\text{CP}} = 12.4$  Hz,  $\text{C}-(S)2$ ), 132.1 ( $\text{C}-4'$ ), 132.4 (d,  $^2J_{\text{CP}} = 9.5$  Hz,  $\text{C}-(R)1$ ), 133.4 ( $\text{C}-9'$ ), 133.9 (d,  $^3J_{\text{CP}} = 12.7$ , Hz,  $\text{C}-9$ ), 134.1 (d,  $^2J_{\text{CP}} = 9.0$  Hz,  $\text{C}-(S)1$ ), 134.1 ( $\text{C}-(R)3$ ), 134.9 ( $\text{C}-(S)3$ ), 136.7 ( $\text{C}-10$ ), 145.2 (d,  $^2J_{\text{CP}} = 9.8$  Hz,  $\text{C}-1$ ), 146.0 ( $\text{C}-2'$ ), 157.8 ( $\text{C}-16$ ), 203.6 (d,  $^3J_{\text{CP}} = 12.5$  Hz,  $\text{C}-\text{K}_3$ ).

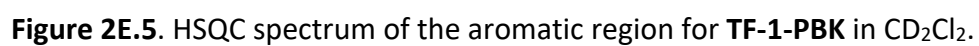
**$^{31}\text{P}$  NMR** (100 MHz,  $\text{CD}_2\text{Cl}_2$ ,  $\delta$ ): 28.5

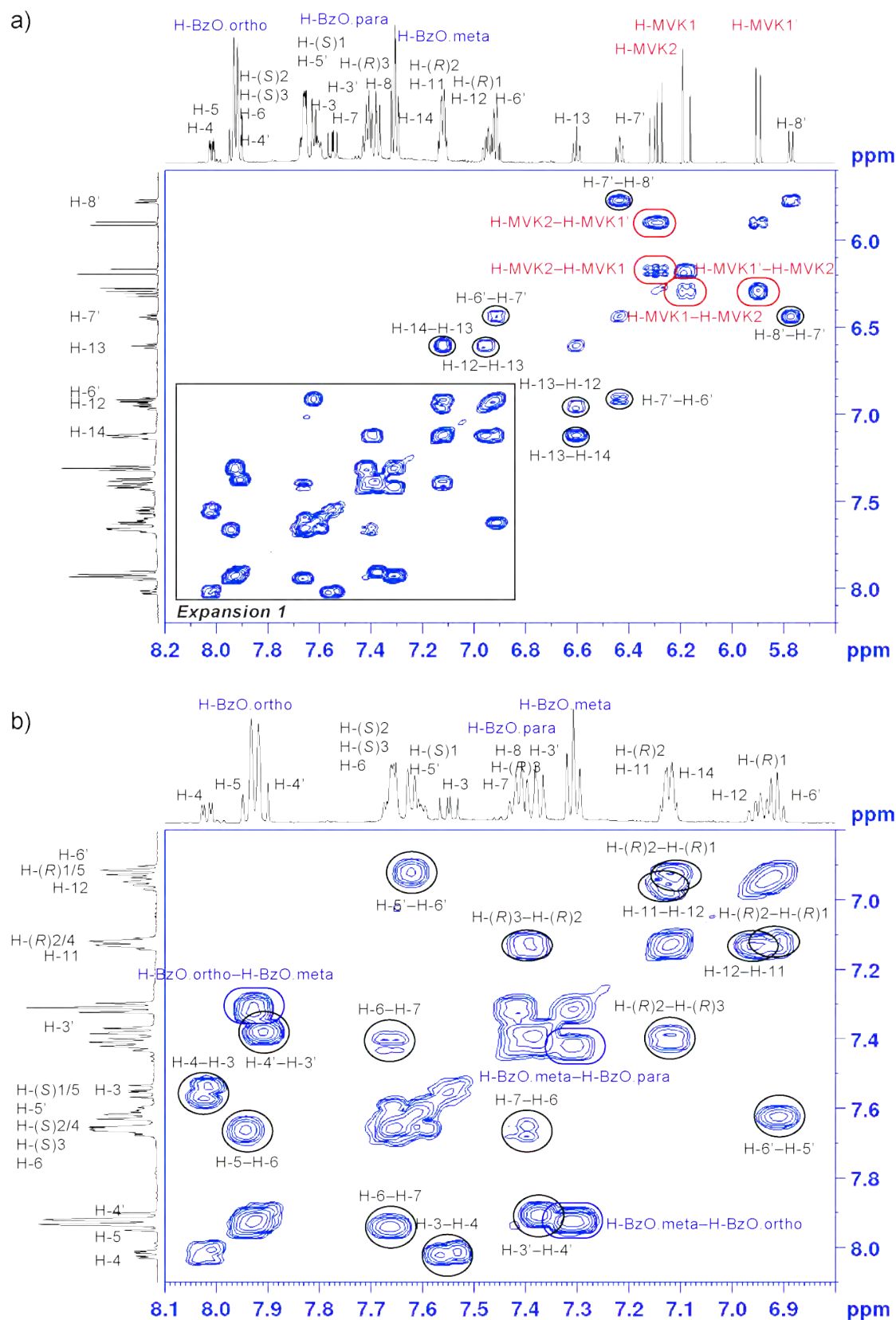




**Figure 2E.4.**  $^{13}\text{C}$  NMR spectrum (150 MHz,  $\text{CD}_2\text{Cl}_2$ ) for TF-1-PBK covering the spectral range a) 140–210 ppm, b) 126–138 ppm, c) 110–125 ppm, d) 18.80–50 ppm.







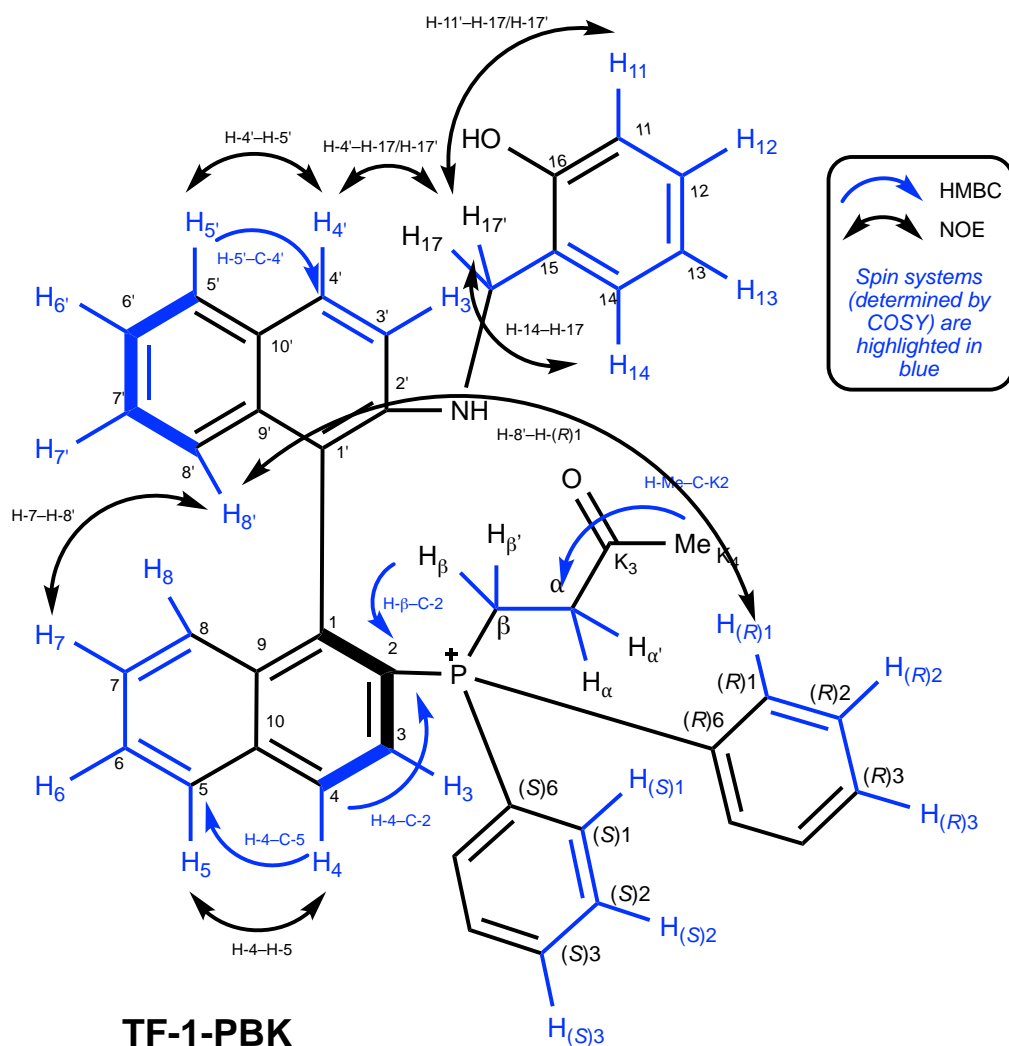
**Figure 2E.6 a)** Complete COSY Spectrum (600 MHz,  $\text{CD}_2\text{Cl}_2$ ) for **TF-1-PBK**. **b)** Expansion of the aromatic region (6.80–7.10 ppm) of **TF-1-PBK**.





**Table 2.3.** Quantitative NOE values for **TF-1-PBK** used for constrained molecular dynamics

| Atoms         | Distance /Å | Atoms      | Distance /Å | Atoms     | Distance /Å |
|---------------|-------------|------------|-------------|-----------|-------------|
| H-(S)1–H-3    | 2.55-3.11   | H-17–H-3'  | 2.2-2.9     | H-β–H-B1  | 3.08-3.76   |
| H-(R)2–H-7'   | 3.7-4.52    | H-17'–H-3' | 2.34-2.86   | H-β–H-A1  | 3.00-3.60   |
| H-(R)2–H-7'   | 3.11-3.81   | H-17'–H-B1 | 2.41-2.95   | H-β–H-17  | 3.60-4.40   |
| H-(R)1–H-3    | 2.82-3.81   | H-3'–NH    | 3.26-3.98   | H-Me–H-13 | 4.26-5.20   |
| H-(R)1–H-(S)1 | 3.16-4.07   | H-14–H-Bn  | 2.41-2.95   | H-α'–H-3  | 3.70-4.40   |
| H-(S)1–NH     | 3.74-4.56   | H-14–H-Bn' | 2.30-2.82   | H-α'–H-A1 | 3.10-3.70   |
| H-3–H-8'      | 3.94-4.82   | H-β–NH     | 2.80-3.40   | BzOo–NH   | 4.49-5.49   |
| H-8–H-8'      | 3.0-3.8     | H-β–H-3'   | 3.8-4.6     | BzOo–CH   | 4.49-5.59   |



**Figure 2E.9.** Key correlations for **TF-1-PBK** determined by 2D NMR spectroscopy, spin systems are shown in blue.

### 2.3.3 Initial Rates

A dry NMR tube charged with (*E*)-*N*-(4-bromobenzylidene)-4-methylbenzenesulfonamide (20 mg, 59  $\mu$ mol) was added catalyst (**TPP** or **TF-1**) (10 mol%, 5.9  $\mu$ mol) and additive (BzOH and/or phenol) (10 mol%, 5.9  $\mu$ mol).  $\text{CD}_2\text{Cl}_2$  was added to make a final concentration of imine 0.15 M, and the mixture heated gently to ensure all of the imine substrate had completely dissolved. Methyl vinyl ketone (168  $\mu$ mol, 3 equiv) was added and the sample immediately analysed by  $^1\text{H}$  NMR spectroscopy. Spectra were collected every minute until 20% conversion

of the imine substrate by  $^1\text{H}$  NMR spectroscopy. Conversion was then plotted as a function of time for phosphine catalysed reactions with or without an acid additive.

#### 2.3.4 Molecular Dynamics

Molecular dynamics were performed using MOE 2015.10. The MMFF94x forcefield was utilised and parameterised with the dichloromethane dielectric constant (8.93). Conformational searches were performed using LowModeMD without NOE constraints. 10000 iterations were performed with a limit of 100 rejections and 10000 conformations. Energy minimisation was performed for each structure generated using an RMS gradient of 0.005 and an iteration limit of 500. A 20 kcal mol $^{-1}$  energy window was searched with RMSD 0.05. Conformations were identified and clustered based on the dihedral angle C-1–C-2–P $^{+}$ –C-(R)6.

Constrained dynamics were performed with NOEs extracted 2D quantitative NOESY experiments with an allowance of  $\pm 10\%$  (see section 2.3.6 for details regarding 2D NOESY experiments).

#### 2.3.5 Homonuclear J-Resolved Spectroscopy

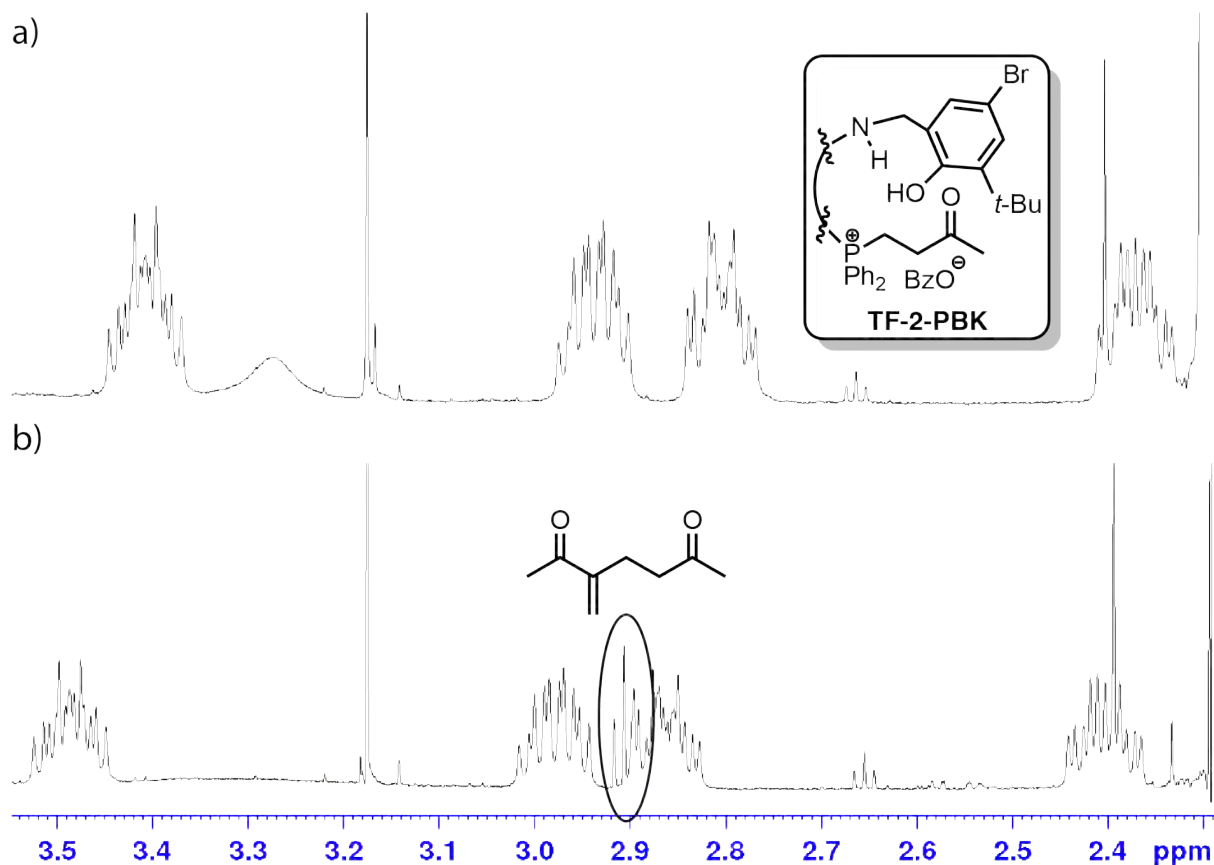
To a sample of **TF-2** (8 mg, 11.5  $\mu\text{mol}$ ) in  $\text{CDCl}_3$  was added freshly recrystallised BzOH (1.5 mg, 11.5  $\mu\text{mol}$ , 1 equiv) and the sample analysed by  $^1\text{H}$  NMR. The temperature was cooled to 278 K, and methyl vinyl ketone (2.2 mg, 31  $\mu\text{mol}$ , 2.7 equiv) was added and the sample allowed to equilibrate at 278 K. A  $^1\text{H}$  NMR spectrum was collected (Figure 2E.10) before a 2D homonuclear J-Resolved (jresqf) experiment was performed on the spectral window 0-5.8 ppm (Figure 2E.11). The spectrum was magnitude multiplied, tilted, symmetrised and rows

extracted for the methylene protons  $H_{\alpha 2.37\text{ppm}}$ ,  $H_{\beta 2.82\text{ppm}}$ ,  $H_{\alpha 2.95\text{ppm}}$  and  $H_{\beta 3.43\text{ppm}}$ .  $^3J_{\text{HH}}$  for  $H_{\alpha}$  and  $H_{\beta}$  were measured and the corresponding dihedral angles determined using the Karplus equation (Eq 1):

$$^3J_{\text{HCCH}} = 9.00 \cos^2 \theta - 0.50 \cos \theta + 0.30 \quad (\text{Eq. 1})$$

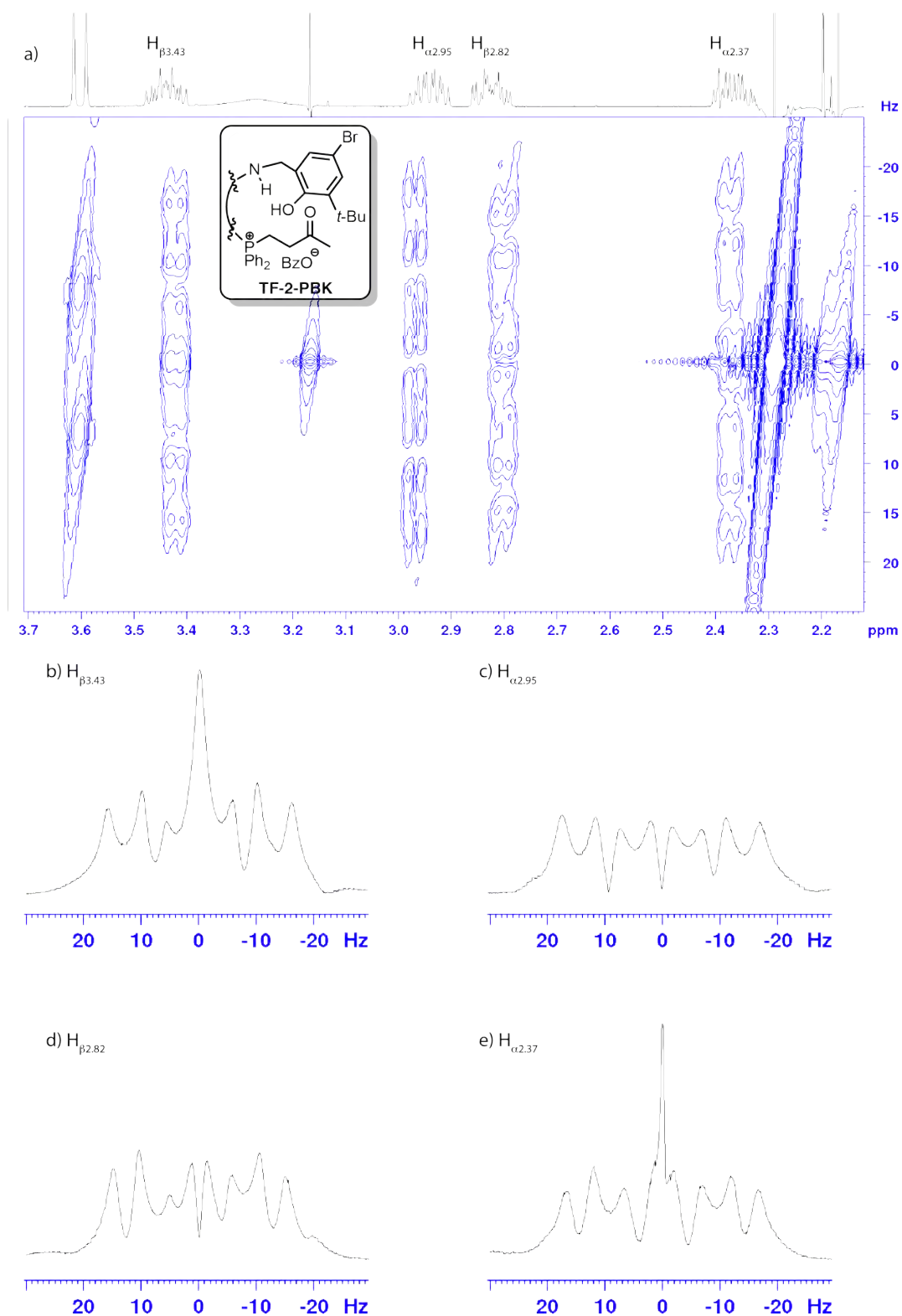
The Karplus equation (Eq. 2) was solved for the P-C-C-C(O) dihedral for the measured coupling constant ( $^3J_{\text{PC(O)}} = 12.88 \text{ Hz}$ ):

$$^3J_{\text{PCCC(O)}} = 14.3 \cos^2 \theta - 1.3 \cos \theta + 0.50 \quad (\text{Eq. 2})$$



**Figure 2E.10.**  $^1\text{H}$  NMR spectrum (600 MHz,  $\text{CDCl}_3$ ) for the phosphonium butanone of **TF-2-PBK** performed at (a) 278 K and (b) 298 K. The Rauhut-Currier side-product is annotated in (b).





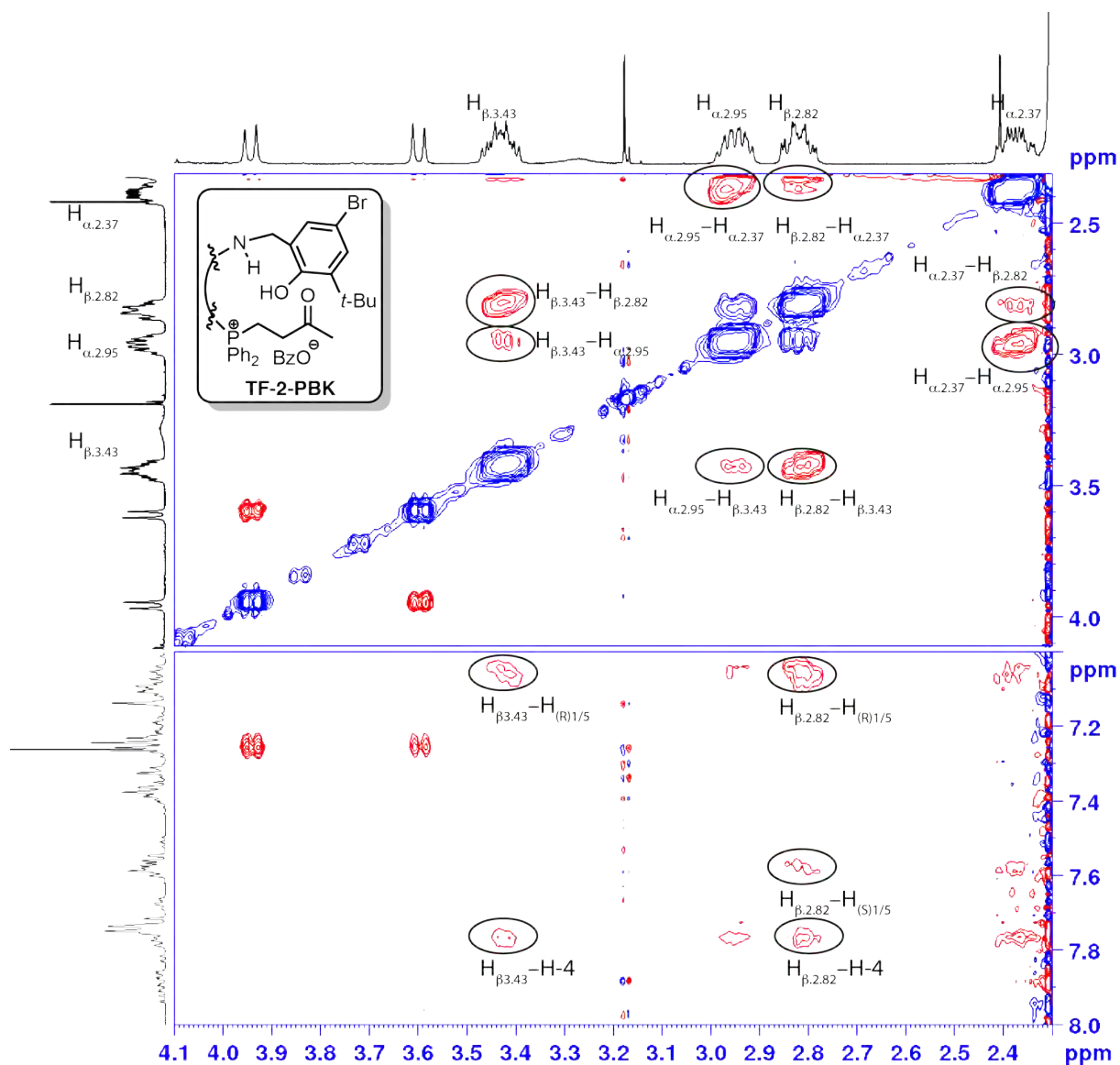
**Figure 2E.11.** a) Homonuclear J-Resolved experiment (600 MHz, CDCl<sub>3</sub>, 278 K) showing expansions for aliphatic protons b) H<sub>β3.43</sub> c) H<sub>α2.95</sub> d) H<sub>β2.82</sub> e) H<sub>α2.37</sub>.

### 2.3.6 2D Quantitative NOESY

To a sample of **TF-2** (8 mg, 11.5  $\mu\text{mol}$ ) in  $\text{CDCl}_3$  was added freshly recrystallised  $\text{BzOH}$  (1.5 mg, 11.5  $\mu\text{mol}$ , 1 eq) and the sample analysed by  $^1\text{H}$  NMR. The temperature was cooled to 278 K, and methyl vinyl ketone (2.2 mg, 31  $\mu\text{mol}$ , 2.7 eq) was added and the sample allowed to equilibrate at 278 K. A  $^1\text{H}$  NMR spectrum was collected of **TF-2-PBK** before a 2D NOESY (noesygpphzs) experiment was performed on the spectral window 0-10 ppm (Figure 2E.12) using mixing time of 400 ms. The strength of the gradient pulse was adjusted to 11.6% using the Bruker zs\_setup pulse program. Equation (3) below was used to convert NOEs to distances,

$$D_{x-y} = D_{\text{H}4'-\text{H}5'} \left( \frac{(\text{NOE}_{\text{H}4'-\text{H}5'} * ns)}{\text{NOE}_{x-y}} \right)^{1/6} \quad (3)$$

Where  $D_{x-y}$  is the intermolecular distance,  $D_{\text{H}4'-\text{H}5'}$  distance between H-4–H-5 (2.48 Å),  $\text{NOE}_{\text{H}4'-\text{H}5'}$  is the H-4'–H-5' NOE, ns is number of spins,  $\text{NOE}_{x-y}$  is the x-y NOE.

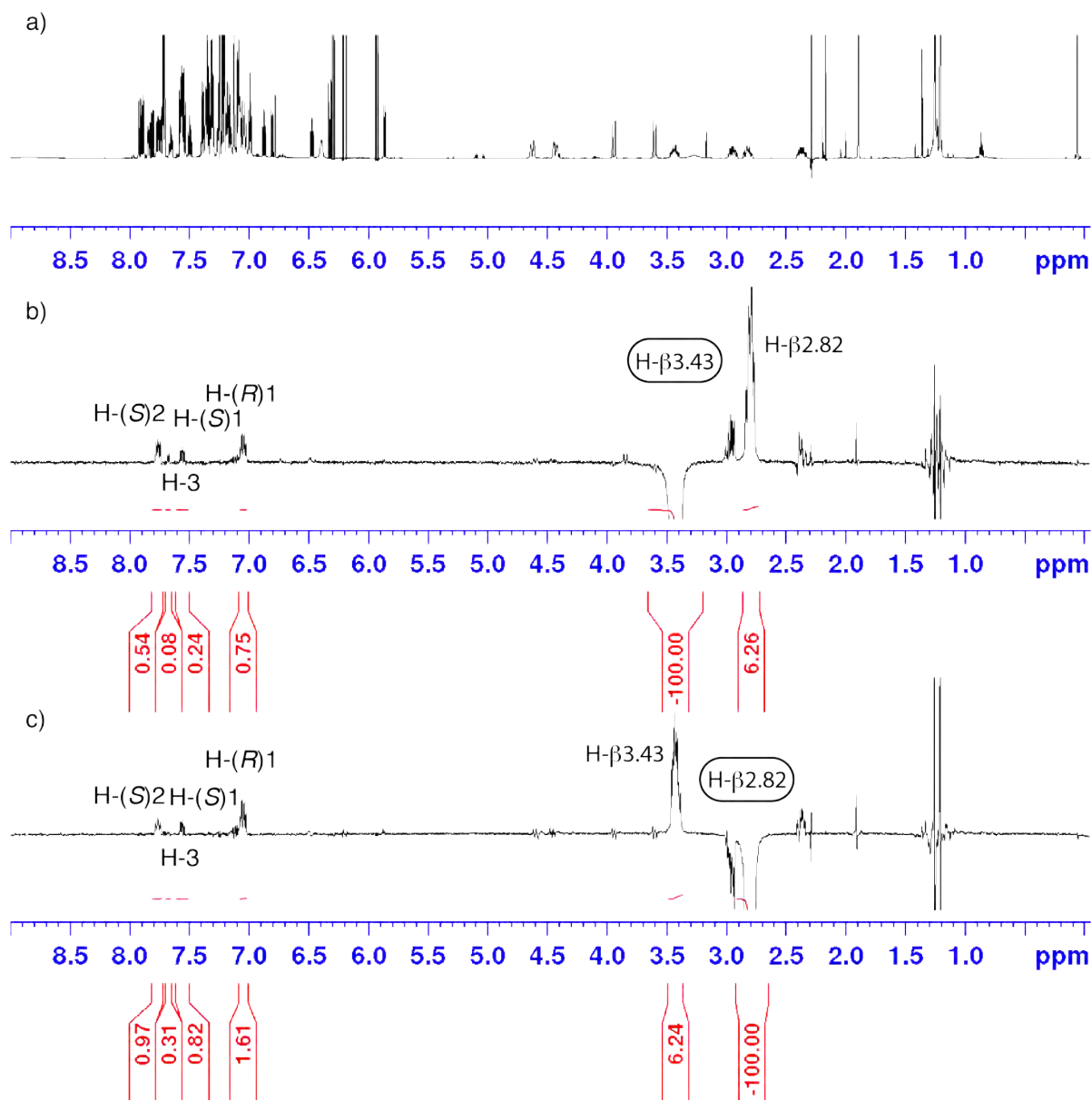


**Figure 2E.12.** TF-2-PBK 2D NOESY spectrum (600 MHz,  $\text{CDCl}_3$ , 278 K) with key NOEs annotated.

### 2.3.7 1D Selective NOESY

To a sample of **TF-2** (8 mg, 11.5  $\mu\text{mol}$ ) in  $\text{CDCl}_3$  was added freshly recrystallised  $\text{BzOH}$  (1.5 mg, 11.5  $\mu\text{mol}$ , 1 eq) and the sample analysed by  $^1\text{H}$  NMR. The temperature was cooled to 278 K, and methyl vinyl ketone (2.2 mg, 31  $\mu\text{mol}$ , 2.7 eq) was added and the sample allowed to equilibrate at 278 K. A  $^1\text{H}$  NMR spectrum was collected of **TF-2-PBK** before a series of 1D

(irradiating 3.43 ppm (2048 Hz), 2.82 ppm (1692 Hz)) selective NOESY (selnoggp) were performed using a 400 ms mixing time and 1024 scans (Figure 2E.13).



**Figure 2E.13.** a) TF-2-PBK  $^1\text{H}$  NMR spectrum (600 MHz,  $\text{CD}_2\text{Cl}_2$ ). b) 1D Selective NOESY spectrum from irradiation of  $\text{H-}\beta$  (3.34 ppm). c) 1D Selective NOESY spectrum from irradiation of  $\text{H-}\beta'$  (2.82 ppm).

### 2.3.8 3D HSQC-NOESY

To a sample of **TF-1** (8 mg, 14.3  $\mu\text{mol}$ ) in  $\text{CD}_2\text{Cl}_2$  was added freshly recrystallised  $^{13}\text{C}_6\text{-BzOH}$  (1.75 mg, 14.3  $\mu\text{mol}$ , 1 eq) and the sample analysed by  $^1\text{H}$  NMR. **MVK** (2.71 mg, 38.6  $\mu\text{mol}$ , 2.7 eq) was added and the sample allowed to equilibrate at room temperature. A  $^{13}\text{C}$ -selective NOESY (hsqcgpnowgx33d) was then performed with 400 ms mixing time and optimised  $^1J_{\text{CH}}$  value of 150 Hz. The spectrum was processed in Topspin 3.6.1.

### 2.3.9 Pulse Programs

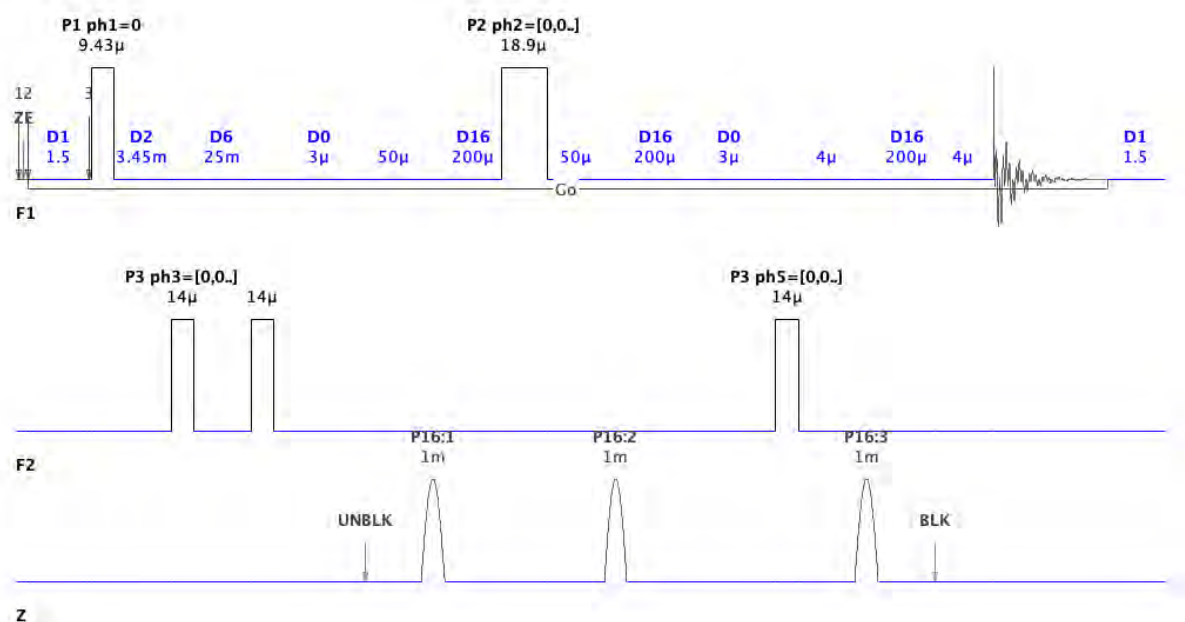


Figure 2E.14. Pulse program (hmbcgplndqf) for 2D HMBC experiments.

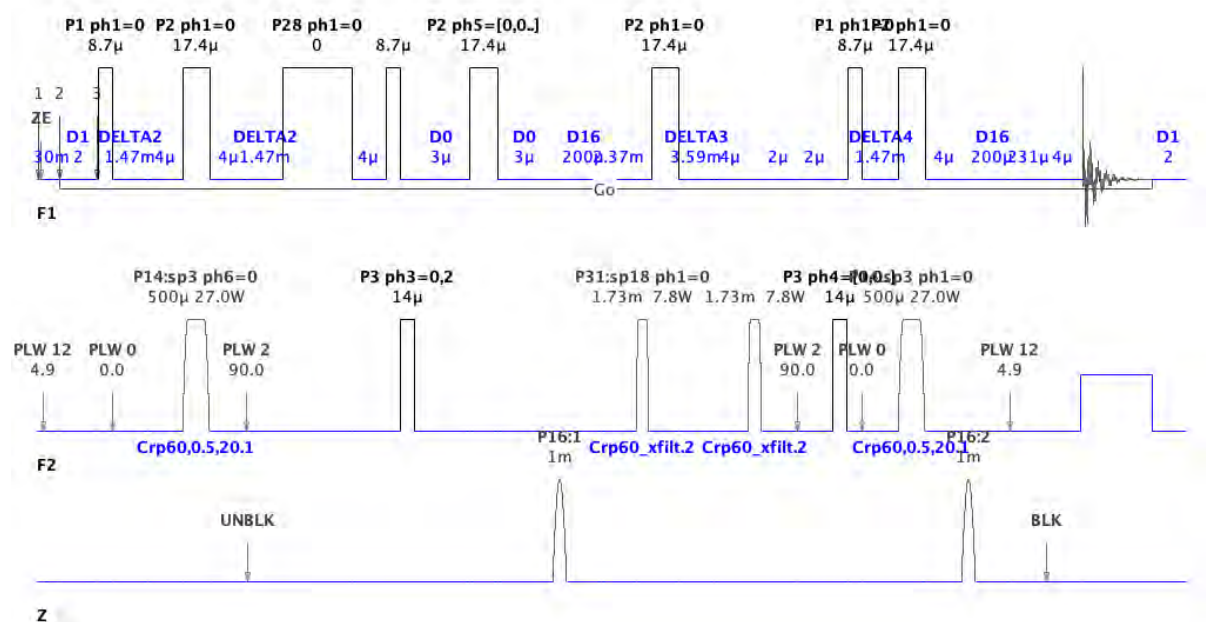
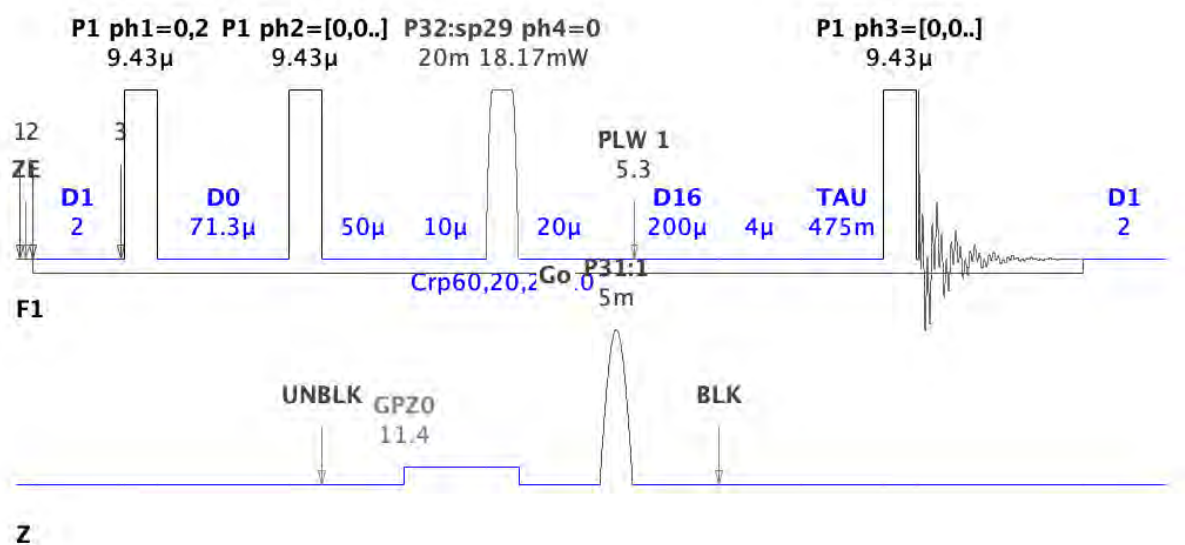
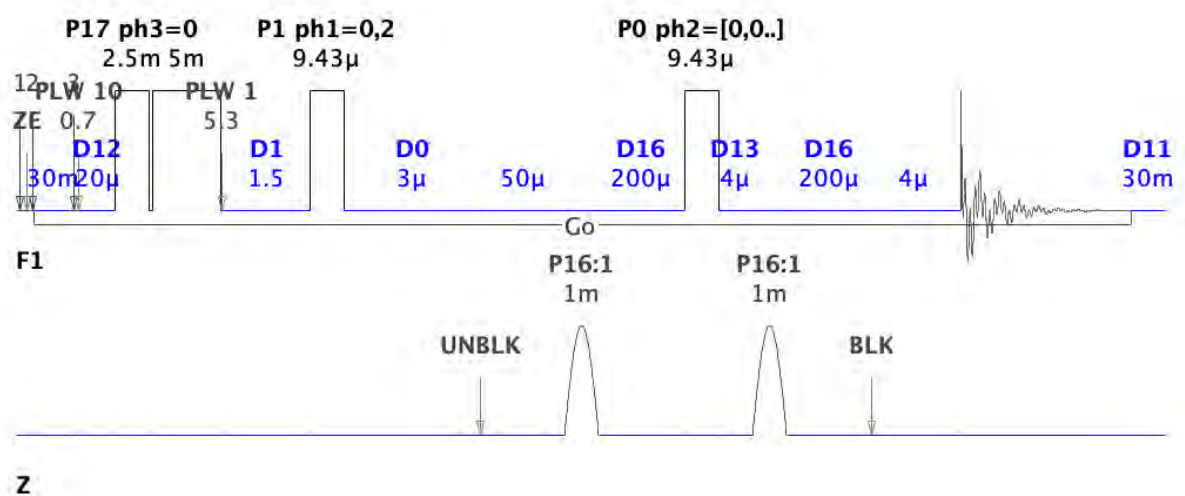


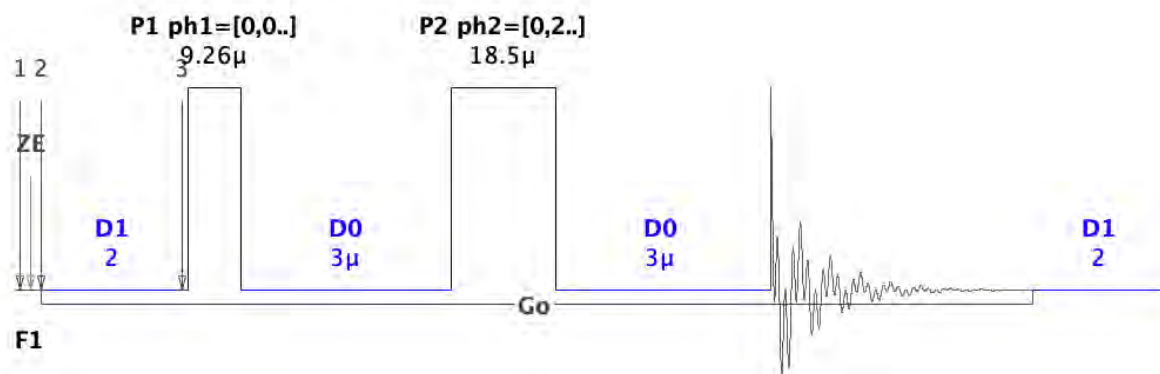
Figure 2E.15. Pulse Program (hsqcedetgpsp.3) for phase-edited HSQC.<sup>43-45</sup>



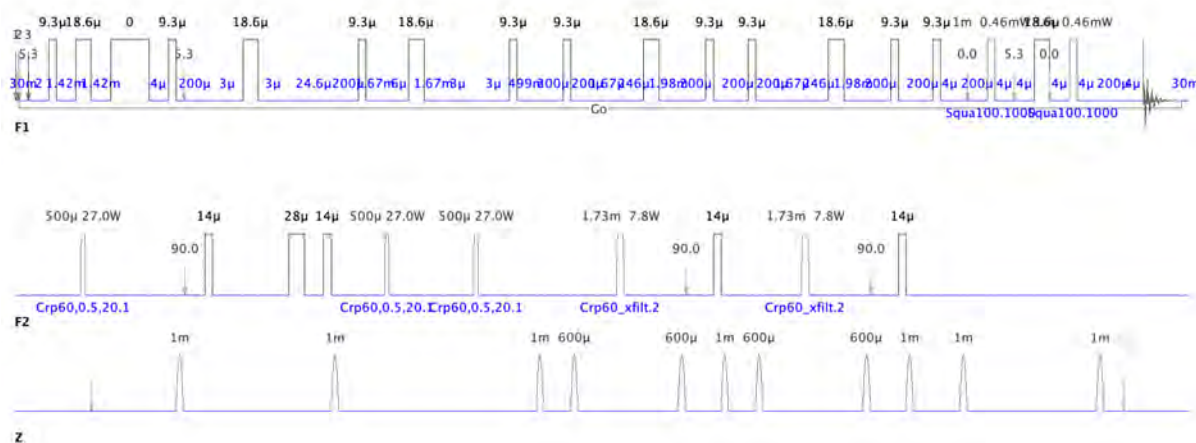
**Figure 2E.16.** Pulse Program (noesygp-phz) for quantitative 2D NOESY experiments.<sup>46-48</sup>



**Figure 2E.17.** Pulse program (cosygppp-qf) for 2D COSY experiments.



**Figure 2E.18.** Pulse program (jresqf) for 2D homonuclear J-Resolved experiments.



**Figure 2E.19.** Pulse program (hsqcgpnwngx33d) for 3D HSQC-NOESY experiments.<sup>44, 49-51</sup>



## 2.4 References

1. Kenny, R.; Liu, F., Trifunctional Organocatalysts: Catalytic Proficiency by Cooperative Activation. *Eur. J. Org. Chem.* **2015**, 2015 (24), 5304-5319.
2. Kenny, R.; Liu, F., Cooperative Trifunctional Organocatalysts for Proficient Proton Transfer Reactions. *Chem. Rec.* **2017**, 17 (5), 535-553.
3. Erkkilä, A.; Majander, I.; Pihko, P. M., Iminium Catalysis. *Chem. Rev.* **2007**, 107 (12), 5416-5470.
4. List, B.; Lerner, R. A.; Barbas, C. F., Proline-Catalyzed Direct Asymmetric Aldol Reactions. *J. Am. Chem. Soc.* **2000**, 122 (10), 2395-2396.
5. Mukherjee, S.; Yang, J. W.; Hoffmann, S.; List, B., Asymmetric Enamine Catalysis. *Chem. Rev.* **2007**, 107 (12), 5471-5569.
6. Bahmanyar, S.; Houk, K. N.; Martin, H. J.; List, B., Quantum Mechanical Predictions of the Stereoselectivities of Proline-Catalyzed Asymmetric Intermolecular Aldol Reactions. *J. Am. Chem. Soc.* **2003**, 125 (9), 2475-2479.
7. Williams, J. E.; Stand, P. J.; Schleyer, P. R., Physical Organic Chemistry: Quantitative Conformational Analysis; Calculation Methods. *Annu. Rev. Phys. Chem.* **1968**, 19 (1), 531-558.
8. Eliel, E. L., Conformational Analysis: 3. In *Encyclopedia of Computational Chemistry*, Schleyer, P. v. R.; Allinger, N. L.; Clark, T.; Gasteiger, J.; Kollman, P. A.; Schaefer, H. F.; Schreiner, P. R., Eds. 2002.
9. Berova, N.; Bari, L. D.; Pescitelli, G., Application of electronic circular dichroism in configurational and conformational analysis of organic compounds. *Chem. Soc. Rev.* **2007**, 36 (6), 914-931.

10. Haasnoot, C. A. G.; de Leeuw, F. A. A. M.; Altona, C., The relationship between proton-proton NMR coupling constants and substituent electronegativities—I: An empirical generalization of the Karplus equation. *Tetrahedron* **1980**, *36* (19), 2783-2792.
11. Contreras, R. H.; Peralta, J. E., Angular dependence of spin-spin coupling constants. *Prog. Nucl. Magn. Reson. Spectrosc.* **2000**, *37* (4), 321-425.
12. Anet, F. A. L.; Bourn, A. J. R., Nuclear Magnetic Resonance Spectral Assignments from Nuclear Overhauser Effects<sup>1</sup>. *J. Am. Chem. Soc.* **1965**, *87* (22), 5250-5251.
13. Neuhaus, D.; Williamson, M. P., *The Nuclear Overhauser Effect in Structural and Conformational Analysis, 2nd Edition*. 2nd ed.; Wiley VCH: New York, 2000.
14. Clore, G. M.; Gronenborn, A. M., Theory and applications of the transferred nuclear Overhauser effect to the study of the conformations of small ligands bound to proteins. *J. Magn. Reson.* **1982**, *48* (3), 402-417.
15. Shuker, S. B.; Hajduk, P. J.; Meadows, R. P.; Fesik, S. W., Discovering High-Affinity Ligands for Proteins: SAR by NMR. *Science* **1996**, *274* (5292), 1531-1534.
16. Meyer, B.; Peters, T., NMR Spectroscopy Techniques for Screening and Identifying Ligand Binding to Protein Receptors. *Angew. Chem., Int. Ed.* **2003**, *42* (8), 864-890.
17. Grošelj, U.; Seebach, D.; Badine, D. M.; Schweizer, W. B.; Beck, A. K.; Krossing, I.; Klose, P.; Hayashi, Y.; Uchimaru, T., Structures of the Reactive Intermediates in Organocatalysis with Diarylprolinol Ethers. *Helv. Chim. Acta* **2009**, *92* (7), 1225-1259.
18. Holland, M. C.; Paul, S.; Schweizer, W. B.; Bergander, K.; Mück-Lichtenfeld, C.; Lakhdar, S.; Mayr, H.; Gilmour, R., Noncovalent Interactions in Organocatalysis: Modulating Conformational Diversity and Reactivity in the MacMillan Catalyst. *Angew. Chem., Int. Ed.* **2013**, *52* (31), 7967-7971.

19. Holland, M. C.; Gilmour, R., Deconstructing Covalent Organocatalysis. *Angew. Chem., Int. Ed.* **2015**, *54* (13), 3862-3871.
20. Renzi, P.; Hioe, J.; Gschwind, R. M., Enamine/Dienamine and Brønsted Acid Catalysis: Elusive Intermediates, Reaction Mechanisms, and Stereoinduction Modes Based on in Situ NMR Spectroscopy and Computational Studies. *Acc. Chem. Res.* **2017**, *50* (12), 2936-2948.
21. Rigling, C.; Kisunzu, J. K.; Duschmalé, J.; Häussinger, D.; Wiesner, M.; Ebert, M.-O.; Wennemers, H., Conformational Properties of a Peptidic Catalyst: Insights from NMR Spectroscopic Studies. *J. Am. Chem. Soc.* **2018**, *140* (34), 10829-10838.
22. Bertelsen, S.; Marigo, M.; Brandes, S.; Dinér, P.; Jørgensen, K. A., Dienamine Catalysis: Organocatalytic Asymmetric  $\gamma$ -Amination of  $\alpha,\beta$ -Unsaturated Aldehydes. *J. Am. Chem. Soc.* **2006**, *128* (39), 12973-12980.
23. List, B.; Hoang, L.; Martin, H. J., New mechanistic studies on the proline-catalyzed aldol reaction. *Proc. Natl. Acad. Sci.* **2004**, *101* (16), 5839-5842.
24. Schmid, M. B.; Zeitler, K.; Gschwind, R. M., The Elusive Enamine Intermediate in Proline-Catalyzed Aldol Reactions: NMR Detection, Formation Pathway, and Stabilization Trends. *Angew. Chem., Int. Ed.* **2010**, *49* (29), 4997-5003.
25. Schmid, M. B.; Zeitler, K.; Gschwind, R. M., Formation and Stability of Prolinol and Prolinol Ether Enamines by NMR: Delicate Selectivity and Reactivity Balances and Parasitic Equilibria. *J. Am. Chem. Soc.* **2011**, *133* (18), 7065-7074.
26. Schmid, M. B.; Zeitler, K.; Gschwind, R. M., Distinct conformational preferences of prolinol and prolinol ether enamines in solution revealed by NMR. *Chem. Sci.* **2011**, *2* (9), 1793-1803.
27. Procházková, E.; Kolmer, A.; Ilgen, J.; Schwab, M.; Kaltschnee, L.; Fredersdorf, M.; Schmidts, V.; Wende, R. C.; Schreiner, P. R.; Thiele, C. M., Uncovering Key Structural Features

of an Enantioselective Peptide-Catalyzed Acylation Utilizing Advanced NMR Techniques. *Angew. Chem., Int. Ed.* **2016**, 55 (51), 15754-15759.

28. Müller, C. E.; Zell, D.; Hrdina, R.; Wende, R. C.; Wanka, L.; Schuler, S. M. M.; Schreiner, P. R., Lipophilic Oligopeptides for Chemo- and Enantioselective Acyl Transfer Reactions onto Alcohols. *J. Org. Chem.* **2013**, 78 (17), 8465-8484.

29. Aue, W. P.; Karhan, J.; Ernst, R. R., Homonuclear broad band decoupling and two - dimensional J - resolved NMR spectroscopy. *J. Chem. Phys.* **1976**, 64 (10), 4226-4227.

30. Ludwig, C.; Viant, M. R., Two-dimensional J-resolved NMR spectroscopy: review of a key methodology in the metabolomics toolbox. *Phytochem. Anal.* **2010**, 21 (1), 22-32.

31. Aggarwal, V. K.; Fulford, S. Y.; Lloyd-Jones, G. C., Reevaluation of the Mechanism of the Baylis–Hillman Reaction: Implications for Asymmetric Catalysis. *Angew. Chem., Int. Ed.* **2005**, 44 (11), 1706-1708.

32. Shi, M.; Chen, L.-H.; Li, C.-Q., Chiral Phosphine Lewis Bases Catalyzed Asymmetric aza-Baylis–Hillman Reaction of N-Sulfonated Imines with Activated Olefins. *J. Am. Chem. Soc.* **2005**, 127 (11), 3790-3800.

33. Buskens, P.; Klankermayer, J.; Leitner, W., Bifunctional Activation and Racemization in the Catalytic Asymmetric Aza-Baylis–Hillman Reaction. *J. Am. Chem. Soc.* **2005**, 127 (48), 16762-16763.

34. Shi, M.; Liu, Y.-H., Traditional Morita–Baylis–Hillman reaction of aldehydes with methyl vinyl ketone co-catalyzed by triphenylphosphine and nitrophenol. *Org. Biomol. Chem.* **2006**, 4 (8), 1468-1470.

35. Lindner, C.; Liu, Y.; Karaghiosoff, K.; Maryasin, B.; Zipse, H., The Aza-Morita–Baylis–Hillman Reaction: A Mechanistic and Kinetic Study. *Chemistry – A European Journal* **2013**, *19* (20), 6429-6434.
36. Anstiss, C.; Garnier, J.-M.; Liu, F., Mechanistic investigations of multidentate organocatalyst-promoted counterion catalysis for fast and enantioselective aza-Morita–Baylis–Hillman reactions at ambient temperature. *Org. Biomol. Chem.* **2010**, *8* (19), 4400-4407.
37. Anstiss, C.; Liu, F., Cooperativity in the counterion catalysis of Morita/Baylis/Hillman reactions promoted by enantioselective trifunctional organocatalysts. *Tetrahedron* **2010**, *66* (29), 5486-5491.
38. Garnier, J.-M.; Anstiss, C.; Liu, F., Enantioselective Trifunctional Organocatalysts for Rate- Enhanced Aza-Morita–Baylis–Hillman Reactions at Room Temperature. *Adv. Synth. Catal.* **2009**, *351* (3), 331-338.
39. Garnier, J.-M.; Liu, F., Trifunctional organocatalyst-promoted counterion catalysis for fast and enantioselective aza-Morita–Baylis–Hillman reactions at ambient temperature. *Org. Biomol. Chem.* **2009**, *7* (7), 1272-1275.
40. Buchanan, G. W.; Benezra, C., Stereochemical dependence of  $^{13}\text{C}$  shieldings and  $^{13}\text{C}$ – $^{31}\text{P}$  couplings in phosphonates of known geometry. Is there a Karplus-type relationship for P–C–C–C coupling? *Can. J. Chem.* **1976**, *54* (2), 231-237.
41. Gorenstein, D. G., Non-biological aspects of phosphorus-31 NMR spectroscopy. *Prog. Nucl. Magn. Reson. Spectrosc.* **1984**, *16*, 1-98.
42. Durig, J. R.; Feng, F. S.; Wang, A.; Phan, H. V., Conformational stability, barriers to internal rotation, ab initio calculations, and vibrational assignment of 2-butanone. *Can. J. Chem.* **1991**, *69* (11), 1827-1844.

43. Willker, W.; Leibfritz, D.; Kerssebaum, R.; Bermel, W., Gradient selection in inverse heteronuclear correlation spectroscopy. *Magn. Reson. Chem.* **1993**, *31* (3), 287-292.
44. Zwahlen, C.; Legault, P.; Vincent, S. J. F.; Greenblatt, J.; Konrat, R.; Kay, L. E., Methods for Measurement of Intermolecular NOEs by Multinuclear NMR Spectroscopy: Application to a Bacteriophage  $\lambda$  N-Peptide/boxB RNA Complex. *J. Am. Chem. Soc.* **1997**, *119* (29), 6711-6721.
45. Boyer, R. D.; Johnson, R.; Krishnamurthy, K., Compensation of refocusing inefficiency with synchronized inversion sweep (CRISIS) in multiplicity-edited HSQC. *J. Magn. Reson.* **2003**, *165* (2), 253-259.
46. Thrippleton, M. J.; Keeler, J., Elimination of Zero-Quantum Interference in Two-Dimensional NMR Spectra. *Angew. Chem., Int. Ed.* **2003**, *42* (33), 3938-3941.
47. Jeener, J.; Meier, B. H.; Bachmann, P.; Ernst, R. R., Investigation of exchange processes by two - dimensional NMR spectroscopy. *J. Chem. Phys.* **1979**, *71* (11), 4546-4553.
48. Wagner, R.; Berger, S., Gradient-Selected NOESY—A Fourfold Reduction of the Measurement Time for the NOESY Experiment. *J. Magn. Reson., Ser. A* **1996**, *123* (1), 119-121.
49. Breeze, A. L., Isotope-filtered NMR methods for the study of biomolecular structure and interactions. *Prog. Nucl. Magn. Reson. Spectrosc.* **2000**, *36* (4), 323-372.
50. Ogura, K.; Terasawa, H.; Inagaki, F., An improved double-tuned and isotope-filtered pulse scheme based on a pulsed field gradient and a wide-band inversion shaped pulse. *J. Biomol. NMR* **1996**, *8* (4), 492-498.
51. Iwahara, J.; Wojciak, J. M.; Clubb, R. T., Improved NMR spectra of a protein–DNA complex through rational mutagenesis and the application of a sensitivity optimized isotope-filtered NOESY experiment. *J. Biomol. NMR* **2001**, *19* (3), 231-241.

## **Chapter 3**

### **Conjugative Catalysis from an aza-MBH**

#### **Proton Shuttle**

### **3.1 Introduction**

#### **3.1.1 Additives improve catalytic proficiency**

Additives have been used extensively in organocatalytic<sup>1-2</sup> and organometallic reactions<sup>3-6</sup> to enhance proficiency by either improving selectivity or altering the reaction mechanism.<sup>7-8</sup> Additives commonly used in organocatalytic reactions include; Brønsted acids, Brønsted bases, inorganic salts, alcohols and phenols, molecular sieves, water and thioureas.<sup>8</sup> A classic example is the addition of water in proline-catalysed aldol reactions.<sup>9-12</sup> Water facilitates proton transfer for activation of the aldehyde and hydrolysis of the imine to regenerate the catalyst.<sup>13-15</sup> Other additives can deoligomerise organometallic structures to release the active monomeric species. Basic additives can regenerate the catalyst by eliminating the product faster, while Brønsted acid additives are typically used to stabilise key intermediates along the reaction coordinate. Deconvoluting the additive effect on catalytic reactions, however, can be difficult sometimes due to the multi-step nature of most reactions, although significant attention has been mainly given particularly to acid additives given their wide range of applications.<sup>9-12, 16</sup>

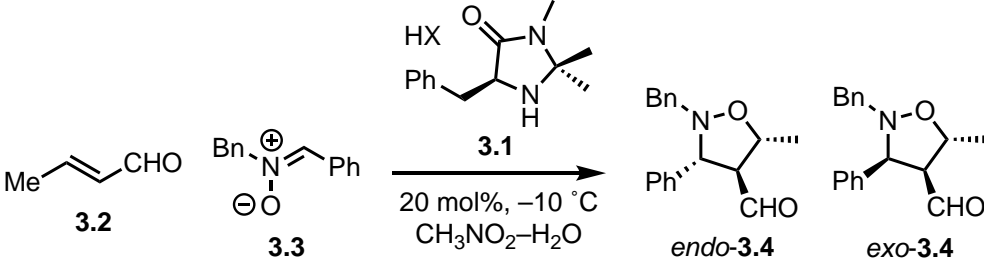
#### **3.1.2 Acid additives exhibit versatile roles in catalysis**

Acid additives are widely utilised in organocatalysis in a variety of different reactions. In many instances, an achiral acid is added to assist a chiral catalyst. Acid additives have a prominent role in iminium<sup>17</sup>, enamine<sup>18</sup> and asymmetric counterion-directed catalysis<sup>19</sup> mediated reactions. Chiral phosphoric acids are also common additives in a diverse array of transformations.<sup>20-23</sup> The acid additive can also achieve its effect through a combination of orbital activation and steric directing through its conjugate base or counterion. A seminal example is MacMillan's Diels–Alder reaction between cinnamaldehyde derivatives and



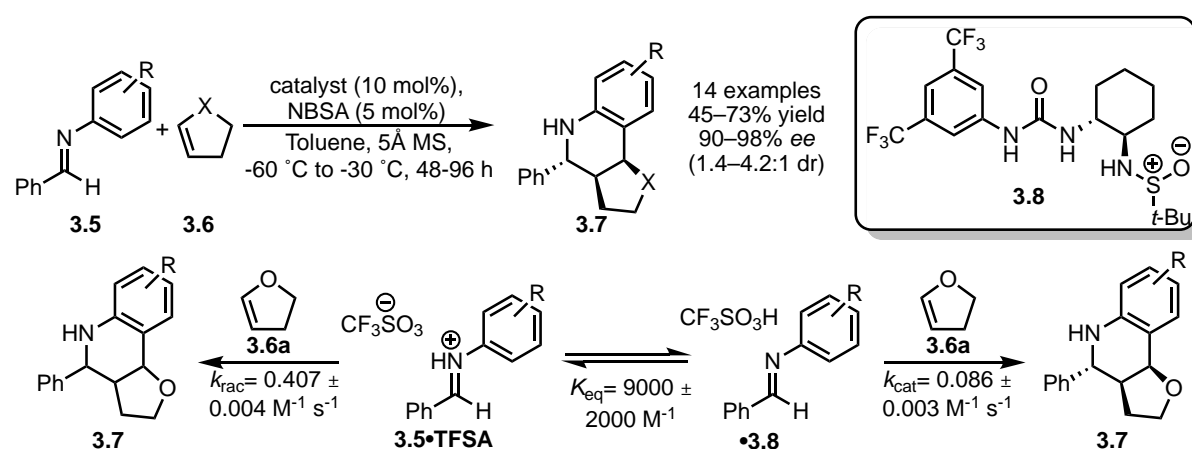
cyclopentadiene catalyst by a chiral amine salt.<sup>24</sup> Proficiency was achieved by LUMO-lowering activation of the  $\alpha,\beta$ -unsaturated aldehydes through the formation of an iminium ion. Essentially, the acid additive facilitates reversible iminium formation that enables covalent activation and cycling of a chiral auxiliary in situ. Some level of counterion effect from the acid additive on stereo- and enantioselectivity was demonstrated for the imidazolidinone salt (**3.1**) in a 1,3-dipolar cycloaddition between crotonaldehyde (**3.2**) and nitrones (**3.3**) to afford isoxazolidines (**3.4**) (Table 3.1).<sup>25</sup> The acid additive HCl provided the best enantioselectivity (95% *ee*, Table 3.1, entry 1), while in the case of TFA, the rate of reaction was accelerated (80 h vs 108 h) but enantioselectivity was noticeably diminished (86% *ee*, Table 3.1, entry 3). The highest selectivity for *endo*-**3.4** over *exo*-**3.4** was achieved with HBr as an additive.

**Table 3.1.** Effect of the Brønsted Acid co-catalyst on the Dipolar Cycloaddition between Crotonaldehyde (**3.2**) and Nitrones (**3.3**).

|  |                   |         |          |                 |                              |
|--|-------------------|---------|----------|-----------------|------------------------------|
| Entry  | HX co-catalyst    | Time /h | Yield /% | <i>endo:exo</i> | <i>ee</i> ( <i>endo</i> ) /% |
| 1  | HCl               | 108     | 70       | 88:12           | 95                           |
| 2  | TfOH              | 101     | 88       | 89:11           | 90                           |
| 3  | TFA               | 80      | 65       | 72:28           | 86                           |
| 4  | HBr               | 80      | 77       | 94:6            | 93                           |
| 5  | HClO <sub>4</sub> | 80      | 86       | 94:6            | 90                           |

In some cases, acid additives may confer diastereo- or enantioselectivity but at the cost of the reaction rate. Jacobsen et al. reported an asymmetric Povarov reaction between *N*-aryl imines (**3.5**) and electron-rich olefins (**3.6**) to form tetrahydroquinolines (**3.7**), which can be catalyzed by triflic acid via imine protonation (Scheme 3.1).<sup>26</sup> Chiral additives, containing multidentate H-bond donors (urea, thiourea, and sulfinamide; **3.8**) and steric-directing groups, can bind to

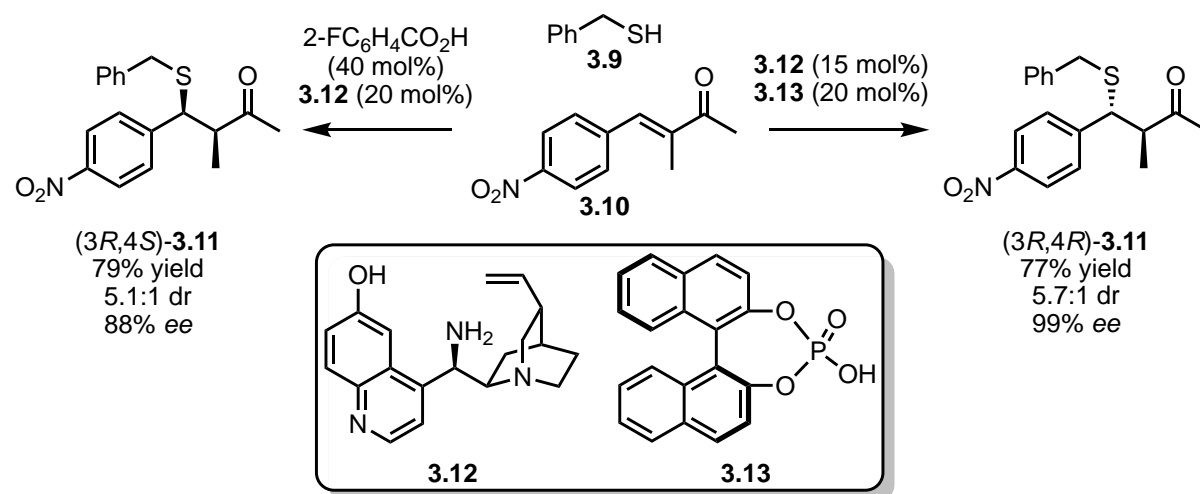
both the triflate counterion and protonated imine in a specific orientation, enabling high facial selectivity (up to 98% *ee*). However, the bulky environment from a chiral additive invariably decelerates, rather than accelerates, the reaction rate in the true sense of catalysis. This illustrates the common difficulty in asymmetric catalysis in which rate acceleration and asymmetric induction often are not achieved in congruence, unless the desired asymmetric pathway is selectively activated, rather than inducing asymmetric induction from the least decelerated pathway by steric hinderance.



**Scheme 3.1.** The povarov reaction catalysed by a chiral thiourea **3.8**.

Melchiorre et al. reported acid additives dictating the stereochemical outcome of a diastereodivergent asymmetric Sulfa-Michael additions of thiols (**3.9**) to  $\alpha$ -branched enone (**3.10**) to yield  $\beta$ -thioether ketones (**3.11**) using a cinchona alkaloid catalyst (**3.12**) (Scheme 3.2).<sup>27</sup> The chiral catalyst has modest selectivity for the *syn* diastereomer (5:1 *dr*) with modest enantioselectivity (65% *ee*). Chiral and achiral acid additives cause modest rate elevation alongside substantial increases in the stereoselectivity (up to 98% *ee*). By switching the acid additive from achiral 2-fluorobenzoic acid to the chiral phosphoric acid **3.13**, the sense of the catalyst's diastereoselectivity could be altered, enabling access to either diastereomer with high enantiopurity. The change in diastereoselectivity was attributed to different

conformations of the ground state structure for the protonated cinchona alkaloid with different counterions.

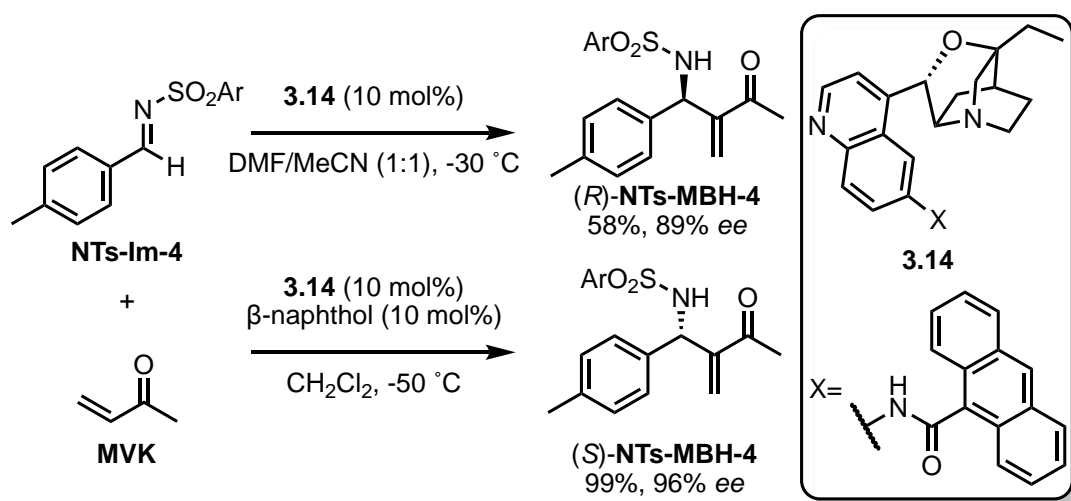


**Scheme 3.2.** Diastereodivergent Sulfa-Michael addition of thiols to  $\alpha$ -branched enones.

### 3.1.3 Acid additive effects in the *aza*-MBH reaction

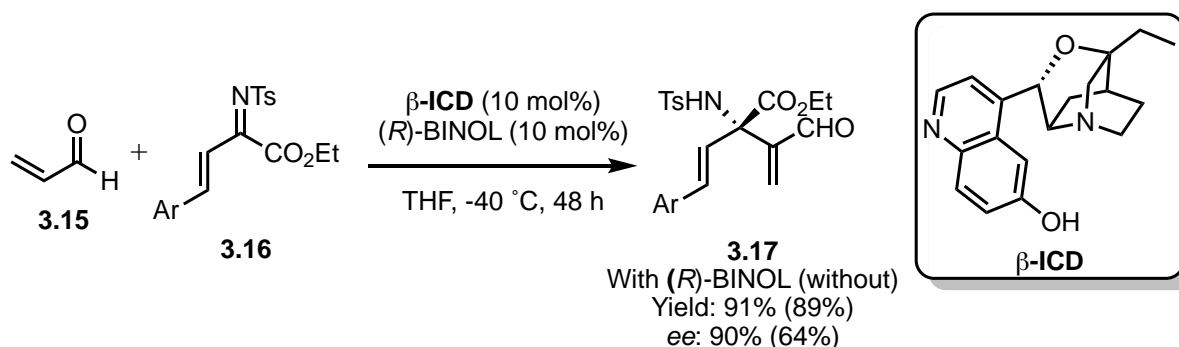
Acid additives have a profound impact on the *aza*-MBH reaction in a highly condition-dependent manner.<sup>28-31</sup> In the absence of protic additives, the proton transfer and elimination step is the rate determining step. Protic species shift the rate-determining step to the Aldol addition.<sup>30, 32-35</sup> Typically, for bifunctional systems, strongly protic additives suppress reactivity through the formation of the inactive ketone tautomer.

Zhu et al. reported a derivatised  $\beta$ -ICD-amide catalyst (**3.14**) for an *aza*-MBH reaction between **NTs-Im-4** and **MVK**, the stereoselectivity of which could be inverted by addition of  $\beta$ -naphthol (Scheme 3.3).<sup>36</sup> Without  $\beta$ -naphthol, the yield of the *aza*-MBH adduct is moderate (58%), and the (*R*)-enantiomer is isolated in high excess (89% ee). Addition of  $\beta$ -naphthol increased the yield (>99%) and yielded the (*S*)-enantiomer with excellent enantioselectivity (96%). The author's proposed that in light of the inversion, the proton transfer was the stereodetermining step.



**Scheme 3.3.** aza-MBH catalysed by  $\beta$ -ICD-amide catalyst **3.14**.

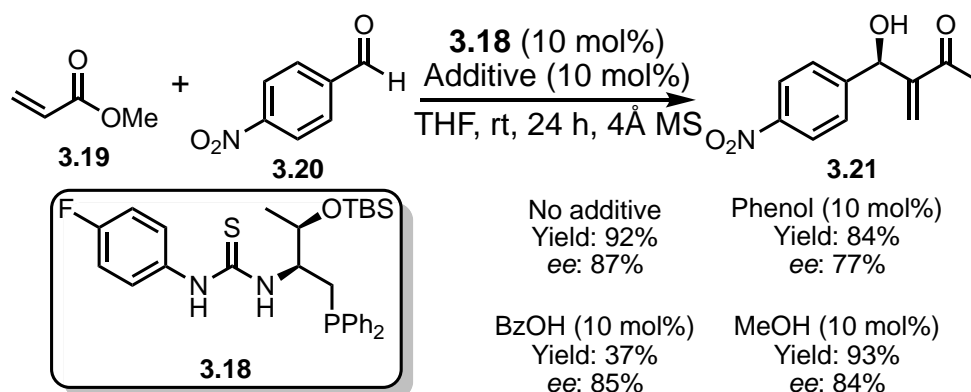
Chen *et al.* reported an asymmetric *aza*-MBH with ketimine (**3.16**) and acrolein (**3.15**) catalysed by  $\beta$ -**ICD** (10 mol%) and (*R*)-BINOL (10 mol%) at  $-40\text{ }^{\circ}\text{C}$  in THF (Scheme 3.4).<sup>37</sup> Without (*R*)-BINOL, the *aza*-MBH adduct (**3.17**) was isolated with 89% yield and 64% *ee*. Addition of (*R*)-BINOL did not lead to a significant change in the reaction rate (89% v.s 91%) but a significant improvement in the asymmetric induction (64% vs 90% *ee*).  $\beta$ -**ICD** and (*R*)-BINOL may self-assemble in solution by hydrogen bonding to promote asymmetric activation.



**Scheme 3.4.** The aza-MBH reaction catalysed by  $\beta$ -**ICD** with improved enantioselectivity in the presence of (*R*)-BINOL.

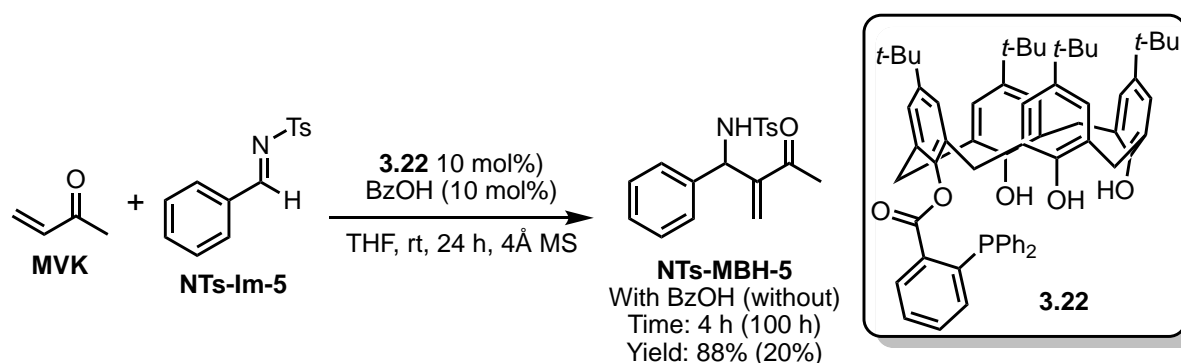
Acid additives are not always conducive to the MBH reaction. Lu *et al.* reported bifunctional phosphine-thiourea catalysts (**3.18**) for the MBH reaction between methyl acrylate (**3.19**) and aromatic aldehydes (**3.20**) (Scheme 3.5)<sup>38</sup> In THF, the catalyst **3.18** yielded the *p*-

nitrobenzaldehyde MBH adduct (**3.21**) with 92% yield and 87% *ee*. The reaction was the most proficient without any additives. Phenol addition caused a decrease in yield (84%), and asymmetric induction (77% *ee*), and BzOH heavily suppressed the reaction (37% yield) due to the formation of the inactive ketone tautomer (See Chapter 2 Section 2.1.3 for discussion of parasitic intermediates in the MBH reaction).



**Scheme 3.5.** aza-MBH catalysed by **3.18** with different protic additives.

Zhong *et al.* reported an acid-activated substituted calix[4]arene catalyst (**3.22**) for the *aza*-MBH reaction (Scheme 3.6).<sup>39</sup> Reactions between the model substrate **NTs-Im-5** and MVK in the absence of a Brønsted acid were slow (100 h) and the aza-MBH adduct **NTs-MBH-5** isolated in a low yield (20%). Acid additives improved the rate (4 h) and yield (88%) with benzoic acid identified as the most effective additive (4 h).



**Scheme 3.6.** acid-activated aza-MBH catalysed by **3.22** and benzoic acid.

Shi *et al.* reported the effect of benzoic acid on a chiral thiourea-phosphine bifunctional organocatalyst **3.23** for the *aza*-MBH reaction between methyl vinyl ketone and aryl NTs imines **NTs-Im-6**.<sup>40</sup> Without any acid additive, the yield and enantioselectivity are low (Table 3.2, Entry 1). All protic additives resulted in rate enhancement, with benzoic acid (Table 3.2, Entry 3) being the most significant in increasing both the yield (96%) and enantioselectivity (87% *ee*). This joint rise of rate and enantioselectivity was observed for other carboxylic acids such as formic acid and 2-iodobenzoic acid however at a less pronounced level. The mechanism of this activated catalysis was not investigated but hypothesised to require proton transfer mediated by the acid additive.

**Table 3.2.** Effect of various additives for the *aza*-MBH catalysed by **3.23**.

| Entry | Additive  | Yield/ % <sup>a</sup> | <i>ee</i> / % <sup>b</sup> |
|-------|---|-----------------------|----------------------------|
| 1     | -   | 12                    | 16                         |
| 2     | HCO <sub>2</sub> H                                  | 30                    | 55                         |
| 3     | BzOH  | 96                    | 87                         |
| 4     | 2-I-C <sub>6</sub> H <sub>4</sub> CO <sub>2</sub> H | 41                    | 76                         |
| 5     | p-nitrophenol                                       | 32                    | 17                         |

a) Isolated Yields. b) Determined by chiral HPLC analysis.

#### 3.1.4 Acid additives in acid switchable trifunctional organocatalysis

In our group's initial report on trifunctional organocatalysts for the *aza*-MBH reaction, we demonstrated that an acid additive was pivotal for rate-coupled asymmetric catalysis. A small acid screen for the *aza*-MBH reaction with the prototype trifunctional organocatalyst **TF-1** was reported (Table 3.3)<sup>41</sup> The highest rate and enantioselectivity for the model *aza*-MBH reaction of **NTs-Im-1** and **MVK** was observed with benzoic acid (Conversion: >95%, *ee*: 92%,

Table 3.3, Entry 3). Rate acceleration was observed for acetic and phosphoric acid (Table 3.3, Entry 2 and 5); however, the sense of the asymmetric induction was inverted. A bulkier acid additive, such as 2-naphthoic acid, lowered the enantioselectivity to 75% (Table 3.3, Entry 10). No conversion was observed for strong acid additives such as 3,5-dinitrobenzoic acid (Table 3.3, Entry 7) or 3,5-dimethoxybenzoic acid (Table 3.3, Entry 8).

**Table 3.3.** Effect of acid additives on trifunctional organocatalysis.

| Entry | Additive   | Time/ h | Conversion/ % <sup>a</sup> | ee/ % <sup>b</sup> |
|-------|--|---------|----------------------------|--------------------|
| 1     | –  | 3       | 10                         | <i>rac</i>         |
| 2     | Acetic acid  | 3       | 20                         | –60 <sup>c</sup>   |
| 3     | BzOH   | 3       | >95                        | 92                 |
| 4     | <i>p</i> -F-C <sub>6</sub> H <sub>4</sub> CO <sub>2</sub> H                                | 5.5     | 57                         | 77                 |
| 5     | Phosphoric acid (H <sub>3</sub> PO <sub>4</sub> )  | 2       | 31                         | –28 <sup>c</sup>   |
| 6     | <i>o</i> -F-C <sub>6</sub> H <sub>4</sub> CO <sub>2</sub> H                                | 3       | 7                          | n.d.               |
| 7     | <i>m</i> -(NO <sub>2</sub> ) <sub>2</sub> -C <sub>6</sub> H <sub>3</sub> CO <sub>2</sub> H | 3.5     | <5                         | n.d.               |
| 8     | <i>m</i> -(MeO) <sub>2</sub> -C <sub>6</sub> H <sub>3</sub> CO <sub>2</sub> H              | 3.5     | <5                         | n.d.               |
| 9     | 1-naphthoic acid   | 15      | 92                         | 72                 |
| 10    | 2-naphthoic acid   | 15      | >95                        | 75                 |

a) Determined by <sup>1</sup>H NMR spectroscopy. b) Determined by chiral HPLC analysis. c) opposite enantiomer observed.

As outlined in Chapter 2, the addition of benzoic acid leads to the formation of a new ground state intermediate PBK that is an unusual ion pair with the conjugate base benzoate constrained by amine Bronsted base and phosphonium centre to maintain perpetual proton shuttling between the tautomeric forms of the PBK. This structural model for the first time suggests that dynamic proton motion is important for catalytic activation and also opens the next set of questions on how the benzoic acid additive may control asymmetric induction along with the rate promotion.

The first question is whether there is some generality to this proficiency control. This question can be answered by examining the switch-on effects of differently substituted benzoic acids and other acids to establish a structure-reactivity relationship (SRR) for identifying contributing factors. The next question is then on how the trifunctional catalysts with different internal Brønsted acidities, due to substitution on the phenol ring, respond to the acid additive to identify other contributing factors underlying PBK activation for rate enhancement. This question can be answered by experimentally assessing the acidity of the  $\alpha$ C-H of the PBK. The third and final question will be on how the carbon-carbon formation and proton-transfer-elimination step respond to the acid additive for asymmetric induction. This is the most difficult question because the reactive intermediate after carbon-carbon bond formation cannot be readily observed for structural characterisation. Indirectly, some insight may be derived by using various imine substrates to probe the final steps (C–C bond formation and proton transfer) of this reaction.

### 3.1.5 Specific aims

The effect of benzoic acid on C–C bond formation and proton transfer will be investigated in this chapter using a combination of kinetics, deuterium incorporation studies and reaction screening. The specific aims of this chapter are:

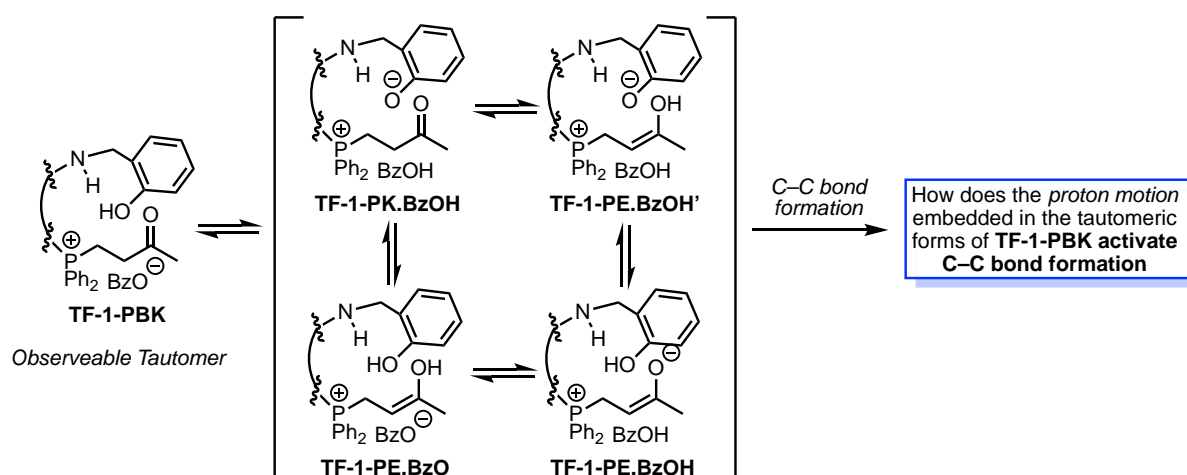
- Establishing a structure reactivity relationship (SRR) for various benzoic acid-type and other additives on catalytic proficiency



- Measuring the relative efficiencies of acid activation for various bifunctional and trifunctional catalysts
- Determining the response profile to the acid additive for a few selected substrates.

### 3.2 Results and Discussion

In this chapter, the cooperativity between the benzoate conjugate base and the phosphonium ketone is investigated using a combination of various acid additives, deuterium incorporation kinetics and different imine substrates. This is intended to validate the structural model for PBK activation and provide some understanding as to how C–C bond formation and proton transfer elimination may be facilitated by the acid additive (Scheme 3.7). The C–C bond formation and proton transfer are nominally presented as two discrete steps; in the course of this chapter, it will be shown that the C–C bond formation and proton transfer are concerted in the case of proficient trifunctional catalysis.

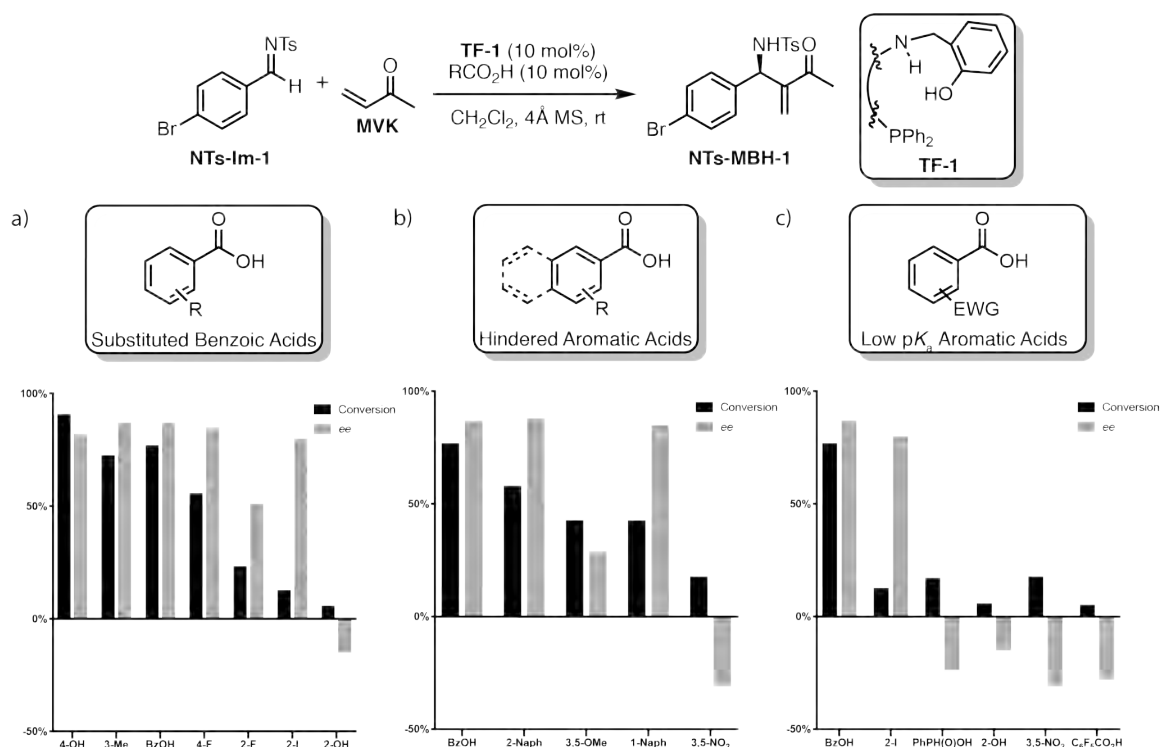


**Scheme 3.7.** Tautomeric forms of TF-1-PBK activate C–C bond formation.

#### 3.2.1 Benzoic acid protonation state is critical for different stages of the reaction

The initial report on the trifunctional system detailed a limited acid screen.<sup>41</sup> In light of this, acids were screened covering three broad and overlapping groups to construct a SRR; 1)

substituted benzoic acids (Figure 3.1a), 2) sterically demanding acids (Figure 3.1b), and 3) low  $pK_a$  aromatic acids (Figure 3.1c). Substituted benzoic acids with electron withdrawing (Br, I, F,  $-\text{NO}_2$ ) and donating (Me,  $-\text{OH}$ ,  $-\text{OMe}$ ) substituents were screened with a model substrate for the *aza*-MBH reaction between **NT-Im-1** and MVK, and the conversion and enantioselectivity were determined after 3 hours (Table 3.4).



**Figure 3.1.** Comparison of the acid additive on rate and *ee* of the **TF-1** catalysed *aza*-MBH reaction with a) substituted benzoic acids, b) hindered aromatic acids and 3) low  $pK_a$  aromatic acids.

**Table 3.4.** Effect of the acid additive on catalytic proficiency.

| Entry | Acid   | pKa  | Conversion <sup>a</sup> /% | Hydrolysis <sup>a,b</sup> /% | ee <sup>c</sup> /% |
|-------|--|------|----------------------------|------------------------------|--------------------|
| 1     | 4-OH-C <sub>6</sub> H <sub>4</sub> CO <sub>2</sub> H                                 | 4.55 | 91                         | 6                            | 81                 |
| 2     | 3-Me-C <sub>6</sub> H <sub>4</sub> CO <sub>2</sub> H                                 | 4.24 | 73                         | 4                            | 87                 |
| 3     | BzOH   | 4.20 | 77                         | 16                           | 87                 |
| 4     | 2-naphthoic acid   | 4.16 | 58                         | 4                            | 88                 |
| 5     | 4-F-C <sub>6</sub> H <sub>4</sub> CO <sub>2</sub> H                                  | 4.15 | 56                         | 10                           | 85                 |
| 6     | 3,5-(OMe) <sub>2</sub> -C <sub>6</sub> H <sub>3</sub> CO <sub>2</sub> H              | 3.97 | 43                         | 8                            | 29                 |
| 7     | 1-naphthoic acid   | 3.67 | 43                         | 9                            | 85                 |
| 8     | 2-F-C <sub>6</sub> H <sub>4</sub> CO <sub>2</sub> H                                  | 3.57 | 24                         | 2                            | 51                 |
| 9     | 2-I-C <sub>6</sub> H <sub>4</sub> CO <sub>2</sub> H                                  | 2.96 | 13                         | 1                            | 80                 |
| 10    | Phenylphosphinic acid  | 2.92 | 17                         | 3                            | -24                |
| 11    | 2-OH-C <sub>6</sub> H <sub>4</sub> CO <sub>2</sub> H                                 | 2.77 | 6                          | 1                            | -14                |
| 12    | 3,5-(NO <sub>2</sub> ) <sub>2</sub> -C <sub>6</sub> H <sub>3</sub> CO <sub>2</sub> H | 2.67 | 18                         | 9                            | -31                |
| 13    | C <sub>6</sub> F <sub>5</sub> -CO <sub>2</sub> H                                     | 2.05 | 5                          | 2                            | -28                |

a) Determined by <sup>1</sup>H NMR spectroscopy. b) Hydrolysis of **NTs-Im-1** to the corresponding aldehyde c) Determined by chiral HPLC analysis.

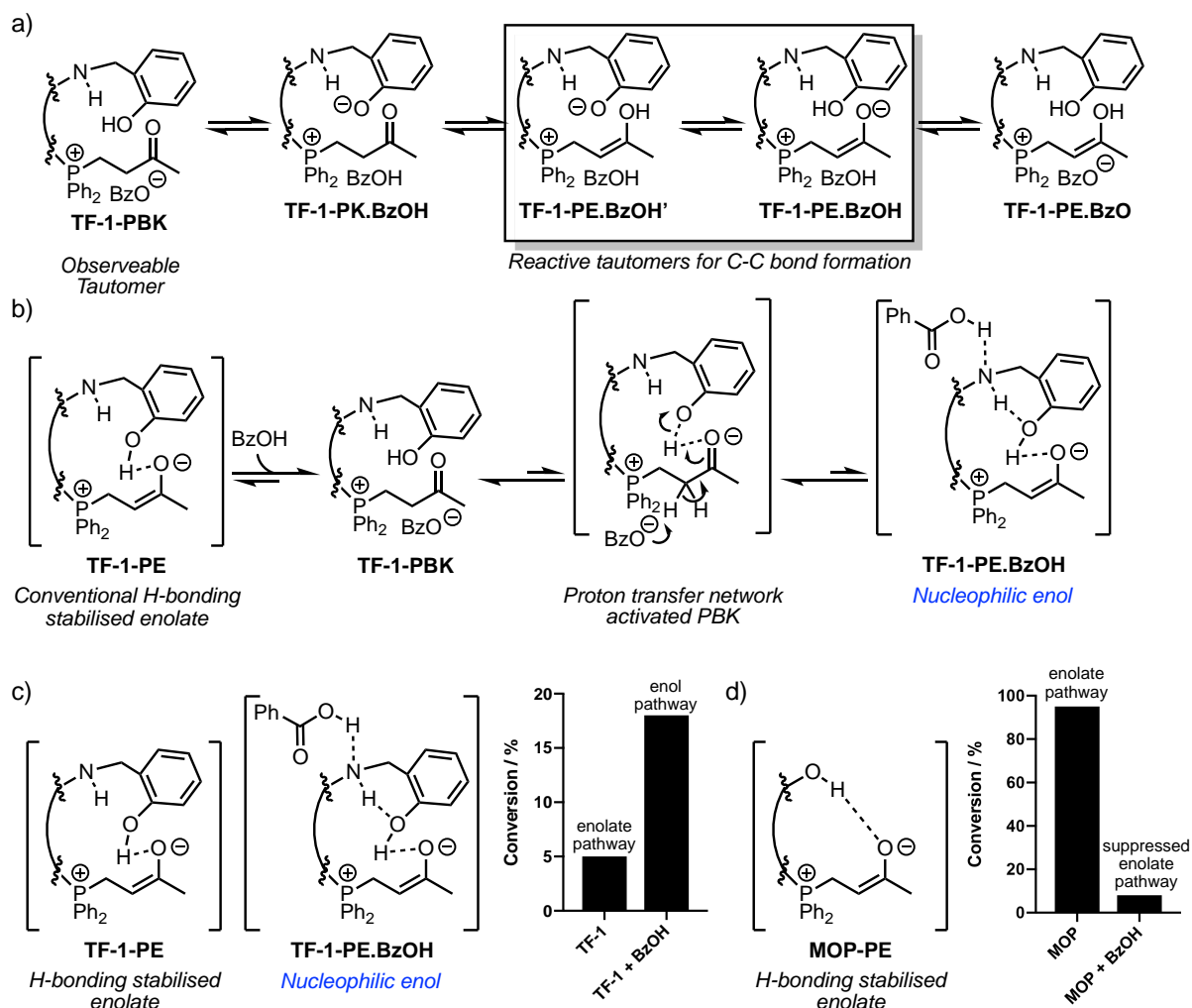
Different catalytic profiles were observed for the three different groups of acids. Group 1 acids (substituted benzoic acids, Figure 3.1a) demonstrate a general trend. As the acidity increased, the rate of reaction decreased, while enantioselectivity was generally high for less acidic additives. Complete conversion was achieved with 4-hydroxybenzoic acid (Table 3.4, Entry 1) whereas only 13% conversion was observed for 2-iodobenzoic acid (Table 3.4, Entry 9) after 3 hours. For bulkier acids (Group 2, Figure 3.1b), the catalytic outcomes seem more complex. The conversion levels for naphthoic acids (Table 3.4, Entries 4 and 7) were consistent with their pK<sub>a</sub> values (lower pK<sub>a</sub>, lower conversion) with the ee values unaffected by the size of the acid. The case of 3,5-dimethoxybenzoic acid (Table 3.4, Entry 6) is interesting as the level of asymmetric induction for this additive is significantly lower than acids with comparable pK<sub>a</sub>, suggesting that the size of the substituents may interfere with the

positioning of the acid which adversely affects both the rate and enantioselectivity. Finally, Group 3 acids (low  $pK_a$ ) are characterised by reduced rates of reaction and low enantioselectivity (Table 3.4, Entries 10–13). The conjugate base is insufficiently basic to deprotonate the PBK preventing tautomerisation; as a result, the conversion is poor.

The acid screening suggests that the acid additive was not limited to activation of the phosphonium benzoate ketone but has a role in the stereodetermining step. For acids with nominally higher  $pK_a$  values, the *ee* of the reaction was consistently higher (80% – 87% *ee*), although there were two exceptions (3,5-OMe= 29% *ee*, Table 3.4, Entry 6; 2-F= 51% *ee*, Table 3.4, Entry 8) possibly due to steric or stereoelectronic reasons. No deleterious effects were observed for 3-methylbenzoic acid (87% *ee*, Table 3.4, Entry 2). The proton transfer elimination is involved in the stereodetermining step; consequently, the steric bulk of 3,5-dimethoxybenzoic acid may alter the orientation of the acid in the stereodetermining step. For stronger acids, the degree of asymmetric induction is small (-15– -31 % *ee*), and the configuration of the MBH adduct is inverted. Essentially, as the ability of the conjugate base of the acid for transferring protons is more and more diminished, the effect of the acid additive on the catalysis becomes less prominent. The reaction then proceeds through primarily via the less organised enolate pathway (e.g. comparable to the case of catalysis without the acid additive) that is slow and low in enantioselectivity.

In summary, benzoic acid and benzoate are involved in different elementary steps during the aza-MBH reaction. The inverse relationship between additive acidity and reaction rate is consistent with the structural model that the benzoate base can deprotonate the  $\alpha$ C-H of **TF-1-PBK**, yielding a *nucleophilic enol* **TF-1-PE.BzOH**. This enol intermediate differs from **TF-1-PE**

(e.g. in the case of catalysis without an acid additive that forms the standard enolate via nucleophilic activation rather than base activation) in that **TF-1-PE.BzOH** is primed for proton transfer, while a standard enolate in typically bifunctional catalysis is stabilised by H-bonding (Scheme 3.8a). Rapid proton motion in **TF-1-PE.BzOH** is mediated by the phenol with concurrent deprotonation by benzoate (Scheme 3.8b). *This novel proton transfer network, connected by the acid and base motifs to establish a low barrier proton transfer pathway (TF-1-PE.BzOH), rather than a conventional rigid H-bonding framework, for enolate stabilisation.* This perpetual proton transfer network is essential in activating the ground state **TF-1-PBK** and primes the following electron exchange in the C–C bond formation via the enol intermediate (**TF-1-PE.BzOH**) that is inaccessible for bifunctional catalysts (Scheme 3.8c,d).<sup>42</sup>

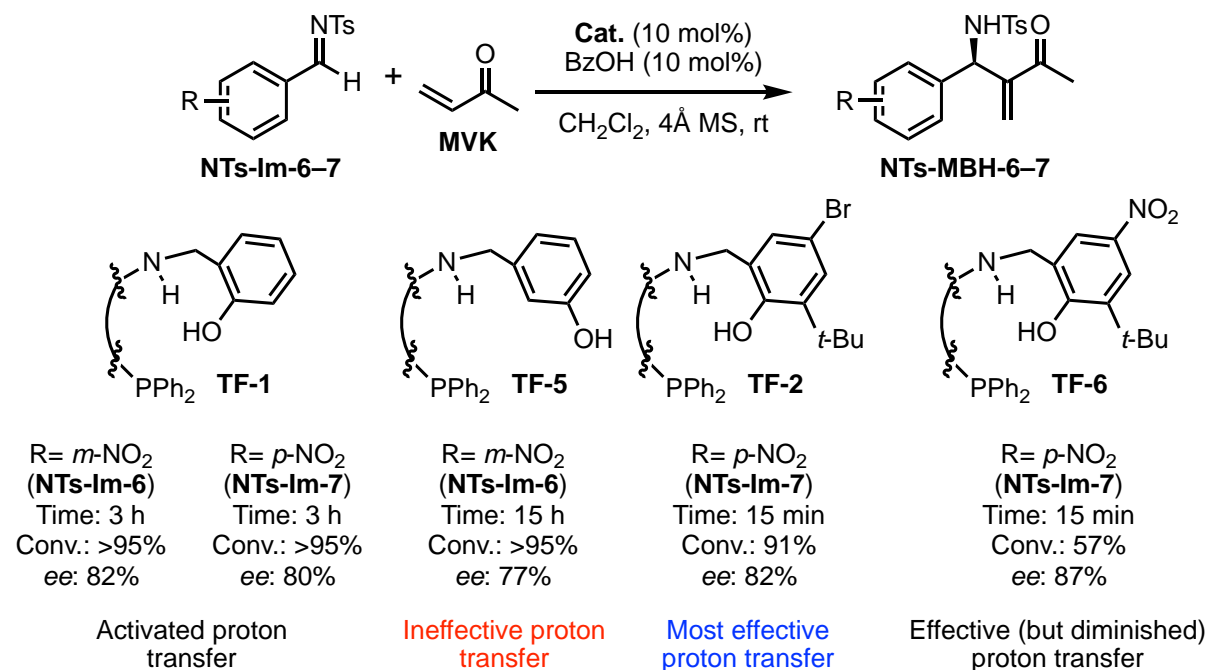


**Scheme 3.8.** a) Tautomers of **TF-1-PBK** highlighting the key tautomers for C-C bond formation. b) **TF-1-PE** and **TF-1-PBK** are in equilibrium in the presence of BzOH, but tautomersation yields the nucleophilic enol **TF-1-PE.BzOH**. c) The trifunctional enol and enolate pathways are distinct. d) BzOH does not activate the enol pathway causing rate suppression for **MOP**.

### 3.2.2 Proton abstraction: Establishing the proton transfer network

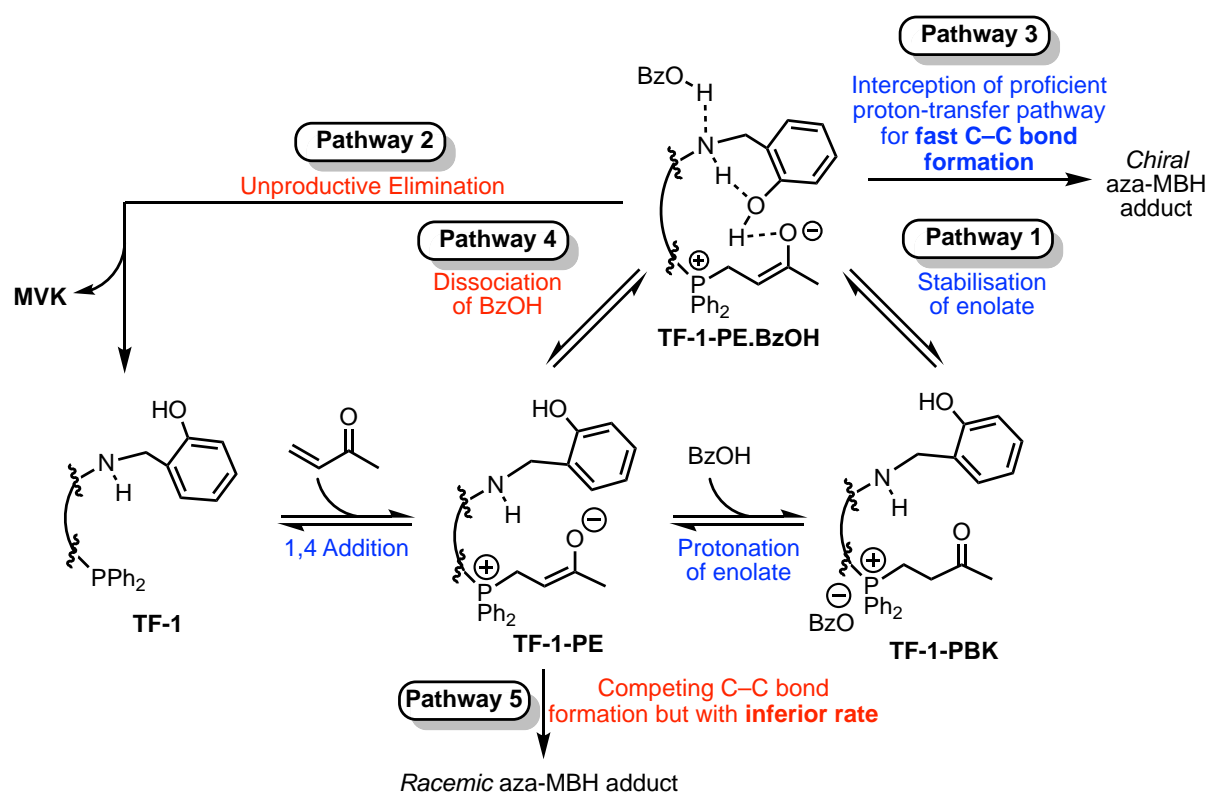
Benzoic acid does not confer catalytic proficiency without cooperativity from the internal Brønsted acid motif (phenol) on the trifunctional organocatalyst.<sup>43</sup> As the phenol becomes more acidic, the proficiency increases first and then becomes diminished. The substantial rate enhancement for **TF-2** (15 min vs 3 hours) is slightly diminished by increasing the phenol acidity further in **TF-6** (57% conversion at 15 min). Furthermore, there is a strict preference for the spatial position of the phenol for optimal rate elevation (Scheme 3.9). The Brønsted acid (phenol) in the 2-position (i.e. **TF-1**) is active with congruent rate elevation and

asymmetric induction through the **PBK** pathway. Moving the phenol to the 3-position (i.e. **TF-5**) sharply decreases the rate with a modest decrease in asymmetric induction. The position and acidity of the phenol are critical for an effective proton transfer pathway to emerge.<sup>41</sup>



**Scheme 3.9.** The phenol position and acidity influences proficiency.

In Chapter 2, no correlation was found between catalytic proficiency and the proportion of the PBK formation relative to the starting phosphine catalyst upon benzoic acid addition, suggesting that the activation of this new ground state is kinetically based. Following deprotonation of the  $\alpha$ C-H of **TF-1-PBK**, the enol **TF-1-PE.BzOH** can proceed down one of four pathways: 1) tautomerisation back to the PBK, 2) retro-Michael addition for recycling catalyst without the proton transfer, 3) C-C bond formation and 4) dissociation of BzOH to **TF-1-PE** (Scheme 3.10).



**Scheme 3.10.** Pathways accessible to **TF-1-PE.BzOH**.

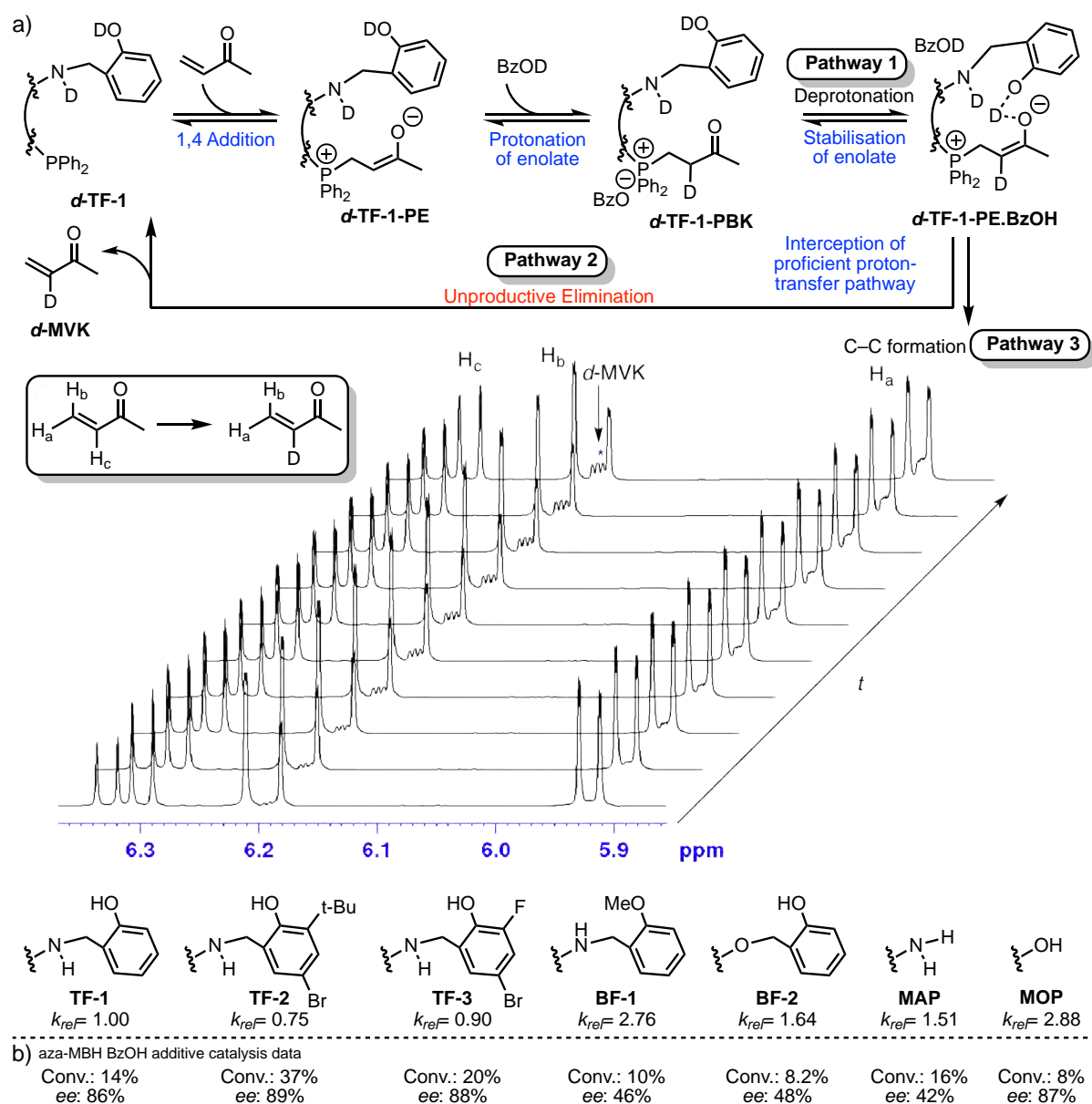
In the absence of the imine substrate following deprotonation of  $\alpha$ -C-H, there is competition between pathway 1 and pathway 2; the equilibrium between these two dictates the proficiency of the PBK intermediate for catalysis. The tautomers of **TF-1-PE.BzOH** are partitioned into two groups; 1) the nucleophilic enol (shown in its observable keto form **TF-1-PBK**, Scheme 3.10) in which benzoic acid is bound closely to facilitate the proton transfer network and 2) the unstabilised enolate **TF-1-PE** in which benzoic acid is loosely held or freely dissociates from the complex (pathway 4). The unstabilised enolate **TF-1-PE** can also form a C-C bond (pathway 5) but this pathway is significantly slower. These dynamic structures rapidly interconvert until the arrival of the substrate to form a C-C bond (pathway 3).

The phenol has a critical role in forming the proton transfer network by donating a hydrogen bond to the enolate **TF-1-PE**. The acidity of the phenol is not only crucial to the stability of the



enolate but also the tautomerisation rate of the enol back to **TF-1-PBK**. If the enolate is not stabilised upon  $\alpha$ C-H deprotonation by the conjugate base benzoate, then the unproductive retro-Michael elimination pathway (Pathway 2) leading to **TF-1** may become dominant. Active proton transfer between phenol Brønsted acid and enolate would diminish the impact of the competing retro-Michael elimination (Pathway 1). Therefore, assessing the relative extent of the retro-Michael elimination would provide some indication of the robustness of the proton transfer network contained within the PBK.

The rate of the retro-Michael elimination was measured by  $^1\text{H}$  NMR (600 MHz,  $\text{CD}_2\text{Cl}_2$ , 293 K) using a panel of *deuterated* trifunctional (***d*<sub>2</sub>-TF-1**, ***d*<sub>2</sub>-TF-2**, ***d*<sub>2</sub>-TF-3**) and bifunctional organocatalysts (***d*-BF-1**, ***d*-BF-2**, ***d*<sub>2</sub>-MAP**, ***d*-MOP**), *deuterated* benzoic acid (BzOD) and MVK. For the prototype trifunctional organocatalyst ***d*-TF-1**, in the presence of BzOD, protonation of **TF-1-PE** proceeds with deuteration at the  $\alpha$ C to yield ***d*-TF-1-PBK**. Retro-Michael elimination will then proceed with the formation of ***d*-MVK** that can be measured as a decrease in the integral of the substituted vinylic proton ( $\text{H}_\text{C}$ : 6.28–6.35 ppm) relative to the terminal protons ( $\text{H}_\text{B}$ : 6.20 ppm and  $\text{H}_\text{A}$ : 5.92 ppm) (Figure 3.2a). Therefore, ratios of deuterium incorporation into the  $\alpha$ C-H of MVK, relative to that of **TF-1**, in a model reaction catalysed by trifunctional and bifunctional organocatalysts were measured (Figure 3.2a). Further details regarding deuteration and optimisation of  $^1\text{H}$  NMR acquisition can be found in Section 3.3.2 Deuteration Studies).



**Figure 3.2.** a) Formation of *d*-MVK and relative rate constants for deuterium incorporation for a panel of catalysts. b) Catalytic profiles for aza-MBH reaction.

The proton transfer network is accelerated by more acidic phenols, and the rate of retro-Michael elimination decreases for more proficient catalysts. Substituted phenols with electron withdrawing groups, such as **TF-2** ( $k_{rel} = 0.75$ ) and **TF-3** ( $k_{rel} = 0.90$ ), presented slower rates of retro-Michael elimination than the prototype **TF-1** ( $k_{rel} = 1.00$ ). This trend is correlated to the catalytic proficiency of the trifunctional organocatalysts (Figure 3.2b). The deuterium incorporation profile suggests that the PBK activation by proton transfer requires

cooperativity between the phenol Brønsted acid and BzOH. As the proton transfer network becomes more competitive (i.e. **TF-2**>**TF-3**>**TF-1**), the measured rate of the retro-Michael addition (deuterium incorporation) decreases. As such, the rate of retro-Michel addition is slower for more proficient trifunctional catalysts.

For bifunctional controls, **BF-2** ( $k_{rel}$ = 1.64) and **BF-1** ( $k_{rel}$ = 2.76), the retro-Michael elimination pathway is, as expected, more dominant than that for **TF-1** ( $k_{rel}$ = 1.00) or the other trifunctional organocatalysts. The methoxy control **BF-1** is unable to form an H-bond to facilitate the proton transfer, and the lack of the amino group (**BF-2**) diminishes benzoic acid association. Both the Brønsted acid (phenol) and the Brønsted base (NH) are therefore required for more active proton transfer, and the lack of either one leads to more prominent elimination of MVK.

For bifunctional catalysts **MOP** ( $k_{rel}$ = 2.88) and **MAP** ( $k_{rel}$ =1.51), the retro-Michael elimination pathway is also more dominant than that for the trifunctional organocatalysts. Rapid elimination for the case of **MOP** may be the result of an unfavourable partition between non-H-bonded and H-bonded geometries. The high rate of elimination suggests non-hydrogen bonded geometry is favoured, contributing to the rapid elimination of MVK from **MOP-PBK** to yield the free phosphine **MOP**. Furthermore, the hydrogen bonding from the **MOP** phenol can stabilise the **MOP** enolate but is not able to promote cooperative proton transfer for the **PBK**. The mode of proton transfer activation is ablated for this catalyst, rendering this **PBK** inactive and parasitic. **MAP**, on the other hand, can form a Brønsted acid-base complex. Dissociation of benzoic acid is diminished, which promotes protonation and tautomerisation back to the **PBK** and reduces the extent of the retro-Michael elimination.

In summary, the deuterium incorporation investigation reveals cooperativity in activating proton transfer between the phenol Brønsted acid, amine Brønsted base, and BzOH, which is consistent with the proton shuttle ion pair structural model. The Brønsted amine provides a binding site for benzoic acid following deprotonation of the phosphonium butanone. This binding site is destabilised for sterically demanding acids. Protonation of the amine by benzoic acid can initiate proton transfer from the amine to phenol and phenol to enolate. The spatial organisation of the different motifs enables this proton transfer network to function. Thus, the novel characteristics of the trifunctional organocatalyst are a result of an active proton transfer network enabled by the conformational geometry, dynamics and spatial organisation of the various motifs that gives rise to the nucleophilic enol (**TF-1-PE.BzOH**).

### **3.2.3 Conjugative catalysis is achieved with recognition of the cognate proton transfer pathway by the substrate**

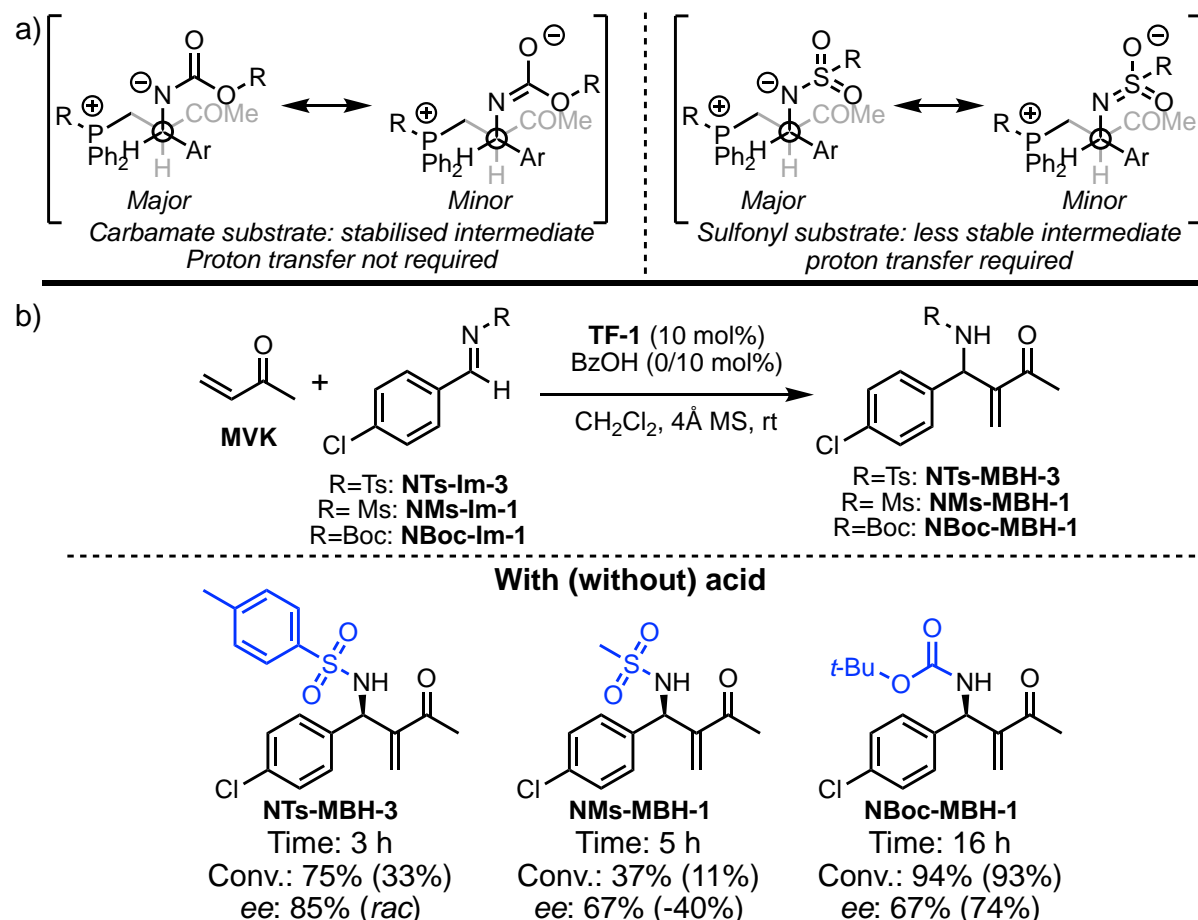
The next set of questions relate to how the activation of the new ground state **PBK** by a cooperative proton transfer network, between the trifunctional catalyst, the enone substrate MVK, and the additive BzOH, configures into the rate and stereo-determining steps (e.g. C-C bond formation and proton-transfer-elimination). Our earlier demonstration that the aldol addition was the rate determining step<sup>44</sup> was confirmed with a large inverse secondary KIE observed for  $\alpha$ -deuterated benzaldimine ( $k_H/k_D = 0.80$ ) (See Section 3.3.3 Measuring secondary kinetic isotope effect for more details). Rate acceleration with  **$\alpha$ -D-NTs-MBH-1** confirms that in the rate-determining-step the imine substrate changes geometry from  $sp^2$  to  $sp^3$  (i.e. the Aldol addition). How the proton transfer network is established after the carbon-carbon bond formation to confer the final proton-transfer-elimination event is likely to be

dependent on the substituent on the aldimine that will need to help stabilise the developing negative charge on the imine nitrogen and also coordinate the next proton transfer events with the nucleophilic enol (Scheme 3.11a).

A test aza-MBH reaction was examined using **TF-1**, MVK, and BzOH in the presence of either a carbaldimine (**NBoc-Im-1**) or sulfonyl aldimine (**NTs-Im-3** and **NMs-Im-1**) substrate as the electrophile (Scheme 3.11b). Sulfonyl or carbamoyl substituents have different charge stabilisation capacity for reacting with the nucleophilic enol.<sup>45</sup> For example, during C–C bond formation, the carbamoyl substituent of the carbaldimine has a higher capacity to stabilise the developing negative charge than the sulfonyl-substituted imine (Scheme 3.11a). For the former the intermediate is stable and proton transfer is not required, while for sulfonyl-substituted substrates the intermediate is less stable and proton transfer is required to ratify the electron exchange of the Aldol-type addition.

First and foremost, BzOH elicited distinct catalysis switching profiles for **NBoc-Im-1** and sulfonylaldimines (**NTs-Im-3** and **NMs-Im-1**). The response to acid activation for the trifunctional organocatalyst **TF-1** was only observed when the imine substrate possessed a sulfonyl substituent (**NTs-Im-3** and **NMs-Im-1**). The **PBK**-mediated pathway via the nucleophilic enol was 3-fold faster than the conventional enolate pathway for imine **NMs-Im-1**, and the sense of the asymmetric induction switched from -40% *ee* without acid to 67% *ee* with BzOH. **NMs-Im-1**, similar to the tosyl-substituted imine **NTs-Im-3**, requires BzOH for enhanced catalytic proficiency. However, the decreased electrophilicity of the mesyl substrate decreases the rate of reaction relative to that of the tosyl substrate. On the contrary, the catalysis with the carbamoyl-substituted imine **NBoc-Im-1** does not respond to the acid

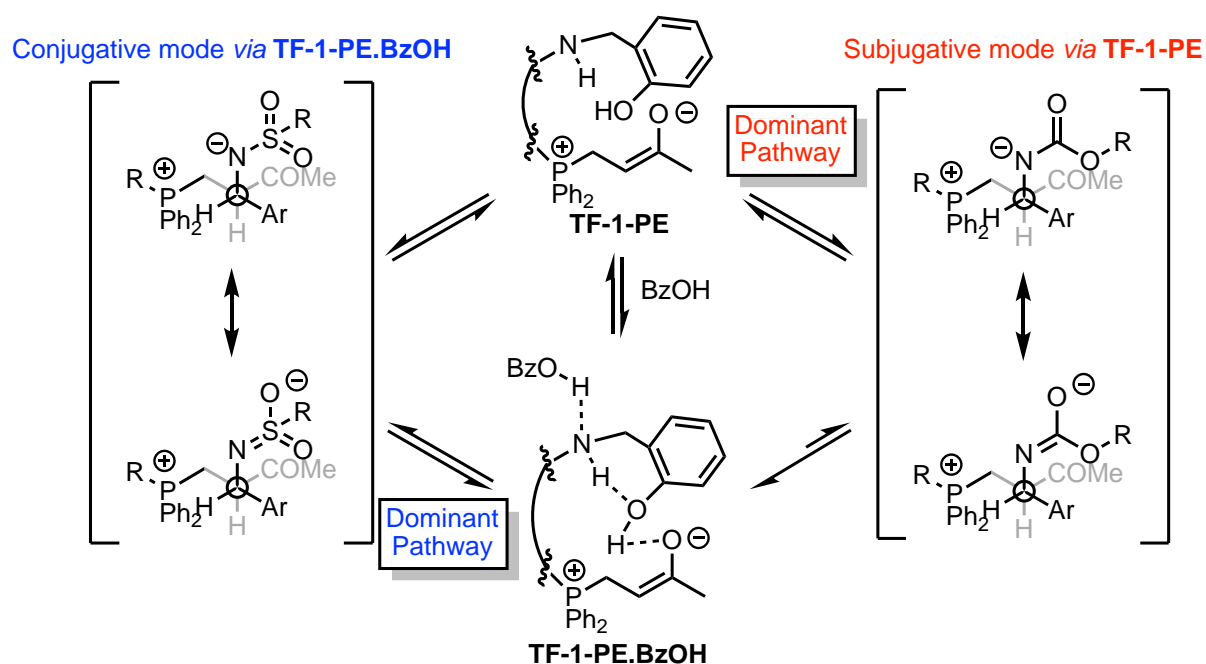
additive. The MBH product **NBoc-MBH-1** are formed through the conventional enolate mechanism and do not require acid additives to initiate proficiency.



**Scheme 3.11.** a) Role of the protecting group in the stabilisation of the aldol adduct. b) Catalysis data for different protecting groups on the substrate.

The enolate (**TF-1-PE**) and nucleophilic enol (**TF-1-PE.BzOH**) give rise to two distinct catalytic modes, subjugative and conjugative (Scheme 3.12). The conventional enolate mechanism is in the *subjugative mode* wherein the trifunctional catalyst is the dominant contributor to rate and enantioselectivity. Carboaldimine (**N-Boc-Im-1**) adopts the subjugative mode via **TF-1-PE** for C–C bond formation (Scheme 3.12, red pathway). The aldol adduct with a carbamoyl group stabilises the aldolate intermediate, negating the need for a rapid proton transfer to occur. On the contrary, tosyl substrates adopt the *conjugative mode* via the nucleophilic enol

(Scheme 3.12, blue pathway). Unlike subjugative catalysis, in the conjugative mode of catalysis, catalyst (**TF-1**) and cofactor (BzOH) cooperate to establish the cognate proton transfer pathway for proficient catalysis. The trifunctional catalyst alone cannot prescribe the conjugative mode, rather- it provides the chiral blueprint to establish a proton network that emerges, in the presence of a cognate imine substrate, to enable C–C bond formation. The nucleophilic enol is only operational if the substrate is capable of recognising the nucleophilic enol's proton motion and extend the proton-transfer network during the C–C bond formation. Critically, the conjugative mode couples the C–C formation to proton transfer, allowing concurrent enhancement of rate and asymmetric induction.

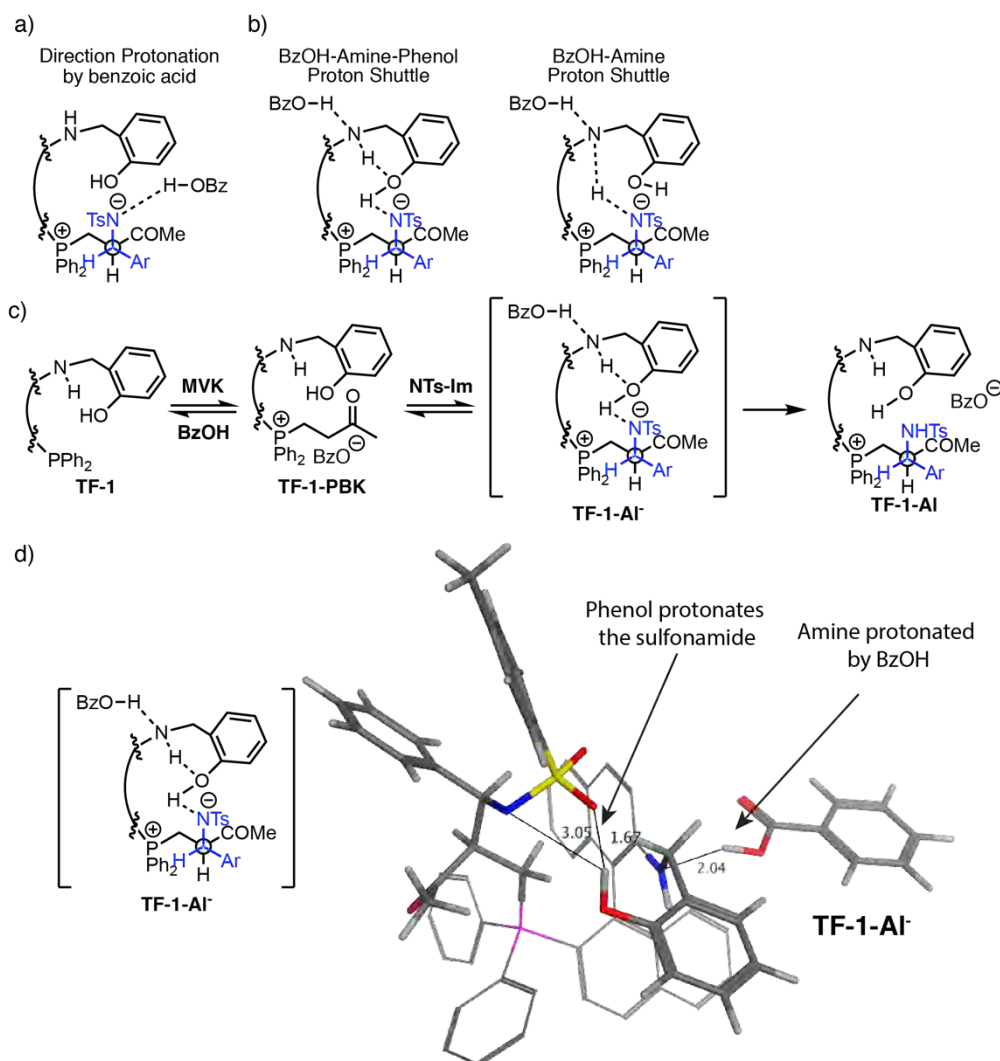


**Scheme 3.12.** Substrate-directed catalytic emergence for **TF-1-PE** and **TF-1-PE.BzOH**.

Two possible proton transfer mechanisms in the conjugative mode to the aldolate (**TF-1-AI'**) are possible; 1) direct protonation of the sulfonamide by benzoic acid (Figure 3.3a) and 2) cooperative protonation of the sulfonamide with a catalyst-acid complex (Figure 3.3b). Retro-Michael elimination and deuterium incorporation studies (Section 3.2.2 above) supports

conjugative catalysis mediated by the acid-catalyst complex with phenol assisting in proton transfer to form the stable C–C bond and yield **TF-1-AI** (Figure 3.3c). The conformation of **TF-1-AI** in the TS for proton transfer to **TF-1-AI** adopts the proton motion facilitating C–C bond formation (Figure 3.3d). Asymmetric induction is lower for sterically demanding acids, such as 3,5-dimethoxybenzoic acid or *ortho*-substituted acid. Additionally, phenol-bearing catalysts yield more proficient catalysis suggesting that the BzOH-amine-phenol proton shuttle is the major contributor. Cooperativity of chemical motifs activates the conjugative mode for proton transfer. The specificity of the conjugative mode (nucleophilic enol, protonation by the proton-transfer network) outcompetes the subjugative pathways (conventional enolate, direct protonation by benzoic acid) to enable rate-coupled asymmetric catalysis.





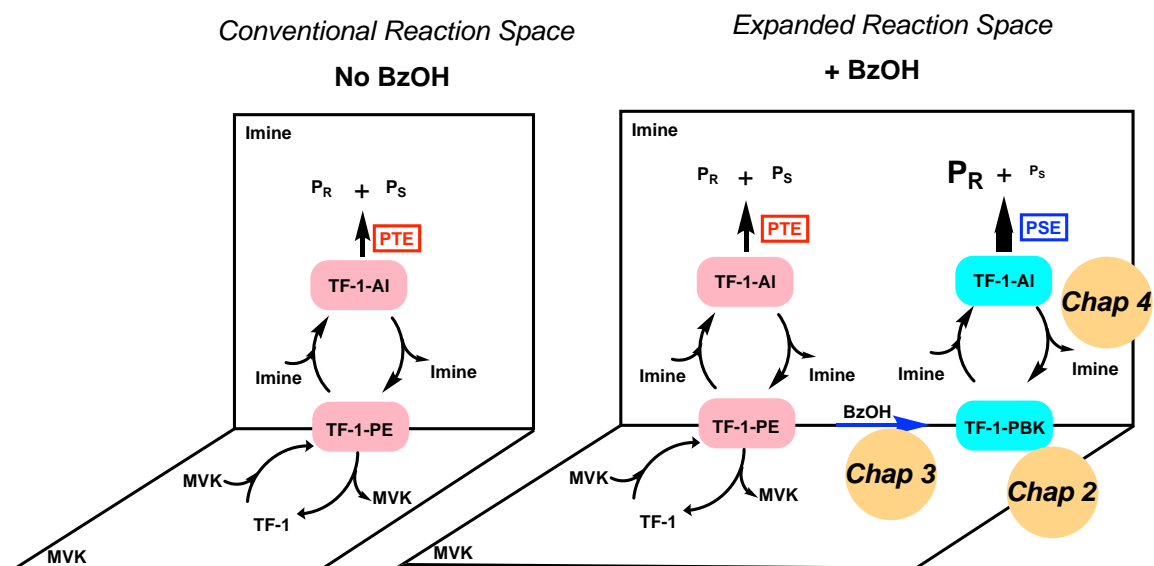
**Figure 3.3.** Possible proton transfer pathways. a) Direct Protonation by benzoic acid. b) Cooperative protonation mediated by BzOH-catalyst complex. c) Formation of the **TF-1-Al<sup>-</sup>** intermediate. d) The structural model for **TF-1-Al<sup>-</sup>** show the conformation amenable to proton transfer.

### 3.2.4 Conclusion

In this chapter, a new mechanism of conjugative catalysis enabled by emergent proton transfer between the initial catalyst (**TF-1**), additive (BzOH), and substrates (**MVK** and sulfonylimine) was outlined in a model aza-MBH reaction. The trifunctional catalyst alone is not able to prescribe this conjugative catalysis, as the proton transfer network is organised by the acid additive and extendable only by a cognate substrate for the key carbon-carbon bond formation to proceed and subsequent proton-transfer-elimination step to ensue. In the

case of sulfonyl imines, conjugative catalysis outcompetes the subjugative pathway (enolate driven, based on H-bonding) via organised proton motion.

The structural model from Chapter 2 is consistent with the acid additive effects examined in this chapter. It appears that the conjugative base of the additive BzOH is integral to all steps, with its constraint motion allowing a proton transfer network to persist over the entire reaction coordinate. The BzOH additive effectively expands the aza-MBH reaction paradigm in which both the conjugative and subjugative pathways are in equilibrium. Cooperativity between the substrate and the counterion are required to select for the proficient conjugative catalysis and shift the mechanism to the conjugative mode in the expanded reaction space. In the next chapter, the characteristics of the imine substrates will be examined in further details to assessing the scope of limits of this conjugative catalysis (Scheme 3.13).



**Scheme 3.13.** BzOH activates a new mechanism for the trifunctional organocatalysed aza-MBH reaction.

### 3.3 Experimental

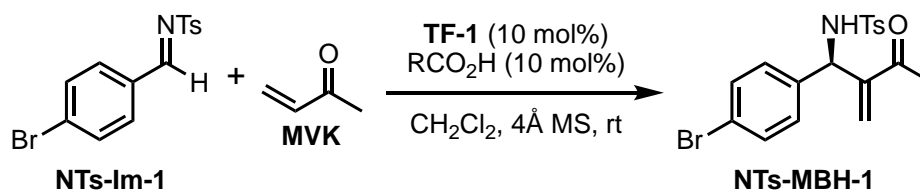
#### 3.3.1 Material and methods

Toluene and THF were distilled from sodium/benzophenone immediately before use. All other reagents were purchased from Sigma-Aldrich Castle Hill. Unless specified, all commercially available reagents were used without further purification. Dichloromethane was distilled from calcium hydride. All air and moisture sensitive reactions were performed under a nitrogen atmosphere. Reactions were magnetically stirred and monitored by thin-layer chromatography (TLC) using silica gel 60 F254 aluminium pre-coated plates from Merck (0.25 mm). Flash column chromatography was performed on silica gel (60 Å, 0.06–0.2 mm, 400 mesh from Scharlau).

All  $^1\text{H}$ ,  $^{13}\text{C}$  and 2D NMR experiments were performed on either a Bruker AVIIIHD 400 MHz NMR Spectrometer equipped with a BBFO SmartProbe (5mm) or DRX600 NMR spectrometer equipped with a TXI (5 mm) Cryoprobe. Chemical shifts were reported in ppm using residual  $\text{CHCl}_3$  ( $\delta_{\text{H}}$ ; 7.26 ppm,  $\delta_{\text{C}}$ ; 77.16 ppm) as an internal reference. All 2D NMR experiments were run with quadrature detection and a relaxation delay of 1–3 s. High power  $1\text{H}$   $\pi/2$  pulses were determined to be  $\sim 9.5$  ms, and  $^{13}\text{C}$  high power  $\pi/2$  pulse was 11.05 ms, and a low power pulse of 65 ms was used for GARP4 decoupling. Gradient pulses were delivered along the z-axis using a 100 step sine program. Heteronuclear single quantum coherence (HSQC) experiments were optimised for a  $^1J_{\text{CH}}$  coupling of 145 Hz and HMBC spectra for a coupling of 20 Hz, using 145 Hz to suppress  $^1J_{\text{CH}}$  couplings. HSQC experiments were performed using the hsqcetgpsi or hsqcedetgpsp.3 (phase-edited HSQC) pulse program, and HMBC experiments were performed using the hmbcgp1pndqf pulse program. HSQC spectra were processed ( $\pi/2$  shifted sine bell squared in both dimensions) phase sensitive and HMBC (sine squared in both dimensions) with magnitude calculation in F1.  $^{13}\text{C}$  spectra were acquired using the UDEFT

sequence. NOESY experiments were performed using the noesygpphys pulse program with a mixing time of 400 ms. All spectra were processed using Bruker TOPSPIN 3.5p17. Trifunctional organocatalyst were prepared following the literature procedure.<sup>41, 46-48</sup>

### 3.3.1 Acid screen

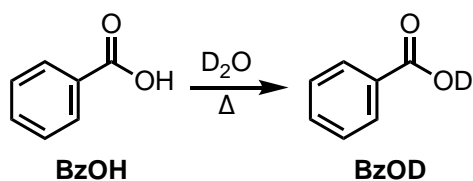


**Scheme 3E.1.** Acid screen for model aza-MBH between **NTs-Im-1** and **MVK** by **TF-1**.

**TF-1** (1.37 mg, 2.4  $\mu$ mol, 10 mol%) and acid (2.4  $\mu$ mol, 10 mol%) in anhydrous **CH<sub>2</sub>Cl<sub>2</sub>** was added to a flame-dried 2 mL vial charged with a stir bar and 4 Å MS. **NTs-Im-1** (8.28 mg, 24  $\mu$ mol) was added in **CH<sub>2</sub>Cl<sub>2</sub>** and the volatiles removed by nitrogen blow down. Anhydrous **CH<sub>2</sub>Cl<sub>2</sub>** (150  $\mu$ L) was added and the vials sonicated to ensure complete dissolution of the reagents. **MVK** (5.15 mg, 73  $\mu$ mol, 3 equiv) was added and the reaction stirred vigorously in a 25 °C sand bath for 3 hours. The volatiles were removed *in vacuo* and the crude material was analysed by <sup>1</sup>H NMR spectroscopy to determine conversion and chiral HPLC to determine enantioselectivity.

### 3.3.2 Deuteration Studies

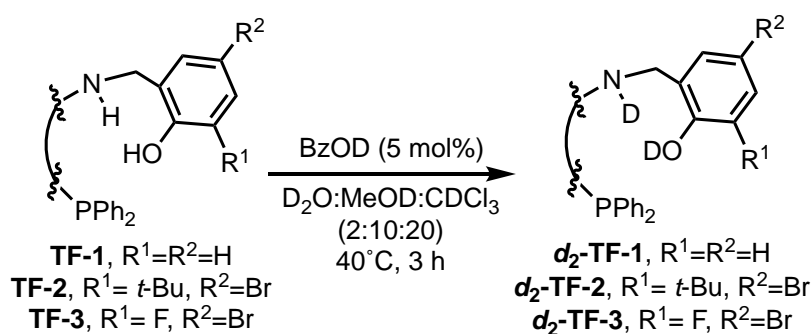
#### 3.3.2.1 Preparation of *d*-Benzoic acid (BzOD)



**Scheme 3E.2.** Deuteration of benzoic acid by D<sub>2</sub>O

Under an inert atmosphere, benzoic acid (500 mg) was recrystallised twice from D<sub>2</sub>O and dried extensively under high vacuum. *d*-Benzoic acid (450 mg) was stored in a desiccator under an inert atmosphere and used within two days of preparation.

#### 3.3.2.2 General Procedure for Deuteration of trifunctional organocatalysts



**Scheme 3E.3** Deuteration of trifunctional organocatalysts

Organocatalysts (18.0 μmol) was added to a flame dried 1.5 mL vial charged with a stir bar. Freshly prepared *d*-Benzoic acid (0.90 μmol, 5 mol%) was added in CDCl<sub>3</sub> (200 μL) and the vessel was purged six times with Argon. MeOD-*d*<sub>4</sub> (100 μL) and D<sub>2</sub>O (20 μL) were added and the mixture heated at 40 °C with stirring for 3 hours. After 3 hours the solvent was removed under reduced pressure at 50 °C. The residue was redissolved in CDCl<sub>3</sub> (100 μL) and the solvent removed under reduced pressure five times to remove residual MeOD-*d*<sub>4</sub> (100 μL) and D<sub>2</sub>O. This procedure yielded deuteration of the organocatalyst exchangeable protons of

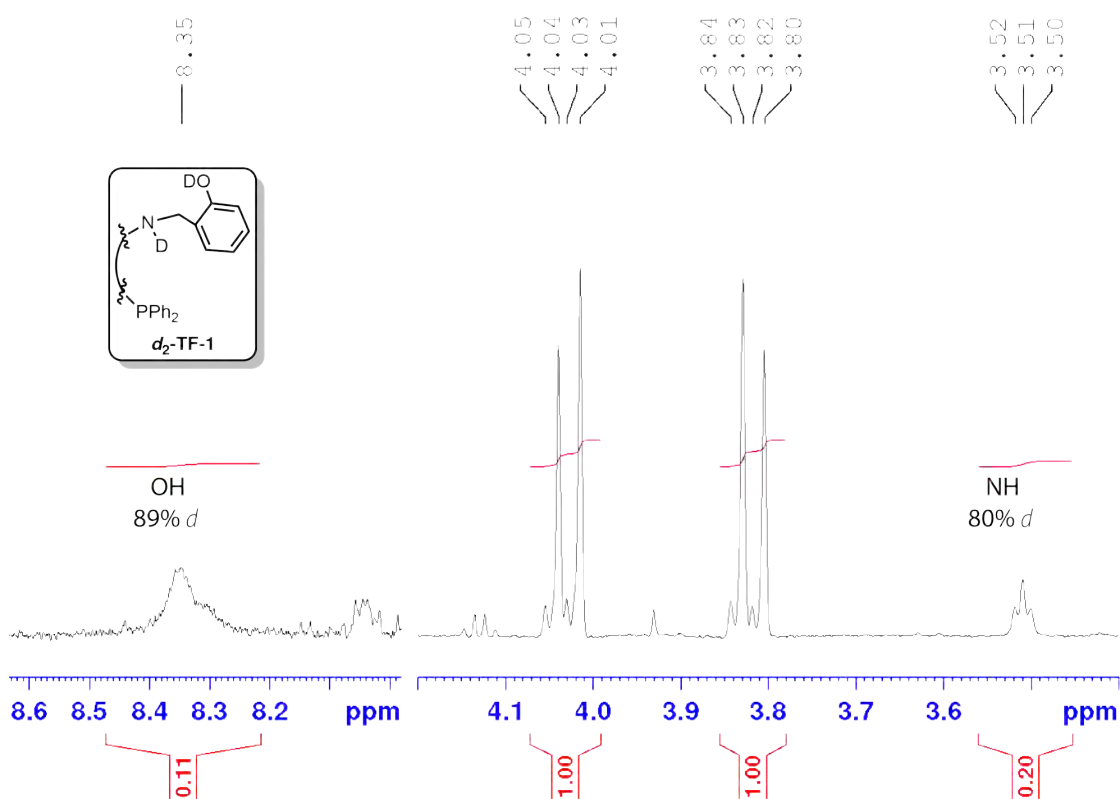
approximately 85% (deuteration of both OD and ND)(Table 3E.1 for full extent of deuteration).

The dry residue was handled under inert conditions and used immediately.

**Table 3E.1.** Proportions of exchangeable protons deuterated.

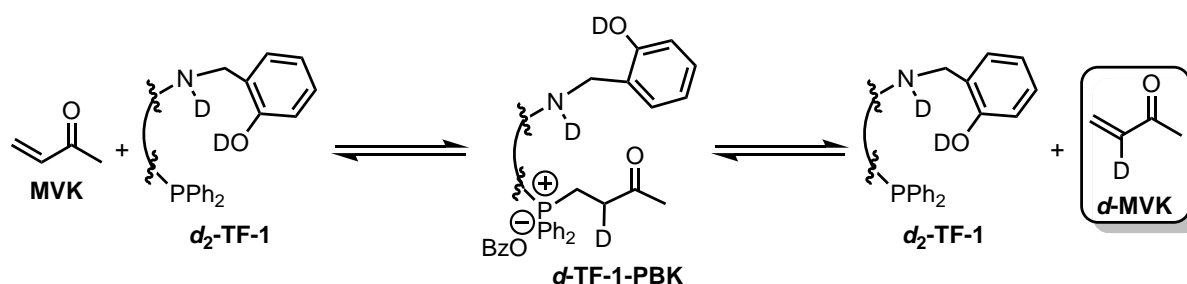
| Catalyst                | Extent of deuteration% |    |    |
|-------------------------|------------------------|----|----|
|                         | 1                      | 2  | 3  |
| <b>TF-1<sup>b</sup></b> | 80                     | 90 | 85 |
| <b>TF-2<sup>b</sup></b> | 85                     | 90 | 85 |
| <b>TF-3<sup>b</sup></b> | 90                     | 90 | 90 |
| <b>BF-1<sup>c</sup></b> | 70                     | 83 | 60 |
| <b>BF-2<sup>d</sup></b> | 90                     | 90 | 85 |
| <b>MAP<sup>e</sup></b>  | 60                     | 60 | 60 |
| <b>MOP<sup>d</sup></b>  | 95                     | 80 | 70 |

a) As measured by <sup>1</sup>H NMR (600 MHz, CD<sub>2</sub>Cl<sub>2</sub>). b) Deuteration of NH and OH. c) Deuteration of NH d) Deuteration of OH. e) Deuteration of NH<sub>2</sub>



**Figure 3E.1.** Characteristic deuteration of **TF-1** with 5 mol% BzOD in CDCl<sub>3</sub> (600 MHz)

### 3.3.2.3 General Procedure for measuring rate of retro-Michael Elimination



**Scheme 3E.4.** Deuteration and elimination of  $d$ -MVK.

The deuterated catalyst was dissolved in  $CD_2Cl_2$  under an Argon atmosphere and transferred to an NMR tube washed with  $CDCl_3$  and dried under reduced pressure. Freshly prepared  $d$ -Benzoic acid was added till a 1:1 ratio with catalyst was obtained as measured by  $^1H$  NMR (600 MHz). Methyl Benzoate (1 equiv) was added as an internal standard. The temperature of the bore was then lowered to 283 K and MVK (5 equiv) was added in one portion. The tube was inverted to ensure thorough mixing before reinjecting into the spectrometer and allowing ketone-phosphine equilibrium to be reached. After the equilibrium was reached in 10 minutes, the temperature was raised to 293 K and  $^1H$  NMR spectra were acquired every 45 seconds for 1 hour. The spectra were then analysed in TopSpin 3.2 with the concentration of ketone and  $d$ -MVK determined for each time point. The concentration of  $d$ -MVK was determined by measuring the integrals of the three vinylic protons of methyl vinyl ketone. These experiments were performed in triplicate for each catalyst and the second order rate constant calculated (**Table 3E.2**).

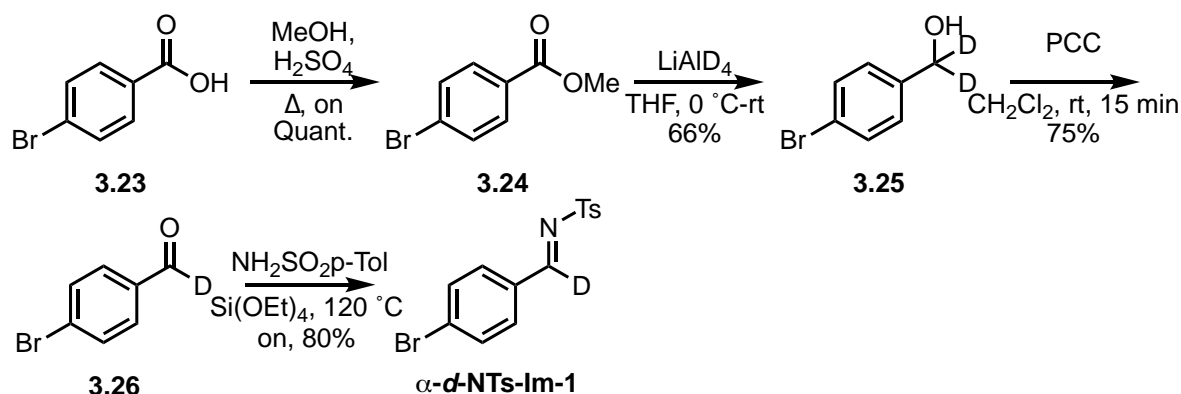
**Table 3E.2.** Summary of the second order rate constant for the elimination of  $d$ -MVK.

| Catalyst    | $k_{obs}$ (second order) | $k_{obs}$ (standardised) <sup>a</sup> |
|-------------|--------------------------|---------------------------------------|
| <b>TF-1</b> | 6.81E-02                 | 100%                                  |
| <b>TF-2</b> | 5.13E-02                 | 75%                                   |
| <b>TF-3</b> | 6.13E-02                 | 90%                                   |
| <b>BF-1</b> | 1.88E-01                 | 276%                                  |
| <b>BF-2</b> | 1.12E-01                 | 164%                                  |
| <b>MAP</b>  | 1.02E-01                 | 151%                                  |
| <b>MOP</b>  | 2.08E-01                 | 306%                                  |

a) Standardised to the elimination of TF-1.

### 3.3.3 Measuring secondary kinetic isotope effect

For secondary KIE ( $2^\circ$  KIE) analysis,<sup>49-52</sup>  $\alpha$ -*d*-NTs-Im-1 was prepared using literature reports from *p*-bromobenzoic acid.<sup>53</sup>



**Scheme 3E.5.** Synthesis of  $\alpha$ -*d*-NTs-Im-1

#### *Methyl 4-Bromobenzoate (3.24)*

4-bromobenzoic acid (**3.23**, 1.00 g, 4.76 mmol) was refluxed in methanol (5 mL) and conc. H<sub>2</sub>SO<sub>4</sub> (250  $\mu$ L, 5 mol%) overnight. The mixture was cooled to room temperature and carefully neutralized with NaHCO<sub>3</sub>. The reaction was diluted with water (5 mL) and extracted three times with EtOAc (20 mL) and the organic extracted washed with brine. The organic phase was dried over sodium sulfate and the solvent removed under reduced pressure to afford the pure methyl ester **3.24** (1.02 g, 100%), which was used without further purification. <sup>1</sup>H NMR (400 MHz, CDCl<sub>3</sub>,  $\delta$ ): 7.91 (d, *J* = 8.5 Hz, 2H), 7.59 (d, *J* = 8.5 Hz, 2H), 3.03 (s, 3H).

#### *d*<sub>2</sub>-4-bromobenzylalcohol (**3.25**)

**3.24** (430 mg, 2.05 mmol) in THF (8.2 mL) was cooled to -20 °C and LiAlD<sub>4</sub> (42.99 mg, 1.02 mmol) was added in small portions over 10 mins under a nitrogen atmosphere and the reaction was warmed to room temperature. After 1 hour the reaction was cooled to 0 °C and



carefully quenched with 1 M HCl. The volatiles were removed *in vacuo* and the residue resuspended in EtOAc (30 mL). The organic phase was washed with water (10 mL) and brine. The organic phase was dried over sodium sulfate and the solvent removed under reduced pressure. The crude alcohol was purified by flash chromatography (15% EtOAc: Hexane) to afford pure **3.25** (255 mg, 66%). <sup>1</sup>H NMR (400 MHz, CDCl<sub>3</sub>, δ): 7.49 (d, *J*= 8.4 Hz, 2H), 7.25 d, *J*= 8.4 Hz, 2H), 1.68 (bs, 1H).

#### *α*d-4-bromobenzaldehyde (**3.26**)

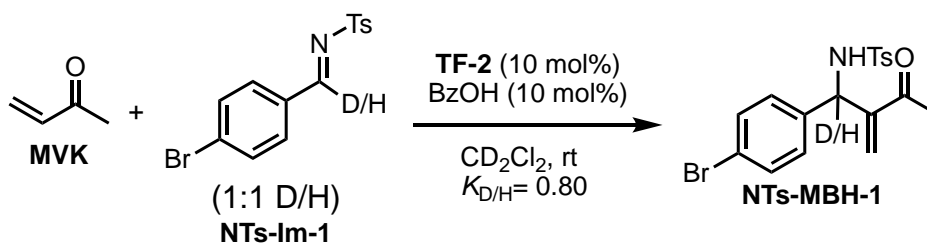
The deuterated alcohol **3.25** (250 mg, 1.32 mmol) was suspended in DCM (12 mL) and PCC (430 mg, 2 mmol) was added in small portions over 10 mins under a nitrogen atmosphere. After 15 minutes, the **reaction had reached** by completion as determined by TLC. The reaction was cooled to 0 °C and carefully quenched with 1 M HCl. The reaction was diluted with DCM (20 mL) and filtered through a bed of celite. The solvent removed under reduced pressure and the crude aldehyde was dry loaded with celite and purified by flash chromatography (5% EtOAc: Hexane) to afford pure **3.26** (200 mg, 75%). <sup>1</sup>H NMR (400 MHz, CDCl<sub>3</sub>, δ): 7.76 (d, *J*= 8.4 Hz, 2H), 7.74 (d, *J*= 8.4 Hz, 2H).

#### (*E*)-*N*-((4-bromophenyl)methylene-*d*)-4-methylbenzenesulfonamide (**α-d-NTs-Im-1**)

Deuterated aldehyde (**3.26**) (175 mg, 0.94 mmol) and p-toluenesulfonamide (164 mg, 0.96 mmol) were suspended in Si(OEt)<sub>4</sub> (587 mg, 2.82 mmol) in a sealed tube under a nitrogen atmosphere. The reaction was heated at 130 °C overnight before cooling the room temperature. The precipitated crude benzaldimine (**α-d-NTs-Im-1**) was recrystallized from EtOAc: Hexane to afford the pure benzaldimine (**α-d-NTs-Im-1**) (252 mg, 78%). <sup>1</sup>H NMR (400

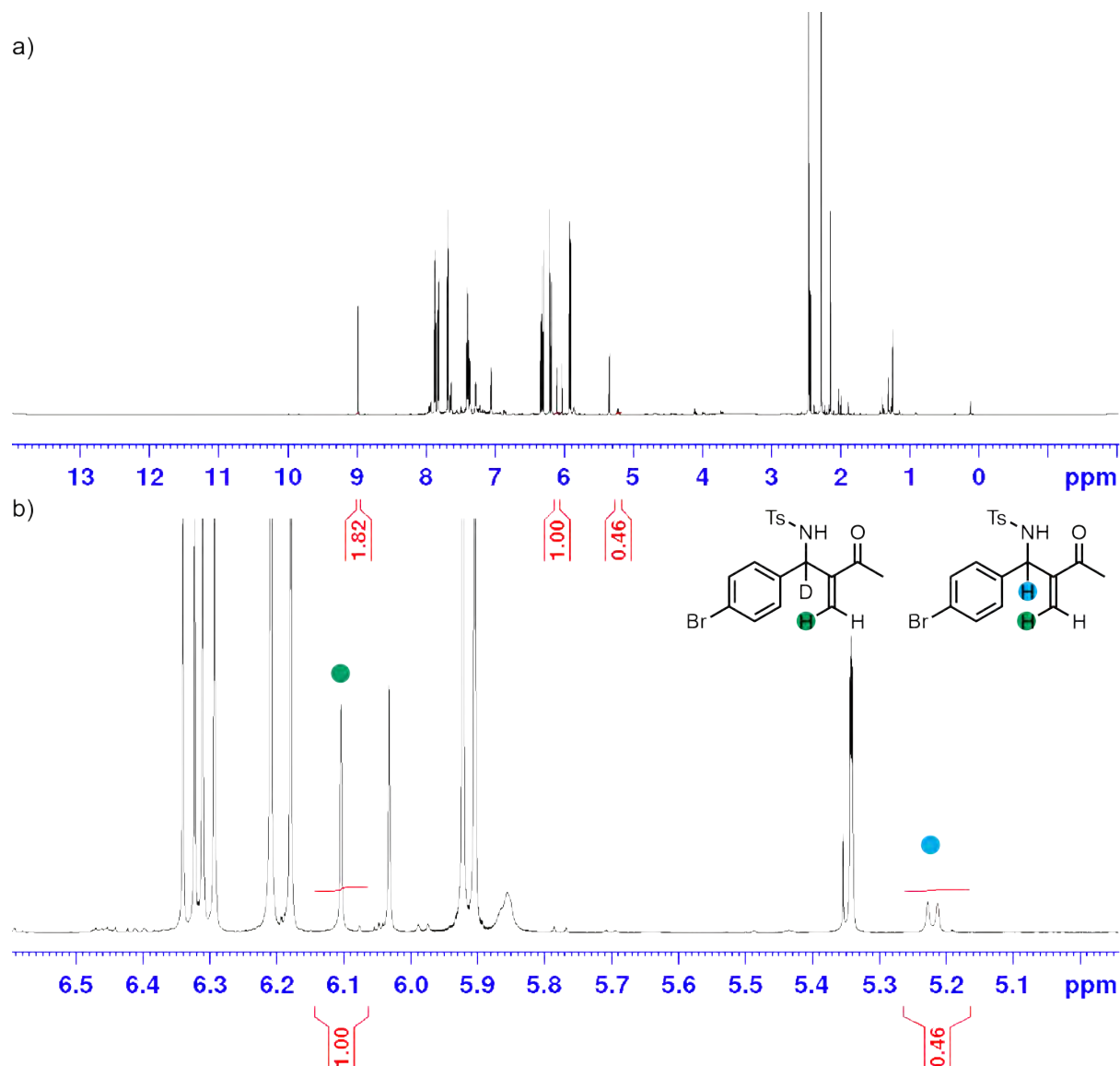
MHz, CDCl<sub>3</sub>,  $\delta$ ): 7.89 (d,  $J$  = 8.0 Hz, 2H), 7.79 (d,  $J$  = 8.6 Hz, 2H), 7.60 (d,  $J$  = 8.6 Hz, 2H), 7.36 (d,  $J$  = 8.0 Hz, 2H), 2.45 (s, 3H).

### 3.3.3.2 Measuring inverse secondary KIE



**Scheme 3E.6.** Reaction to perform 2° KIE analysis of the acid-regulated aza-MBH.

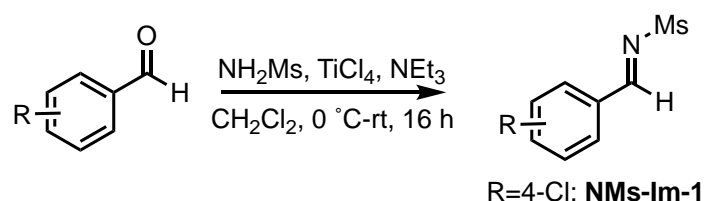
To a 1:1 mixture of  $\alpha$ -d-NTs-MBH-1 (12.43 mg, 0.04 mmol) and NTs-MBH-1 (12.43 mg, 0.04 mmol) in CD<sub>2</sub>Cl<sub>2</sub> was added catalyst **TF-2** (0.008 mmol, 10 mol%), and benzoic acid (0.97 mg, 0.008 mmol, 10 mol%). Methyl vinyl ketone (7.71 mg, 0.11 mmol) was added and the reaction monitored by <sup>1</sup>H NMR spectroscopy (600 MHz) with a 4 s relaxation delay. 4 scans were performed for each experiment with a 60 s delay between experiments. The reaction was monitored until the reaction had reached 20% conversion, as determined by the ratio between the imine proton and benzylic proton of the aza-MBH product. The amount of deuterated substrate was determined by subtracting the integral of the benzylic proton (5.20 ppm) from the vinyl proton (6.08 ppm).



**Figure 3E.1.** a)  $^1\text{H}$  NMR spectrum (600 MHz,  $\text{CD}_2\text{Cl}_2$ , 298 K) of the crude reaction mixture with  $\alpha$ -*d*-NTs-Im-1- and  $\alpha$ -*d*-NTs-Im-1 catalysed by TF-2. b)  $^1\text{H}$  NMR expansion (4.90-6.60 ppm) highlighting the key proton 5.21 ppm (NTs-MBH-1) and 6.10 ppm ( $\alpha$ -*d*-NTs-MBH-1, NTs-MBH-1).

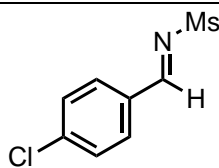
### 3.3.4 Preparation of imine substrates

#### 3.3.4.1 General procedure for preparation of *N*-Ms protected imines (**N-Ms-Im-1**)



**Scheme 3E.7** TiCl<sub>4</sub> catalysed mesyl imine formation.

In a 100 mL round bottom flask charged with a stir bar was added methanesulfonamide (3.15 mmol, 1 equiv), DCM (25 mL), aldehyde (3.31 mmol, 1.05 equiv) and NEt<sub>3</sub> (1.5 mL, 3.5 equiv). The solution was stirred and cooled to 0 °C. A freshly prepared solution of TiCl<sub>4</sub> in anhydrous CH<sub>2</sub>Cl<sub>2</sub> (1 M, 3.5 mL, 1.1 equiv) was added dropwise over 15 mins. The solution was allowed to slowly warm to room temperature over 2 hours and stirred for 16 hours. The crude mixture was filtered through a pad of celite, and the celite was washed three times with DCM before evaporating the solvent under reduced pressure. Anhydrous toluene (20 mL) was added, and the solution refluxed for 2 hours. The mixture was filtered through celite, washed three times with DCM and solvent evaporated under reduced pressure to afford analytically pure *N*-Mesyl protected imines which was used without further purification.



**NMs-Im-1**

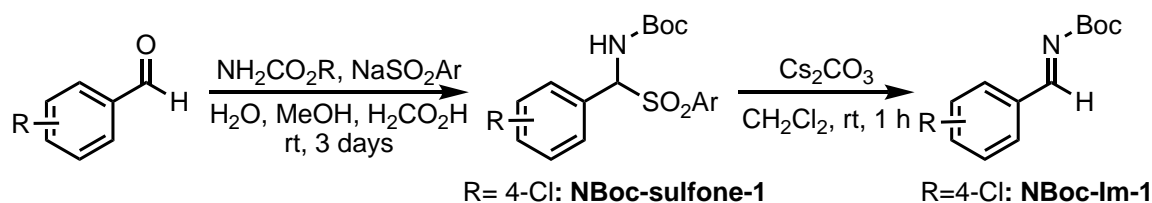
(*E*)-*N*-(4-chlorobenzylidene)methanesulfonamide (**NMs-Im-1**)

**<sup>1</sup>H NMR** (400 MHz, CDCl<sub>3</sub>, δ): 8.99 (s, 1H), 7.89 (d, *J* = 8.4 Hz, 2H), 7.51 (d, *J* = 8.4 Hz, 2H), 3.13 (s, 3H)

**<sup>13</sup>C NMR** (100 MHz, CDCl<sub>3</sub>, δ): 170.4, 141.9, 132.5, 130.7, 129.9, 40.4.

**MS (ESI)**: 279.1 [M+2-PrOH+H]

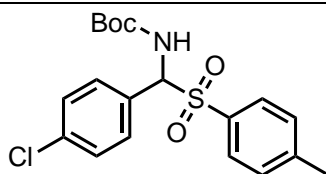
### 3.3.4.2 General procedure for *N*-Boc imine (NBoc-Im-1)



**Scheme 3E.8.** Preparation of *N*-Boc substrates via sulfones.

To a 50 mL round bottom flask charged with a stirring bar was added aldehyde (4 mmol), carbamate (2.67 mmol, 0.67 equiv) and *p*-toluenesulfonic acid sodium salt (8 mmol, 2 equiv). A solvent mixture of water (6 mL), methanol (3 mL) and formic acid (2 mL) were added, and the mixture sonicated until material had dissolved. The reaction was stirred at room temperature for three days before collecting the precipitate and washing with water and cold ether. The crude material was then triturated with ether to yield analytically pure carbamate sulfone.

The sulfone was dissolved in freshly distilled DCM, and anhydrous  $\text{Cs}_2\text{CO}_3$  (10 equiv) was added. The reaction was vigorously stirred for 45 minutes before filtering the heterogeneous mixture through celite. The precipitate was washed three times with DCM and filtrate concentrated under reduced pressure to afford analytically pure carbamate imines.



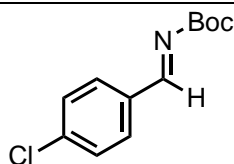
**NBoc-sulfone-1**

*tert*-butyl ((4-chlorophenyl)(tosyl)methyl)carbamate (**NBoc-sulfone-1**)

$^1\text{H}$  NMR (400 MHz,  $\text{CDCl}_3$ ,  $\delta$ ): 7.77 (d,  $J$ = 8.1 Hz, 2H), 7.38 (m, 4H), 7.34 (d,  $J$ = 8.1 Hz, 2H), 5.86 Hz (1H,  $J$ = 10.6 Hz, 1H), 5.71 (b, 1H), 2.43 (s, 3H), 1.26 (s, 9H).

$^{13}\text{C}$  NMR (100 MHz,  $\text{CDCl}_3$ ,  $\delta$ ): 153.59, 145.35, 136.07, 133.62, 130.31, 229.87, 129.59, 129.02, 128.73, 81.42, 73.31, 28.04, 21.74

**MS (ESI):** 240.1 [ $\text{M}+\text{H}-\text{Ts}$ ]



**NBoc-Im-1**

*tert*-butyl (*E*)-(4-chlorobenzylidene)carbamate (**NBoc-Im-1**)

**<sup>1</sup>H NMR** (400 MHz, CDCl<sub>3</sub>, δ): 8.82 (s, 1H), 7.84 (d, *J* = 8.5 Hz, 2H), 7.44 (d, *J* = 8.5 Hz, 2H), 1.58 (s, 9H).

**<sup>13</sup>C NMR** (CDCl<sub>3</sub>, 100 MHz, δ): 168.4, 162.5, 139.9, 132.6, 131.4, 129.4, 82.6, 28.0

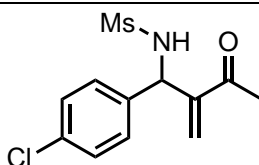
**MS (ESI)**: 240.1 [M+H]

---

### 3.3.4.3 General procedure for aza-MBH reaction.

Catalyst (2.5 μmol), imine (25 μmol) and benzoic acid (2.5 μmol) were combined in a 1.5 mL Teflon capped vial with 4Å molecular sieves. MVK (75 μmol) was added to the mixture and the reaction diluted to a total volume of 200 μL. Aliquots of the reaction mixture were taken and volatiles removed via nitrogen blow down. The residue was redissolved in CDCl<sub>3</sub> to determine conversion to product and analysed by chiral HPLC.

---



**NMs-MBH-1**

*N*-(1-(4-chlorophenyl)-2-methylene-3-oxobutyl)methanesulfonamide (**NMs-MBH-1**)

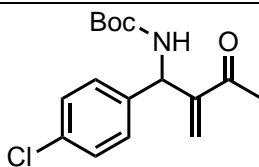
**<sup>1</sup>H NMR** (100 MHz, CDCl<sub>3</sub>, δ): 7.27 (m, 4H), 6.28 (s, 1H), 6.15 (s, 1H), 5.71 (d, *J* = 9.0 Hz, 1H), 5.43 (d, *J* = 9.0 Hz, 1H), 2.87 (s, 3H), 2.33 (s, 3H)

**<sup>13</sup>C NMR** (100 MHz, CDCl<sub>3</sub>, δ): δ 199.0, 147.3, 137.9, 133.9, 129.3, 129.0, 128.7, 128.1, 58.4, 41.9, 26.7

**MS (ESI)**: 333.1 [M+ 2Na-H]

**Chiral HPLC**: 60:40 Hex/2-PrOH, Whelk-01 Column, RT<sub>1</sub> 15.50 min, RT<sub>2</sub> 18.00 min

---



**NBoc-MBH-1**

*tert*-butyl (1-(4-chlorophenyl)-2-methylene-3-oxobutyl)carbamate (**NBoc-MBH-1**)

**<sup>1</sup>H NMR** (400 MHz, CDCl<sub>3</sub>, δ): 7.26 (d, *J*= 8.0 Hz, 2H), 7.19 (d, *J*= 8.0 Hz, 2H), 6.22 (s, 1H), 6.12 (s, 1H), 5.59 (d, *J*= 8.6 Hz), 5.54 (br, 1H), 2.30 (s, 3H), 1.44 (s, 9H).

**<sup>13</sup>C NMR** (100 MHz, CDCl<sub>3</sub>, δ): 199.0, 155.1, 147.6, 139.0, 133.4, 133.2, 130.2, 128.5, 127.6, 80.1, 55.9, 28.5, 26.7.

**MS (ESI):** 254.1 [M-*t*-Bu], 193.1 [M-NHBoc]

**Chiral HPLC:** Mobile Phase 75:25 Hex/2-PrOH, Chiralpak AD-H column RT<sub>1</sub>: 15.6 min, RT<sub>2</sub>: 16.5 min.

---

### 3.4 References

1. Zhou, Y.; Shan, Z., Chiral Diols: A New Class of Additives for Direct Aldol Reaction Catalyzed by L-Proline. *J. Org. Chem.* **2006**, *71* (25), 9510-9512.
2. Brière, J.-F.; Oudeyer, S.; Dalla, V.; Levacher, V., Recent advances in cooperative ion pairing in asymmetric organocatalysis. *Chem. Soc. Rev.* **2012**, *41* (5), 1696-1707.
3. Lautens, M.; Fagnou, K., Effects of Halide Ligands and Protic Additives on Enantioselectivity and Reactivity in Rhodium-Catalyzed Asymmetric Ring-Opening Reactions. *J. Am. Chem. Soc.* **2001**, *123* (29), 7170-7171.
4. Faller, J. W.; Lavoie, A. R.; Parr, J., Chiral Poisoning and Asymmetric Activation. *Chem. Rev.* **2003**, *103* (8), 3345-3368.
5. Shul'pin, G. B., Metal-catalyzed hydrocarbon oxygenations in solutions: the dramatic role of additives: a review. *J. Mol. Catal. A: Chem.* **2002**, *189* (1), 39-66.
6. Johnson, J. B.; Rovis, T., More than Bystanders: The Effect of Olefins on Transition-Metal-Catalyzed Cross-Coupling Reactions. *Angew. Chem., Int. Ed.* **2008**, *47* (5), 840-871.
7. Vogl, E. M.; Gröger, H.; Shibasaki, M., Towards Perfect Asymmetric Catalysis: Additives and Cocatalysts. *Angew. Chem., Int. Ed.* **1999**, *38* (11), 1570-1577.
8. Hong, L.; Sun, W.; Yang, D.; Li, G.; Wang, R., Additive Effects on Asymmetric Catalysis. *Chem. Rev.* **2016**, *116* (6), 4006-4123.
9. Raj, M.; Singh, V. K., Organocatalytic reactions in water. *Chem. Commun.* **2009**, (44), 6687-6703.
10. Brogan, A. P.; Dickerson, T. J.; Janda, K. D., Enamine-Based Aldol Organocatalysis in Water: Are They Really "All Wet"? *Angew. Chem., Int. Ed.* **2006**, *45* (48), 8100-8102.
11. Blackmond, D. G.; Armstrong, A.; Coombe, V.; Wells, A., Water in Organocatalytic Processes: Debunking the Myths. *Angew. Chem., Int. Ed.* **2007**, *46* (21), 3798-3800.



12. Hayashi, Y., In Water or in the Presence of Water? *Angew. Chem., Int. Ed.* **2006**, *45* (48), 8103-8104.
13. Dickerson, T. J.; Janda, K. D., Aqueous Aldol Catalysis by a Nicotine Metabolite. *J. Am. Chem. Soc.* **2002**, *124* (13), 3220-3221.
14. Rogers, C. J.; Dickerson, T. J.; Janda, K. D., Kinetic isotope and thermodynamic analysis of the nornicotine-catalyzed aqueous aldol reaction. *Tetrahedron* **2006**, *62* (2), 352-356.
15. Dickerson, T. J.; Lovell, T.; Meijler, M. M.; Noodleman, L.; Janda, K. D., Nornicotine Aqueous Aldol Reactions: Synthetic and Theoretical Investigations into the Origins of Catalysis. *J. Org. Chem.* **2004**, *69* (20), 6603-6609.
16. Chen, M.; Sun, J., How Understanding the Role of an Additive Can Lead to an Improved Synthetic Protocol without an Additive: Organocatalytic Synthesis of Chiral Diarylmethyl Alkynes. *Angew. Chem., Int. Ed.* **2017**, *56* (39), 11966-11970.
17. Erkkilä, A.; Majander, I.; Pihko, P. M., Iminium Catalysis. *Chem. Rev.* **2007**, *107* (12), 5416-5470.
18. Mukherjee, S.; Yang, J. W.; Hoffmann, S.; List, B., Asymmetric Enamine Catalysis. *Chem. Rev.* **2007**, *107* (12), 5471-5569.
19. Mahlau, M.; List, B., Asymmetric Counteranion-Directed Catalysis: Concept, Definition, and Applications. *Angew. Chem., Int. Ed.* **2013**, *52* (2), 518-533.
20. Parmar, D.; Sugiono, E.; Raja, S.; Rueping, M., Complete Field Guide to Asymmetric BINOL-Phosphate Derived Brønsted Acid and Metal Catalysis: History and Classification by Mode of Activation; Brønsted Acidity, Hydrogen Bonding, Ion Pairing, and Metal Phosphates. *Chem. Rev.* **2014**, *114* (18), 9047-9153.
21. Akiyama, T.; Mori, K., Stronger Brønsted Acids: Recent Progress. *Chem. Rev.* **2015**, *115* (17), 9277-9306.

22. Connon, S. J., Chiral Phosphoric Acids: Powerful Organocatalysts for Asymmetric Addition Reactions to Imines. *Angew. Chem., Int. Ed.* **2006**, 45 (24), 3909-3912.
23. Terada, M., Chiral Phosphoric Acids as Versatile Catalysts for Enantioselective Transformations. *Synthesis* **2010**, 2010 (12), 1929-1982.
24. Ahrendt, K. A.; Borths, C. J.; MacMillan, D. W. C., New Strategies for Organic Catalysis: The First Highly Enantioselective Organocatalytic Diels–Alder Reaction. *J. Am. Chem. Soc.* **2000**, 122 (17), 4243-4244.
25. Jen, W. S.; Wiener, J. J. M.; MacMillan, D. W. C., New Strategies for Organic Catalysis: The First Enantioselective Organocatalytic 1,3-Dipolar Cycloaddition. *J. Am. Chem. Soc.* **2000**, 122 (40), 9874-9875.
26. Xu, H.; Zuend, S. J.; Woll, M. G.; Tao, Y.; Jacobsen, E. N., Asymmetric Cooperative Catalysis of Strong Brønsted Acid–Promoted Reactions Using Chiral Ureas. *Science* **2010**, 327 (5968), 986-990.
27. Tian, X.; Cassani, C.; Liu, Y.; Moran, A.; Urakawa, A.; Galzerano, P.; Arceo, E.; Melchiorre, P., Diastereodivergent Asymmetric Sulfa-Michael Additions of  $\alpha$ -Branched Enones using a Single Chiral Organic Catalyst. *J. Am. Chem. Soc.* **2011**, 133 (44), 17934-17941.
28. Robiette, R.; Aggarwal, V. K.; Harvey, J. N., Mechanism of the Morita–Baylis–Hillman Reaction: A Computational Investigation. *J. Am. Chem. Soc.* **2007**, 129 (50), 15513-15525.
29. Aggarwal, V. K.; Fulford, S. Y.; Lloyd-Jones, G. C., Reevaluation of the Mechanism of the Baylis–Hillman Reaction: Implications for Asymmetric Catalysis. *Angew. Chem., Int. Ed.* **2005**, 44 (11), 1706-1708.
30. Aggarwal, V. K.; Emme, I.; Fulford, S. Y., Correlation between pKa and Reactivity of Quinuclidine-Based Catalysts in the Baylis–Hillman Reaction: Discovery of Quinuclidine as

Optimum Catalyst Leading to Substantial Enhancement of Scope. *J. Org. Chem.* **2003**, *68* (3), 692-700.

31. Price, K. E.; Broadwater, S. J.; Jung, H. M.; McQuade, D. T., Baylis–Hillman Mechanism: A New Interpretation in Aprotic Solvents. *Org. Lett.* **2005**, *7* (1), 147-150.
32. Yamada, Y. M. A.; Ikegami, S., Efficient Baylis–Hillman reactions promoted by mild cooperative catalysts and their application to catalytic asymmetric synthesis. *Tetrahedron Lett.* **2000**, *41* (13), 2165-2169.
33. Aggarwal, V. K.; Fulford, S. Y.; Lloyd-Jones, G. C., Reevaluation of the Mechanism of the Baylis–Hillman Reaction: Implications for Asymmetric Catalysis. *Angew. Chem. Int. Ed.* **2005**, *44* (11), 1706-1708.
34. Park, K.-S.; Kim, J.; Choo, H.; Chong, Y., Octanol-Accelerated Baylis–Hillman Reaction. *Synlett* **2007**, *2007* (3), 395-398.
35. Gomes, J. C.; Jr, M. T. R.; Moyano, A.; Coelho, F., Efficient Catalysis of Aqueous Morita–Baylis–Hillman Reactions of Cyclic Enones by a Bicyclic Imidazolyl Alcohol. *Eur. J. Org. Chem.* **2012**, *2012* (35), 6861-6866.
36. Abermil, N.; Masson, G.; Zhu, J., Invertible Enantioselectivity in 6′ -Deoxy-6′ -acylamino- $\beta$ -isocupreidine-Catalyzed Asymmetric Aza-Morita–Baylis–Hillman Reaction: Key Role of Achiral Additive. *Org. Lett.* **2009**, *11* (20), 4648-4651.
37. Yao, Y.; Li, J.-L.; Zhou, Q.-Q.; Dong, L.; Chen, Y.-C., Enantioselective Aza-Morita–Baylis–Hillman Reaction with Ketimines and Acrolein Catalyzed by Organic Assemblies. *Chemistry – A European Journal* **2013**, *19* (29), 9447-9451.
38. Han, X.; Wang, Y.; Zhong, F.; Lu, Y., Enantioselective Morita–Baylis–Hillman reaction promoted by l-threonine-derived phosphine–thiourea catalysts. *Org. Biomol. Chem.* **2011**, *9* (19), 6734-6740.

39. Shen, Y.; Tang, Q.; Zhang, C.; Zhong, W., 2-(Diphenylphosphino)benzoyl-Substituted Calix[4]arene: Efficient Organocatalyst in Aza-Morita-Baylis-Hillman Reaction of N-Sulfonated Imines with Methyl Vinyl Ketone. *Synlett* **2012**, 23 (05), 741-746.
40. Shi, Y.-L.; Shi, M., Chiral Thiourea-Phosphine Organocatalysts in the Asymmetric Aza-Morita-Baylis-Hillman Reaction. *Adv. Synth. Catal.* **2007**, 349 (13), 2129-2135.
41. Garnier, J.-M.; Anstiss, C.; Liu, F., Enantioselective Trifunctional Organocatalysts for Rate- Enhanced Aza-Morita-Baylis-Hillman Reactions at Room Temperature. *Adv. Synth. Catal.* **2009**, 351 (3), 331-338.
42. A. Berkessel; Gröger, H., *Asymmetric Organocatalysis: From Biomimetic Concepts to Applications in Asymmetric Synthesis*. 1st ed.; Wiley-VCH: Weinheim, 2005.
43. Garnier, J.-M.; Liu, F., Trifunctional organocatalyst-promoted counterion catalysis for fast and enantioselective aza-Morita-Baylis-Hillman reactions at ambient temperature. *Org. Biomol. Chem.* **2009**, 7 (7), 1272-1275.
44. Anstiss, C.; Garnier, J.-M.; Liu, F., Mechanistic investigations of multidentate organocatalyst-promoted counterion catalysis for fast and enantioselective aza-Morita-Baylis-Hillman reactions at ambient temperature. *Org. Biomol. Chem.* **2010**, 8 (19), 4400-4407.
45. Chataigner, I.; Panel, C.; Gérard, H.; Piettre, S. R., Sulfonyl vs. carbonyl group: which is the more electron-withdrawing? *Chem. Commun.* **2007**, (31), 3288-3290.
46. Anstiss, C.; Garnier, J.-M.; Liu, F., Mechanistic investigations of multidentate organocatalyst-promoted counterion catalysis for fast and enantioselective aza-Morita-Baylis-Hillman reactions at ambient temperature. *Org. Biomol. Chem.* **2010**, 8 (19), 4400-4407.

47. Anstiss, C.; Liu, F., Cooperativity in the counterion catalysis of Morita/Baylis/Hillman reactions promoted by enantioselective trifunctional organocatalysts. *Tetrahedron* **2010**, *66* (29), 5486-5491.
48. Garnier, J.-M.; Liu, F., Trifunctional organocatalyst-promoted counterion catalysis for fast and enantioselective aza-Morita-Baylis-Hillman reactions at ambient temperature. *Org. Biomol. Chem.* **2009**, *7* (7), 1272-1275.
49. Gajewski, J. J.; Bocian, W.; Harris, N. J.; Olson, L. P.; Gajewski, J. P., Secondary Deuterium Kinetic Isotope Effects in Irreversible Additions of Hydride and Carbon Nucleophiles to Aldehydes: A Spectrum of Transition States from Complete Bond Formation to Single Electron Transfer. *J. Am. Chem. Soc.* **1999**, *121* (2), 326-334.
50. Westaway, K. C., Using kinetic isotope effects to determine the structure of the transition states of S<sub>N</sub>2 reactions. In *Advances in Physical Organic Chemistry*, Richard, J. P., Ed. Academic Press: 2006; Vol. 41, pp 217-273.
51. Northrop, D. B., Deuterium and tritium kinetic isotope effects on initial rates. *Methods Enzymol.* **1982**, *87* (Enzyme Kinet. Mech.), 607-625.
52. Streitwieser, A.; Jagow, R. H.; Fahey, R. C.; Suzuki, S., Kinetic Isotope Effects in the Acetolyses of Deuterated Cyclopentyl Tosylates<sup>1,2</sup>. *J. Am. Chem. Soc.* **1958**, *80* (9), 2326-2332.
53. Jiang, M.; Shi, M., Aluminum Chloride-Mediated Acylation of Methylenecyclobutanes. A Facile Synthetic Protocol for the Construction of Substituted Cyclopentenones. *Org. Lett.* **2008**, *10* (11), 2239-2242.

## **Chapter 4**

# **Scope of the Trifunctional Conjugative Catalysis in the aza-MBH Model System**

## 4.1 Introduction

In this chapter, the conjugative catalysis mode outlined in Chapter 3 will be tested with new heterocyclic substrates. Substrate bearing nitrogens are challenging due to potential interference from additional Brønsted base motifs with proton transfer unless the proton motion can be specified with high fidelity in the proton transfer network.

### 4.1.1 Nitrogen Heterocycles in organocatalysis

Nitrogen heterocycles are one of the most abundant epitopes in small molecule drugs.<sup>1-2</sup> In particular, pyridine heterocycles not only are common pharmaceutical moieties,<sup>3-5</sup> but also are used as catalysts, because of the basicity of the pyridinyl nitrogen and its involvement in proton shuttling, hydrogen bonding or metal chelation.<sup>6</sup> For example, chelation to transition metals can provide a chiral environment around the metal centre.<sup>7-10</sup> As an organocatalytic motif, pyridine motifs can function as a nucleophile<sup>11-15</sup>, or hydrogen bond donors as the pyridinium salt.<sup>16-17</sup> Pyridines also enable fundamental processes such as proton transfer in low-barrier H-bonds to be studied.<sup>18</sup>

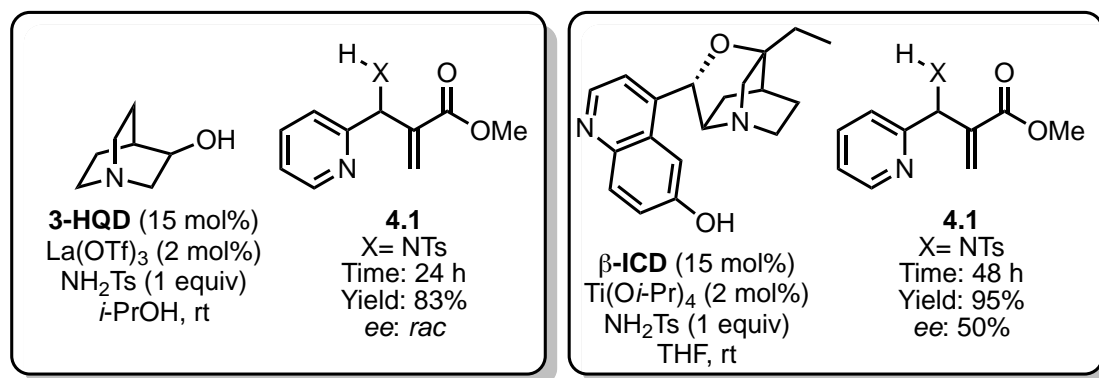
Due to the different functional roles of pyridines employing them as substrates, rather than catalysts, can be challenging. For example, pyridine carboxaldehyde, and carbaldimines are under-represented as substrates in hydrogen-bond activated organocatalytic reactions due to the capacity of the pyridinyl nitrogen can hijack stereospecific proton transfer eroding stereoselectivity.<sup>19-21</sup> In light of the mechanistic work presented in Chapter 2 and 3 of this thesis, the next interesting question is if and how an emergent proton transfer network can be established for heterocyclic substrates with complex characteristics.

#### 4.1.2 Pyridine carboxaldehyde as aza-MBH substrates.

Pyridinyl substrates are underrepresented in the enantioselective MBH and aza-MBH reaction. This is somewhat surprising given the potential utility of MBH adducts in pharmaceutical synthesis.<sup>22-24</sup> Below reports of asymmetric catalysis with 2-pyridinyl and 3-pyridinyl substrates will be outlined.

##### 4.1.2.1 2-carboxypyridine substrates

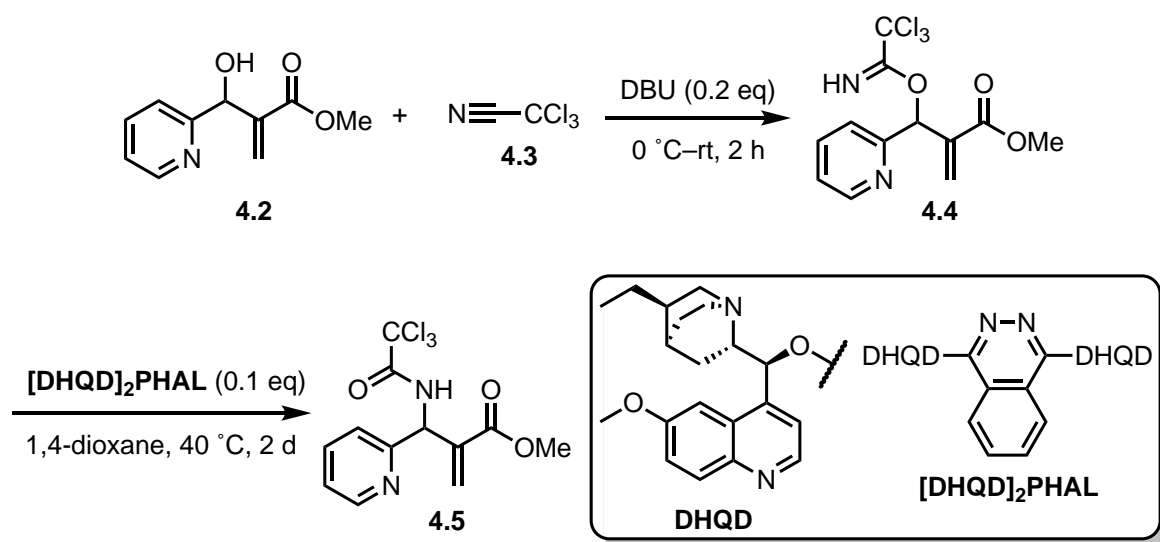
Adolfsson et al. published the first report of a *racemic in situ* aza-MBH with 2-pyridinecarboxaldehyde (**Figure 4.1**).<sup>25</sup> To suppress the formation of the undesired MBH adduct, the pyridinyl aldimine was formed over 24 hours before adding methyl acrylate. The reaction was catalysed with  $\text{La}(\text{OTf})_3$  and 3-hydroxyquinuclidine (**3-HQD**) with 4Å MS. The aza-MBH adduct was isolated with 83% yield as well as the MBH adduct as a minor product (7%). Substituting  $\text{La}(\text{OTf})_3$  for  $\text{Ti}(\text{Oi-Pr})_4$  improved the isolated yield for the aza-MBH reaction to 92%.<sup>26</sup> Immediate addition of methyl acrylate decreased the yield of the aza-MBH adduct (80%). An enantioselective variant was reported with  $\beta$ -ICD employed as the chiral catalyst.<sup>27</sup> However, the enantioselectivity of the reaction was only moderate (50% ee).



**Figure 4.1.** 2-Pyridine aza-MBH adducts and catalysts used for the transformation.



2-pyridinecarboxaldehyde has also been used in a *racemic* MBH reaction as a part of a multistep synthesis of quinolines.<sup>28</sup> Jørgensen et al. reported an indirect method for preparation of chiral aza-MBH adducts from *racemic* MBH trichloroacetimidates (**Scheme 4.1**).<sup>29</sup> *Racemic* MBH adducts (**4.2**) were prepared and transformed with DBU and **4.3** into *O*-allylic trichloroacetimidates (**4.4**). A [1,3]-sigmatropic rearrangement of acetimidate **4.4** by **[DHQD]<sub>2</sub>PHAL** yielded the trichloroacetamide aza-MBH adduct **4.5** with 64% yield and 87% *ee*. The procedure yields the aza-MBH adduct with high enantiopurity, but the need for an indirect methodology demonstrates that this is a challenging class of substrate for the aza-MBH reaction.

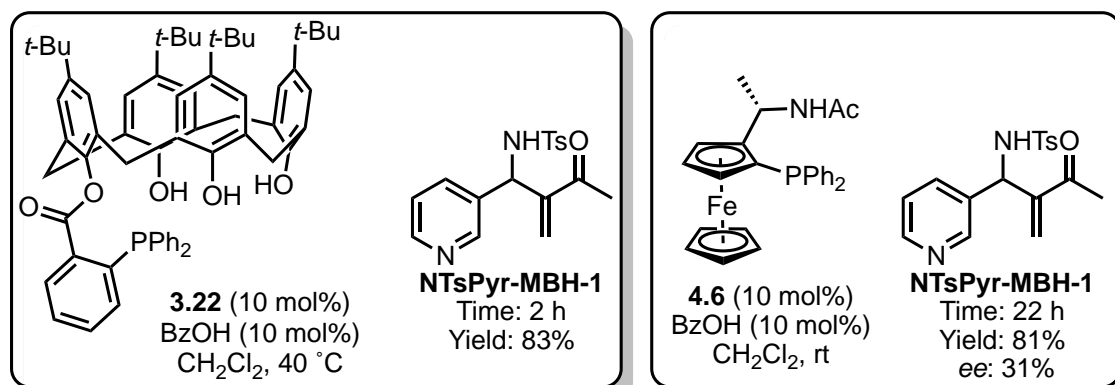


**Scheme 4.1.** Indirect synthesis of aza-MBH adducts by [1,3]-sigmatropic rearrangement.

#### 4.1.2.3 3-Pyridine carboxaldehyde

The initial report of a *racemic* 3-pyridinyl aza-MBH adduct was from the corresponding MBH acetate and DABCO via  $S_N2'$  substitution.<sup>30</sup> Gajda et al. reported the formation of *racemic* *N*-Boc aza-MBH adducts from the corresponding *N*-Boc sulfone in low yields (51%) over five days.<sup>31</sup> Zhong et al. reported a substituted calix[4]arene phosphine organocatalyst **3.22** which required benzoic acid (BzOH) to enhance the rate of a *racemic* aza-MBH reaction of a variety

of substituted aryl *N*-Ts benzaldimines including a pyridinyl adduct (**NTsPyr-MBH-1**).<sup>32</sup> In 2015, the Zhong group reported a derivatised ferrocene bifunctional organocatalyst **4.6**.<sup>33</sup> The reaction was dependent upon the addition of BzOH to achieve high yields of **NTsPyr-MBH-1** (81%), but the enantioselectivity was poor (31%).

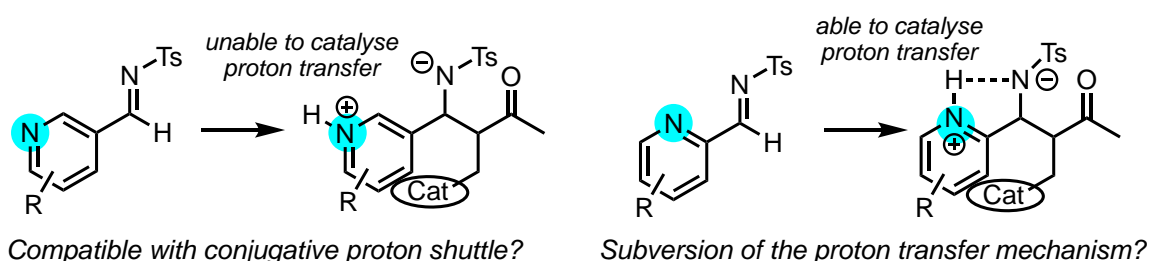


**Figure 4.2.** 3-pyridine NTs aza-MBH adducts (**NTsPyr-MBH-1**) and the catalysts used for the transformation.

#### 4.1.3 Proton motion specificity in conjugative catalysis

In Chapter 3, conjugative catalysis for a model aza-MBH reaction involving organised proton transfer between the acid additive (BzOH) and a cognate sulfonyl imine substrate was outlined. In the conjugative mode, the trifunctional catalyst, substrates and counterion together facilitate fast and enantioselective proton transfer for catalytic proficiency. In this chapter, the specificity of the cognate proton transfer process will be examined by testing additional heterocyclic substrates for the aza-MBH reaction. Conjugative catalysis is highly selective based on cooperativity between motifs so may be more tolerant of H-bond donors or acceptors such as pyridine containing substrates. Additional proton stationary sites (Brønsted base) from the pyridinyl nitrogen may not perturb the generation and deployment of the cooperative proton network if their positions are not spatially aligned.

2- and 3-substituted pyridines are examined next as they could potentially influence the conjugative proton transfer pathway and challenge the specificity of the proton motion (**Scheme 4.2**). The pyridinyl nitrogen in the 3-position may be unable to act as an intermediary in proton transfer catalysis as it is further removed from the bond formation site. Conversely, if the pyridinyl nitrogen is in the 2-position proton transfer may interfere with the cognate proton transfer pathway and decrease the enantioselectivity due to the proximity between the nitrogen and sulfonamidate.



**Scheme 4.2.** Potential effects of the pyridine nitrogen base on proton-transfer catalysis.

#### 4.1.4 Specific aims

The specific aims of this chapter are:

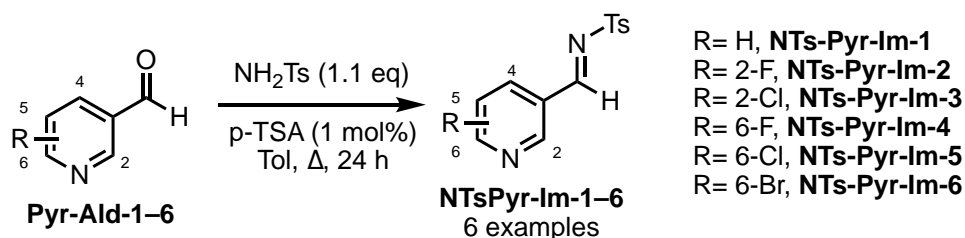
- Prepare a series of 2- and 3-pyridinyl substrates for the aza-MBH reaction;
- Determine if the position of the substrate Brønsted base interferes with proton motion;
- Establish if the conjugative mode is adoptable for new pyridine substrates.

#### 4.2 Results and Discussion

In this chapter, first a milder method for preparation of pyridinyl substrates was developed. Next, the effect of the pyridinyl nitrogen Brønsted base on trifunctional catalysis was determined. Finally, the catalytic profile for 3-pyridine substrates with different acids and loading was determined.

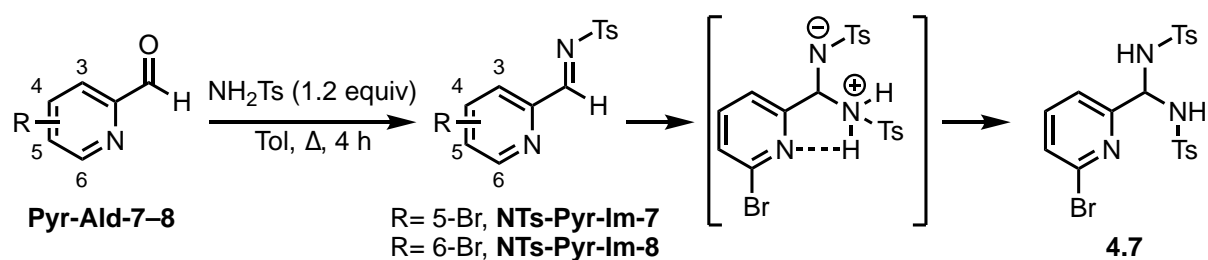
#### 4.2.1 Synthesis of pyridine substrates

Preparation of *N*-Ts pyridinyl aldimine substrates **NTsPyr-Im-1–6** (**Scheme 4.3**) using methods for the aryl analogues proved unsuccessful due to facile polymerisation of the aldehyde and degradation via the Cannizzaro reaction. In addition, hydrolysis of the imine product was more pronounced due to hydroxide generated *in situ* by the pyridinyl Brønsted base with water, and molecular sieves were ineffective in preventing this hydrolysis. Reactions were then performed with a Dean-Stark apparatus under an inert atmosphere in refluxing toluene using *p*-toluenesulfonic acid (1 mol%) as a catalyst. Complete conversion for the model aldehyde, 3-pyridinecarboxaldehyde (**Pyr-Ald-1**) to the imine **NTsPyr-Im-1**, was elicited in 24 hours with an isolated yield of 85% after recrystallisation from EtOAc/hexane. This method was successful for a range of halogen-substituted 3-pyridinecarboxaldehydes (**Scheme 4.3**).



**Scheme 4.3.** Synthesis of substituted 3-pyridinecarboxaldehydes.

The preparation of 2-pyridinyl carbaldimine was more difficult than 3-pyridinyl carbaldimine. Optimised conditions identified for 3-formyl pyridines resulted in an isolated yield of **NTsPyr-Im-8** below 10% due to the formation of a bis-sulfonamide side-product **4.7** (**Scheme 4.4**) and polymerisation. After formation of **NTsPyr-Im-8**, the pyridinyl nitrogen can promote formation of **4.7** by catalysing proton transfer for the addition of a second equivalent of *p*-toluenesulfonamide to prevent the tetrahedral intermediate from collapsing, (**Scheme 4.4**).



**Scheme 4.4.** Formation of the bis-sulfonamide product.

More mild reaction conditions were screened to minimise the formation of **4.7**, including lowering the reaction temperature from 100 °C to 60 °C, adding excess 4Å MS and using aldehyde in excess (1.05 equiv). At 60 °C, the bis-sulfonamide side-product **4.7** was still the major product, while lowering the temperature further to 40 °C with excess 4Å MS yielded the 2-pyridinyl NTs imine **NTsPyr-Im-7** and **NTsPyr-Im-8** without the formation of **4.7**.

#### 4.2.2 Profile of catalyst response to BzOH activation using a representative pyridinyl imine substrate

The model pyridinyl substrates **NTsPyr-Im-1**, was first employed to determine if the pyridinyl imine substrates were capable of recognising and accessing the conjugative catalysis by proficient proton transfer pathway. Bifunctional and trifunctional organocatalysts were screened to determine the effect of BzOH on the catalysis of the model substrate (**Table 4.1**).

**Table 4.1.** Effect of BzOH on catalysis for a series of catalysts.

| Entry | Catalyst          | Time/ m | BzOH (10 mol%)             |                           | BzOH (0 mol%)              |                           |
|-------|-------------------|---------|----------------------------|---------------------------|----------------------------|---------------------------|
|       |                   |         | Conversion <sup>a</sup> /% | <i>ee</i> /% <sup>b</sup> | Conversion <sup>a</sup> /% | <i>ee</i> /% <sup>b</sup> |
| 1     | <b>TF-1</b>       | 30      | 34                         | 89                        | 3                          | nd                        |
| 2     | <b>TF-2</b>       | 30      | 62                         | 88                        | nd                         | nd                        |
| 3     | <b>TF-3</b>       | 30      | 62                         | 84                        | 13 (>95%) <sup>c</sup>     | nd (30) <sup>c</sup>      |
| 4     | <b>BF-2</b>       | 30      | 11                         | 57                        | 16                         | 89                        |
| 5     | <b>MAP</b>        | 30      | 22                         | 41                        | 11                         | <i>rac</i>                |
| 6     | <b>MOP</b>        | 30      | 8                          | 78                        | 90                         | 82                        |
| 7     | <b>TPP-Phenol</b> | 30      | 90                         | <i>rac</i>                | >95                        | <i>rac</i>                |

a) Determined by <sup>1</sup>H NMR spectroscopy b) Determined by chiral HPLC c) determined after 24 hours

Consistent with the trifunctional proton transfer model developed for aromatic substrates (Chapter 2 and 3), catalysis proceeds through the conjugative mode for trifunctional organocatalysts for **NTsPyr-Im-1** (Table 4.1, Entries 1–3), suggesting the enolate pathway in the subjugative mode was ineffective for 3-pyridinyl substrates. Without BzOH (the subjugative mode), **TF-2** is unable to catalyse the aza-MBH reaction (Table 4.1, Entry 2), addition of BzOH induces the conjugative mode and concurrent elevation of rate (62% conversion after 30 min) and *ee* (88% *ee*). Complete conversion for **NTsPyr-Im-1** was observed with TPP and phenol within 30 minutes in the absence of acid (Table 4.1, Entry 7) with a modest decrease in rate with BzOH (90% conversion). A similar catalytic profile was observed for **MAP**, with the addition of BzOH doubling the rate of reaction and elevating the level of asymmetric induction (41% *ee*)(Table 4.1, Entry 5).

Bifunctional catalyst **MOP** proceeded with high rates without acid (Table 4.1, Entry 6), and BzOH addition led to a 10-fold decrease in the rate of reaction while the level of

enantioselectivity was consistent between the reaction with (78% *ee*) and without acid (82% *ee*). This is a clear example of the conventional enolate pathway operating in the subjugative mode, and the rate reduction induced by BzOH is a result of the parasitic **MOP-PBK** (Chapter 2). Mild suppression of the reactive pathway was also observed upon addition of BzOH to the amine bifunctional control **BF-2** (**Table 4.1**, Entry 4), intriguingly enantioselectivity decreased significantly from 89% to 57%. One possible explanation is that in the absence of a proton-transfer network, bifunctional **BF-2** adopts the subjugative mode of catalysis via H-bonding. BzOH shifts the mechanism from the subjugative to a proton transfer network. The underdeveloped network likely lacks the amine stationary point for proton transfer, thus decreasing the enantioselectivity.

Congruent elevation of rate and asymmetric induction for **NTsPyr-Im-1** is the most efficient for amine-containing catalysts **TF-1–TF-3** with BzOH (**Table 4.1**, Entries 1–3), proceeding through the **PBK**-mediated proton transfer pathway. The conventional trifunctional enolate mechanism (reactions without BzOH), were ineffective for all trifunctional organocatalysts **TF-1–TF-3**. For catalyst **TF-3** after 24 hours without BzOH, the conventional enolate pathway reached complete conversion with poor asymmetric induction (30% *ee*, **Table 4.1**, Entry 3). BzOH activated the cognate conjugative catalysis for the pyridinyl substrate **NTsPyr-Im-1** resulting in consistent elevation of rate and *ee* for the trifunctional systems. The high rate and excellent level of asymmetric induction (78–89% *ee*) are consistent with the mechanistic model derived for the aromatic substrates. The spatial organisation of the proton transfer network was specific enough to tolerate the substrate's additional protonation site. Catalyst **TF-2** was identified as the most proficient catalyst for the 3-pyridinyl substrate **NTsPyr-Im-1** and was employed to examine the scope of the 3-pyridinyl and 2-pyridinyl substrates.

#### 4.2.3 Effect of the nitrogen (Brønsted base) position on deploying the proton shuttle

The effect of the pyridinyl nitrogen on the proton transfer mechanism was examined using the most proficient catalyst **TF-2** in a model aza-MBH reaction with MVK and 2- and 3-pyridinyl *N*-Ts aldimines. 3-pyridinyl substrates were analysed after 30 minutes for conversion and enantioselectivity and 2-pyridinyl substrates after 1 hour (Table 4.2).

**Table 4.2.** Conversion and enantioselectivity for pyridine substrates catalysed by TF-2.

|       |          | MVK                 | X= 3-Pyr: NTsPyr-lm-1-6<br>X= 2-Pyr: MTsPyr-lm-7-8 |   | X= 3-Pyr: NTsPyr-MBH-1-6<br>X= 2-Pyr: MTsPyr-MBH-7-8 |  |                        |
|-------|----------|---------------------|--|---|--|--|------------------------|
| Entry | Pyridine | R                   | Time   | BzOH (10 mol%)<br>Conversion <sup>a</sup> | <i>ee</i> <sup>b</sup>                               | BzOH (0 mol%)<br>Conversion <sup>a</sup> | <i>ee</i> <sup>b</sup> |
| 1     |          | H (NTsPyr-MBH-1)    | 30   | 62  | 88   | nd <sup>c</sup>                          | nd                     |
| 2     |          | 2-F (NTsPyr-MBH-2)  | 30   | 33  | 60   | nd <sup>c</sup>                          | nd                     |
| 3     |          | 2-Cl (NTsPyr-MBH-3) | 30   | 30  | 70   | nd <sup>c</sup>                          | nd                     |
| 4     |          | 6-F (NTsPyr-MBH-4)  | 30   | 63  | 82   | nd <sup>c</sup>                          | nd                     |
| 5     |          | 6-Cl (NTsPyr-MBH-5) | 30   | 62  | 91   | nd <sup>c</sup>                          | nd                     |
| 6     |          | 6-Br (NTsPyr-MBH-6) | 30   | 64  | 84   | nd <sup>c</sup>                          | nd                     |
| 7     |          | 5-Br (NTsPyr-MBH-7) | 60   | >95                                       | 50   | 50                                       | 50                     |
| 8     |          | 6-Br (NTsPyr-MBH-8) | 60   | 90  | 43   | 25                                       | 30                     |

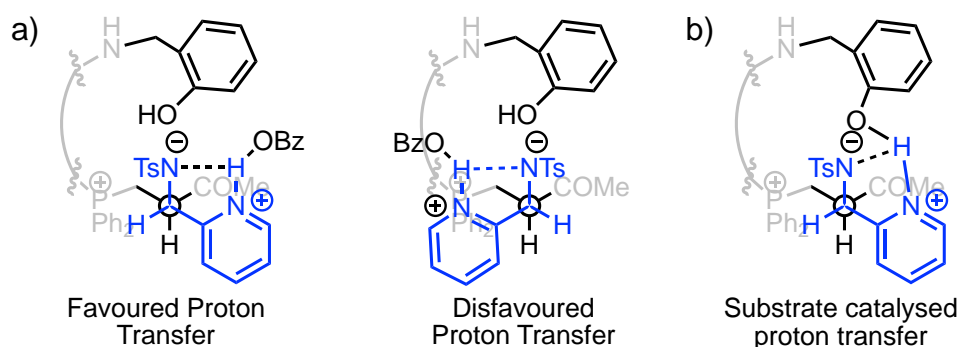
a) As determined by  $^1\text{H}$  NMR spectroscopy. b) As determined by chiral HPLC. See Appendix for more details regarding mobile phase, flow rate and column. c) <5% conversion as determined by  $^1\text{H}$  NMR spectroscopy.



For both the 3-pyridinyl and 2-pyridinyl substrates, BzOH was able to activate proton transfer for conjugative catalysis. Without BzOH, there was no conversion for 3-pyridinyl substrates (**NTsPyr-Im-1–6**) over thirty minutes with **TF-2** (Table 4.2, Entries 1–6), while the addition of BzOH led to moderate to good enantioselectivities (60–91%) with conversions ranging from 30–64% over 30 minutes. Substituents at the 2-position on 3-pyridinyl substrates (**NTsPyr-Im-2–3**) likely invoked steric clashing with the phenol motif, lowering the rate and enantioselectivity (2-F (**NTsPyr-MBH-2**)= 60% *ee*; 2-Cl (**NTsPyr-MBH-3**)= 70% *ee*; Table 4.2, Entries 2 and 3). Substitution at the 6-position (**NTsPyr-Im-4–6**) appeared to be well tolerated with good conversions (62–64%) and enantioselectivity (82–91% *ee*) (Table 4.2, Entries 4–6). The catalytic profile for **NTsPyr-Im-1–6** parallels aryl tosyl aldimines (Chapter 3).

For the 2-pyridinyl substrates (**NTsPyr-Im-7–8**), the conventional enolate mechanism appeared to be more active compared to 3-pyridinyl substrates (Table 4.2, Entries 7 and 8). Asymmetric induction for **NTsPyr-MBH-7** was identical with and without BzOH (*ee*= 50%), however with BzOH, the reaction rate became significantly faster (Table 4.2, Entry 7). Likewise, for **NTsPyr-MBH-8**, the enantioselectivities with or without BzOH are similar (Table 4.2, Entry 8). These substrates are the first examples of the trifunctional catalytic system where the conjugative mode of catalysis is the dominant pathway. Significant levels of conversion and enantioselectivities could be observed for *N*-tosyl aldimines via the conventional enolate intermediate without BzOH activation. The origin of the 2-pyridinyl reactivity is unclear. With BzOH, protonation of the pyridinyl nitrogen (Brønsted base) by BzOH yields a pyridinium conjugate acid as proton transfer intermediate that significantly accelerates the reaction without changing the level or sense of the asymmetric induction, likely by directing proton transfer to either diastereomer of the aldol adduct (**Scheme 4.5a**). Steric clashing between

the catalyst BINAP scaffold and the tosyl group is the key factor for the observed stereoselectivity of the reaction. Moreover, the protonation of the pyridinyl nitrogen may assist in stabilisation of the sulfonamide negative charge. In the absence of the additive, the pyridine base may also catalyse the proton transfer by shuttling the proton from the phenol to the sulfonamide (**Scheme 4.5b**).

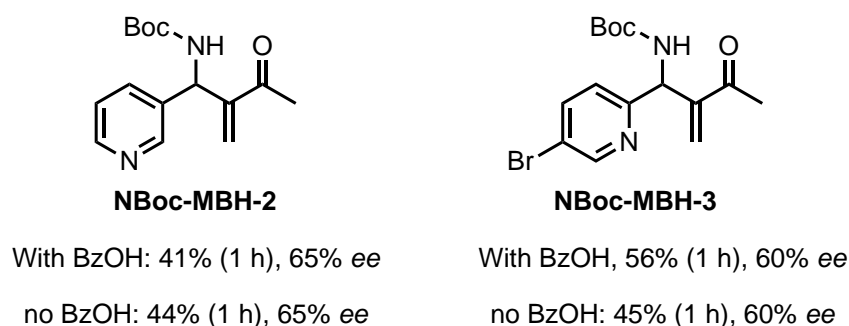


**Scheme 4.5.** Proton transfer catalysed by the pyridine nitrogen base a) with acid and b) without acid.

In summary, 3-pyridinyl *N*-tosyl imines are able to adopt the conjugative catalysis mode in the presence of BzOH while 2-pyridinyl analogues are unable to and can proceed through the subjugative pathway. This confirms the initial hypothesis that the position of the additional Brønsted base on the substrate can only be tolerated if it is not in a position to interfere with organized proton transfer. The specificity of the proton transfer network can be disrupted if the additional Brønsted base can orchestrate alternate proton transfer pathways.

To further test how the stability of the pyridinyl aldolate can alter the activity of the conventional subjugative catalysis (enolate formation) in competition with the BzOH activated conjugative catalysis (nucleophilic enol formation), carbamoyl-substituted, 2- or 3-pyridinyl imines were prepared and subjected to a model aza-MBH reaction with MVK and **TF-2** (**Scheme 4.6**). The profile for pyridinyl carbamates parallels aryl carbamates. For the 3-

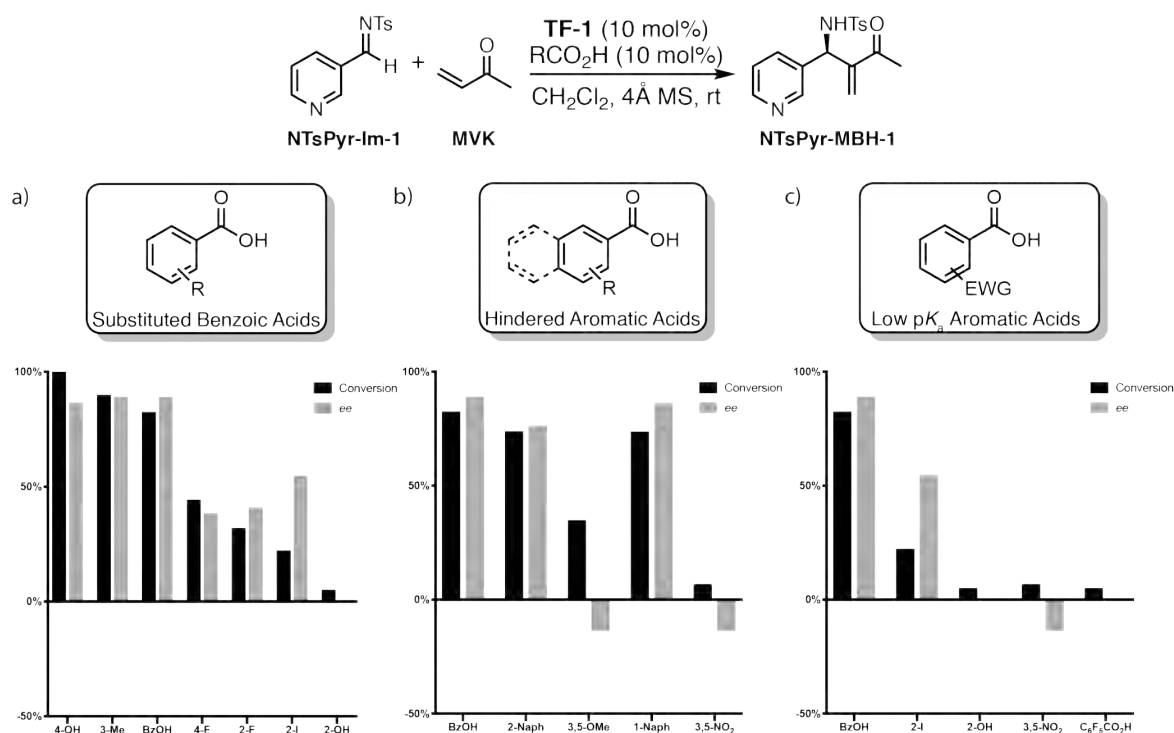
pyridinyl *N*-Boc imine **NBoc-Im-2**, BzOH addition exhibited no influence on the rate nor enantioselectivity (Scheme 4.6, **NBoc-MBH-2**). Likewise, for the 2-pyridinyl analogue, no change in conversion or *ee* occurs with the addition of BzOH (Scheme 4.6, **NBoc-MBH-3**). Unlike the *N*-tosyl case, where C–C bond formation and proton transfer are organised by BzOH to become likely concerted in conjugative catalysis, the *N*-carbamoyl imines are only able to proceed via subjugative catalysis by forming the stabilised aldolate. In addition, this confirms the conjugative mode requires the cooperative action of catalyst (with the appropriate geometry), co-factor and substrate.



**Scheme 4.6.** Effect of the substrate protecting group on reaction outcome for **TF-1**.

#### 4.2.4 Effect of the acid additive on catalytic proficiency for 3-pyridinyl imine substrates

In Chapter 3, it was shown that the identity and acidity of the acid additive influences the tautomerisation of the PBK and proton transfer in conjugative catalysis. Both aryl and 3-pyridinyl *N*-tosyl imine substrates require BzOH for proficient catalysis, therefore a range of acid additives, covering three broad groups of aromatic acids (substituted (Group 1), sterically hindered (Group 2) and lower  $pK_a$  (Group 3)), were tested to determine the effect of the acid additive on rate and enantioselectivity for **TF-1** catalysed reactions. Conversion and enantioselectivity were determined after 90 mins for the aza-MBH reaction between model substrate **NTsPyr-Im-1** and **MVK** (Figure 4.3 and Table 4.3).



**Figure 4.3.** Effect of the acid additive on rate and ee of the **TF-1** catalysed aza-MBH reaction with a) substituted BzOHs, b) hindered aromatic acids and 3) low pK<sub>a</sub> aromatic acids.

**Table 4.3.** Effect of the acid additive on catalytic proficiency for model pyridine substrates.

| <chem>N#Cc1ccncc1C=O</chem> + <chem>CC(=O)C=C</chem> $\xrightarrow[\text{CH}_2\text{Cl}_2, 4\text{\AA MS, rt}]{\text{TF-1 (10 mol\%)}, \text{RCO}_2\text{H (10 mol\%)}}$ <chem>CC(=O)C=C[C@H](N#Cc1ccncc1)C(=O)N#Cc1ccncc1</chem> |  |                 |                             |                     |
|---|--|-----------------|-----------------------------|---------------------|
| NTsPyr-Im-1      MVK  |  | NTsPyr-MBH-1    |                             |                     |
| Entry   | Acid   | pK <sub>a</sub> | Conversion <sup>a</sup> / % | ee <sup>b</sup> / % |
| 1   | 4-OH-C <sub>6</sub> H <sub>4</sub> CO <sub>2</sub> H                                 | 4.55            | 100                         | 86                  |
| 2   | 3-Me-C <sub>6</sub> H <sub>4</sub> CO <sub>2</sub> H                                 | 4.24            | 90                          | 89                  |
| 3   | BzOH   | 4.20            | 82                          | 89                  |
| 4   | 2-naphthoic acid   | 4.16            | 74                          | 76                  |
| 5   | 4-F-C <sub>6</sub> H <sub>4</sub> CO <sub>2</sub> H                                  | 4.15            | 44                          | 38                  |
| 6   | 3,5-(OMe) <sub>2</sub> -C <sub>6</sub> H <sub>3</sub> CO <sub>2</sub> H              | 3.97            | 35                          | -14                 |
| 7   | 1-naphthoic acid   | 3.67            | 74                          | 86                  |
| 8   | 2-F-C <sub>6</sub> H <sub>4</sub> CO <sub>2</sub> H                                  | 3.57            | 32                          | 41                  |
| 9   | 2-I-C <sub>6</sub> H <sub>4</sub> CO <sub>2</sub> H                                  | 2.96            | 22                          | 55                  |
| 10  | 2-OH-C <sub>6</sub> H <sub>4</sub> CO <sub>2</sub> H                                 | 2.77            | 5                           | 0                   |
| 11  | 3,5-(NO <sub>2</sub> ) <sub>2</sub> -C <sub>6</sub> H <sub>3</sub> CO <sub>2</sub> H | 2.67            | 6                           | -14                 |
| 12  | C <sub>6</sub> F <sub>5</sub> -CO <sub>2</sub> H                                     | 2.05            | 5                           | 0                   |

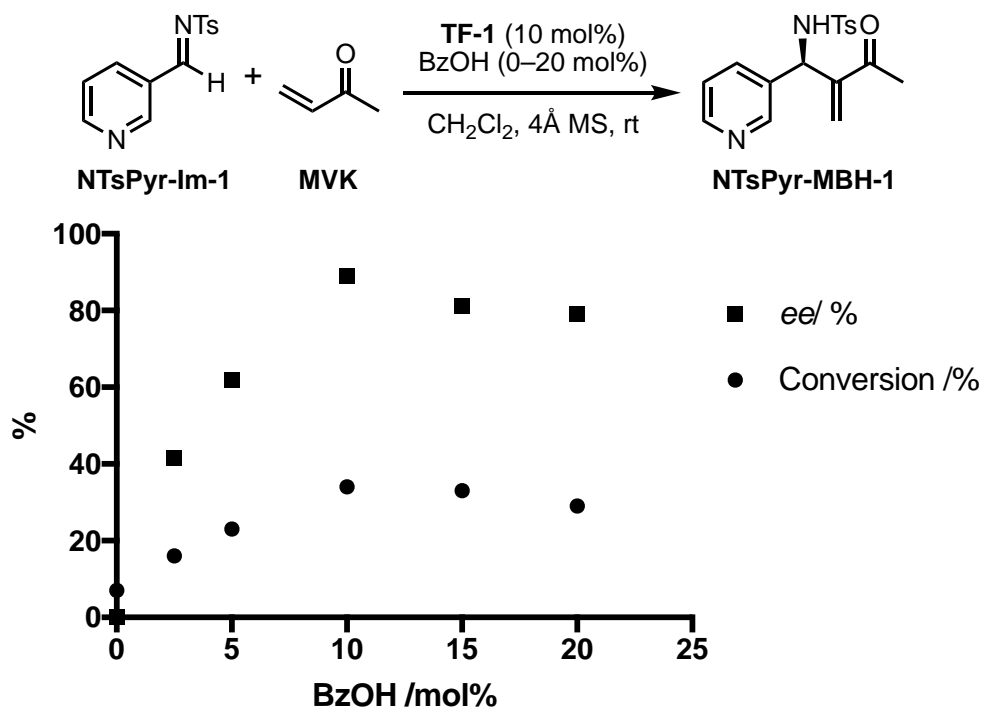
a) Determined by <sup>1</sup>H NMR spectroscopy. Note: no hydrolysis was observed in these reactions. b) Determined by chiral HPLC analysis.

Across the three different groups (substituted acids (Group 1; **Figure 4.3a**), sterically hindered acids (Group 2; **Figure 4.3b**), lower  $pK_a$  acids (Group 3; **Figure 4.3c**), **NTsPyr-Im-1** responded to acid additives with a similar profile to that for benzaldimines (**NTs-Im-1**, Chapter 3, Figure 3.1). The rate of reaction decreases as the acidity of the additive increases (**Figure 4.3c**, **Table 4.3**) as stronger acids become more suppressive of tautomerisation of the PBK. Moreover, the pyridinyl Brønsted base is unable to substitute for benzoate and catalyse tautomerisation of these PBK. The high reactivity of pyridinyl substrates towards the aza-MBH reaction is due to the activating effect of the electron deficient pyridinyl ring.

Close analogues of BzOH (Group 1 acids; **Figure 4.3a**) are highly effective in catalysis activation as the enantioselectivity and rate of reaction are coupled to a greater extent than the case for the aryl imines. For acids such as BzOH and 2-naphthoic acid (with  $pK_a$  above 3), the enantioselectivity was generally excellent (76–89% *ee*). Rate and enantioselectivity decrease simultaneously as the strength of the acid additive increases (**Table 4.3**). For sterically more demanding BzOH acids (**Figure 4.3b**), 1-naphthoic (**Table 4.3**, Entry 7; 74% conversion) and 2-naphthoic acid (**Table 4.3**, Entry 4; 74% conversion) appear highly effective on catalysis activation whereas 3,5-dimethoxyBzOH proceeds with sluggish conversion (35%) and poor enantioselectivity (-14% *ee*). This profile parallels that for benzaldimines suggesting pyridinyl substrates may proceed through a similar mechanistic pathway by conjugative catalysis.

At this point, it is unclear whether the proficient conjugative catalysis involves a 1:1 stoichiometric relationship between trifunctional organocatalyst and BzOH or if excess acid would facilitate additional roles. By altering the loading of BzOH, insight can be gained into the nature of the trifunctional proton transfer pathway. For a model aza-MBH reaction with

**TF-1** (10 mol%), MVK, and **NTsPyr-Im-1**, the loading BzOH was altered from 0–20 mol% and the effect on enantioselectivity and conversion was measured in 30 min. (**Figure 4.4**, **Table 4.4**).

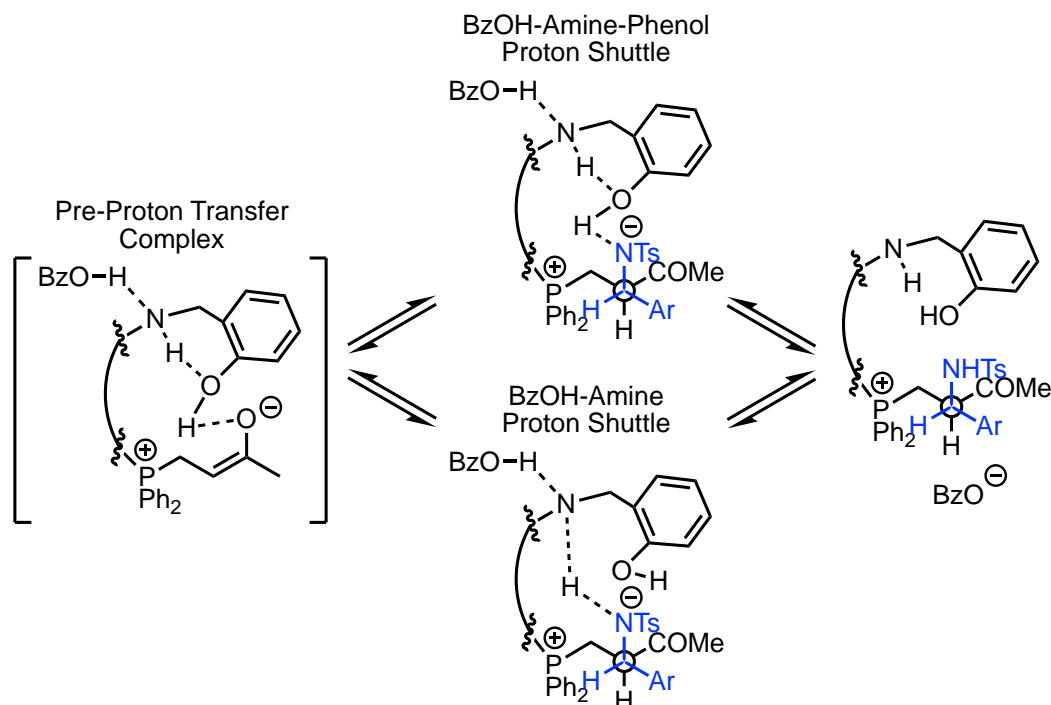


**Figure 4.4.** Effect of BzOH loading on catalytic proficiency for model substrate **NTsPyr-Im-1**.

**Table 4.4.** Effect of BzOH loading on catalytic proficiency for model substrate **NTsPyr-Im-1**.

|   |
|---|
| <chem>Nc1ccc(cc1)C(=O)Nc2ccc(cc2)C(=O)Nc3ccc(cc3)C(=O)Nc4ccc(cc4)C(=O)Nc5ccc(cc5)C(=O)Nc6ccc(cc6)C(=O)Nc7ccc(cc7)C(=O)Nc8ccc(cc8)C(=O)Nc9ccc(cc9)C(=O)Nc10ccc(cc10)C(=O)Nc11ccc(cc11)C(=O)Nc12ccc(cc12)C(=O)Nc13ccc(cc13)C(=O)Nc14ccc(cc14)C(=O)Nc15ccc(cc15)C(=O)Nc16ccc(cc16)C(=O)Nc17ccc(cc17)C(=O)Nc18ccc(cc18)C(=O)Nc19ccc(cc19)C(=O)Nc20ccc(cc20)C(=O)Nc21ccc(cc21)C(=O)Nc22ccc(cc22)C(=O)Nc23ccc(cc23)C(=O)Nc24ccc(cc24)C(=O)Nc25ccc(cc25)C(=O)Nc26ccc(cc26)C(=O)Nc27ccc(cc27)C(=O)Nc28ccc(cc28)C(=O)Nc29ccc(cc29)C(=O)Nc30ccc(cc30)C(=O)Nc31ccc(cc31)C(=O)Nc32ccc(cc32)C(=O)Nc33ccc(cc33)C(=O)Nc34ccc(cc34)C(=O)Nc35ccc(cc35)C(=O)Nc36ccc(cc36)C(=O)Nc37ccc(cc37)C(=O)Nc38ccc(cc38)C(=O)Nc39ccc(cc39)C(=O)Nc40ccc(cc40)C(=O)Nc41ccc(cc41)C(=O)Nc42ccc(cc42)C(=O)Nc43ccc(cc43)C(=O)Nc44ccc(cc44)C(=O)Nc45ccc(cc45)C(=O)Nc46ccc(cc46)C(=O)Nc47ccc(cc47)C(=O)Nc48ccc(cc48)C(=O)Nc49ccc(cc49)C(=O)Nc50ccc(cc50)C(=O)Nc51ccc(cc51)C(=O)Nc52ccc(cc52)C(=O)Nc53ccc(cc53)C(=O)Nc54ccc(cc54)C(=O)Nc55ccc(cc55)C(=O)Nc56ccc(cc56)C(=O)Nc57ccc(cc57)C(=O)Nc58ccc(cc58)C(=O)Nc59ccc(cc59)C(=O)Nc60ccc(cc60)C(=O)Nc61ccc(cc61)C(=O)Nc62ccc(cc62)C(=O)Nc63ccc(cc63)C(=O)Nc64ccc(cc64)C(=O)Nc65ccc(cc65)C(=O)Nc66ccc(cc66)C(=O)Nc67ccc(cc67)C(=O)Nc68ccc(cc68)C(=O)Nc69ccc(cc69)C(=O)Nc70ccc(cc70)C(=O)Nc71ccc(cc71)C(=O)Nc72ccc(cc72)C(=O)Nc73ccc(cc73)C(=O)Nc74ccc(cc74)C(=O)Nc75ccc(cc75)C(=O)Nc76ccc(cc76)C(=O)Nc77ccc(cc77)C(=O)Nc78ccc(cc78)C(=O)Nc79ccc(cc79)C(=O)Nc80ccc(cc80)C(=O)Nc81ccc(cc81)C(=O)Nc82ccc(cc82)C(=O)Nc83ccc(cc83)C(=O)Nc84ccc(cc84)C(=O)Nc85ccc(cc85)C(=O)Nc86ccc(cc86)C(=O)Nc87ccc(cc87)C(=O)Nc88ccc(cc88)C(=O)Nc89ccc(cc89)C(=O)Nc90ccc(cc90)C(=O)Nc91ccc(cc91)C(=O)Nc92ccc(cc92)C(=O)Nc93ccc(cc93)C(=O)Nc94ccc(cc94)C(=O)Nc95ccc(cc95)C(=O)Nc96ccc(cc96)C(=O)Nc97ccc(cc97)C(=O)Nc98ccc(cc98)C(=O)Nc99ccc(cc99)C(=O)Nc100ccc(cc100)C(=O)Nc101ccc(cc101)C(=O)Nc102ccc(cc102)C(=O)Nc103ccc(cc103)C(=O)Nc104ccc(cc104)C(=O)Nc105ccc(cc105)C(=O)Nc106ccc(cc106)C(=O)Nc107ccc(cc107)C(=O)Nc108ccc(cc108)C(=O)Nc109ccc(cc109)C(=O)Nc110ccc(cc110)C(=O)Nc111ccc(cc111)C(=O)Nc112ccc(cc112)C(=O)Nc113ccc(cc113)C(=O)Nc114ccc(cc114)C(=O)Nc115ccc(cc115)C(=O)Nc116ccc(cc116)C(=O)Nc117ccc(cc117)C(=O)Nc118ccc(cc118)C(=O)Nc119ccc(cc119)C(=O)Nc120ccc(cc120)C(=O)Nc121ccc(cc121)C(=O)Nc122ccc(cc122)C(=O)Nc123ccc(cc123)C(=O)Nc124ccc(cc124)C(=O)Nc125ccc(cc125)C(=O)Nc126ccc(cc126)C(=O)Nc127ccc(cc127)C(=O)Nc128ccc(cc128)C(=O)Nc129ccc(cc129)C(=O)Nc130ccc(cc130)C(=O)Nc131ccc(cc131)C(=O)Nc132ccc(cc132)C(=O)Nc133ccc(cc133)C(=O)Nc134ccc(cc134)C(=O)Nc135ccc(cc135)C(=O)Nc136ccc(cc136)C(=O)Nc137ccc(cc137)C(=O)Nc138ccc(cc138)C(=O)Nc139ccc(cc139)C(=O)Nc140ccc(cc140)C(=O)Nc141ccc(cc141)C(=O)Nc142ccc(cc142)C(=O)Nc143ccc(cc143)C(=O)Nc144ccc(cc144)C(=O)Nc145ccc(cc145)C(=O)Nc146ccc(cc146)C(=O)Nc147ccc(cc147)C(=O)Nc148ccc(cc148)C(=O)Nc149ccc(cc149)C(=O)Nc150ccc(cc150)C(=O)Nc151ccc(cc151)C(=O)Nc152ccc(cc152)C(=O)Nc153ccc(cc153)C(=O)Nc154ccc(cc154)C(=O)Nc155ccc(cc155)C(=O)Nc156ccc(cc156)C(=O)Nc157ccc(cc157)C(=O)Nc158ccc(cc158)C(=O)Nc159ccc(cc159)C(=O)Nc160ccc(cc160)C(=O)Nc161ccc(cc161)C(=O)Nc162ccc(cc162)C(=O)Nc163ccc(cc163)C(=O)Nc164ccc(cc164)C(=O)Nc165ccc(cc165)C(=O)Nc166ccc(cc166)C(=O)Nc167ccc(cc167)C(=O)Nc168ccc(cc168)C(=O)Nc169ccc(cc169)C(=O)Nc170ccc(cc170)C(=O)Nc171ccc(cc171)C(=O)Nc172ccc(cc172)C(=O)Nc173ccc(cc173)C(=O)Nc174ccc(cc174)C(=O)Nc175ccc(cc175)C(=O)Nc176ccc(cc176)C(=O)Nc177ccc(cc177)C(=O)Nc178ccc(cc178)C(=O)Nc179ccc(cc179)C(=O)Nc180ccc(cc180)C(=O)Nc181ccc(cc181)C(=O)Nc182ccc(cc182)C(=O)Nc183ccc(cc183)C(=O)Nc184ccc(cc184)C(=O)Nc185ccc(cc185)C(=O)Nc186ccc(cc186)C(=O)Nc187ccc(cc187)C(=O)Nc188ccc(cc188)C(=O)Nc189ccc(cc189)C(=O)Nc190ccc(cc190)C(=O)Nc191ccc(cc191)C(=O)Nc192ccc(cc192)C(=O)Nc193ccc(cc193)C(=O)Nc194ccc(cc194)C(=O)Nc195ccc(cc195)C(=O)Nc196ccc(cc196)C(=O)Nc197ccc(cc197)C(=O)Nc198ccc(cc198)C(=O)Nc199ccc(cc199)C(=O)Nc200ccc(cc200)C(=O)Nc201ccc(cc201)C(=O)Nc202ccc(cc202)C(=O)Nc203ccc(cc203)C(=O)Nc204ccc(cc204)C(=O)Nc205ccc(cc205)C(=O)Nc206ccc(cc206)C(=O)Nc207ccc(cc207)C(=O)Nc208ccc(cc208)C(=O)Nc209ccc(cc209)C(=O)Nc210ccc(cc210)C(=O)Nc211ccc(cc211)C(=O)Nc212ccc(cc212)C(=O)Nc213ccc(cc213)C(=O)Nc214ccc(cc214)C(=O)Nc215ccc(cc215)C(=O)Nc216ccc(cc216)C(=O)Nc217ccc(cc217)C(=O)Nc218ccc(cc218)C(=O)Nc219ccc(cc219)C(=O)Nc220ccc(cc220)C(=O)Nc221ccc(cc221)C(=O)Nc222ccc(cc222)C(=O)Nc223ccc(cc223)C(=O)Nc224ccc(cc224)C(=O)Nc225ccc(cc225)C(=O)Nc226ccc(cc226)C(=O)Nc227ccc(cc227)C(=O)Nc228ccc(cc228)C(=O)Nc229ccc(cc229)C(=O)Nc230ccc(cc230)C(=O)Nc231ccc(cc231)C(=O)Nc232ccc(cc232)C(=O)Nc233ccc(cc233)C(=O)Nc234ccc(cc234)C(=O)Nc235ccc(cc235)C(=O)Nc236ccc(cc236)C(=O)Nc237ccc(cc237)C(=O)Nc238ccc(cc238)C(=O)Nc239ccc(cc239)C(=O)Nc240ccc(cc240)C(=O)Nc241ccc(cc241)C(=O)Nc242ccc(cc242)C(=O)Nc243ccc(cc243)C(=O)Nc244ccc(cc244)C(=O)Nc245ccc(cc245)C(=O)Nc246ccc(cc246)C(=O)Nc247ccc(cc247)C(=O)Nc248ccc(cc248)C(=O)Nc249ccc(cc249)C(=O)Nc250ccc(cc250)C(=O)Nc251ccc(cc251)C(=O)Nc252ccc(cc252)C(=O)Nc253ccc(cc253)C(=O)Nc254ccc(cc254)C(=O)Nc255ccc(cc255)C(=O)Nc256ccc(cc256)C(=O)Nc257ccc(cc257)C(=O)Nc258ccc(cc258)C(=O)Nc259ccc(cc259)C(=O)Nc260ccc(cc260)C(=O)Nc261ccc(cc261)C(=O)Nc262ccc(cc262)C(=O)Nc263ccc(cc263)C(=O)Nc264ccc(cc264)C(=O)Nc265ccc(cc265)C(=O)Nc266ccc(cc266)C(=O)Nc267ccc(cc267)C(=O)Nc268ccc(cc268)C(=O)Nc269ccc(cc269)C(=O)Nc270ccc(cc270)C(=O)Nc271ccc(cc271)C(=O)Nc272ccc(cc272)C(=O)Nc273ccc(cc273)C(=O)Nc274ccc(cc274)C(=O)Nc275ccc(cc275)C(=O)Nc276ccc(cc276)C(=O)Nc277ccc(cc277)C(=O)Nc278ccc(cc278)C(=O)Nc279ccc(cc279)C(=O)Nc280ccc(cc280)C(=O)Nc281ccc(cc281)C(=O)Nc282ccc(cc282)C(=O)Nc283ccc(cc283)C(=O)Nc284ccc(cc284)C(=O)Nc285ccc(cc285)C(=O)Nc286ccc(cc286)C(=O)Nc287ccc(cc287)C(=O)Nc288ccc(cc288)C(=O)Nc289ccc(cc289)C(=O)Nc290ccc(cc290)C(=O)Nc291ccc(cc291)C(=O)Nc292ccc(cc292)C(=O)Nc293ccc(cc293)C(=O)Nc294ccc(cc294)C(=O)Nc295ccc(cc295)C(=O)Nc296ccc(cc296)C(=O)Nc297ccc(cc297)C(=O)Nc298ccc(cc298)C(=O)Nc299ccc(cc299)C(=O)Nc300ccc(cc300)C(=O)Nc301ccc(cc301)C(=O)Nc302ccc(cc302)C(=O)Nc303ccc(cc303)C(=O)Nc304ccc(cc304)C(=O)Nc305ccc(cc305)C(=O)Nc306ccc(cc306)C(=O)Nc307ccc(cc307)C(=O)Nc308ccc(cc308)C(=O)Nc309ccc(cc309)C(=O)Nc310ccc(cc310)C(=O)Nc311ccc(cc311)C(=O)Nc312ccc(cc312)C(=O)Nc313ccc(cc313)C(=O)Nc314ccc(cc314)C(=O)Nc315ccc(cc315)C(=O)Nc316ccc(cc316)C(=O)Nc317ccc(cc317)C(=O)Nc318ccc(cc318)C(=O)Nc319ccc(cc319)C(=O)Nc320ccc(cc320)C(=O)Nc321ccc(cc321)C(=O)Nc322ccc(cc322)C(=O)Nc323ccc(cc323)C(=O)Nc324ccc(cc324)C(=O)Nc325ccc(cc325)C(=O)Nc326ccc(cc326)C(=O)Nc327ccc(cc327)C(=O)Nc328ccc(cc328)C(=O)Nc329ccc(cc329)C(=O)Nc330ccc(cc330)C(=O)Nc331ccc(cc331)C(=O)Nc332ccc(cc332)C(=O)Nc333ccc(cc333)C(=O)Nc334ccc(cc334)C(=O)Nc335ccc(cc335)C(=O)Nc336ccc(cc336)C(=O)Nc337ccc(cc337)C(=O)Nc338ccc(cc338)C(=O)Nc339ccc(cc339)C(=O)Nc340ccc(cc340)C(=O)Nc341ccc(cc341)C(=O)Nc342ccc(cc342)C(=O)Nc343ccc(cc343)C(=O)Nc344ccc(cc344)C(=O)Nc345ccc(cc345)C(=O)Nc346ccc(cc346)C(=O)Nc347ccc(cc347)C(=O)Nc348ccc(cc348)C(=O)Nc349ccc(cc349)C(=O)Nc350ccc(cc350)C(=O)Nc351ccc(cc351)C(=O)Nc352ccc(cc352)C(=O)Nc353ccc(cc353)C(=O)Nc354ccc(cc354)C(=O)Nc355ccc(cc355)C(=O)Nc356ccc(cc356)C(=O)Nc357ccc(cc357)C(=O)Nc358ccc(cc358)C(=O)Nc359ccc(cc359)C(=O)Nc360ccc(cc360)C(=O)Nc361ccc(cc361)C(=O)Nc362ccc(cc362)C(=O)Nc363ccc(cc363)C(=O)Nc364ccc(cc364)C(=O)Nc365ccc(cc365)C(=O)Nc366ccc(cc366)C(=O)Nc367ccc(cc367)C(=O)Nc368ccc(cc368)C(=O)Nc369ccc(cc369)C(=O)Nc370ccc(cc370)C(=O)Nc371ccc(cc371)C(=O)Nc372ccc(cc372)C(=O)Nc373ccc(cc373)C(=O)Nc374ccc(cc374)C(=O)Nc375ccc(cc375)C(=O)Nc376ccc(cc376)C(=O)Nc377ccc(cc377)C(=O)Nc378ccc(cc378)C(=O)Nc379ccc(cc379)C(=O)Nc380ccc(cc380)C(=O)Nc381ccc(cc381)C(=O)Nc382ccc(cc382)C(=O)Nc383ccc(cc383)C(=O)Nc384ccc(cc384)C(=O)Nc385ccc(cc385)C(=O)Nc386ccc(cc386)C(=O)Nc387ccc(cc387)C(=O)Nc388ccc(cc388)C(=O)Nc389ccc(cc389)C(=O)Nc390ccc(cc390)C(=O)Nc391ccc(cc391)C(=O)Nc392ccc(cc392)C(=O)Nc393ccc(cc393)C(=O)Nc394ccc(cc394)C(=O)Nc395ccc(cc395)C(=O)Nc396ccc(cc396)C(=O)Nc397ccc(cc397)C(=O)Nc398ccc(cc398)C(=O)Nc399ccc(cc399)C(=O)Nc400ccc(cc400)C(=O)Nc401ccc(cc401)C(=O)Nc402ccc(cc402)C(=O)Nc403ccc(cc403)C(=O)Nc404ccc(cc404)C(=O)Nc405ccc(cc405)C(=O)Nc406ccc(cc406)C(=O)Nc407ccc(cc407)C(=O)Nc408ccc(cc408)C(=O)Nc409ccc(cc409)C(=O)Nc410ccc(cc410)C(=O)Nc411ccc(cc411)C(=O)Nc412ccc(cc412)C(=O)Nc413ccc(cc413)C(=O)Nc414ccc(cc414)C(=O)Nc415ccc(cc415)C(=O)Nc416ccc(cc416)C(=O)Nc417ccc(cc417)C(=O)Nc418ccc(cc418)C(=O)Nc419ccc(cc419)C(=O)Nc420ccc(cc420)C(=O)Nc421ccc(cc421)C(=O)Nc422ccc(cc422)C(=O)Nc423ccc(cc423)C(=O)Nc424ccc(cc424)C(=O)Nc425ccc(cc425)C(=O)Nc426ccc(cc426)C(=O)Nc427ccc(cc427)C(=O)Nc428ccc(cc428)C(=O)Nc429ccc(cc429)C(=O)Nc430ccc(cc430)C(=O)Nc431ccc(cc431)C(=O)Nc432ccc(cc432)C(=O)Nc433ccc(cc433)C(=O)Nc434ccc(cc434)C(=O)Nc435ccc(cc435)C(=O)Nc436ccc(cc436)C(=O)Nc437ccc(cc437)C(=O)Nc438ccc(cc438)C(=O)Nc439ccc(cc439)C(=O)Nc440ccc(cc440)C(=O)Nc441ccc(cc441)C(=O)Nc442ccc(cc442)C(=O)Nc443ccc(cc443)C(=O)Nc444ccc(cc444)C(=O)Nc445ccc(cc445)C(=O)Nc446ccc(cc446)C(=O)Nc447ccc(cc447)C(=O)Nc448ccc(cc448)C(=O)Nc449ccc(cc449)C(=O)Nc450ccc(cc450)C(=O)Nc451ccc(cc451)C(=O)Nc452ccc(cc452)C(=O)Nc453ccc(cc453)C(=O)Nc454ccc(cc454)C(=O)Nc455ccc(cc455)C(=O)Nc456ccc(cc456)C(=O)Nc457ccc(cc457)C(=O)Nc458ccc(cc458)C(=O)Nc459ccc(cc459)C(=O)Nc460ccc(cc460)C(=O)Nc461ccc(cc461)C(=O)Nc462ccc(cc462)C(=O)Nc463ccc(cc463)C(=O)Nc464ccc(cc464)C(=O)Nc465ccc(cc465)C(=O)Nc466ccc(cc466)C(=O)Nc467ccc(cc467)C(=O)Nc468ccc(cc468)C(=O)Nc469ccc(cc469)C(=O)Nc470ccc(cc470)C(=O)Nc471ccc(cc471)C(=O)Nc472ccc(cc472)C(=O)Nc473ccc(cc473)C(=O)Nc474ccc(cc474)C(=O)Nc475ccc(cc475)C(=O)Nc476ccc(cc476)C(=O)Nc477ccc(cc477)C(=O)Nc478ccc(cc478)C(=O)Nc479ccc(cc479)C(=O)Nc480ccc(cc480)C(=O)Nc481ccc(cc481)C(=O)Nc482ccc(cc482)C(=O)Nc483ccc(cc483)C(=O)Nc484ccc(cc484)C(=O)Nc485ccc(cc485)C(=O)Nc486ccc(cc486)C(=O)Nc487ccc(cc487)C(=O)Nc488ccc(cc488)C(=O)Nc489ccc(cc489)C(=O)Nc490ccc(cc490)C(=O)Nc491ccc(cc491)C(=O)Nc492ccc(cc492)C(=O)Nc493ccc(cc493)C(=O)Nc494ccc(cc494)C(=O)Nc495ccc(cc495)C(=O)Nc496ccc(cc496)C(=O)Nc497ccc(cc497)C(=O)Nc498ccc(cc498)C(=O)Nc499ccc(cc499)C(=O)Nc500ccc(cc500)C(=O)Nc501ccc(cc501)C(=O)Nc502ccc(cc502)C(=O)Nc503ccc(cc503)C(=O)Nc504ccc(cc504)C(=O)Nc505ccc(cc505)C(=O)Nc506ccc(cc506)C(=O)Nc507ccc(cc507)C(=O)Nc508ccc(cc508)C(=O)Nc509ccc(cc509)C(=O)Nc510ccc(cc510)C(=O)Nc511ccc(cc511)C(=O)Nc512ccc(cc512)C(=O)Nc513ccc(cc513)C(=O)Nc514ccc(cc514)C(=O)Nc515ccc(cc515)C(=O)Nc516ccc(cc516)C(=O)Nc517ccc(cc517)C(=O)Nc518ccc(cc518)C(=O)Nc519ccc(cc519)C(=O)Nc520ccc(cc520)C(=O)Nc521ccc(cc521)C(=O)Nc522ccc(cc522)C(=O)Nc523ccc(cc523)C(=O)Nc524ccc(cc524)C(=O)Nc525ccc(cc525)C(=O)Nc526ccc(cc526)C(=O)Nc527ccc(cc527)C(=O)Nc528ccc(cc528)C(=O)Nc529ccc(cc529)C(=O)Nc530ccc(cc530)C(=O)Nc531ccc(cc531)C(=O)Nc532ccc(cc532)C(=O)Nc533ccc(cc533)C(=O)Nc534ccc(cc534)C(=O)Nc535ccc(cc535)C(=O)Nc536ccc(cc536)C(=O)Nc537ccc(cc537)C(=O)Nc538ccc(cc538)C(=O)Nc539ccc(cc539)C(=O)Nc540ccc(cc540)C(=O)Nc541ccc(cc541)C(=O)Nc542ccc(cc542)C(=O)Nc543ccc(cc543)C(=O)Nc544ccc(cc544)C(=O)Nc545ccc(cc545)C(=O)Nc546ccc(cc546)C(=O)Nc547ccc(cc547)C(=O)Nc548ccc(cc548)C(=O)Nc549ccc(cc549)C(=O)Nc550ccc(cc550)C(=O)Nc551ccc(cc551)C(=O)Nc552ccc(cc552)C(=O)Nc553ccc(cc553)C(=O)Nc554ccc(cc554)C(=O)Nc555ccc(cc555)C(=O)Nc556ccc(cc556)C(=O)Nc557ccc(cc557)C(=O)Nc558ccc(cc558)C(=O)Nc559ccc(cc559)C(=O)Nc560ccc(cc560)C(=O)Nc561ccc(cc561)C(=O)Nc562ccc(cc562)C(=O)Nc563ccc(cc563)C(=O)Nc564ccc(cc564)C(=O)Nc565ccc(cc565)C(=O)Nc566ccc(cc566)C(=O)Nc567ccc(cc567)C(=O)Nc568ccc(cc568)C(=O)Nc569ccc(cc569)C(=O)Nc570ccc(cc570)C(=O)Nc571ccc(cc571)C(=O)Nc572ccc(cc572)C(=O)Nc573ccc(cc573)C(=O)Nc574ccc(cc574)C(=O)Nc575ccc(cc575)C(=O)Nc576ccc(cc576)C(=O)Nc577ccc(cc577)C(=O)Nc578ccc(cc578)C(=O)Nc579ccc(cc579)C(=O)Nc580ccc(cc580)C(=O)Nc581ccc(cc581)C(=O)Nc582ccc(cc582)C(=O)Nc583ccc(cc583)C(=O)Nc584ccc(cc584)C(=O)Nc585ccc(cc585)C(=O)Nc586ccc(cc586)C(=O)Nc587ccc(cc587)C(=O)Nc588ccc(cc588)C(=O)Nc589ccc(cc589)C(=O)Nc590ccc(cc590)C(=O)Nc591ccc(cc591)C(=O)Nc592ccc(cc592)C(=O)Nc593ccc(cc593)C(=O)Nc594ccc(cc594)C(=O)Nc595ccc(cc595)C(=O)Nc596ccc(cc596)C(=O)Nc597ccc(cc597)C(=O)Nc598ccc(cc598)C(=O)Nc599ccc(cc599)C(=O)Nc600ccc(cc600)C(=O)Nc601ccc(cc601)C(=O)Nc602ccc(cc602)C(=O)Nc603ccc(cc603)C(=O)Nc604ccc(cc604)C(=O)Nc605ccc(cc605)C(=O)Nc606ccc(cc606)C(=O)Nc607ccc(cc607)C(=O)Nc608ccc(cc608)C(=O)Nc609ccc(cc609)C(=O)Nc610ccc(cc610)C(=O)Nc611ccc(cc611)C(=O)Nc612ccc(cc612)C(=O)Nc613ccc(cc613)C(=O)Nc614ccc(cc614)C(=O)Nc615ccc(cc615)C(=O)Nc616ccc(cc616)C(=O)Nc617ccc(cc617)C(=O)Nc618ccc(cc618)C(=O)Nc619ccc(cc619)C(=O)Nc620ccc(cc620)C(=O)Nc621ccc(cc621)C(=O)Nc622ccc(cc622)C(=O)Nc623ccc(cc623)C(=O)Nc624ccc(cc624)C(=O)Nc625ccc(cc625)C(=O)Nc626ccc(cc626)C(=O)Nc627ccc(cc627)C(=O)Nc628ccc(cc628)C(=O)Nc629ccc(cc629)C(=O)Nc630ccc(cc630)C(=O)Nc631ccc(cc631)C(=O)Nc632ccc(cc632)C(=O)Nc633ccc(cc633)C(=O)Nc634ccc(cc634)C(=O)Nc635ccc(cc635)C(=O)Nc636ccc(cc636)C(=O)Nc637ccc(cc637)C(=O)Nc638ccc(cc638)C(=O)Nc639ccc(cc639)C(=O)Nc640ccc(cc640)C(=O)Nc641ccc(cc641)C(=O)Nc642ccc(cc642)C(=O)Nc643ccc(cc643)C(=O)Nc644ccc(cc644)C(=O)Nc645ccc(cc645)C(=O)Nc646ccc(cc646)C(=O)Nc647ccc(cc647)C(=O)Nc648ccc(cc648)C(=O)Nc649ccc(cc649)C(=O)Nc650ccc(cc650)C(=O)Nc651ccc(cc651)C(=O)Nc652ccc(cc652)C(=O)Nc653ccc(cc653)C(=O)Nc654ccc(cc654)C(=O)Nc655ccc(cc655)C(=O)Nc656ccc(cc656)C(=O)Nc657ccc(cc657)C(=O)Nc658ccc(cc658)C(=O)Nc659ccc(cc659)C(=O)Nc660ccc(cc660)C(=O)Nc661ccc(cc661)C(=O)Nc662ccc(cc662)C(=O)Nc663ccc(cc663)C(=O)Nc664ccc(cc664)C(=O)Nc665ccc(cc665)C(=O)Nc666ccc(cc666)C(=O)Nc667ccc(cc667)C(=O)Nc668ccc(cc668)C(=O)Nc669ccc(cc669)C(=O)Nc670ccc(cc670)C(=O)Nc671ccc(cc671)C(=O)Nc672ccc(cc672)C(=O)Nc673ccc(cc673)C(=O)Nc674ccc(cc674)C(=O)Nc675ccc(cc675)C(=O)Nc676ccc(cc676)C(=O)Nc677ccc(cc677)C(=O)Nc678ccc(cc678)C(=O)Nc679ccc(cc679)C(=O)Nc680ccc(cc680)C(=O)Nc681ccc(cc681)C(=O)Nc682ccc(cc682)C(=O)Nc683ccc(cc683)C(=O)Nc684ccc(cc684)C(=O)Nc685ccc(cc685)C(=O)Nc686ccc(cc686)C(=O)Nc687ccc(cc687)C(=O)Nc688ccc(cc688)C(=O)Nc689ccc(cc689)C(=O)Nc690ccc(cc690)C(=O)Nc691ccc(cc691)C(=O)Nc692ccc(cc692)C(=O)Nc693ccc(cc693)C(=O)Nc694ccc(cc694)C(=O)Nc695ccc(cc695)C(=O)Nc696ccc(cc696)C(=O)Nc697ccc(cc697)C(=O)Nc698ccc(cc698)C(=O)Nc699ccc(cc699)C(=O)Nc700ccc(cc700)C(=O)Nc701ccc(cc701)C(=O)Nc702ccc(cc702)C(=O)Nc703ccc(cc703)C(=O)Nc704ccc(cc704)C(=O)Nc705ccc(cc705)C(=O)Nc706ccc(cc706)C(=O)Nc707ccc(cc707)C(=O)Nc708ccc(cc708)C(=O)Nc709ccc(cc709)C(=O)Nc710ccc(cc710)C(=O)Nc711ccc(cc711)C(=O)Nc712ccc(cc712)C(=O)Nc713ccc(cc713)C(=O)Nc714ccc(cc714)C(=O)Nc715ccc(cc715)C(=O)Nc716ccc(cc716)C(=O)Nc717ccc(cc717)C(=O)Nc718ccc(cc718)C(=O)Nc719ccc(cc719)C(=O)Nc720ccc(cc720)C(=O)Nc721ccc(cc721)C(=O)Nc722ccc(cc722)C(=O)Nc723ccc(cc723)C(=O)Nc724ccc(cc724)C(=O)Nc725ccc(cc725)C(=O)Nc726ccc(cc726)C(=O)Nc727ccc(cc727)C(=O)Nc728ccc(cc728)C(=O)Nc729ccc(cc729)C(=O)Nc730ccc(cc730)C(=O)Nc731ccc(cc731)C(=O)Nc732ccc(cc732)C(=O)Nc733ccc(cc733)C(=O)Nc734ccc(cc734)C(=O)Nc735ccc</chem> |
|---|

BzOH (**Table 4.4**, Entry 4); higher loading of BzOH caused no further elevation. BzOH loading as low as 2.5 mol% (25% with respect to **TF-1**) doubles the rate compared to the reaction without acid and has a lower level of asymmetric induction (42%; **Table 4.4**, Entry 2). Increasing the equivalents of BzOH above 10 mol% (1:1 ratio to **TF-1**) causes minimal changes in the rate (**Table 4.4**, Entry 5-6) but a large decrease in the enantioselectivity of the reaction. The hypothesised proton transfer network is supported by the response to the amount of the acid additive (**Figure 4.5**). With a substoichiometric amount of BzOH, the asymmetric induction is lower due to a decrease in the proportion of substrates proceeding through conjugative pathway facilitated by the proton-transfer network. With superstoichiometric amounts of BzOH, non-specific protonation of the aldolate occurs alongside the stereospecific protonation via the proton-transfer pathway.



**Figure 4.5.** Proton transfer network mediated by the cooperative action of chemical motifs.

#### 4.2.5 Conclusion

In this chapter, 3-pyridinyl *N*-tosyl imine substrates, analogous to their aryl counterparts, are shown to be effective substrates for conjugative catalysis in the aza-MBH reaction. These substrates require BzOH to organize the proton transfer network to achieve high rates and enantioselectivities. The conjugative mode of catalysis is only accessible for 3-pyridinyl *N*-tosyl imines substrates. *N*-Boc and 2-pyridinyl *N*-tosyl imines proceed through the subjugative mode of catalysis via the conventional enolate-driven pathway. The proton transfer network in this mode of conjugative catalysis is shown to tolerate additional proton stationary points (e.g. an additional Bronsted base) as long as it is not in close proximity. In the next chapter, the question of if this mode of catalysis could be utilised in organising a kinetically differentiated reaction network will be explored. In particular, the asymmetric potential of this proton network-based catalysis for chirality propagation will be investigated in an asymmetric aza-MBH–Soai ripple reaction.



## 4.3 Experimental

### 4.3.1 Materials and Methods

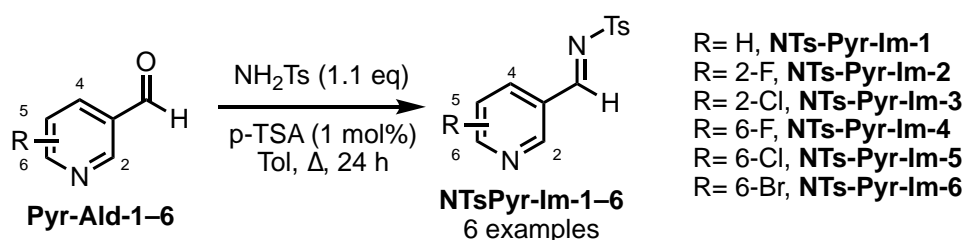
Toluene and THF were distilled from sodium/benzophenone immediately before use. All other reagents were purchased from Sigma-Aldrich Castle Hill. Unless specified, all commercially available reagents were used without further purification. Dichloromethane was distilled from calcium hydride. All air and moisture sensitive reactions were performed under a nitrogen atmosphere. Reactions were magnetically stirred and monitored by thin-layer chromatography (TLC) using silica gel 60 F254 aluminium pre-coated plates from Merck (0.25 mm). Flash column chromatography was performed on silica gel (60 Å, 0.06–0.2 mm, 400 mesh from Scharlau).

All  $^1\text{H}$ ,  $^{13}\text{C}$  and 2D NMR experiments were performed on either a Bruker AVIIIHD 400 MHz NMR Spectrometer equipped with a BBFO SmartProbe (5mm) or DRX600 NMR spectrometer equipped with a TXI (5 mm) Cryoprobe. Chemical shifts were reported in ppm using residual  $\text{CHCl}_3$  ( $\delta_{\text{H}}$ ; 7.26 ppm,  $\delta_{\text{C}}$ ; 77.16 ppm) as an internal reference. All 2D NMR experiments were run with quadrature detection and a relaxation delay of 1–3 s. High power  $1\text{H}$   $\pi/2$  pulses were determined to be  $\sim 9.5$  ms, and  $^{13}\text{C}$  high power  $\pi/2$  pulse was 11.05 ms, and a low power pulse of 65 ms was used for GARP4 decoupling. Gradient pulses were delivered along the z-axis using a 100 step sine program. Heteronuclear single quantum coherence (HSQC) experiments were optimised for a  $^1J_{\text{CH}}$  coupling of 145 Hz and HMBC spectra for a coupling of 20 Hz, using 145 Hz to suppress  $^1J_{\text{CH}}$  couplings. HSQC experiments were performed using the hsqcetgpsi or hsqcedetgpsp.3 (phase-edited HSQC) pulse program, and HMBC experiments were performed using the hmbcgp1pndqf pulse program. HSQC spectra were processed ( $\pi/2$  shifted sine bell squared in both dimensions) phase sensitive and HMBC (sine squared in both dimensions) with magnitude calculation in F1.  $^{13}\text{C}$  spectra were acquired using the UDEFT

sequence. NOESY experiments were performed using the noesygpshz pulse program with a mixing time of 400 ms. All spectra were processed using Bruker TOPSPIN 3.5p17. Trifunctional organocatalyst were prepared following the literature procedure.<sup>34-37</sup>

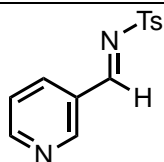
### 4.3.2 Synthesis of imine

#### 4.3.2.1 General Procedure for NTs 3-pyridine carbaldimines (NTsPyr-Im-1–6)



**Scheme 4E.1.** Synthesis of 3-Pyridine substrates **NTsPyr-Im-1–6**.

To a flame dried round bottom flask charged with a stir bar was added aldehyde (10 mmol), *p*-toluenesulfonamide (11.0 mmol) and a *p*-toluenesulfonic acid (0.010 mmol). Anhydrous toluene (10 mL) was added, a Dean-Stark apparatus was attached, and the reaction was placed under an inert atmosphere. The mixture was refluxed for 24 hours and the solvent was then removed under reduced pressure to afford the crude N-Tosyl protected imines (**NTsPyr-Im-1–6**) which were recrystallised from ethyl acetate-hexane to yield analytically pure imine.



**NTsPyr-Im-1**

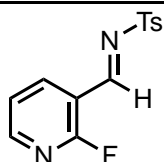
(*E*)-4-methyl-*N*-(pyridin-3-ylmethylene)benzenesulfonamide (**NTsPyr-Im-1**)

**<sup>1</sup>H NMR** (400 MHz, CDCl<sub>3</sub>, δ): 9.09 (s, 1H), 9.05 (s, 1H), 8.81 (d, *J* = 4.9 Hz, 1H), 8.27 (d, *J* = 4.9 Hz, 1H), 7.89 (d, *J* = 4.9 Hz, 2H), 7.44 (dd, *J* = 7.9, 4.9 Hz, 2H), 7.37 (d, *J* = 8.0 Hz, 2H), 2.45 (s, 3H).

**<sup>13</sup>C NMR** (100 MHz, CDCl<sub>3</sub>, δ): 167.7, 155.2, 153.1, 145.2, 137.0, 134.6, 130.1, 128.4, 124.2, 21.82.

**MS (ESI):** 261.1 [M+H]

---



**NTsPyr-Im-2**

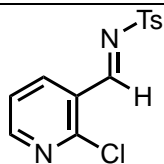
(*E*)-*N*-((2-fluoropyridin-3-yl)methylene)-4-methylbenzenesulfonamide (**NTsPyr-Im-2**)

**<sup>1</sup>H NMR** (400 MHz, CDCl<sub>3</sub>, δ): 9.25 (s, 1H), 8.50 (ddd, *J* = 9.1, 7.4, 1.9 Hz, 1H), 8.45 (ddd, *J* = 4.8, 2.1, 0.9 Hz, 1H), 7.89 (d, *J* = 8.3 Hz, 2H), 7.37 (d, *J* = 8.3 Hz, 2H), 7.33 (m, 1H).

**<sup>13</sup>C NMR** (100 MHz, CDCl<sub>3</sub>, δ): 163.8 (d, 248.6 Hz), 162.6 (d, 1.2 Hz), 154.1, 153.9, 140.3 (2.1 Hz), 134.2, 130.1, 128.6, 126.6, 122.5 (d, 4.4 Hz), 115.8, 115.3, 21.9

**MS (ESI):** 279.0 [M+H]

---



**NTsPyr-Im-3**

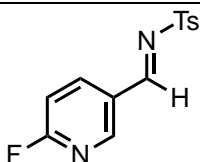
(*E*)-*N*-((2-chloropyridin-3-yl)methylene)-4-methylbenzenesulfonamide (**NTsPyr-Im-3**)

**<sup>1</sup>H NMR** (400 MHz, CDCl<sub>3</sub>, δ): 9.41 (s, 1H), 8.58 (dd, *J* = 4.7, 1.9 Hz, 1H), 8.46 (dd, *J* = 7.8 Hz, 1.9 Hz, 1H), 7.90 (d, *J* = 8.3 Hz, 2H), 7.37 (m, 3H), 2.46 (s, 3H)

**<sup>13</sup>C NMR** (100 MHz, CDCl<sub>3</sub>, δ): 165.90, 154.7, 154.6, 145.4, 138.9, 134.1, 130.1, 128.6, 126.9, 123.2, 21.8

**MS (ESI):** 295.0 [M+H]

---



**NTsPyr-lm-4**

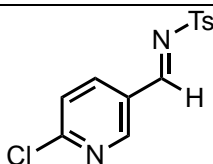
(*E*)-*N*-((6-fluoropyridin-3-yl)methylene)-4-methylbenzenesulfonamide (**NTsPyr-lm-4**)

**<sup>1</sup>H NMR** (400 MHz, CDCl<sub>3</sub>, δ): 9.09 (d, *J* = 1.8 Hz, 1H), 8.84 (dd, *J* = 1.4 Hz, 1H), 8.67 (d, *J* = 2.8 Hz, 1H), 7.98 (ddd, *J* = 8.4 Hz, 2.8 Hz, 1.7 Hz, 1H), 7.89 (d, *J* = 8.4 Hz, 2H), 7.37 (d, *J* = 8.4 Hz, 2H), 2.45 (1H, s)

**<sup>13</sup>C NMR** (100 MHz, CDCl<sub>3</sub>, δ): 166.2 (d, *J* = 2.2 Hz), 159.5 (d, *J* = 260.5 Hz), 149.0 (d, *J* = 4.3 Hz), 145.5, 144.2, 143.9, 134.2, 130.1, 128.5, 122.3 (d, *J* = 19.1 Hz), 21.9

**MS (ESI):** 279.0 [M+H]

---



**NTsPyr-lm-5**

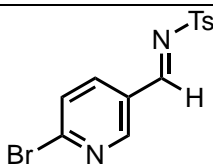
(*E*)-*N*-((6-chloropyridin-3-yl)methylene)-4-methylbenzenesulfonamide (**NTsPyr-lm-5**)

**<sup>1</sup>H NMR** (400 MHz, CDCl<sub>3</sub>, δ): 9.05 (s, 1H), 8.81 (d, *J* = 2.1 Hz, 1H), 8.22 (dd, *J* = 8.4, 2.4 Hz, 1H), 7.88 (d, *J* = 8.3 Hz, 2H), 7.46 (d, *J* = 8.4 Hz, 2H), 7.36 (d, *J* = 8.4 Hz, 2H), 2.45 (s, 3H).

**<sup>13</sup>C NMR** (100 MHz, CDCl<sub>3</sub>, δ): 166.2, 157.5, 153.2, 145.4, 139.1, 134.4, 130.1, 128.4, 127.4, 125.3, 21.8

**MS (ESI):** 295 [M+H]

---



**NTsPyr-lm-6**

(*E*)-*N*-((6-bromopyridin-3-yl)methylene)-4-methylbenzenesulfonamide (**NTsPyr-lm-6**)

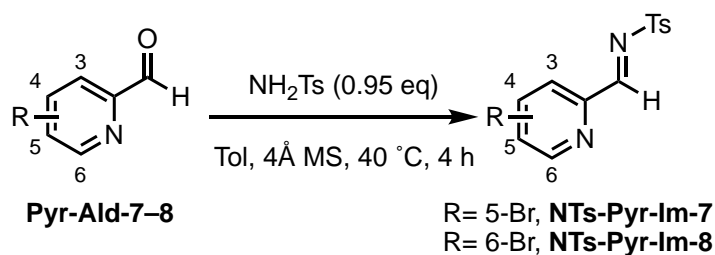
**<sup>1</sup>H NMR** (400 MHz, CDCl<sub>3</sub>, δ): δ 9.05 (s, 1H), 8.77 (d, *J* = 2.2 Hz, 1H), 8.10 (dd, *J* = 8.3, 2.4 Hz, 1H), 7.87 (d, *J* = 8.3 Hz, 1H), 7.62 (d, *J* = 8.3 Hz, 2H), 7.36 (d, *J* = 8.3 Hz, 2H), 2.45 (s, 3H).

**<sup>13</sup>C NMR** (100 MHz, CDCl<sub>3</sub>, δ): 166.4, 153.3, 148.8, 145.4, 138.5, 134.3, 130.1, 129.1, 128.4, 127.7, 21.8.

**MS (ESI):** 338.9 [M+H], 340.9 [M+H]

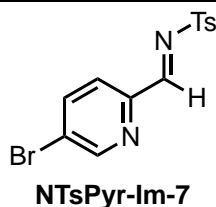
---

#### 4.3.2.2 General Procedure for NTs 2-pyridine carbaldimines



**Scheme 4E.2.** Synthesis of 2-Pyridine substrates (**NTs-Pyr-Im-7-8**).

To a flame dried round bottom flask charged with a stir bar was added aldehyde (10 mmol) and p-toluenesulfonamide (9.5 mmol) and 4 Å MS. Anhydrous, degassed toluene (10 mL) was added and the reaction was placed under an inert atmosphere. The mixture was vigorously stirred at 40 °C and monitored by  $^1\text{H}$  NMR spectroscopy. After complete consumption of the sulfonamide, the reaction was passed through a pad of celite. The pad was washed extensively with ethyl acetate and the solvent removed *in vacuo* to afford the crude N-Tosyl protected imines which were recrystallised from ethyl acetate-hexane to yield analytically pure imine.

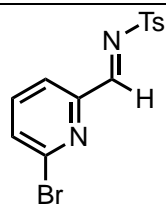


(*E*)-*N*-((5-bromopyridin-2-yl)methylene)-4-methylbenzenesulfonamide (**NTsPyr-Im-7**)

$^1\text{H}$  NMR (400 MHz,  $\text{CDCl}_3$ ,  $\delta$ ): 8.94 (s, 1H), 8.81 (d,  $J$  = 2.0 Hz, 1H), 8.04 (d,  $J$  = 8.4 Hz, 1H), 7.95 (dd,  $J$  = 8.4, 2.1 Hz, 1H), 7.88 (d,  $J$  = 8.3 Hz, 2H), 7.37 (d,  $J$  = 8.3 Hz, 2H), 2.45 (s, 3H).

$^{13}\text{C}$  NMR (100 MHz,  $\text{CDCl}_3$ ,  $\delta$ ): 169.1, 151.9, 149.8, 145.4, 139.8, 133.9, 130.1, 128.7, 126.1, 125.0, 21.8

**MS (ESI):** 338.9 [M+H], 340.9 [M+H]



**NTsPyr-Im-8**

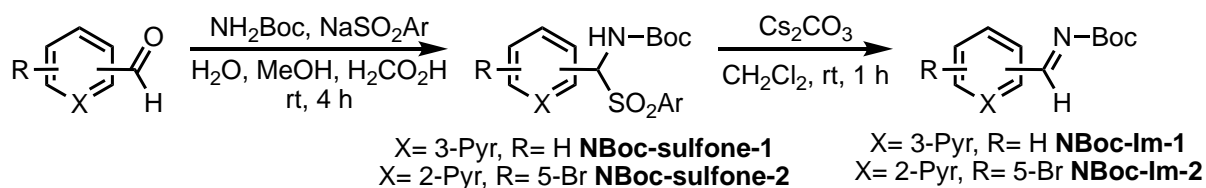
(*E*)-*N*-((6-bromopyridin-2-yl)methylene)-4-methylbenzenesulfonamide (**NTsPyr-Im-8**)

**<sup>1</sup>H NMR** (400 MHz, CDCl<sub>3</sub>, δ): 8.89 (s, 1H), 8.16 (dd, *J* = 6.9, 1.6 Hz, 1H), 7.89 (d, *J* = 7.9 Hz, 2H), 7.69 (m, 2H), 7.39 (d, *J* = 7.9 Hz, 2H), 2.45 (s, 2H).

**<sup>13</sup>C NMR** (CDCl<sub>3</sub>, 100 MHz) δ 168.5, 153.4, 145.5, 142.6, 139.3, 133.5, 132.8, 130.2, 128.8, 122.8, 21.8.

**MS (ESI):** 338.9 [M+H], 340.9 [M+H]

#### 4.3.2.3 General Procedure for NBoc pyridine carbaldimines



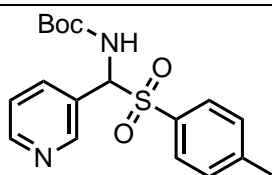
**Scheme 4E.3.** Synthesis of NBoc protected imines.

To a 50 mL round bottom flask charged with a stirring bar was added aldehyde (4 mmol), carbamate (2.67 mmol, 0.67 equiv) and toluenesulfinic acid sodium salt (8 mmol, 2 equiv). A solvent mixture of water (6 mL), methanol (3 mL) and formic acid (2 mL) was added and the mixture sonicated until material had dissolved. The reaction was stirred at room temperature for 4 hours before collecting the precipitate and washing with water and cold ether. The crude material was then triturated with ether to yield analytically pure carbamate sulfone.

The sulfone was dissolved in freshly distilled DCM and anhydrous Cs<sub>2</sub>CO<sub>3</sub> (10 equiv) was added.

The reaction was vigorously stirred for 45 minutes before filtering the heterogeneous mixture

through celite. The precipitate was washed three times with DCM and filtrate concentrated under reduced pressure to afford analytically pure carbamate imines.



**NBoc-sulfone-2**

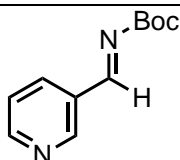
*tert*-butyl (pyridin-3-yl(tosyl)methyl)carbamate (**NBoc-sulfone-2**)

**<sup>1</sup>H NMR** (400 MHz, CDCl<sub>3</sub>, δ): 8.86 (s, 2H), 7.85 (d, *J* = 7.9 Hz, 1H), 7.83 (d, *J* = 7.8 Hz, 2H), 7.34 (m 3H), 6.26 (d, *J* = 10.8 Hz, 1H), 5.96 (d, *J* = 10.8 Hz, 1H), 2.42 (s, 3H), 1.25 (s, 9H)

**<sup>13</sup>C NMR** (100 MHz, CDCl<sub>3</sub>, δ): δ 153.7, 150.8, 150.1, 145.6, 136.5, 133.3, 129.8, 129.6, 126.7, 123.6, 81.5, 72.1, 28.1, 21.8

**MS (ESI):** 363.1 [M+H]

---



**NBoc-lm-2**

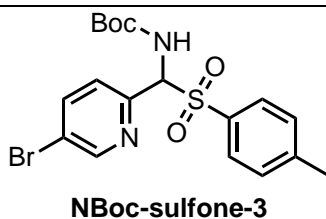
*tert*-butyl (*E*)-(pyridin-3-ylmethylene)carbamate (**NBoc-lm-2**)

**<sup>1</sup>H NMR** (400 MHz, CDCl<sub>3</sub>, δ): 8.99 (d, *J* = 1.8 Hz, 1H), 8.86 (s, 1H), 8.74 (dd, *J* = 4.8, 1.7 Hz, 1H), 8.25 (dt, *J* = 7.9, 1.9 Hz, 1H), 7.39 (dd, *J* = 7.9 Hz, 4.8 Hz, 1H) 1.57 (s, 9H).

**<sup>13</sup>C NMR** (100 MHz, CDCl<sub>3</sub>, δ): 166.8, 162.1, 154.0, 152.3, 135.9, 129.9, 124.0, 82.9, 27.9

**MS (ESI):** 207.1 [M+H]

---



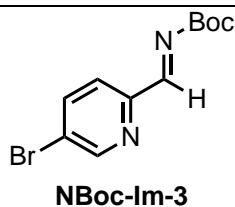
*tert*-butyl ((5-bromopyridin-2-yl)(tosyl)methyl)carbamate (**NBoc-sulfone-3**)

**<sup>1</sup>H NMR** (400 MHz, CDCl<sub>3</sub>, δ): 8.67 (d, *J* = 1.9 Hz, 1H), 7.90 (dd, *J* = 8.3, 2.3 Hz, 1H), 7.78 (d, *J* = 8.2 Hz, 2H), 7.53 (d, *J* = 8.2 Hz, 1H), 7.33 (d, *J* = 8.0 Hz, 2H), 7.72 (d, *J* = 9.4 Hz, 1H), 5.96 (d, *J* = 9.4 Hz, 1H), 2.43 (s, 3H), 1.26 (s, 9H).

**<sup>13</sup>C NMR** (100 MHz, CDCl<sub>3</sub>, δ): 153.7, 150.8, 146.8, 145.4, 139.4, 133.4, 130.0, 129.8, 126.7, 122.1, 81, 74.2, 28.4, 28.1, 21.2

**MS (ESI):** 339 [M-Boc]

---



*tert*-butyl (*E*)-((5-bromopyridin-2-yl)methylene)carbamate (**NBoc-Im-3**)

**<sup>1</sup>H NMR** (400 MHz, CDCl<sub>3</sub>, δ): 8.76 (m 1H), 8.74 (s, 1H), 8.03 (d, *J* = 8.4 Hz, 1H), 7.93 (dd, *J* = 8.4, 2.3 Hz, 1H), 1.58 (s, 9H)

**<sup>13</sup>C NMR** (100 MHz, CDCl<sub>3</sub>, δ): 167.7, 161.8, 151.4, 139.6, 129.9, 124.8, 123.6, 83.2, 28.0

**MS (ESI):** 285 [M+H]

---

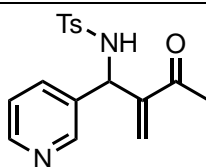
### 4.3.3 General procedures for catalysis

#### 4.3.3.1 Pyridine aza-MBH

Trifunctional catalyst (2.4 μmol, 10 mol%) and BzOH (2.4 μmol, 10 mol%) in anhydrous CH<sub>2</sub>Cl<sub>2</sub> was added to a flame-dried 2 mL vial charged with a stir bar and 4 Å MS. **PGPyr-Im-1** (24 μmol) was added in CH<sub>2</sub>Cl<sub>2</sub> and the volatiles removed by nitrogen blow down. Anhydrous CH<sub>2</sub>Cl<sub>2</sub> (150 μL) was added and the vials sonicated to ensure complete dissolution of the reagents. Methyl vinyl ketone (5.15 mg, 73 μmol, 3 equiv) was added and the reaction stirred vigorously



in a 25 °C sand bath for 3 hours. The volatiles were removed *in vacuo* and the crude material was analysed by  $^1\text{H}$  NMR spectroscopy to determine conversion and chiral HPLC to determine enantioselectivity



**NTsPyr-MBH-1**

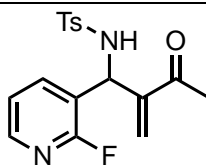
4-methyl-*N*-(2-methylene-3-oxo-1-(pyridin-3-yl)butyl)benzenesulfonamide (**NTsPyr-MBH-1**)

$^1\text{H}$  NMR (400 MHz,  $\text{CDCl}_3$ ,  $\delta$ ): 8.41 (dd,  $J$  = 4.8 Hz, 1.4 Hz, 1H), 8.30 (d,  $J$  = 2.7 Hz, 1H), 7.64 (d,  $J$  = 8.3 Hz, 2H), 7.53 (dt,  $J$  = 7.8, 1.6 Hz, 1H), 7.23 (d,  $J$  = 8.3 Hz, 2H), 7.14 (dd,  $J$  = 7.8 Hz, 4.8 Hz, 1H), 6.13 (s, 1H), 6.10 (s, 1H), 6.07 (d,  $J$  = 8.6 Hz, 1H), 2.40 (s, 3H), 2.16 (s, 3H).

$^{13}\text{C}$  NMR ( $\text{CDCl}_3$ , 100 MHz)  $\delta$  198.9, 148.9, 148.2, 145.7, 143.8, 137.5, 134.8, 134.3, 129.8, 129.3, 127.3, 123.4, 57.4, 26.3, 21.6.

**MS (ESI):** 331.1 [ $\text{M} + \text{H}$ ]

**Chiral HPLC:** 80:20 Hex/2-PrOH ( $0.7 \text{ mL min}^{-1}$ ), Chiralpak AD-H,  $\text{RT}_1$  36.40 min,  $\text{RT}_2$  38.54 min



**NTsPyr-MBH-2**

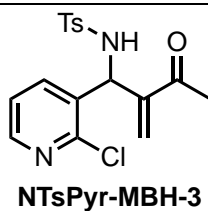
*N*-(1-(2-fluoropyridin-3-yl)-2-methylene-3-oxobutyl)-4-methylbenzenesulfonamide (**NTsPyr-MBH-2**)

$^1\text{H}$  NMR (400 MHz,  $\text{CDCl}_3$ ,  $\delta$ ): 8.01 (dt,  $J$  = 4.8, 1.5 Hz, 1H), 7.76 (ddd,  $J$  = 9.7, 7.8, 1.9 Hz, 1H), 7.63 (d,  $J$  = 8.3 Hz, 2H), 7.19 (d,  $J$  = 8.1 Hz, 2H), 7.04 (ddd,  $J$  = 7.4, 4.9, 1.8 Hz, 1H), 6.14 (s, 1H), 6.10 (s, 1H), 5.40 (br, 1H), 2.37 (s, 3H), 2.17 (s, 3H)

$^{13}\text{C}$  NMR (100 MHz,  $\text{CDCl}_3$ ,  $\delta$ ): 199.2, 146.8, 146.6, 144.4, 143.8, 140.0, 139.9, 137.4, 129.8, 129.7, 127.2, 121.6, 121.5, 121.4, 121.2, 54.2, 26.3, 21.6

**MS (ESI):** 349.1 [ $\text{M} + \text{H}$ ]

**Chiral HPLC:** 80:20 Hex/2-PrOH ( $0.7 \text{ mL min}^{-1}$ ), Chiralpak AD-H Column,  $\text{RT}_1$ : 21.46 min,  $\text{RT}_2$ : 25.49 min



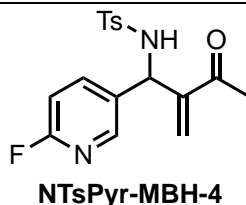
*N*-(1-(2-chloropyridin-3-yl)-2-methylene-3-oxobutyl)-4-methylbenzenesulfonamide (**NTsPyr-MBH-3**)

**<sup>1</sup>H NMR** (400 MHz, CDCl<sub>3</sub>, δ): 8.19 (dd, *J* = 4.7, 1.9 Hz, 1H), 7.76 (dd, *J* = 7.9, 1.9 Hz, 1H), 7.61 (d, *J* = 8.3 Hz, 2H), 7.17 (d, *J* = 8.3 Hz, 2H), 7.08 (dd, *J* = 7.7, 4.7 Hz, 1H), 6.16 (s, 1H), 6.00 (b, 1H), 5.53 (d, *J* = 9.2 Hz, 1H), 2.36 (s, 2H), 2.19 (s, 3H)

**<sup>13</sup>C NMR** (100 MHz, CDCl<sub>3</sub>, δ): 199.3, 149.5, 148.7, 143.9, 143.8, 138.5, 137.2, 132.9, 130.9, 129.7, 127.3, 122.6, 56.5, 26.5, 21.6.

**MS (ESI):** 365.1 [M+ H]

**Chiral HPLC:** 80:20 Hex/2-PrOH (0.7 mL min<sup>-1</sup>), Chiralpak AD-H Column, RT<sub>1</sub>: 21.46 min, RT<sub>2</sub>: 25.49 min



*N*-(1-(6-fluoropyridin-3-yl)-2-methylene-3-oxobutyl)-4-methylbenzenesulfonamide (**NTsPyr-MBH-4**)

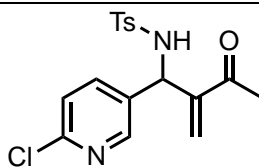
**<sup>1</sup>H NMR** (400 MHz, CDCl<sub>3</sub>, δ): 8.26 (m, 1H), 8.14 (m, 1H), 7.26 (d, *J* = 8.0 Hz, 2H), 7.24 (m, 3H), 6.10 (m, 3H), 5.29 (d, *J* = 9.3 Hz, 1H), 2.40 (s, 3H), 2.16 (s, 3H).

**<sup>13</sup>C NMR** (100 MHz, CDCl<sub>3</sub>, δ): 198.8, 160.6, 158.1, 145.4, 143.96, 143.8 (d, 4 Hz), 137.4, 137.4, 137.1, 136.8, 129.8, 129.7, 127.3, 121.3 (d, 19.3 Hz), 57.0, 26.3, 21.6.

**MS (ESI):** 349.1 [M+ H]

**Chiral HPLC:** 80:20 Hex/2-PrOH (0.7 mL min<sup>-1</sup>), Chiralpak AD-H Column, RT<sub>1</sub>: 27.35 min, RT<sub>2</sub>: 30.13 min

---



**NTsPyr-MBH-5**

*N*-(1-(6-chloropyridin-3-yl)-2-methylene-3-oxobutyl)-4-methylbenzenesulfonamide (**NTsPyr-MBH-5**)

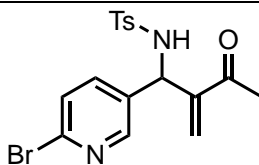
**<sup>1</sup>H NMR** (400 MHz, CDCl<sub>3</sub>, δ): 8.07 (d, *J* = 2.6 Hz, 1H), 7.62 (d, *J* = 8.2 Hz, 2H), 7.50 (dd, *J* = 8.3, 2.5 Hz, 1H), 7.23 (d, *J* = 8.1 Hz, 2H), 7.15 (d, *J* = 8.3 Hz, 1H), 6.12 (s, 1H), 6.08 (s, 1H), 5.99 (b, 1H), 5.26 (d, *J* = 9.3 Hz, 1H), 2.41 (s, 3H), 2.16 (s, 3H).

**<sup>13</sup>C NMR** (100 MHz, CDCl<sub>3</sub>, δ): 198.9, 150.8, 147.9, 145.4, 143.9, 137.4, 137.2, 133.8, 129.8, 129.7, 127.3, 124.1, 57.2, 29.8, 26.3, 21.7.

**MS (ESI):** 365.1 [M+ H]

**Chiral HPLC:** 80:20 Hex/2-PrOH (0.7 mL min<sup>-1</sup>), Chiralpak AD-H Column, RT<sub>1</sub>: 29.70 min, RT<sub>2</sub>: 39.11 min

---



**NTsPyr-MBH-6**

*N*-(1-(6-bromopyridin-3-yl)-2-methylene-3-oxobutyl)-4-methylbenzenesulfonamide (**NTsPyr-MBH-6**)

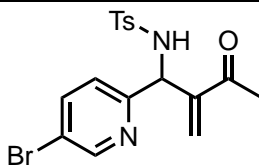
**<sup>1</sup>H NMR** (400 MHz, CDCl<sub>3</sub>, δ): 8.06 (d, *J* = 2.4 Hz, 1H), 7.61 (d, *J* = 8.2 Hz, 2H), 7.40 (dd, *J* = 7.2, 2.5 Hz, 1H), 7.23 (d, *J* = 8.1 Hz, 2H), 6.12 (s, 1H), 6.08 (s, 1H), 5.97 (m, 1H), 5.24 (d, *J* = 9.2 Hz, 2H), 2.41 (s, 3H), 2.16 (s, 3H)

**<sup>13</sup>C NMR** (100 MHz, CDCl<sub>3</sub>, δ): 198.9, 148.6, 145.4, 141.3, 137.3, 136.9, 134.3, 129.8, 129.6, 127.9, 127.3, 56.9, 26.3, 21.7.

**MS (ESI):** 408.9 [M+ H] 410.9 [M+H]

**Chiral HPLC:** 80:20 Hex/2-PrOH (0.7 mL min<sup>-1</sup>), Chiralpak AD-H Column, RT<sub>1</sub>: 26.94 min, RT<sub>2</sub>: 34.84 min

---



**NTsPyr-MBH-7**

*N*-(1-(5-bromopyridin-2-yl)-2-methylene-3-oxobutyl)-4-methylbenzenesulfonamide (**NTsPyr-MBH-7**)

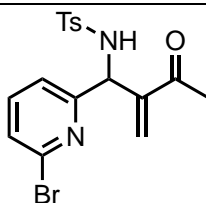
**<sup>1</sup>H NMR** (400 MHz, CDCl<sub>3</sub>, δ): 8.44 (d, *J* = 2.0 Hz, 1H), 7.64 (m, 3H), 7.20 (m, 3H), 6.34 (d, *J* = 8.7 Hz, 1H), 6.11 (s, 1H), 6.09 (s, 1H), 5.39 (d, *J* = 8.7 Hz, 1H), 2.40 (s, 3H), 2.33 (s, 3H).

**<sup>13</sup>C NMR** (100 MHz, CDCl<sub>3</sub>, δ): 198.8, 156.2, 149.8, 146.6, 143.5, 139.3, 137.3, 129.6, 128.7, 127.3, 123.7, 119.5, 27.5, 26.2, 21.6.

**MS (ESI):** 408.9 [M+ H] 410.9 [M+H]

**Chiral HPLC:** 80:20 Hex/2-PrOH (0.7 mL min<sup>-1</sup>), Chiralpak AD-H Column, RT<sub>1</sub>: 23.84 min, RT<sub>2</sub>: 24.80 min

---



**NTsPyr-MBH-8**

*N*-(1-(6-bromopyridin-2-yl)-2-methylene-3-oxobutyl)-4-methylbenzenesulfonamide (**NTsPyr-MBH-8**)

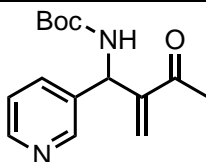
**<sup>1</sup>H NMR** (400 MHz, CDCl<sub>3</sub>, δ): 7.62 (d, *J* = 8.3 Hz, 2H), 7.34 (dd, *J* = 8.3 Hz, 1H), 7.21 (m, 4H), 6.26 (d, *J* = 8.9 Hz, 1H), 6.10 (s, 1H), 6.09 (s, 1H), 5.39 (d, *J* = 8.9 Hz, 1H), 2.36 (s, 3H), 2.23 (s, 3H).

**<sup>13</sup>C NMR** (100 MHz, CDCl<sub>3</sub>, δ): 198.8, 158.9, 146.3, 143.5, 141.2, 138.9, 137.2, 129.5, 128.8, 127.3, 126.9, 121.2, 57.3, 26.2, 21.6

**MS (ESI):** 408.9 [M+ H] 410.9 [M+H]

**Chiral HPLC:** 85:15 Hex/2-PrOH (0.7 mL min<sup>-1</sup>), Chiralpak AD-H Column, RT<sub>1</sub>: 24.79 min, RT<sub>2</sub>: 29.24 min

---



**NBoc-MBH-2**

*tert*-butyl (2-methylene-3-oxo-1-(pyridin-3-yl)butyl)carbamate (**NBoc-MBH-2**)

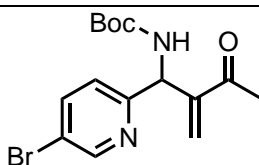
**<sup>1</sup>H NMR** (400 MHz, CDCl<sub>3</sub>, δ): 8.48 (d, *J* = 1.4 Hz, 1H), 8.46 (dd, *J* = 4.8, 1.4 Hz), 7.60 (dd, *J* = 7.9, 3.8 Hz), 7.21 (dd, *J* = 7.9, 4.8 Hz, 1H), 6.26 (s, 1H), 6.18 (s, 1H), 5.65 (m, 2H), 2.31 (s, 3H), 1.43 (s, 9H).

**<sup>13</sup>C NMR** (100 MHz, CDCl<sub>3</sub>, δ): 198.9, 155.1, 148.7, 148.3, 147.0, 136.1, 134.2, 128.3, 123.4, 80., 54.7, 28.4, 26.6.

**MS (ESI)**: 277.1 [M+ H]

**Chiral HPLC**: 80:20 Hex/2-PrOH (0.7 mL min<sup>-1</sup>), Chiralpak AD-H Column, RT<sub>1</sub>: 10.83 min, RT<sub>2</sub>: 14.21 min

---



**NBoc-MBH-3**

*tert*-butyl (1-(5-bromopyridin-2-yl)-2-methylene-3-oxobutyl)carbamate (**NBoc-MBH-3**)

**<sup>1</sup>H NMR** (400 MHz, CDCl<sub>3</sub>, δ): 8.17 (d, *J* = 2.5 Hz, 1H), 7.42 (dd, *J* = 8.3, 2.6 Hz, 1H), 7.33 (d, *J* = 8.2 Hz, 2H), 6.21 (s, 1H), 6.13 (s, 1H), 5.93 (b, 1H), 5.53 (d, *J* = 8.9 Hz, 1H), 2.25 (s, 3H), 1.37 (s, 9H).

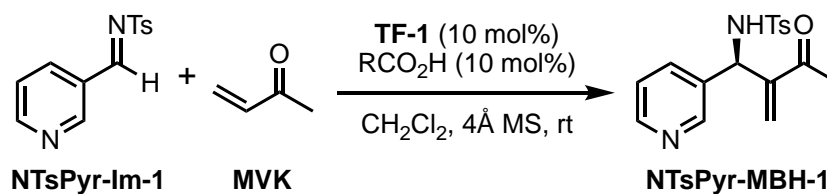
**<sup>13</sup>C NMR** (100 MHz, CDCl<sub>3</sub>, δ): 198.9, 155.0, 148.6, 146.6, 140.9, 136.9, 135.8, 128.8, 127.8, 80.4, 54.3, 28.4, 26.5

**MS (ESI)**: 355.0 [M+ H] 357.0 [M+H]

**Chiral HPLC**: 85:15 Hex/2-PrOH (0.7 mL min<sup>-1</sup>), Chiralpak AD-H Column, RT<sub>1</sub>: 8.93 min, RT<sub>2</sub>: 9.93 min

---

#### 4.3.3.2 Acid screen



**Scheme 4E.4.** Acid screen for **NTsPyr-Im-1** with **TF-1**.

**TF-1** (1.37 mg, 2.4  $\mu$ mol, 10 mol%) and acid (2.4  $\mu$ mol, 10 mol%) in anhydrous **CH<sub>2</sub>Cl<sub>2</sub>** was added to a flame-dried 2 mL vial charged with a stir bar and 4 Å MS. **NTsPyr-Im-1** (8.28 mg, 24  $\mu$ mol) was added in **CH<sub>2</sub>Cl<sub>2</sub>** and the volatiles removed by nitrogen blow down. Anhydrous **CH<sub>2</sub>Cl<sub>2</sub>** (150  $\mu$ L) was added and the vials sonicated to ensure complete dissolution of the reagents. Methyl vinyl ketone (5.15 mg, 73  $\mu$ mol, 3 equiv) was added and the reaction stirred vigorously in a 25 °C sand bath for 3 hours. The volatiles were removed *in vacuo* and the crude material was analysed by <sup>1</sup>H NMR spectroscopy to determine conversion and chiral HPLC to determine enantioselectivity

#### 4.5 References

1. Vitaku, E.; Smith, D. T.; Njardarson, J. T., Analysis of the Structural Diversity, Substitution Patterns, and Frequency of Nitrogen Heterocycles among U.S. FDA Approved Pharmaceuticals. *J. Med. Chem.* **2014**, *57* (24), 10257-10274.
2. Taylor, R. D.; MacCoss, M.; Lawson, A. D. G., Rings in Drugs. *J. Med. Chem.* **2014**, *57* (14), 5845-5859.
3. Kiuru, P.; Yli - Kauhaluoma, J., Pyridine and Its Derivatives. In *Heterocycles in Natural Product Synthesis*, Majumdar, K. C.; Chattopadhyay, S. K., Eds. Wiley-VCH Verlag GmbH & Co. KGaA: Weinheim, Germany: 2011; pp 267-297.
4. Baumann, M.; Baxendale, I. R., An overview of the synthetic routes to the best selling drugs containing 6-membered heterocycles. *Beilstein J. Org. Chem.* **2013**, *9*, 2265-2319.
5. Vitaku, E.; Smith, D. T.; Njardarson, J. T., Analysis of the Structural Diversity, Substitution Patterns, and Frequency of Nitrogen Heterocycles among U.S. FDA Approved Pharmaceuticals. *J. Med. Chem.* **2014**, *57* (24), 10257-10274.
6. Chu, L.; Shang, M.; Tanaka, K.; Chen, Q.; Pissarnitski, N.; Streckfuss, E.; Yu, J.-Q., Remote Meta-C-H Activation Using a Pyridine-Based Template: Achieving Site-Selectivity via the Recognition of Distance and Geometry. *ACS Cent. Sci.* **2015**, *1* (7), 394-399.
7. Rudolph, J.; Reddy, K. L.; Chiang, J. P.; Sharpless, K. B., Highly Efficient Epoxidation of Olefins Using Aqueous H<sub>2</sub>O<sub>2</sub> and Catalytic Methyltrioxorhenium/Pyridine: Pyridine-Mediated Ligand Acceleration. *J. Am. Chem. Soc.* **1997**, *119* (26), 6189-6190.
8. Grützmacher, H., Cooperating Ligands in Catalysis. *Angew. Chem., Int. Ed.* **2008**, *47* (10), 1814-1818.
9. Gibson, V. C.; Redshaw, C.; Solan, G. A., Bis(imino)pyridines: Surprisingly Reactive Ligands and a Gateway to New Families of Catalysts. *Chem. Rev.* **2007**, *107* (5), 1745-1776.

10. Kuhl, N.; Hopkinson, M. N.; Wencel - Delord, J.; Glorius, F., Beyond Directing Groups: Transition - Metal - Catalyzed C-H Activation of Simple Arenes. *Angew. Chem., Int. Ed.* **2012**, *51* (41), 10236-10254.
11. Scriven, E. F. V., 4-Dialkylaminopyridines: super acylation and alkylation catalysts. *Chem. Soc. Rev.* **1983**, *12* (2), 129-161.
12. Fu, G. C., Enantioselective Nucleophilic Catalysis with “Planar-Chiral” Heterocycles. *Acc. Chem. Res.* **2000**, *33* (6), 412-420.
13. Fu, G. C., Asymmetric Catalysis with “Planar-Chiral” Derivatives of 4-(Dimethylamino)pyridine. *Acc. Chem. Res.* **2004**, *37* (8), 542-547.
14. Yamada, S.; Misono, T.; Iwai, Y.; Masumizu, A.; Akiyama, Y., New Class of Pyridine Catalyst Having a Conformation Switch System: Asymmetric Acylation of Various sec-Alcohols. *J. Org. Chem.* **2006**, *71* (18), 6872-6880.
15. De Rycke, N.; Couty, F.; David, O. R. P., Increasing the Reactivity of Nitrogen Catalysts. *Chemistry – A European Journal* **2011**, *17* (46), 12852-12871.
16. Peng, Z.; Takenaka, N., Applications of Helical - Chiral Pyridines as Organocatalysts in Asymmetric Synthesis. *Chem. Rec.* **2013**, *13* (1), 28-42.
17. Auvil, T. J.; Schafer, A. G.; Mattson, A. E., Design Strategies for Enhanced Hydrogen-Bond Donor Catalysts. *Eur. J. Org. Chem.* **2014**, *2014* (13), 2633-2646.
18. Smirnov, S. N.; Golubev, N. S.; Denisov, G. S.; Benedict, H.; Schah-Mohammed, P.; Limbach, H.-H., Hydrogen/Deuterium Isotope Effects on the NMR Chemical Shifts and Geometries of Intermolecular Low-Barrier Hydrogen-Bonded Complexes. *J. Am. Chem. Soc.* **1996**, *118* (17), 4094-4101.



19. McGarrigle, E. M.; Myers, E. L.; Illa, O.; Shaw, M. A.; Riches, S. L.; Aggarwal, V. K., Chalcogenides as Organocatalysts. *Chem. Rev.* **2007**, *107* (12), 5841-5883.
20. Trost, B. M.; Brindle, C. S., The direct catalytic asymmetric aldol reaction. *Chem. Soc. Rev.* **2010**, *39* (5), 1600-1632.
21. Rueping, M.; Antonchick, A. P., Organocatalytic Enantioselective Reduction of Pyridines. *Angew. Chem., Int. Ed.* **2007**, *46* (24), 4562-4565.
22. Narendar Reddy, T.; Jayathirtha Rao, V., Importance of Baylis-Hillman adducts in modern drug discovery. *Tetrahedron Lett.* **2018**, *59* (30), 2859-2875.
23. Basavaiah, D.; Reddy, B. S.; Badsara, S. S., Recent Contributions from the Baylis-Hillman Reaction to Organic Chemistry. *Chem. Rev.* **2010**, *110* (9), 5447-5674.
24. Lima-Junior, C. G.; Vasconcellos, M. L. A. A., Morita-Baylis-Hillman adducts: Biological activities and potentialities to the discovery of new cheaper drugs. *Bioorg. Med. Chem.* **2012**, *20* (13), 3954-3971.
25. Balan, D.; Adolfsson, H., Selective Formation of  $\alpha$ -Methylene- $\beta$ -amino acid Derivatives through the Aza Version of the Baylis-Hillman Reaction. *J. Org. Chem.* **2001**, *66* (19), 6498-6501.
26. Balan, D.; Adolfsson, H., Titanium Isopropoxide as Efficient Catalyst for the Aza-Baylis-Hillman Reaction. Selective Formation of  $\alpha$ -Methylene- $\beta$ -amino Acid Derivatives. *J. Org. Chem.* **2002**, *67* (7), 2329-2334.
27. Balan, D.; Adolfsson, H., Chiral quinuclidine-based amine catalysts for the asymmetric one-pot, three-component aza-Baylis-Hillman reaction. *Tetrahedron Lett.* **2003**, *44* (12), 2521-2524.
28. Pathak, R.; Madapa, S.; Batra, S., Trifluoroacetic acid: a more effective and efficient reagent for the synthesis of 3-arylmethylene-3,4-dihydro-1H-quinolin-2-ones and 3-

arylmethyl-2-aminoquinolines from Baylis-Hillman derivatives via Claisen rearrangement. *Tetrahedron* **2007**, 63 (2), 451-460.

29. Kobbelgaard, S.; Brandes, S.; Jorgensen, K. A., Asymmetric organocatalyzed [1,3]-sigmatropic rearrangements. *Chemistry – A European Journal* **2008**, 14 (5), 1464-1471.

30. Kim, J. N.; Lee, H. J.; Lee, K. Y.; Gong, J. H., Regioselective Allylic Amination of the Baylis-Hillman Adducts: An Easy and Practical Access to the Baylis-Hillman Adducts of N-Tosylimines. *Synlett* **2002**, 2002 (01), 0173-0175.

31. Gajda, A.; Gajda, T., N-Carbamate Protected  $\alpha$ -Amidoalkyl-p-tolylsulfones: Convenient Substrates in the aza-Morita-Baylis-Hillman Reaction. *J. Org. Chem.* **2008**, 73 (21), 8643-8646.

32. Imura, Y.; Shimojoh, N.; Moriyama, K.; Togo, H., Aza-Morita-Baylis-Hillman reaction with ion-supported Ph<sub>3</sub>P. *Tetrahedron* **2012**, 68 (10), 2319-2325.

33. Hu, H.; Tang, Q.; Tu, A.; Zhong, W., Chiral Bifunctional Ferrocenylphosphines as New Catalysts for aza-Morita-Baylis-Hillman Reactions of N-Sulfonated Imines with Methyl Vinyl Ketone. *Curr. Organocatal.* **2015**, 2 (1), 58-63.

34. Anstiss, C.; Garnier, J.-M.; Liu, F., Mechanistic investigations of multidentate organocatalyst-promoted counterion catalysis for fast and enantioselective aza-Morita-Baylis-Hillman reactions at ambient temperature. *Org. Biomol. Chem.* **2010**, 8 (19), 4400-4407.

35. Anstiss, C.; Liu, F., Cooperativity in the counterion catalysis of Morita/Baylis/Hillman reactions promoted by enantioselective trifunctional organocatalysts. *Tetrahedron* **2010**, 66 (29), 5486-5491.

36. Garnier, J.-M.; Anstiss, C.; Liu, F., Enantioselective Trifunctional Organocatalysts for Rate-Enhanced Aza-Morita-Baylis-Hillman Reactions at Room Temperature. *Adv. Synth. Catal.* **2009**, 351 (3), 331-338.

37. Garnier, J.-M.; Liu, F., Trifunctional organocatalyst-promoted counterion catalysis for fast and enantioselective aza-Morita-Baylis-Hillman reactions at ambient temperature. *Org. Biomol. Chem.* **2009**, 7 (7), 1272-1275.

## **Chapter 5**

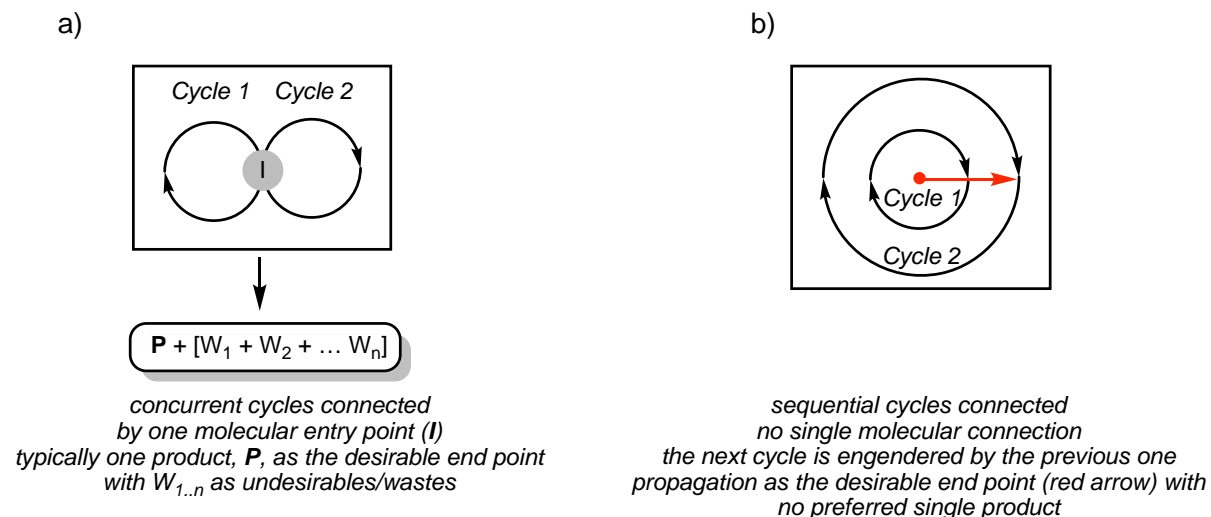
### **Propagation of Chirality via an aza-MBH–Soai**

#### **Asymmetric Ripple**

## 5.1 Introduction

### 5.1.1 A suprareaction network by continuous chiral propagation

The current paradigm for chemical reactivity organisation focuses on molecular connections between different cycles or pathways to achieve specific bond formation events. For example, a conjoined reaction pathway will have two separate but concurrent cycles with one species acting as a focal point for the two cycles.<sup>1-3</sup> The success of this type of reaction network is measured by its endpoint, defined by the level of conversion of starting materials to typically one desired end product (Scheme 5.1a). If a single product outcome is not the target (e.g. prebiotic reaction cycles without elaborate reaction engineering or knowledge of a desired product), then reaction cycles can be connected in a sequential manner (Scheme 5.1b). In such cases, the connectivity manifests as how well the entire chemical information produced in the first cycle is being incorporated productively in the 2<sup>nd</sup> cycle (red arrow, Scheme 5.1b).



**Scheme 5.1.** a) Conjoined reaction pathway yielding a single product. b) Sequential reactions cycles

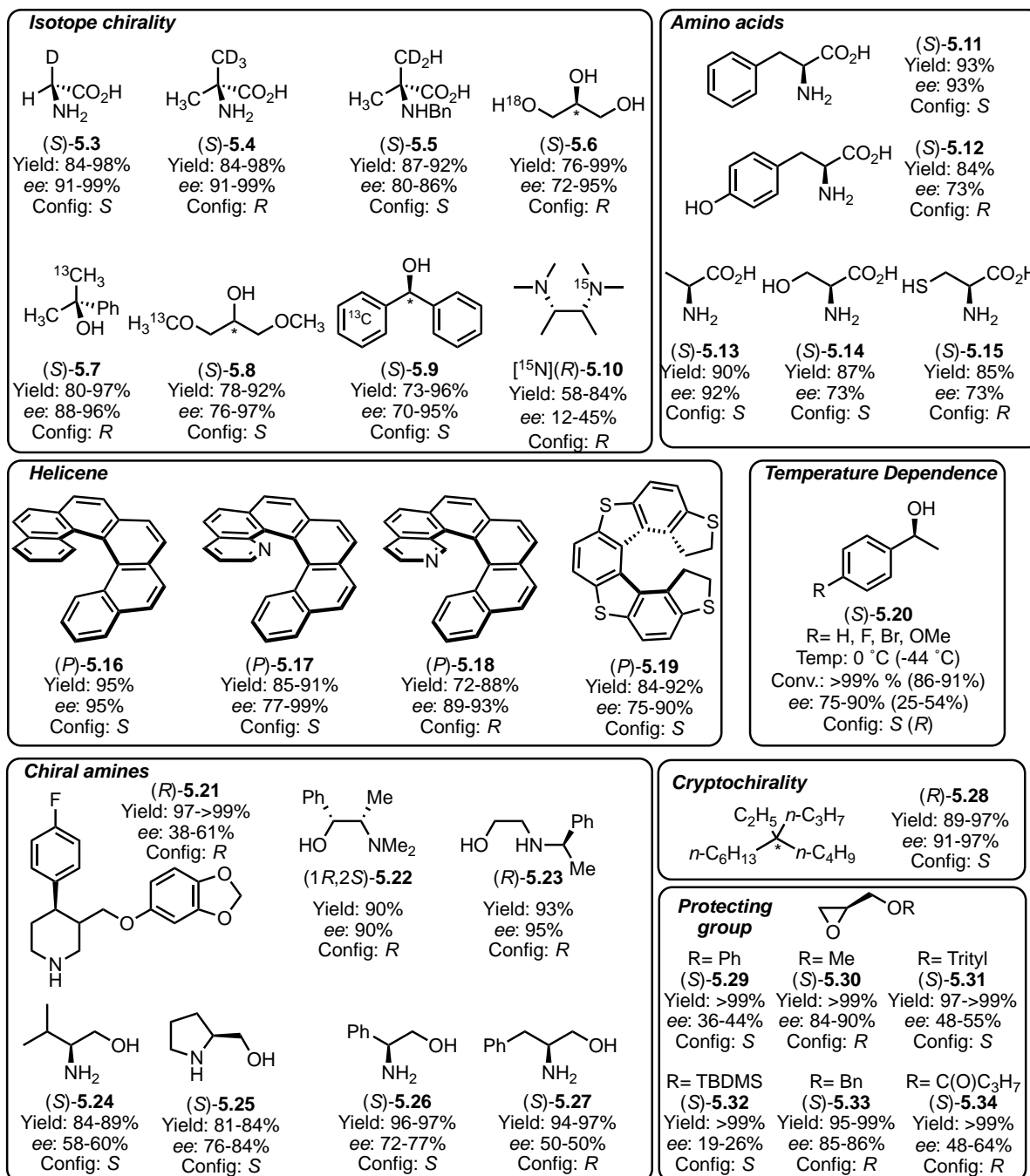
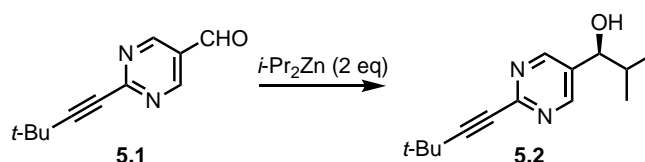
If a reaction network were to continue, then factors that promote information propagation rather than endpoint conversions would be of primary importance. The Soai reaction illuminates a mechanism by which chiral information is propagated from an initial point of

chirality via asymmetric autocatalysis and is an excellent propagative component to explore a new paradigm of continuous and propagative reaction network.<sup>4-5</sup> However, the Soai reaction initiates homochirality transfer mode with little growth in chemical diversity (i.e. only one chiral entity at the end). This raises the next question of how another reaction component may integrate with the Soai reaction to begin to construct a propagative reaction network in which both chirality and chemical diversity can expand.

### **5.1.2 Chirality propagation by the asymmetric autocatalytic Soai reaction**

#### **5.1.2.1 Known chiral initiators for the Soai reaction**

Unlike its limited substrate scope, the Soai reaction can be initiated by a variety of chiral compounds with proficient asymmetric autocatalysis. Many different scaffolds have been used to initiate chiral information transfer including organic molecules, circularly polarised light-mediated photoequilibrium<sup>6-7</sup>, inorganic and organic crystals<sup>8-19</sup>, isotopically labelled substrates<sup>20</sup>. A significant amount of attention has been given to isotopically chiral initiators, amino acids, helices, amines and simple building blocks. The absolute configuration of the resulting chiral pyrimidine alkanol is dependent upon the initiator. However, it is not possible to predict the absolute configuration of the alkanol based upon the absolute configuration of structurally similar substrates. A selection of organic initiators organised by compound class can be seen in Scheme 5.2,



**Scheme 5.2.** Chiral Initiators for the Soai reaction with the configuration of 5.2 shown.

As aforementioned, the configuration of the alkanol cannot be predicted by the configuration of the initiator. This is best demonstrated by three separate case studies involving amino acids, helicene derivatives and glycidyl ethers. As expected in all cases, each pair of enantiomers

transfer the opposite sense of chirality to the alkanol product — however, different amino acids with the same configuration yield different configurations.<sup>21</sup> For example, L-tyrosine ((*S*)-**5.12**) induces (*R*)-configuration while L-phenylalanine ((*S*)-**5.11**) induces (*S*). Likewise, L-alanine ((*S*)-**5.13**) and L-serine ((*S*)-**5.14**) induce (*S*)-configuration, whereas L-cysteine ((*S*)-**5.15**) yields the (*R*)-enantiomer. Helicene analogues **5.16–5.19** demonstrated the same phenomenon; the unsubstituted helicene (*P*)-**5.16** and quinoline derivative (*P*)-**5.17** yields the (*S*)-enantiomer whereas isoquinoline (*P*)-**5.18** induces the (*R*)-enantiomer.<sup>22-23</sup> Finally, glycidyl ethers **5.29–5.34** display no consistent trend in the configuration of the alkanol. Phenyl ((*S*)-**5.29**), trityl ((*S*)-**5.31**) and TBDMS ((*S*)-**5.32**) ethers induce the (*S*)-enantiomer, while methyl ((*S*)-**5.30**), benzyl ((*S*)-**5.33**) and isopropyl acetate ((*S*)-**5.34**) analogues yield the (*R*) enantiomer.<sup>24</sup>

The configuration of the pyrimidinyl alkanol has also been shown to be affected by the temperature for a series of *para*-substituted phenylethanol derivatives ((*S*)-**5.20**). All substrates yielded (*S*)-**5.2** at room temperature with high degrees of enantio excess (75–90% *ee*). However, upon cooling to –44 °C, the sense of asymmetry induction inverted and (*R*)-**5.2** was isolated in lower enantiopurity (25–54% *ee*). Unexpected temperature dependence and unpredictable configurations between analogous substrates underline the mechanistic complexity of the reaction.

The Soai reaction is a useful model system to explore how an initial kinetic differentiation between a *racemic* and asymmetric pathway can propagate heterochirality transfer as a precursor for homochirality. In principle, a chiral initiator does not have to be a single type of chiral compound. It is possible that an asymmetric catalytic reaction product mixture could



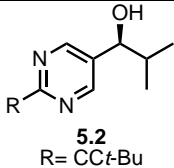
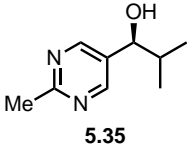
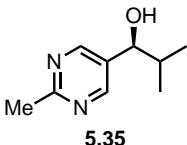
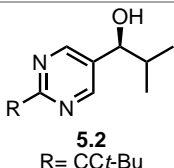
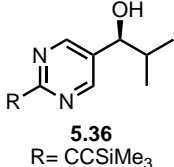
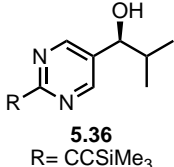
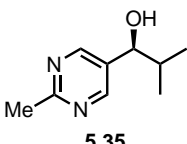
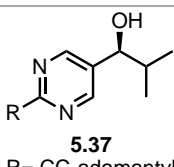
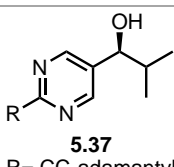
be used to initiate the Soai amplification reaction. In this type of reaction network, the Soai chirality propagation is used as a read-out for gauging the level of information integrity within the system. However, replacing a simple chiral initiator with the entire chemical outputs of an asymmetric reaction means that many competitive pathways can potentially derail the Soai propagation. The next section summaries significant mechanistic findings on the likely complexes in the Soai reaction that give rise to chiral amplification.

#### 5.1.2.1 Complexes in the Soai reaction for chirality amplification

Determining the mechanism by which high levels of asymmetry are induced independently of initial chiral purity is a complex question. The mechanism of the Soai chiral amplification has been extensively reviewed and over the past decade, the mechanism chiral amplification in the Soai reaction has been debated by several groups..<sup>19, 25</sup> A summary of the key mechanistic investigations can be seen in Table 5.1.

The mechanistic investigations into the Soai have focused upon identifying the nature of the active catalyst. Initially, the reactive catalyst form of **5.36** was proposed to be a homochiral dimer<sup>26</sup> which was proposed to be a bimetallic dimer with N,O complexation.<sup>27</sup> Blackmond and Brown demonstrated that the rate of reaction was proportion to the *ee* of the autocatalyst **5.35**.<sup>27</sup> The homo- and heterochiral dimers of **5.36** were characterised by <sup>1</sup>H and 2D NMR spectroscopy and the two complexes were shown to interconvert rapidly.<sup>28</sup>

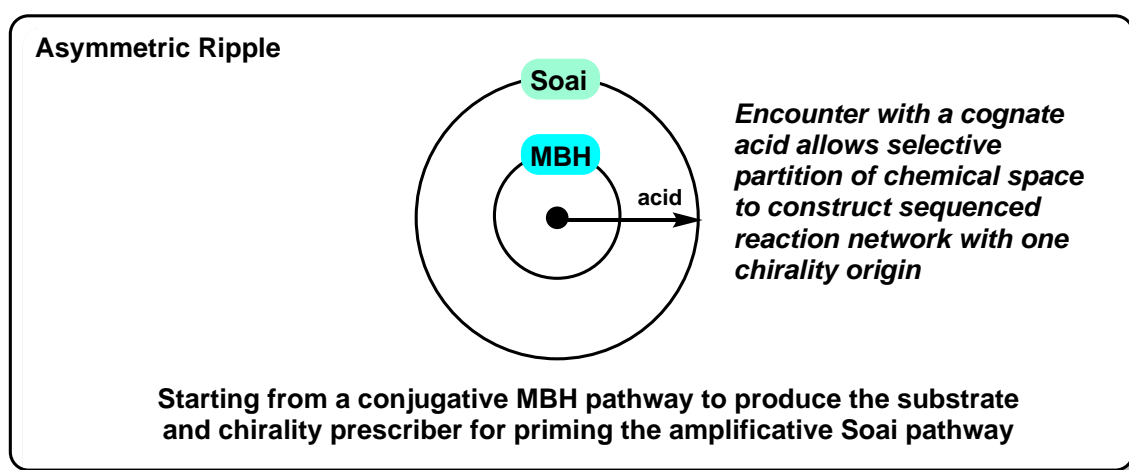
**Table 5.1.** Key mechanistic investigations of the asymmetric autocatalytic Soai reaction.

| Author                                | Year | Catalyst  | Methods                                | Key findings  |
|---------------------------------------|------|---|--|---|
| Soai <sup>26</sup>                    | 2001 |  <p><b>5.2</b><br/>R = CCt-Bu</p>                | HPLC of initial rates                  | Reaction can proceed through monomeric or dimeric catalyst. Origin of chiral amplification unclear.   |
| Blackmond and Brown <sup>27</sup>     | 2001 |  <p><b>5.35</b></p>                              | Reaction microcalorimetry              | Reaction with <i>racemic</i> catalyst proceeds at exactly half the rate of enantiopure. Catalyst is a macrocyclic homochiral bimetallic dimer (N, O chelation). Heterochiral dimer is unreactive.                 |
| Buhse <sup>29</sup>                   | 2003 |   | Kinetic modelling                      | High concentration of the homochiral dimer is required for catalysis. Autocatalysis and chiral amplification are the results of the entire scheme.  |
| Blackmond and Buono <sup>30</sup>     | 2003 |  <p><b>5.35</b></p>                              | Reaction microcalorimetry              | Mechanism is different at higher loading of <i>i</i> -Pr <sub>2</sub> Zn. Pre-complexation of organozinc to aldehyde which can interact with the homochiral dimer in a tetrameric TS.                             |
| Soai <sup>31</sup>                    | 2003 |  <p><b>5.2</b><br/>R = CCt-Bu</p>               | Kinetic analysis                       | Asymmetric amplification arises from heterochiral trimers being significantly more stable than homochiral dimers.   |
| Brown <sup>28</sup>                   | 2003 |  <p><b>5.36</b><br/>R = CCSiMe<sub>3</sub></p> | <sup>1</sup> H and 2D NMR spectroscopy | <i>i</i> -Pr <sub>2</sub> Zn binds to pyrimidine nitrogen not the carbonyl. Homo- and heterochiral dimer rapidly interconvert and structures are different. Heterochiral dimer has an internal plane of symmetry. |
| Brown <sup>32</sup>                   | 2007 |  <p><b>5.36</b><br/>R = CCSiMe<sub>3</sub></p> | DFT and 2D NMR spectroscopy            | Sterics of the isopropyl group favour the formation of a square-macrocycle-square tetramer.   |
| Schiafiino and Ercolani <sup>33</sup> | 2008 |  <p><b>5.35</b></p>                            | DFT                                    | Chirality transfer is achieved by a hexamer. Isopropyl group and the $\gamma$ -pyrimidinic nitrogen biases the complex towards <i>anti</i> -arrangement which propagates chirality.                               |
| Blackmond and Brown <sup>34</sup>     | 2010 |  <p><b>5.37</b><br/>R = CC-adamantyl</p>       | Kinetic analysis                       | Maximum rate observed at 36-42% substrate conversion. Induction period is shorter at low temperature. Supports higher order oligomers propagate chirality.  |
| Blackmond and Brown <sup>35</sup>     | 2012 |  <p><b>5.37</b><br/>R = CC-adamantyl</p>       | 2D NMR spectroscopy                    | A transient zinc acetal intermediate is observed as the reaction initiates comprised of three pyrimidine units.   |

Significant kinetic modelling was performed based on the dimer model. However, the kinetics and amplification of the reaction could not be accurately modelled.<sup>29</sup> As such, higher order-oligomers were considered.<sup>32, 36</sup> The high fidelity of the reaction was proposed to be the results of a hexameric transition state, generated from the homochiral dimers, involving two equivalents of alkanol, aldehyde and organozinc reagent.<sup>33</sup> The pyrimidinyl nitrogen plays a key role in complexing the zinc reagent which also drives enantioselectivity due to the steric bulk of the isopropyl group.<sup>32</sup> This model predicts that the homochiral complex of **5.38** directs the addition of the isopropyl group through an *anti*-conformation.<sup>32</sup> Over the past decade, the mechanistic understanding has matured, however, the exact nature of the intermediate in chirality transfer is unclear.

### 5.1.3 Building an aza-MBH-Soai reaction system

The aza-MBH reaction and Soai reaction both provide excellent model systems to explore origins of catalytic proficiency by coordinated proton transfer and how this can be expanded into a chiral propagation network, or an “asymmetric ripple” (Scheme 5.3).



**Scheme 5.3.** Propagation of MBH reaction into the Soai space.

In Chapters 2, 3 and 4 the details of the enantioselective proton transfer network that gives rise to regulated catalysis for the trifunctional system in the aza-MBH model system was enumerated. In this expanded MBH reaction space (i.e. the conjugative catalysis mode), proficient catalysis emerges when networked proton motion can be recognised by the cognate substrate. In the absence of this recognition (i.e. subjugative catalysis), the reaction proceeds through slow and conventional pathway without chiral information transfer. Consequently, this kinetic differentiation by proton motion recognition of two substrates makes this aza-MBH reaction an interesting precursor to Soai amplification. In this case, this kinetically differentiated MBH reaction is not merely an initiator but may engender the appropriate temporal sequencing for the Soai amplification to propagate the heterochirality transfer to achieve concurrent expansion of chirality and chemical diversity.

#### **5.1.4 Specific aims**

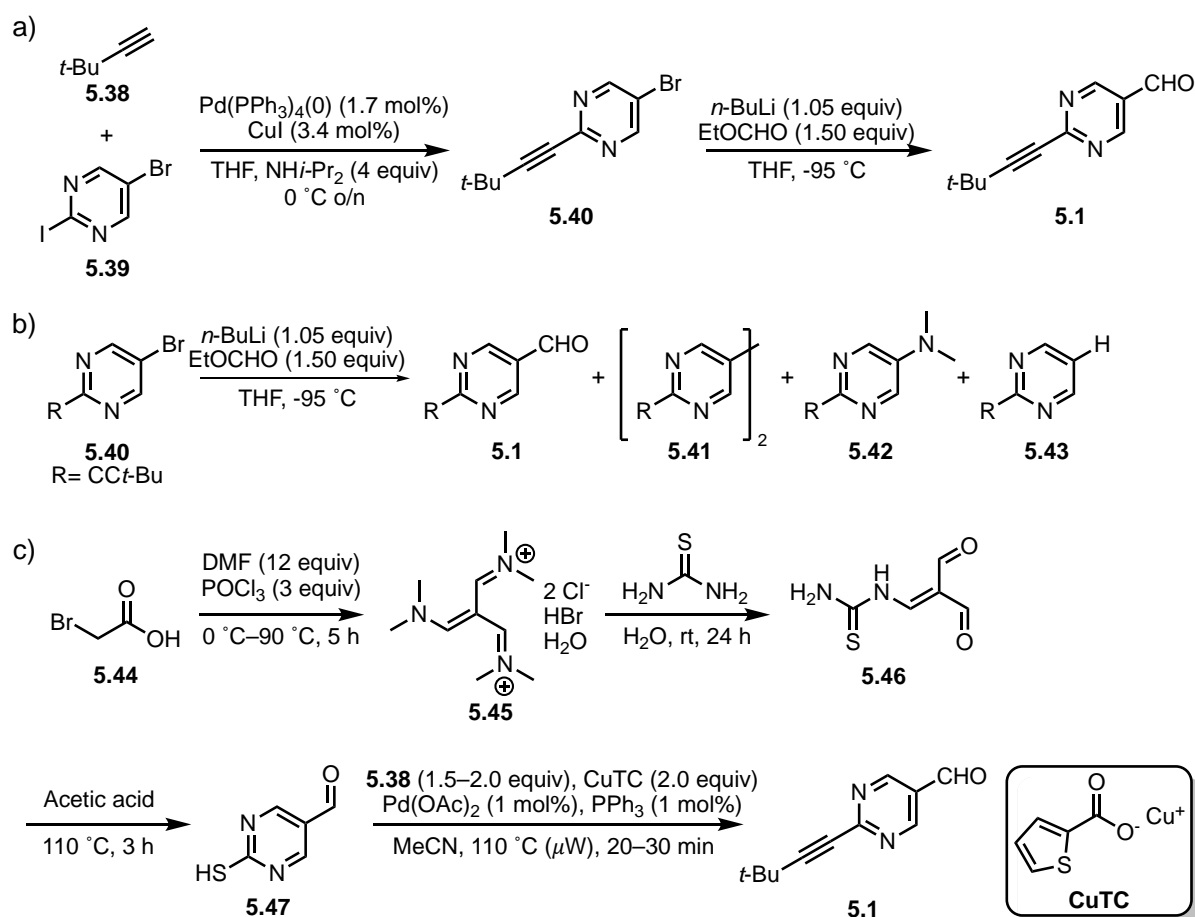
The specific aims of this chapter are:

- Develop a robust and high yielding synthesis of Soai aldehydes;
- Measure the Soai amplification outcomes with enantiopure aza-MBH adducts;
- Demonstrate the Soai amplification with crude aza-MBH reaction mixtures containing the aza-MBH adduct as the major constituent;
- Demonstrate the role of the BzOH additive on the Soai amplification initiated with crude aza-MBH reaction mixtures .

## 5.2 Results and discussion

The investigation begins first with optimising a scalable and robust synthesis of Soai aldehyde substrates via Barbier-type lithium-halogen exchange. Next, the capacity for isolated enantioenriched aza-MBH adducts in initiating the Soai reaction was examined before the eventual demonstration of how the conjugative aza-MBH catalysis is more efficiently propagated by the Soai into an asymmetric ripple.

### 5.2.1 Development of a more robust synthesis of Soai Aldehydes



**Scheme 5.4.** a) Synthesis of substrates for the Soai Reaction via lithium-halogen exchange. B) Side-product from the lithium-halogen exchange. c) Alternate synthesis by desulfurative cross coupling.

The typical synthetic route for a Soai-type pyrimidine aldehyde consists of two steps from commercially available 5-bromo-2-iodopyrimidine (**5.39**); 1) Sonagoshira cross-coupling 2)

lithium-halogen exchange and quench with a formyl group donor (Scheme 5.4a). The Sonagoshira cross-coupling is robust, proceeding with high yields (>90%) and low catalyst loading (1.7 mol%) for a wide range of alkynes. The lithium-halogen exchange is less robust, proceeding in yields below 60% due to; dimerisation (**5.41**); amination (dimethylamine by-product mediated)(**5.42**); and protonation (adventitious water)(**5.43**) (Scheme 5.4b). Hintermann et al. developed a desulfurative cross-coupling from mercapto aldehyde **5.47** in yields up to 86% for a variety of alkyne substrates (Scheme 5.4c).<sup>37</sup> The four-step synthesis begins from bromoacetic acid **5.44** by converting it to the Arnold salt **5.45** via a Vilsmeier–Haack reaction.<sup>38</sup> Addition of thiourea yields **5.46** which can undergo acid catalysed ring closure to yield thiol **5.47**. While this is a successful route, it is significantly longer than the lithium-halogen exchange route. Consequently, a more robust method for installation of the formyl group was explored using Barbier-type conditions.

Under Barbier-type conditions, the lithiate is formed in the presence of the electrophile (ethyl formate (EtOCHO) or DMF).<sup>39-41</sup> This in situ approach limits unproductive side reactions from occurring by immediately quenching the aryl lithiate as it is formed. Crude yields, of **5.43** and the major side product **5.1**, and isolated yields for Barbier-type formylation of pyrimidine **5.40** with EtOCHO and DMF are summarised in Table 5.2 (Entries 2–5).

**Table 5.2.** Barbier-type formylation of pyrimidine **5.40**.

| Entry          | Scale /mg | Electrophile       | Crude Yields <sup>a</sup> /% |            | Isolated Yield <b>5.1</b> /% |
|----------------|-----------|--------------------|------------------------------|------------|------------------------------|
|                |           |                    | <b>5.43</b>                  | <b>5.1</b> |                              |
| 1 <sup>b</sup> | 1000      | EtOCHO (1.2 equiv) | <5                           | >95        | 42                           |
| 2 <sup>c</sup> | 500       | EtOCHO (1.0 equiv) | <5                           | 62         | 58                           |
| 3 <sup>c</sup> | 500       | DMF (1.0 equiv)    | <5                           | >95        | 22                           |
| 4 <sup>d</sup> | 1000      | EtOCHO (1.2 equiv) | 16                           | 79         | 72                           |
| 5 <sup>e</sup> | 3000      | EtOCHO (1.5 equiv) | 10                           | 90         | 82                           |

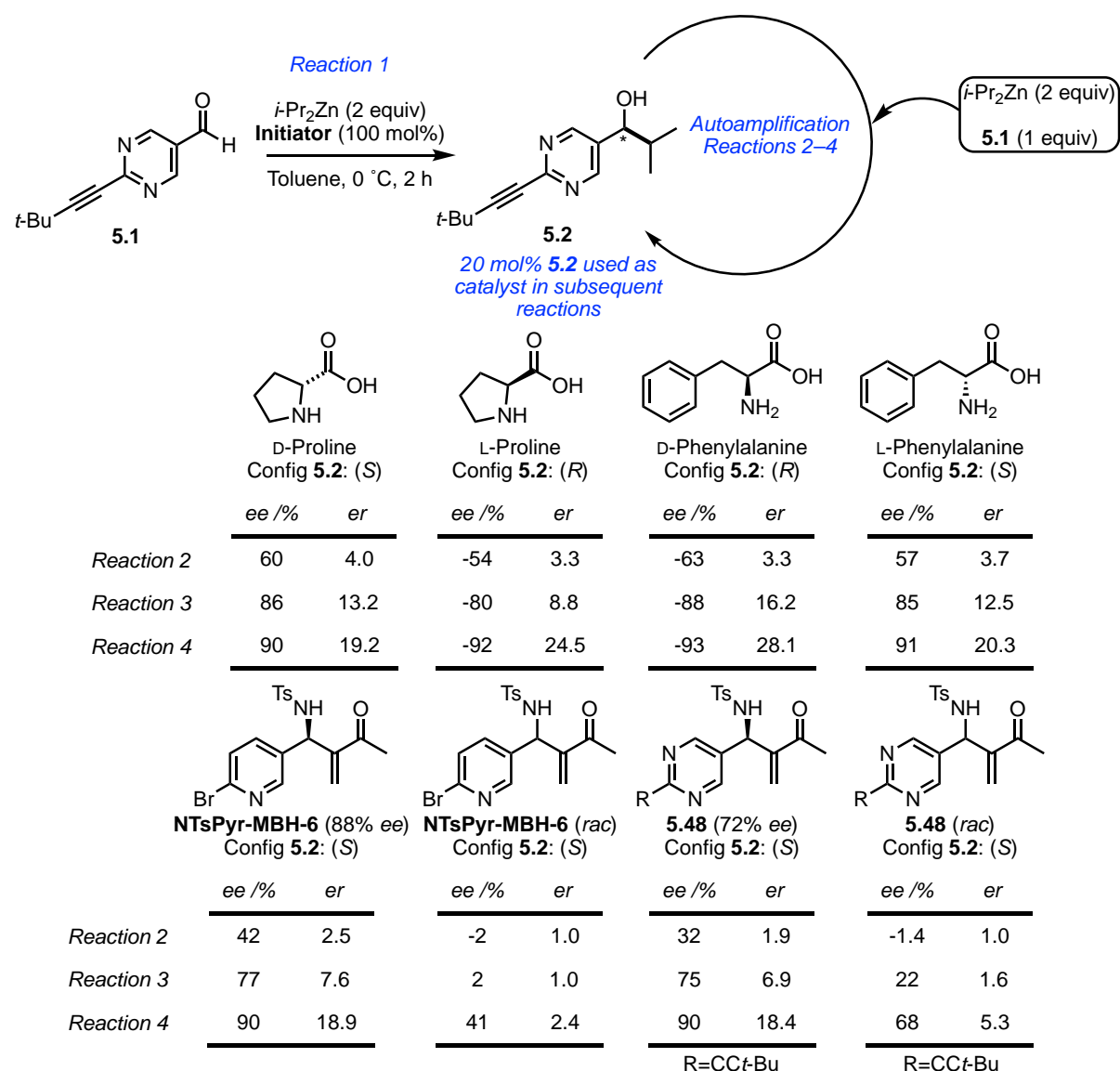
a) Yield as determined by <sup>1</sup>H NMR spectroscopy b) 1.05 equiv *n*-BuLi, 1.20 equiv EtOCHO preforming the heteroaryl lithiate. c) 1.0 equiv *n*-BuLi, 1.0 equiv Electrophile, d) 1.20 equiv *n*-BuLi and EtOCHO, e) 1.50 equiv *n*-BuLi and EtOCHO.

Barbier-type conditions with EtOCHO resulted in an improved but modest isolated yield for **5.1** (58%) with recovery of starting material **5.40** (31%, Table 5.2, Entry 3). Isolated yields when quenching with DMF (22%, Table 5.2, Entry 3) and the standard approach to the lithium-halogen exchange with ethyl formate (42%, Table 5.2, Entry 1) was significantly lower than Barbier-type conditions. Increasing the equivalents of *n*-BuLi and the EtOCHO to 1.2 and 1.5 increased the isolated yield of **5.1** to 72% and 82% respectively (Table 5.2, Entries 4 and 5). The operationally robust Barbier-type conditions yielded **5.1** in the highest reported yields.

### 5.2.2 Enantioenriched aza-MBH adducts as chiral initiators for the Soai reaction

Initial control experiments were performed to determine if asymmetric autocatalysis was reproducible using known initiators (proline and phenylalanine) and the methodology outlined in the introduction (for more information see 5.4.3.2 Soai Reaction– Method A in the experimental).<sup>42</sup> In brief, pyrimidine alkanol **5.2** generated during Reaction 1 was used without purification in the second reaction as the chiral initiator. Due to the small scale of the first reaction (<2mg) the enantioselectivity cannot be reliably measured. This process is

repeated for a total of four reactions per replicate for each chiral initiator. The absolute configuration of **5.2** catalysed by D-proline and L-phenylalanine is the (*S*) enantiomer and L-proline and D-phenylalanine yield the (*R*) enantiomer.<sup>42</sup> These configurations were used to assign the stereochemistry of the enantiomers detected by chiral HPLC. The results of these control experiments are summarised in Figure 5.1.



**Figure 5.1.** Enantioselectivity for control chiral initiators.

Control experiments for the four known chiral initiators successfully activated autocatalytic chiral amplification and were consistent with published data.<sup>42</sup> Chirality of D-Proline was transferred to the Soai product with modest stereoselectivity in the second reaction (60% ee),

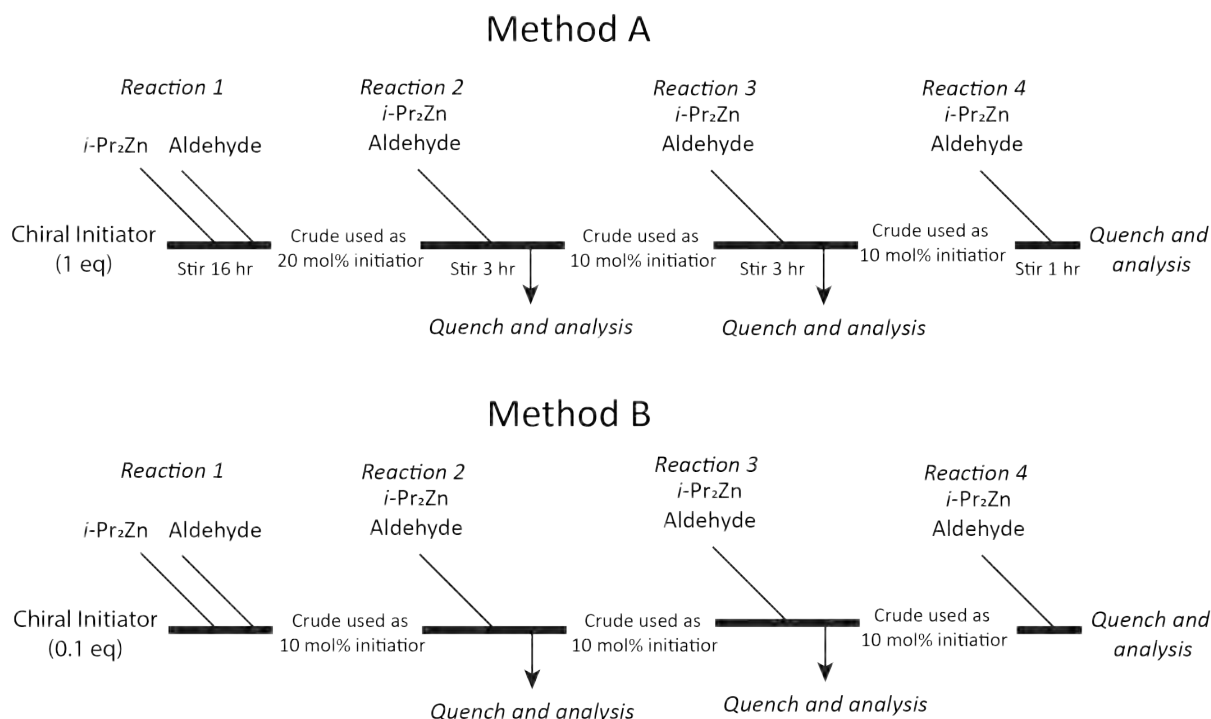


which further amplified to give a total *ee* of 90% in the fourth reaction. Likewise, L-proline conferred the opposite sense of asymmetry and amplified from an *ee* of -54% in the second reaction to -92%. Furthermore, the control reactions of phenylalanine amplified from modest *ee* (D= -63%; L= 58%) to excellent *ee* in the fourth reaction (D= -93%; L= 91%).

Pyrimidyl substrate have previously been reported for the MBH reaction by Soai et al. and in light of this the N-tosyl imine of **5.1** was prepared and successfully catalysed as a substrate for the aza-MBH reaction.<sup>43</sup> Isolated MBH adducts, **NTsPyr-MBH-6** (87% *ee* and *racemic*) and **5.48** (78% *ee* and *racemic*), were successful in initiating the Soai reaction. Chiral pyridine initiator **NTsPyr-MBH-6** produced an *ee* of 42% *ee* in the second reaction, which increased further to 77% and 90% in the third and fourth reactions, respectively. Initially, little chiral initiation was observed for *racemic* adduct **NTsPyr-MBH-6** in the second (-2% *ee*) and third amplification rounds (2% *ee*) before a moderate amplification outcome in the fourth reaction (41% *ee*).

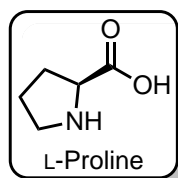
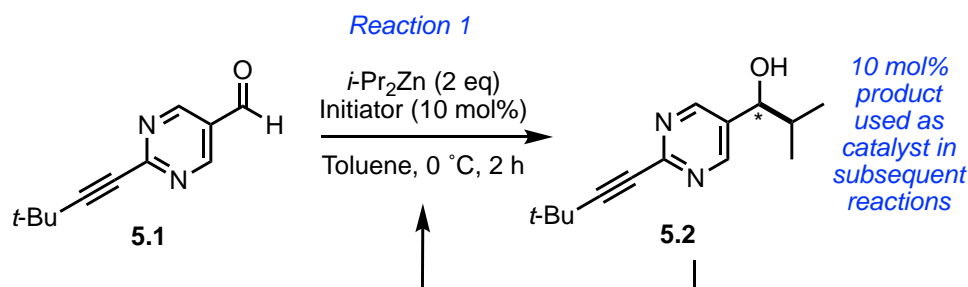
Pyrimidine initiator **5.48** (72% *ee*) was also an effective initiator, with chiral amplification of 32% *ee* in the second round to 90% *ee* in the fourth round. The *racemic* adduct **5.48** was less effective as a chiral inducer. No enantioenrichment was observed for the second reaction (-1.4% *ee*) before modest increases for the third (22% *ee*) and fourth reaction (68% *ee*). Both sets of experiments demonstrate that isolated *aza*-MBH adducts are capable of acting as a chiral inducing agent for the Soai reaction. More importantly, the single-point chiral information stored by the catalyst can be transferred through the *aza*-MBH adduct. For this system, chirality is only transmitted via the cognate proton transfer network.

Seeking to determine the effectiveness of the initiators, an alternate method for the Soai amplification was developed, for more details see 5.4.3.3 Soai Reaction– Method B in the experimental section. In this method, the initiator was used as a 10 mol% additive, and the reaction was sampled after 2 hours (Figure 5.2).

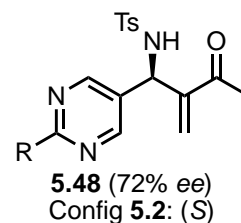
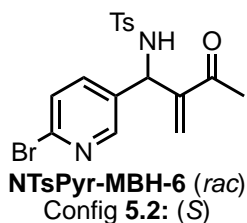
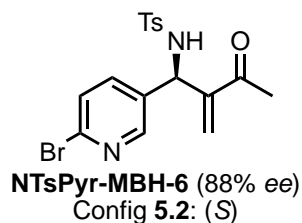


**Figure 5.2.** Comparison of methodology for the Soai reaction.

For Method B, the scale of the first reaction increases from 2 mg to 8 mg allowing for the reaction to be sampled after the first reaction so the chirality transfer from the initiator can be directly measured. Control experiments with L-Proline (>99.95% *ee*) were performed in triplicate to demonstrate that this method would reproduce the expected chiral amplification outcomes (Figure 5.3). Chirality transfer is efficient in the first reaction and can be assessed for each round of chiral transfer amplification. L-Proline successfully induced asymmetry in the first reaction with an *ee* of  $-50 \pm 7\%$  amplifying to excellent levels of enantiopurity by the third reaction ( $-95 \pm 1\%$  *ee*).



|            | Replicate 1                          |       | Replicate 2                          |       | Replicate 3                          |       |
|------------|--------------------------------------|-------|--------------------------------------|-------|--------------------------------------|-------|
|            | L-Proline<br>Config <b>5.2</b> : (R) |       | L-Proline<br>Config <b>5.2</b> : (R) |       | L-Proline<br>Config <b>5.2</b> : (R) |       |
|            | ee/ %                                | er    | ee/ %                                | er    | ee/ %                                | er    |
| Reaction 1 | -58                                  | 3.75  | -48                                  | 2.91  | -45                                  | 2.59  |
| Reaction 2 | -90                                  | 18.24 | -87                                  | 14.48 | -88                                  | 15.29 |
| Reaction 3 | -96                                  | 48.60 | -96                                  | 48.47 | -94                                  | 32.73 |



|            | ee/ %  | er           | ee/ %  | er           | ee/ %  | er           |
|------------|--------|--------------|--------|--------------|--------|--------------|
| Reaction 1 | 13 ± 4 | 1.30 ± 0.18  | rac    | 1.00         | 11 ± 1 | 1.24 ± 0.051 |
| Reaction 2 | 72 ± 2 | 6.15 ± 0.72  | 8 ± 2  | 1.18 ± 0.076 | 61 ± 7 | 4.53 ± 1.68  |
| Reaction 3 | 83 ± 2 | 10.69 ± 1.95 | 31 ± 3 | 1.92 ± 0.19  | 70 ± 4 | 5.80 ± 1.54  |

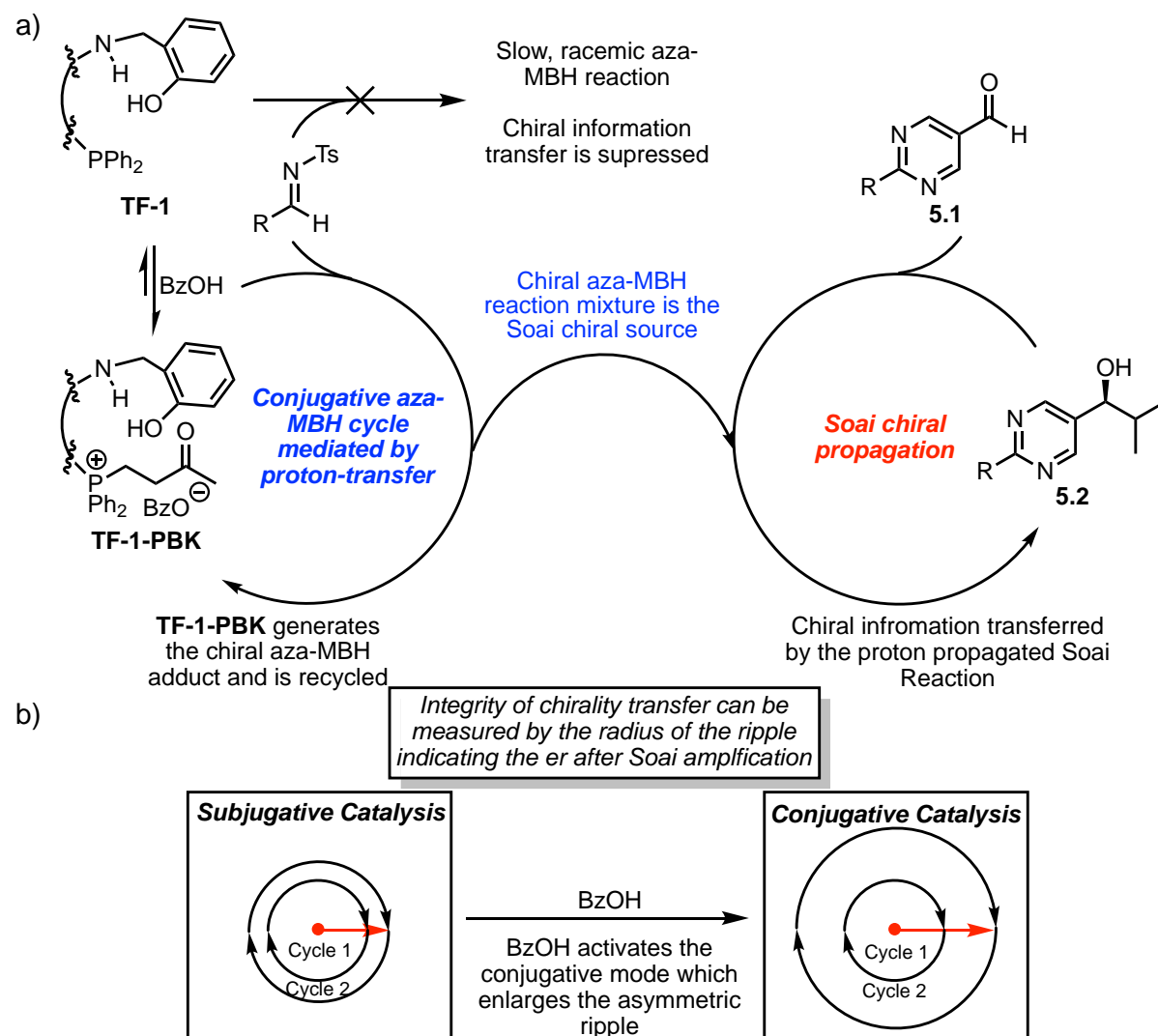
R= CC*t*-Bu

**Figure 5.3.** Asymmetric amplification of **5.1** using alternate methodology with L-Proline and isolate *aza*-MBH adducts.

Chiral MBH adducts **NTsPyr-MBH-6** (12 ± 4% ee; 1 ± 1 er) and **5.48** (11 ± 1% ee; 1 ± 0.30 er) initiated asymmetric amplification with a modest induction observed in the first reaction. This propagated to excellent enantioselectivities over three reactions (**NTsPyr-MBH-6**= 83 ± 2% ee; **5.48**= 70 ± 4% ee). For chirality to amplify quickly, there must be an initial imbalance to propagate. Induction with the *racemic* adduct was diminished, the degree of asymmetric

induction in the final reaction was significantly lower ( $30 \pm 3\%$  ee) than the enantioenriched counterparts.

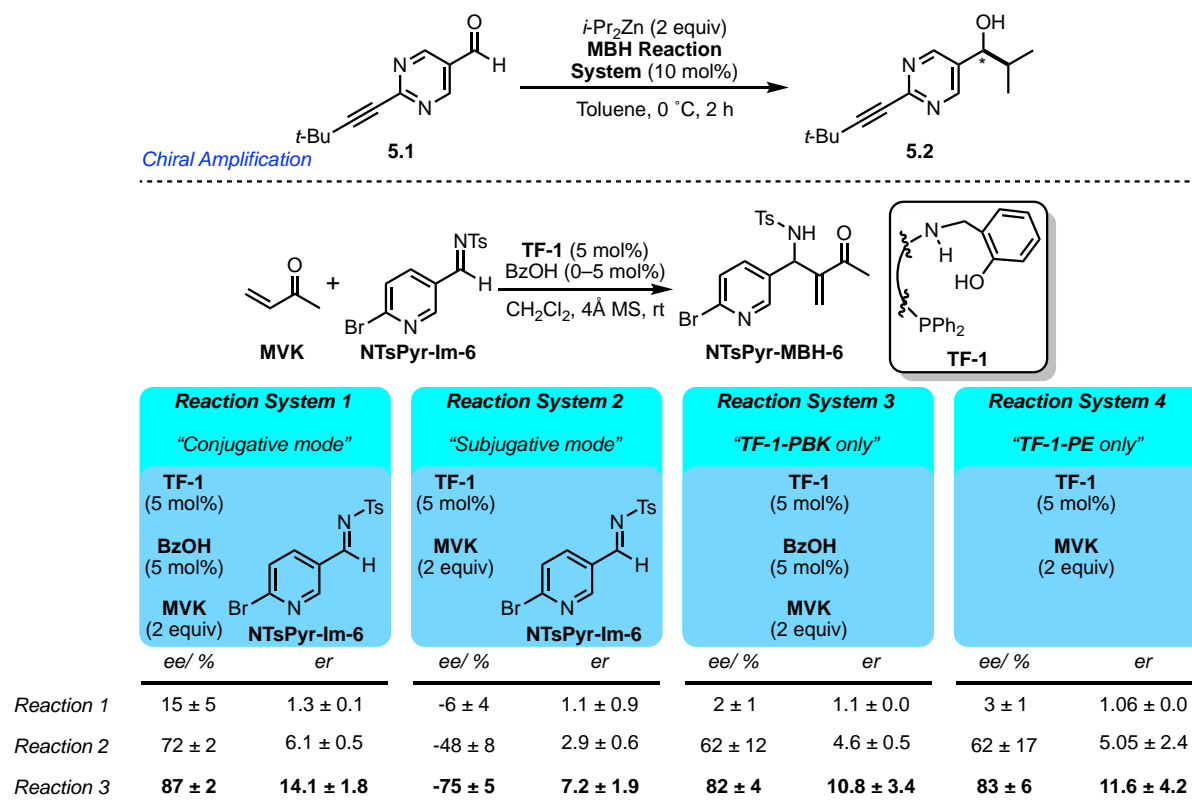
### 5.2.3 A proton-shuttle driven aza-MBH reaction as a chiral initiator for the Soai reaction



**Scheme 5.5.** a) Reaction cycles connect the aza-MBH and Soai. b) The size of the asymmetric ripple is a measure of the integrity of chirality transfer indicating the *er* outcome of the Soai reaction.

In the conjugative catalysis mode of the aza-MBH reaction, substrate recognition of the proton motion embedded in **TF-1-PBK** leads to proficient chirality transfer for enabling the

subsequent Soai reaction (Scheme 5.5a). In the subjugative mode (reactions without BzOH), the chiral information of the trifunctional catalyst is not transferred to the MBH product, thus reducing the chiral information propagation via the Soai reaction (Scheme 5.5b, ripple on the left). In the conjugative mode, the asymmetric aza-MBH reaction with BzOH is highly proficient and may result in faster chiral amplification in the Soai reaction (e.g. larger *er* ratios after the same number of amplification rounds represented by a larger radius of the ripple) (Scheme 5.5b, ripple on the right). However, having both the initial chiral catalyst and its chiral progeny, the aza-MBH product, in the same Soai reaction may or may not lead to synergistic chirality amplification.



**Figure 5.4.** Soai reactions initiated by various modes of the aza-MBH catalysis.

The conjugate *aza*-MBH reaction was found to achieve the greatest amplification of chirality in the first round of chiral amplification (15 ± 5% *ee*; Figure 5.4, reaction system 1). In the absence of BzOH (subjugative catalysis)(Figure 5.4, reaction system 2), the configuration of

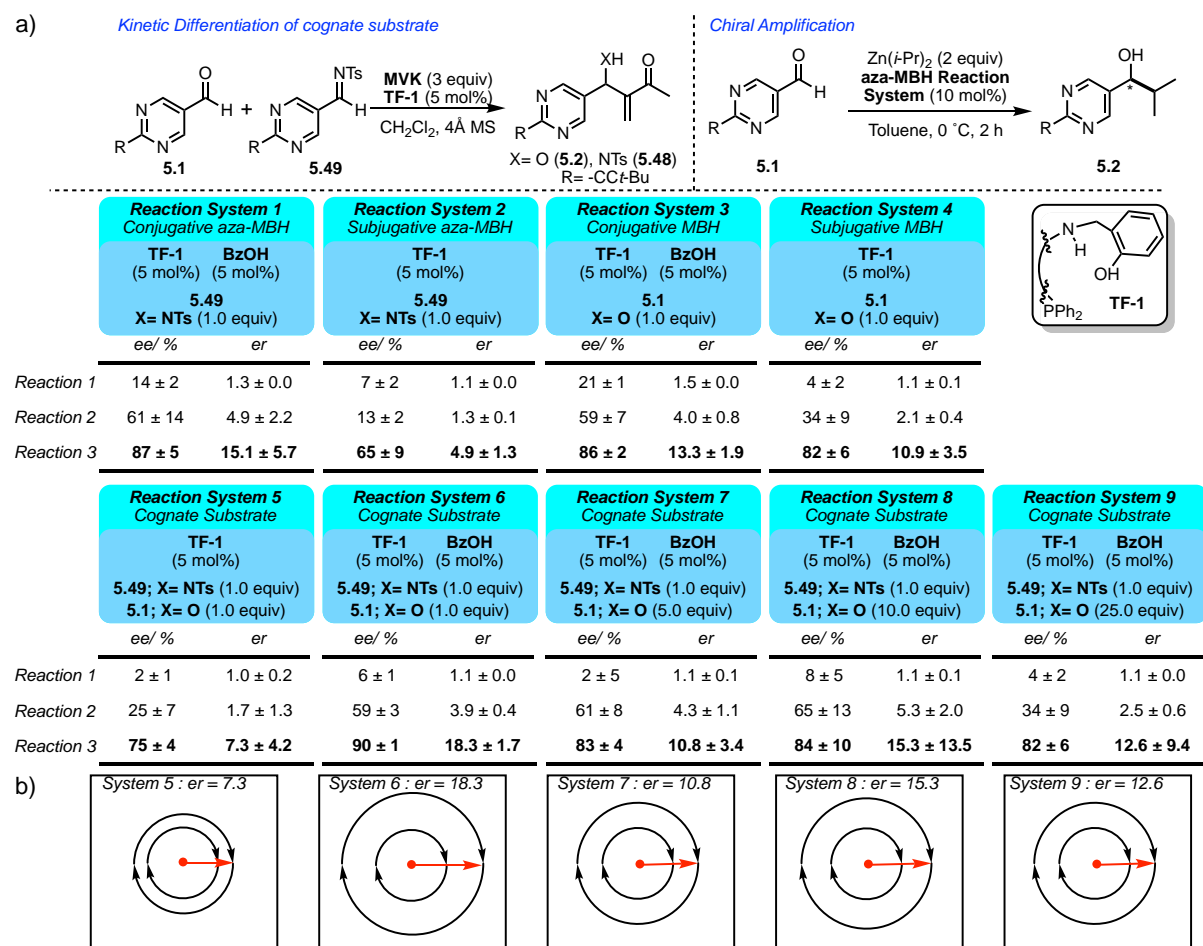
the Soai amplification was inverted with reduced *ee* ( $-6 \pm 4\%$  *ee*). After three rounds of asymmetric amplification, the conjugative aza-MBH reaction (reaction system 1) yielded the adduct **5.2** in high enantiopurity ( $87 \pm 2\%$  *ee*) while reaction system 2 (subjugative *aza*-MBH reaction) yielded **5.2** with  $-75 \pm 5\%$  *ee*. Trifunctional catalysts alone as the **PBK** (**TF-1-PBK**, reaction system 3) or **PE** (**TF-1-PE**, reaction system 4) are also capable of inducing chirality in the Soai reaction. With two chiral sources (both trifunctional catalyst and the aza-MBH adduct **NTsPyr-MBH-6** in reaction system 1) present, the sense of the Soai asymmetry remained the same as that for reaction system 3 and 4.

#### 5.2.4 A kinetically differentiated MBH reaction for engendering the Soai reaction

In the MBH reaction space, aldehydes and imine are both legitimate substrates. The aldehyde **5.1**, however, is unreactive in the conjugative mode for the MBH reaction while the corresponding imine **5.49** is reactive. BzOH allows kinetic differentiation of substrate in the conjugative aza-MBH catalysis, which leaves the aldehyde substrate for the subsequent Soai reaction. This would then represent a kinetically differentiated aza-MBH-Soai reaction ripple, rather than another cascade reaction sequence.

Two sets of reaction systems were developed to examine the effect of the conjugative and subjugative modes on chirality propagation via the Soai reaction (Figure 5.5). The first set of reaction systems examines the effect of the conjugative and subjugative mode on chirality propagation for a model aza-MBH reaction with **5.49** (reaction systems 1–2) and MBH with **5.1** (reaction systems 3–4). In the second set of reaction systems (reaction systems 5–9), the effect of the conjugative mode enabling kinetic differentiation of imine and aldehyde substrates is exploited to demonstrate that the conjugative mode gives rise to the largest

asymmetric ripple. A greater degree of asymmetric amplification in the Soai reaction was induced by the catalysis in the conjugative mode with the largest degree of chirality transfer was observed for a competitive reaction between the imine substrates **5.49** and aldehyde **5.1** (reaction system 6,  $90 \pm 1\%$  ee).



**Figure 5.5.** a) Proton-transfer temporal sequenced *aza*-MBH–Soai reaction. b) Size of the asymmetric ripple induced by proton transfer.

BzOH was integral in increasing the size of the asymmetric ripple for the *aza*-MBH (Reaction System 1 and 2) and MBH (Reaction System 3 and 4) induced reaction systems. The conjugative proton transfer pathway induced by BzOH increases the extent of chiral amplification (reaction system 1;  $87 \pm 5\%$  ee) compared to the subjugative pathway (reaction system 2;  $65 \pm 9\%$  ee). In the cases of reaction system 3 ( $86 \pm 2\%$  ee) and 4 ( $82 \pm 6\%$  ee), there

is no difference between the subjugative and conjugative pathway, consequently, there is no difference in the final degree of asymmetric induction. There is no conversion of **5.1** to the MBH adduct as it is an incompatible substrate for the trifunctional organocatalysed reaction. The increase in the number of chemical entities induced by benzoic acid in reaction system 3 does not cause a decrease in the size of the asymmetric ripple. This model system demonstrates that increased chemical complexity does not hinder chemical information transfer.

BzOH differentiated the imine and aldehyde substrates enabling greater chiral amplification for five competition experiments (reaction systems 5–9). Chirality was amplified for all systems, however, the conjugative mode (i.e. reactions with BzOH) was required for higher degrees of asymmetry (up to  $90 \pm 1\%$  ee). The greatest amplification was observed for the conjugative reaction system 6 (1.0 equiv **5.1**,  $90 \pm 1\%$  ee). While the lowest degree of chirality transfer was observed in the subjugative-mode reaction system (reaction system 5,  $75 \pm 4\%$  ee). Initial aldehyde loading is only detrimental to asymmetric induction when in large excess (25 equiv **5.1**, reaction system 9).

In many instances of organic reactions, diversity is undesirable as the focus is on isolating a single compound in high yields and purity. This approach is not conducive to developing complex systems that possibly start from a wide range of chemical reactions and mixtures. This model reaction network demonstrates that complexity can be instrumental in transforming chemical information with chiral integrity. The reaction systems 5 and 6 demonstrate the importance of chemical diversity and highlight how an additional chemical entity (BzOH with an additional proton source) can activate new pathways (kinetic



differentiation of substrates) to facilitate a larger asymmetric ripple. Thus is shown that expansion of chiral information and chemical diversity is achievable concurrently.

### 5.3 Conclusion

Chiral information is an essential component for the initiation and propagation of life. Proton transfer, a ubiquitous process, provides a basis by which complex reaction mixtures are partitioned into select pathways. Proton transfer offers a method by which two analogous molecules can be directed towards two different pathways. This kinetic differentiation strategy is able to partition the reactivities of an imine and aldehyde substrate in the conjugative mode of an asymmetric aza-MBH reaction, which then allowed a temporally sequenced aza-MBH-Soai ripple to proceed. In this simple model system, a single catalyst molecule translates chirality 20 molecules of the aza-MBH adduct which propagates into 20000 molecules of Soai pyrimidine alkanol. This enhancement of both chirality (heterochirality transfer) and chemical diversity is a useful mechanism in exploring expansionary chiral information propagation..

## 5.4 Experimental

### 5.4.1 Materials and methods

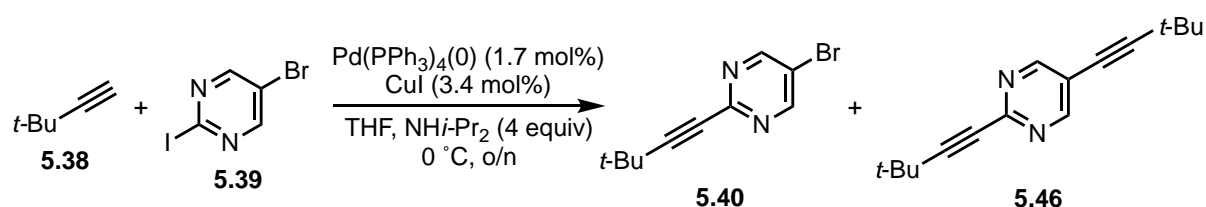
5-bromo-2-iodopyrimidine, 3,3-dimethyl-1-butyne and diisopropylamine were purchased from Oakwood Chemicals and used without further purification. Tetrakis(triphenylphosphine)palladium (0) ( $\text{PdPPh}_3)_4$  (0)) was prepared following the known literature procedure reported by Coulson immediately before use.<sup>44</sup> Copper Iodide was purified as previously reported before use.<sup>45</sup> *n*-butyllithium (2 M in hexane) was purchased from Sigma Aldrich and titrated against menthol/1,10-phenanthroline in THF immediately before use.  $\text{Zn}i\text{-Pr}_2$  was purchased from Sigma Aldrich and titrated against  $\text{LiCl}/\text{I}_2$  in anhydrous THF before use. Toluene and THF were distilled from sodium/benzophenone immediately before use. All other reagents were purchased from Sigma-Aldrich Castle Hill. Unless specified, all commercially available reagents were used without further purification. Dichloromethane was distilled from calcium hydride. All air and moisture sensitive reactions were performed under a nitrogen atmosphere. Reactions were magnetically stirred and monitored by thin-layer chromatography (TLC) using silica gel 60 F254 aluminium pre-coated plates from Merck (0.25 mm). Flash column chromatography was performed on silica gel (60 Å, 0.06–0.2 mm, 400 mesh from Scharlau).

All  $^1\text{H}$ ,  $^{13}\text{C}$  and 2D NMR experiments were performed on either a Bruker AVIIIHD 400 MHz NMR Spectrometer equipped with a BBFO SmartProbe (5mm) or DRX600 NMR spectrometer equipped with a TXI (5 mm) Cryoprobe. Chemical shifts were reported in ppm using residual  $\text{CHCl}_3$  ( $\delta_{\text{H}}$ ; 7.26 ppm,  $\delta_{\text{C}}$ ; 77.16 ppm) as an internal reference. All 2D NMR experiments were run with quadrature detection and a relaxation delay of 1–3 s. High power  $^1\text{H}$   $\pi/2$  pulses were determined to be ~9.5 ms, and  $^{13}\text{C}$  high power  $\pi/2$  pulse was 11.05 ms, and a low power pulse

of 65 ms was used for GARP4 decoupling. Gradient pulses were delivered along the z-axis using a 100 step sine program. Heteronuclear single quantum coherence (HSQC) experiments were optimised for a  $^1J_{\text{CH}}$  coupling of 145 Hz and HMBC spectra for a coupling of 20 Hz, using 145 Hz to suppress  $^1J_{\text{CH}}$  couplings. HSQC experiments were performed using the hsqcetgpsi or hsqcedetgpsp.3 (phase-edited HSQC) pulse program, and HMBC experiments were performed using the hmbcgp1pndqf pulse program. HSQC spectra were processed ( $\pi/2$  shifted sine bell squared in both dimensions) phase sensitive and HMBC (sine squared in both dimensions) with magnitude calculation in F1.  $^{13}\text{C}$  spectra were acquired using the UDEFT sequence. NOESY experiments were performed using the noesygp1phz pulse program with a mixing time of 400 ms. All spectra were processed using Bruker TOPSPIN 3.5p17. Trifunctional organocatalyst were prepared following the literature procedure.<sup>46-49</sup>

## 5.4.2 Synthesis of Soai Aldehydes via Lithium Halogen Exchange

### 5.4.2.1 Sonagoshira cross-coupling



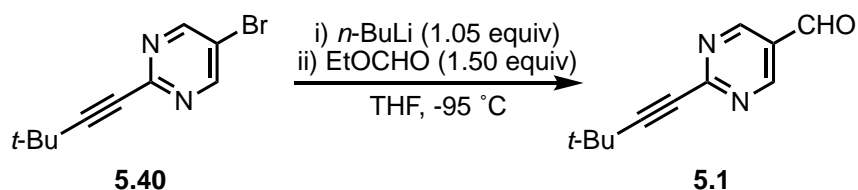
**Scheme 5E.1.** Preparation of **5.40** by Sonagoshira cross-coupling

5-Bromo-2-iodopyrimidine (**5.39**, 3.00 g, 10.53 mmol),  $\text{Pd(PPh}_3)_4(0)$  (206.87 mg, 0.18 mmol), copper iodide (68.19 mg, 0.38 mmol) were added to a flame dried 50 mL Schlenk flask and placed under an Ar atmosphere. Freshly distilled THF (17 mL) and diisopropylamine (5.90 mL, 42.1 mmol, 4 equiv) were added at  $0^\circ\text{C}$ . The mixture was then degassed (freeze-pump-thawed) before adding 3,3-dimethyl-1-butyne (**5.38**, 1.35 mL, 11.05 mmol, 1.05 equiv) over 30

mins at 0 °C. The reaction was stirred vigorously overnight at 0 °C and monitored by  $^1\text{H}$  NMR. Upon complete consumption of starting material, the reaction was poured through a pad of celite, and the filter cake washed extensively with EtOAc. The filtrate was concentrated *in vacuo* and the crude product resuspended in celite and ethyl acetate. The crude was then purified by flash chromatography (5–10% EtOAc/Hexane) to afford **5.40** as a white powder (2.51 g, 95.6%).  $^1\text{H}$  NMR (400MHz,  $\text{CDCl}_3$   $\delta$ ): 8.73 (s, 2H), 1.37 (s, 9H);  $^{13}\text{C}$  NMR (100MHz,  $\text{CDCl}_3$   $\delta$ ): 188.4, 158.4, 156.6, 126.4, 103.3, 79.2, 30.4, 28.4

The purified material was then recrystallised from heptane to remove the bisalkylation product (**5.46**).

#### 5.4.2.2 Lithium Halogen Exchange and trapping with Ethyl Formate

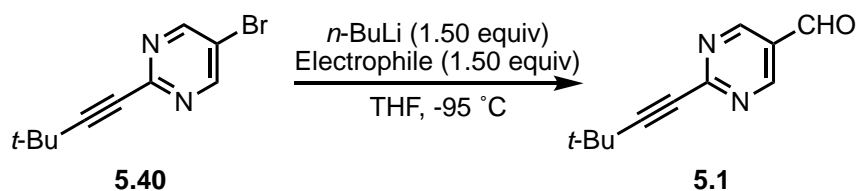


**Scheme 5E.2.** Preparation of **5.1** by Lithium-halogen exchange and formylation.

Pyrimidine bromide **5.40** (2.0 g, 8.36 mmol) was transferred to a 250 mL flame-dried Schlenk flask charged with a stir bar, and complexed water was removed with toluene by azeotropic distillation under reduced pressure. The dry material was then melted under an inert atmosphere to remove trace water. After cooling to room temperature, the flask was placed under an Ar atmosphere, and freshly distilled THF (85 mL) was added. The mixture was stirred vigorously and then cooled to -95 °C ( $\text{N}_2(\text{l})/\text{hexane}$ ) and this temperature was maintained throughout the reaction.  $n\text{-BuLi}$  (1.8 M in hexanes, 4.88 mL) was then added over 20 minutes via a syringe pump. The dark orange mixture was then stirred for 5 minutes before adding

ethyl formate (1.02 mL, 12.5 mmol, 1.5 equiv) in THF (5 mL) over 10 minutes via a syringe pump. The reaction was stirred at -95 °C for a further 10 minutes before adding HCl (2 M in Et<sub>2</sub>O, 4.4 mL) via a syringe pump over 10 minutes. The reaction was warmed to room temperature, and the THF removed *in vacuo*. The residue was resuspended with EtOAc (50 mL) and washed with NaHCO<sub>3</sub> (3 x 25 mL), brine (25 mL) and dried over sodium sulphate. The crude material was suspended in celite and purified by flash chromatography (5-15% EtOAc: Hexane). Fractions containing product were collected and reduced *in vacuo* to afford a yellow solid. This was transferred to a 100 mL Schlenk flask, and the aldehyde product was purified by sublimation under reduced pressure to afford **5.1** as a white powder (727 mg, 46%). Spectroscopic data was consistent with the literature reports.<sup>37</sup> The product could also be recrystallised from boiling heptane.

#### 5.4.2.3 Formylation via Barbier-type conditions.



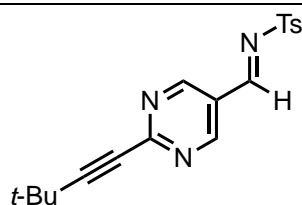
**Scheme 5E.3.** Preparation of **5.1** by Barbier-type formylation.

Pyrimidine bromide **20** (3.14 g, 13.14 mmol) was transferred to a 250 mL flame-dried Schlenk flask charged with a stir bar, and complexed water was removed with toluene by azeotropic distillation under reduced pressure. The dry material was then melted under an inert atmosphere to remove trace water. After cooling to room temperature, the flask was placed under an Ar atmosphere, and freshly distilled THF (130 mL) was added. Ethyl formate (1.50 mL, 18.40 mmol, 1.4 equiv) was added, and the reaction was cooled to -95 °C (N<sub>2</sub>(l)/Hexane). *n*-BuLi (2.5 M in hexanes, 7.36 mL) was then added dropwise over 10 minutes. The dark

orange mixture was then stirred for 10 minutes before quenching with acetic acid (2.1 mL, 36.80 mmol, 2.8 equiv). The reaction was warmed to room temperature before adding water (20 mL) and removing the volatiles *in vacuo*. The residue was resuspended in ether (75 mL) and carefully quenched with NaHCO<sub>3</sub>. Water (50 mL) was added, and the aqueous layer was extracted with ether (3 x 30 mL). The combined organic layers were washed with brine (25 mL) and dried over sodium sulphate. The crude material was suspended in celite and purified by flash chromatography (5–25% EtOAc: Hexane) to afford pyrimidine aldehyde **5.1** (2.02 g, 82%) which contained trace reductive debromination side product. The material was further purified by recrystallisation from ethyl acetate/hexane. Spectroscopic data was consistent with the literature reports.<sup>37</sup>

#### 5.4.2.4 Data for compound 5.48 and 5.49

Compound **5.49** was prepared using the general procedure for 3-pyridine carbaldimines established in Chapter 4.



**5.49**

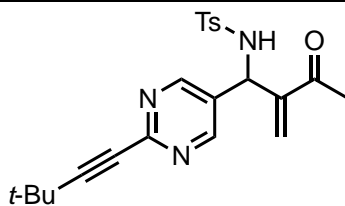
(*E*)-*N*-((2-(3,3-dimethylbut-1-yn-1-yl)pyrimidin-5-yl)methylene)-4-methylbenzenesulfonamide (**5.49**)

**<sup>1</sup>H NMR** (400 MHz, CDCl<sub>3</sub>, δ): 9.12 (s, 2H), 9.03 (s, 1H), 7.90 (d, *J* = 8.3 Hz, 2H), 7.38, (d, *J* = 8.3 Hz, 2H), 2.46 (s, 3H), 1.39 (s, 9H).

**<sup>13</sup>C NMR** (100 MHz, CDCl<sub>3</sub>, δ): 164.5, 159.0, 156.7, 145.6, 134.1, 130.2, 128.6, 124.1, 103.8, 30.3, 28.4, 21.9

**MS (ESI):** 342.1 [M+ H]

---



**5.48**

*N*-(1-(2-(3,3-dimethylbut-1-yn-1-yl)pyrimidin-5-yl)-2-methylene-3-oxobutyl)-4-methylbenzenesulfonamide (**5.48**)

**<sup>1</sup>H NMR** (400 MHz, CDCl<sub>3</sub>, δ): 8.41 (s, 2H), 7.63 (d, *J* = 8.3, 2H), 7.24 (d, *J* = 8.3 Hz, 2H), 6.16 (s, 1H), 6.13 (s, 1H), 5.82 (d, *J* = 9.5 Hz, 1H), 5.23 (d, *J* = 9.5 Hz, 1H), 2.42 (s, 3H), 2.18 (s, 3H), 1.35 (s, 9H).

**<sup>13</sup>C NMR** (100 MHz, CDCl<sub>3</sub>, δ): 198.8, 155.5, 144.8, 144.2, 137.3, 130.4, 130.1, 129.9, 127.3, 98.6, 56.2, 30.5, 28.0, 26.3, 21.7.

**MS (ESI)**: 412 [M+ H]

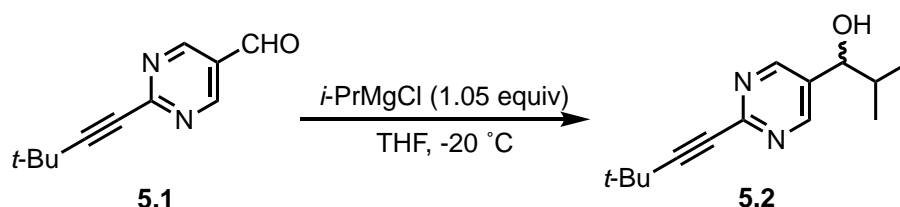
**Chiral HPLC**: 60:40 Hex/2-PrOH (0.7 mL min<sup>-1</sup>), Whelk-01 Column, RT<sub>1</sub>: 21.4 min, RT<sub>2</sub>: 24.86 min

---

### 5.4.3 Soai Reaction

All glassware used for Soai amplification reaction was performed with new and unused disposable 4 mL vials. Vials and stir bars for the reaction were washed with 6.0 M nitric, distilled water and ethanol (99.95%). Vials and stir bars were stored in a 120 °C oven overnight before use. Gastight disposable syringes and needles were used and disposed of after sampling each reaction to ensure no contamination between different conditions.

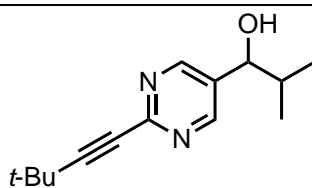
#### 5.4.3.1 Preparation of Racemic Standard



**Scheme 5E.4.** Preparation of *racemic* **5.2**

**5.1** (25 mg, 0.13 mmol) was dissolved in THF (1.3 mL) and cooled to -20 °C. *i*-PrMgCl (1 M in Et<sub>2</sub>O, 139 µL, 1.05 equiv) was added dropwise over 5 minutes. The reaction was stirred for 10 minutes, allowed to warm to room temperature, and carefully quenched with NH<sub>4</sub>Cl (200 µL). THF was removed *in vacuo* and the residue resuspended in EtOAc (15 mL). The reaction was washed with NaHCO<sub>3</sub> (3 x 10 mL), water (2 x 1 mL) and then dried over sodium sulfate. The solvent was removed *in vacuo*, and the crude product was purified by flash chromatography (20% EtOAc: Hexane) to afford **5.2** as a white solid (17 mg, 55%). Spectroscopic data was consistent with the literature.<sup>15</sup>





**5.2**

1-(2-(3,3-dimethylbut-1-yn-1-yl)pyrimidin-5-yl)-2-methylpropan-1-ol (**5.2**)

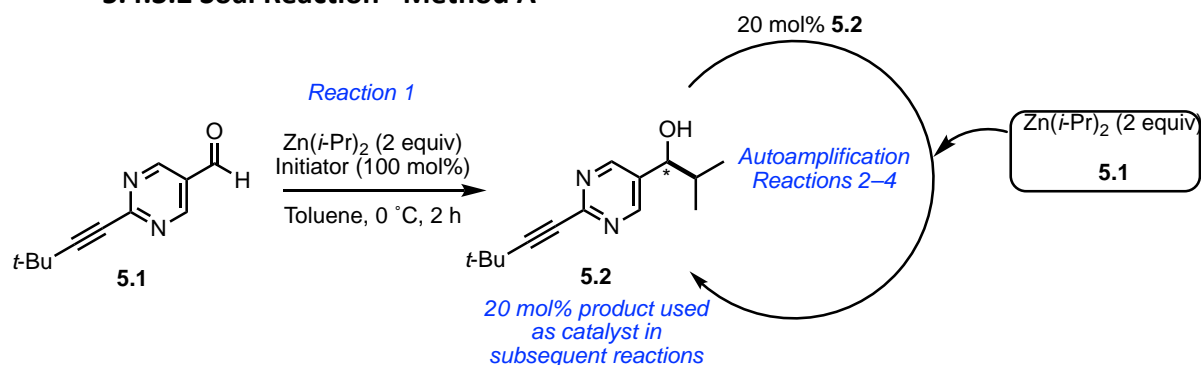
**<sup>1</sup>H NMR** (400 MHz, CDCl<sub>3</sub>, δ): 8.62 (s, 2H), 4.51 (d, *J* = 6.1 Hz), 1.97 (m, 1H), 1.37 (s, 9H), 0.95 (d, *J* = 6.7 Hz, 3H), 0.87 (d, *J* = 6.7 Hz, 3H).

**<sup>13</sup>C NMR** (100 MHz, CDCl<sub>3</sub>, δ): 155.7, 153.3, 134.4, 97.9, 78.5, 75.3, 35.3, 30.5, 27.9, 18.5, 17.5.

**MS (ESI):** *m/z*, need to do [M+ H]

**Chiral HPLC:** 95:5 Hex/2-PrOH (0.7 mL min<sup>-1</sup>), Chiralpak AD-H Column, RT<sub>1</sub>: 13.12 min, RT<sub>2</sub>: 14.63 min

#### 5.4.3.2 Soai Reaction– Method A



**Scheme 5E.5.** The Soai reaction using Method A.

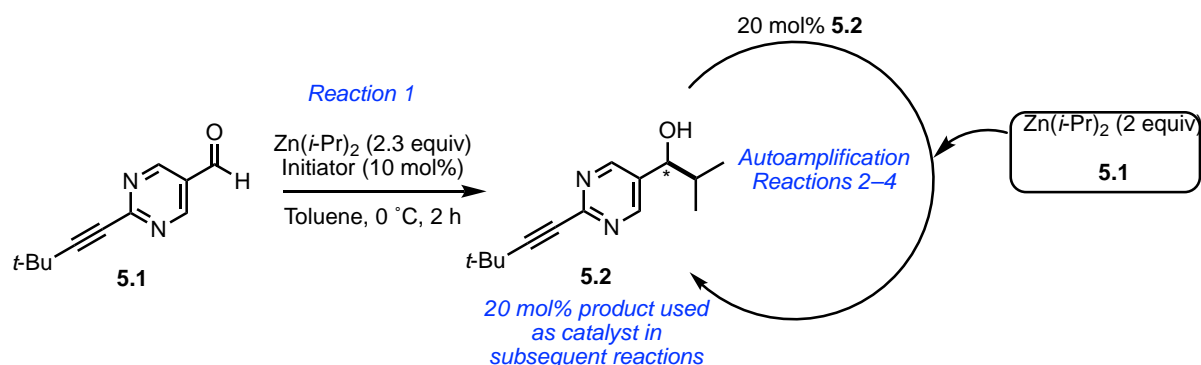
#### Reaction 1– Chiral Initiation

The chiral initiator (0.01 mmol, 1 equiv) was added to a flame-dried 4 mL vial, and the vessel was purged 8 times with Ar. Toluene (100 μL) was added, and the mixture was stirred for cooled to 0 °C before adding Zn*i*-Pr<sub>2</sub> (90 μL, 0.05 mmol, 5 equiv) dropwise over 2 minutes. The reaction was stirred for a further 5 minutes before adding a solution of **5.1** in toluene (2.00 mg, 0.01 mmol, 1 equiv, 500 μL) over 30 minutes and then left to stir overnight at 0 °C.

#### Reaction 2-4 – Chiral Propagation

Toluene (150  $\mu\text{L}$ ) and  $\text{Zn}(\text{i-Pr})_2$  (94  $\mu\text{L}$ , 0.86 mmol, 2 equiv) were added before dropwise addition of **5.1** in toluene (8.00 mg, 0.043 mmol, 1 equiv, 320  $\mu\text{L}$ ). The reaction was stirred for three hours at 0  $^\circ\text{C}$  before removing an aliquot of the reaction (840  $\mu\text{L}$ ) and adding toluene (450  $\mu\text{L}$ ),  $\text{Zn}(\text{i-Pr})_2$  (191  $\mu\text{L}$ , 0.17 mmol, 2 equiv) and a solution of **5.1** in toluene (16.21 mg, 0.086 mmol, 1 equiv, 430  $\mu\text{L}$ ). The reaction was stirred for one hour at 0  $^\circ\text{C}$  before removing an aliquot of the reaction (1.30 mL) and adding toluene (450  $\mu\text{L}$ ),  $\text{Zn}(\text{i-Pr})_2$  (144  $\mu\text{L}$ , 0.13 mmol, 2 equiv) and a solution of **5.1** in toluene (12.16 mg, 0.065 mmol, 1 equiv, 484  $\mu\text{L}$ ). Reactions were quenched with the slow addition of HCl (1M, 3 equiv) and then careful addition of  $\text{NaHCO}_3$  (sat., 9 equiv). The aqueous phase was extracted with DCM (5 x 10 mL) and the organic phase dried over sodium sulphate. The combined organic phase was reduced *in vacuo* and crude **5.2** analysed by chiral HPLC.

#### 5.4.3.3 Soai Reaction– Method B



**Scheme 5E.6.** The Soai reaction using Method B.

#### Reaction 1– Chirality Initiation

The chiral initiator (4  $\mu\text{mol}$ ) in a flame-dried, 4 mL vial charged with a stir bar was dissolved in anhydrous toluene (1.00 mL) and placed under an inert atmosphere. The reaction was cooled to 0  $^\circ\text{C}$  and  $\text{Zn}(\text{i-Pr})_2$  (1M in toluene, 100  $\mu\text{L}$ , 2.3 equiv) was added dropwise, and the reaction was stirred vigorously for 30 minutes. Aldehyde **5.1** (8.00 mg, 0.043 mmol) was

dissolved in toluene (575  $\mu$ L) and added dropwise over 2 minutes. The reaction was then stirred for 2 hours before removing an aliquot and quenching with 2-propanol (2 mL). The quenched reaction was evaporated to dryness, resuspended in 2-propanol (2 mL), filtered and analysed by chiral HPLC.

#### Reaction 2 and 3 – Chiral Propagation

To the remaining reaction mixture was added toluene (600  $\mu$ L), and  $\text{Zn-Pr}_2$  (1M in toluene, 100  $\mu$ L, 2.3 equiv) was added dropwise and stirred for 10 minutes. A toluene solution of aldehyde **5.1** (8.00 mg, 0.043 mmol, 575  $\mu$ L) was dissolved in toluene (575  $\mu$ L) and added dropwise over 2 minutes. The reaction was stirred for one hour, and an aliquot was removed and quenched with 2-propanol (2 mL). The solvent was evaporated to dryness, resuspended in 2-propanol (2 mL), filtered and analysed by chiral HPLC. The remaining unquenched reaction mixture was used to repeat the reaction at the same scale (toluene (600  $\mu$ L),  $\text{Zn-Pr}_2$  (1M in toluene, 100  $\mu$ L, 2.3 equiv) and aldehyde **5.1** in toluene (8.00 mg, 0.043 mmol, 575  $\mu$ L).

## 5.5 References

1. Lee, J. M.; Na, Y.; Han, H.; Chang, S., Cooperative multi-catalyst systems for one-pot organic transformations. *Chem. Soc. Rev.* **2004**, 33 (5), 302-312.
2. Seayad, J.; List, B., Asymmetric organocatalysis. *Org. Biomol. Chem.* **2005**, 3 (5), 719-724.
3. Zhou, J., Recent Advances in Multicatalyst Promoted Asymmetric Tandem Reactions. *Chem. - Asian J.* **2010**, 5 (3), 422-434.
4. Bissette, A. J.; Fletcher, S. P., Mechanisms of Autocatalysis. *Angew. Chem., Int. Ed.* **2013**, 52 (49), 12800-12826.
5. Soai, K.; Kawasaki, T., Asymmetric Autocatalysis with Amplification of Chirality. In *Amplification of Chirality*, Soai, K., Ed. Springer Berlin Heidelberg: Berlin, Heidelberg, 2008; pp 1-33.
6. Sato, I.; Sugie, R.; Matsueda, Y.; Furumura, Y.; Soai, K., Asymmetric Synthesis Utilizing Circularly Polarized Light Mediated by the Photoequilibrium of Chiral Olefins in Conjunction with Asymmetric Autocatalysis. *Angew. Chem., Int. Ed.* **2004**, 43 (34), 4490-4492.
7. Kawasaki, T.; Sato, M.; Ishiguro, S.; Saito, T.; Morishita, Y.; Sato, I.; Nishino, H.; Inoue, Y.; Soai, K., Enantioselective Synthesis of Near Enantiopure Compound by Asymmetric Autocatalysis Triggered by Asymmetric Photolysis with Circularly Polarized Light. *J. Am. Chem. Soc.* **2005**, 127 (10), 3274-3275.
8. Sato, I.; Kadowaki, K.; Soai, K., Asymmetric Synthesis of an Organic Compound with High Enantiomeric Excess Induced by Inorganic Ionic Sodium Chlorate. *Angew. Chem., Int. Ed.* **2000**, 39 (8), 1510-1512.

9. Kawasaki, T.; Suzuki, K.; Hakoda, Y.; Soai, K., Achiral Nucleobase Cytosine Acts as an Origin of Homochirality of Biomolecules in Conjunction with Asymmetric Autocatalysis. *Angew. Chem., Int. Ed.* **2008**, *47* (3), 496-499.
10. Kawasaki, T.; Harada, Y.; Suzuki, K.; Tobita, T.; Florini, N.; Pályi, G.; Soai, K., Enantioselective Synthesis Utilizing Enantiomorphous Organic Crystal of Achiral Benzils as a Source of Chirality in Asymmetric Autocatalysis. *Org. Lett.* **2008**, *10* (18), 4085-4088.
11. Mineki, H.; Hanasaki, T.; Matsumoto, A.; Kawasaki, T.; Soai, K., Asymmetric autocatalysis initiated by achiral nucleic acid base adenine: implications on the origin of homochirality of biomolecules. *Chem. Commun.* **2012**, *48* (85), 10538-10540.
12. Shindo, H.; Shirota, Y.; Niki, K.; Kawasaki, T.; Suzuki, K.; Araki, Y.; Matsumoto, A.; Soai, K., Asymmetric Autocatalysis Induced by Cinnabar: Observation of the Enantioselective Adsorption of a 5-Pyrimidyl Alkanol on the Crystal Surface. *Angew. Chem., Int. Ed.* **2013**, *52* (35), 9135-9138.
13. Kawasaki, T.; Uchida, M.; Kaimori, Y.; Sasagawa, T.; Matsumoto, A.; Soai, K., Enantioselective Synthesis Induced by the Helical Molecular Arrangement in the Chiral Crystal of Achiral Tris(2-hydroxyethyl) 1,3,5-Benzenetricarboxylate in Conjunction with Asymmetric Autocatalysis. *Chem. Lett.* **2013**, *42* (7), 711-713.
14. Mineki, H.; Kaimori, Y.; Kawasaki, T.; Matsumoto, A.; Soai, K., Enantiodivergent formation of a chiral cytosine crystal by removal of crystal water from an achiral monohydrate crystal under reduced pressure. *Tetrahedron: Asymmetry* **2013**, *24* (21), 1365-1367.
15. Hitosugi, S.; Matsumoto, A.; Kaimori, Y.; Iizuka, R.; Soai, K.; Isobe, H., Asymmetric Autocatalysis Initiated by Finite Single-Wall Carbon Nanotube Molecules with Helical Chirality. *Org. Lett.* **2014**, *16* (3), 645-647.

16. Matsumoto, A.; Ide, T.; Kaimori, Y.; Fujiwara, S.; Soai, K., Asymmetric Autocatalysis Triggered by Chiral Crystal of Achiral Ethylenediamine Sulfate. *Chem. Lett.* **2015**, 44 (5), 688-690.
17. Matsumoto, A.; Ozawa, H.; Inumaru, A.; Soai, K., Asymmetric induction by retgersite, nickel sulfate hexahydrate, in conjunction with asymmetric autocatalysis. *New J. Chem.* **2015**, 39 (9), 6742-6745.
18. Matsumoto, A.; Kaimori, Y.; Uchida, M.; Omori, H.; Kawasaki, T.; Soai, K., Achiral Inorganic Gypsum Acts as an Origin of Chirality through Its Enantiotopic Surface in Conjunction with Asymmetric Autocatalysis. *Angew. Chem., Int. Ed.* **2017**, 56 (2), 545-548.
19. Soai, K.; Kawasaki, T.; Matsumoto, A., Asymmetric autocatalysis of pyrimidyl alkanol and related compounds. Self-replication, amplification of chirality and implication for the origin of biological enantioenriched chirality. *Tetrahedron* **2018**, 74 (16), 1973-1990.
20. Kawasaki, T.; Shimizu, M.; Nishiyama, D.; Ito, M.; Ozawa, H.; Soai, K., Asymmetric autocatalysis induced by meteoritic amino acids with hydrogen isotope chirality. *Chem. Commun.* **2009**, (29), 4396-4398.
21. Sato, I.; Ohgo, Y.; Igarashi, H.; Nishiyama, D.; Kawasaki, T.; Soai, K., Determination of absolute configurations of amino acids by asymmetric autocatalysis of 2-alkynylpyrimidyl alkanol as a chiral sensor. *J. Organomet. Chem.* **2007**, 692 (9), 1783-1787.
22. Sato, I.; Yamashima, R.; Kadowaki, K.; Yamamoto, J.; Shibata, T.; Soai, K., Asymmetric induction by helical hydrocarbons: [6]- and [5]helicenes. *Angew. Chem., Int. Ed.* **2001**, 40 (6), 1096-1098.
23. Matsumoto, A.; Yonemitsu, K.; Ozaki, H.; Misek, J.; Stary, I.; Stara, I. G.; Soai, K., Reversal of the sense of enantioselectivity between 1- and 2-aza[6]helicenes used as chiral inducers of asymmetric autocatalysis. *Org. Biomol. Chem.* **2017**, 15 (6), 1321-1324.

24. Welch, C. J.; Zawatzky, K.; Makarov, A. A.; Fujiwara, S.; Matsumoto, A.; Soai, K., Can the analyte-triggered asymmetric autocatalytic Soai reaction serve as a universal analytical tool for measuring enantiopurity and assigning absolute configuration? *Org. Biomol. Chem.* **2017**, *15* (1), 96-101.
25. Soai, K.; Kawasaki, T.; Matsumoto, A., Asymmetric Autocatalysis of Pyrimidyl Alkanol and Its Application to the Study on the Origin of Homochirality. *Acc. Chem. Res.* **2014**, *47* (12), 3643-3654.
26. Sato, I.; Omiya, D.; Tsukiyama, K.; Ogi, Y.; Soai, K., Evidence of asymmetric autocatalysis in the enantioselective addition of diisopropylzinc to pyrimidine-5-carbaldehyde using chiral pyrimidyl alkanol. *Tetrahedron: Asymmetry* **2001**, *12* (14), 1965-1969.
27. Blackmond, D. G.; McMillan, C. R.; Ramdeehul, S.; Schorm, A.; Brown, J. M., Origins of Asymmetric Amplification in Autocatalytic Alkylzinc Additions. *J. Am. Chem. Soc.* **2001**, *123* (41), 10103-10104.
28. Gridnev, I. D.; Serafimov, J. M.; Brown, J. M., Solution Structure and Reagent Binding of the Zinc Alkoxide Catalyst in the Soai Asymmetric Autocatalytic Reaction. *Angew. Chem., Int. Ed.* **2004**, *43* (37), 4884-4887.
29. Buhse, T., A tentative kinetic model for chiral amplification in autocatalytic alkylzinc additions. *Tetrahedron: Asymmetry* **2003**, *14* (8), 1055-1061.
30. Buono, F. G.; Blackmond, D. G., Kinetic Evidence for a Tetrameric Transition State in the Asymmetric Autocatalytic Alkylation of Pyrimidyl Aldehydes. *J. Am. Chem. Soc.* **2003**, *125* (30), 8978-8979.
31. Sato, I.; Omiya, D.; Igarashi, H.; Kato, K.; Ogi, Y.; Tsukiyama, K.; Soai, K., Relationship between the time, yield, and enantiomeric excess of asymmetric autocatalysis of chiral 2-

alkynyl-5-pyrimidyl alkanol with amplification of enantiomeric excess. *Tetrahedron: Asymmetry* **2003**, *14* (8), 975-979.

32. Klankermayer, J.; Gridnev, I. D.; Brown, J. M., Role of the isopropyl group in asymmetric autocatalytic zinc alkylations. *Chem. Commun.* **2007**, (30), 3151-3153.

33. Schiaffino, L.; Ercolani, G., Unraveling the Mechanism of the Soai Asymmetric Autocatalytic Reaction by First - Principles Calculations: Induction and Amplification of Chirality by Self - Assembly of Hexamolecular Complexes. *Angew. Chem., Int. Ed.* **2008**, *47* (36), 6832-6835.

34. Quaranta, M.; Gehring, T.; Odell, B.; Brown, J. M.; Blackmond, D. G., Unusual Inverse Temperature Dependence on Reaction Rate in the Asymmetric Autocatalytic Alkylation of Pyrimidyl Aldehydes. *J. Am. Chem. Soc.* **2010**, *132* (43), 15104-15107.

35. Gehring, T.; Quaranta, M.; Odell, B.; Blackmond, D. G.; Brown, J. M., Observation of a Transient Intermediate in Soai's Asymmetric Autocatalysis: Insights from <sup>1</sup>H NMR Turnover in Real Time. *Angew. Chem., Int. Ed.* **2012**, *51* (38), 9539-9542.

36. Matsumoto, A.; Abe, T.; Hara, A.; Tobita, T.; Sasagawa, T.; Kawasaki, T.; Soai, K., Crystal Structure of the Isopropylzinc Alkoxide of Pyrimidyl Alkanol: Mechanistic Insights for Asymmetric Autocatalysis with Amplification of Enantiomeric Excess. *Angew. Chem., Int. Ed.* **2015**, *54* (50), 15218-15221.

37. Maltsev, O. V.; Pöthig, A.; Hintermann, L., Synthesis of Soai Aldehydes for Asymmetric Autocatalysis by Desulfurative Cross-Coupling. *Org. Lett.* **2014**, *16* (5), 1282-1285.

38. Arnold, Z., Note on the formylation of chloro- and bromoacetic acid. *Collect. Czech. Chem. Commun.* **1965**, *30*, 2125-2127.



39. Blomberg, C.; Hartog, F. A., The Barbier Reaction - A One-Step Alternative for Syntheses via Organomagnesium Compounds. *Synthesis* **1977**, 1977 (01), 18-30.
40. Molle, G.; Bauer, P., The Barbier synthesis: a one-slip Grignard reaction? *J. Am. Chem. Soc.* **1982**, 104 (12), 3481-3487.
41. Blomberg, C., *The Barbier Reaction and Related One-Step Processes*. Springer Berlin Heidelberg: Berlin, Heidelberg, 1993.
42. Sato, I.; Ohgo, Y.; Igarashi, H.; Nishiyama, D.; Kawasaki, T.; Soai, K., Determination of absolute configurations of amino acids by asymmetric autocatalysis of 2-alkynylpyrimidyl alkanol as a chiral sensor. *Journal of Organometallic Chemistry* **2007**, 692, 1783-1787.
43. Hayase, T.; Shibata, T.; Soai, K.; Wakatsuki, Y., An enantioselective Baylis–Hillman reaction catalyzed by chiral phosphines under atmospheric pressure. *Chem. Commun.* **1998**, (12), 1271-1272.
44. Coulson, D. R.; Satek, L. C.; Grim, S. O., Tetrakis(triphenylphosphine)palladium(0). In *Inorganic Syntheses*, Cotton, F. A., Ed. 1972.
45. Armarego, W. L. F.; Chai, C. L. L., Chapter 5 - Purification of Inorganic and Metal-Organic Chemicals: (Including Organic compounds of B, Bi, P, Se, Si, and ammonium and metal salts of organic acids). In *Purification of Laboratory Chemicals (Sixth Edition)*, Butterworth-Heinemann: Oxford, 2009; pp 445-576.
46. Anstiss, C.; Garnier, J.-M.; Liu, F., Mechanistic investigations of multidentate organocatalyst-promoted counterion catalysis for fast and enantioselective aza-Morita-Baylis-Hillman reactions at ambient temperature. *Org. Biomol. Chem.* **2010**, 8 (19), 4400-4407.
47. Anstiss, C.; Liu, F., Cooperativity in the counterion catalysis of Morita/Baylis/Hillman reactions promoted by enantioselective trifunctional organocatalysts. *Tetrahedron* **2010**, 66 (29), 5486-5491.

48. Garnier, J.-M.; Anstiss, C.; Liu, F., Enantioselective Trifunctional Organocatalysts for Rate- Enhanced Aza-Morita–Baylis–Hillman Reactions at Room Temperature. *Adv. Synth. Catal.* **2009**, 351 (3), 331-338.
49. Garnier, J.-M.; Liu, F., Trifunctional organocatalyst-promoted counterion catalysis for fast and enantioselective aza-Morita-Baylis-Hillman reactions at ambient temperature. *Org. Biomol. Chem.* **2009**, 7 (7), 1272-1275.

## **Chapter 6**

### **Conclusions and Future Directions**

## 6.1 Conclusions

This thesis began with the initial aim of addressing the mechanism complexity of the acid-regulated trifunctional organocatalysed aza-MBH reaction. In this thesis, the effect of proton motion in a model proton transfer reaction (aza-MBH) has been demonstrated. The chapters within this thesis have demonstrated that proton motion is the basis behind the activation of ground state **PBK** and is essential for C–C bond formation. In this thesis, an asymmetric ripple in the Soai reaction has been employed as a method of reading the chemical output of a system.

In **chapter two**, a solution structure model of **TF-1-PBK** was developed by 2D NMR and molecular mechanics. It was shown that unlike bifunctional PBK (i.e. **MOP-PBK**), that **TF-1-PBK** is not a parasitic intermediate. Proton motion, facilitated by the conformational bias of **TF-1-PBK** and embedded within the tautomeric forms of **TF-1-PBK**, activates the ground state for C–C bond formation.

In **chapter three**, the role of the acid additive in trifunctional catalysis was investigated. A structure-reactivity relationship (SRR) demonstrated that the nature and identity of the acid additive can dictate the activation of **TF-1-PBK** and directs proton transfer to the aldolate (**TF-1-AI**). The acid additive also accelerates proton motion in the trifunctional PBKs (**TF-1-3**) contributing to a slower elimination of **MVK** (deuterium incorporation kinetics). Finally, the role of BzOH in expanding the aza-MBH reaction into a new paradigm with conjugative and subjugative pathways was shown with a set of substrates with different protecting groups.

In **chapter four**, new heterocyclic substrates (pyridines) for the aza-MBH were prepared and tested to identify the scope of the trifunctional conjugative mode. 3-pyridine substrates were compliant with the conjugative mode of catalysis while 2-pyridine substrates can only adopt an asymmetric subjugative mode.

In **chapter five**, an asymmetric ripple connecting the aza-MBH and Soai reaction was developed. A more robust synthesis of the Soai aldehyde **5.1** was developed using Barbier-type conditions and ethyl formate. The size of the asymmetric ripple in the Soai reaction was also shown to be dependent upon the addition of benzoic acid (and adoption of the conjugative mode of trifunctional catalysis).

## 6.2 Future Directions

The model trifunctional system has demonstrated the role of proton motion and how it can be utilised for catalytic proficiency. From the mechanistic model developed in this work further developments to the catalytic system can be rationally designed to expand further into a different reaction space. Additionally, new catalysts for other model reactions can be developed based upon the dynamics of proton transfer.

In relation to the aza-MBH reaction, there is opportunity to explore new heteroaryl substrates includes furans and pyrroles. In addition, the scope of heteroaryl aldehyde substrates and their capacity to facilitate proton transfer can be investigated. Furthermore, the substrate scope of carbamoyl imine can be expanded further to identify if the mechanism can be shifted to the conjugative mode. Likewise, the effect of the different aza-MBH adducts (different protecting groups, aryl vs heteroaryl) on the asymmetric ripple in the Soai reaction can also

be explored. Finally, the capacity of proton transfer to propagate chirality can be explored in other model systems. This is of particular relevance to prebiotic chemistry and is an avenue that can be explored further.

# Appendix

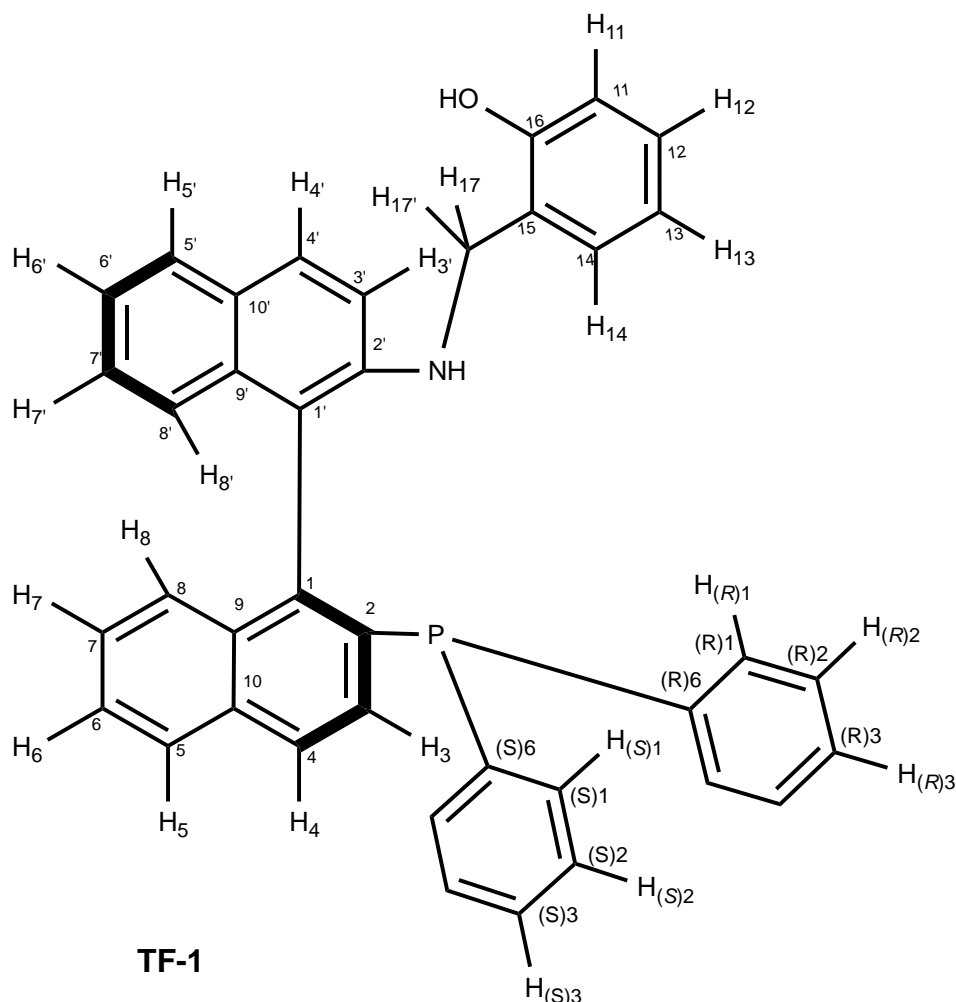
## Table of contents

|   |      |
|---|------|
| <b>A.1 catalyst spectra and assignments.</b>  | A-4  |
| <b>A.1.1 Catalyst TF-1</b>  | A-4  |
| <b>A.1.2 Partial assignments for the phosphonium butanone for pbk</b>   | A-11 |
| <b>A.2 <sup>1</sup>H NMR, <sup>13</sup>C nmr and chiral hplc traces for substrates in chapter 3, 4 and 5.</b>     | A-14 |
| <i>(E)</i> -N-(4-chlorobenzylidene)methanesulfonamide ( <b>NMs-Im-1</b> )   | A-14 |
| <i>(E)</i> -4-methyl-N-(pyridin-3-ylmethylene)benzenesulfonamide ( <b>NTsPyr-Im-1</b> )                           | A-17 |
| <i>(E)</i> -N-((2-fluoropyridin-3-yl)methylene)-4-methylbenzenesulfonamide ( <b>NTsPyr-Im-2</b> )                 | A-20 |
| <i>(E)</i> -N-((2-chloropyridin-3-yl)methylene)-4-methylbenzenesulfonamide ( <b>NTsPyr-Im-3</b> )                 | A-23 |
| <i>(E)</i> -N-((6-fluoropyridin-3-yl)methylene)-4-methylbenzenesulfonamide ( <b>NTsPyr-Im-4</b> )                 | A-26 |
| <i>(E)</i> -N-((6-chloropyridin-3-yl)methylene)-4-methylbenzenesulfonamide ( <b>NTsPyr-Im-5</b> )                 | A-31 |
| <i>(E)</i> -N-((6-bromopyridin-3-yl)methylene)-4-methylbenzenesulfonamide ( <b>NTsPyr-Im-6</b> )                  | A-32 |
| <i>(E)</i> -N-((5-bromopyridin-2-yl)methylene)-4-methylbenzenesulfonamide ( <b>NTsPyr-Im-7</b> )                  | A-35 |
| <i>(E)</i> -N-((6-bromopyridin-2-yl)methylene)-4-methylbenzenesulfonamide ( <b>NTsPyr-Im-8</b> )                  | A-38 |
| <i>(E)</i> -N-((2-(3,3-dimethylbut-1-yn-1-yl)pyrimidin-5-yl)methylene)-4-methylbenzenesulfonamide ( <b>5.49</b> ) | A-41 |
| <i>tert</i> -butyl ((4-chlorophenyl)(tosyl)methyl)carbamate ( <b>NBoc-sulfone-1</b> )                             | A-44 |
| <i>tert</i> -butyl ( <i>e</i> )-(4-chlorobenzylidene)carbamate ( <b>NBoc-Im-1</b> )                               | A-47 |
| <i>tert</i> -butyl (pyridin-3-yl(tosyl)methyl)carbamate ( <b>NBoc-sulfone-2</b> )                                 | A-50 |
| <i>tert</i> -butyl ( <i>e</i> )-(pyridin-3-ylmethylene)carbamate ( <b>NBoc-Im-2</b> )                             | A-53 |
| <i>tert</i> -butyl ((5-bromopyridin-2-yl)(tosyl)methyl)carbamate ( <b>NBoc-sulfone-3</b> )                        | A-56 |
| <i>tert</i> -butyl ( <i>e</i> )-((5-bromopyridin-2-yl)methylene)carbamate ( <b>NBoc-Im-3</b> )                    | A-59 |



|   |       |
|---|-------|
| <i>N</i> -(1-(4-chlorophenyl)-2-methylene-3-oxobutyl)methanesulfonamide ( <b>NMs-MBH-1</b> ) .....                                  | A-62  |
| 4-methyl- <i>N</i> -(2-methylene-3-oxo-1-(pyridin-3-yl)butyl)benzenesulfonamide ( <b>NTsPyr-MBH-1</b> ) .....                       | A-66  |
| <i>N</i> -(1-(2-fluoropyridin-3-yl)-2-methylene-3-oxobutyl)-4-methylbenzenesulfonamide ( <b>NTsPyr-MBH-2</b> ) .....                | A-70  |
| <i>N</i> -(1-(2-chloropyridin-3-yl)-2-methylene-3-oxobutyl)-4-methylbenzenesulfonamide ( <b>NTsPyr-MBH-3</b> ) .....                | A-74  |
| <i>N</i> -(1-(6-fluoropyridin-3-yl)-2-methylene-3-oxobutyl)-4-methylbenzenesulfonamide ( <b>NTsPyr-MBH-4</b> ) .....                | A-78  |
| <i>N</i> -(1-(6-chloropyridin-3-yl)-2-methylene-3-oxobutyl)-4-methylbenzenesulfonamide ( <b>NTsPyr-MBH-5</b> ) .....                | A-82  |
| <i>N</i> -(1-(6-bromopyridin-3-yl)-2-methylene-3-oxobutyl)-4-methylbenzenesulfonamide ( <b>NTsPyr-MBH-6</b> ) .....                 | A-86  |
| <i>N</i> -(1-(5-bromopyridin-2-yl)-2-methylene-3-oxobutyl)-4-methylbenzenesulfonamide ( <b>NTsPyr-MBH-7</b> ) .....                 | A-90  |
| <i>N</i> -(1-(6-bromopyridin-2-yl)-2-methylene-3-oxobutyl)-4-methylbenzenesulfonamide ( <b>NTsPyr-MBH-8</b> ) .....                 | A-94  |
| <i>tert</i> -butyl (1-(4-chlorophenyl)-2-methylene-3-oxobutyl)carbamate ( <b>NBoc-MBH-1</b> ) .....                                 | A-98  |
| <i>tert</i> -butyl (2-methylene-3-oxo-1-(pyridin-3-yl)butyl)carbamate ( <b>NBoc-MBH-2</b> ) .....                                   | A-102 |
| <i>tert</i> -butyl (1-(5-bromopyridin-2-yl)-2-methylene-3-oxobutyl)carbamate ( <b>NBoc-MBH-3</b> ) .....                            | A-106 |
| <i>N</i> -(1-(2-(3,3-dimethylbut-1-yn-1-yl)pyrimidin-5-yl)-2-methylene-3-oxobutyl)-4-methylbenzenesulfonamide ( <b>5.48</b> ) ..... | A-110 |
| 1-(2-(3,3-dimethylbut-1-yn-1-yl)pyrimidin-5-yl)-2-methylpropan-1-ol ( <b>5.2</b> ) .....  | A-114 |

### A.1.1 Catalyst TF-1



**<sup>1</sup>H NMR** (600 MHz, CD<sub>2</sub>Cl<sub>2</sub>, δ): 3.51 (s, 1H, NH), 3.76-3.79 (dd, 1H, H17), 4.01-4.04 (dd, 1H, H-17') 6.65 (d, *J* = 8.2 Hz, 1H, H-11), 6.76-6.79 (m, 2H, H-13, H-8'), 6.88 (d, *J* = 7.7 Hz, H-14), 7.02-7.06 (m, 2H, H-(*R*)1/5), 7.07-7.11 (m, 2H, H-12, H-7'), 7.17-7.23 (m, 3H, H-8, H-(*R*)2/B4), 7.23-7.27 (m, 5H, H-3', H-(*S*)1/5, H6', H-(*R*)3), 7.32-7.37 (m, 3H, H-7, H-(*S*)2/A4), 7.37-7.40 (m, 1H, H-(*S*)3), 7.40-7.43 (dd, 1H, H-3), 7.52-7.56 (m, 1H, H-6), 7.80-7.83 (d, 1H, H-5') 7.89-7.92 (d, 1H, H-4') 7.92-7.97 (m, 2H, H-4, H-5), 8.03 (b, 1H, OH).

**<sup>13</sup>C NMR** (100 MHz, CD<sub>2</sub>Cl<sub>2</sub>, δ): 45.5 (C-17), 115.5 (C-3'), 116.6 (C-11), 120.0 (C-13), 120.6 (C-13), 120.5-120.6 (d, *J*=8.41 Hz C-1') 120.4 (C15, C6'-), 125.0 (C-8'), 126.0 (C-8), 126.9 (C-7'), 127.5 (C-7), 127.6 (C-6), 128.2 (C-5'), 128.5-128.6 (C-5, C-14, C-(*S*)2/4, C-(*R*)3) 128.9 (C-9', C-12), 129.1 (d, C-4), 129.2 (C-(*R*)2/4), 129.3 (C-(*S*)3), 130.1 (C-4'), 130.6 (C-3), 133.2 (d, C-9), 133.5 (d, C-(*S*)1/5), 133.9 (C-10'), 134.3 (d, C-(*R*)1/5), 134.6 (C10), 137.2 (d, C-(*R*)6/(*S*)6), 137.4 (dd, C-2), 140.6 (d, C-1), 143.7 (C-2'), 157.0 (C-16).

A-3

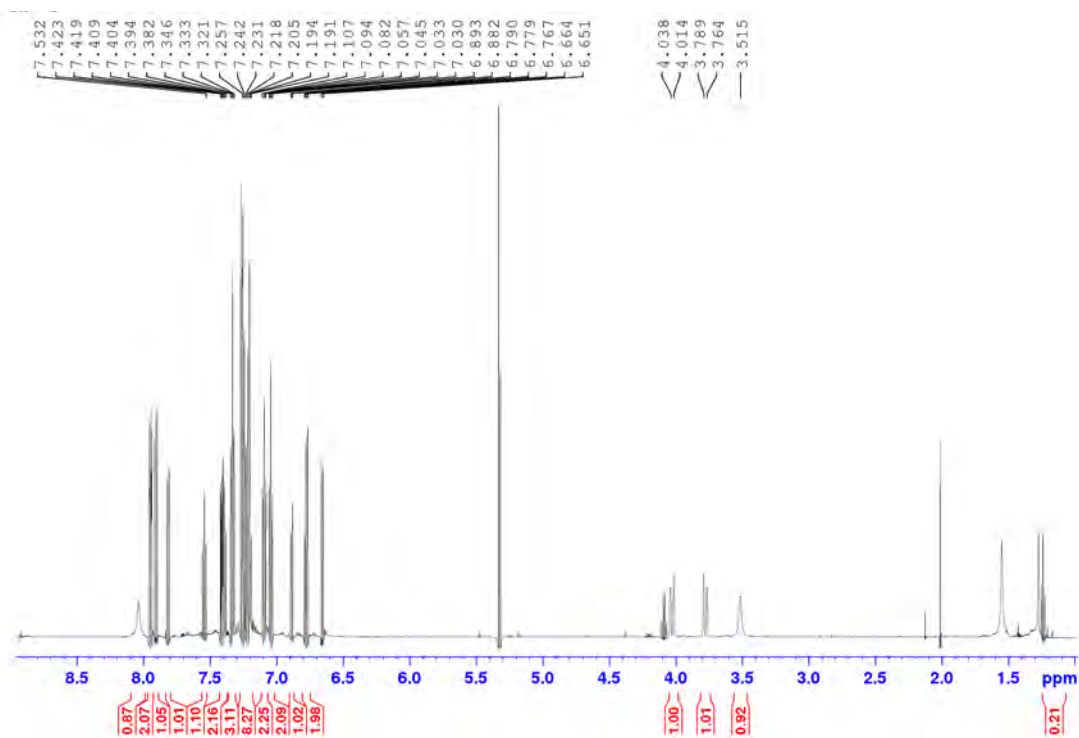


Figure A.2  $^1\text{H}$  NMR spectrum (600 MHz,  $\text{CD}_2\text{Cl}_2$ ) for TF-1.

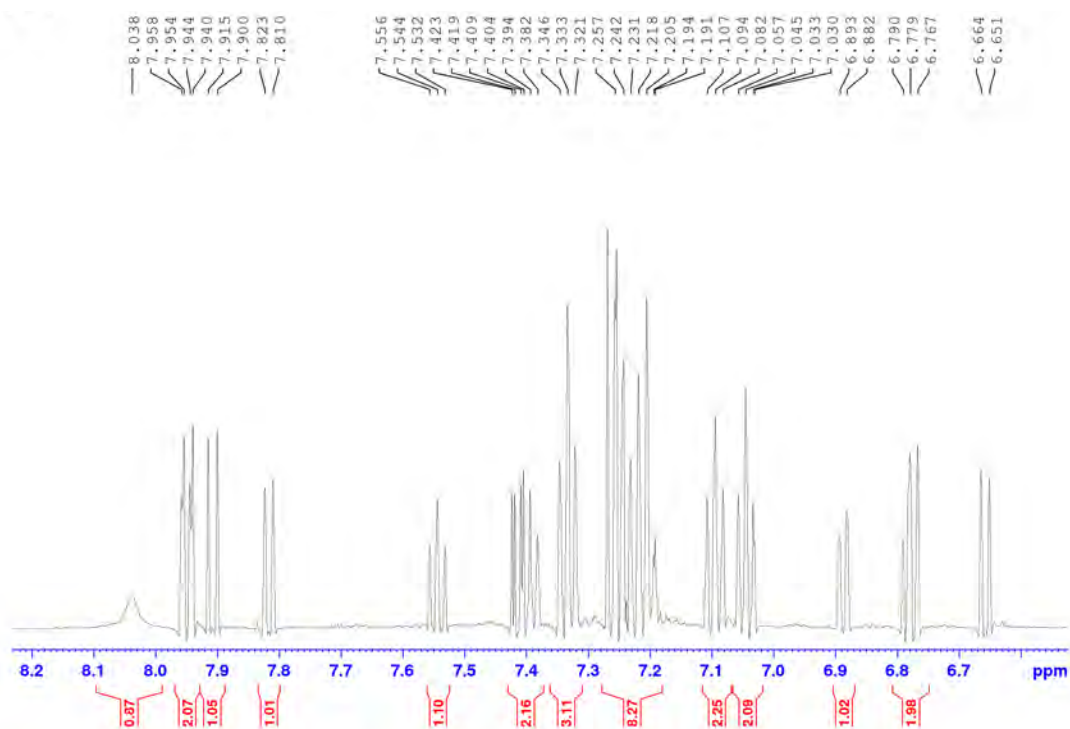
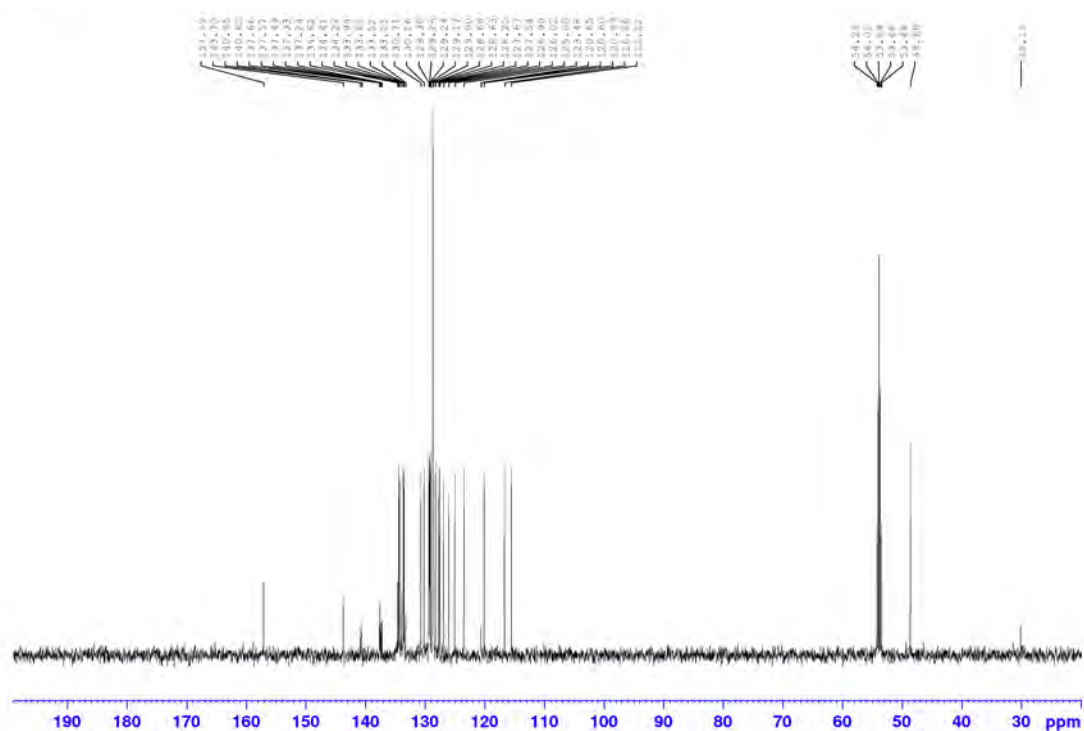
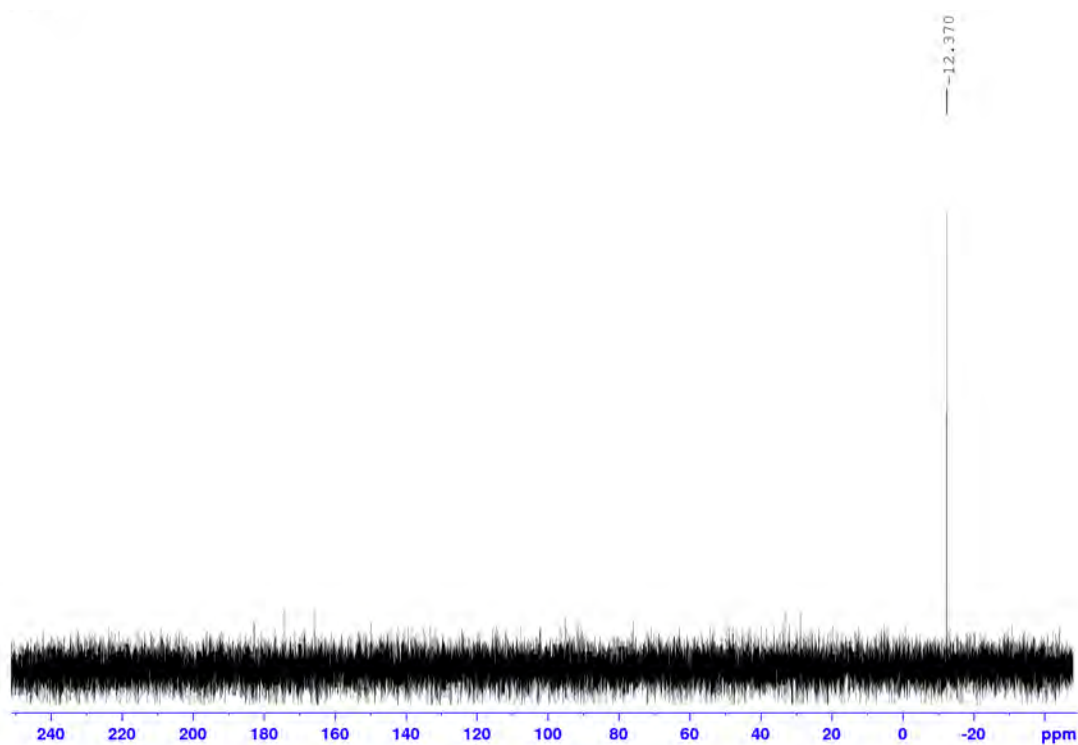
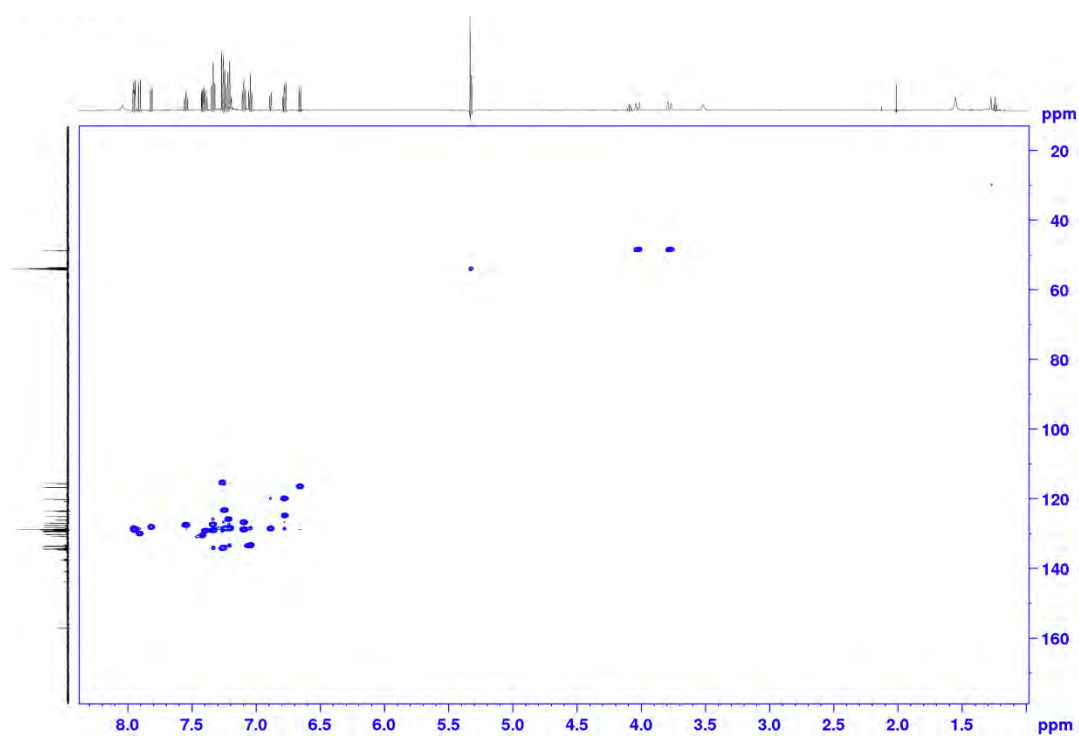


Figure A.3  $^1\text{H}$  NMR spectrum (600 MHz,  $\text{CD}_2\text{Cl}_2$ ) of the aromatic region for TF-1.

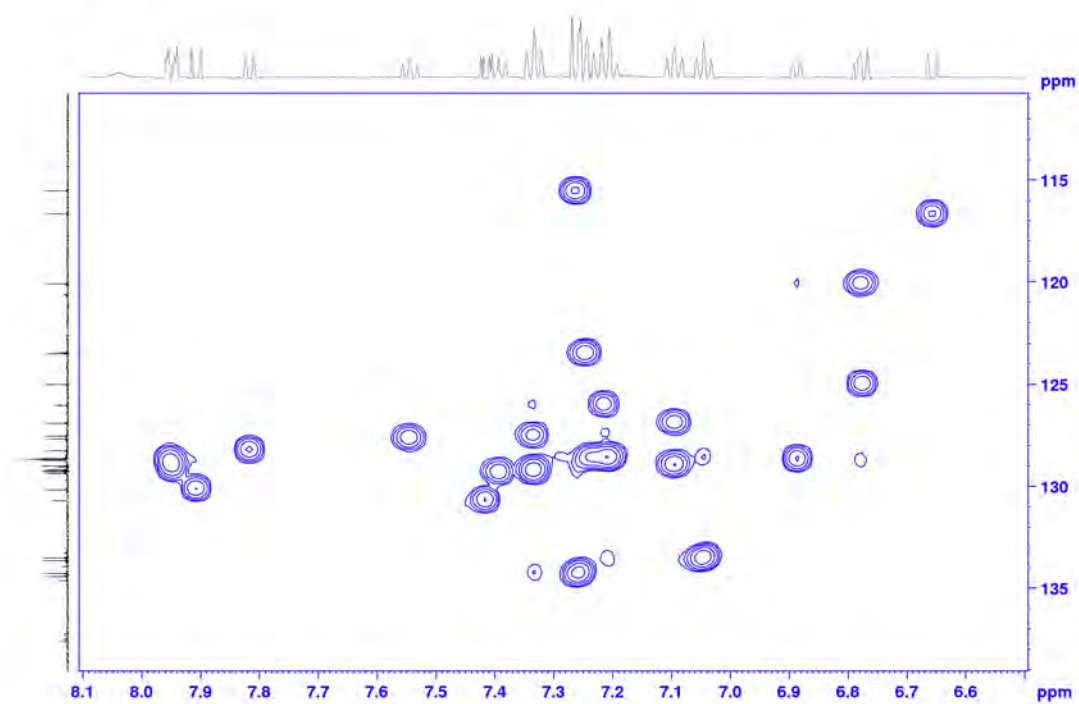




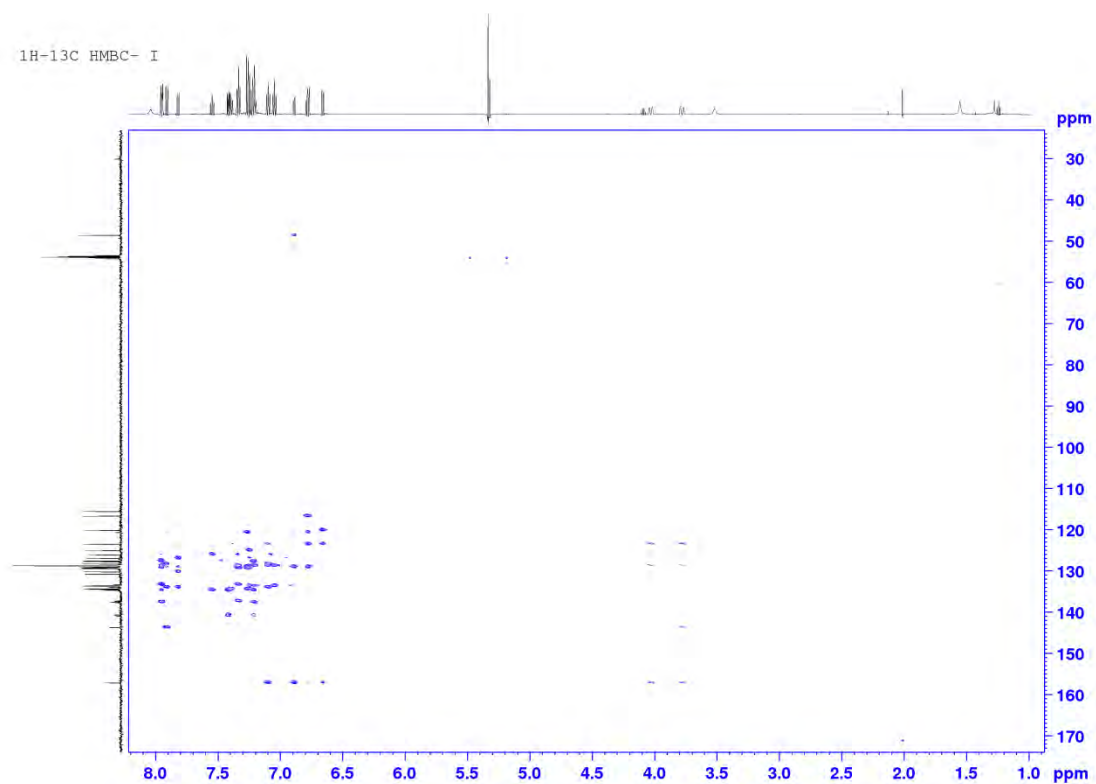
**Figure A.6**  $^{31}\text{P}$  NMR spectrum (167 MHz,  $\text{CD}_2\text{Cl}_2$ ) for **TF-1**.



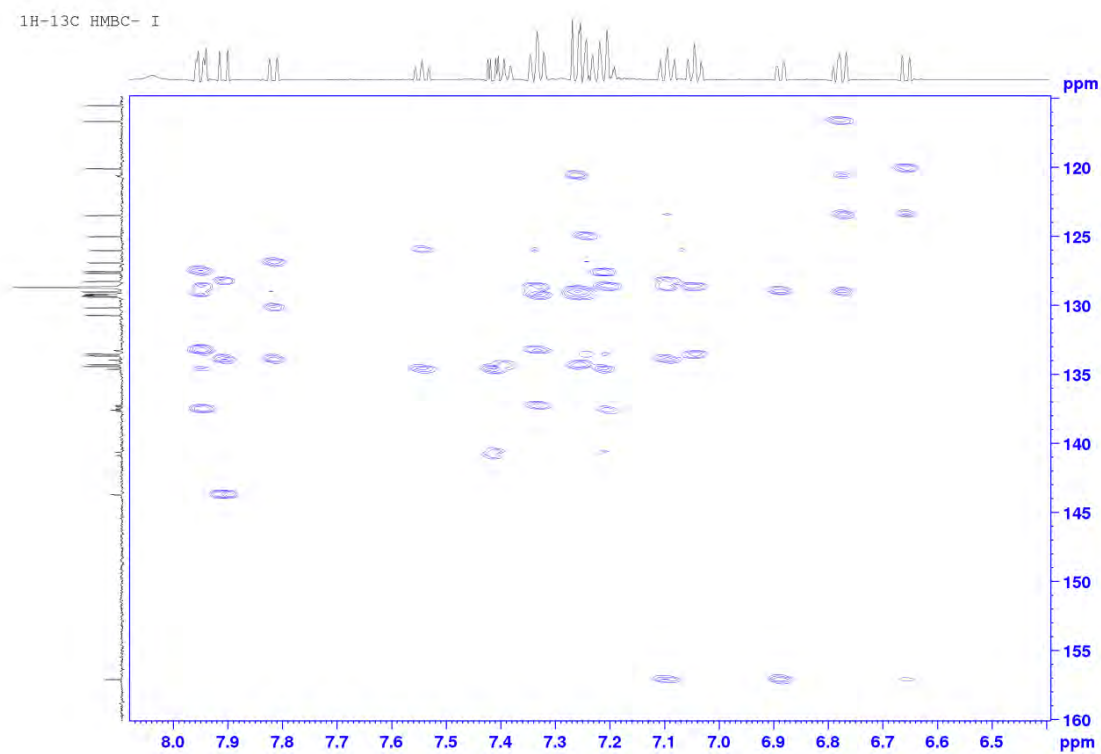
**Figure A.7**  $^1\text{H}$ – $^{13}\text{C}$  HSQC spectrum (600 MHz,  $\text{CD}_2\text{Cl}_2$ ) for **TF-1**.



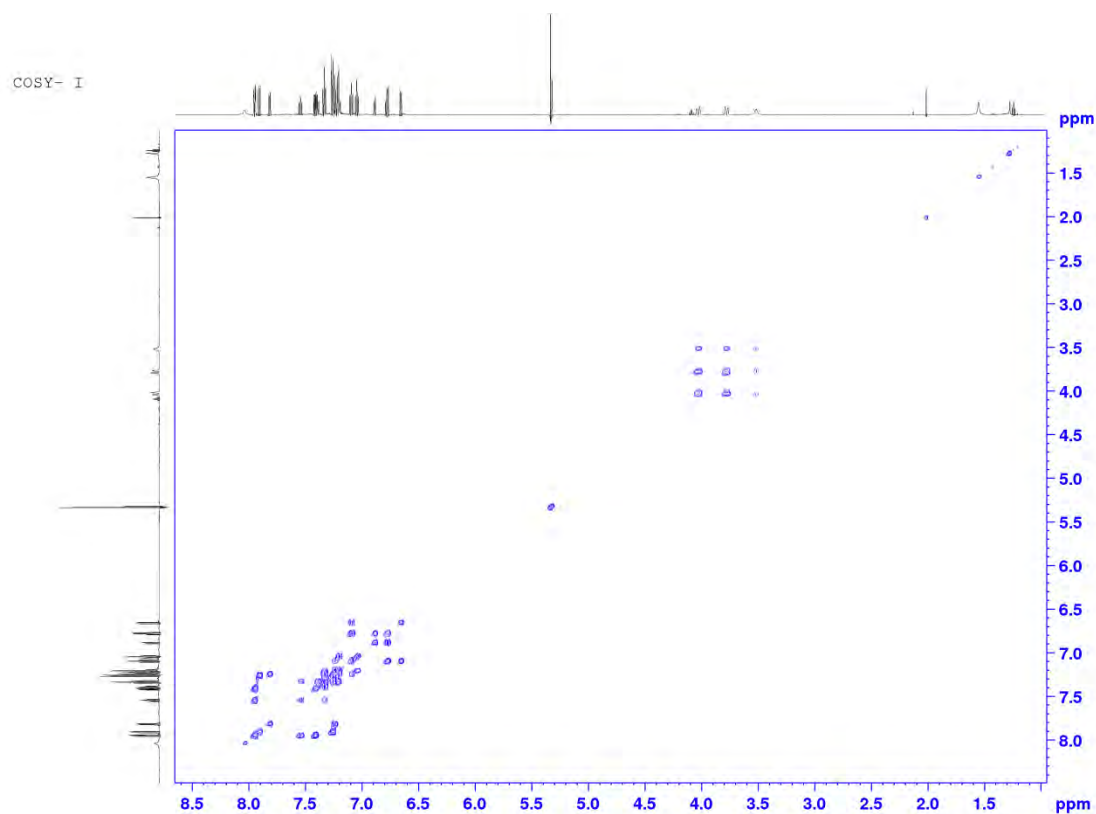
**Figure A.8**  $^1\text{H}$ – $^{13}\text{C}$  HSQC spectrum (600 MHz,  $\text{CD}_2\text{Cl}_2$ ) of the aromatic region for **TF-1**.



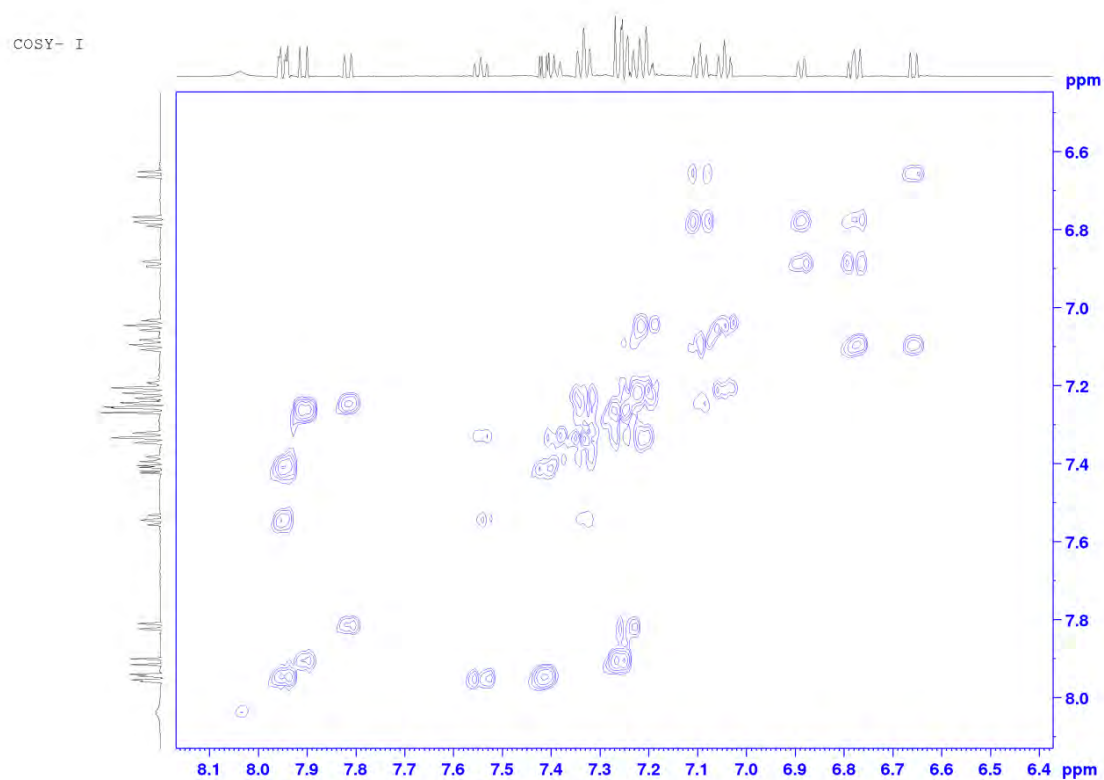
**Figure A.9**  $^1\text{H}$ – $^{13}\text{C}$  HMBC spectrum (600 MHz,  $\text{CD}_2\text{Cl}_2$ ) for **TF-1**.



**Figure A.10**  $^1\text{H}$ – $^{13}\text{C}$  HMBC spectrum (600 MHz,  $\text{CD}_2\text{Cl}_2$ ) of the aromatic region for **TF-1**.



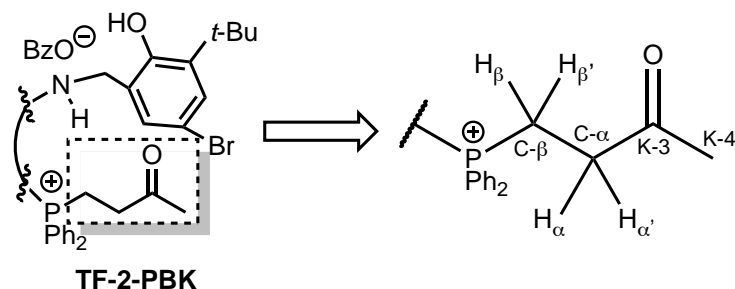
**Figure A.11**  $^1\text{H}$ – $^1\text{H}$  COSY spectrum (600 MHz,  $\text{CD}_2\text{Cl}_2$ ) for **TF-1**.



**Figure A.12**  $^1\text{H}$ – $^1\text{H}$  HSQC spectrum (600 MHz,  $\text{CD}_2\text{Cl}_2$ ) of the aromatic region for **TF-1**.



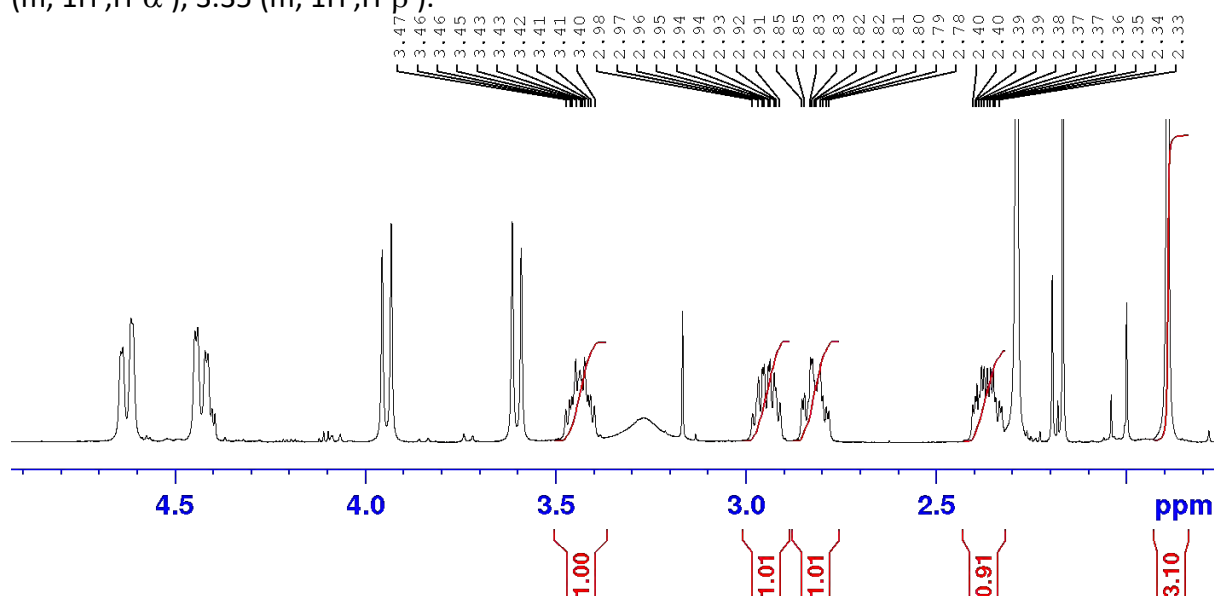
### A.1.2 Partial assignments for the phosphonium butanone for PBK



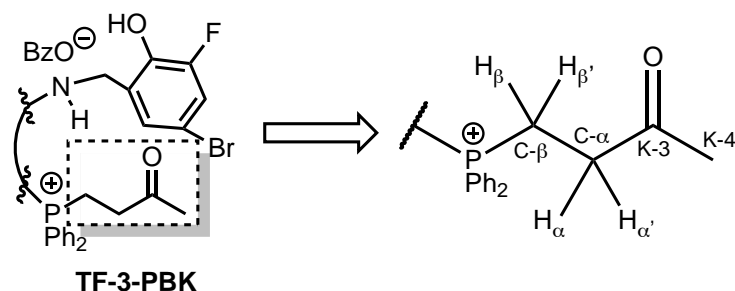
**Figure A.13** TF-2-PBK partial assignment map for the PBK

$^1\text{H}$  NMR (600 MHz,  $\text{CDCl}_3$ ,  $\delta$ ): 1.89 (s, 3H, H-Me), 2.34 (m, 1H, H- $\alpha$ ), 2.82 (m, 1H, H- $\beta$ ), 2.95 (m, 1H, H- $\alpha'$ ), 3.43 (m, 1H, H- $\beta'$ ).

$^1\text{H}$  NMR (600 MHz,  $\text{CD}_2\text{Cl}_2$ ,  $\delta$ ): 1.85 (s, 3H, H-Me), 2.36 (m, 1H, H- $\alpha$ ), 2.67 (m, 1H, H- $\beta$ ), 2.82 (m, 1H, H- $\alpha'$ ), 3.35 (m, 1H, H- $\beta'$ ).

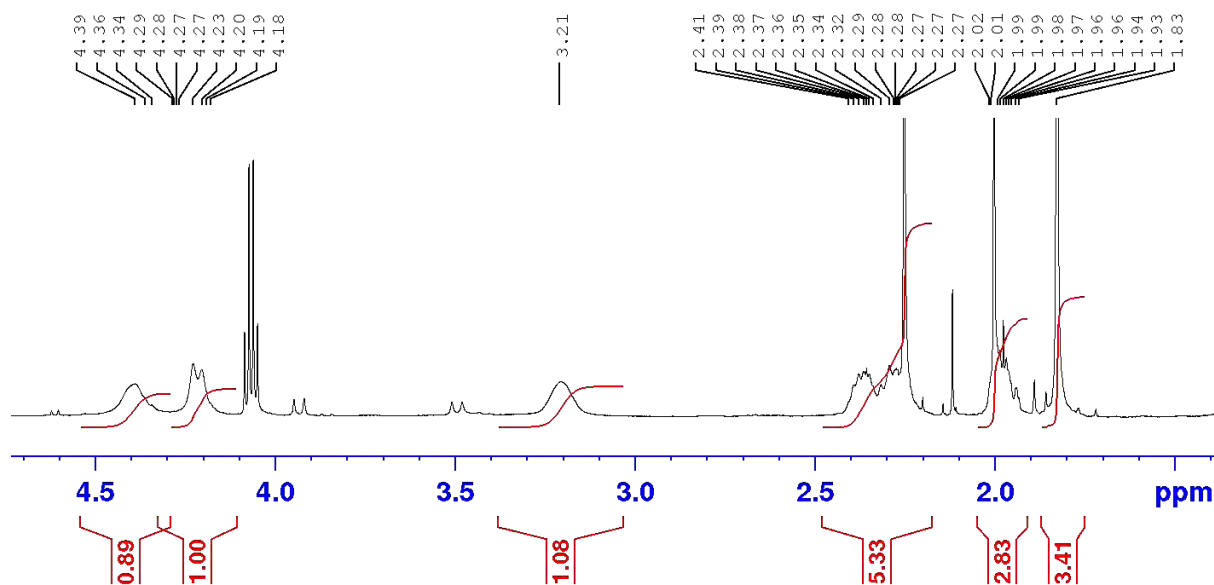


**Figure A.14**  $^1\text{H}$  NMR spectrum (600 MHz,  $\text{CD}_2\text{Cl}_2$ ) of phosphonium butanone for **TF-2-PBK**

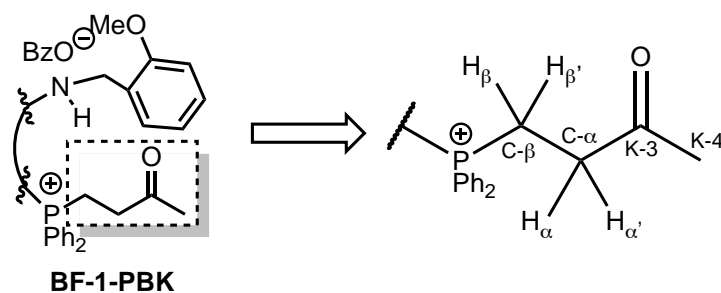


**Figure A.15** TF-3-PBK partial assignment map for the PBK

$^1\text{H}$  NMR (600 MHz,  $\text{CD}_2\text{Cl}_2$ ,  $\delta$ ): 1.82 (s, 3H, H-Me), 1.95 (m, 1H, H- $\alpha$ ), 2.28 (m, 1H, H- $\beta$ ), 2.38 (m, 1H, H- $\alpha'$ ), 3.21 (m, 1H, H- $\beta'$ ).

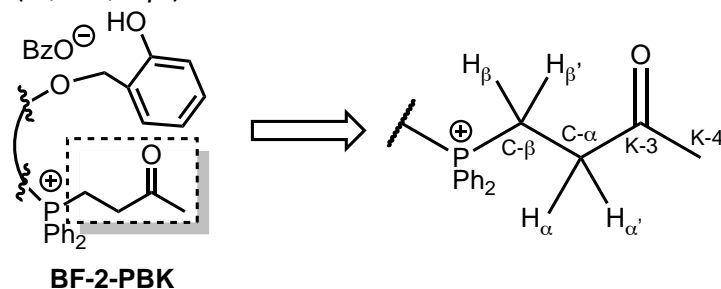


**Figure A.16**  $^1\text{H}$  NMR spectrum (600 MHz,  $\text{CD}_2\text{Cl}_2$ ) of phosphonium butanone for **TF-3-PBK**



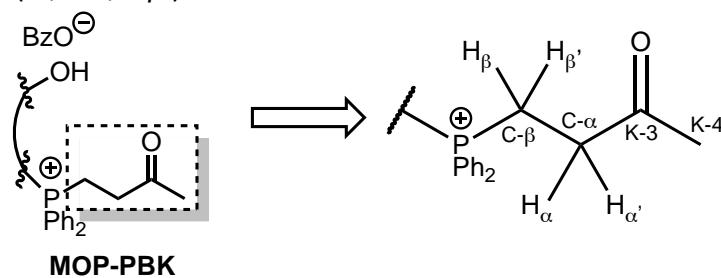
**Figure A.17** **BF-1-PBK** partial assignment map for the PBK

$^1\text{H}$  NMR (600 MHz,  $\text{CD}_2\text{Cl}_2$ ,  $\delta$ ): 1.90 (s, 3H, H-Me), 2.06 (m, 1H, H- $\alpha$ ), 2.45 (m, 1H, H- $\beta$ ), 2.63 (m, 1H, H- $\alpha'$ ), 3.16 (m, 1H, H- $\beta'$ ).



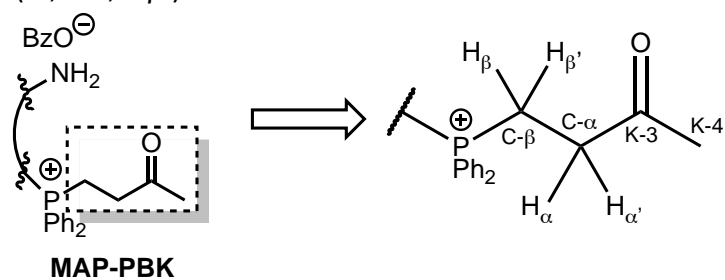
**Figure A.18** **BF-2-PBK** partial assignment map for the PBK

$^1\text{H}$  NMR (600 MHz,  $\text{CD}_2\text{Cl}_2$ ,  $\delta$ ): 1.89 (s, 3H, H-Me), 2.20 (m, 1H, H- $\alpha$ ), 2.63 (m, 1H, H- $\beta$ ), 2.96 (m, 1H, H- $\alpha'$ ), 3.52 (m, 1H, H- $\beta'$ ).



**Figure A.19** **MOP-PBK** partial assignment map for the PBK

**$^1\text{H}$  NMR** (600 MHz,  $\text{CD}_2\text{Cl}_2$ ,  $\delta$ ): 2.02 (s, 3H, H-Me), 2.49 (m, 1H, H- $\alpha$ ), 3.01 (m, 1H, H- $\beta$ ), 3.10 (m, 1H, H- $\alpha'$ ), 3.45 (m, 1H, H- $\beta'$ ).

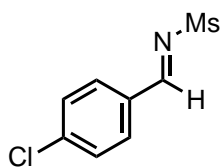


**Figure A.20** MAP-PBK partial assignment map for the PBK

**$^1\text{H}$  NMR** (600 MHz,  $\text{CD}_2\text{Cl}_2$ ,  $\delta$ ): 1.90 (s, 3H, H-Me), 2.38 (m, 1H, H- $\alpha$ ), 2.71 (m, 2H, H- $\beta$ , H- $\alpha'$ ), 3.26 (m, 1H, H- $\beta'$ ).

## A.2 <sup>1</sup>H NMR, <sup>13</sup>C NMR and Chiral HPLC Traces for substrates in Chapter 3, 4 and 5.

---



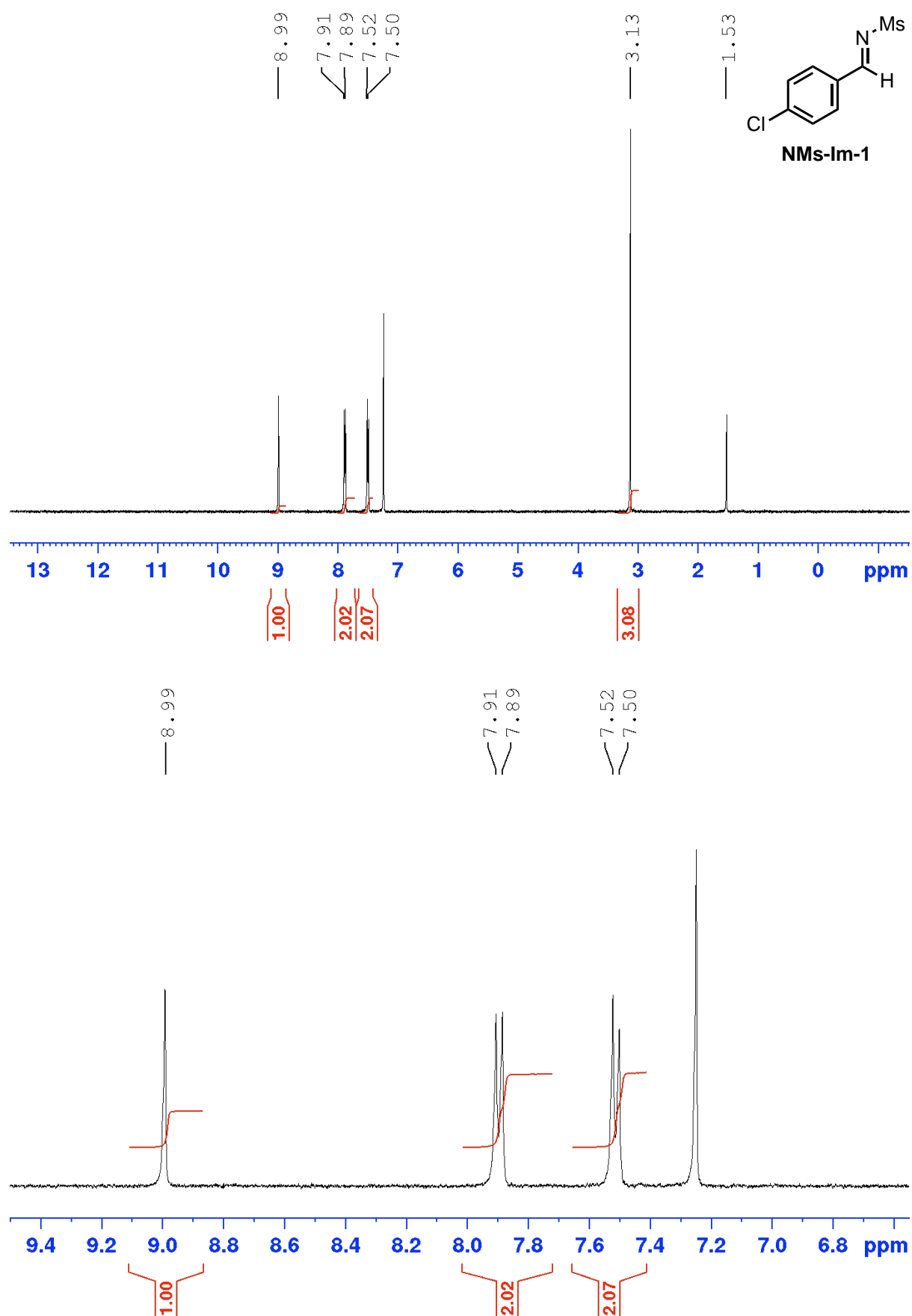
**NMs-lm-1**

***(E)-N-(4-chlorobenzylidene)methanesulfonamide (NMs-lm-1)***

**<sup>1</sup>H NMR** (400 MHz, CDCl<sub>3</sub>, δ): 8.99 (s, 1H), 7.89 (d, *J* = 8.4 Hz, 2H), 7.51 (d, *J* = 8.4 Hz), 3.13 (s, 3H)

**<sup>13</sup>C NMR** (100 MHz, CDCl<sub>3</sub>, δ): 170.4, 141.9, 132.5, 130.7, 129.9, 40.4.

**MS (ESI)**: 279.1 [M+IsoProp+H]



**Figure A.21**  $^1\text{H}$  NMR spectrum (400 MHz,  $\text{CDCl}_3$ ) for **NMs-Im-1**.

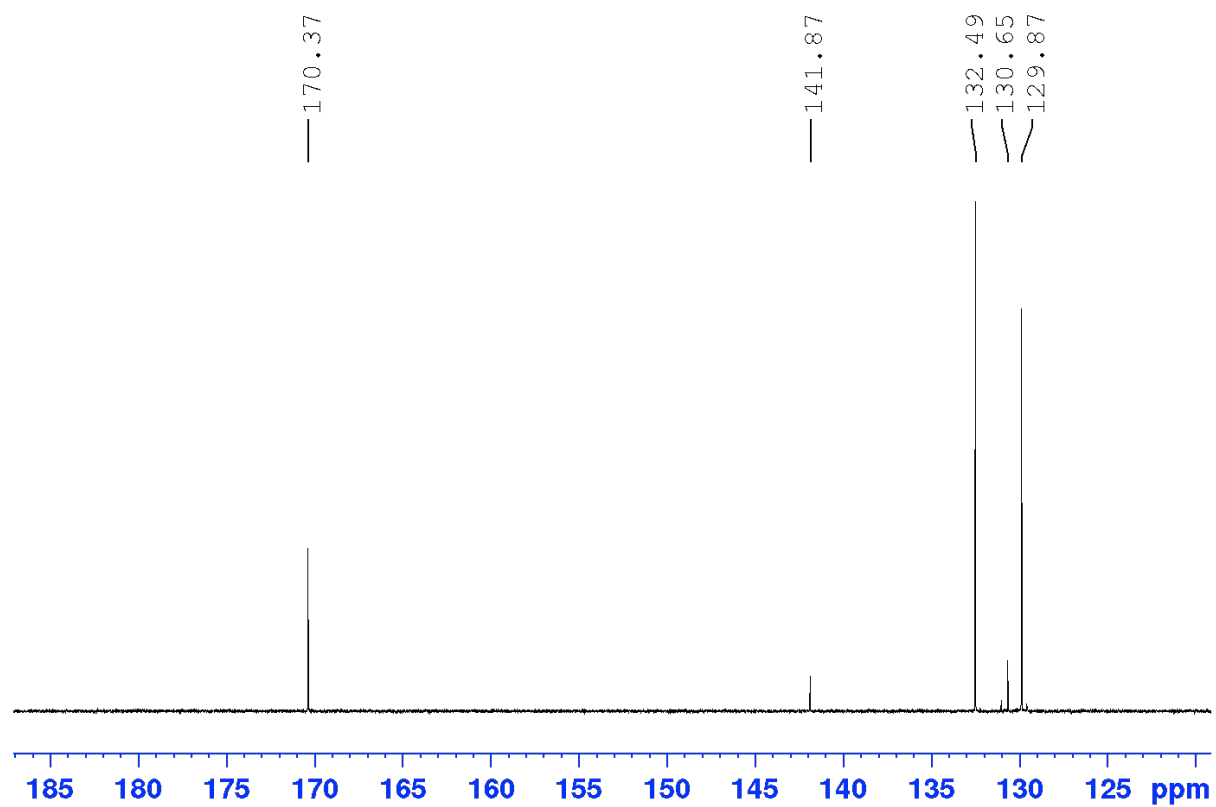
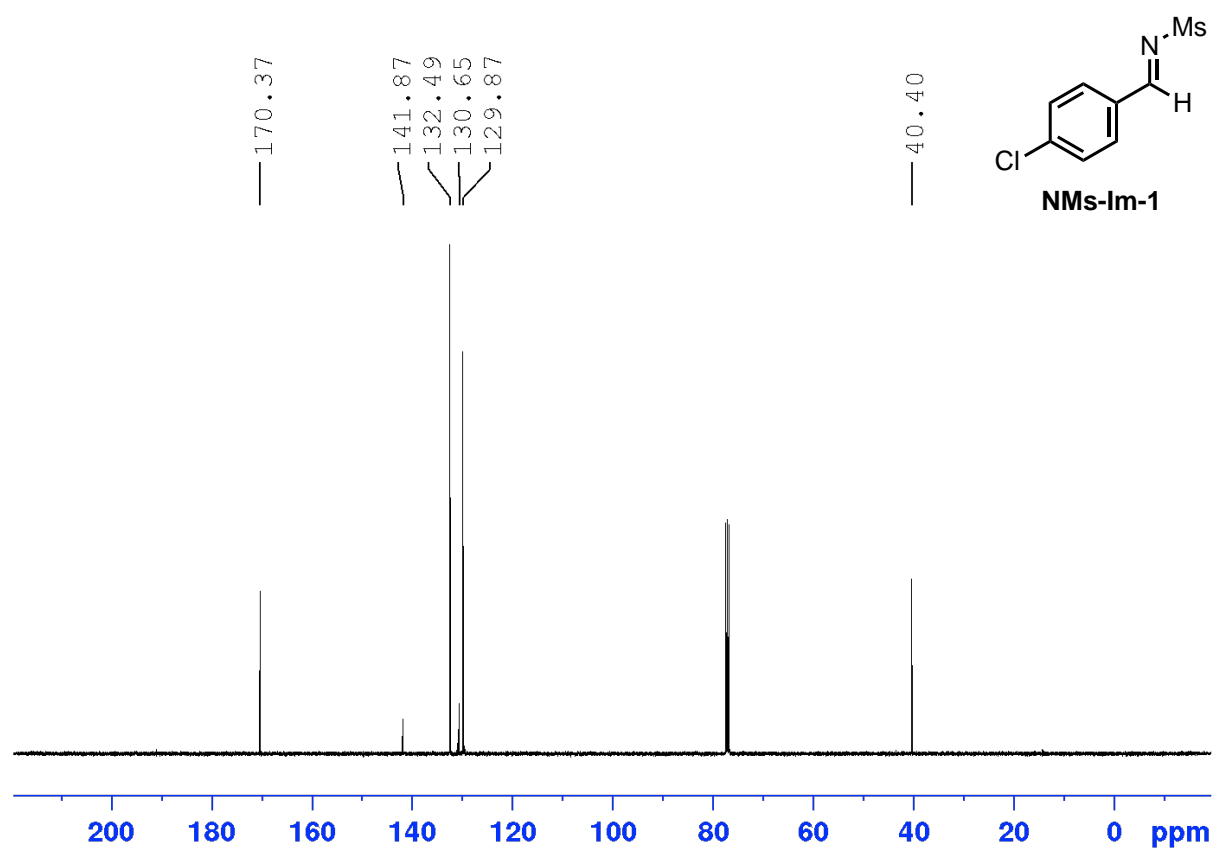
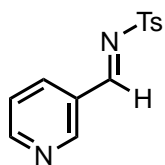


Figure A.22. <sup>13</sup>C NMR spectrum (100 MHz, CDCl<sub>3</sub>) for NMs-Im-1.



**NTsPyr-lm-1**

***(E)-4-methyl-N-(pyridin-3-ylmethylene)benzenesulfonamide (NTsPyr-lm1)***

**<sup>1</sup>H NMR** (400 MHz, CDCl<sub>3</sub>, δ): 9.09 (s, 1H), 9.05 (s, 1H), 8.81 (d, *J* = 4.9 Hz, 1H), 8.27 (d, *J* = 4.9 Hz, 1H), 7.89 (d, *J* = 4.9 Hz, 2H), 7.44 (dd, *J* = 7.9, 4.9 Hz, 2H), 7.37 (d, *J* = 8.0 Hz, 2H), 2.45 (s, 3H).

**<sup>13</sup>C NMR** (100 MHz, CDCl<sub>3</sub>, δ): 167.7, 155.2, 153.1, 145.2, 137.0, 134.6, 130.1, 128.4, 124.2, 21.82.

**MS (ESI):** 261.1 [M+H]

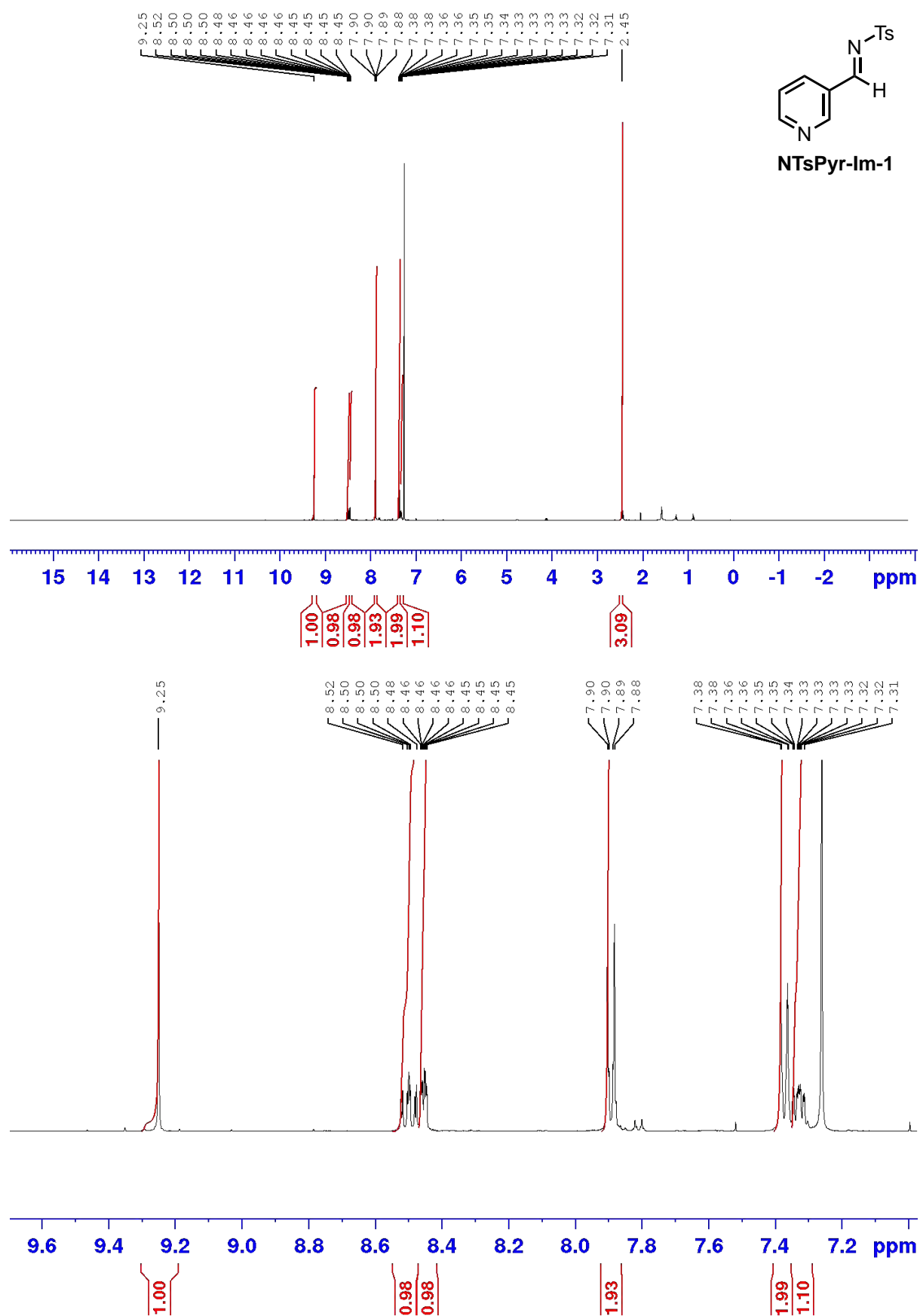


Figure A.23 <sup>1</sup>H NMR spectrum (400 MHz, CDCl<sub>3</sub>) for NTsPyr-Im1.



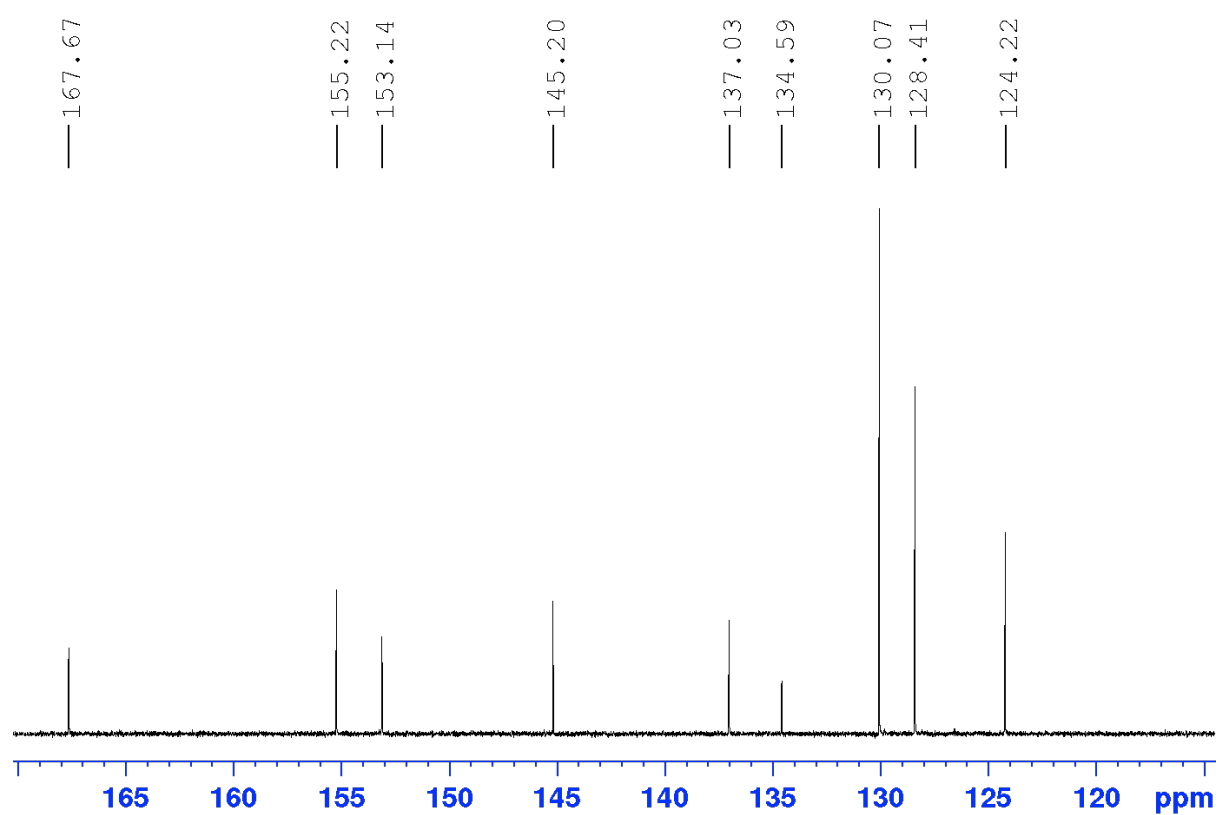
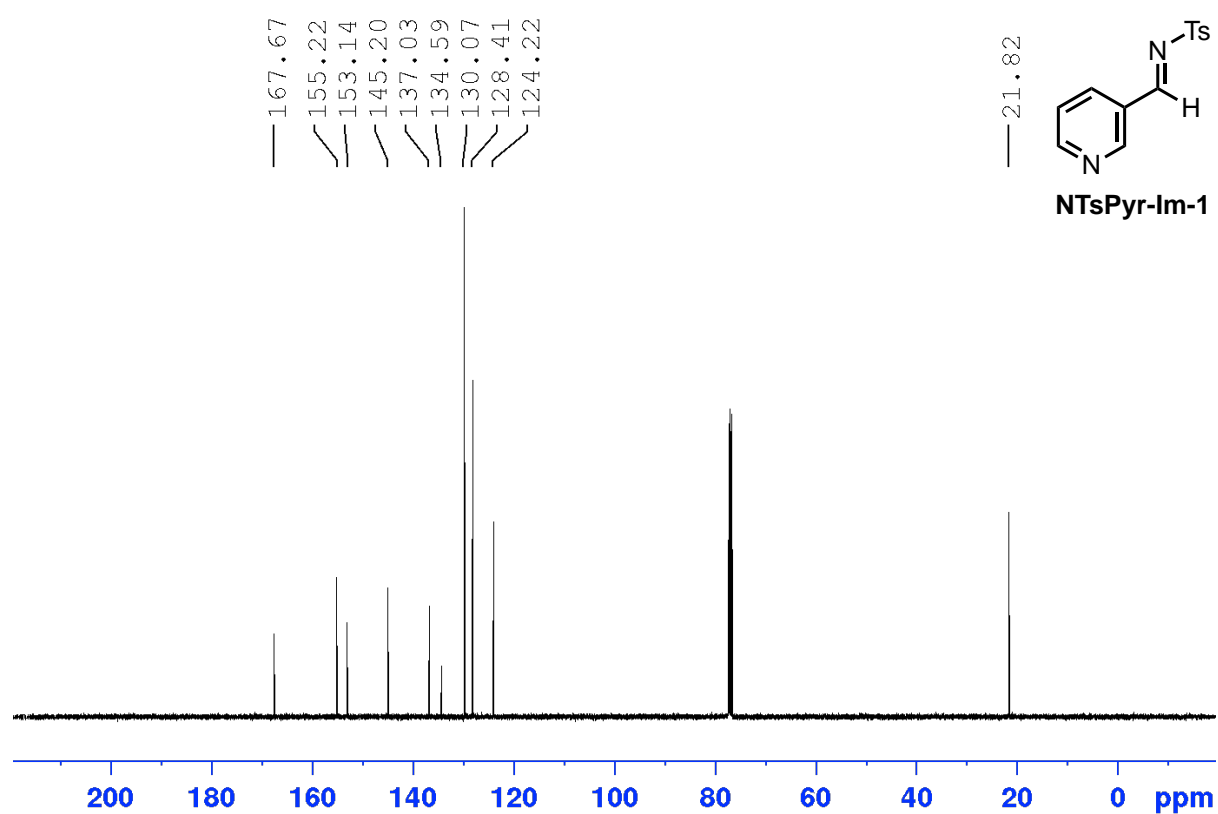
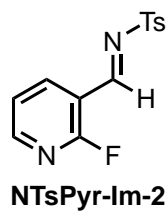


Figure A.24  $^{13}\text{C}$  NMR spectrum (100 MHz,  $\text{CDCl}_3$ ) for NTsPyr-lm1.



***(E)-N-((2-fluoropyridin-3-yl)methylene)-4-methylbenzenesulfonamide (NTsPyr-lm2)***

**<sup>1</sup>H NMR** (400 MHz, CDCl<sub>3</sub>, δ): 9.25 (s, 1H), 8.50 (ddd, *J*= 9.1, 7.4, 1.9 Hz, 1H), 8.45 (ddd, *J*= 4.8, 2.1, 0.9 Hz, 1H), 7.89 (d, *J*= 8.3 Hz, 2H), 7.37 (d, *J*= 8.3 Hz, 2H), 7.33 (m, 1H).

**<sup>13</sup>C NMR** (100 MHz, CDCl<sub>3</sub>, δ): 163.8 (d, 248.6 Hz), 162.6 (d, 1.2 Hz), 154.1, 153.9, 140.3 (2.1 Hz), 134.2, 130.1, 128.6, 126.6, 122.5 (d, 4.4 Hz), 115.8, 115.3, 21.9

**MS (ESI):** 279 [M+H]

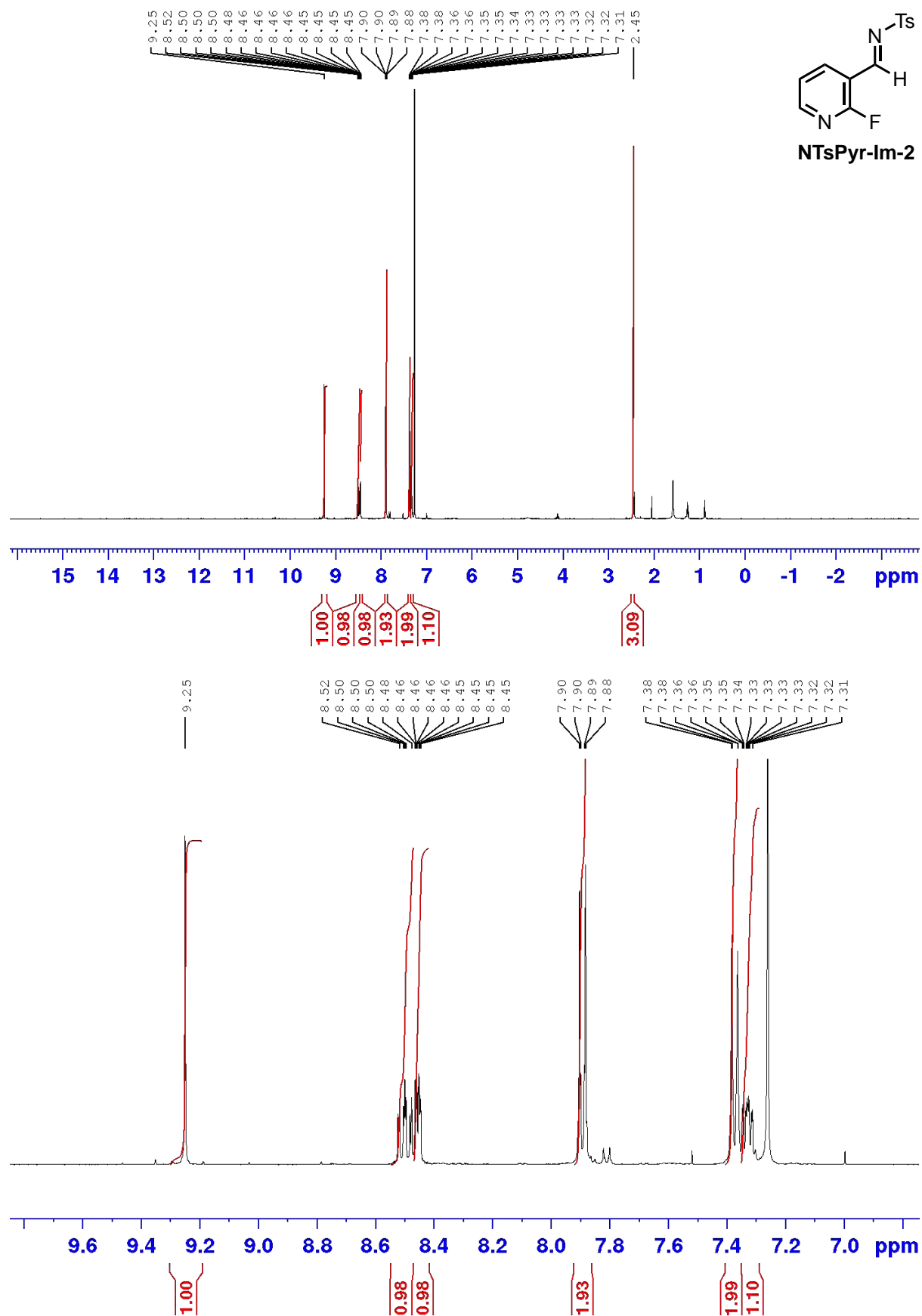


Figure A.25  $^1\text{H}$  NMR spectrum (400 MHz,  $\text{CDCl}_3$ ) for NTsPyr-Im2.

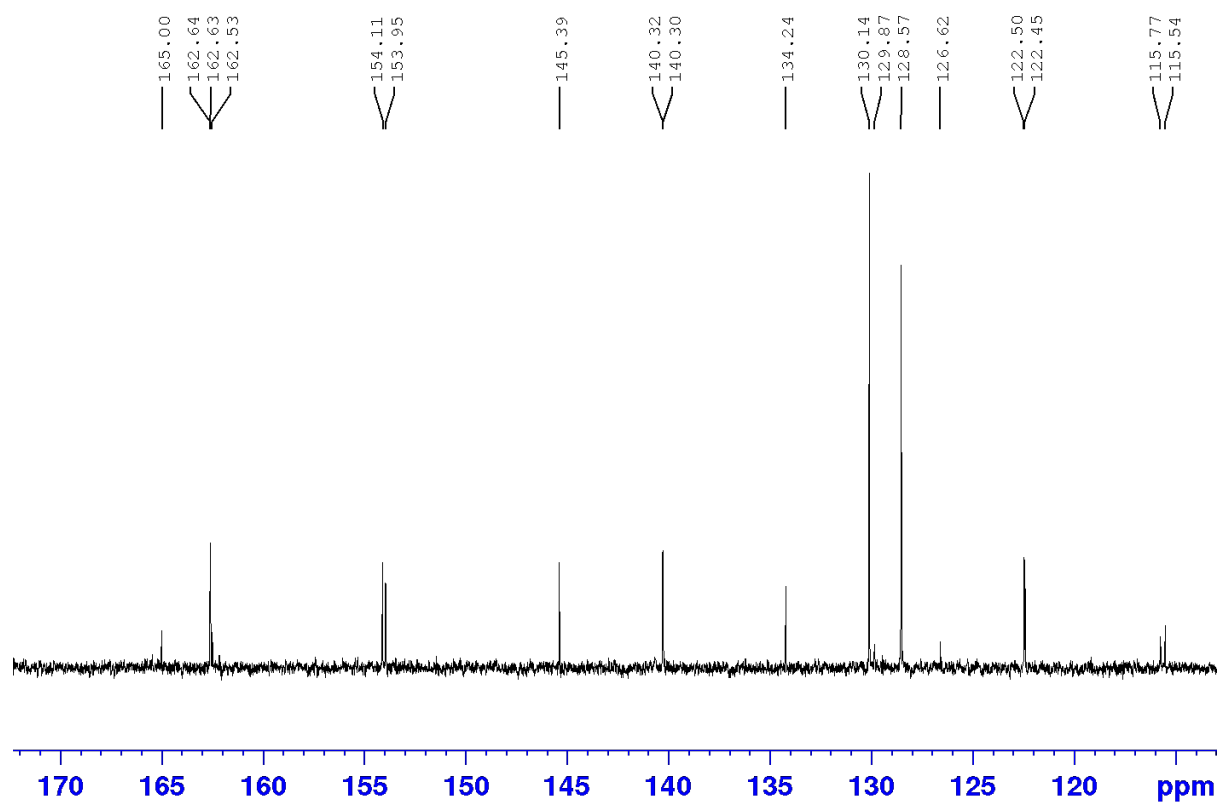
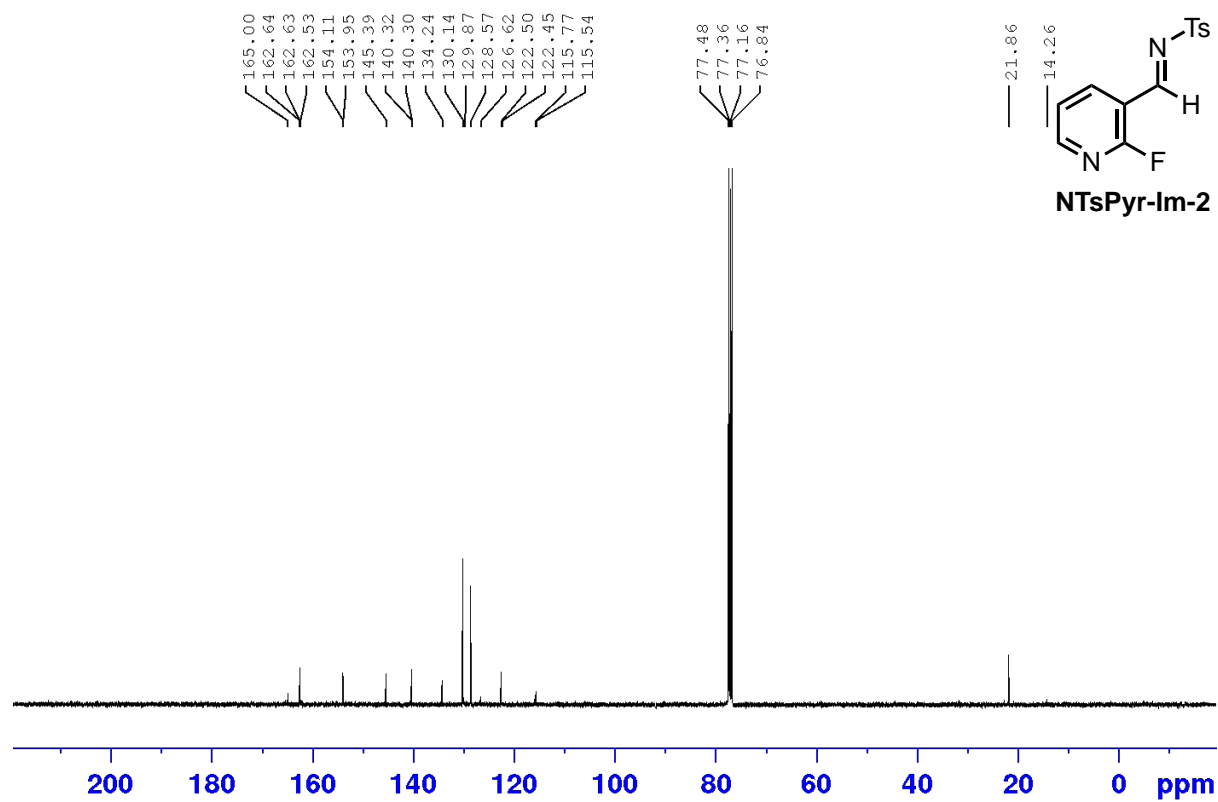
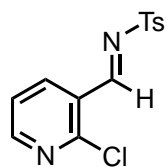


Figure A.26  $^{13}\text{C}$  NMR spectrum (100 MHz,  $\text{CDCl}_3$ ) for NTsPyr-Im2.



**NTsPyr-Im3**

**(E)-N-((2-chloropyridin-3-yl)methylene)-4-methylbenzenesulfonamide (NTsPyr-**

**Im3)**

**<sup>1</sup>H NMR** (400 MHz, CDCl<sub>3</sub>, δ): 9.41 (s, 1H), 8.58 (dd, *J* = 4.7, 1.9 Hz, 1H), 8.46 (dd, *J* = 7.8 Hz, 1.9 Hz, 1H), 7.90 (d, *J* = 8.3 Hz, 2H), 7.37 (m, 3H), 2.46 (s, 3H)

**<sup>13</sup>C NMR** (100 MHz, CDCl<sub>3</sub>, δ): 165.90, 154.7, 154.6, 145.4, 138.9, 134.1, 130.1, 128.6, 126.9, 123.2, 21.8

**MS (ESI):** 295 [M+H]

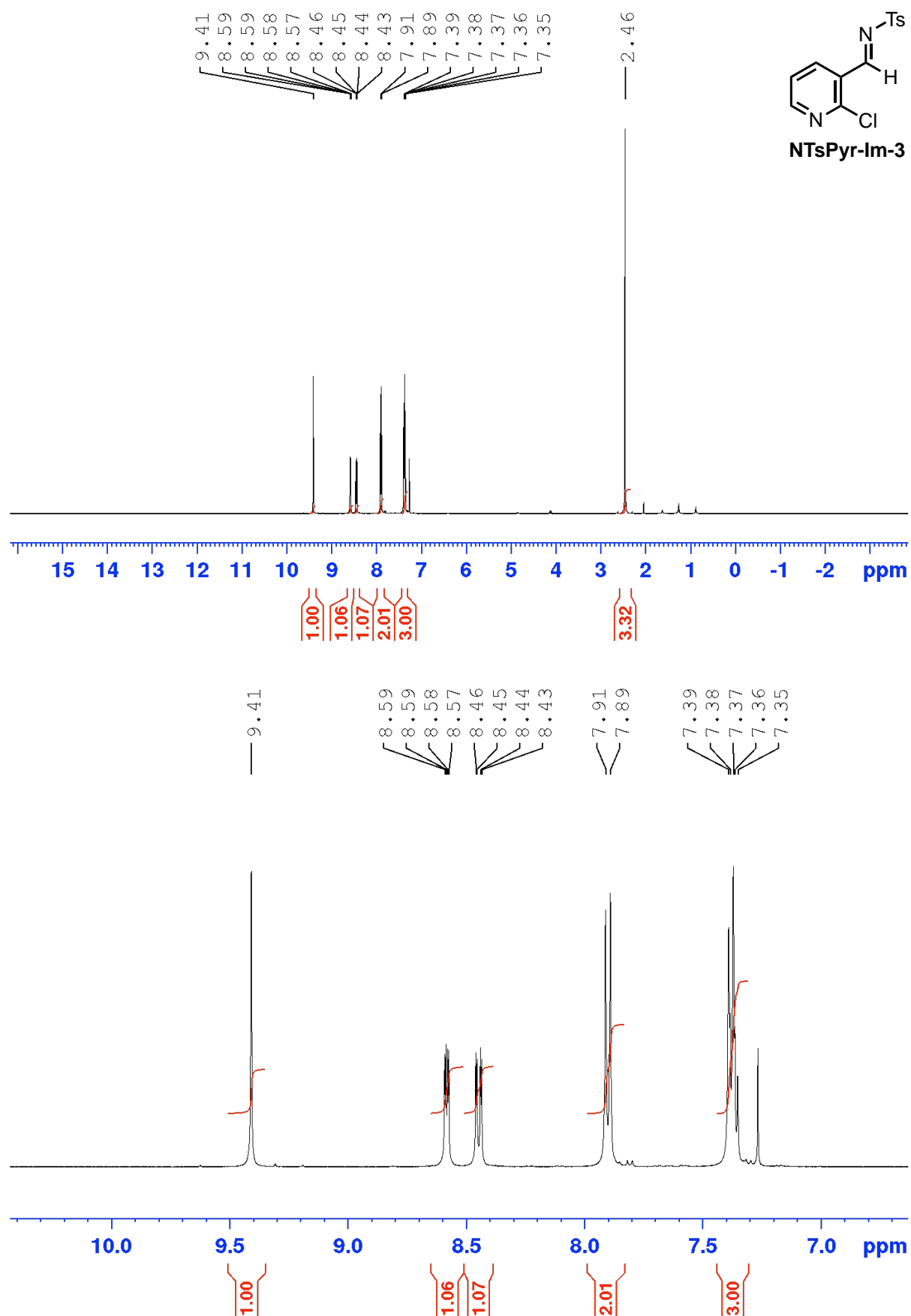


Figure A.27  $^1\text{H}$  NMR spectrum (400 MHz,  $\text{CDCl}_3$ ) for NTsPyr-Im3.

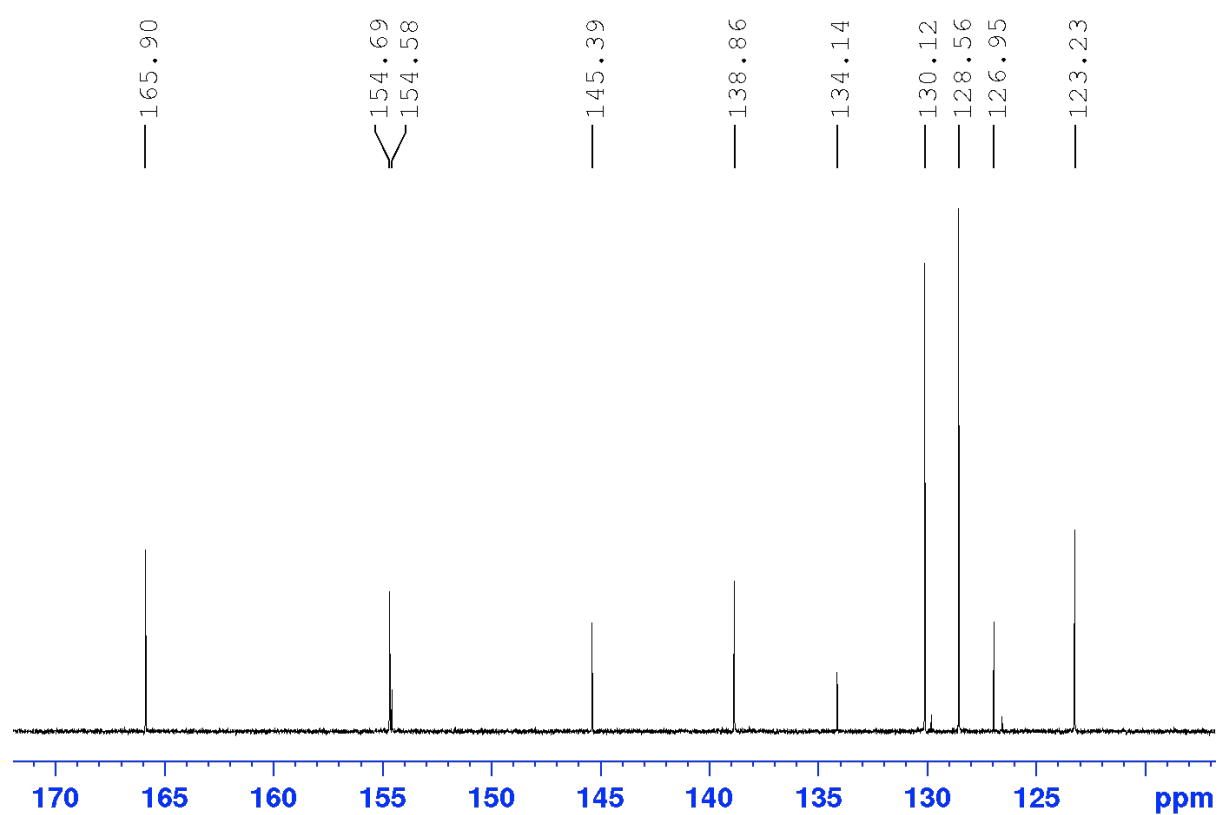
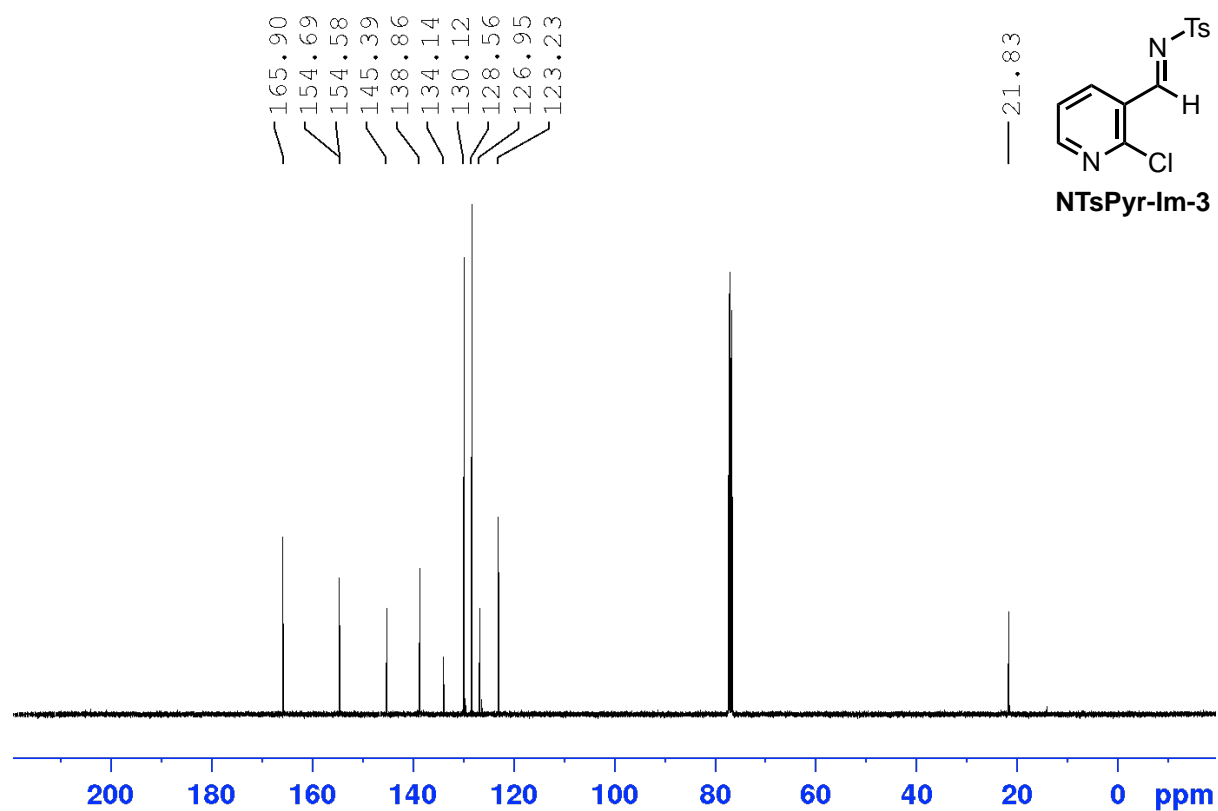
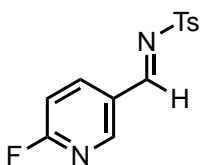


Figure A.28 <sup>13</sup>C NMR spectrum (100 MHz, CDCl<sub>3</sub>) for NTsPyr-lm3.



**NTsPyr-lm-4**

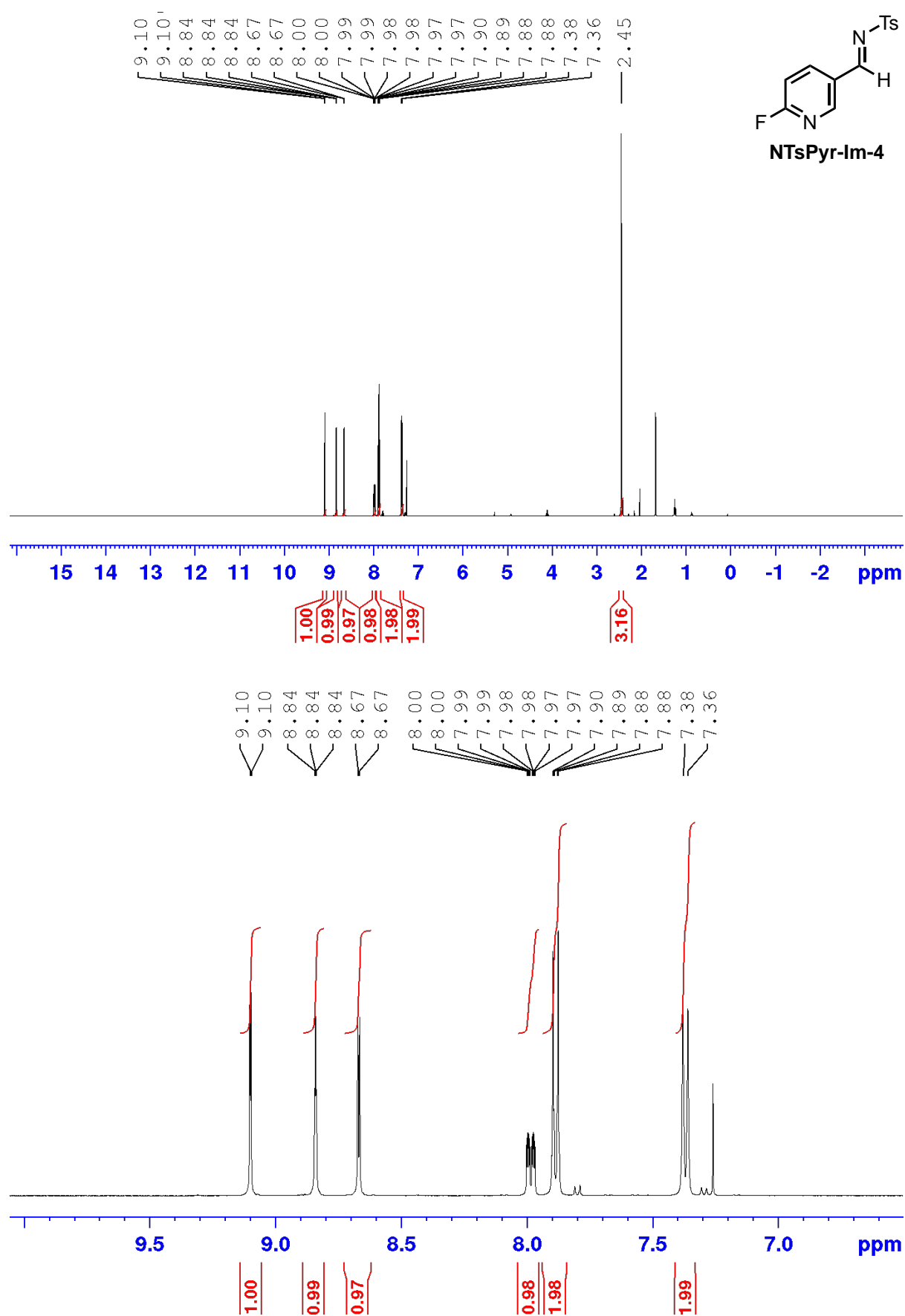
***(E)-N-((6-fluoropyridin-3-yl)methylene)-4-methylbenzenesulfonamide (NTsPyr-lm4)***

**<sup>1</sup>H NMR** (400 MHz, CDCl<sub>3</sub>, δ): 9.09 (d, *J* = 1.8 Hz, 1H), 8.84 (dd, *J* = 1.4 Hz, 1H), 8.67 (d, *J* = 2.8 Hz, 1H), 7.98 (ddd, *J* = 8.4 Hz, 2.8 Hz, 1.7 Hz, 1H), 7.89 (d, *J* = 8.4 Hz, 2H), 7.37 (d, *J* = 8.4 Hz, 2H), 2.45 (1H, s)

**<sup>13</sup>C NMR** (100 MHz, CDCl<sub>3</sub>, δ): 166.2 (d, *J* = 2.2 Hz), 159.5 (d, *J* = 260.5 Hz), 149.0 (d, *J* = 4.3 Hz), 145.5, 144.2, 143.9, 134.2, 130.1, 128.5, 122.3 (d, *J* = 19.1 Hz), 21.9

**MS (ESI):** 279 [M+H], 311 [M+CH<sub>3</sub>OH+H]





**Figure A.29**  $^1\text{H}$  NMR spectrum (400 MHz,  $\text{CDCl}_3$ ) for **NTsPyr-Im4**.

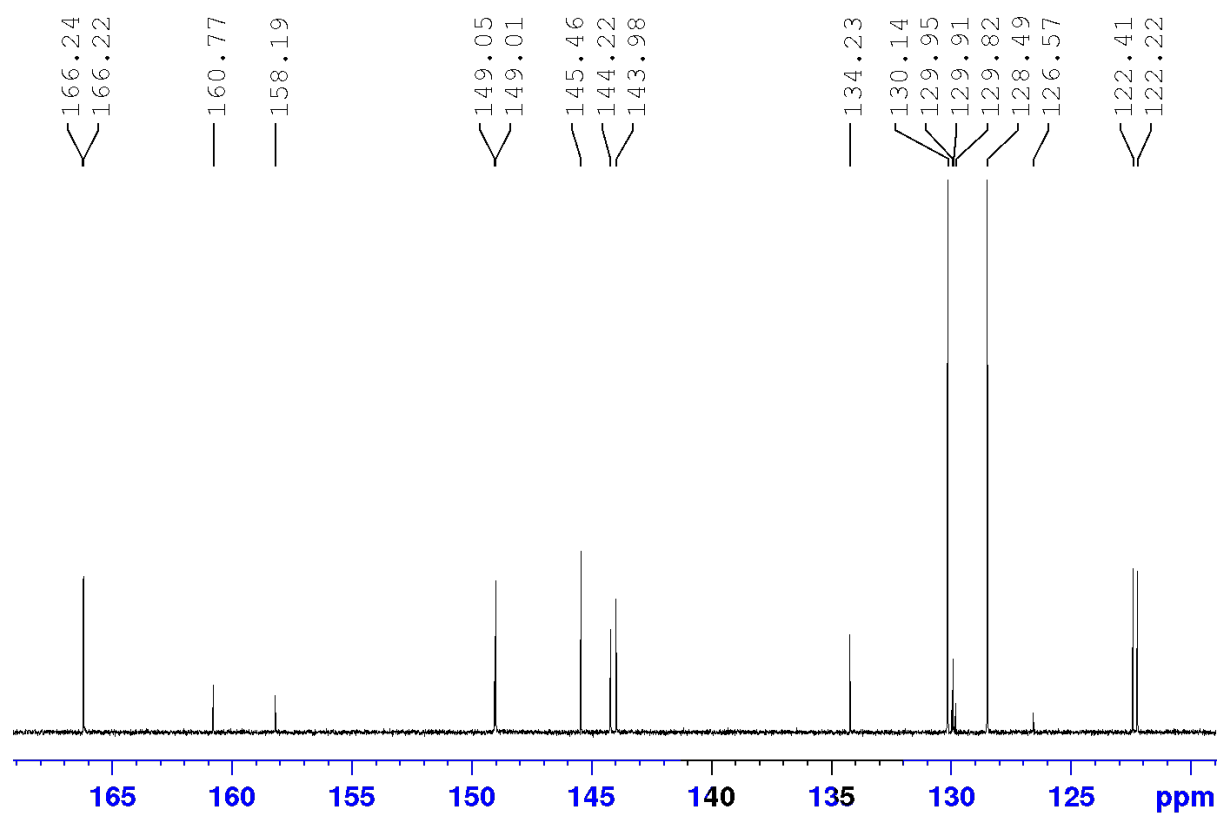
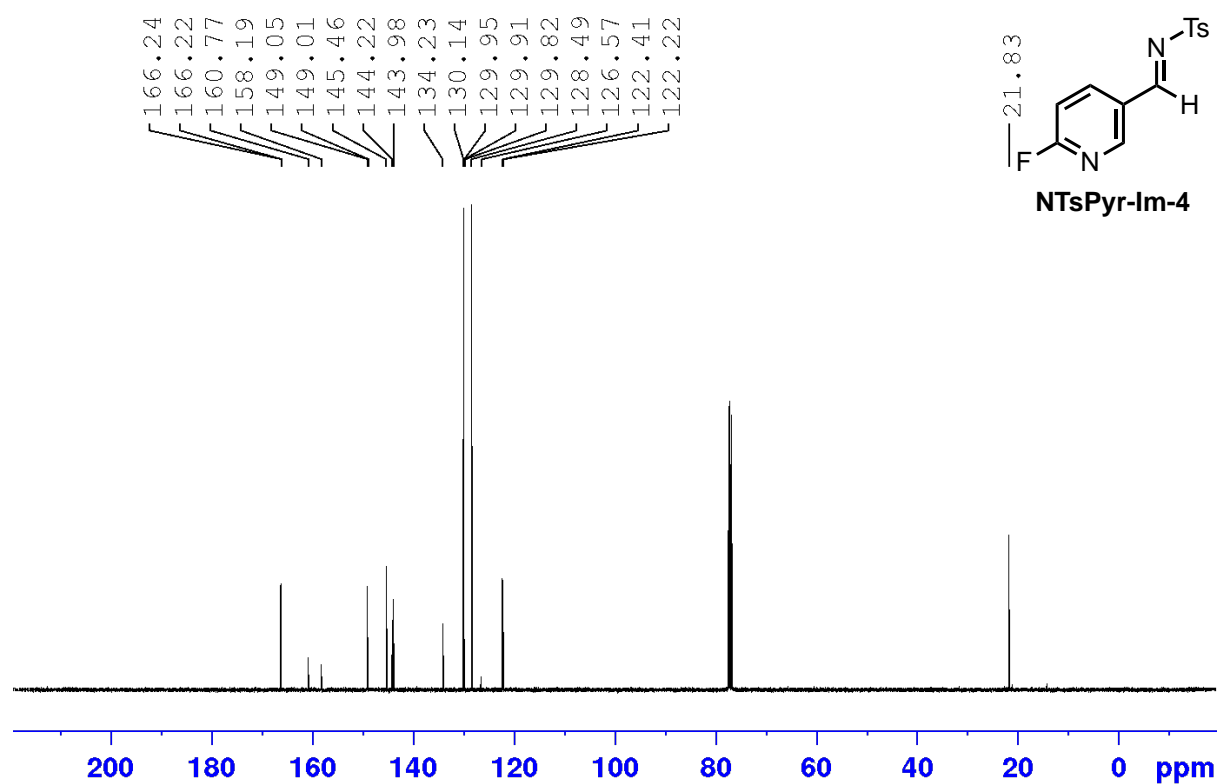
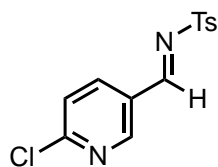


Figure A.30 <sup>13</sup>C NMR spectrum (100 MHz, CDCl<sub>3</sub>) for NTsPyr-Im4.



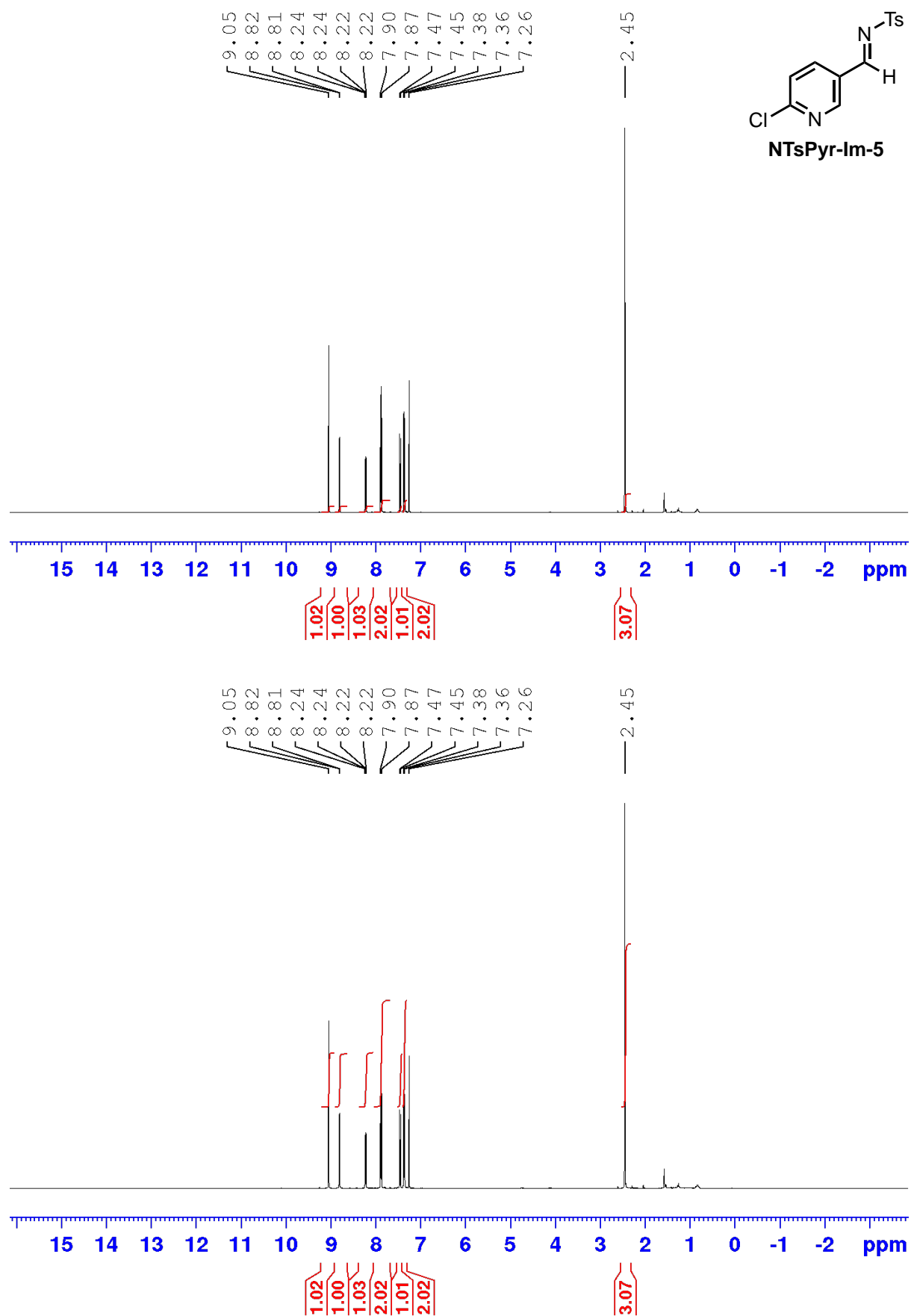
**NTsPyr-Im-5**

**(E)-N-((6-chlororopyridin-3-yl)methylene)-4-methylbenzenesulfonamide (NTsPyr-Im5)**

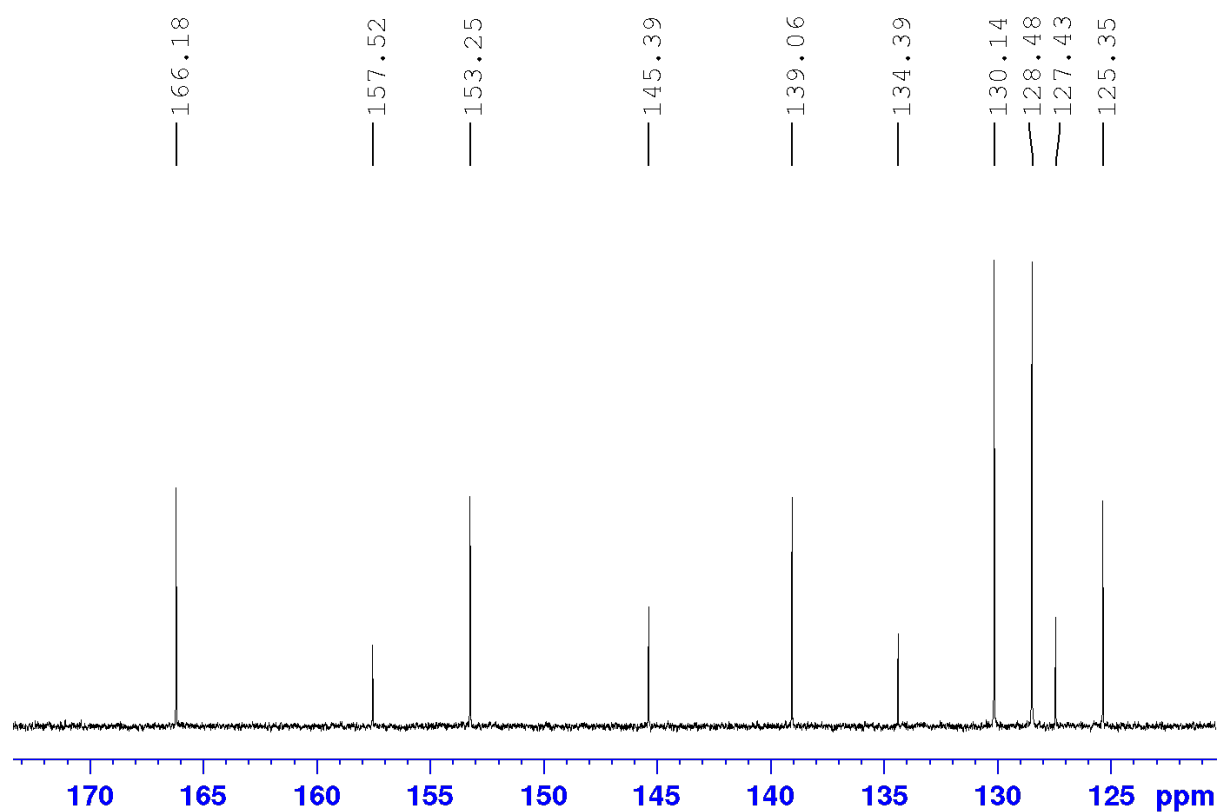
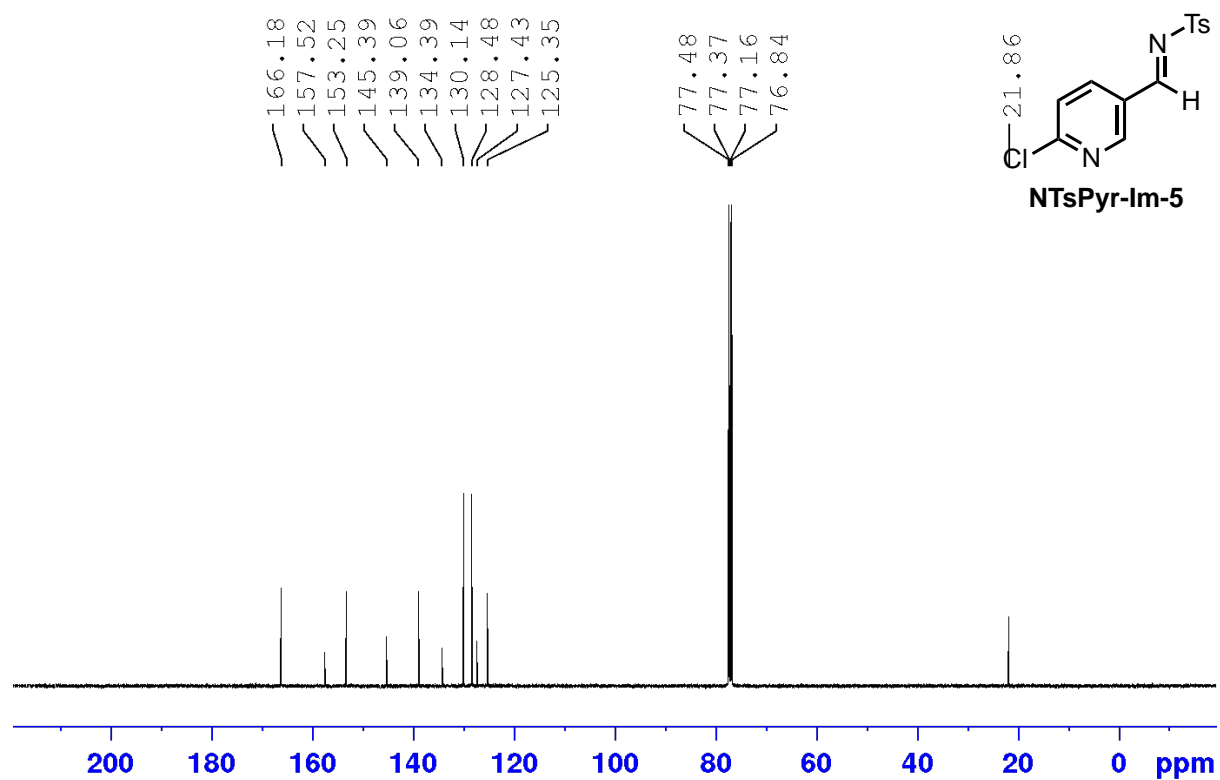
**<sup>1</sup>H NMR** (400 MHz, CDCl<sub>3</sub>, δ): 9.05 (s, 1H), 8.81 (d, *J* = 2.1 Hz, 1H), 8.22 (dd, *J* = 8.4, 2.4 Hz, 1H), 7.88 (d, *J* = 8.3 Hz, 2H), 7.46 (d, *J* = 8.4 Hz, 2H), 7.36 (d, *J* = 8.4 Hz, 2H), 2.45 (s, 3H).

**<sup>13</sup>C NMR** (100 MHz, CDCl<sub>3</sub>, δ): 166.2, 157.5, 153.2, 145.4, 139.1, 134.4, 130.1, 128.4, 127.4, 125.3, 21.8

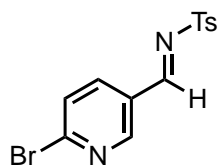
**MS (ESI)**: 295 [M+H]



**Figure A.31**  $^1\text{H}$  NMR spectrum (400 MHz,  $\text{CDCl}_3$ ) for NTsPyr-lm5.



**Figure A.32**  $^{13}\text{C}$  NMR spectrum (100 MHz,  $\text{CDCl}_3$ ) for NTsPyr-lm5.



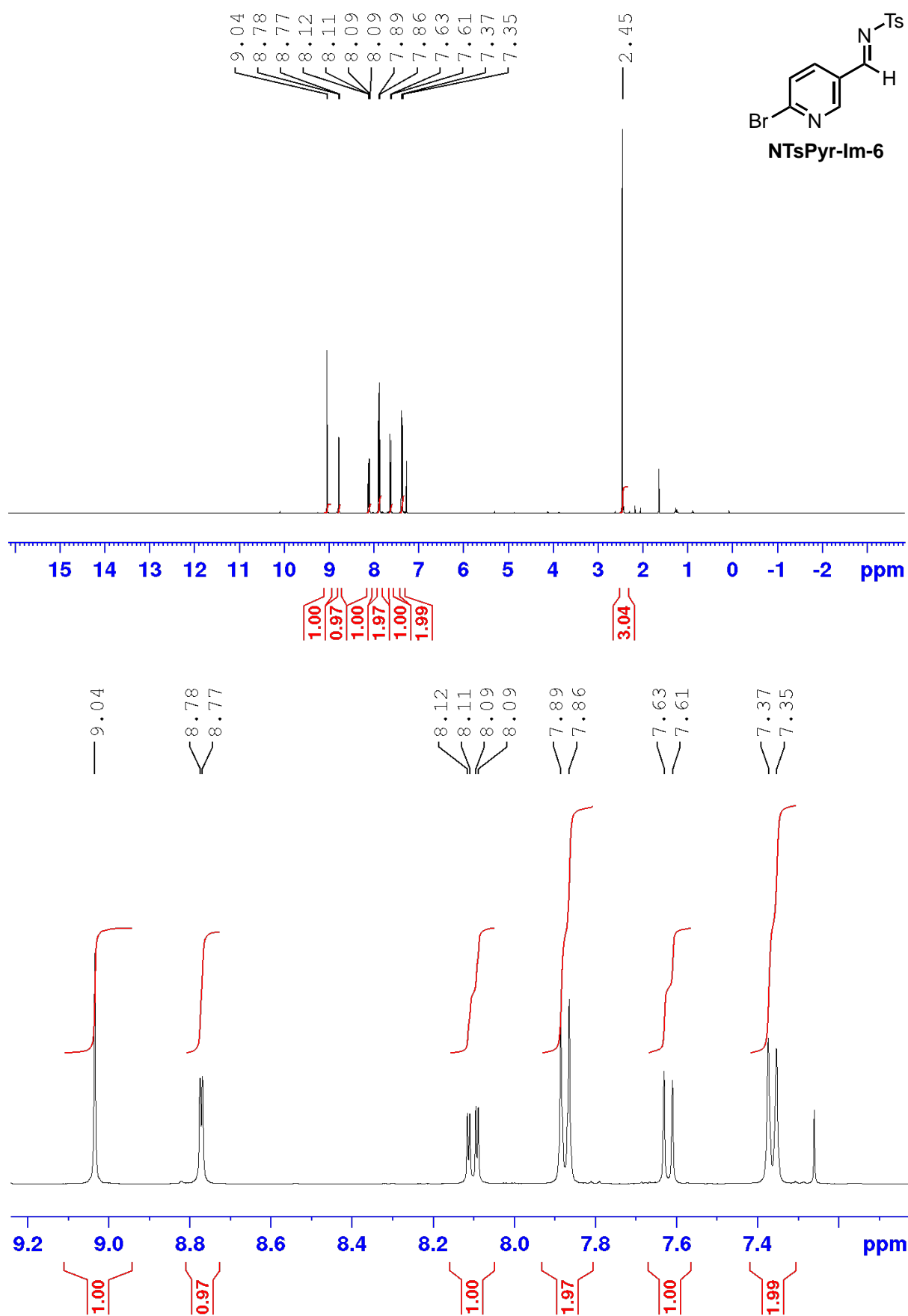
**NTsPyr-Im-6**

***(E)-N-((6-bromopyridin-3-yl)methylene)-4-methylbenzenesulfonamide (NTsPyr-Im6)***

**<sup>1</sup>H NMR** (400 MHz, CDCl<sub>3</sub>, δ): δ 9.05 (s, 1H), 8.77 (d, *J* = 2.2 Hz, 1H), 8.10 (dd, *J* = 8.3, 2.4 Hz, 1H), 7.87 (d, *J* = 8.3 Hz, 1H), 7.62 (d, *J* = 8.3 Hz, 2H), 7.36 (d, *J* = 8.3 Hz, 2H), 2.45 (s, 3H).

**<sup>13</sup>C NMR** (100 MHz, CDCl<sub>3</sub>, δ): 166.4, 153.3, 148.8, 145.4, 138.5, 134.3, 130.1, 129.1, 128.4, 127.7, 21.8.

**MS (ESI):** 338.9 [M+H], 340.9 [M+H]



**Figure A.33**  $^1\text{H}$  NMR spectrum (400 MHz,  $\text{CDCl}_3$ ) for **NTsPyr-Im6**.

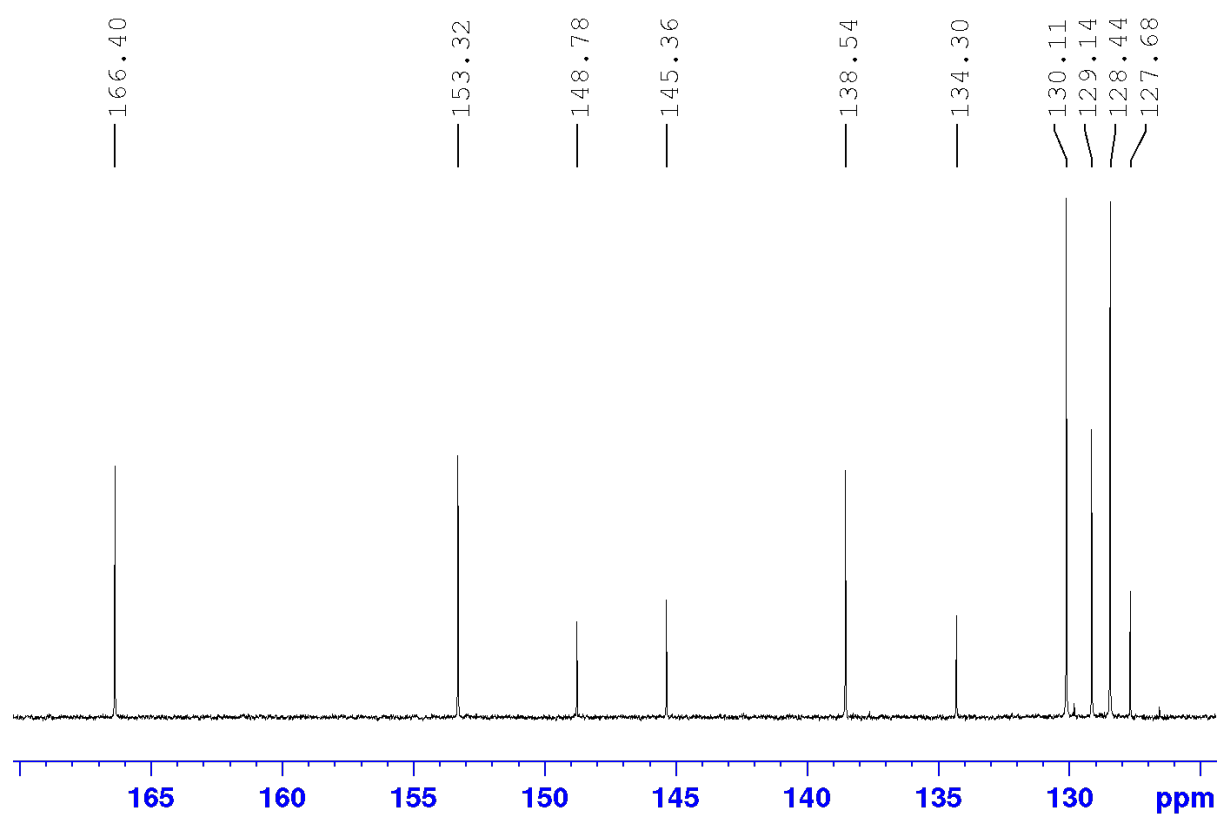
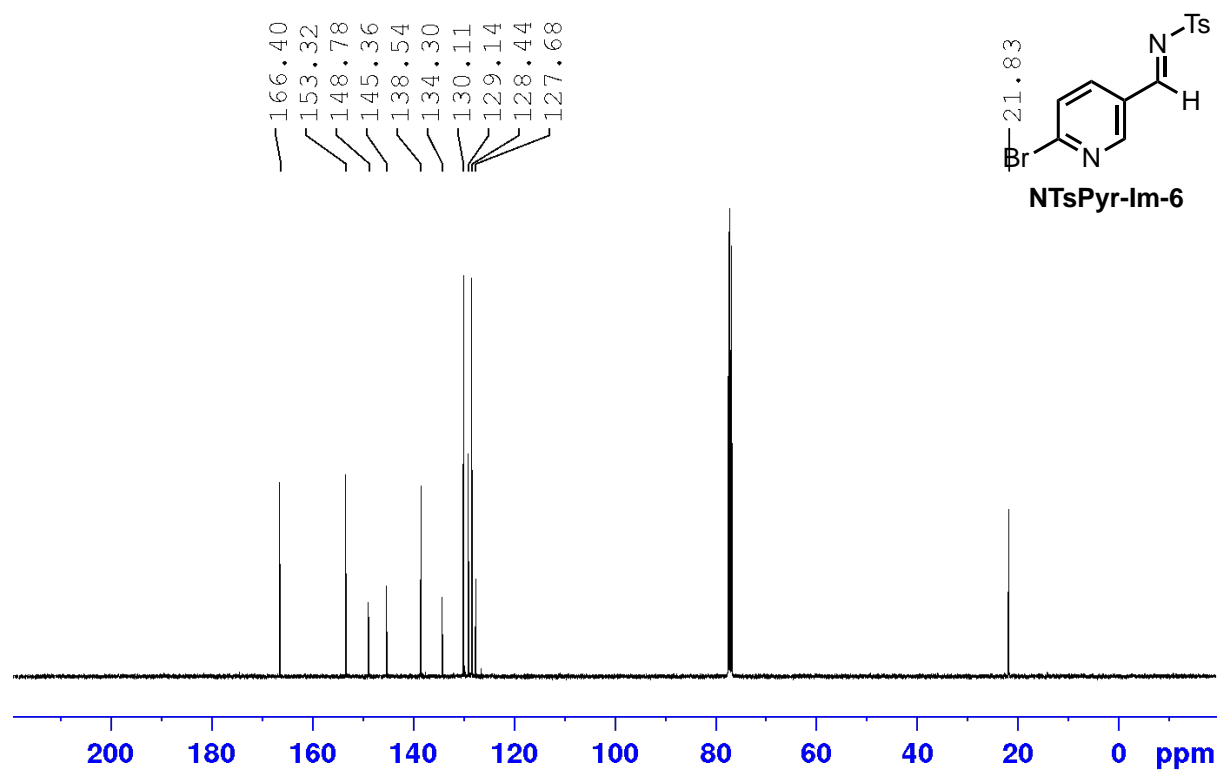
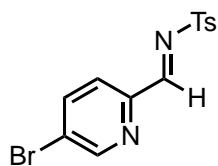


Figure A.34 <sup>13</sup>C NMR spectrum (100 MHz, CDCl<sub>3</sub>) for NTsPyr-lm6.





**NTsPyr-lm-7**

***(E)-N-((5-bromopyridin-2-yl)methylene)-4-methylbenzenesulfonamide (NTsPyr-lm7)***

**<sup>1</sup>H NMR** (400 MHz, CDCl<sub>3</sub>, δ): 8.94 (s, 1H), 8.81 (d, *J* = 2.0 Hz, 1H), 8.04 (d, *J* = 8.4 Hz, 1H), 7.95 (dd, *J* = 8.4, 2.1 Hz, 1H), 7.88 (d, *J* = 8.3 Hz, 2H), 7.37 (d, *J* = 8.3 Hz, 2H), 2.45 (s, 3H).

**<sup>13</sup>C NMR** (100 MHz, CDCl<sub>3</sub>, δ): 169.1, 151.9, 149.8, 145.4, 139.8, 133.9, 130.1, 128.7, 126.1, 125.0, 21.8

**MS (ESI):** 338.9 [M+H], 340.9 [M+H]

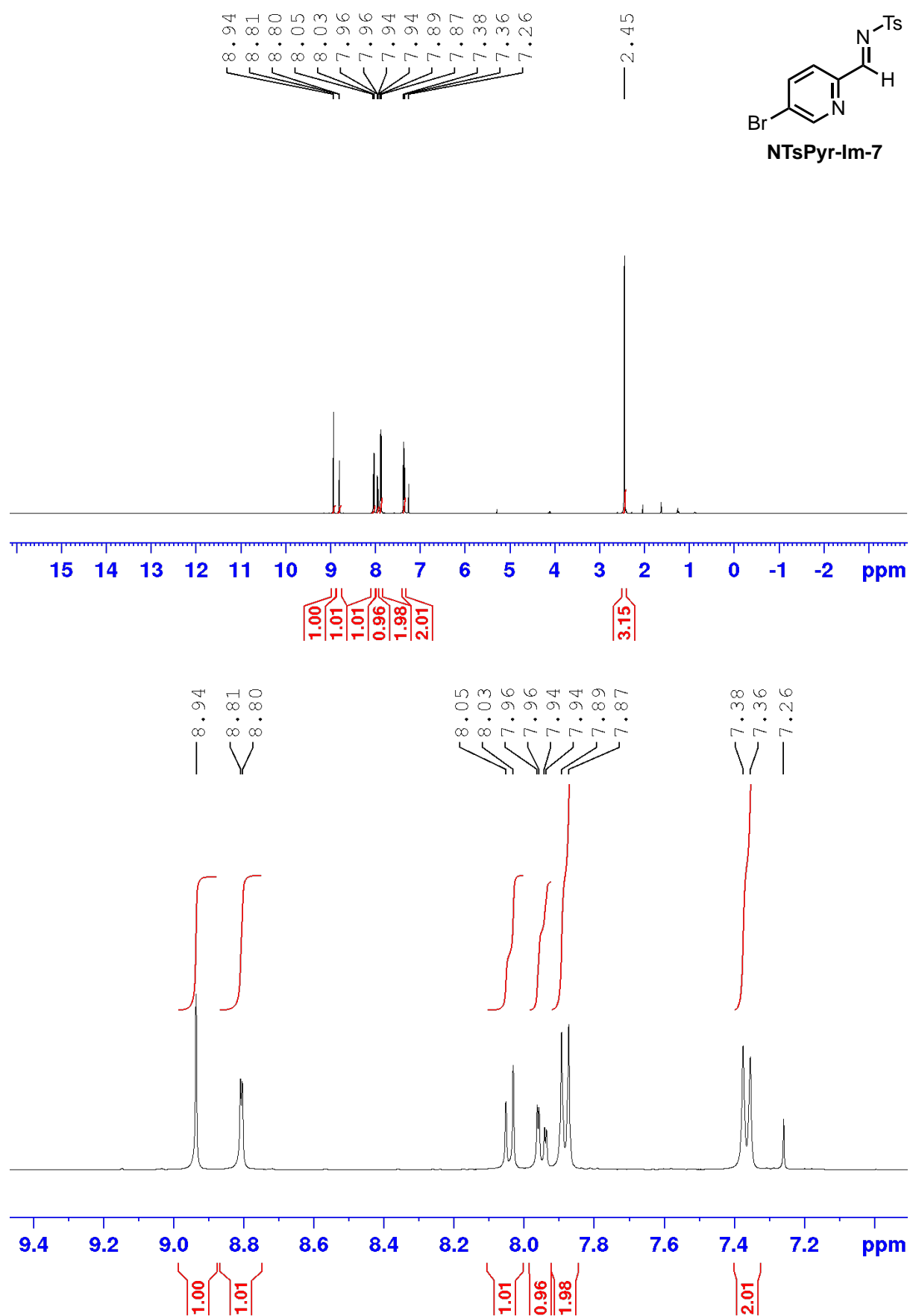


Figure A.35 <sup>1</sup>H NMR spectrum (400 MHz, CDCl<sub>3</sub>) for NTsPyr-lm7.

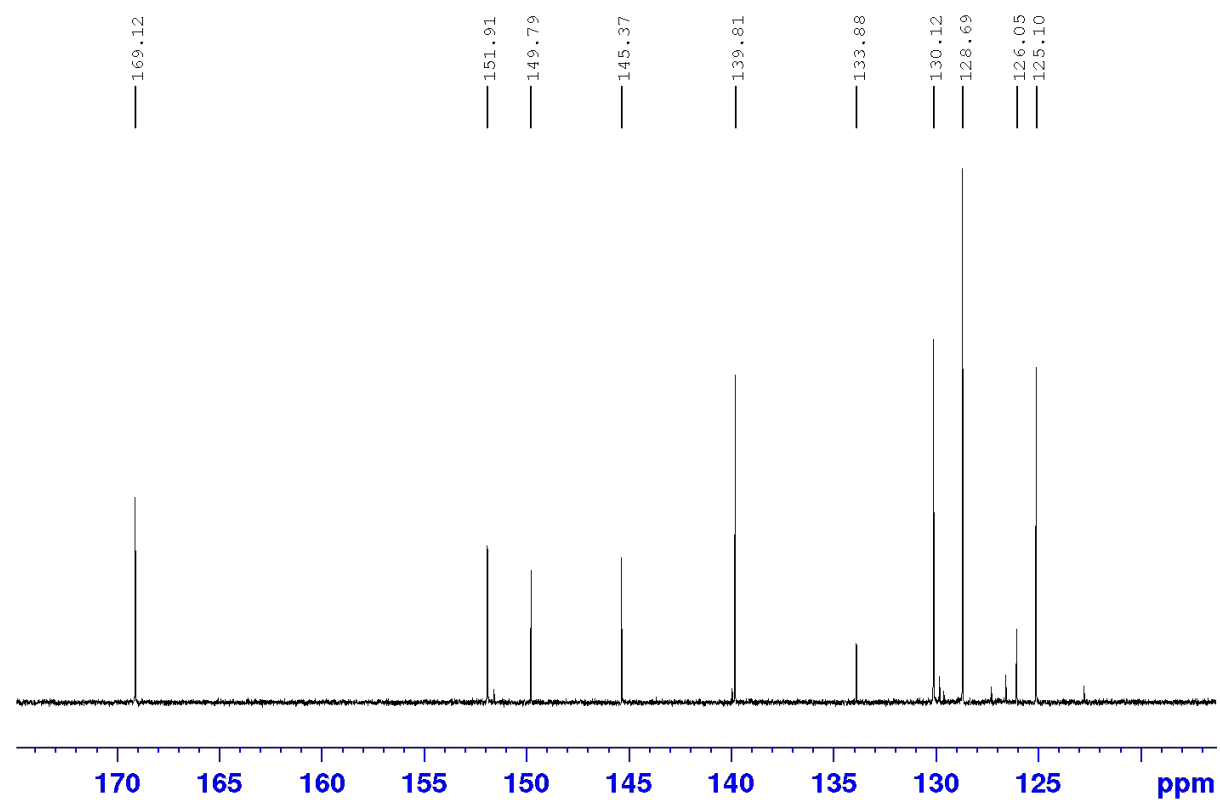
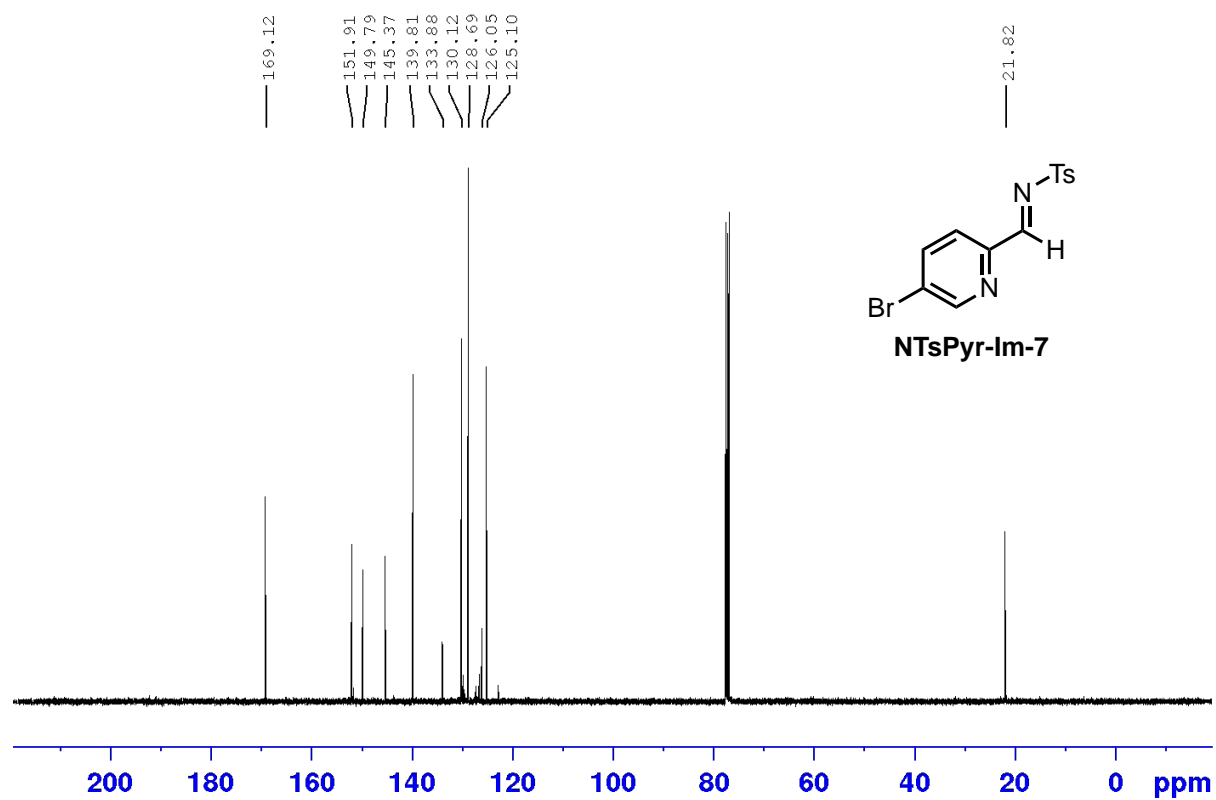
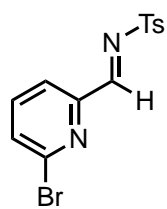


Figure A.36 <sup>13</sup>C NMR spectrum (100 MHz, CDCl<sub>3</sub>) for NTsPyr-Im7.



**NTsPyr-Im-8**

***(E)-N-((6-bromopyridin-2-yl)methylene)-4-methylbenzenesulfonamide (NTsPyr-Im8)***

**<sup>1</sup>H NMR** (400 MHz, CDCl<sub>3</sub>, δ): 8.89 (s, 1H), 8.16 (dd, *J* = 6.9, 1.6 Hz, 1H), 7.89 (d, *J* = 7.9 Hz, 2H), 7.69 (m, 2H), 7.39 (d, *J* = 7.9 Hz, 2H), 2.45 (s, 2H).

**<sup>13</sup>C NMR** (CDCl<sub>3</sub>, 100 MHz) δ 168.5, 153.4, 145.5, 142.6, 139.3, 133.5, 132.8, 130.2, 128.8, 122.8, 21.8.

**MS (ESI)**: 338.9 [M+H], 340.9 [M+H]

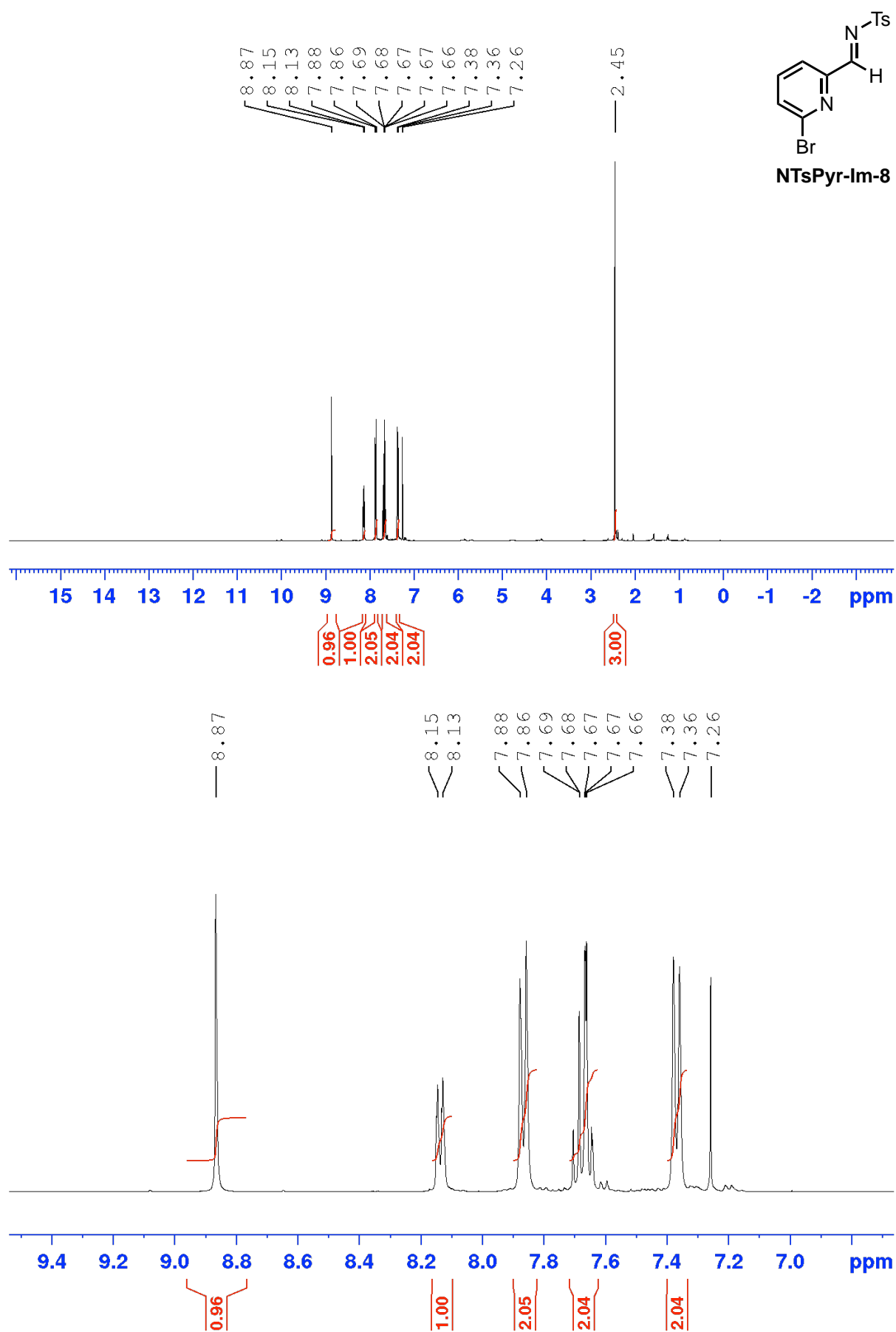


Figure A.37 <sup>1</sup>H NMR spectrum (400 MHz, CDCl<sub>3</sub>) for NTsPyr-Im8.

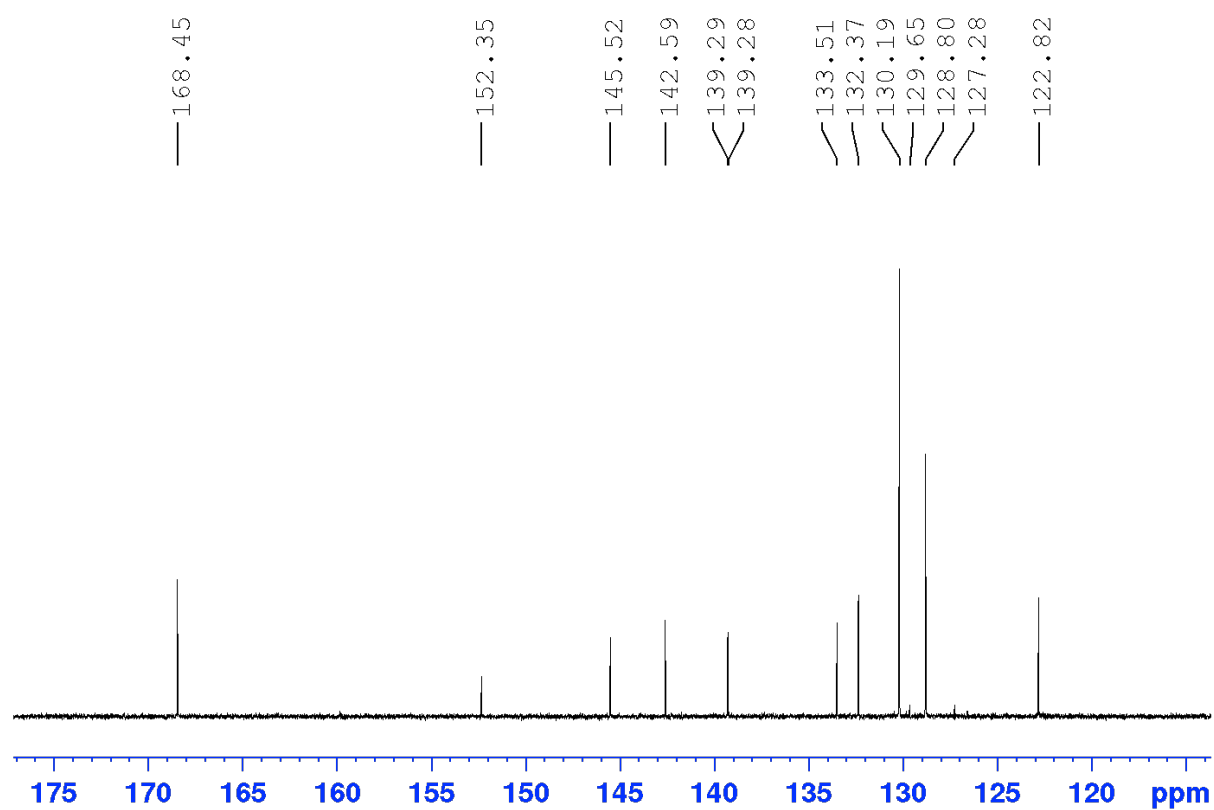
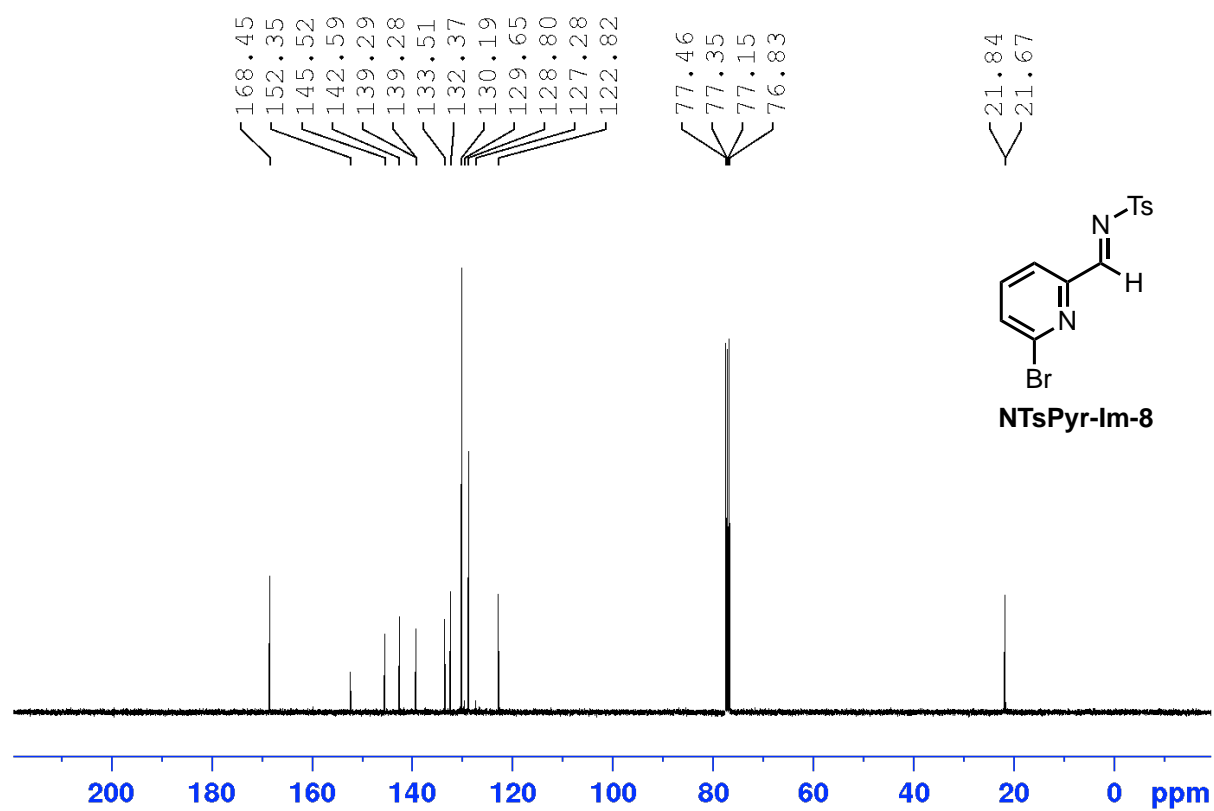
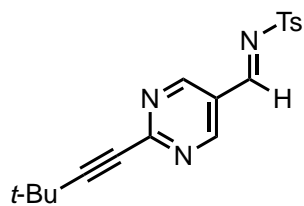


Figure A.38 <sup>13</sup>C NMR spectrum (100 MHz, CDCl<sub>3</sub>) for NTsPyr-Im8.



**5.49**

**(E)-N-((2-(3,3-dimethylbut-1-yn-1-yl)pyrimidin-5-yl)methylene)-4-**

**methylbenzenesulfonamide (5.49)**

**<sup>1</sup>H NMR** (400 MHz, CDCl<sub>3</sub>, δ): 9.12 (s, 2H), 9.03 (s, 1H), 7.90 (d, *J* = 8.3 Hz, 2H), 7.38, (d, *J* = 8.3 Hz, 2H), 2.46 (s, 3H), 1.39 (s, 9H).

**<sup>13</sup>C NMR** (100 MHz, CDCl<sub>3</sub>, δ): 164.5, 159.0, 156.7, 145.6, 134.1, 130.2, 128.6, 124.1, 103.8, 30.3, 28.4, 21.9

**MS (ESI):** 342.1 [M+H]

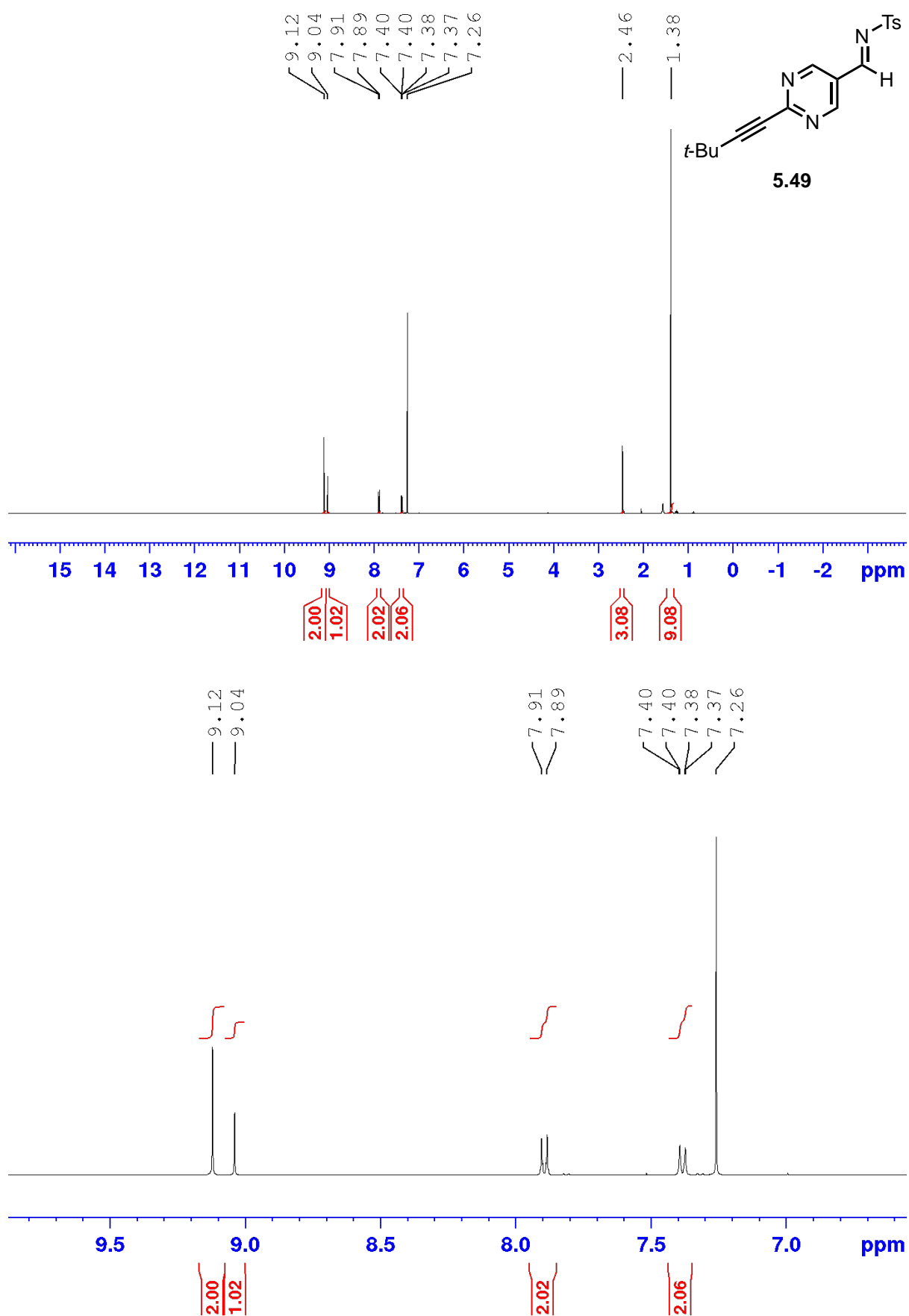


Figure A.39 <sup>1</sup>H NMR spectrum (400 MHz, CDCl<sub>3</sub>) for **5.49**.



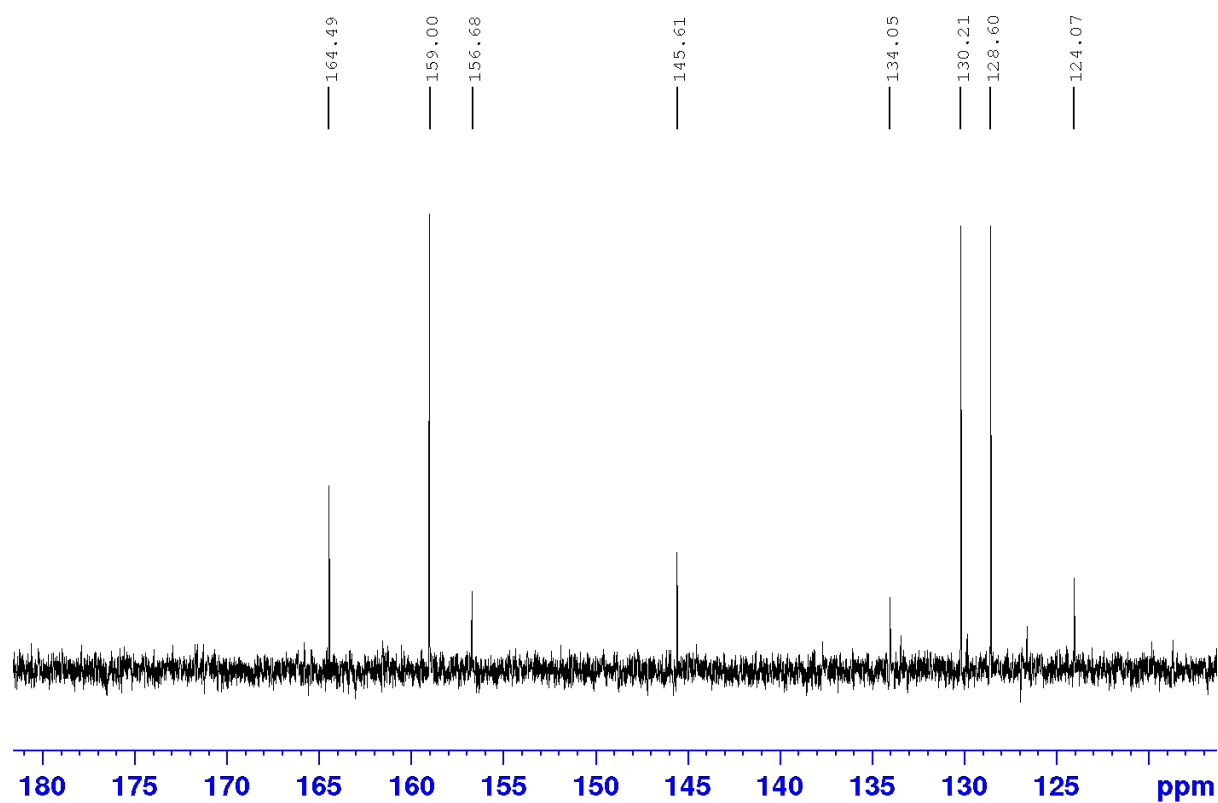
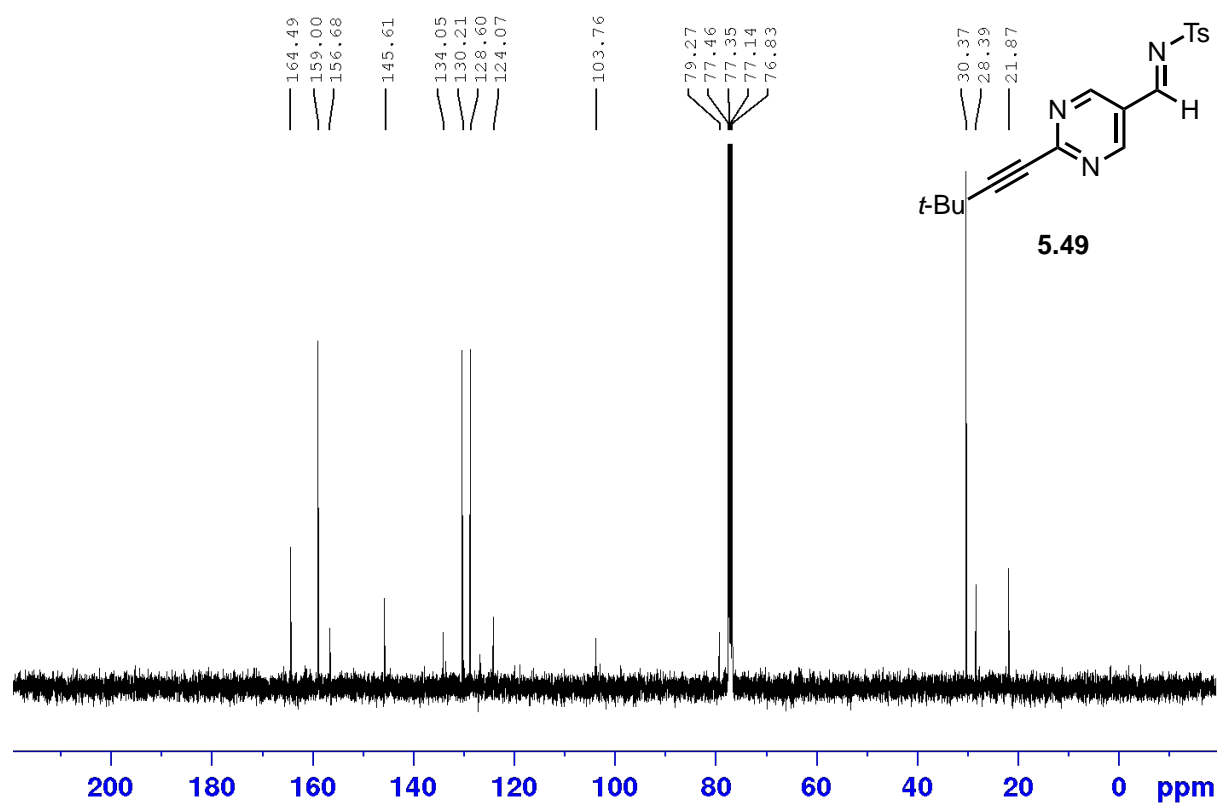
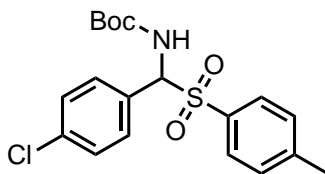


Figure A.40  $^{13}\text{C}$  NMR spectrum (100 MHz,  $\text{CDCl}_3$ ) for 5.49.



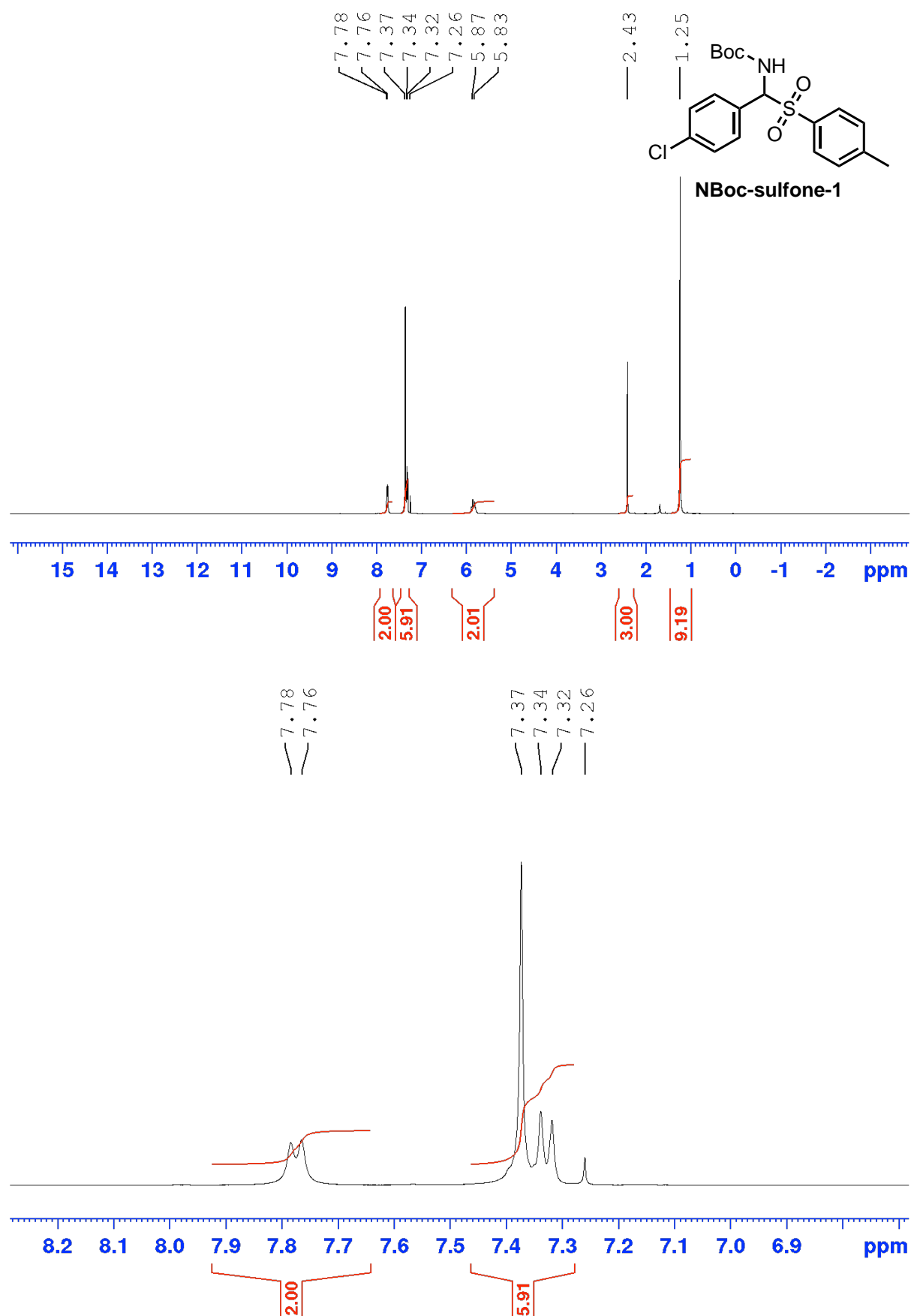
**NBoc-sulfone-1**

***tert*-butyl ((4-chlorophenyl)(tosyl)methyl)carbamate (NBoc-sulfone-1)**

**<sup>1</sup>H NMR** (400 MHz, CDCl<sub>3</sub>, δ): 7.77 (d, *J*= 8.1 Hz, 2H), 7.38 (m, 4H), 7.34 (d, *J*= 8.1 Hz, 2H), 5.86 Hz (1H, *J*= 10.6 Hz, 1H), 5.71 (b, 1H), 2.43 (s, 3H), 1.26 (s, 9H).

**<sup>13</sup>C NMR** (100 MHz, CDCl<sub>3</sub>, δ): 153.59, 145.35, 136.07, 133.62, 130.31, 229.87, 129.59, 129.02, 128.73, 81.42, 73.31, 28.04, 21.74

**MS (ESI):** 240.1 [M-Ts]



**Figure A.41**  $^1\text{H}$  NMR spectrum (400 MHz,  $\text{CDCl}_3$ ) for **NBoc-sulfone-1**.

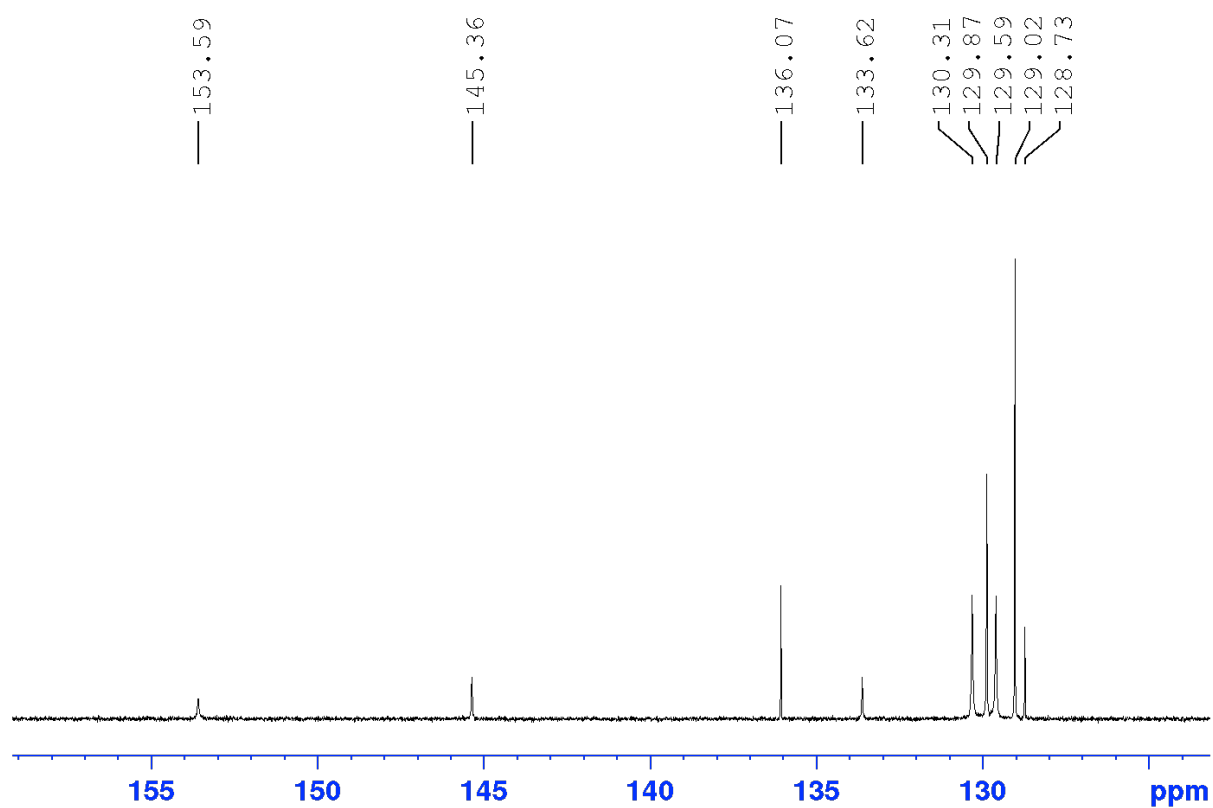
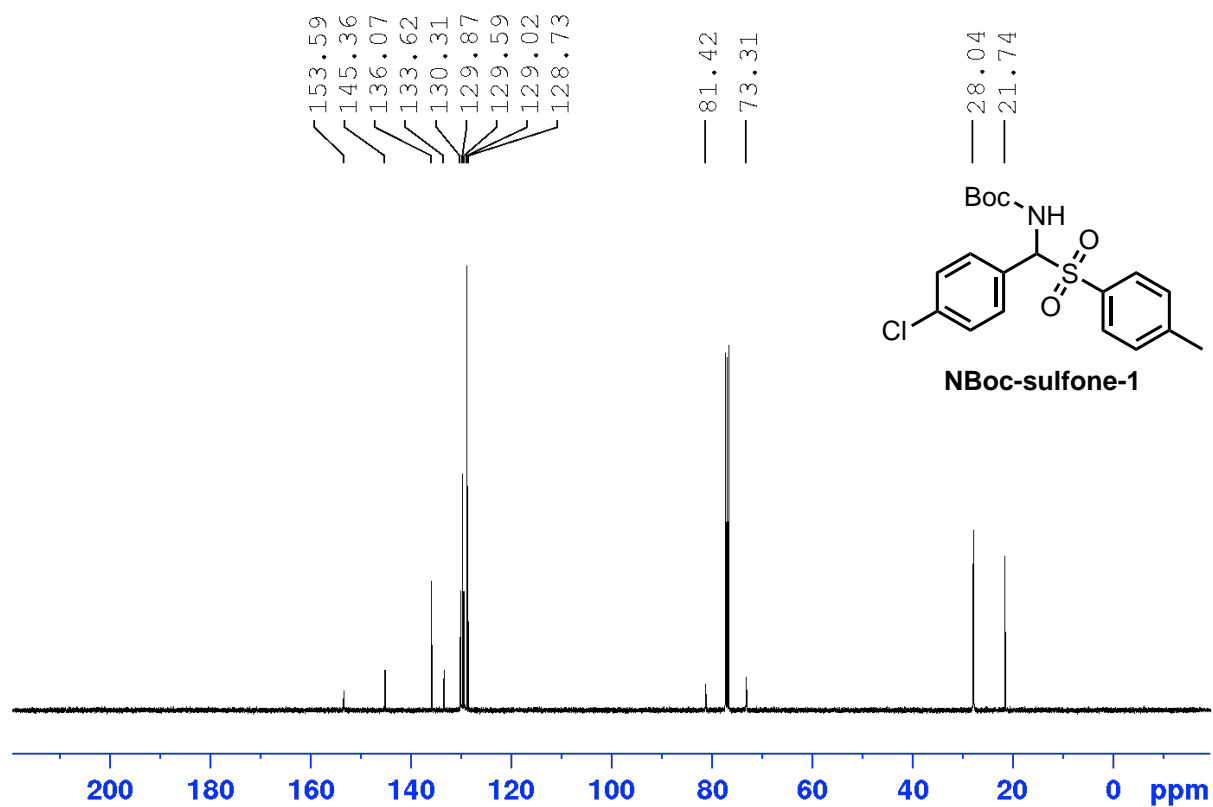
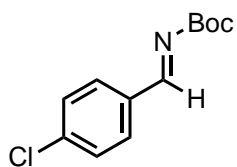


Figure A.42 <sup>1</sup>H NMR spectrum (400 MHz, CDCl<sub>3</sub>) for NBoc-sulfone-1.



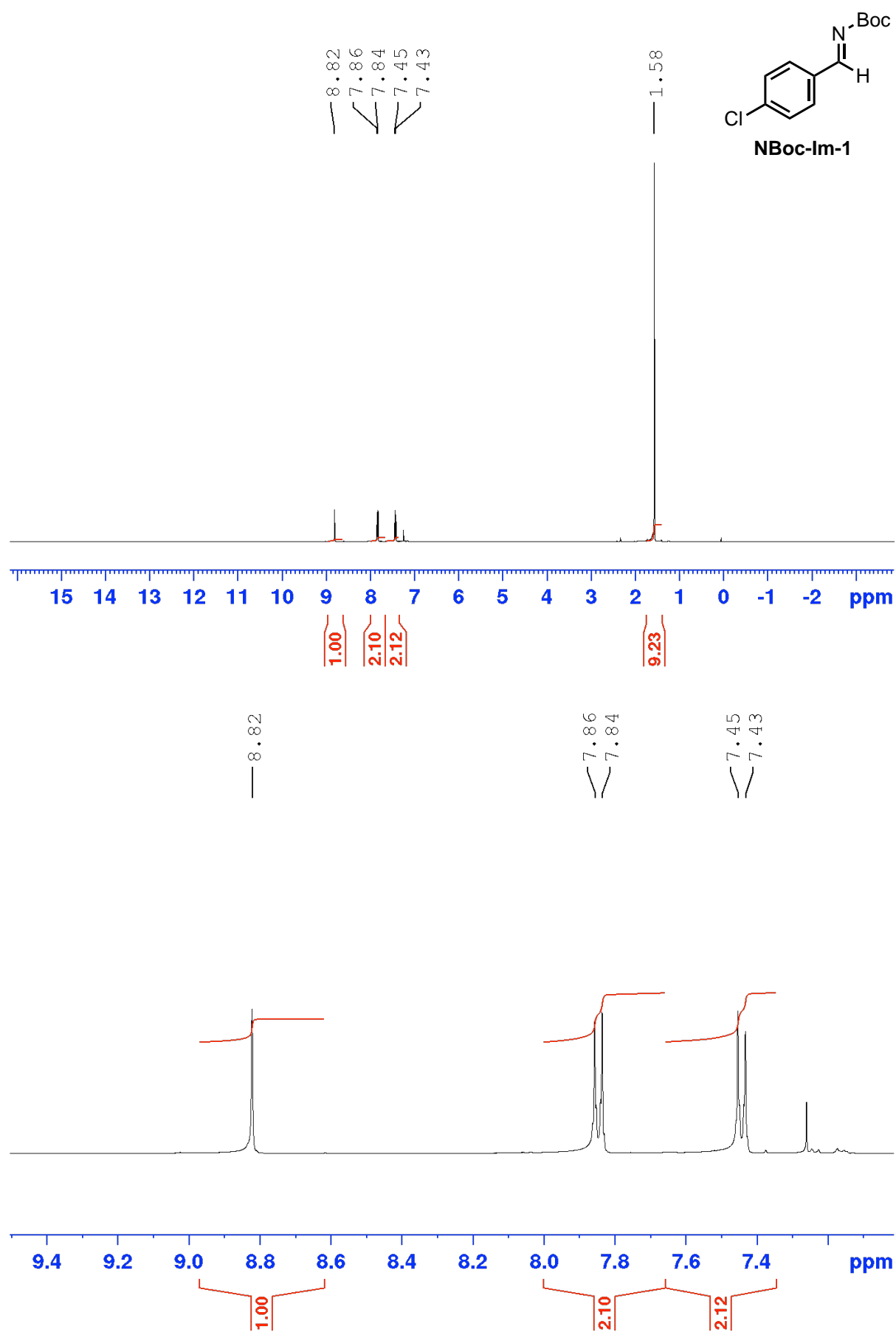
**NBoc-lm-1**

***tert*-butyl (*E*)-(4-chlorobenzylidene)carbamate (NBoc-lm1)**

**<sup>1</sup>H NMR** (400 MHz, CDCl<sub>3</sub>, δ): 8.82 (s, 1H), 7.84 (d, *J* = 8.5 Hz, 2H), 7.44 (d, *J* = 8.5 Hz, 2H), 1.58 (s, 9H).

**<sup>13</sup>C NMR** (CDCl<sub>3</sub>, 100 MHz) δ 168.4, 162.5, 139.9, 132.6, 131.4, 129.4, 82.6, 28.0

**MS (ESI):** 240.1 [M+H]



**Figure A.43**  $^1\text{H}$  NMR spectrum (400 MHz,  $\text{CDCl}_3$ ) for **NBoc-Im1**.

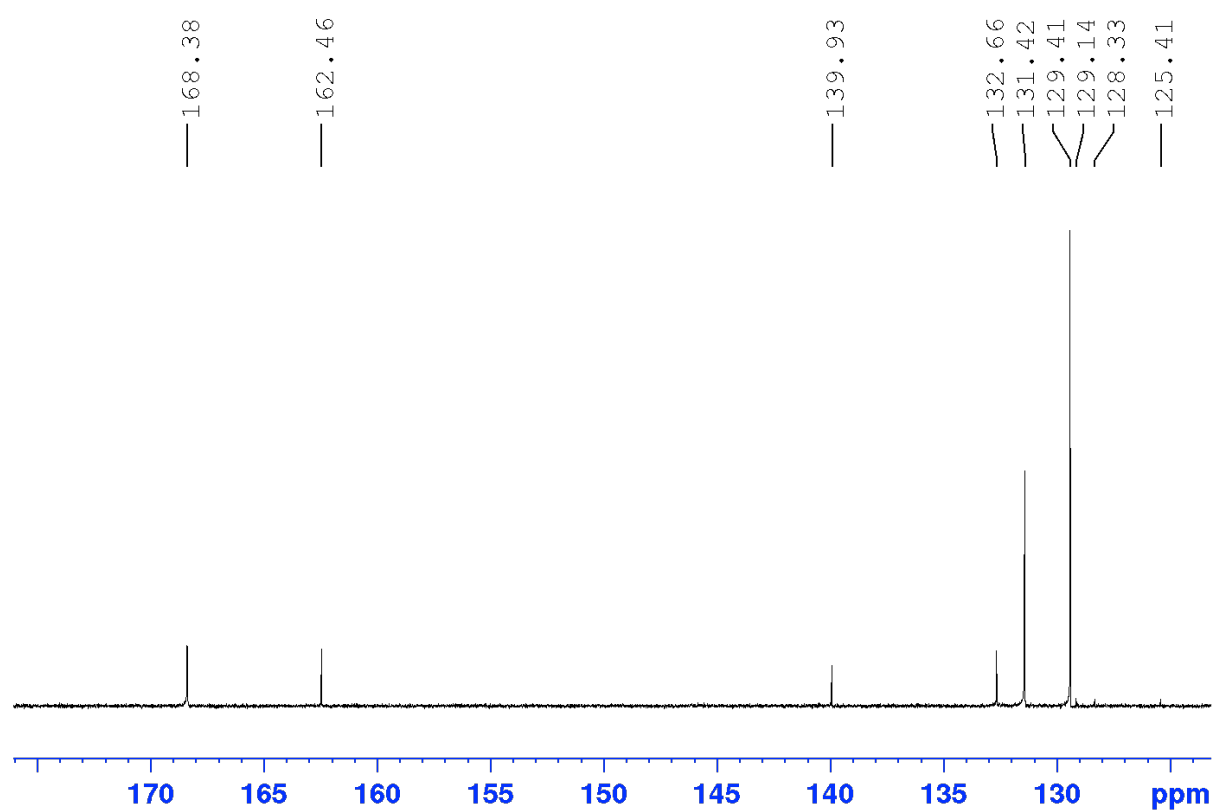
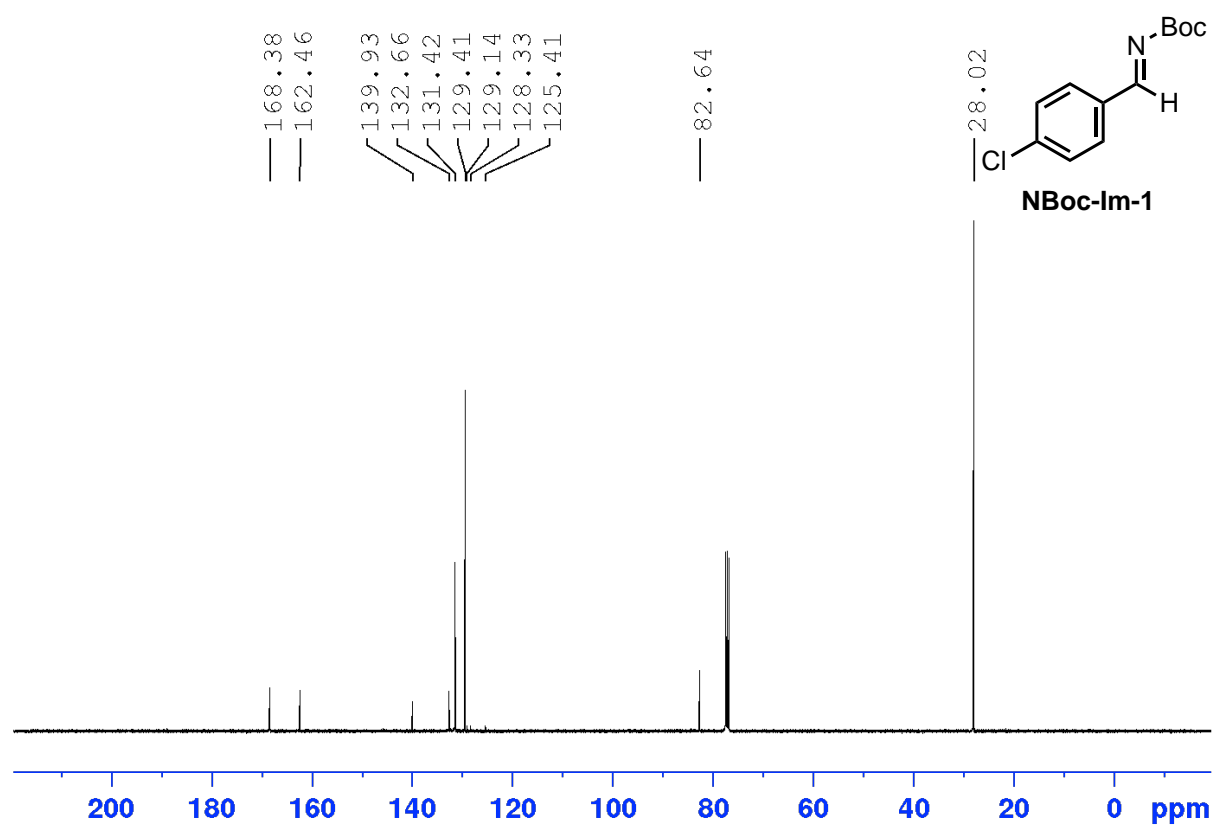
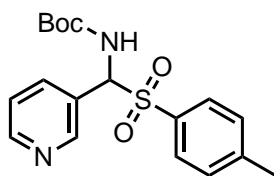


Figure A.44 <sup>13</sup>C NMR spectrum (100 MHz, CDCl<sub>3</sub>) for NBoc-Im1.



**NBoc-sulfone-2**

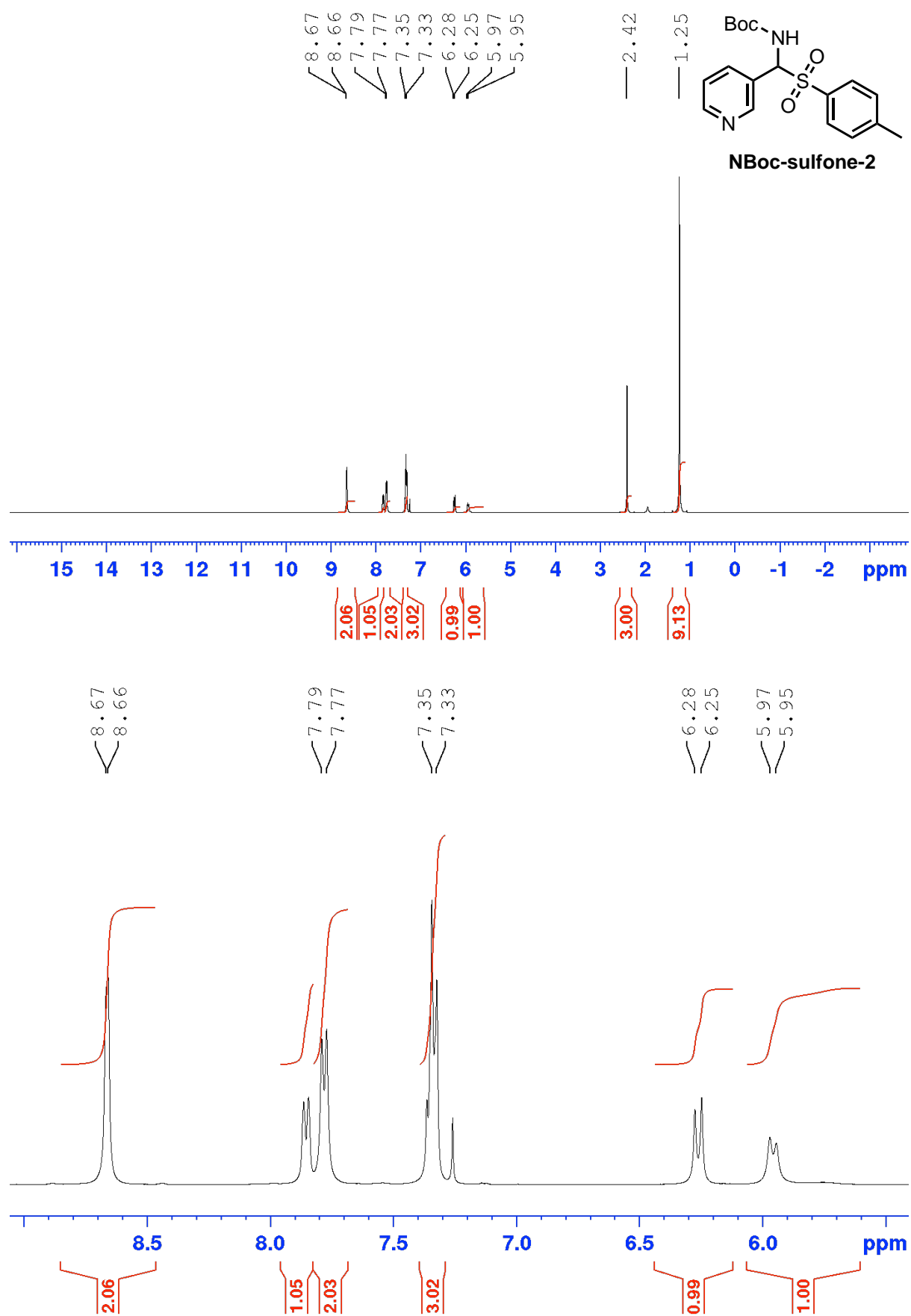
***tert-butyl (pyridin-3-yl(tosyl)methyl)carbamate (NBoc-sulfone-2)***

**<sup>1</sup>H NMR** (400 MHz, CDCl<sub>3</sub>, δ): 8.86 (s, 2H), 7.85 (d, *J* = 7.9 Hz, 1H), 7.83 (d, *J* = 7.8 Hz, 2H), 7.34 (m 3H), 6.26 (d, *J* = 10.8 Hz, 1H), 5.96 (d, *J* = 10.8 Hz, 1H), 2.42 (s, 3H), 1.25 (s, 9H)

**<sup>13</sup>C NMR** (100 MHz, CDCl<sub>3</sub>, δ): δ 153.7, 150.8, 150.1, 145.6, 136.5, 133.3, 129.8, 129.6, 126.7, 123.6, 81.5, 72.1, 28.1, 21.8

**MS (ESI):** 363.1 [M+H]





**Figure A.45** <sup>1</sup>H NMR spectrum (400 MHz, CDCl<sub>3</sub>) for **NBoc-sulfone-2**.

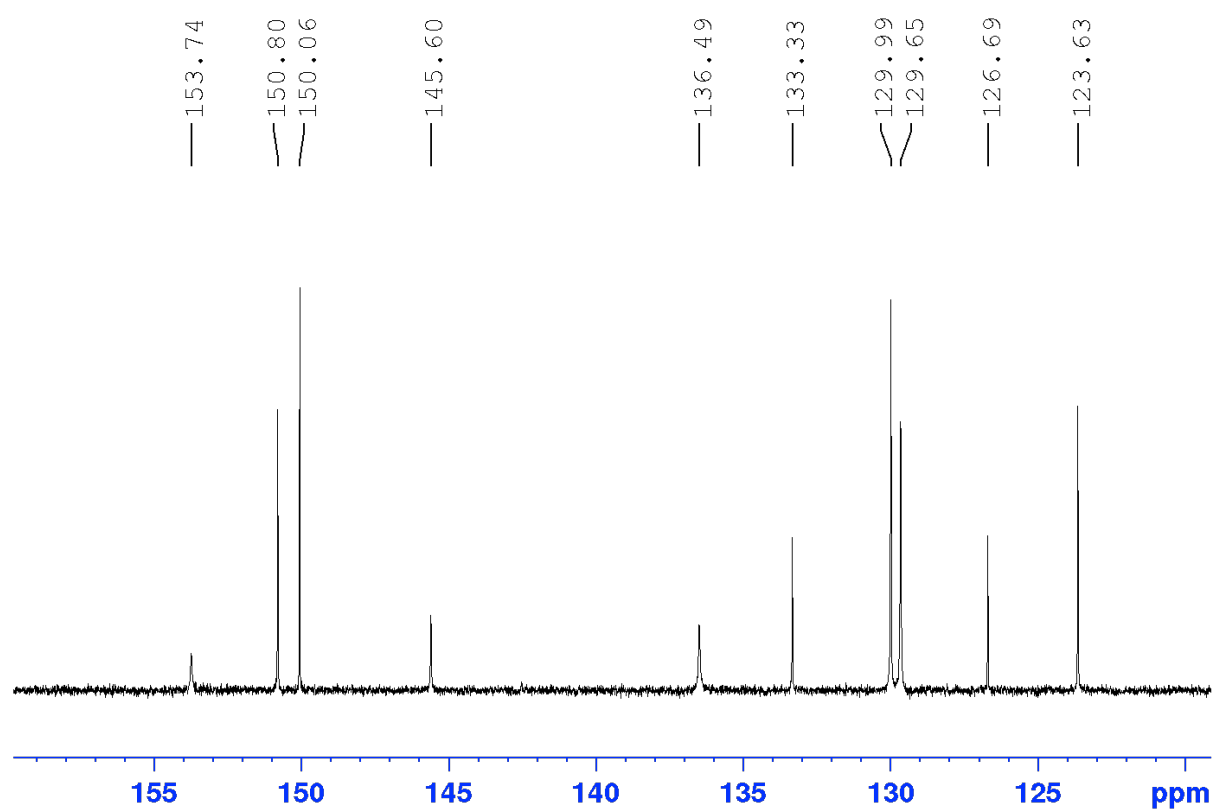
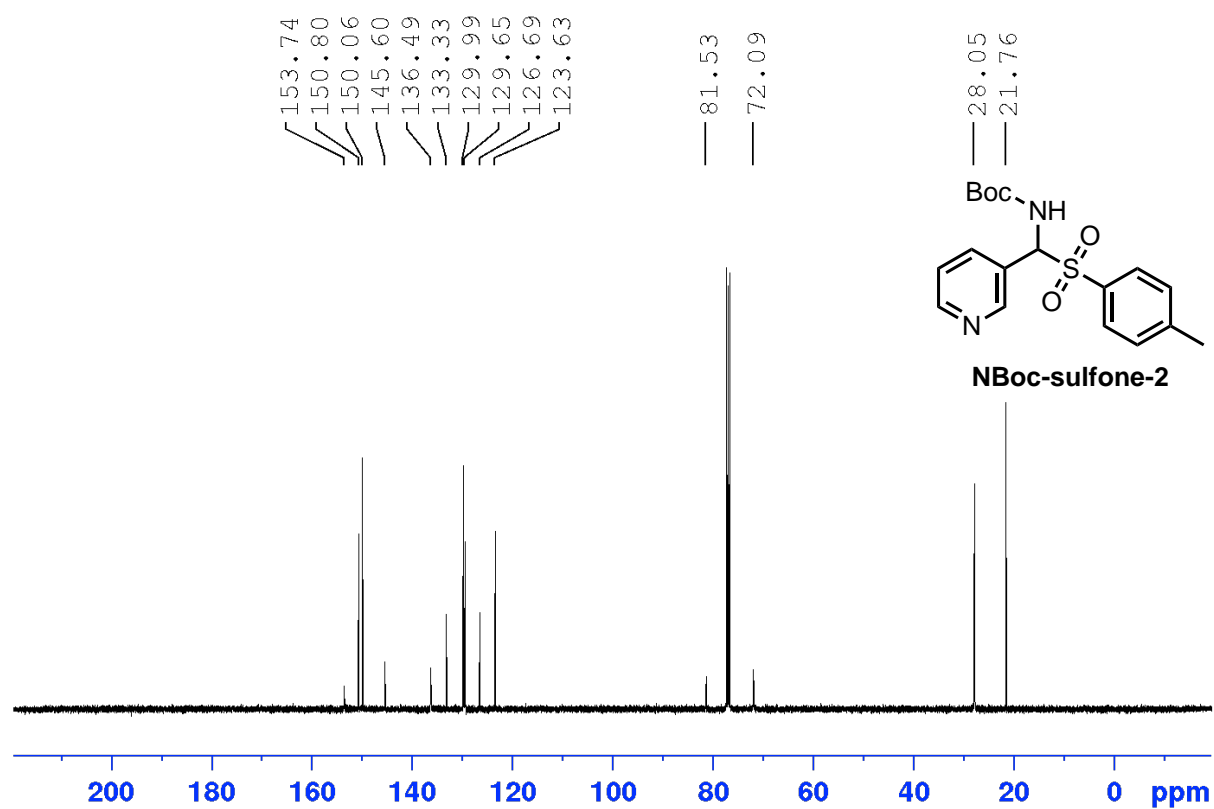
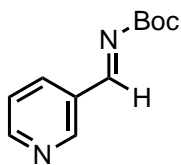


Figure A.46  $^{13}\text{C}$  NMR spectrum (100 MHz,  $\text{CDCl}_3$ ) for NBoc-sulfone-2.



**NBoc-lm-2**

***tert-butyl (E)-(pyridin-3-ylmethylene)carbamate (NBoc-lm2)***

**<sup>1</sup>H NMR** (400 MHz, CDCl<sub>3</sub>, δ): 8.99 (d, *J*= 1.8 Hz, 1H), 8.86 (s, 1H), 8.74 (dd, *J*= 4.8, 1.7 Hz, 1H), 8.25 (dt, *J*= 7.9, 1.9 Hz, 1H), 7.39 (dd, *J*= 7.9 Hz, 4.8 Hz, 1H) 1.57 (s, 9H).

**<sup>13</sup>C NMR** (100 MHz, CDCl<sub>3</sub>, δ): 166.8, 162.1, 154.0, 152.3, 135.9, 129.9, 124.0, 82.9, 27.9

**MS (ESI):** 207.1 [M+H]

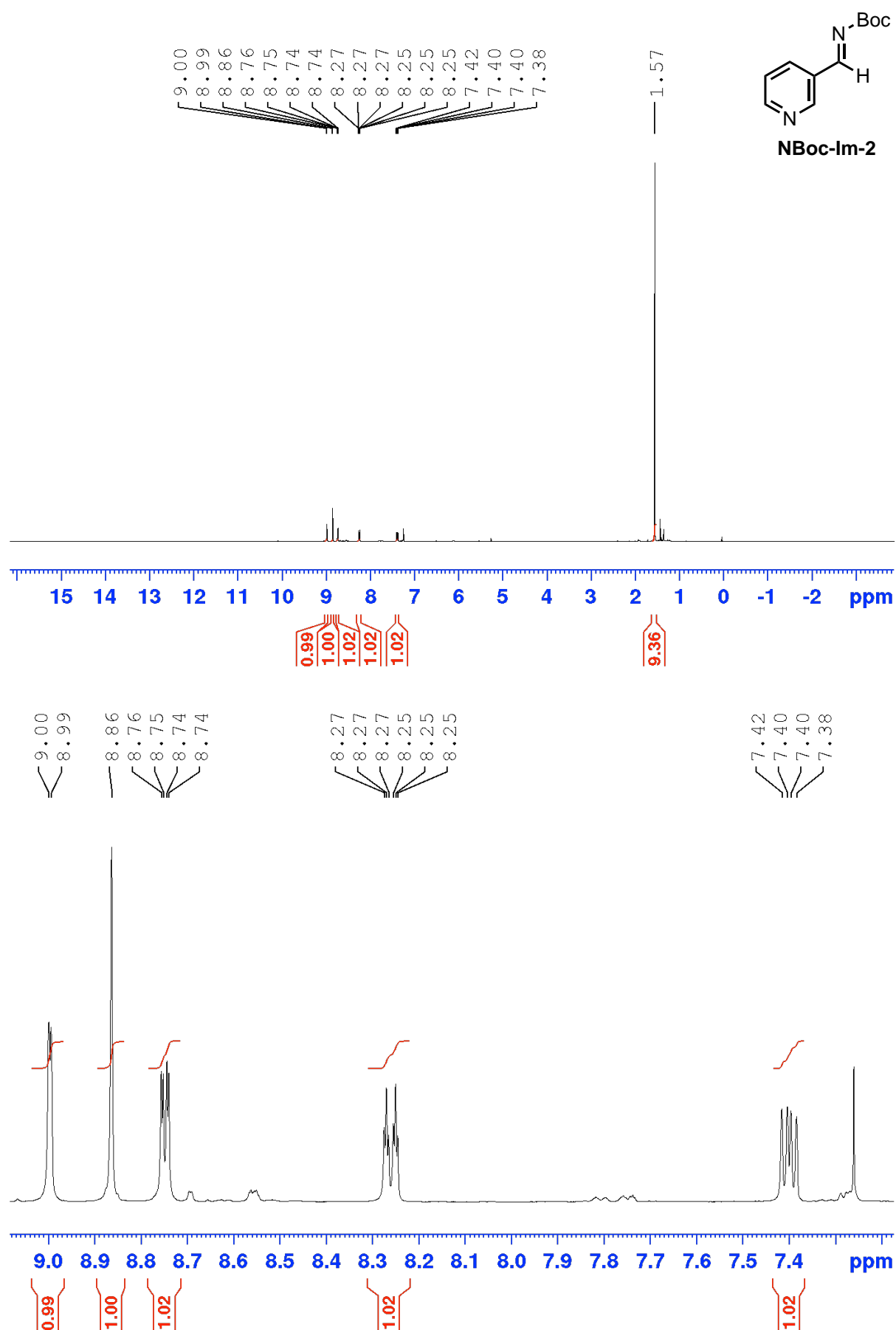
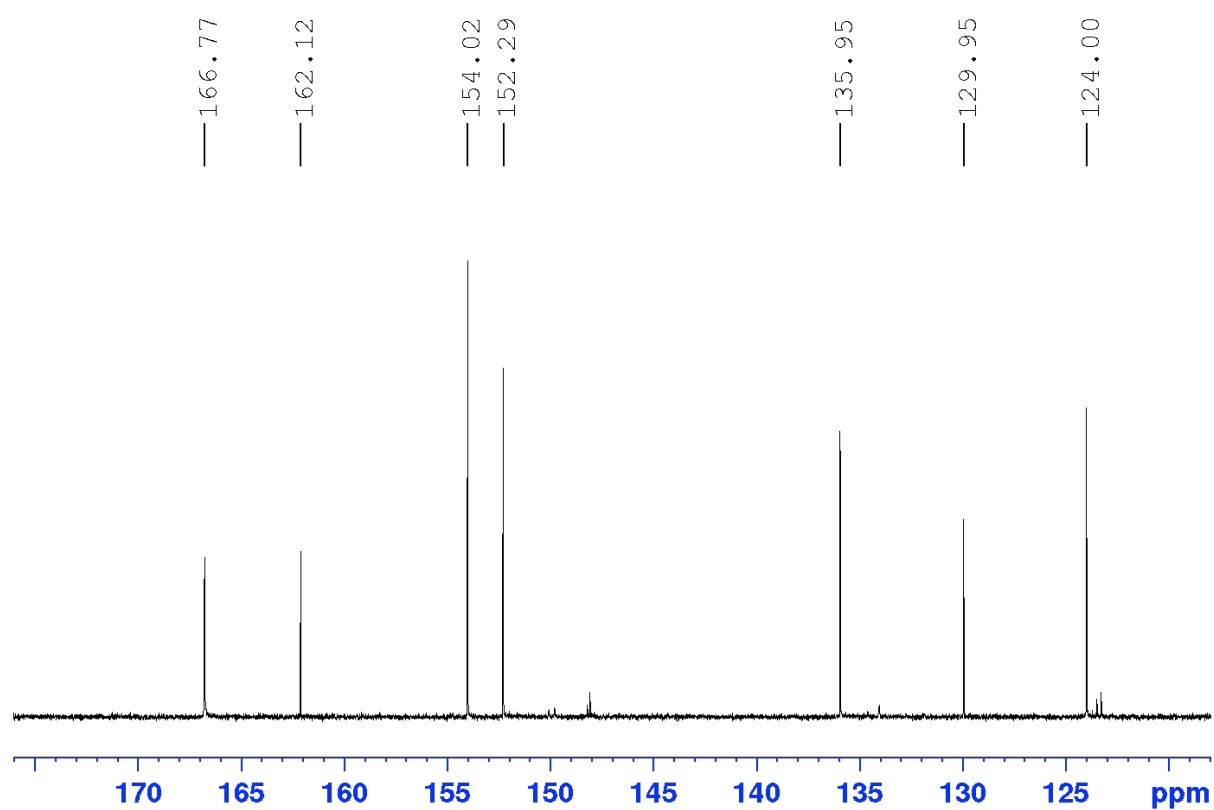
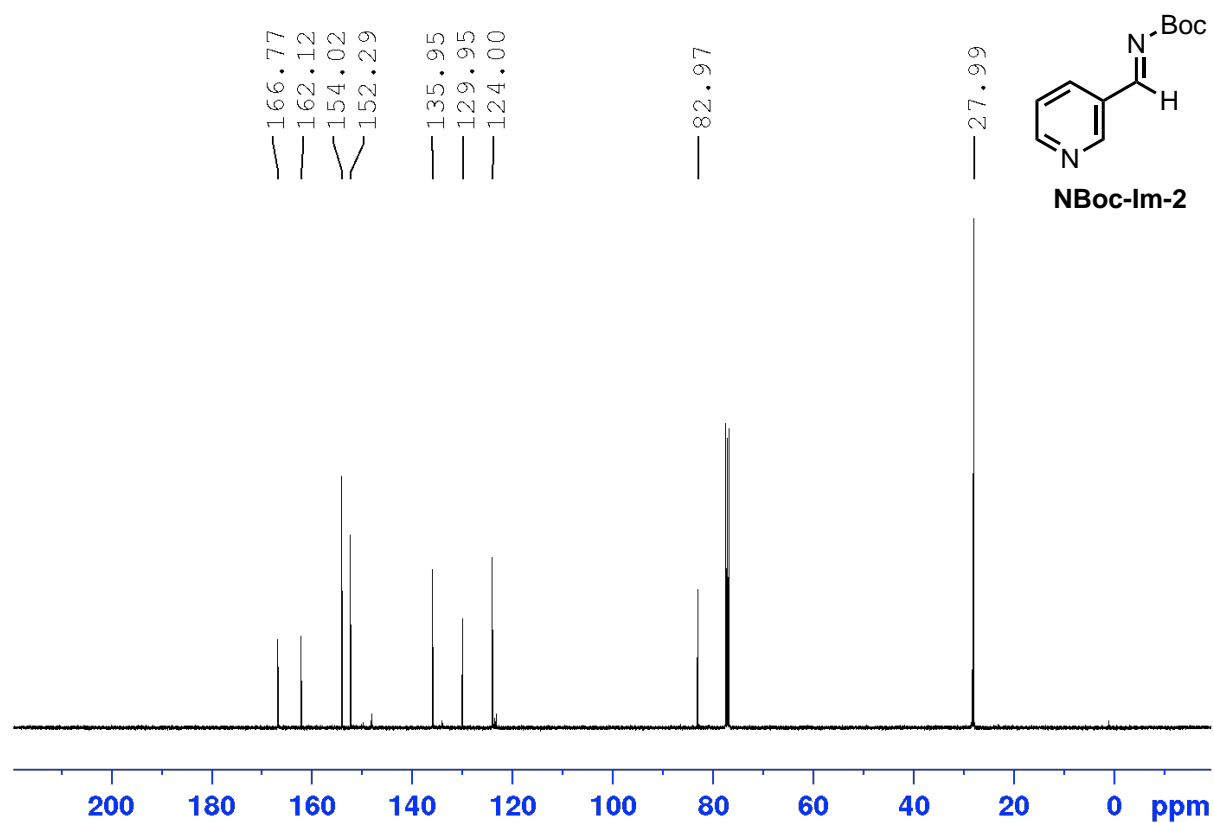
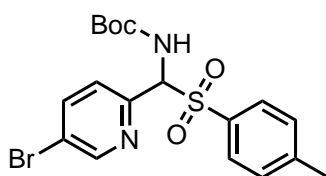


Figure A.47 <sup>1</sup>H NMR spectrum (400 MHz, CDCl<sub>3</sub>) for NBoc-Im2.



**Figure A.48** <sup>13</sup>C NMR spectrum (100 MHz, CDCl<sub>3</sub>) for NBoc-Im2.



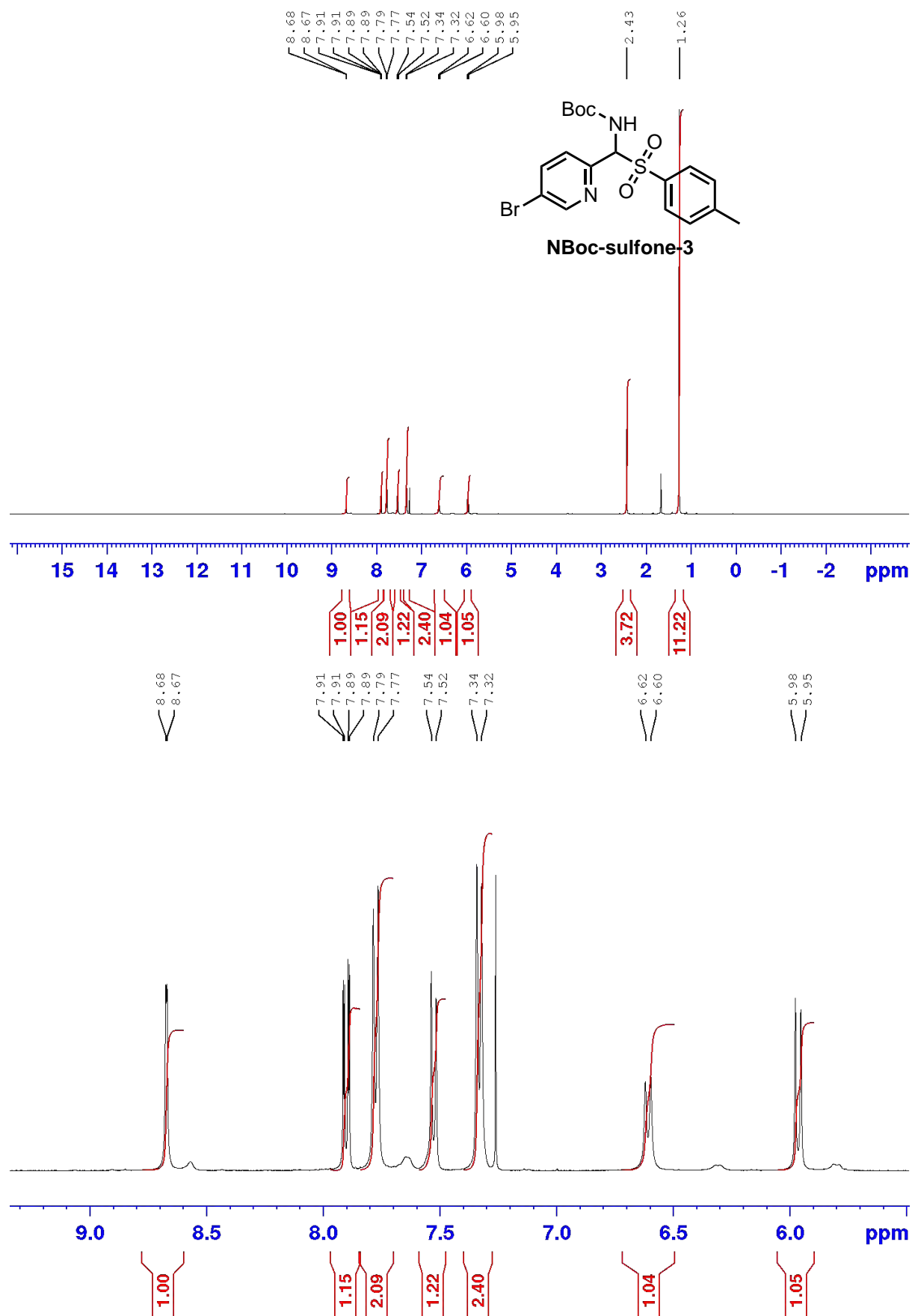
**NBoc-sulfone-3**

***tert-butyl ((5-bromopyridin-2-yl)(tosyl)methyl)carbamate (NBoc-sulfone-3)***

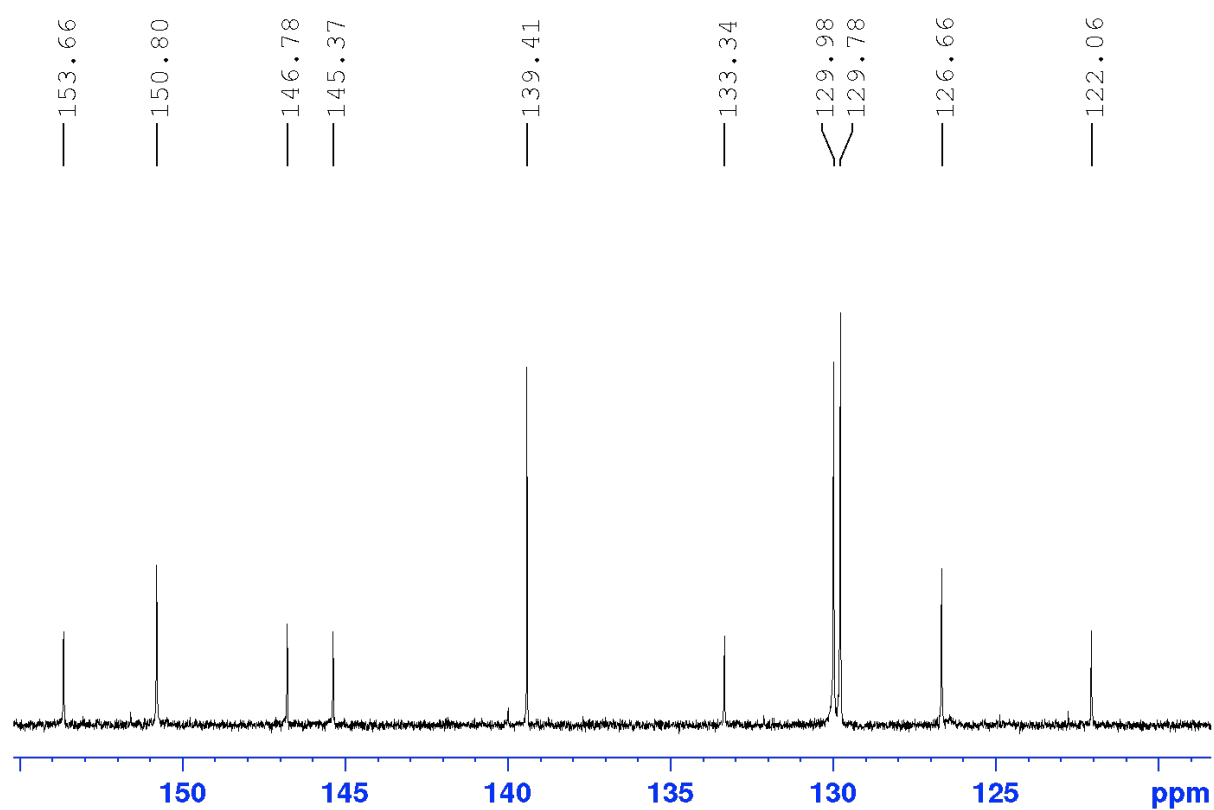
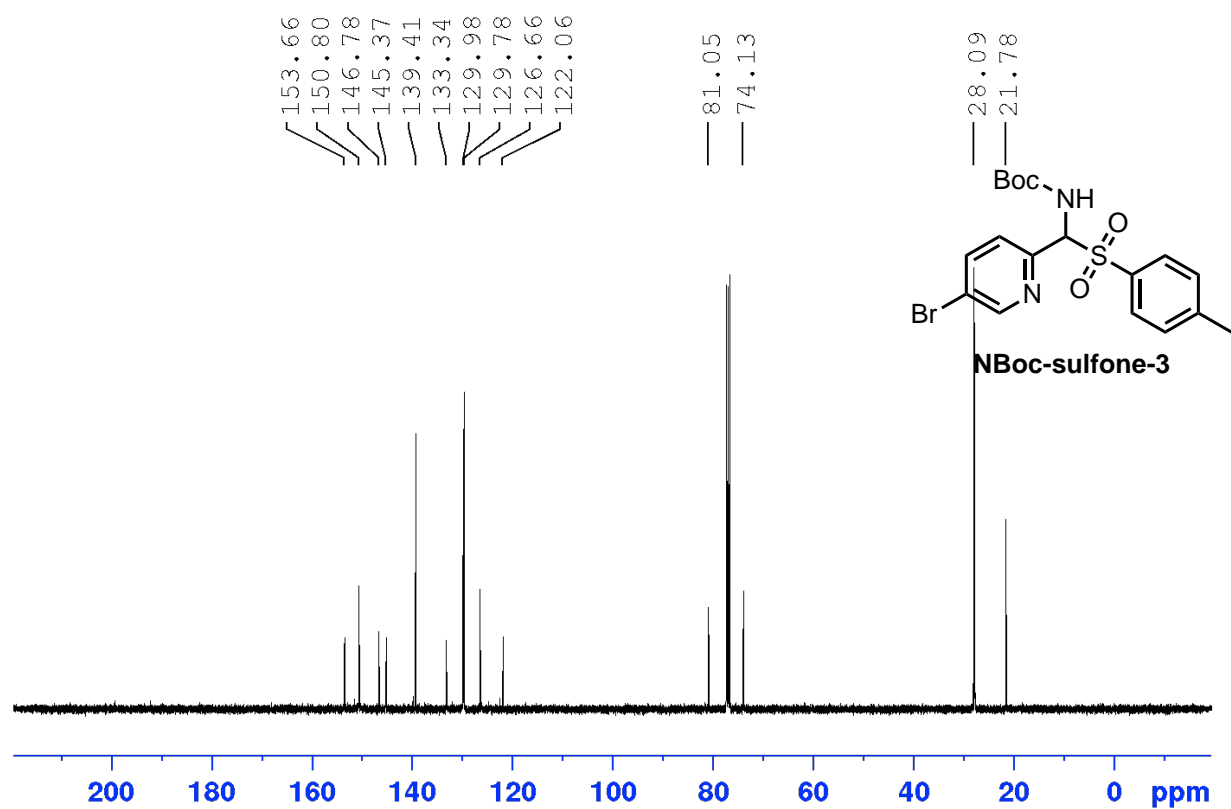
**<sup>1</sup>H NMR** (400 MHz, CDCl<sub>3</sub>, δ): 8.67 (d, *J* = 1.9 Hz, 1H), 7.90 (dd, *J* = 8.3, 2.3 Hz, 1H), 7.78 (d, *J* = 8.2 Hz, 2H), 7.53 (d, *J* = 8.2 Hz, 1H), 7.33 (d, *J* = 8.0 Hz, 2H), 7.72 (d, *J* = 9.4 Hz, 1H), 5.96 (d, *J* = 9.4 Hz, 1H), 2.43 (s, 3H), 1.26 (s, 9H).

**<sup>13</sup>C NMR** (100 MHz, CDCl<sub>3</sub>, δ): 153.7, 150.8, 146.8, 145.4, 139.4, 133.4, 130.0, 129.8, 126.7, 122.1, 81, 74.2, 28.4, 28.1, 21.2

**MS (ESI):** 339 [M-Boc]

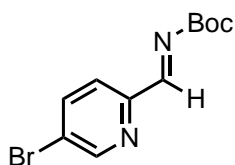


**Figure A.49**  $^1\text{H}$  NMR spectrum (400 MHz,  $\text{CDCl}_3$ ) for **NBoc-sulfone-3**



**Figure A.50**  $^{13}\text{C}$  NMR spectrum (100 MHz,  $\text{CDCl}_3$ ) for NBoc-sulfone-3.





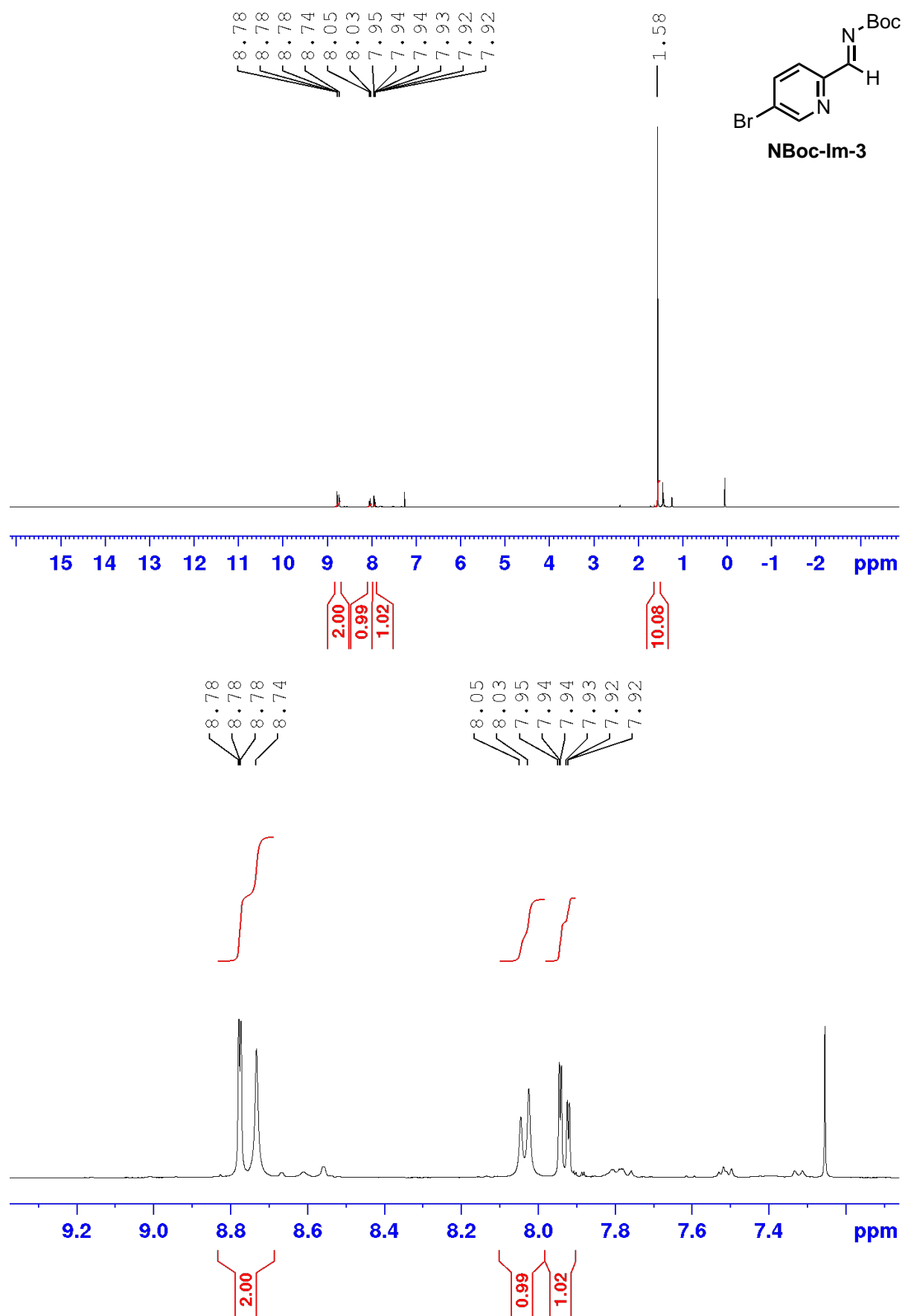
**NBoc-Im-3**

***tert-butyl (E)-((5-bromopyridin-2-yl)methylene)carbamate (NBoc-Im3)***

**<sup>1</sup>H NMR** (400 MHz, CDCl<sub>3</sub>, δ): 8.76 (m 1H), 8.74 (s, 1H), 8.03 (d, *J* = 8.4 Hz, 1H), 7.93 (dd, *J* = 8.4, 2.3 Hz, 1H), 1.58 (s, 9H)

**<sup>13</sup>C NMR** (100 MHz, CDCl<sub>3</sub>, δ): 167.7, 161.8, 151.4, 139.6, 129.9, 124.8, 123.6, 83.2, 28.0

**MS (ESI):** 285 [M+H]



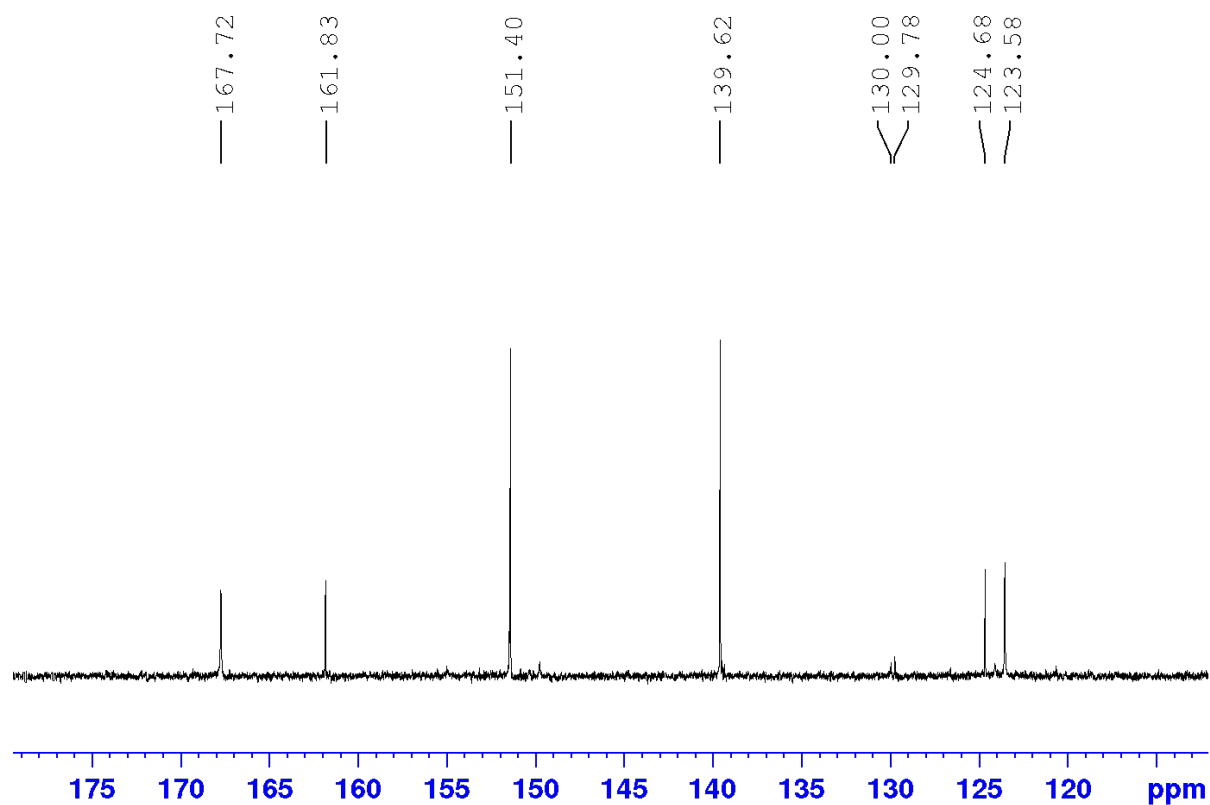
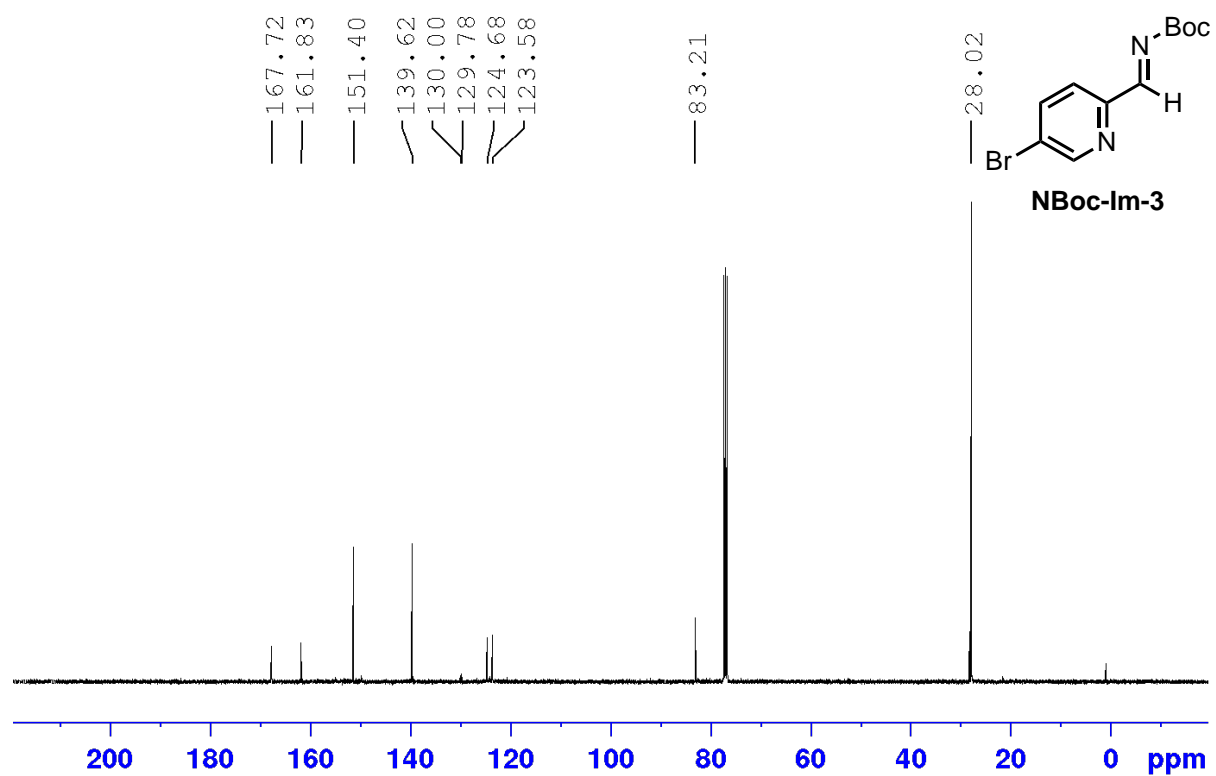
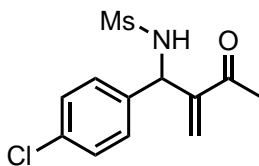


Figure A.52 <sup>13</sup>C NMR spectrum (100 MHz, CDCl<sub>3</sub>) for NBoc-Im3.



**NMs-MBH-1**

***N*-(1-(4-chlorophenyl)-2-methylene-3-oxobutyl)methanesulfonamide (NMs-MBH-1)**

**<sup>1</sup>H NMR** (100 MHz, CDCl<sub>3</sub>, δ): 7.27 (m, 4H), 6.28 (s, 1H), 6.15 (s, 1H), 5.71 (d, *J* = 9.0 Hz, 1H), 5.43 (d, *J* = 9.0 Hz, 1H), 2.87 (s, 3H), 2.33 (s, 3H).

**<sup>13</sup>C NMR** (100 MHz, CDCl<sub>3</sub>, δ): δ 199.0, 147.3, 137.9, 133.9, 129.3, 129.0, 128.7, 128.1, 58.4, 41.9, 26.7

**MS (ESI):** 333.1 [M+2Na-H]

**Chiral HPLC:** 60:40 Hex/*i*-PrOH, Whelk-01 Column, RT<sub>1</sub> 15.50 min, RT<sub>2</sub> 18.00 min

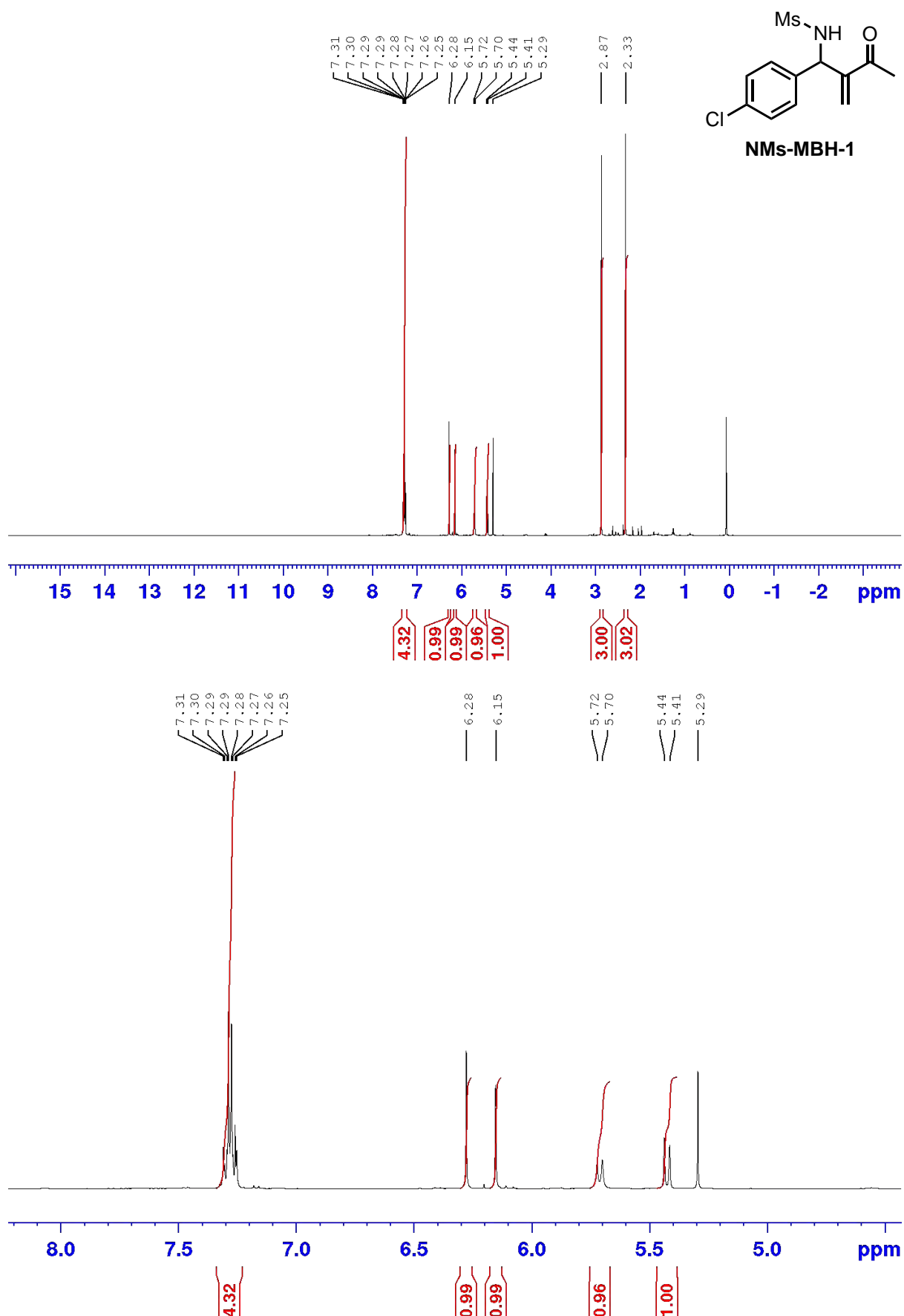
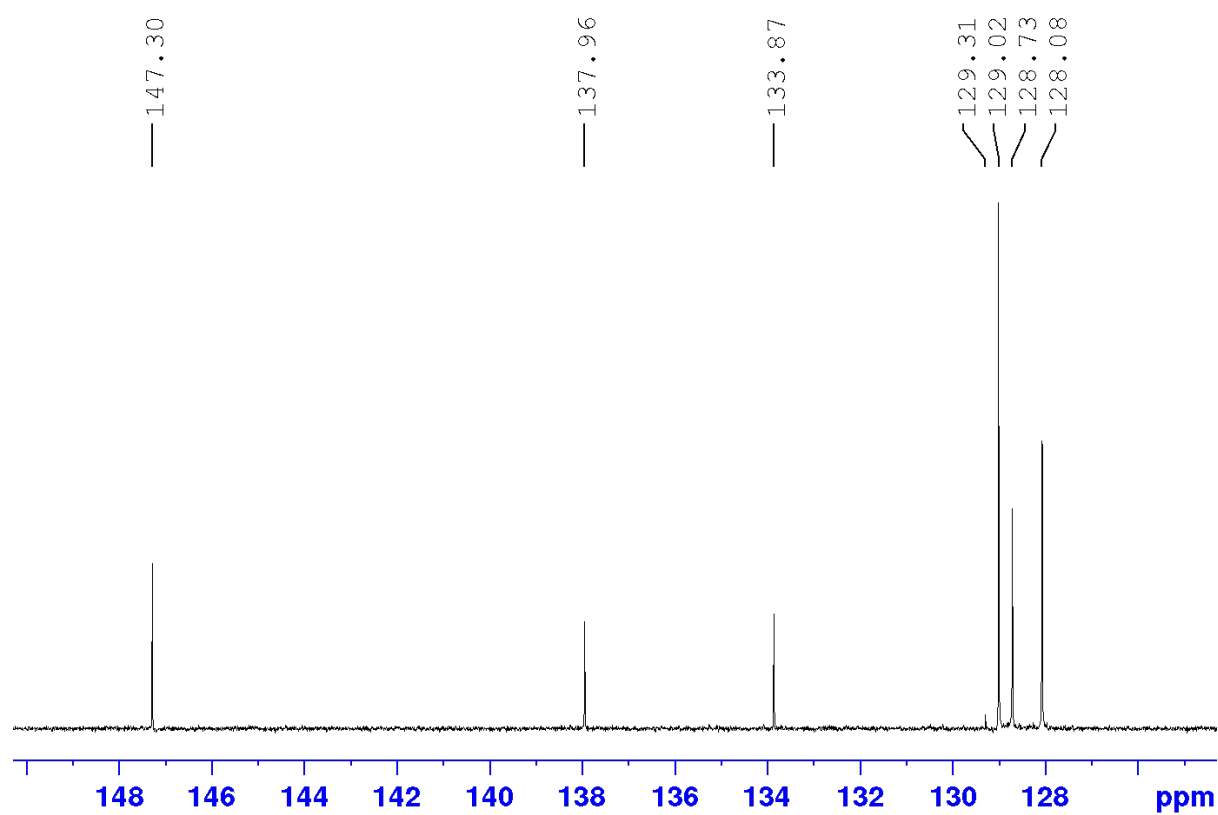
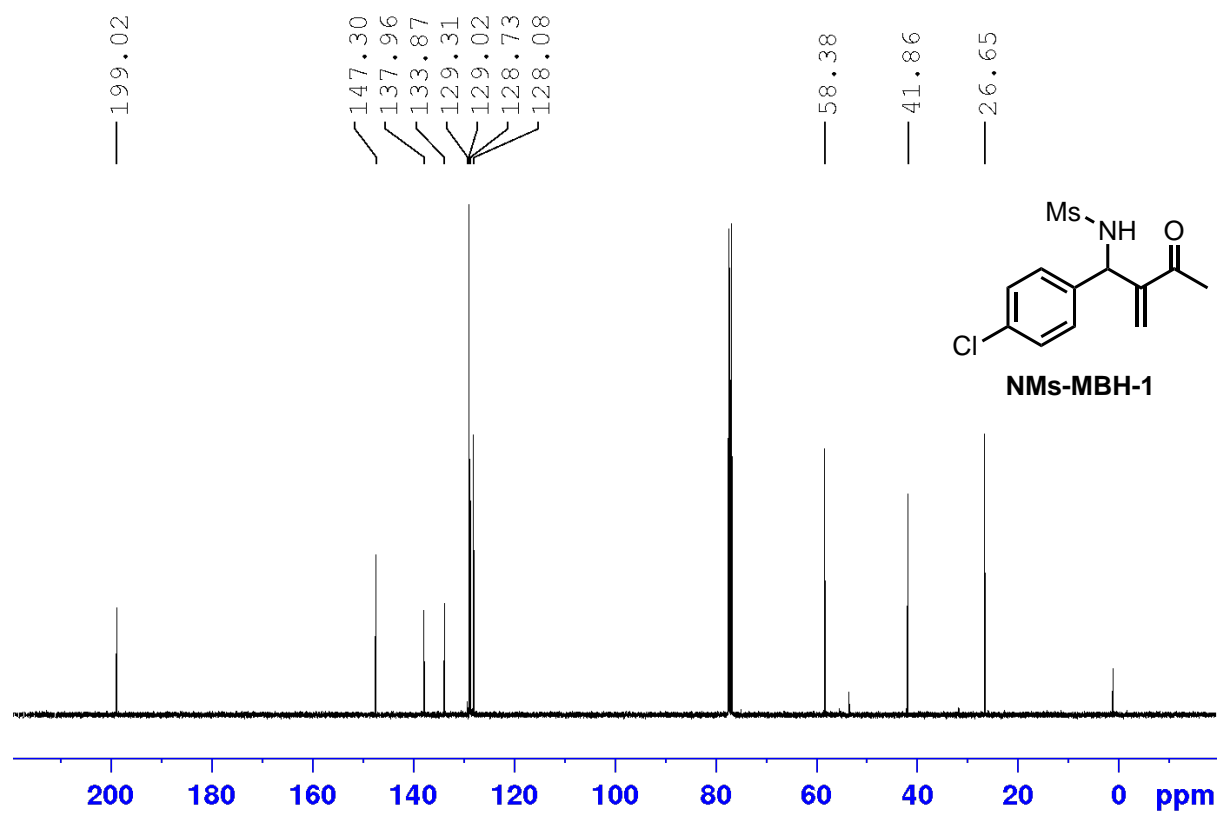
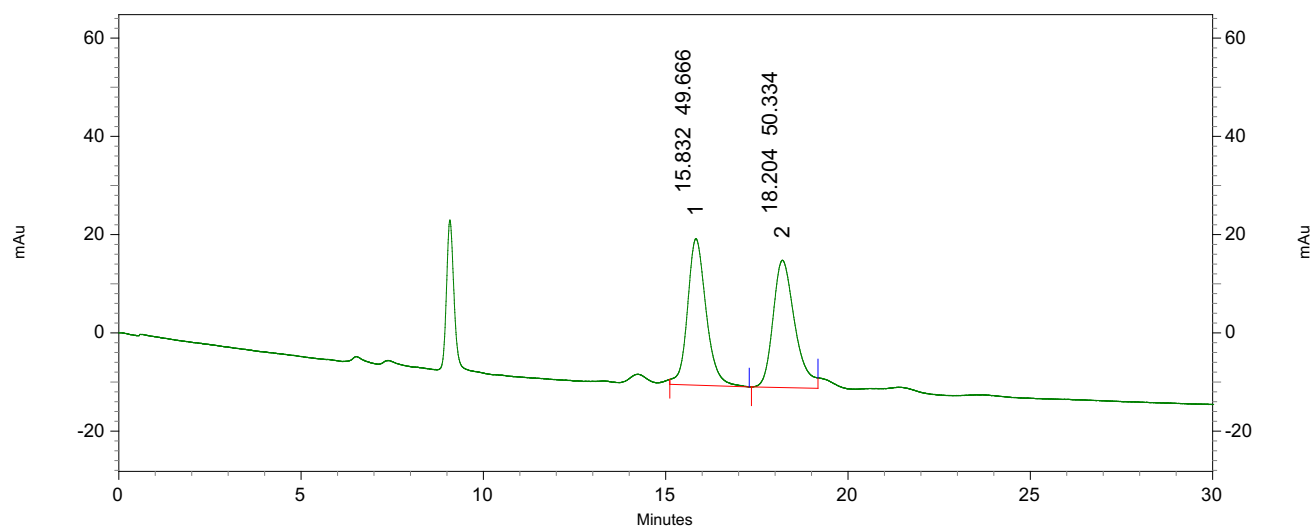


Figure A.53  $^1\text{H}$  NMR spectrum (400 MHz,  $\text{CDCl}_3$ ) for NMs-MBH-1.-



**Figure A.54**  $^{13}\text{C}$  NMR spectrum (100 MHz,  $\text{CDCl}_3$ ) for NMs-MBH-1.

### Racemic HPLC Trace

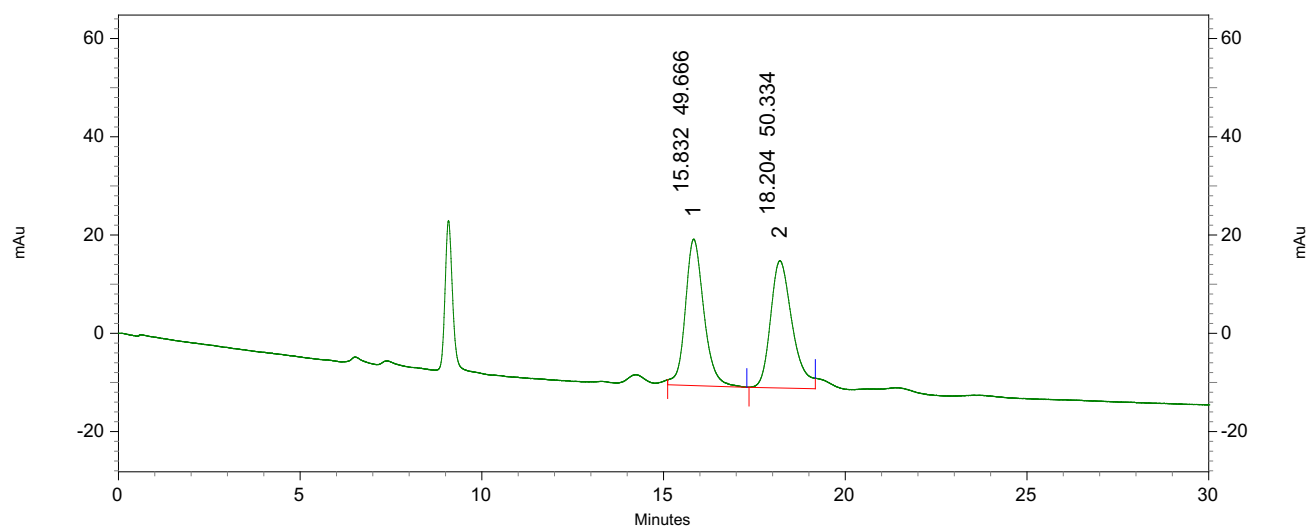


#### 4: 220 nm, 4 nm Results

| Pk # | Retention Time | Area    | Area % |
|------|----------------|---------|--------|
| 1    | 15.832         | 1057718 | 49.67  |
| 2    | 18.204         | 1071929 | 50.33  |

|        |  |         |        |
|--------|--|---------|--------|
| Totals |  | 2129647 | 100.00 |
|--------|--|---------|--------|

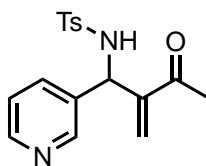
### Chiral HPLC Trace



#### 4: 220 nm, 4 nm Results

| Pk # | Retention Time | Area     | Area % |
|------|----------------|----------|--------|
| 1    | 15.744         | 68238426 | 86.39  |
| 2    | 18.456         | 10754022 | 13.61  |

|        |  |          |        |
|--------|--|----------|--------|
| Totals |  | 78992448 | 100.00 |
|--------|--|----------|--------|



**NTsPyr-MBH-1**

**4-methyl-N-(2-methylene-3-oxo-1-(pyridin-3-yl)butyl)benzenesulfonamide  
(NTsPyr-MBH-1)**

**<sup>1</sup>H NMR** (400 MHz, CDCl<sub>3</sub>, δ): 8.41 (dd, *J* = 4.8 Hz, 1.4 Hz, 1H), 8.30 (d, *J* = 2.7 Hz, 1H), 7.64 (d, *J* = 8.3 Hz, 2H), 7.53 (dt, *J* = 7.8, 1.6 Hz, 1H), 7.23 (d, *J* = 8.3 Hz, 2H), 7.14 (dd, *J* = 7.8 Hz, 4.8 Hz, 1H), 6.13 (s, 1H), 6.10 (s, 1H), 6.07 (d, *J* = 8.6 Hz, 1H), 2.40 (s, 3H), 2.16 (s, 3H).

**<sup>13</sup>C NMR** (CDCl<sub>3</sub>, 100 MHz) δ 198.9, 148.9, 148.2, 145.7, 143.8, 137.5, 134.8, 134.3, 129.8, 129.3, 127.3, 123.4, 57.4, 26.3, 21.6.

**MS (ESI):** 331.1 [M+ H]

**Chiral HPLC:** 80:20 Hex/*i*-PrOH, Chiralpak AD-H, RT<sub>1</sub> 36.40 min, RT<sub>2</sub> 38.54 min



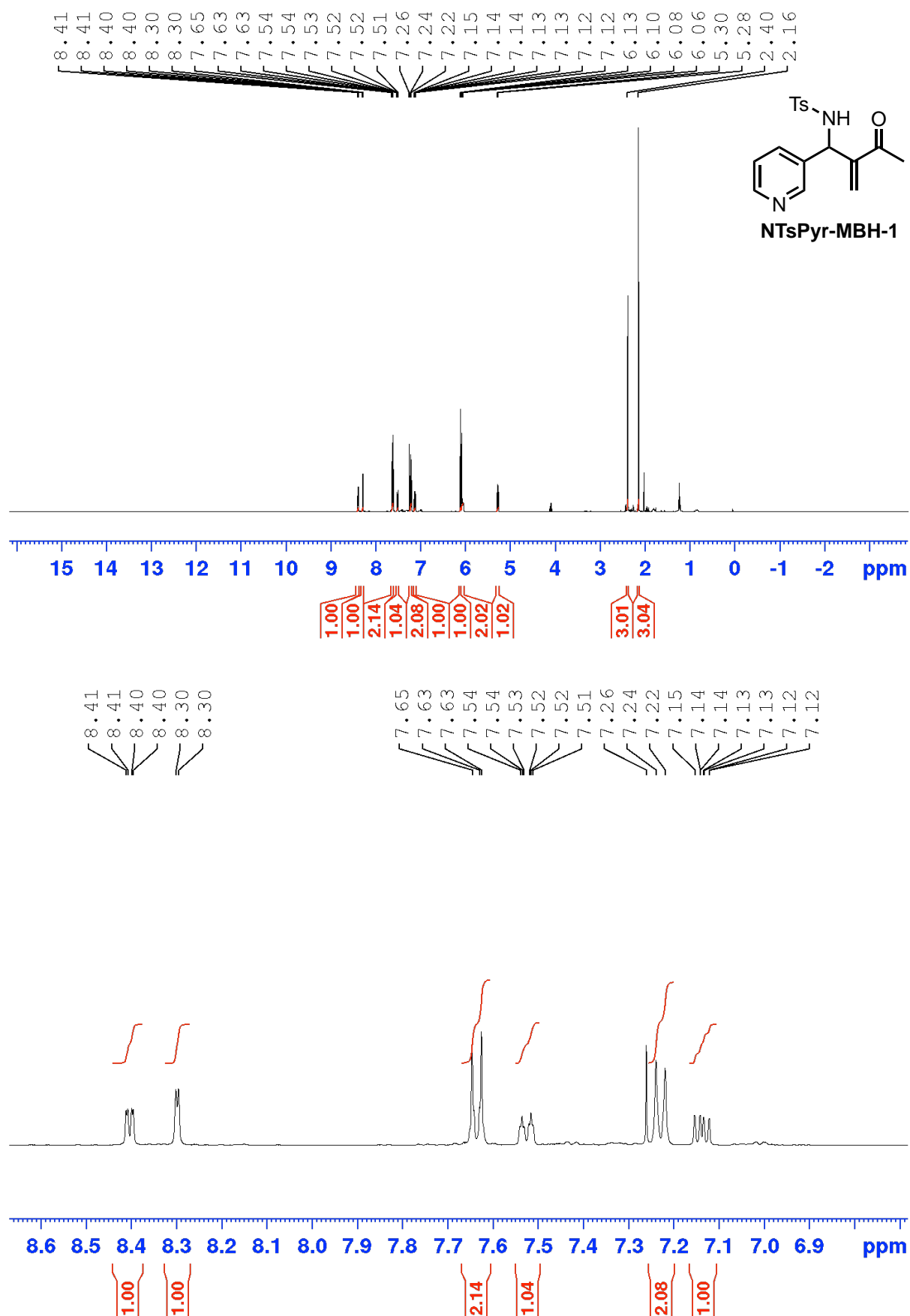


Figure A.55 <sup>1</sup>H NMR spectrum (400 MHz, CDCl<sub>3</sub>) for NTsPyr-MBH-1.

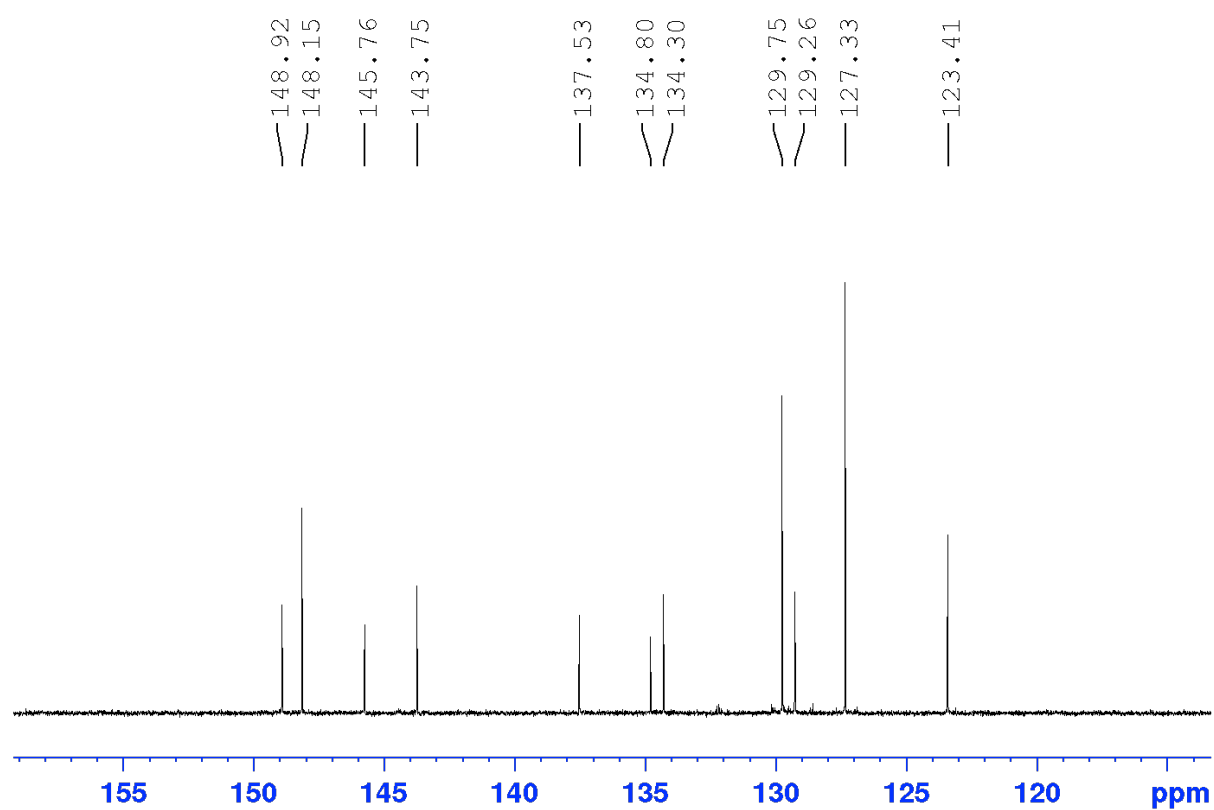
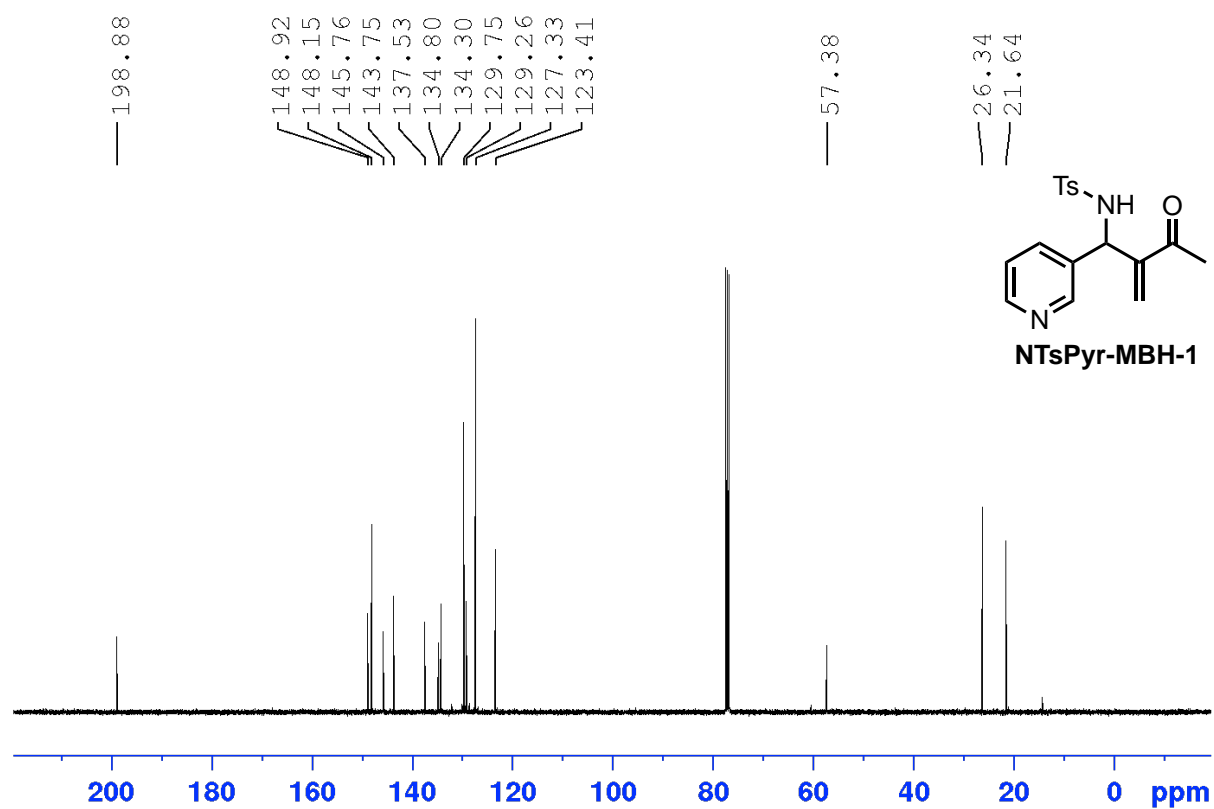
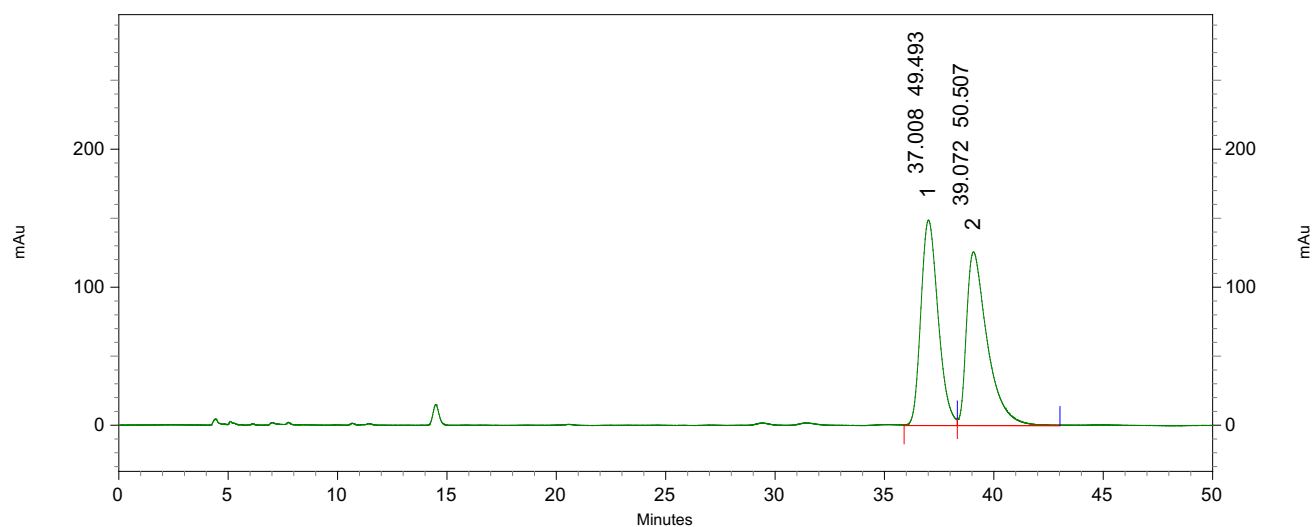


Figure A.56  $^{13}\text{C}$  NMR spectrum (100 MHz,  $\text{CDCl}_3$ ) for NTsPyr-MBH-1.

### Racemic HPLC Trace

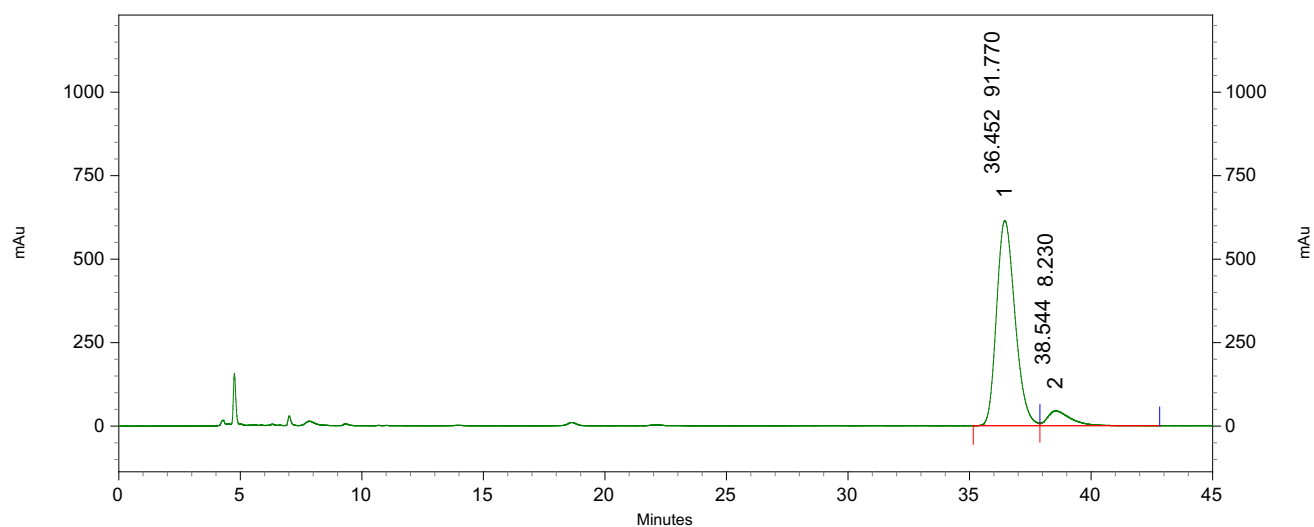


#### 4: 220 nm, 4 nm Results

| Pk # | Retention Time | Area    | Area % |
|------|----------------|---------|--------|
| 1    | 37.008         | 8157256 | 49.49  |
| 2    | 39.072         | 8324405 | 50.51  |

|        |  |          |        |
|--------|--|----------|--------|
| Totals |  | 16481661 | 100.00 |
|--------|--|----------|--------|

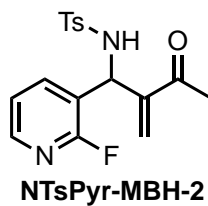
### Chiral HPLC Trace



#### 4: 220 nm, 4 nm Results

| Pk # | Retention Time | Area     | Area % |
|------|----------------|----------|--------|
| 1    | 36.452         | 32355929 | 91.77  |
| 2    | 38.544         | 2901823  | 8.23   |

|        |  |          |        |
|--------|--|----------|--------|
| Totals |  | 35257752 | 100.00 |
|--------|--|----------|--------|



***N*-(1-(2-fluoropyridin-3-yl)-2-methylene-3-oxobutyl)-4-methylbenzenesulfonamide (NTsPyr-MBH-2)**

**<sup>1</sup>H NMR** (400 MHz, CDCl<sub>3</sub>, δ): 8.01 (dt, *J* = 4.8, 1.5 Hz, 1H), 7.76 (ddd, *J* = 9.7, 7.8, 1.9 Hz, 1H), 7.63 (d, *J* = 8.3 Hz, 2H), 7.19 (d, *J* = 8.1 Hz, 2H), 7.04 (ddd, *J* = 7.4, 4.9, 1.8 Hz, 1H), 6.14 (s, 1H), 6.10 (s, 1H), 5.40 (br, 1H), 2.37 (s, 3H), 2.17 (s, 3H)

**<sup>13</sup>C NMR** (100 MHz, CDCl<sub>3</sub>, δ): 199.2, 146.8, 146.6, 144.4, 143.8, 140.0, 139.9, 137.4, 129.8, 129.7, 127.2, 121.6, 121.5, 121.4, 121.2, 54.2, 26.3, 21.6

**MS (ESI):** 349.1 [M+ H]

**Chiral HPLC:** 80:20 Hex/*i*-PrOH, Chiralpak AD-H Column, RT<sub>1</sub>: 21.46 min, RT<sub>2</sub>: 25.49 min

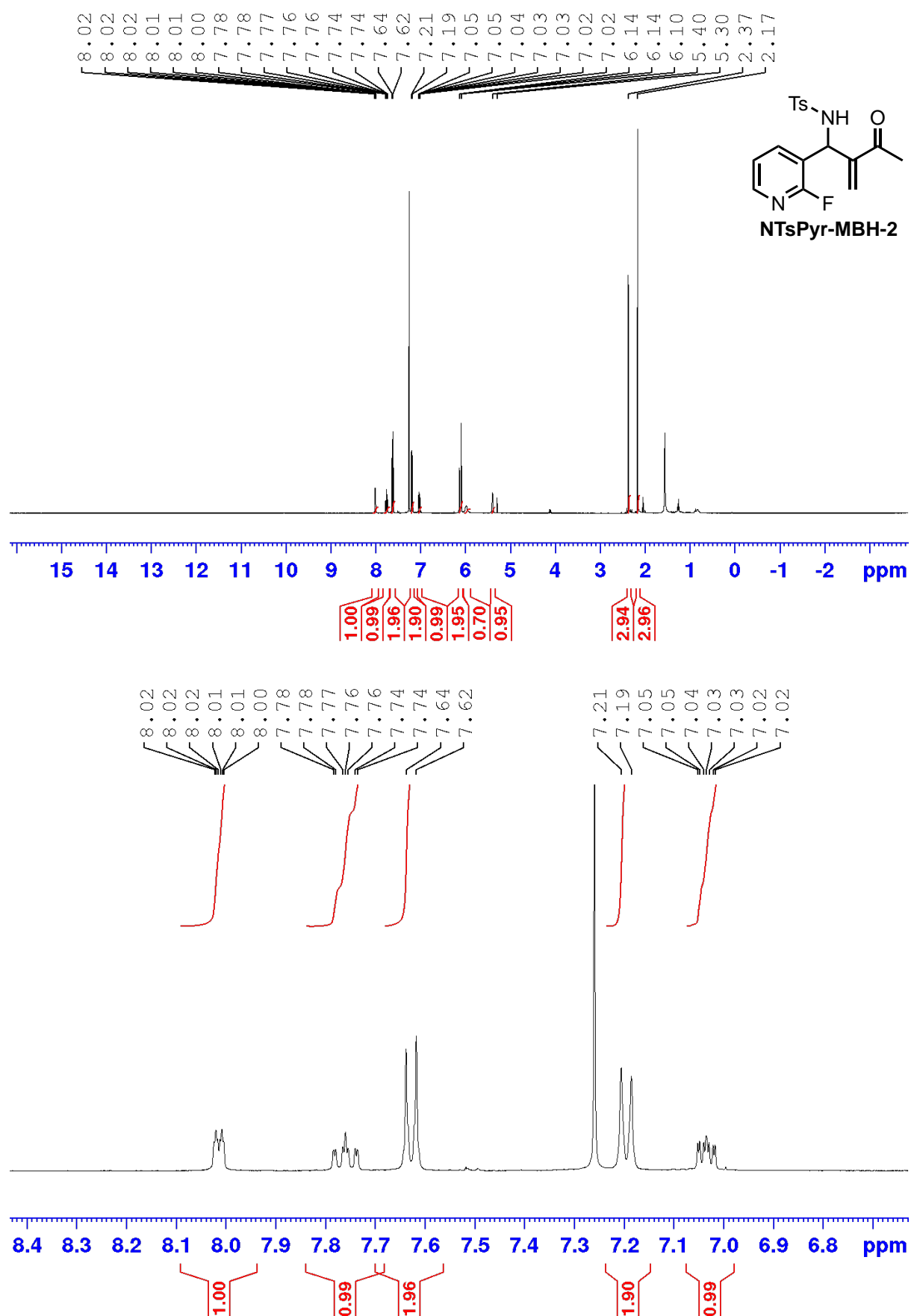


Figure A.57 <sup>1</sup>H NMR spectrum (400 MHz, CDCl<sub>3</sub>) for NTsPyr-MBH-2.

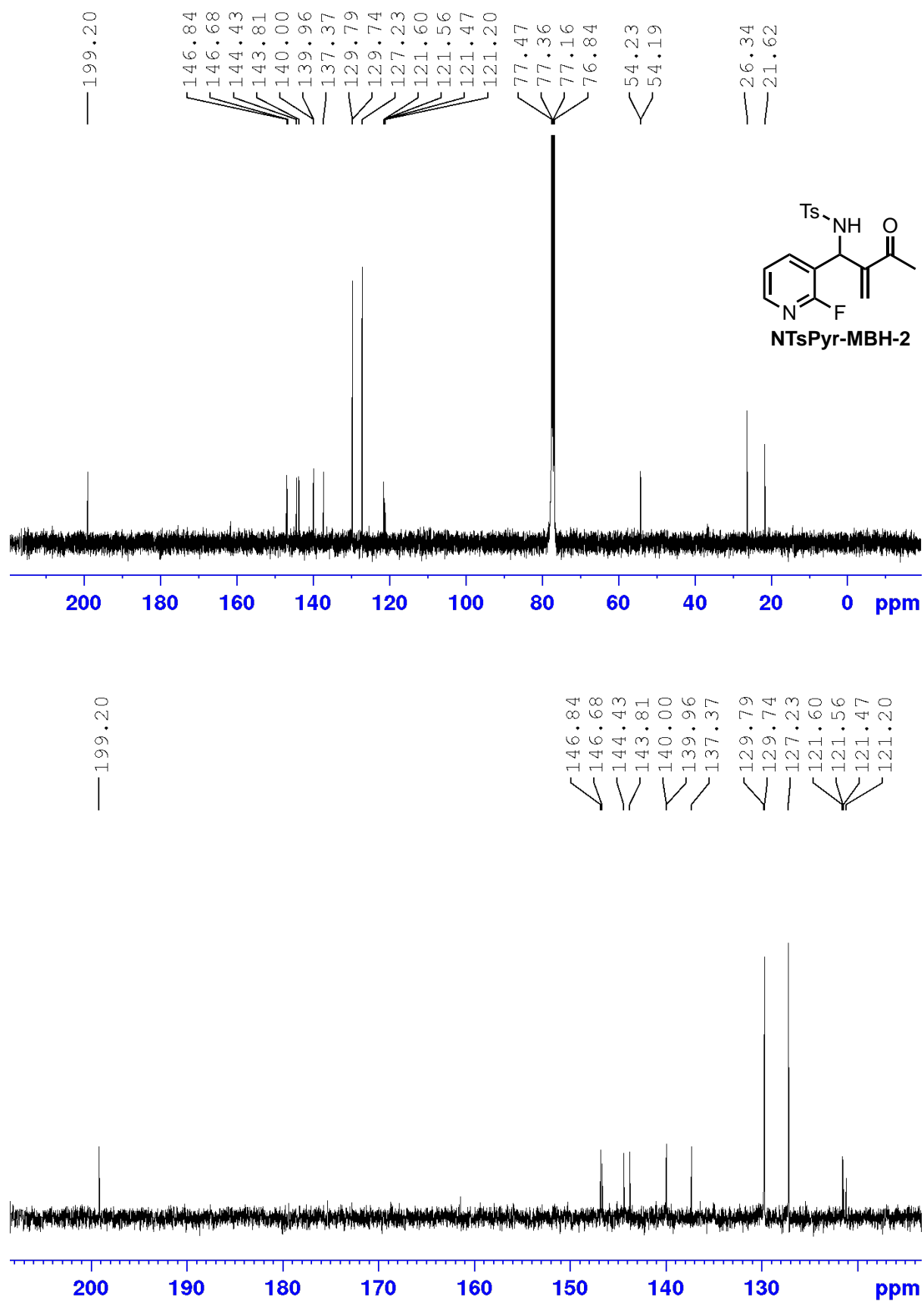
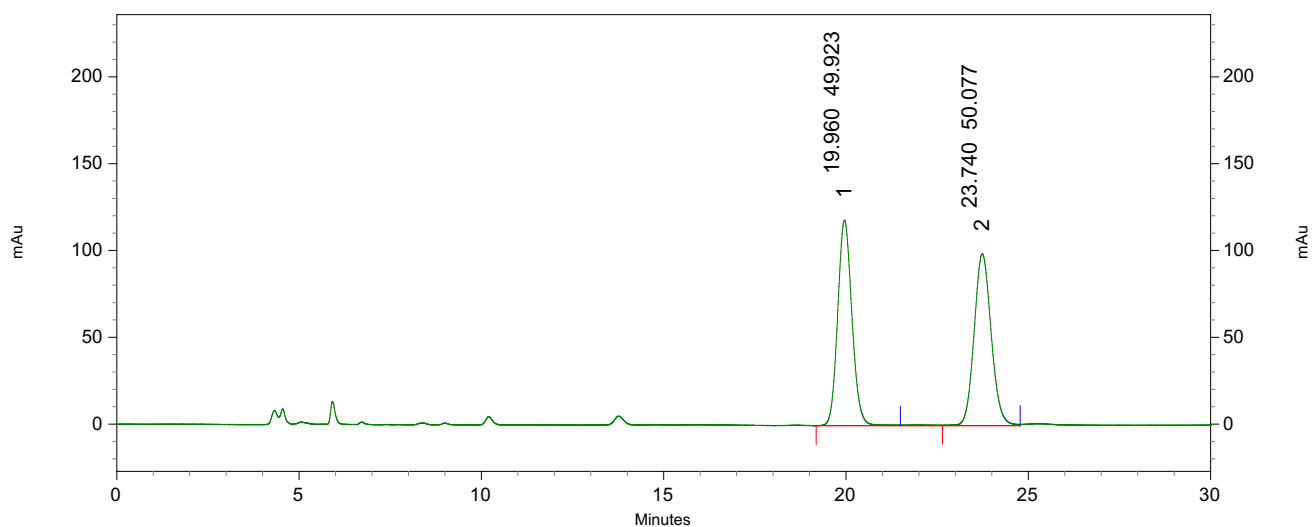


Figure A.58 <sup>13</sup>C NMR spectrum (100 MHz, CDCl<sub>3</sub>) for NTsPyr-MBH-2.

### Racemic HPLC Trace

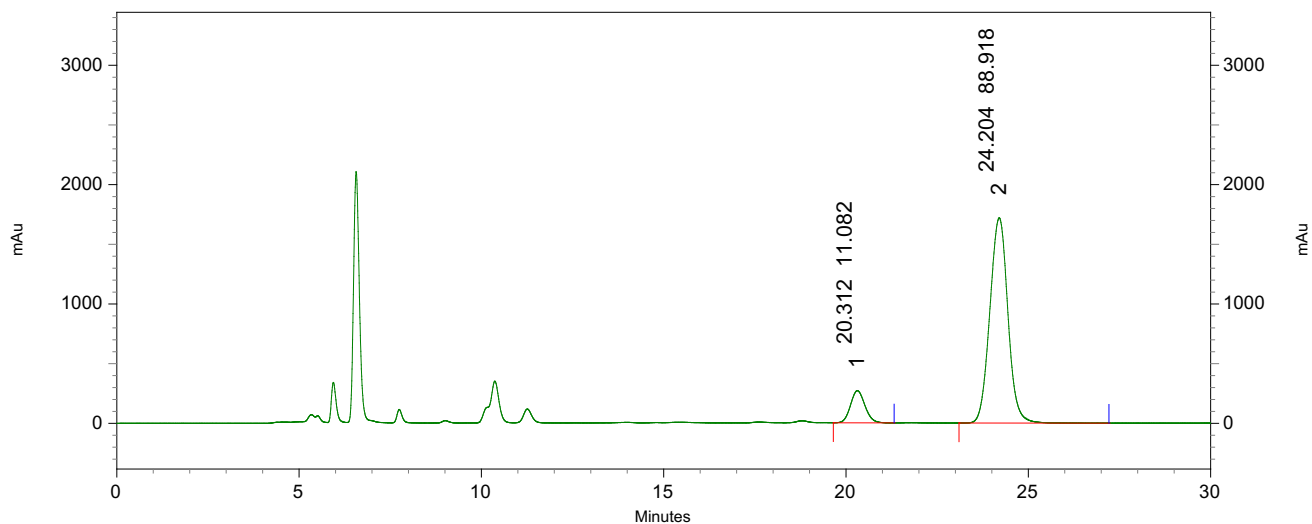


#### 4: 220 nm, 4 nm Results

| Pk # | Retention Time | Area    | Area % |
|------|----------------|---------|--------|
| 1    | 19.960         | 3209803 | 49.92  |
| 2    | 23.740         | 3219762 | 50.08  |

|        |  |         |        |
|--------|--|---------|--------|
| Totals |  | 6429565 | 100.00 |
|--------|--|---------|--------|

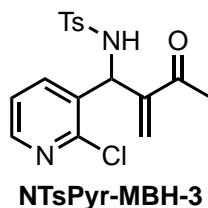
### Chiral HPLC Trace



#### 4: 220 nm, 4 nm Results

| Pk # | Retention Time | Area     | Area % |
|------|----------------|----------|--------|
| 1    | 20.312         | 7375528  | 11.08  |
| 2    | 24.204         | 59179757 | 88.92  |

|        |  |          |        |
|--------|--|----------|--------|
| Totals |  | 66555285 | 100.00 |
|--------|--|----------|--------|



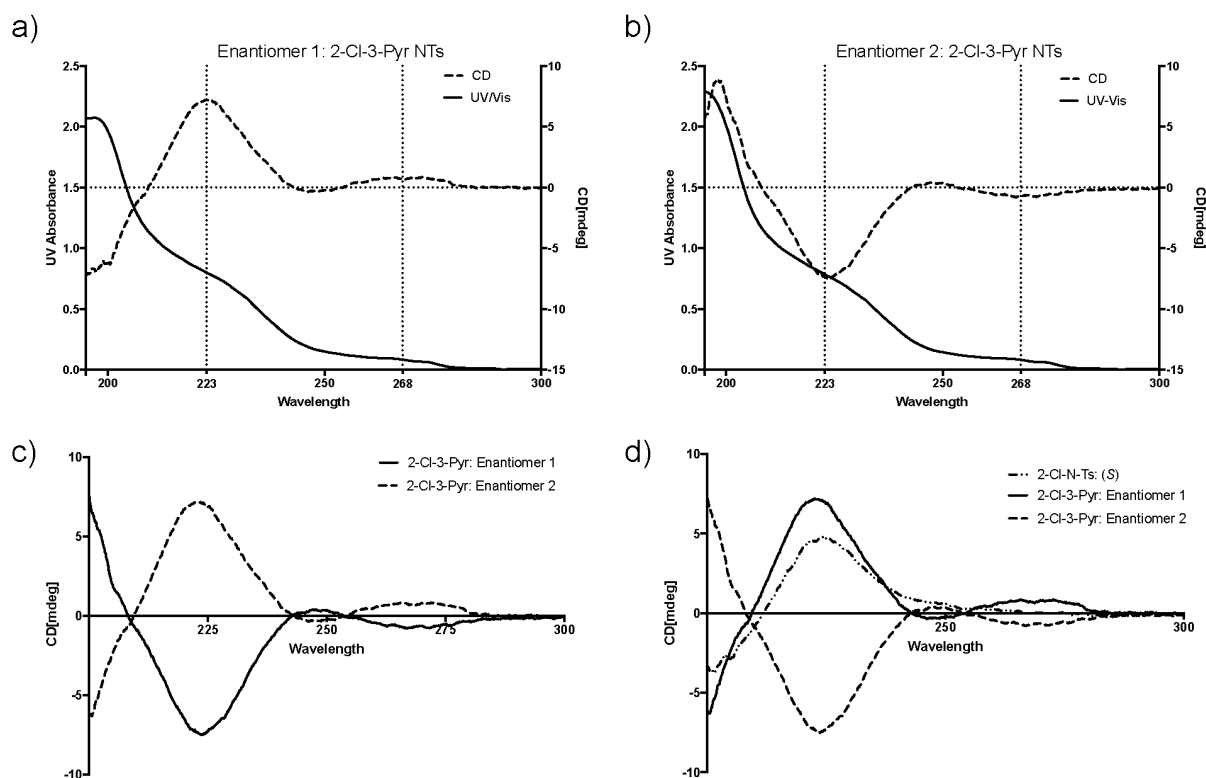
***N*-(1-(2-chloropyridin-3-yl)-2-methylene-3-oxobutyl)-4-methylbenzenesulfonamide (NTsPyr-MBH-3)**

**<sup>1</sup>H NMR** (400 MHz, CDCl<sub>3</sub>, δ): 8.19 (dd, *J* = 4.7, 1.9 Hz, 1H), 7.76 (dd, *J* = 7.9, 1.9 Hz, 1H), 7.61 (d, *J* = 8.3 Hz, 2H), 7.17 (d, *J* = 8.3 Hz, 2H), 7.08 (dd, *J* = 7.7, 4.7 Hz, 1H), 6.16 (s, 1H), 6.00 (b, 1H), 5.53 (d, *J* = 9.2 Hz, 1H), 2.36 (s, 2H), 2.19 (s, 3H)

**<sup>13</sup>C NMR** (100 MHz, CDCl<sub>3</sub>, δ): 199.3, 149.5, 148.7, 143.9, 143.8, 138.5, 137.2, 132.9, 130.9, 129.7, 127.3, 122.6, 56.5, 26.5, 21.6.

**MS (ESI):** 365.1 [M+ H]

**Chiral HPLC:** 80:20 Hex/*i*-PrOH, Chiralpak AD-H Column, RT<sub>1</sub>: 21.46 min, RT<sub>2</sub>: 25.49 min



**Figure A.59** CD Spectra for isolated enantiomers for **NTsPyr-MBH-3** a) First eluting enantiomer. b) Second eluting enantiomer. c) Comparison of CD traces for (*R*)- and (*S*)-**NTsPyr-MBH-3**. d) Comparison of **NTsPyr-MBH-3** with (*R*)-**NTs-MBH-5** adducts.



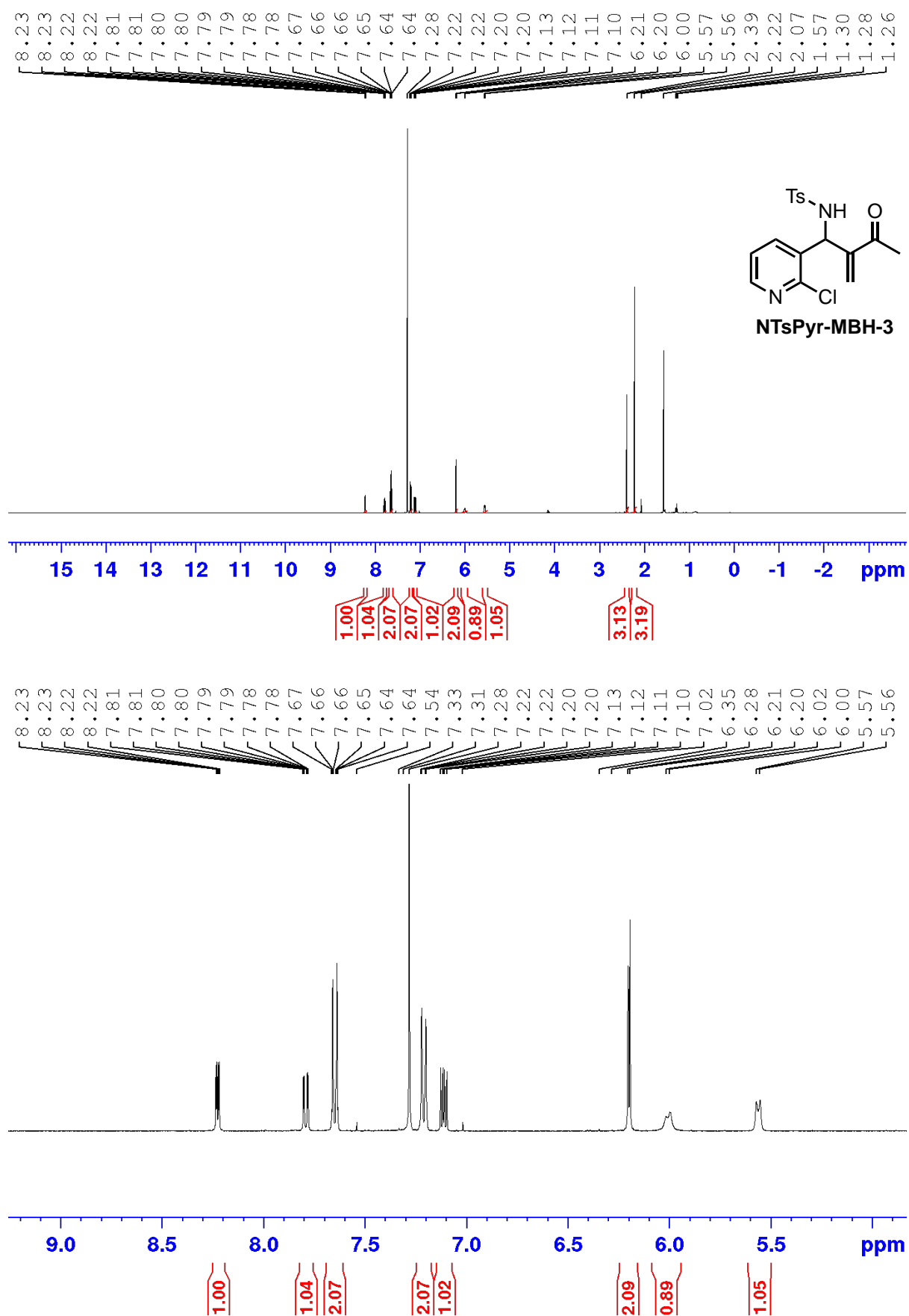
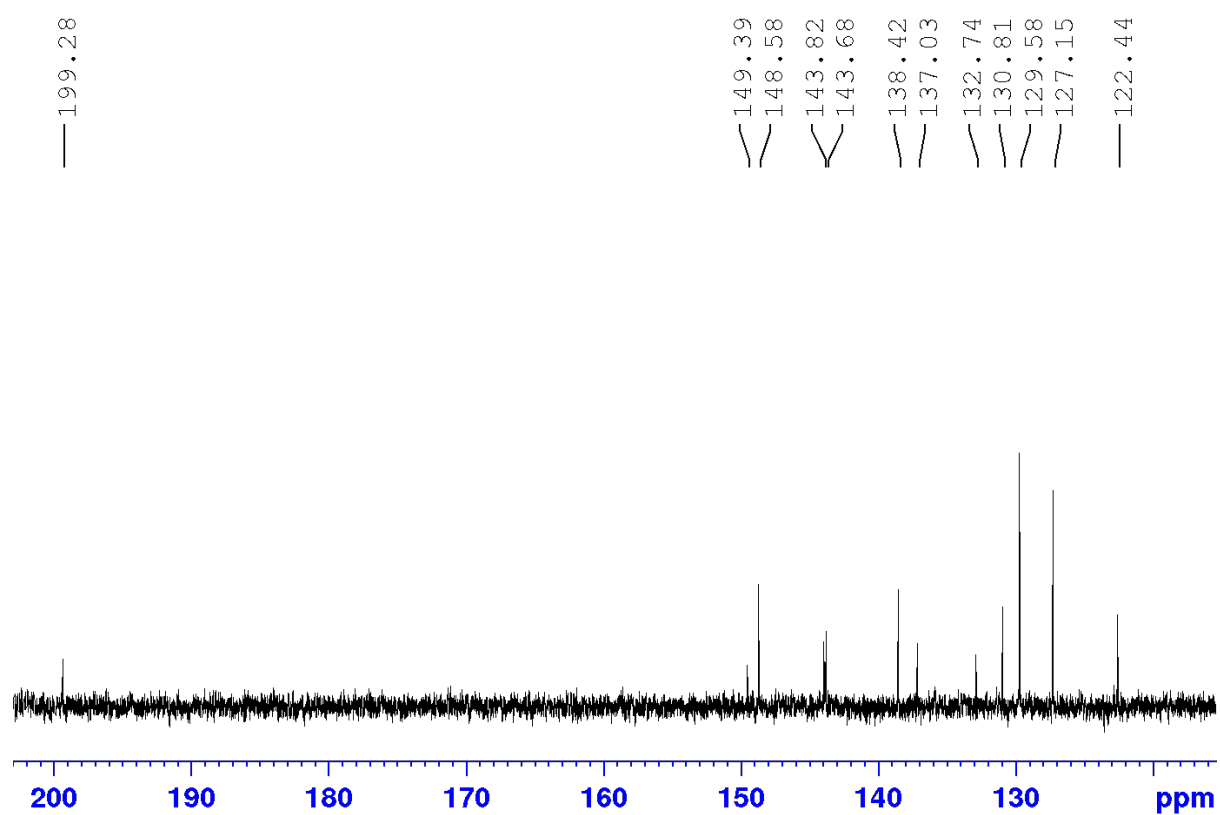
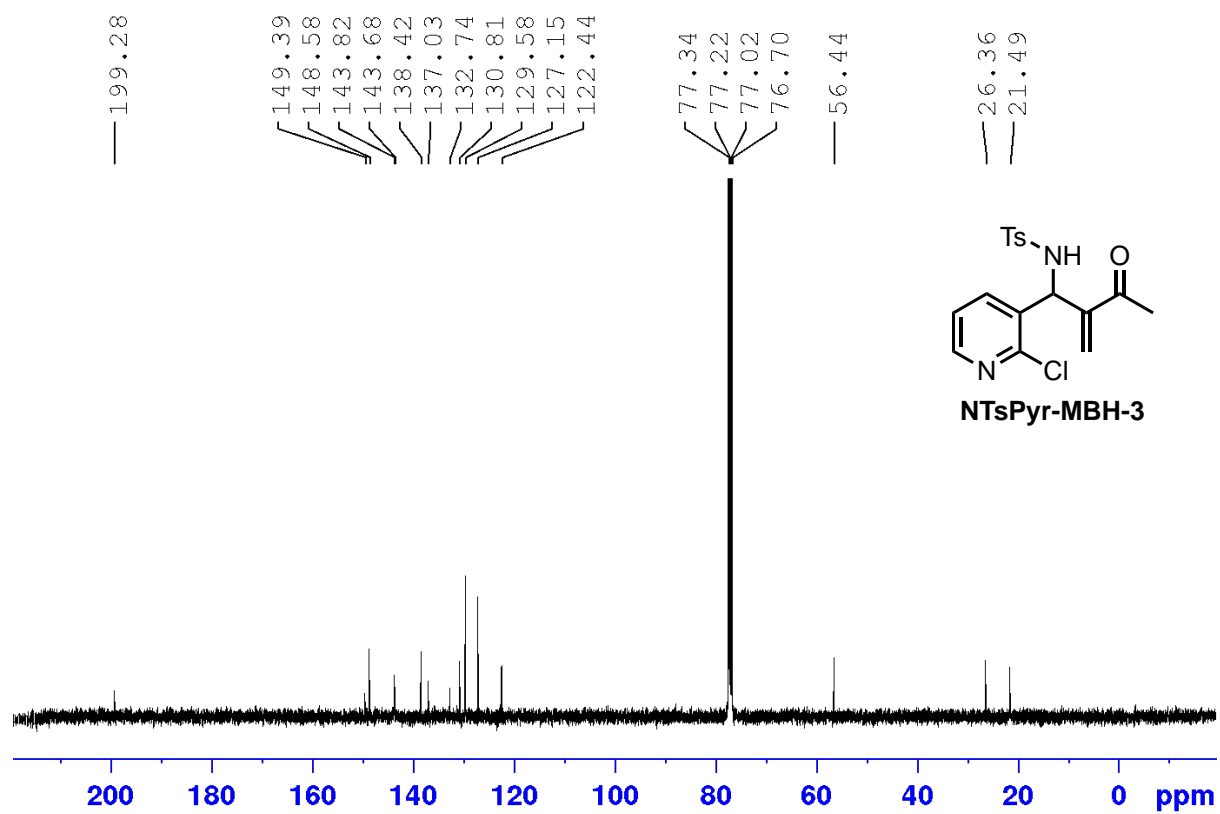
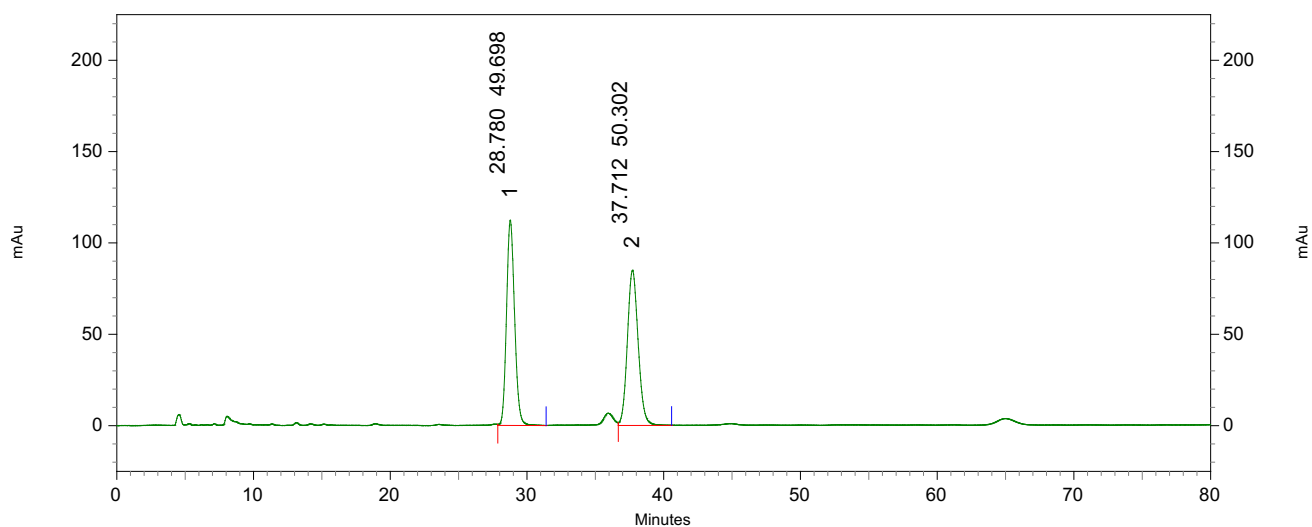


Figure A.60 <sup>1</sup>H NMR spectrum (400 MHz, CDCl<sub>3</sub>) for NTsPyr-MBH-3.



**Figure A.61** <sup>13</sup>C NMR spectrum (100 MHz, CDCl<sub>3</sub>) for NTsPyr-MBH-3.

### Racemic HPLC Trace

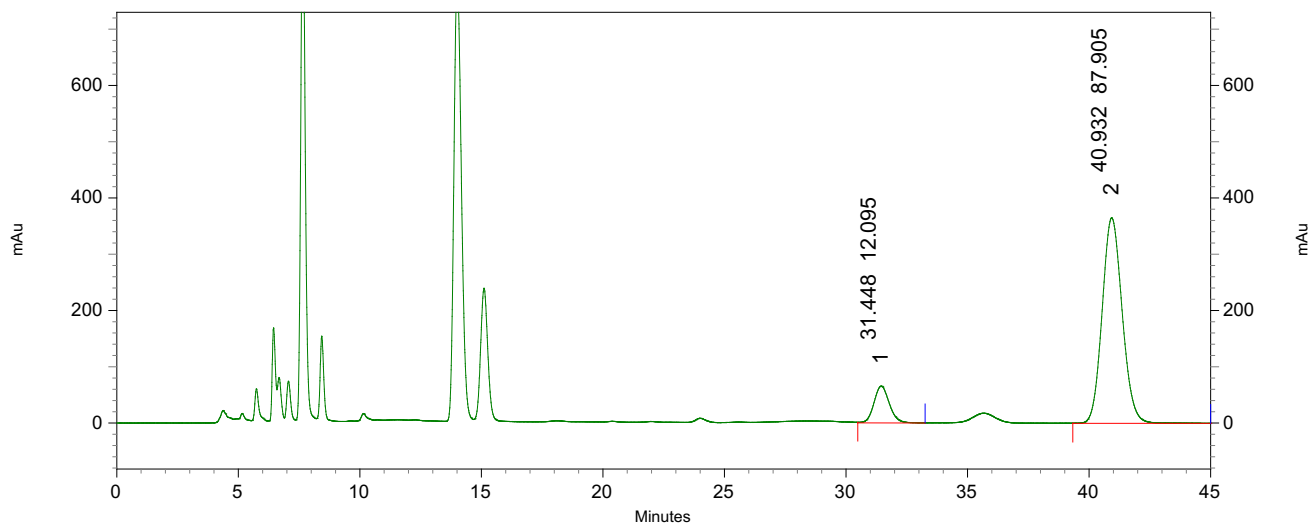


#### 4: 220 nm, 4 nm Results

| Pk # | Retention Time | Area    | Area % |
|------|----------------|---------|--------|
| 1    | 28.780         | 4617709 | 49.70  |
| 2    | 37.712         | 4673817 | 50.30  |

|        |  |         |        |
|--------|--|---------|--------|
| Totals |  | 9291526 | 100.00 |
|--------|--|---------|--------|

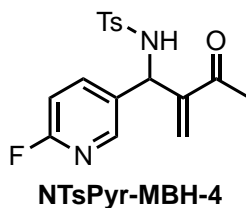
### Chiral HPLC Trace



#### 4: 220 nm, 4 nm Results

| Pk # | Retention Time | Area     | Area % |
|------|----------------|----------|--------|
| 1    | 31.448         | 2877294  | 12.09  |
| 2    | 40.932         | 20911963 | 87.91  |

|        |  |          |        |
|--------|--|----------|--------|
| Totals |  | 23789257 | 100.00 |
|--------|--|----------|--------|



***N-(1-(6-fluoropyridin-3-yl)-2-methylene-3-oxobutyl)-4-methylbenzenesulfonamide***  
**(NTsPyr-MBH-4)**

**<sup>1</sup>H NMR** (400 MHz, CDCl<sub>3</sub>, δ): 8.26 (m, 1H), 8.14 (m, 1H), 7.26 (d, *J*= 8.0 Hz, 2H), 7.24 (m, 3H), 6.10 (m, 3H), 5.29 (d, *J*= 9.3 Hz, 1H), 2.40 (s, 3H), 2.16 (s, 3H).

**<sup>13</sup>C NMR** (100 MHz, CDCl<sub>3</sub>, δ): 198.8, 160.6, 158.1, 145.4, 143.96, 143.8 (d, 4 Hz), 137.4, 137.4, 137.1, 136.8, 129.8, 129.7, 127.3, 121.3 (d, 19.3 Hz), 57.0, 26.3, 21.6.

**MS (ESI):** 349.1 [M+ H]

**Chiral HPLC:** 80:20 Hex/*i*-PrOH (0.7 mL min<sup>-1</sup>), Chiralpak AD-H Column, RT<sub>1</sub>: 27.35 min, RT<sub>2</sub>: 30.13 min

---

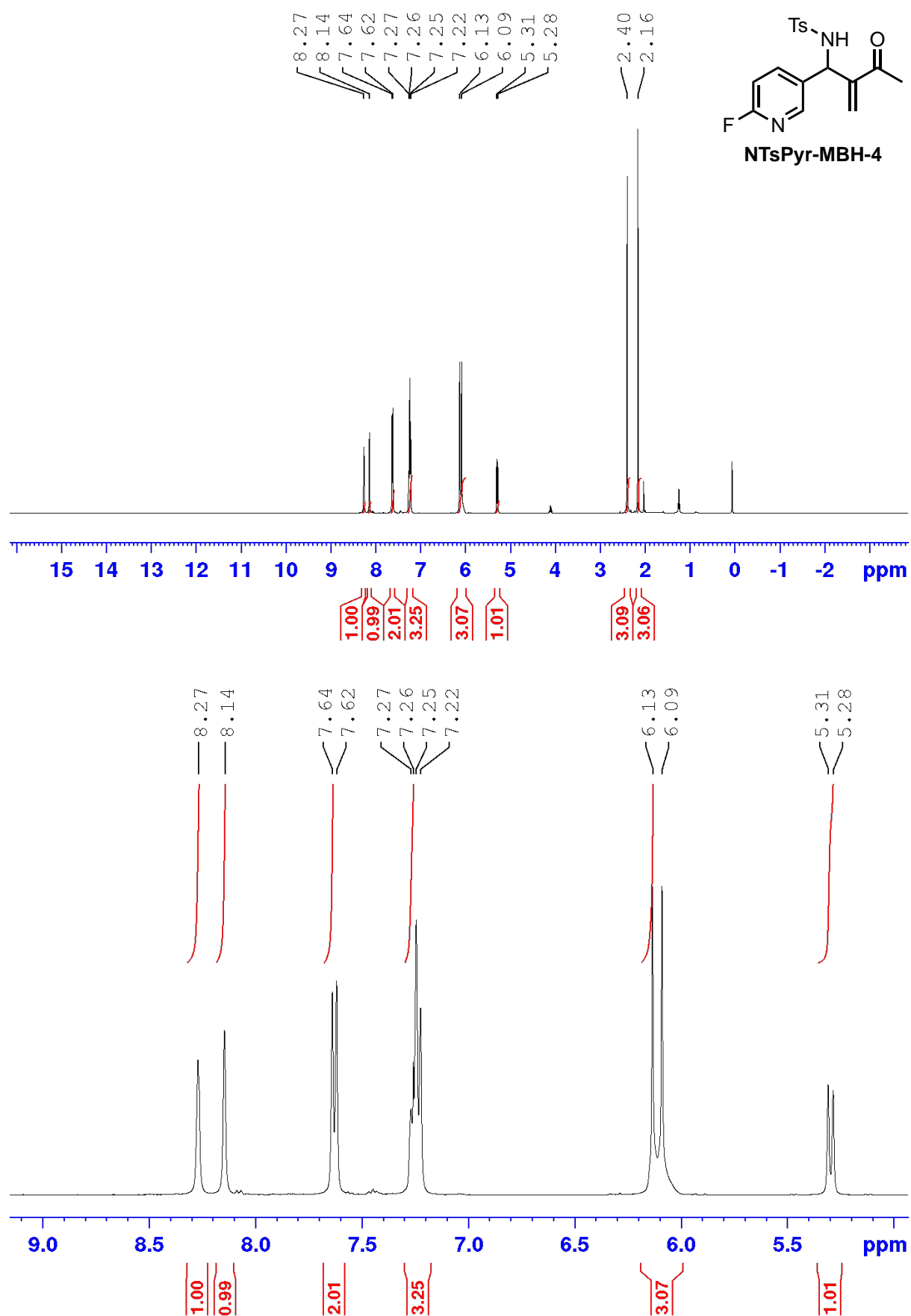
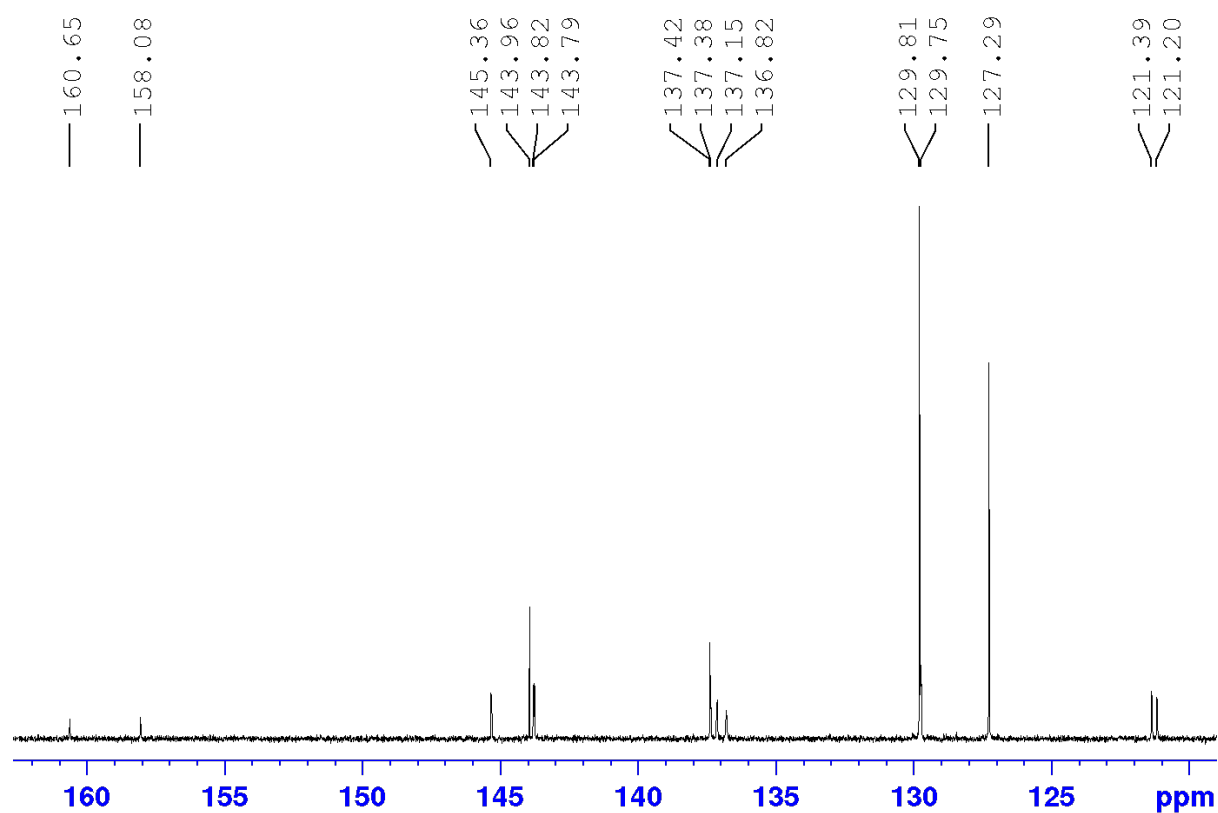
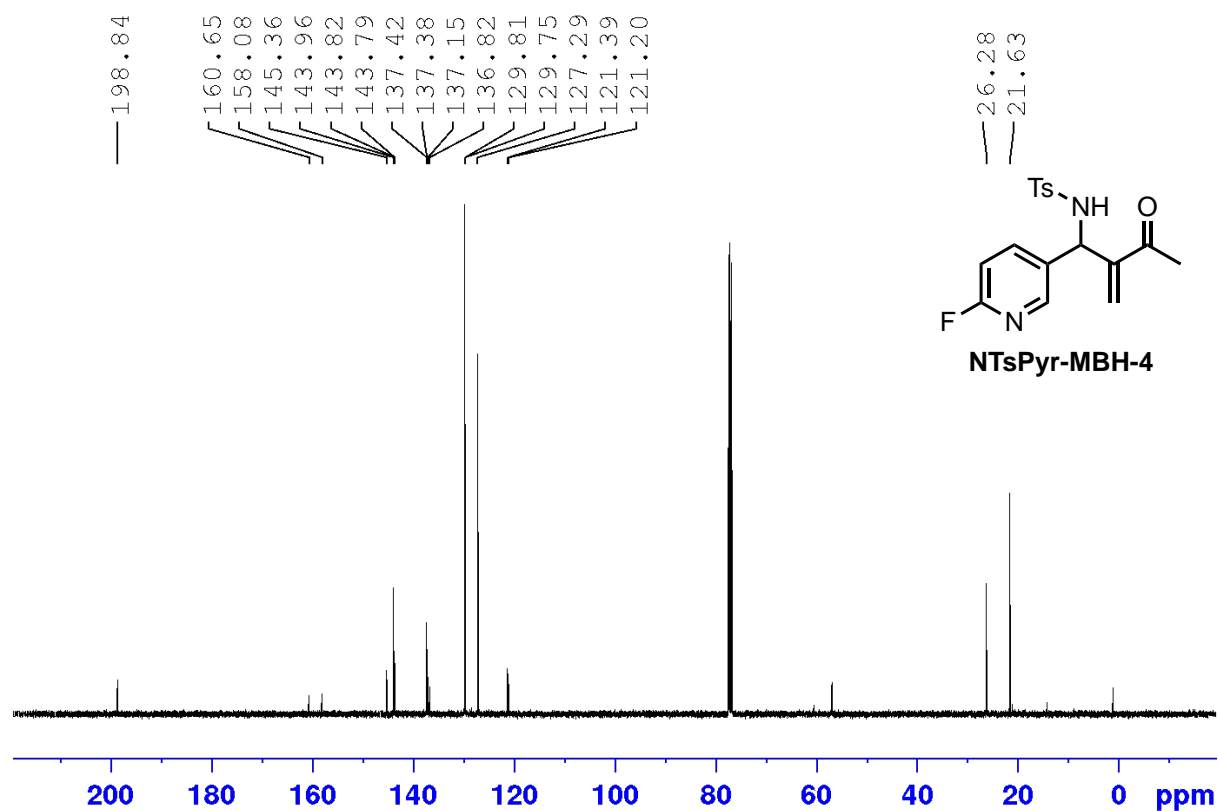
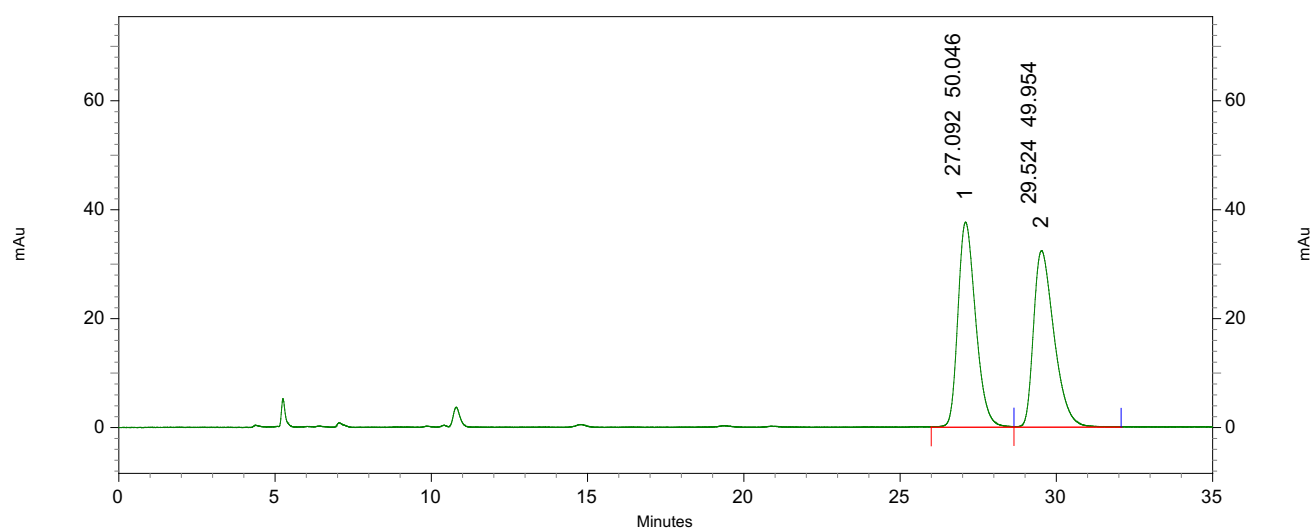


Figure A.62 <sup>1</sup>H NMR spectrum (400 MHz, CDCl<sub>3</sub>) for NTsPyr-MBH-4.



**Figure A.63**  $^{13}\text{C}$  NMR spectrum (100 MHz,  $\text{CDCl}_3$ ) for NTsPyr-MBH-4.

### Racemic HPLC Trace

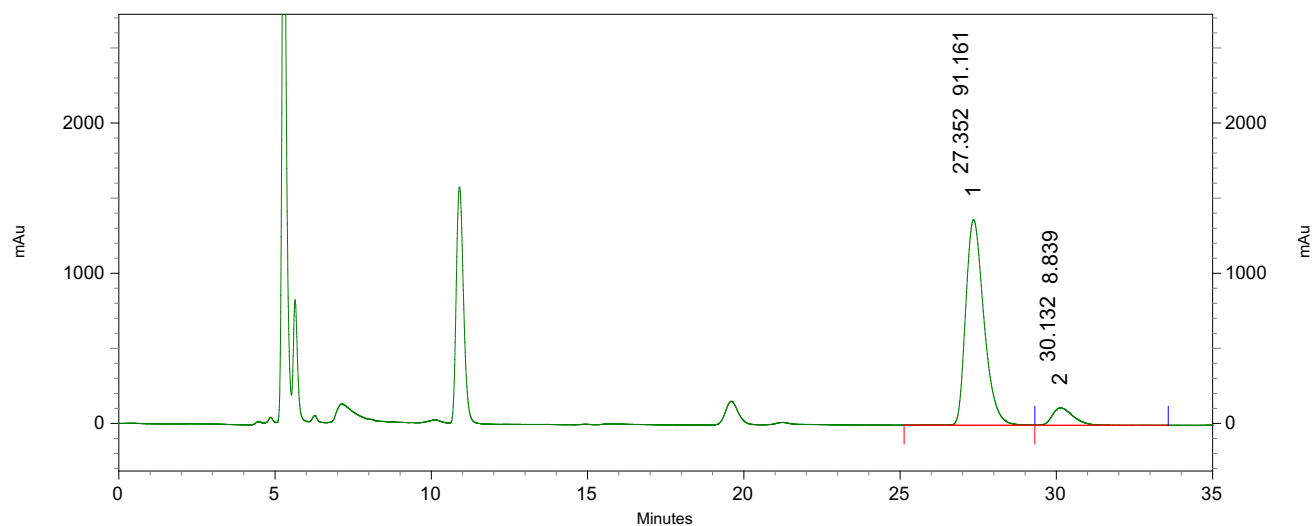


### 3: 254 nm, 4 nm Results

| Pk # | Retention Time | Area    | Area % |
|------|----------------|---------|--------|
| 1    | 27.092         | 1485320 | 50.05  |
| 2    | 29.524         | 1482599 | 49.95  |

|        |  |         |        |
|--------|--|---------|--------|
| Totals |  | 2967919 | 100.00 |
|--------|--|---------|--------|

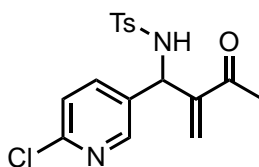
### Chiral HPLC Trace



### 4: 220 nm, 4 nm Results

| Pk # | Retention Time | Area     | Area % |
|------|----------------|----------|--------|
| 1    | 27.352         | 55278108 | 91.16  |
| 2    | 30.132         | 5359453  | 8.84   |

|        |  |          |        |
|--------|--|----------|--------|
| Totals |  | 60637561 | 100.00 |
|--------|--|----------|--------|



**NTsPyr-MBH-5**

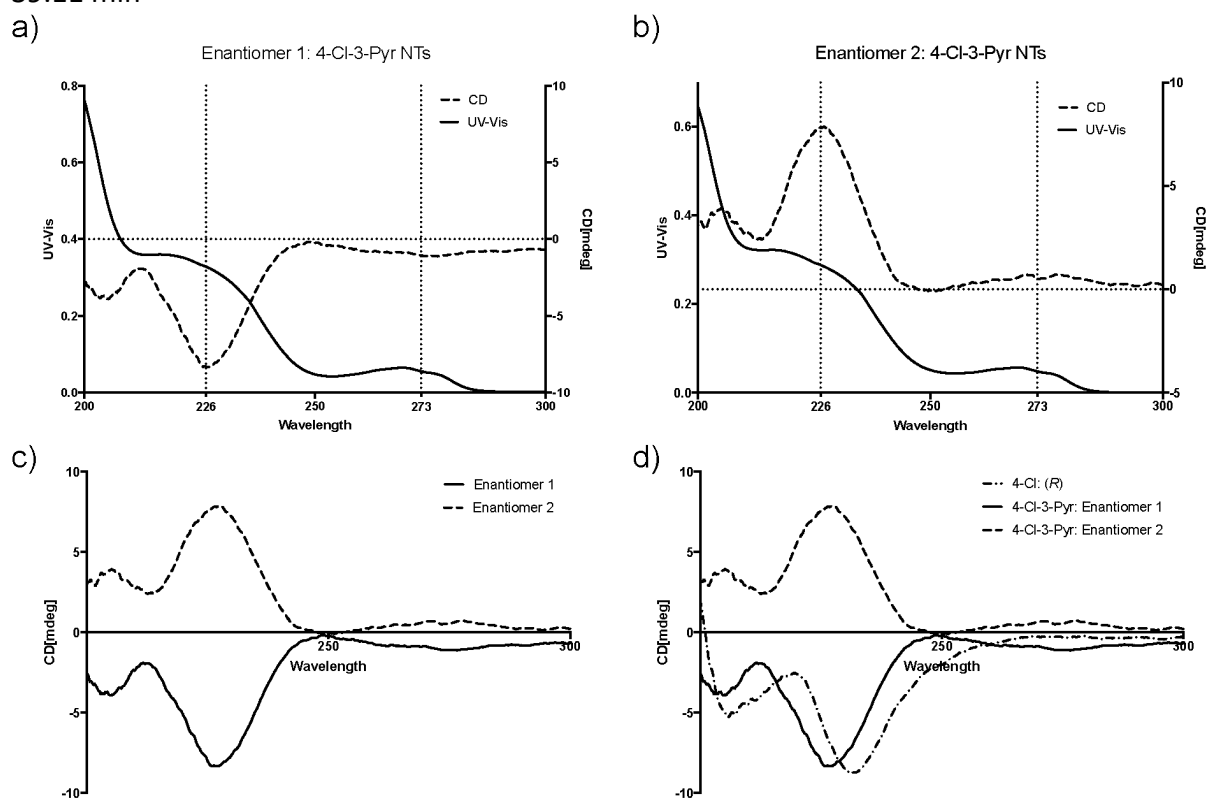
***N*-(1-(6-chloropyridin-3-yl)-2-methylene-3-oxobutyl)-4-methylbenzenesulfonamide (NTsPyr-MBH-5)**

**<sup>1</sup>H NMR** (400 MHz, CDCl<sub>3</sub>, δ): 8.07 (d, *J* = 2.6 Hz, 1H), 7.62 (d, *J* = 8.2 Hz, 2H), 7.50 (dd, *J* = 8.3, 2.5 Hz, 1H), 7.23 (d, *J* = 8.1 Hz, 2H), 7.15 (d, *J* = 8.3 Hz, 1H), 6.12 (s, 1H), 6.08 (s, 1H), 5.99 (b, 1H), 5.26 (d, *J* = 9.3 Hz, 1H), 2.41 (s, 3H), 2.16 (s, 3H).

**<sup>13</sup>C NMR** (100 MHz, CDCl<sub>3</sub>, δ): 198.9, 150.8, 147.9, 145.4, 143.9, 137.4, 137.2, 133.8, 129.8, 129.7, 127.3, 124.1, 57.2, 29.8, 26.3, 21.7.

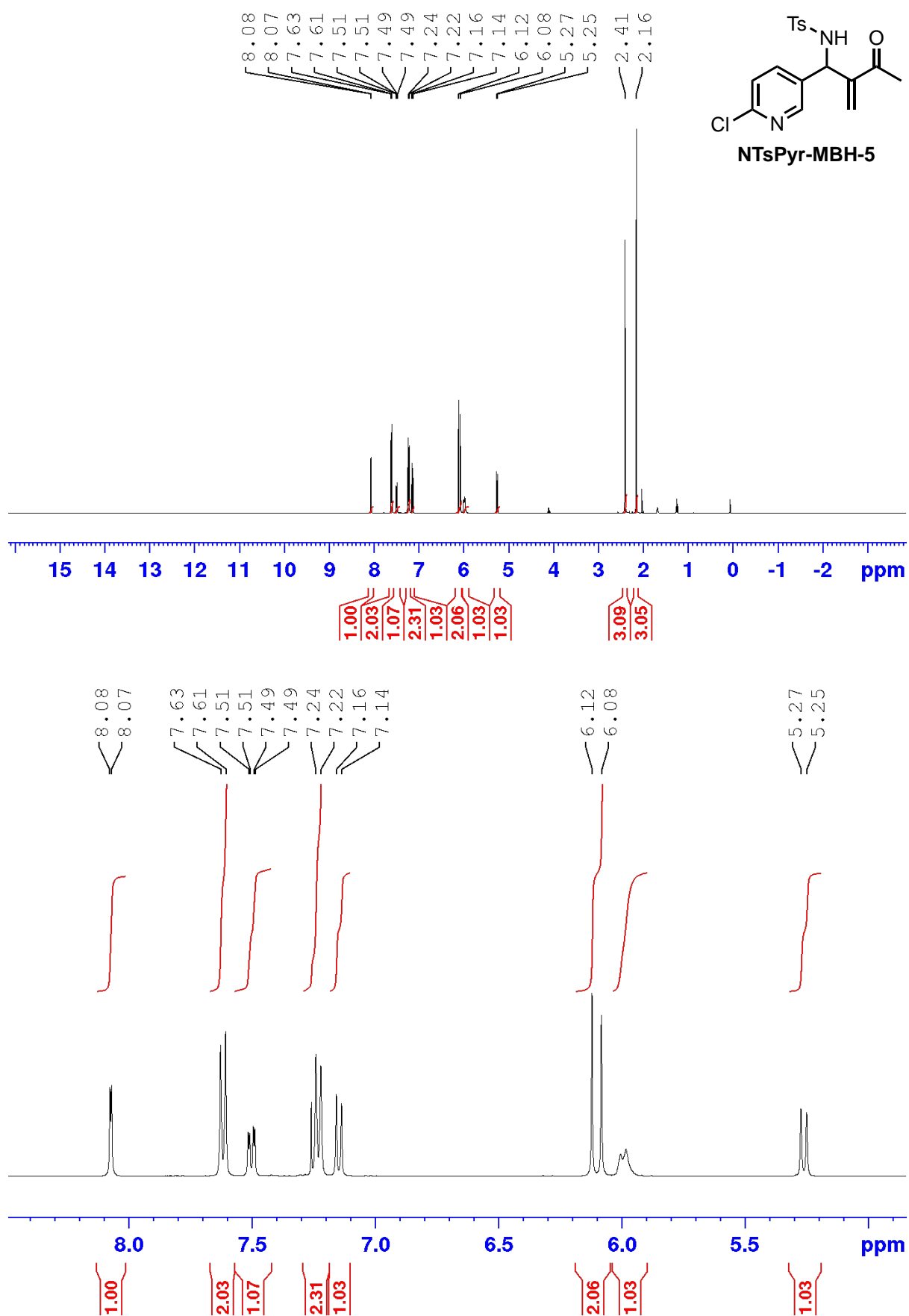
**MS (ESI):** 365.1 [M+ H]

**Chiral HPLC:** 80:20 Hex/*i*-PrOH (0.7 mL min<sup>-1</sup>), Chiralpak AD-H Column, RT<sub>1</sub>: 29.70 min, RT<sub>2</sub>: 39.11 min



**Figure A.64** CD Spectra for isolated enantiomers for **NTsPyr-MBH-5** a) First eluting enantiomer. b) Second eluting enantiomer. c) Comparison of CD traces for (*R*)- and (*S*)-**NTsPyr-MBH-5**. d) Comparison of **NTsPyr-MBH-5** with (*R*)-**NTs-MBH-3** adducts.





**Figure A.65** <sup>1</sup>H NMR spectrum (400 MHz, CDCl<sub>3</sub>) for NTsPyr-MBH-5.

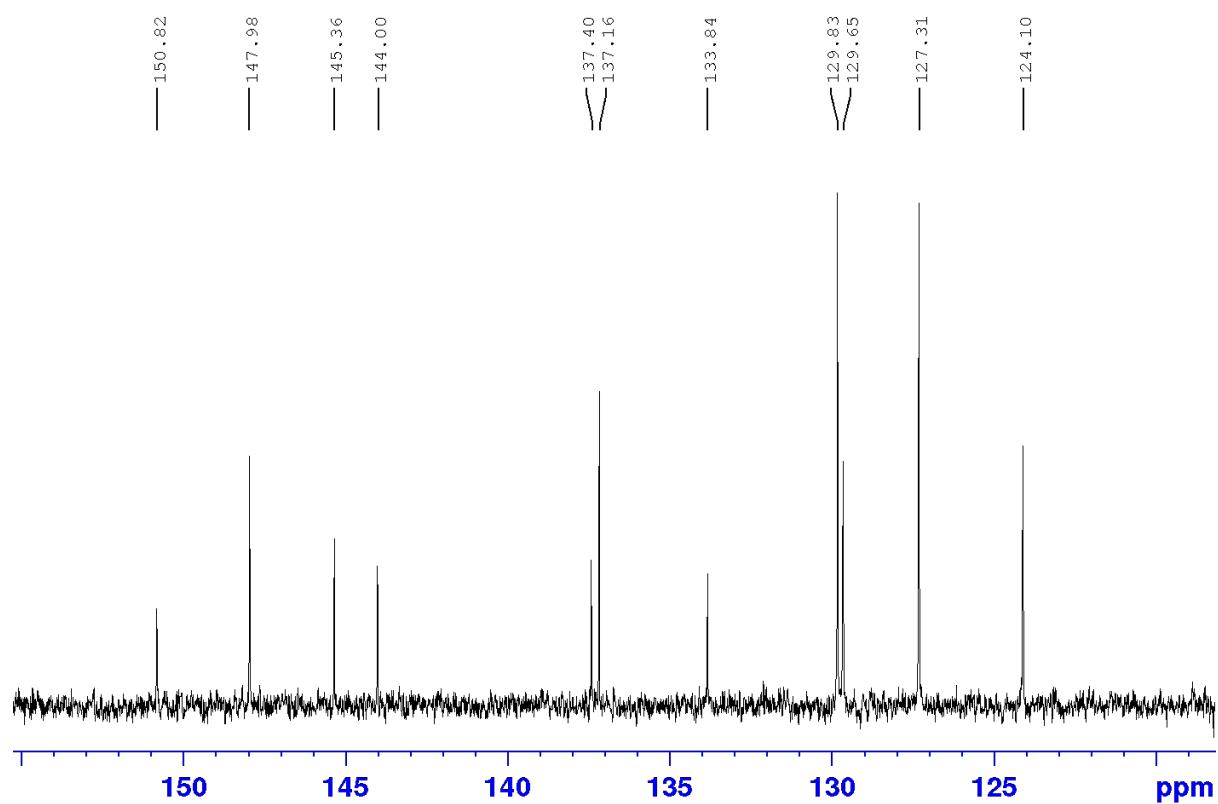
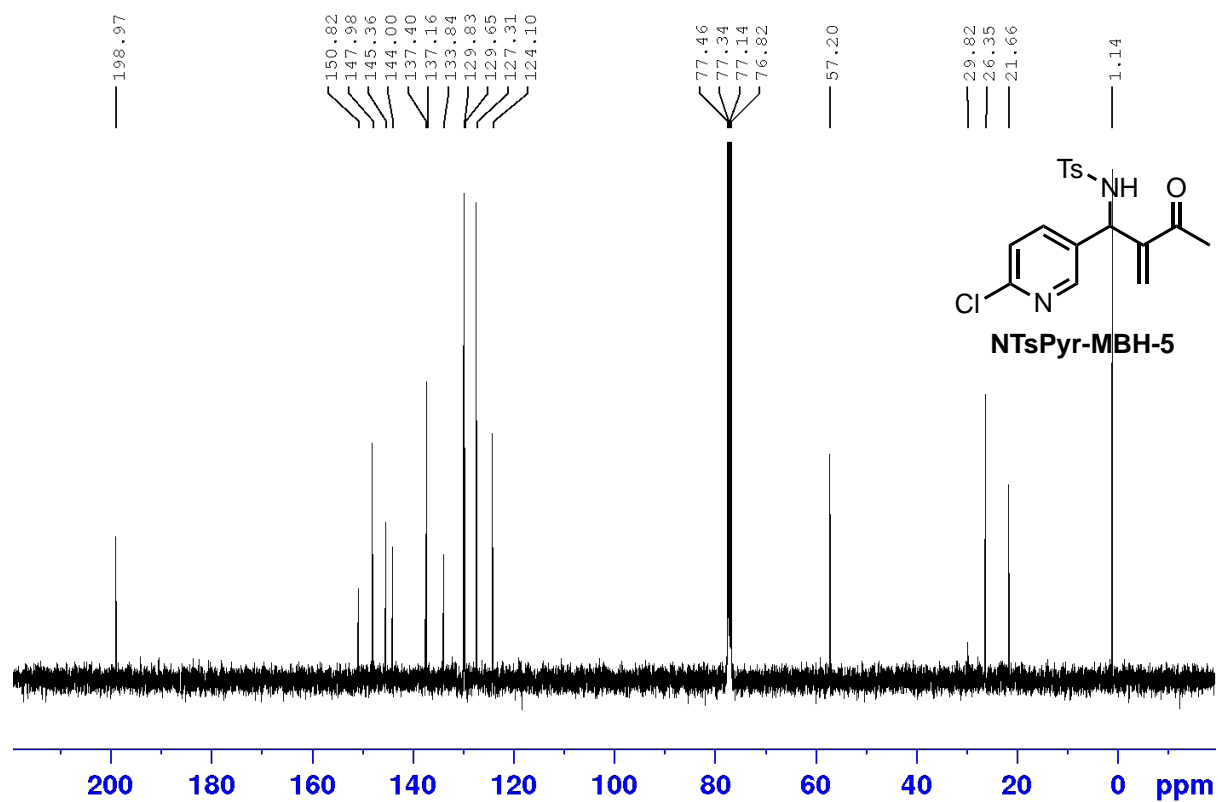
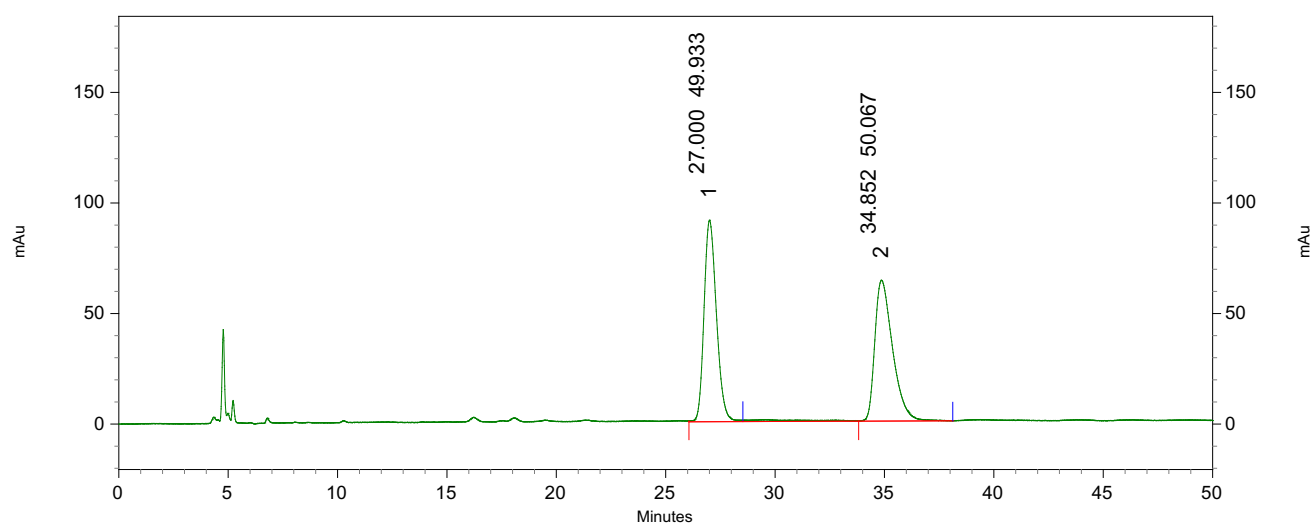


Figure A.66  $^{13}\text{C}$  NMR spectrum (100 MHz,  $\text{CDCl}_3$ ) for NTsPyr-MBH-5.

### Racemic HPLC Trace

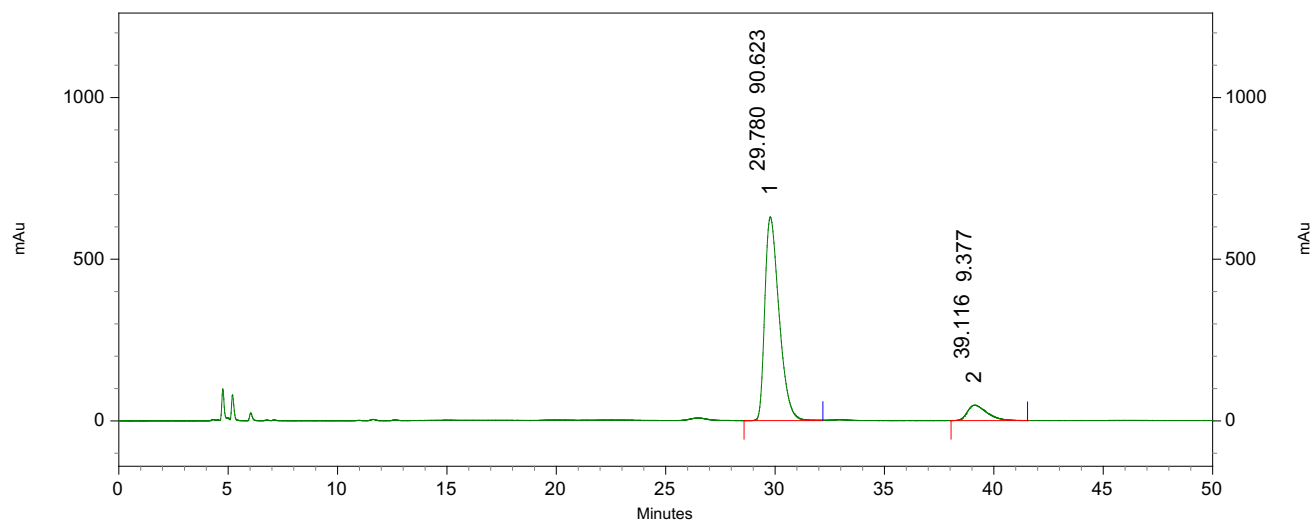


#### 4: 220 nm, 4 nm Results

| Pk # | Retention Time | Area    | Area % |
|------|----------------|---------|--------|
| 1    | 27.000         | 3589857 | 49.93  |
| 2    | 34.852         | 3599494 | 50.07  |

|        |  |         |        |
|--------|--|---------|--------|
| Totals |  | 7189351 | 100.00 |
|--------|--|---------|--------|

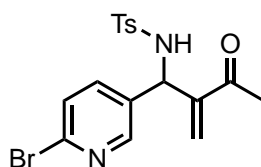
### Chiral HPLC Trace



#### 4: 220 nm, 4 nm Results

| Pk # | Retention Time | Area     | Area % |
|------|----------------|----------|--------|
| 1    | 29.780         | 28448426 | 90.62  |
| 2    | 39.116         | 2943582  | 9.38   |

|        |  |          |        |
|--------|--|----------|--------|
| Totals |  | 31392008 | 100.00 |
|--------|--|----------|--------|



**NTsPyr-MBH-6**

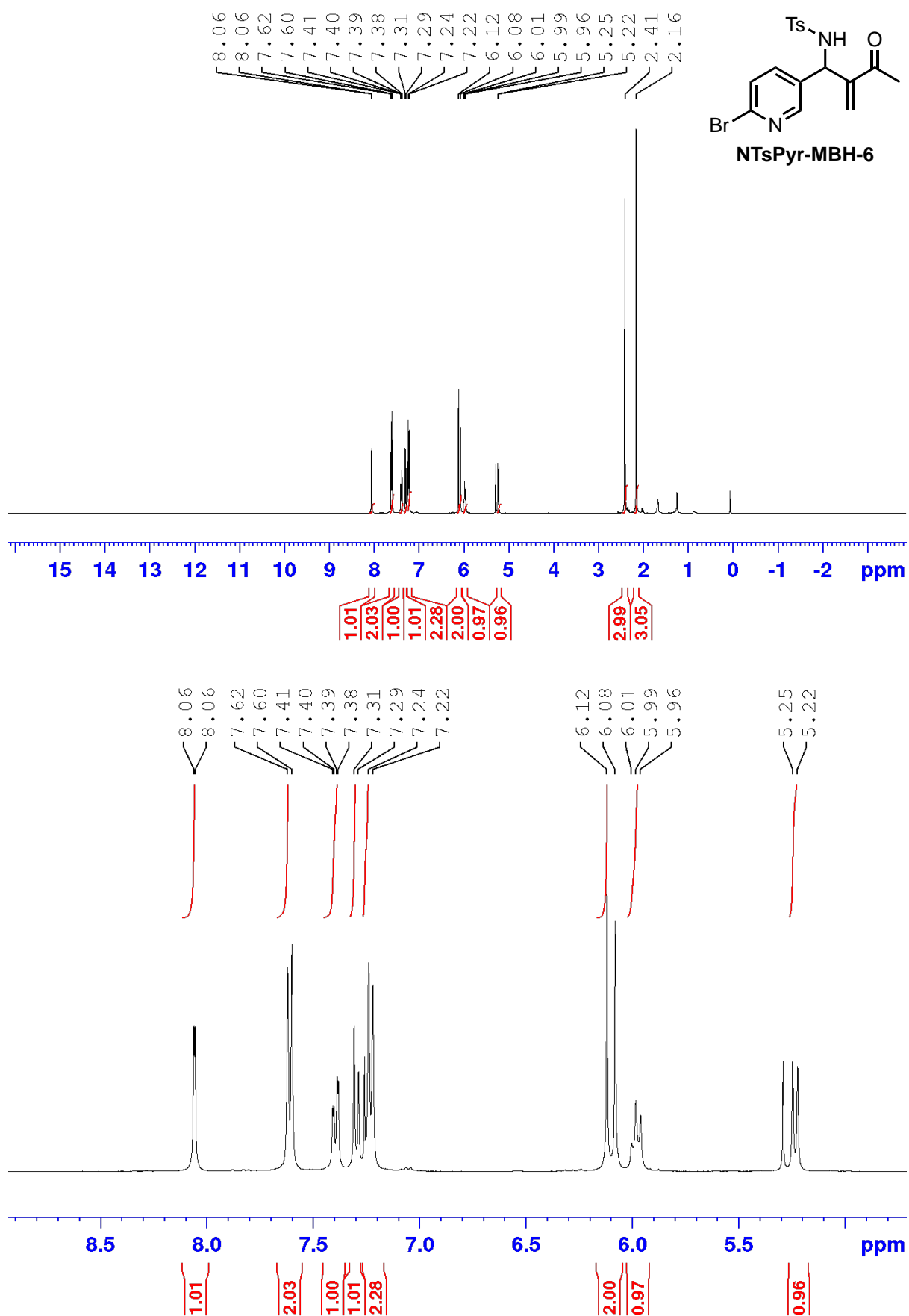
***N*-(1-(6-bromopyridin-3-yl)-2-methylene-3-oxobutyl)-4-methylbenzenesulfonamide**  
(NTsPyr-MBH-6)

**<sup>1</sup>H NMR** (400 MHz, CDCl<sub>3</sub>, δ): 8.06 (d, *J* = 2.4 Hz, 1H), 7.61 (d, *J* = 8.2 Hz, 2H), 7.40 (dd, *J* = 7.2, 2.5 Hz, 1H), 7.23 (d, *J* = 8.1 Hz, 2H), 6.12 (s, 1H), 6.08 (s, 1H), 5.97 (m, 1H), 5.24 (d, *J* = 9.2 Hz, 2H), 2.41 (s, 3H), 2.16 (s, 3H)

**<sup>13</sup>C NMR** (100 MHz, CDCl<sub>3</sub>, δ): 198.9, 148.6, 145.4, 141.3, 137.3, 136.9, 134.3, 129.8, 129.6, 127.9, 127.3, 56.9, 26.3, 21.7.

**MS (ESI)**: 408.9 [M+ H], 410.9 [M+H]

**Chiral HPLC**: 80:20 Hex/*i*-PrOH (0.7 mL min<sup>-1</sup>), Chiralpak AD-H Column, RT<sub>1</sub>: 26.94 min, RT<sub>2</sub>: 34.84 min



**Figure A.67** <sup>1</sup>H NMR spectrum (400 MHz, CDCl<sub>3</sub>) for NTsPyr-MBH-6.

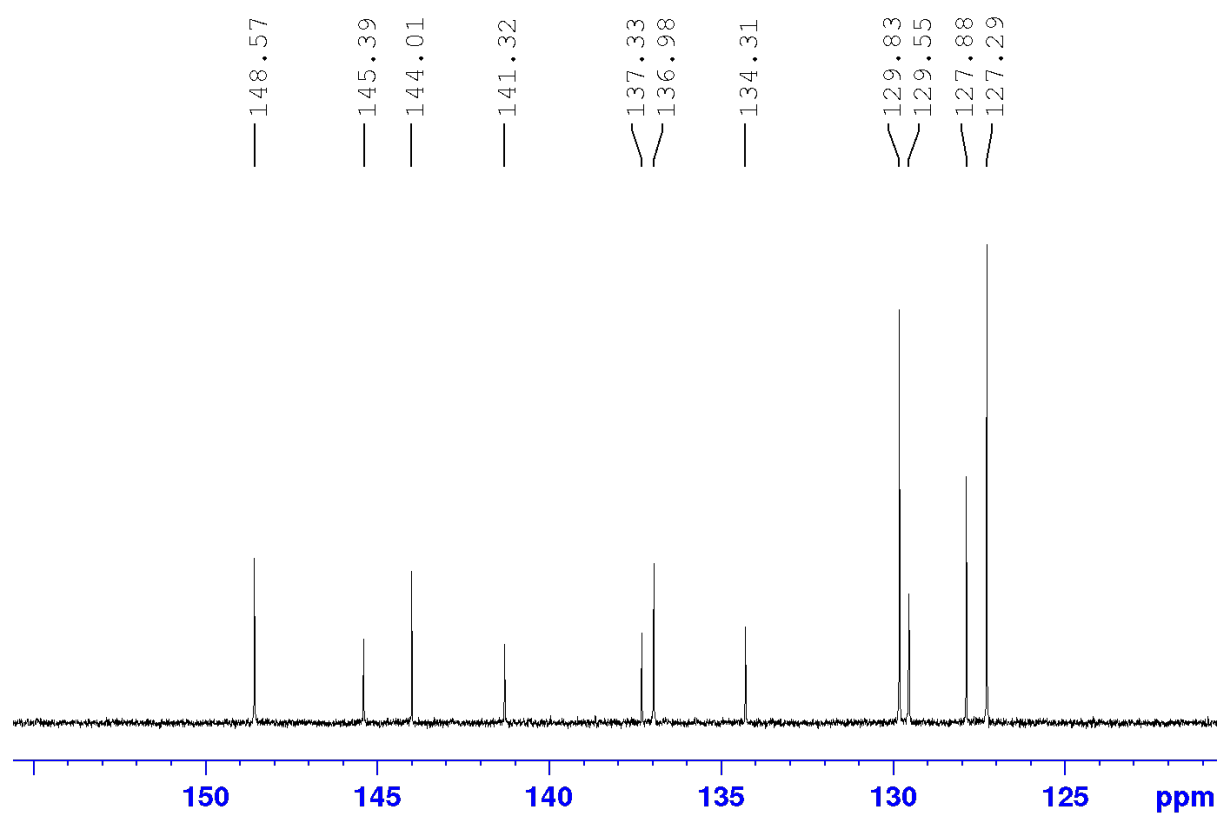
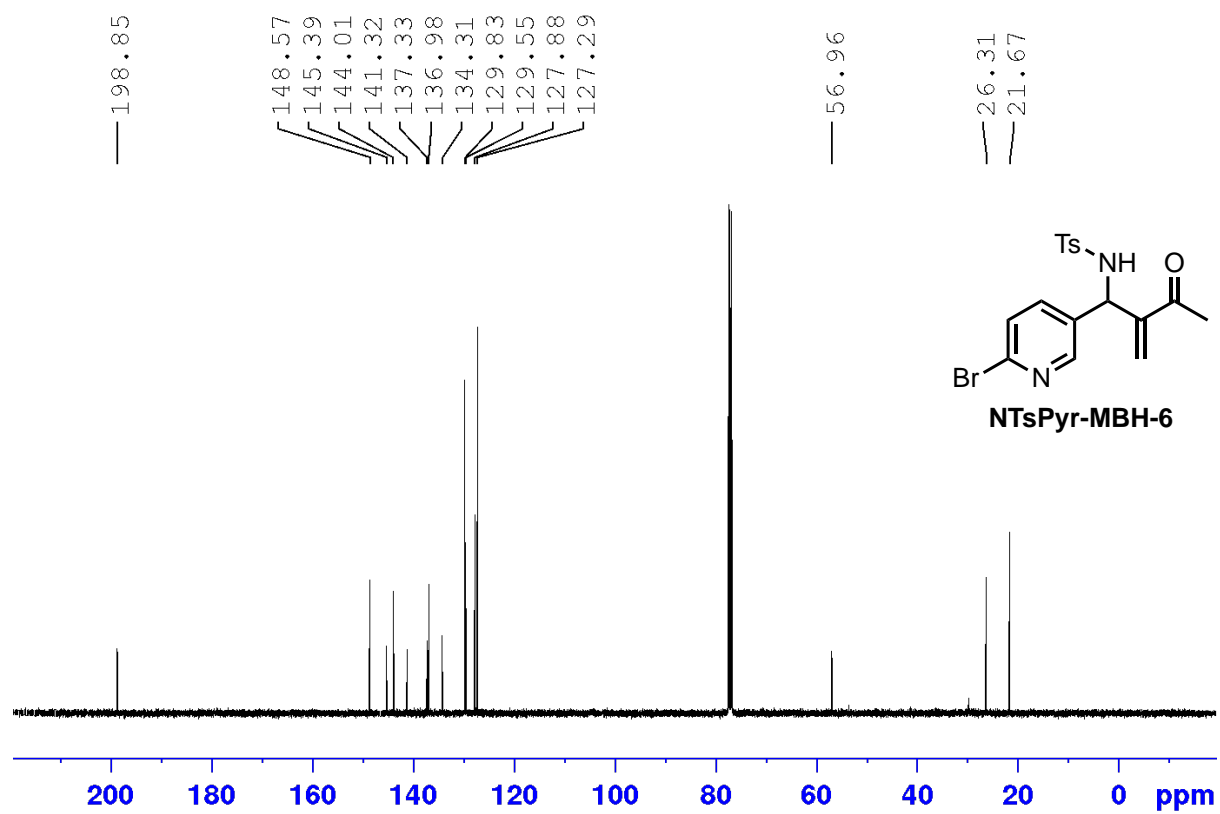
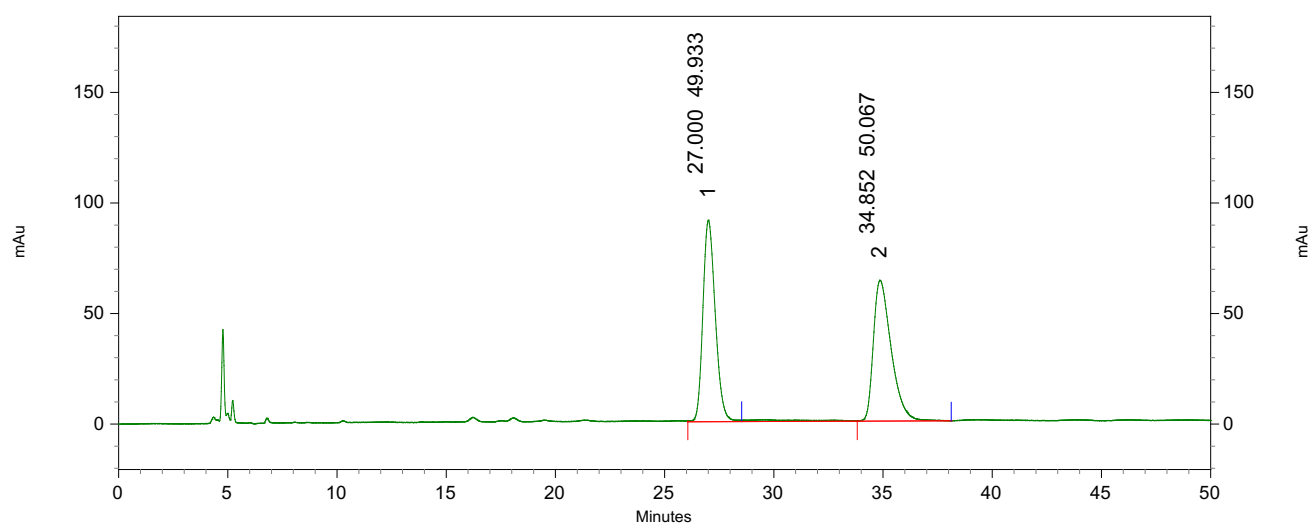


Figure A.68 <sup>13</sup>C NMR spectrum (100 MHz, CDCl<sub>3</sub>) for NTsPyr-MBH-6.

### Racemic HPLC Trace

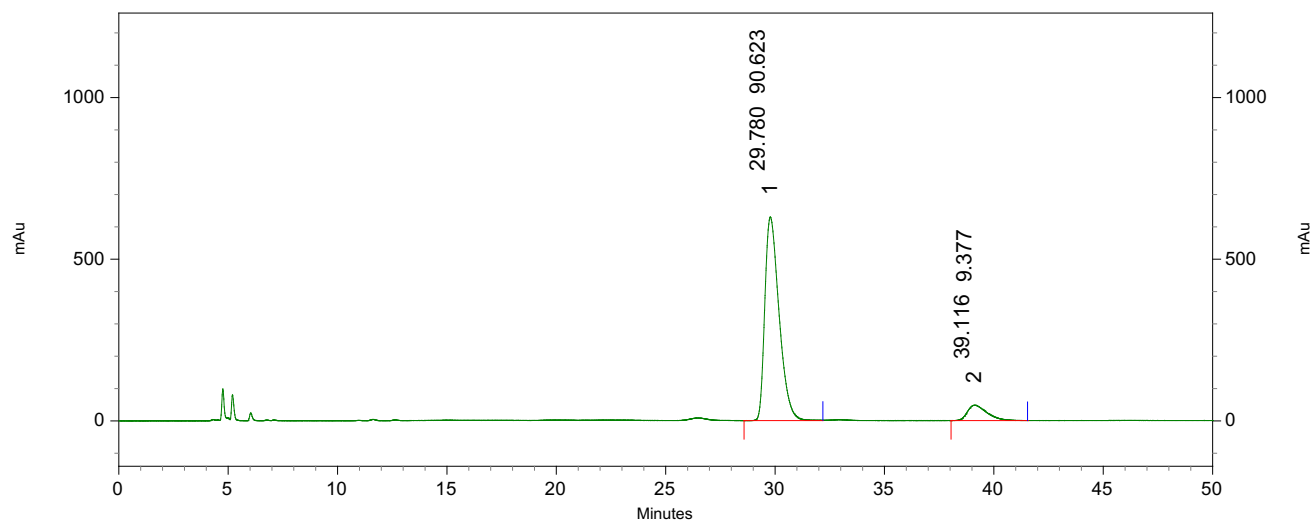


#### 4: 220 nm, 4 nm Results

| Pk # | Retention Time | Area    | Area % |
|------|----------------|---------|--------|
| 1    | 27.000         | 3589857 | 49.93  |
| 2    | 34.852         | 3599494 | 50.07  |

|        |  |         |        |
|--------|--|---------|--------|
| Totals |  | 7189351 | 100.00 |
|--------|--|---------|--------|

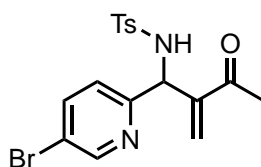
### Chiral HPLC Trace



#### 4: 220 nm, 4 nm Results

| Pk # | Retention Time | Area     | Area % |
|------|----------------|----------|--------|
| 1    | 29.780         | 28448426 | 90.62  |
| 2    | 39.116         | 2943582  | 9.38   |

|        |  |          |        |
|--------|--|----------|--------|
| Totals |  | 31392008 | 100.00 |
|--------|--|----------|--------|



**NTsPyr-MBH-7**

***N*-(1-(5-bromopyridin-2-yl)-2-methylene-3-oxobutyl)-4-methylbenzenesulfonamide (NTsPyr-MBH-7)**

**<sup>1</sup>H NMR** (400 MHz, CDCl<sub>3</sub>, δ): 8.44 (d, *J* = 2.0 Hz, 1H), 7.64 (m, 3H), 7.20 (m, 3H), 6.34 (d, *J* = 8.7 Hz, 1H), 6.11 (s, 1H), 6.09 (s, 1H), 5.39 (d, *J* = 8.7 Hz, 1H), 2.40 (s, 3H), 2.33 (s, 3H).

**<sup>13</sup>C NMR** (100 MHz, CDCl<sub>3</sub>, δ): 198.8, 156.2, 149.8, 146.6, 143.5, 139.3, 137.3, 129.6, 128.7, 127.3, 123.7, 119.5, 27.5, 26.2, 21.6.

**MS (ESI):** 409.0 [M+ H], 411.0 [M+H]

**Chiral HPLC:** 80:20 Hex/*i*-PrOH (0.7 mL min<sup>-1</sup>), Chiralpak AD-H Column, RT<sub>1</sub>: 23.84 min, RT<sub>2</sub>: 24.80 min



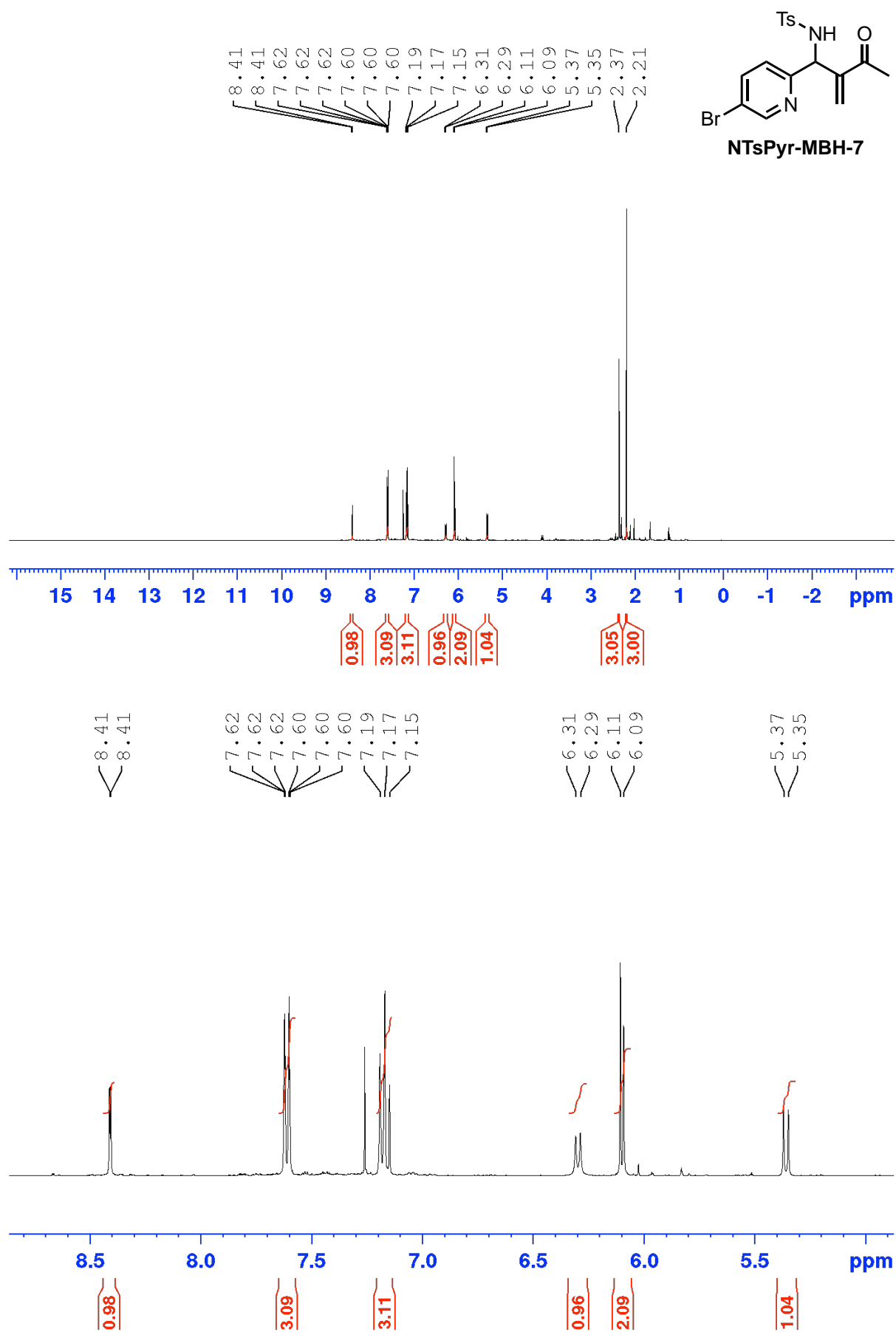
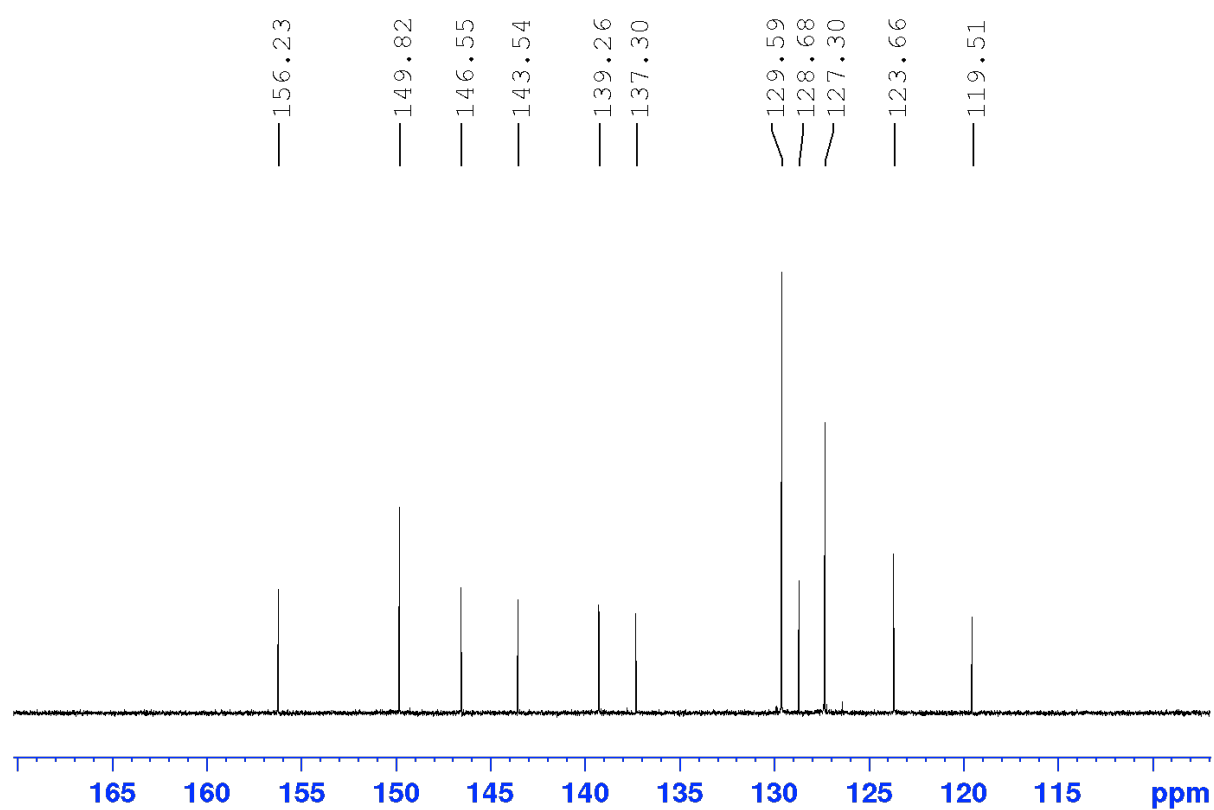
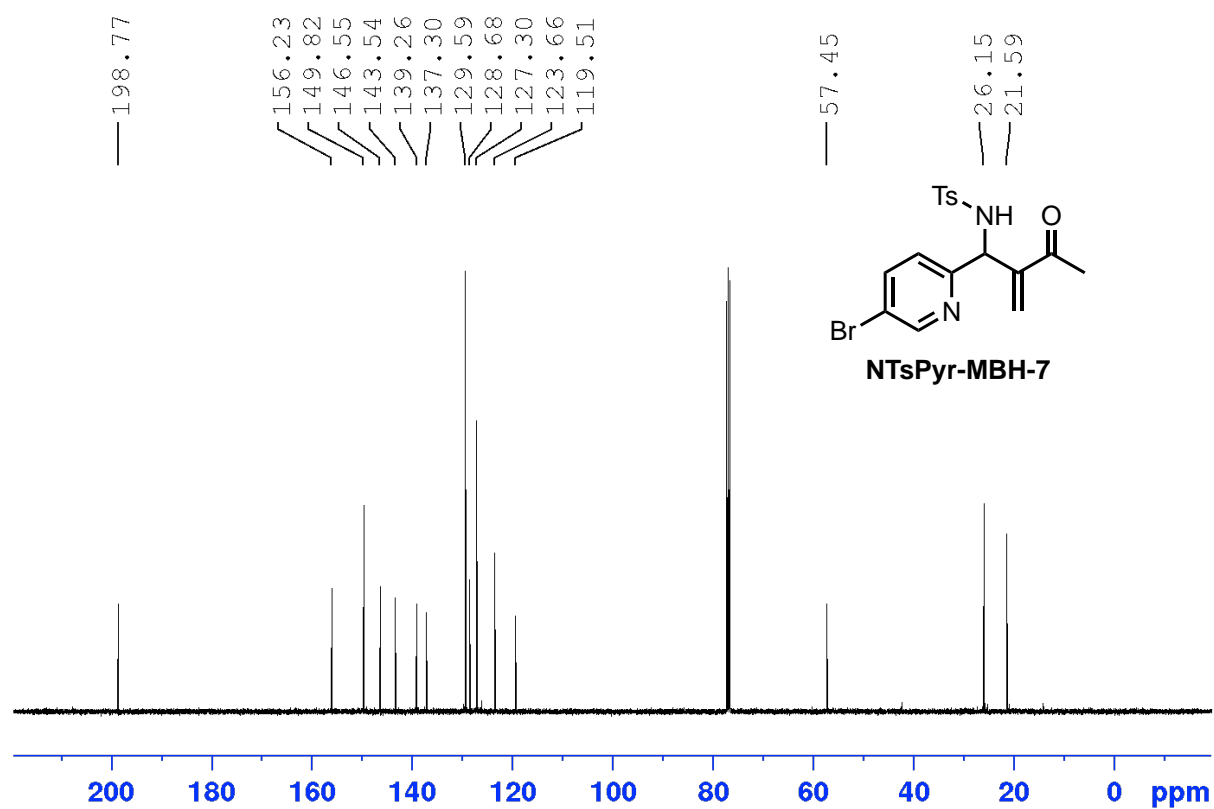
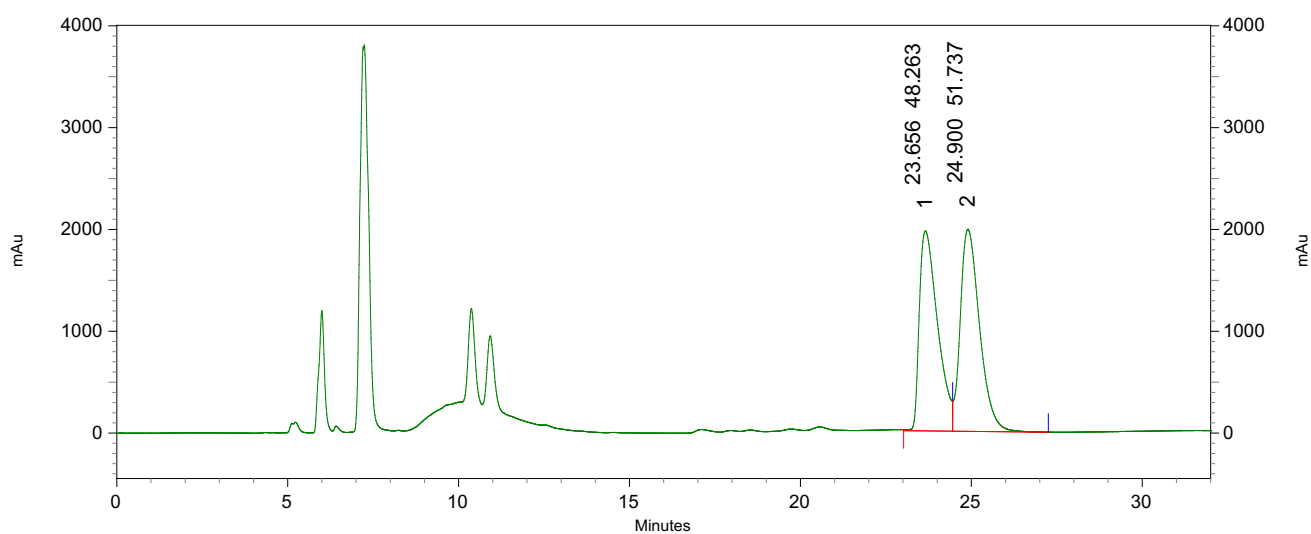


Figure A.69 <sup>1</sup>H NMR spectrum (400 MHz, CDCl<sub>3</sub>) for NTsPyr-MBH-12.



**Figure A.70** <sup>13</sup>C NMR spectrum (100 MHz, CDCl<sub>3</sub>) for NTsPyr-MBH-12.

### Racemic HPLC Trace

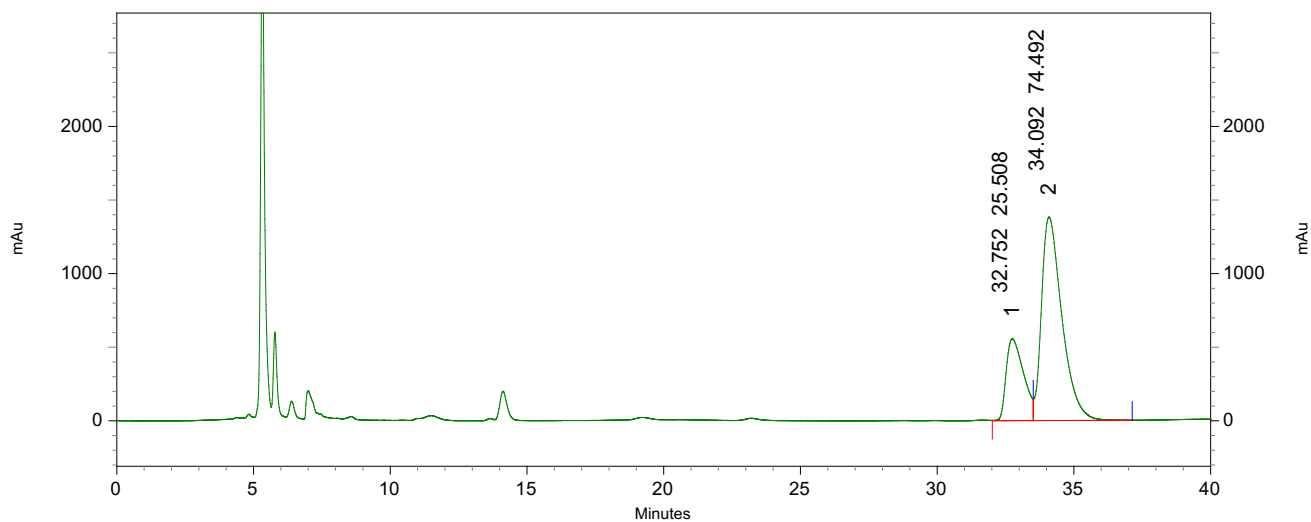


#### 4: 220 nm, 4 nm Results

| Pk # | Retention Time | Area     | Area % |
|------|----------------|----------|--------|
| 1    | 23.656         | 72668849 | 48.26  |
| 2    | 24.900         | 77900309 | 51.74  |

|        |  |           |        |
|--------|--|-----------|--------|
| Totals |  | 150569158 | 100.00 |
|--------|--|-----------|--------|

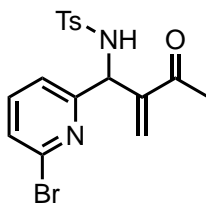
### Chiral HPLC Trace



#### 4: 220 nm, 4 nm Results

| Pk # | Retention Time | Area     | Area % |
|------|----------------|----------|--------|
| 1    | 32.752         | 24573955 | 25.51  |
| 2    | 34.092         | 71763907 | 74.49  |

|        |  |          |        |
|--------|--|----------|--------|
| Totals |  | 96337862 | 100.00 |
|--------|--|----------|--------|



**NTsPyr-MBH-8**

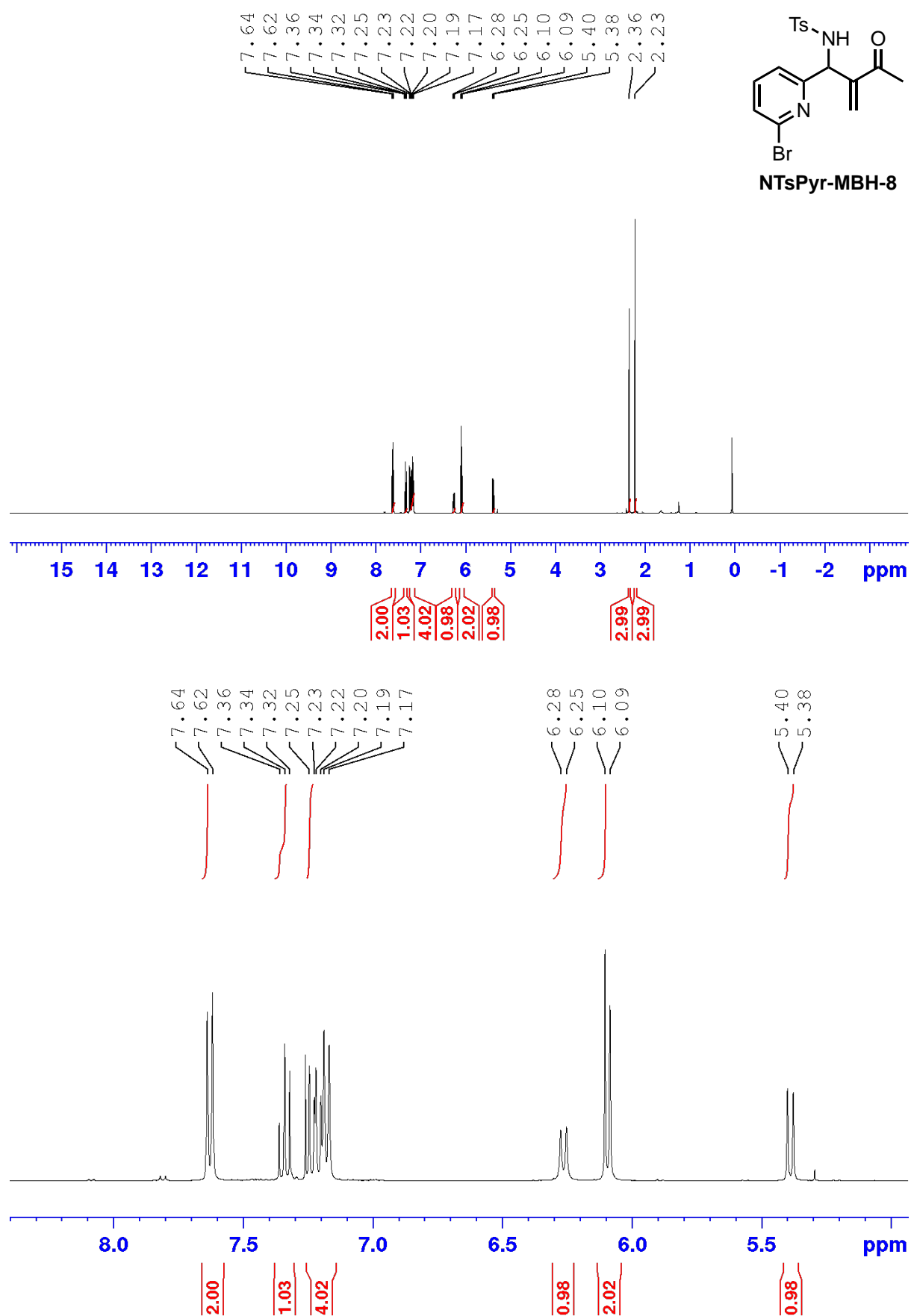
***N*-(1-(6-bromopyridin-2-yl)-2-methylene-3-oxobutyl)-4-methylbenzenesulfonamide (NTsPyr-MBH-8)**

**<sup>1</sup>H NMR** (400 MHz, CDCl<sub>3</sub>, δ): 7.62 (d, *J*= 8.3 Hz, 2H), 7.34 (dd, *J*= 8.3 Hz, 1H), 7.21 (m, 4H), 6.26 (d, *J*= 8.9 Hz, 1H), 6.10 (s, 1H), 6.09 (s, 1H), 5.39 (d, *J*= 8.9 Hz, 1H), 2.36 (s, 3H), 2.23 (s, 3H).

**<sup>13</sup>C NMR** (100 MHz, CDCl<sub>3</sub>, δ): 198.8, 158.9, 146.3, 143.5, 141.2, 138.9, 137.2, 129.5, 128.8, 127.3, 126.9, 121.2, 57.3, 26.2, 21.6

**MS (ESI):** 408.9 [M+ H], 410.9 [M+H]

**Chiral HPLC:** 85:15 Hex/*i*-PrOH (0.7 mL min<sup>-1</sup>), Chiralpak AD-H Column, RT<sub>1</sub>: 24.79 min, RT<sub>2</sub>: 29.24 min



**Figure A.71** <sup>1</sup>H NMR spectrum (400 MHz, CDCl<sub>3</sub>) for NTsPyr-MBH-8.

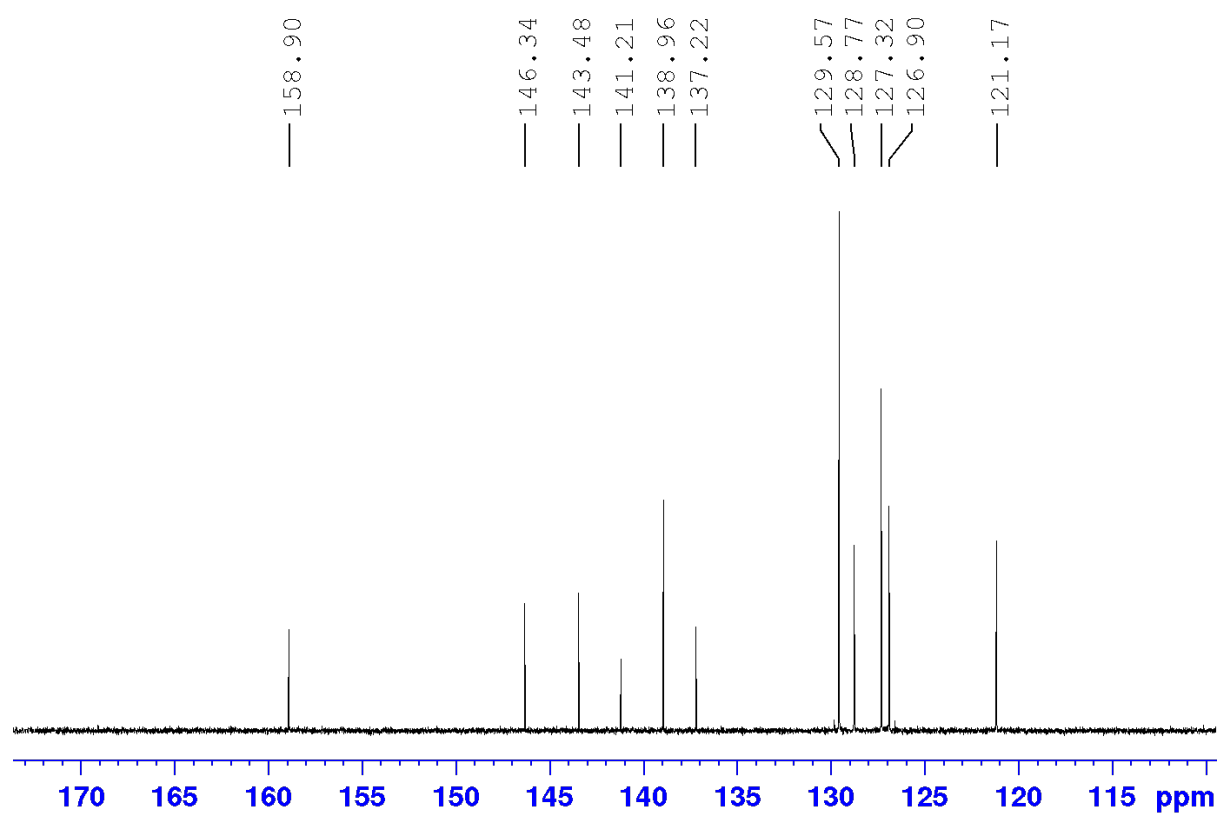
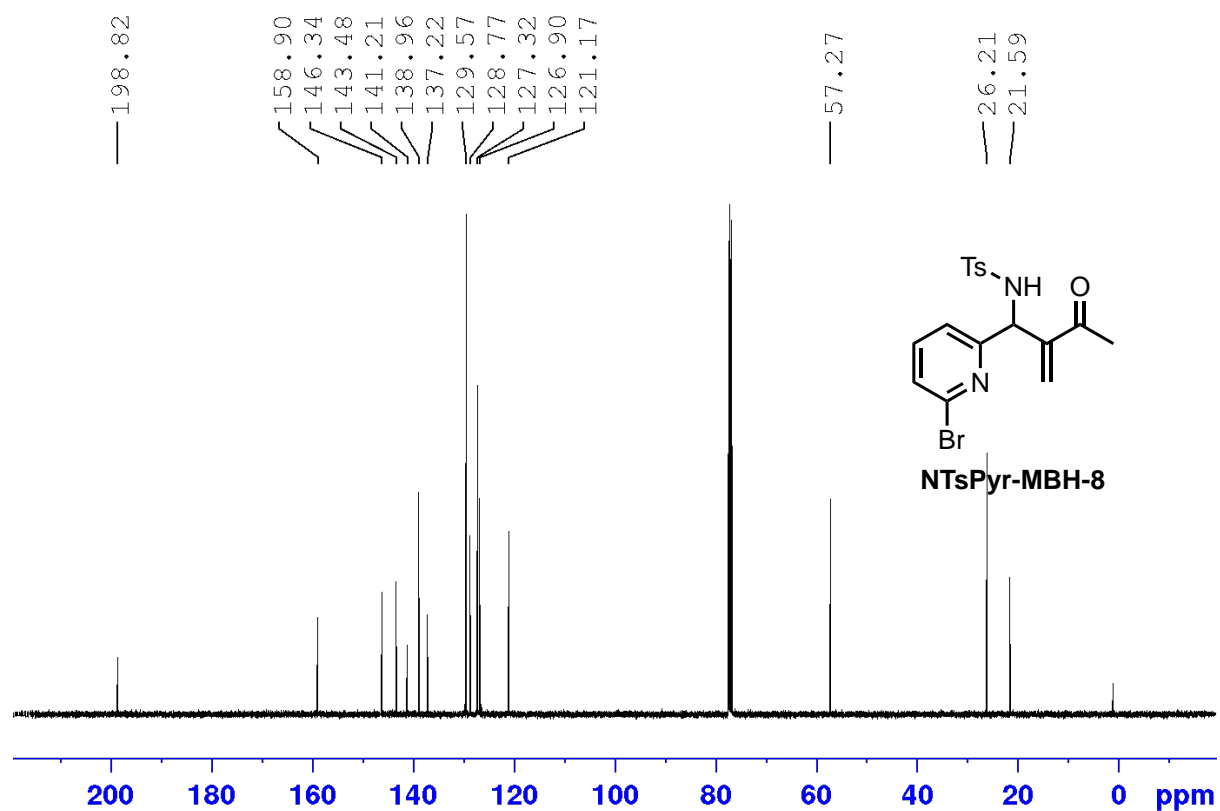
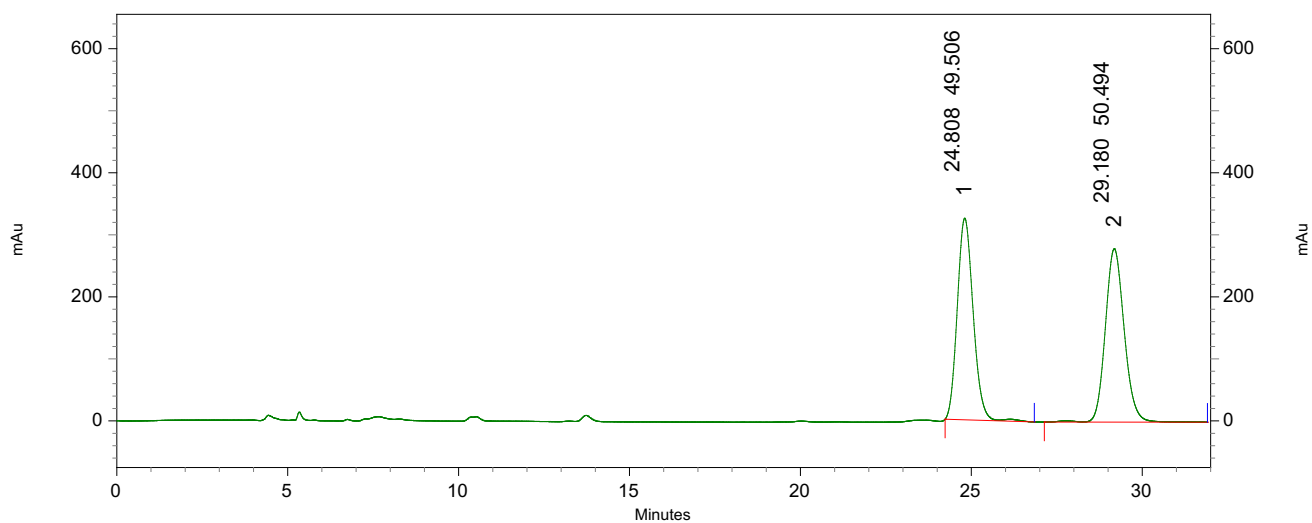


Figure A.72 <sup>13</sup>C NMR spectrum (100 MHz, CDCl<sub>3</sub>) for NTsPyr-MBH-8.

### Racemic HPLC Trace

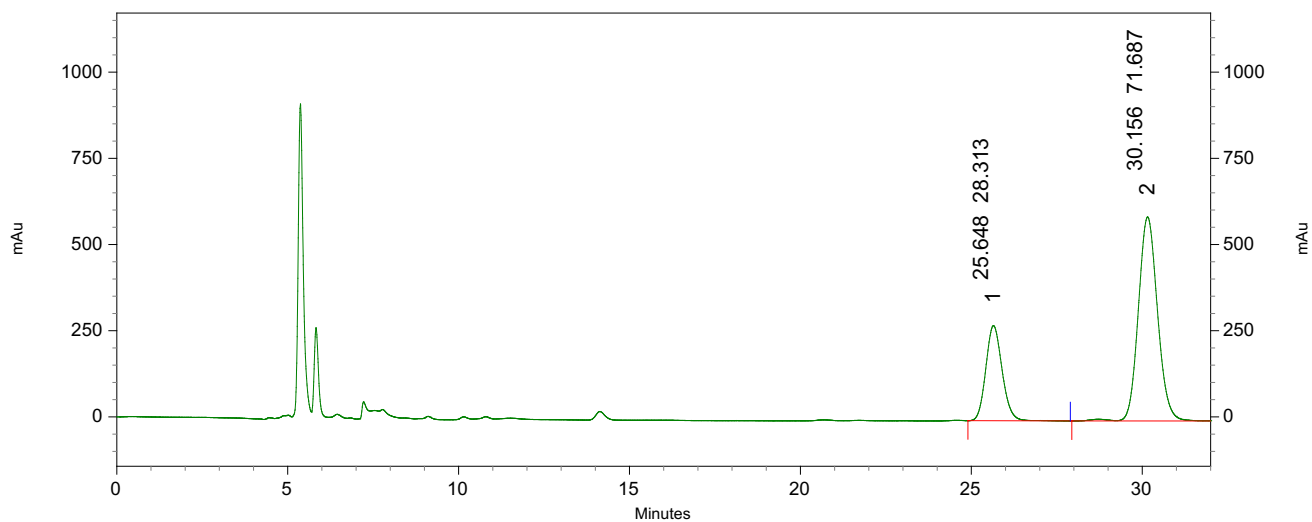


#### 4: 220 nm, 4 nm Results

| Pk # | Retention Time | Area     | Area % |
|------|----------------|----------|--------|
| 1    | 24.808         | 10523479 | 49.51  |
| 2    | 29.180         | 10733492 | 50.49  |

|        |  |          |        |
|--------|--|----------|--------|
| Totals |  | 21256971 | 100.00 |
|--------|--|----------|--------|

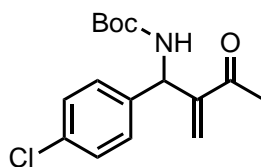
### Chiral HPLC Trace



#### 4: 220 nm, 4 nm Results

| Pk # | Retention Time | Area     | Area % |
|------|----------------|----------|--------|
| 1    | 25.648         | 9143515  | 28.31  |
| 2    | 30.156         | 23150612 | 71.69  |

|        |  |          |        |
|--------|--|----------|--------|
| Totals |  | 32294127 | 100.00 |
|--------|--|----------|--------|



**NBoc-MBH-1**

***tert-butyl (1-(4-chlorophenyl)-2-methylene-3-oxobutyl)carbamate (NBoc-MBH-1)***

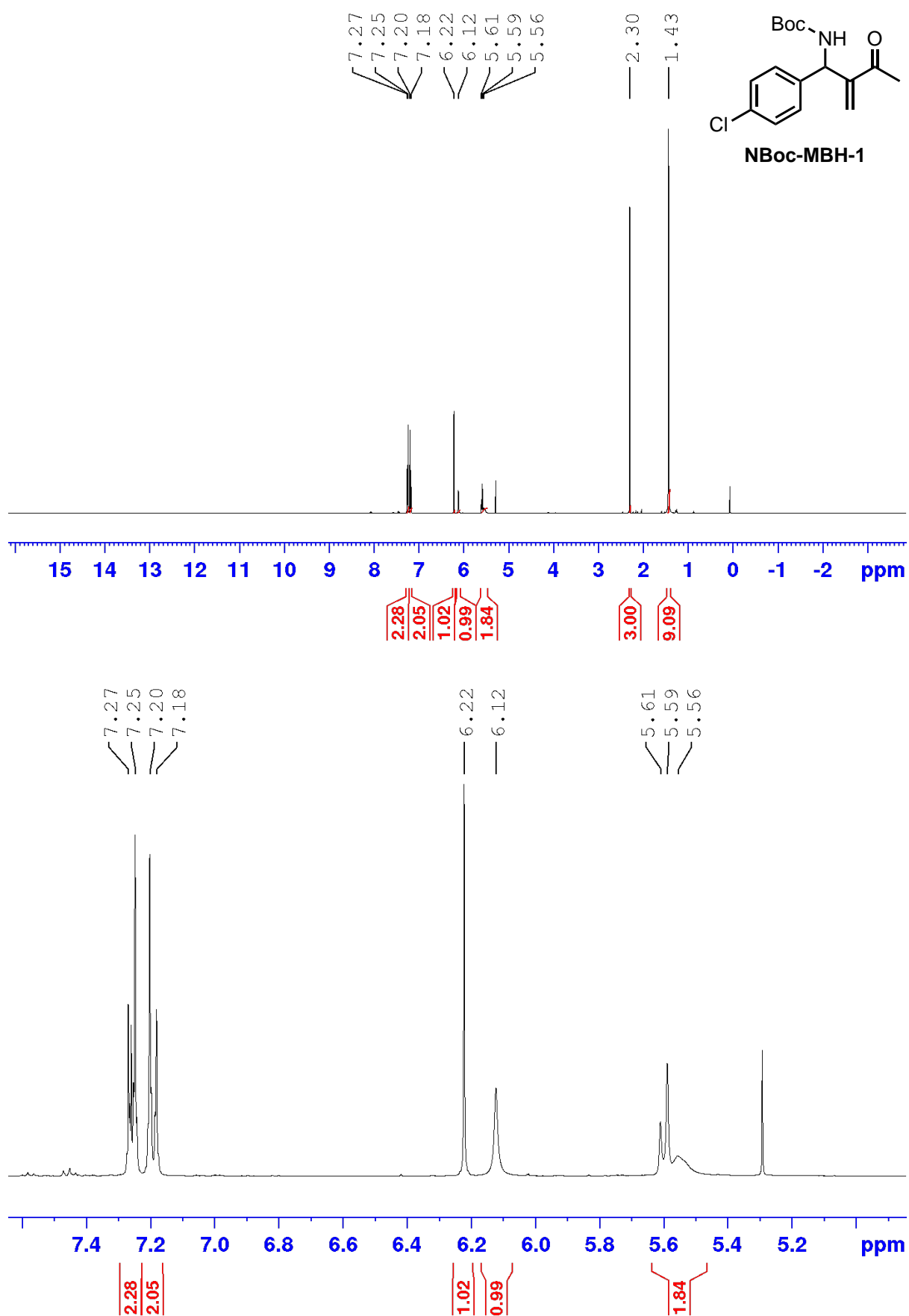
**<sup>1</sup>H NMR** (400 MHz, CDCl<sub>3</sub>, δ): 7.26 (d, *J* = 8.0 Hz, 2H), 7.19 (d, *J* = 8.0 Hz, 2H), 6.22 (s, 1H), 6.12 (s, 1H), 5.59 (d, *J* = 8.6 Hz), 5.54 (br, 1H), 2.30 (s, 3H), 1.44 (s, 9H).

**<sup>13</sup>C NMR** (100 MHz, CDCl<sub>3</sub>, δ): 199.0, 155.1, 147.6, 139.0, 133.4, 133.2, 130.2, 128.5, 127.6, 80.1, 55.9, 28.5, 26.7.

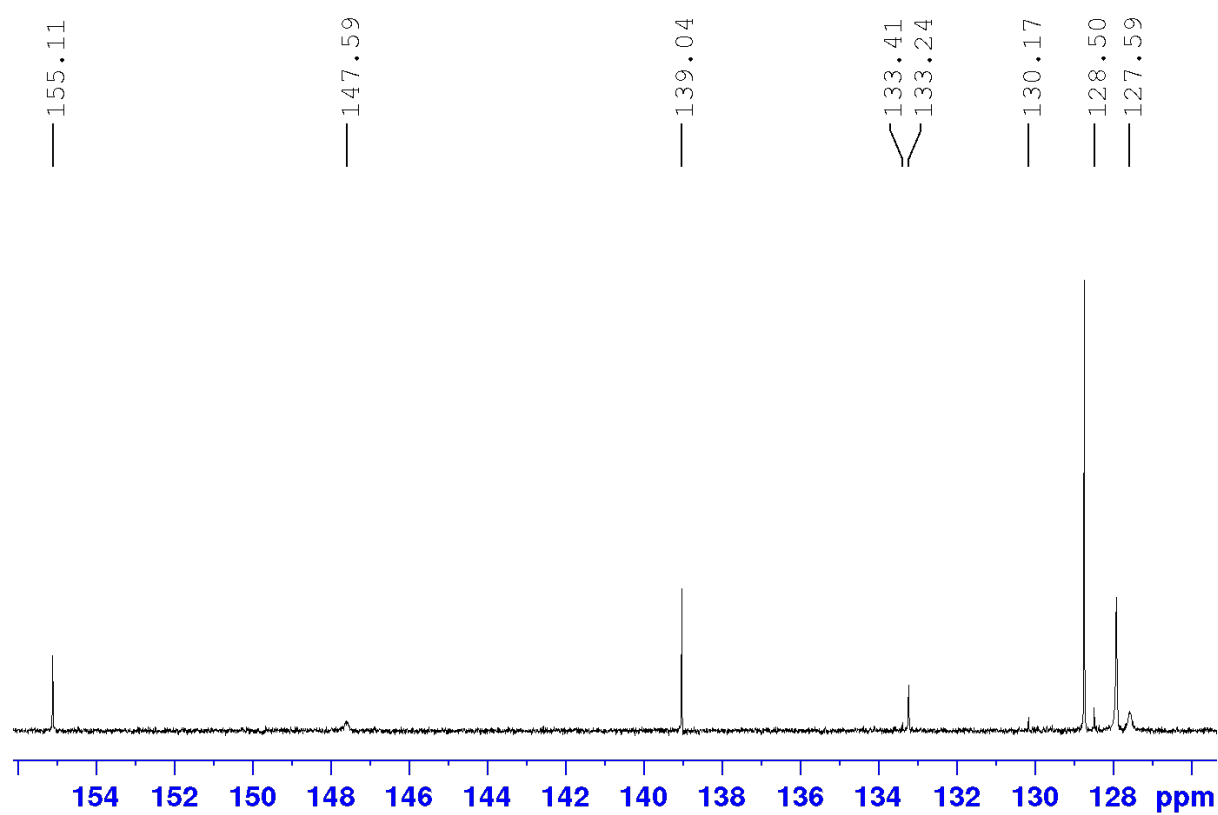
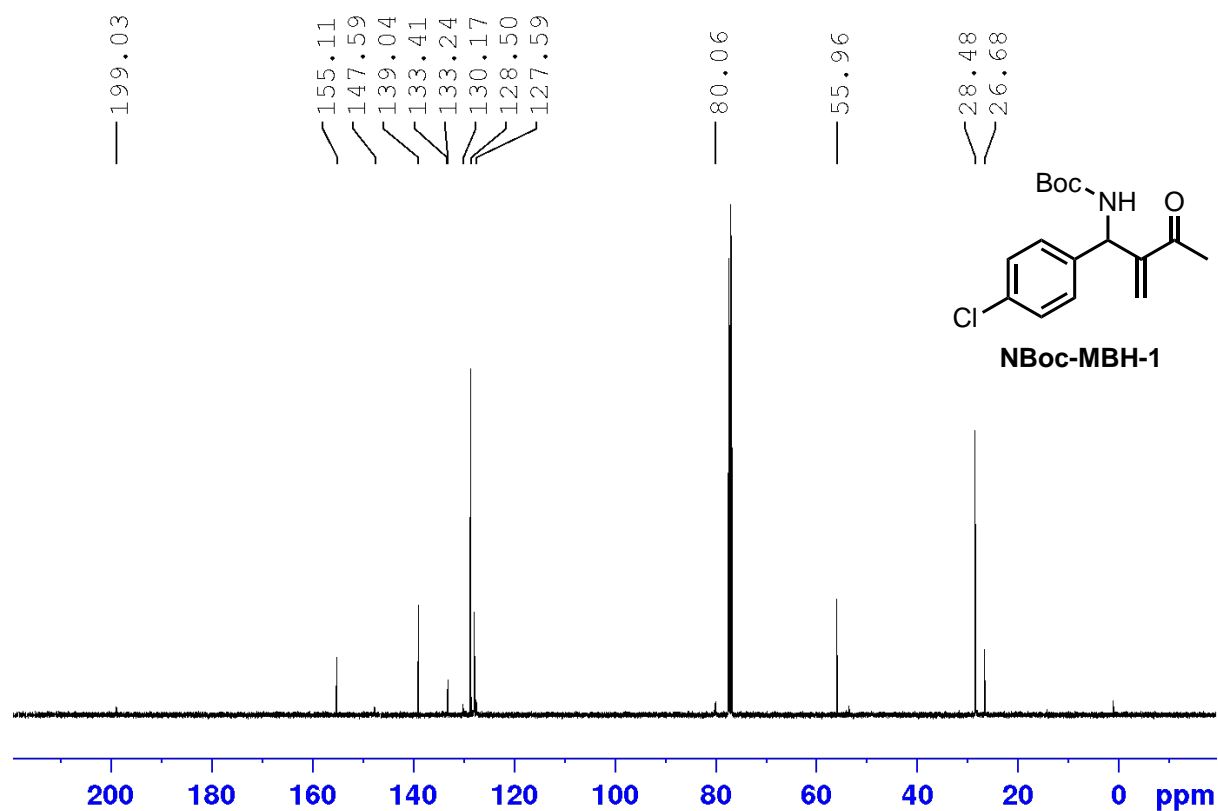
**MS (ESI):** 254.1 [M- t-Bu], 193.1 [M- NHBoc]

**Chiral HPLC:** Mobile Phase 75:25 Hex/*i*-PrOH, Chiralpak AD-H column RT<sub>1</sub>: 15.6 min, RT<sub>2</sub>: 16.5 min.



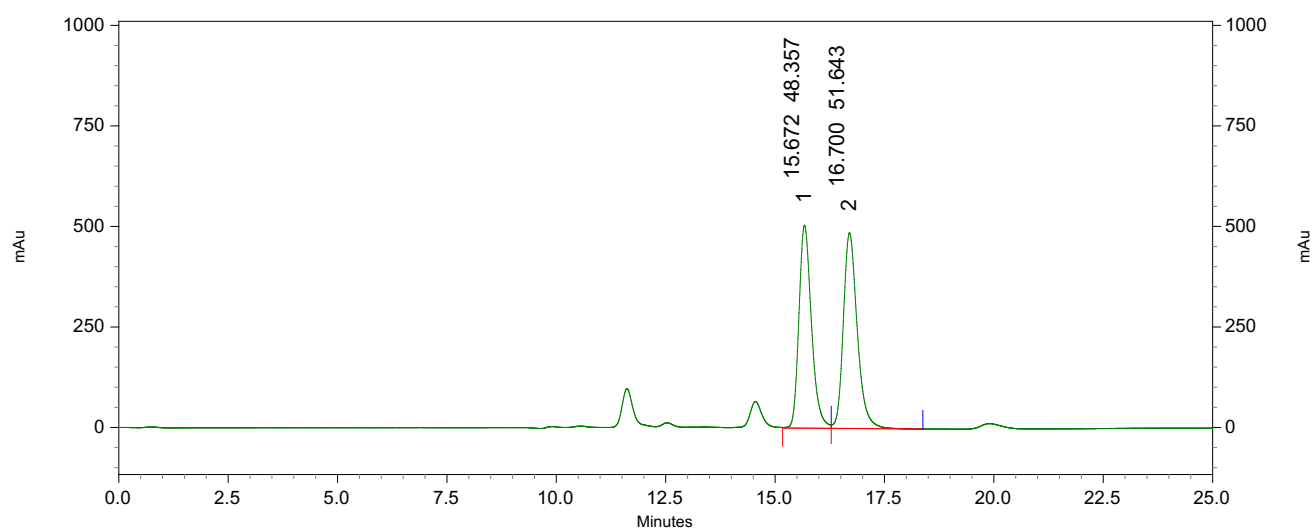


**Figure A.73**  $^1\text{H}$  NMR spectrum (400 MHz,  $\text{CDCl}_3$ ) for **NBoc-MBH-1**



**Figure A.74** <sup>13</sup>C NMR spectrum (100 MHz, CDCl<sub>3</sub>) for NBoc-MBH-1

### Racemic HPLC Trace

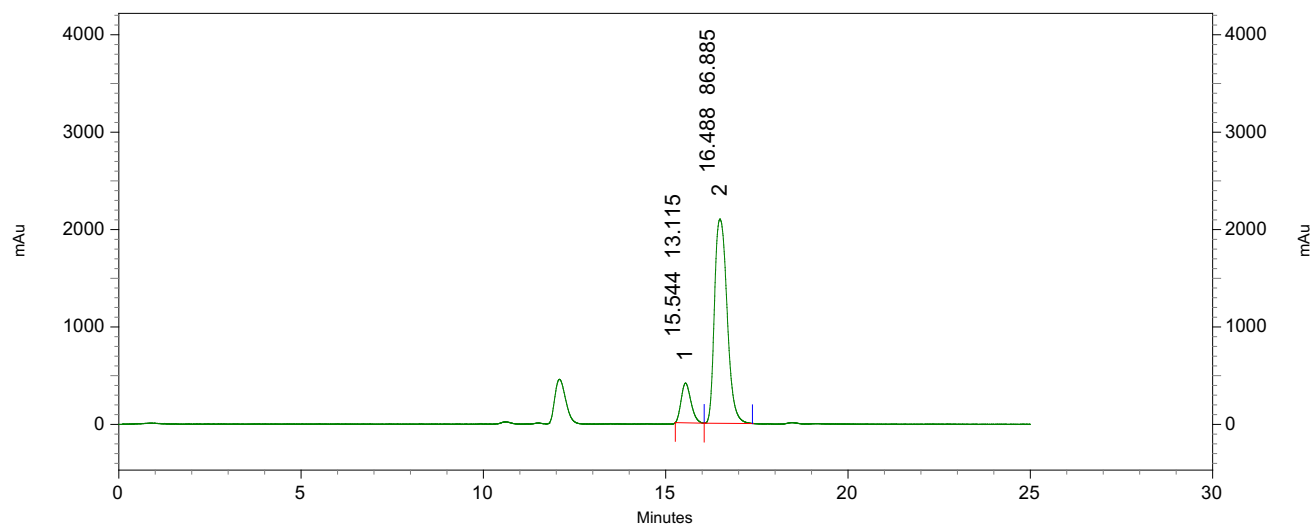


### 4: 220 nm, 4 nm Results

| Pk # | Retention Time | Area     | Area % |
|------|----------------|----------|--------|
| 1    | 15.672         | 10072981 | 48.36  |
| 2    | 16.700         | 10757342 | 51.64  |

|        |  |          |        |
|--------|--|----------|--------|
| Totals |  | 20830323 | 100.00 |
|--------|--|----------|--------|

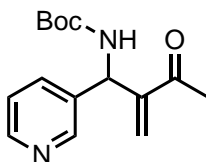
### Chiral HPLC Trace



### 4: 220 nm, 4 nm Results

| Pk # | Retention Time | Area     | Area % |
|------|----------------|----------|--------|
| 1    | 15.540         | 5792228  | 13.31  |
| 2    | 16.492         | 37722116 | 86.69  |

|        |  |          |        |
|--------|--|----------|--------|
| Totals |  | 43516284 | 100.00 |
|--------|--|----------|--------|



**NBoc-MBH-2**

***tert-butyl (2-methylene-3-oxo-1-(pyridin-3-yl)butyl)carbamate (NBoc-MBH-2)***

**<sup>1</sup>H NMR** (400 MHz, CDCl<sub>3</sub>, δ): 8.48 (d, *J* = 1.4 Hz, 1H), 8.46 (dd, *J* = 4.8, 1.4 Hz), 7.60 (dd, *J* = 7.9, 3.8 Hz), 7.21 (dd, *J* = 7.9, 4.8 Hz, 1H), 6.26 (s, 1H), 6.18 (s, 1H), 5.65 (m, 2H), 2.31 (s, 3H), 1.43 (s, 9H).

**<sup>13</sup>C NMR** (100 MHz, CDCl<sub>3</sub>, δ): 198.9, 155.1, 148.7, 148.3, 147.0, 136.1, 134.2, 128.3, 123.4, 80., 54.7, 28.4, 26.6.

**MS (ESI):** 277.1 [M+ H]

**Chiral HPLC:** 80:20 Hex/*i*-PrOH (0.7 mL min<sup>-1</sup>), Chiralpak AD-H Column, RT<sub>1</sub>: 10.83 min, RT<sub>2</sub>: 14.211 min

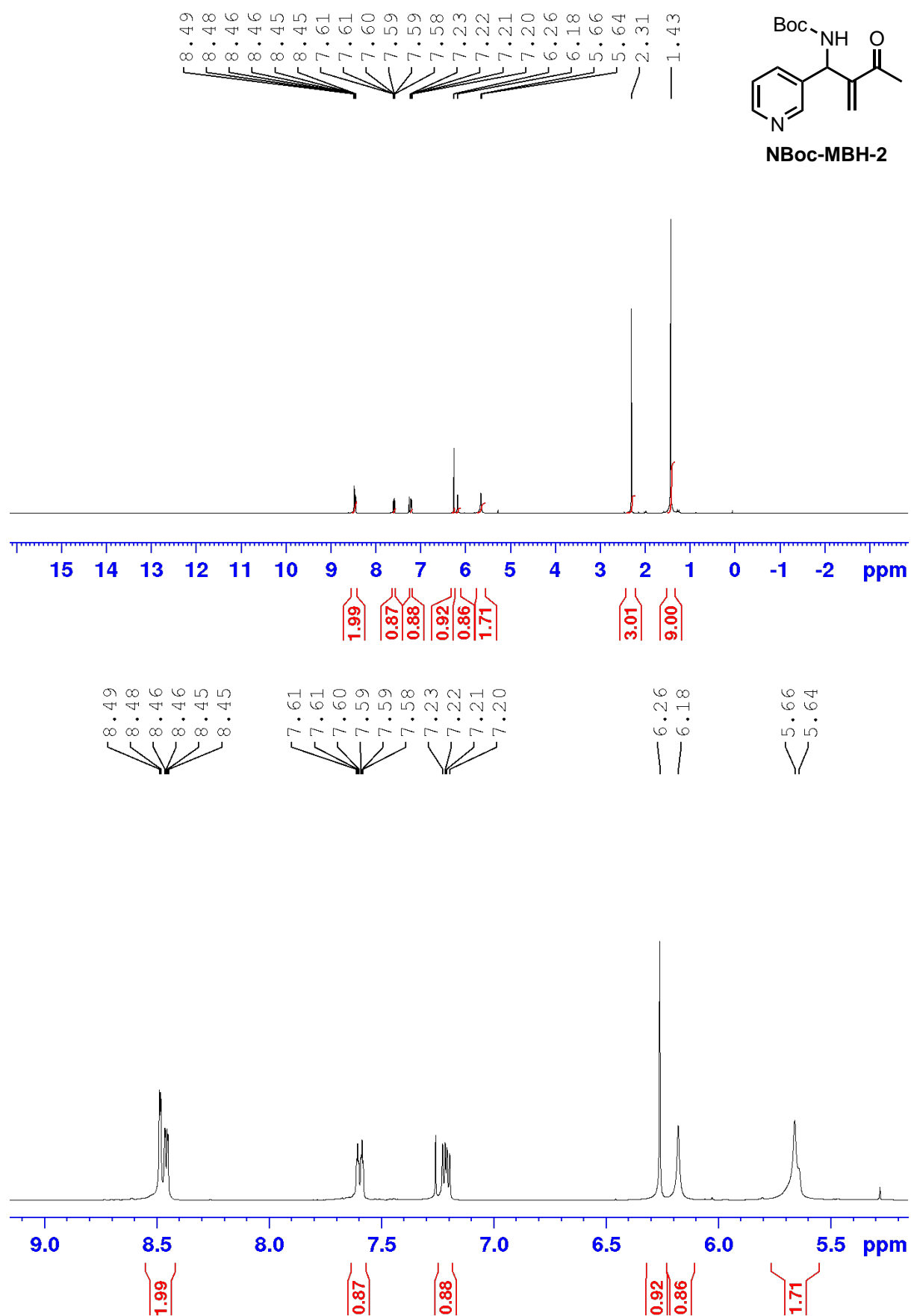


Figure A.75  $^1\text{H}$  NMR spectrum (400 MHz,  $\text{CDCl}_3$ ) for NBoc-MBH-2

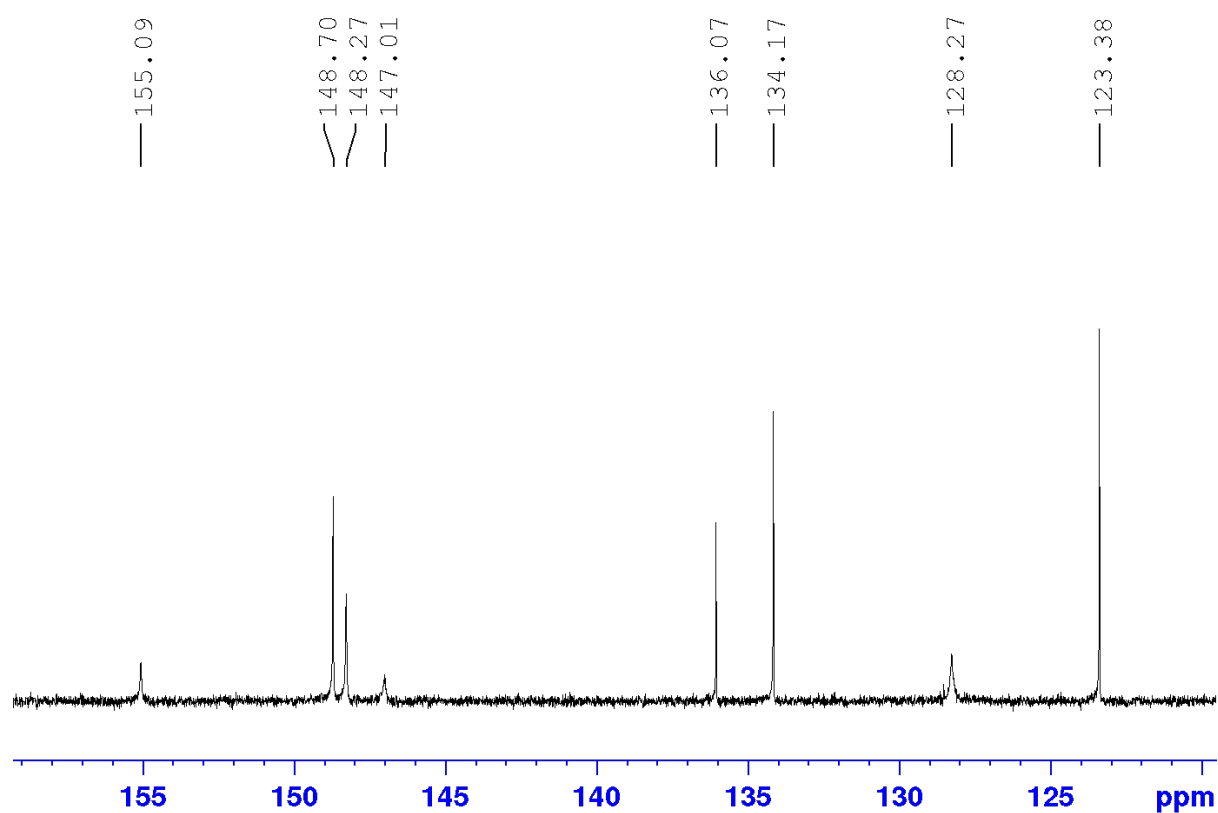
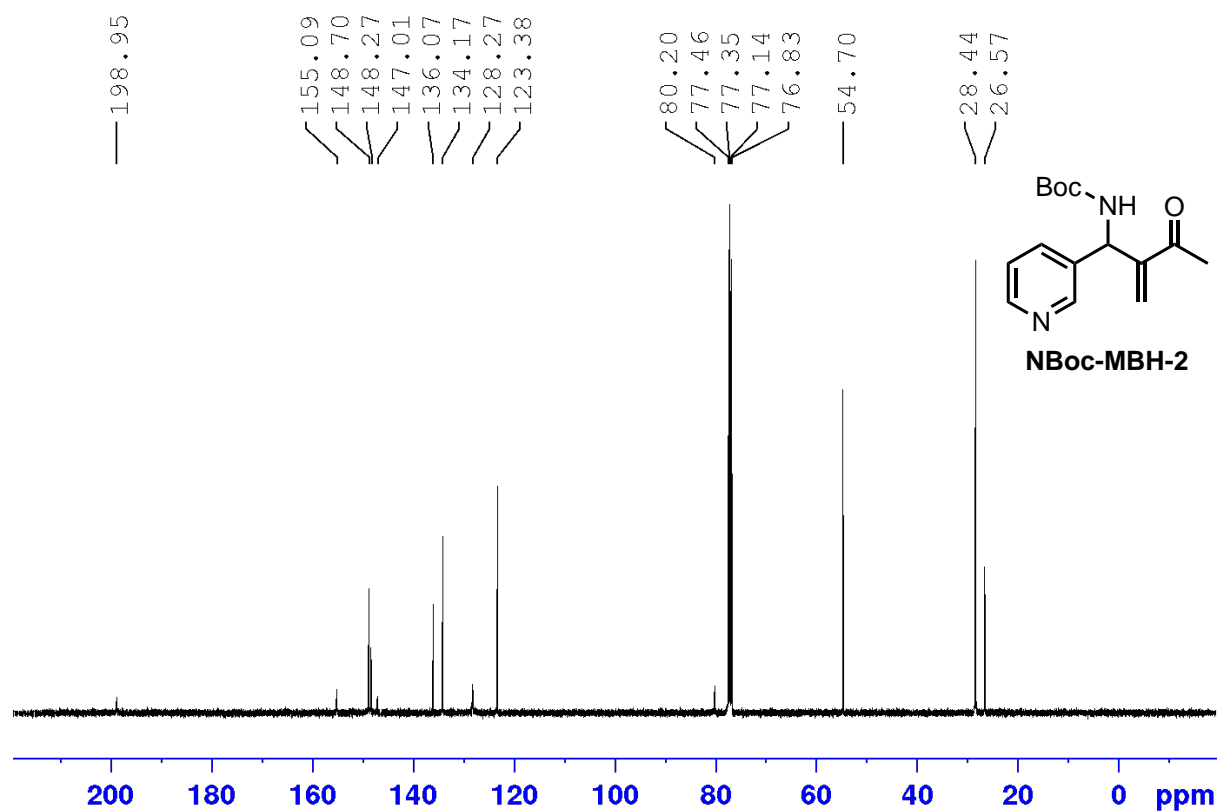
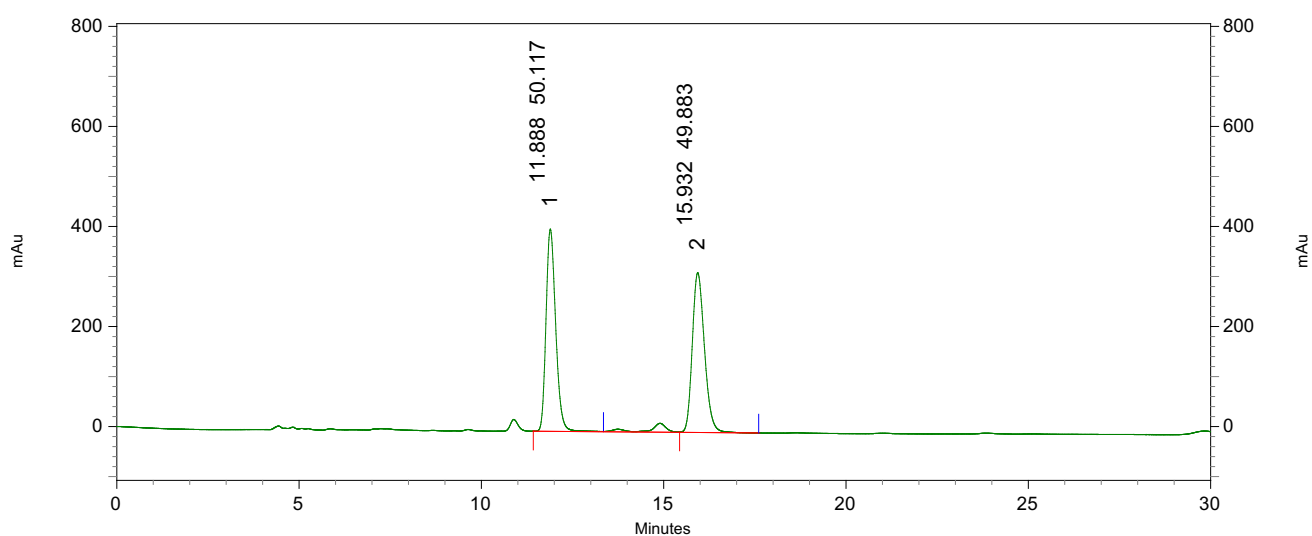


Figure A.76 <sup>13</sup>C NMR spectrum (100 MHz, CDCl<sub>3</sub>) for NBoc-MBH-2

### Racemic HPLC Trace

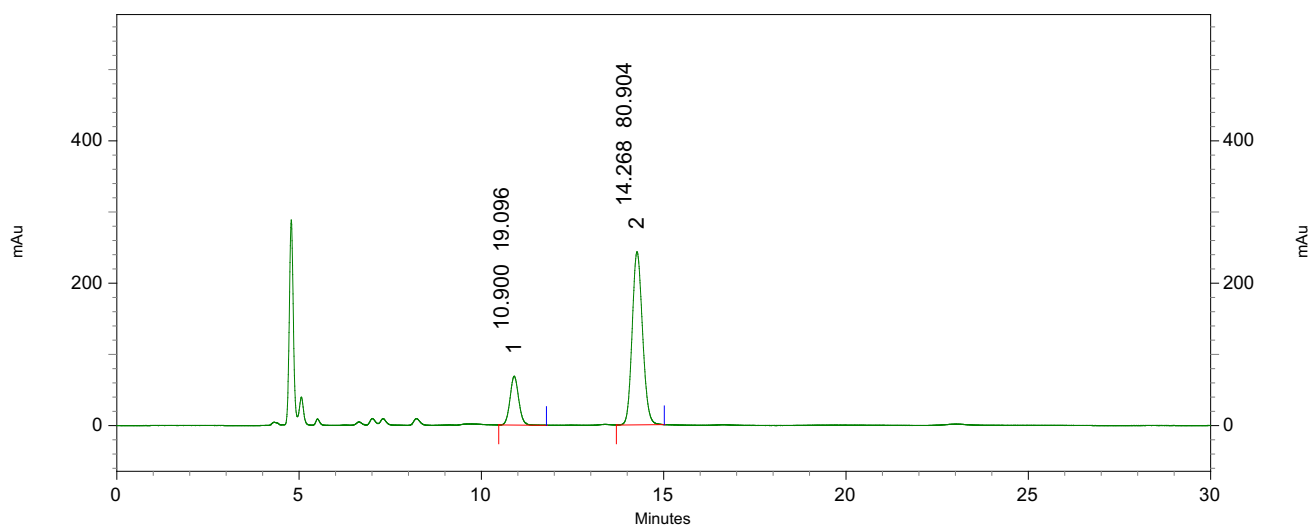


### 4: 220 nm, 4 nm Results

| Pk # | Retention Time | Area    | Area % |
|------|----------------|---------|--------|
| 1    | 11.888         | 7462505 | 50.12  |
| 2    | 15.932         | 7427755 | 49.88  |

|        |  |          |        |
|--------|--|----------|--------|
| Totals |  | 14890260 | 100.00 |
|--------|--|----------|--------|

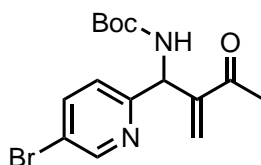
### Chiral HPLC Trace



### 4: 220 nm, 4 nm Results

| Pk # | Retention Time | Area    | Area % |
|------|----------------|---------|--------|
| 1    | 10.900         | 1134491 | 19.10  |
| 2    | 14.268         | 4806373 | 80.90  |

|        |  |         |        |
|--------|--|---------|--------|
| Totals |  | 5940864 | 100.00 |
|--------|--|---------|--------|



**NBoc-MBH-3**

***tert-butyl (1-(5-bromopyridin-2-yl)-2-methylene-3-oxobutyl)carbamate (NBoc-MBH-3)***

**<sup>1</sup>H NMR** (400 MHz, CDCl<sub>3</sub>, δ): 8.17 (d, *J* = 2.5 Hz, 1H), 7.42 (dd, *J* = 8.3, 2.6 Hz, 1H), 7.33 (d, *J* = 8.2 Hz, 2H), 6.21 (s, 1H), 6.13 (s, 1H), 5.93 (b, 1H), 5.53 (d, *J* = 8.9 Hz, 1H), 2.25 (s, 3H), 1.37 (s, 9H).

**<sup>13</sup>C NMR** (100 MHz, CDCl<sub>3</sub>, δ): 198.9, 155.0, 148.6, 146.6, 140.9, 136.9, 135.8, 128.8, 127.8, 80.4, 54.3, 28.4, 26.5

**MS (ESI):** 355 [M+H], 357 [M+H]

**Chiral HPLC:** 80:20 Hex/*i*-PrOH (0.7 mL min<sup>-1</sup>), Chiralpak AD-H Column, RT<sub>1</sub>: 10.83 min, RT<sub>2</sub>: 14.211 min



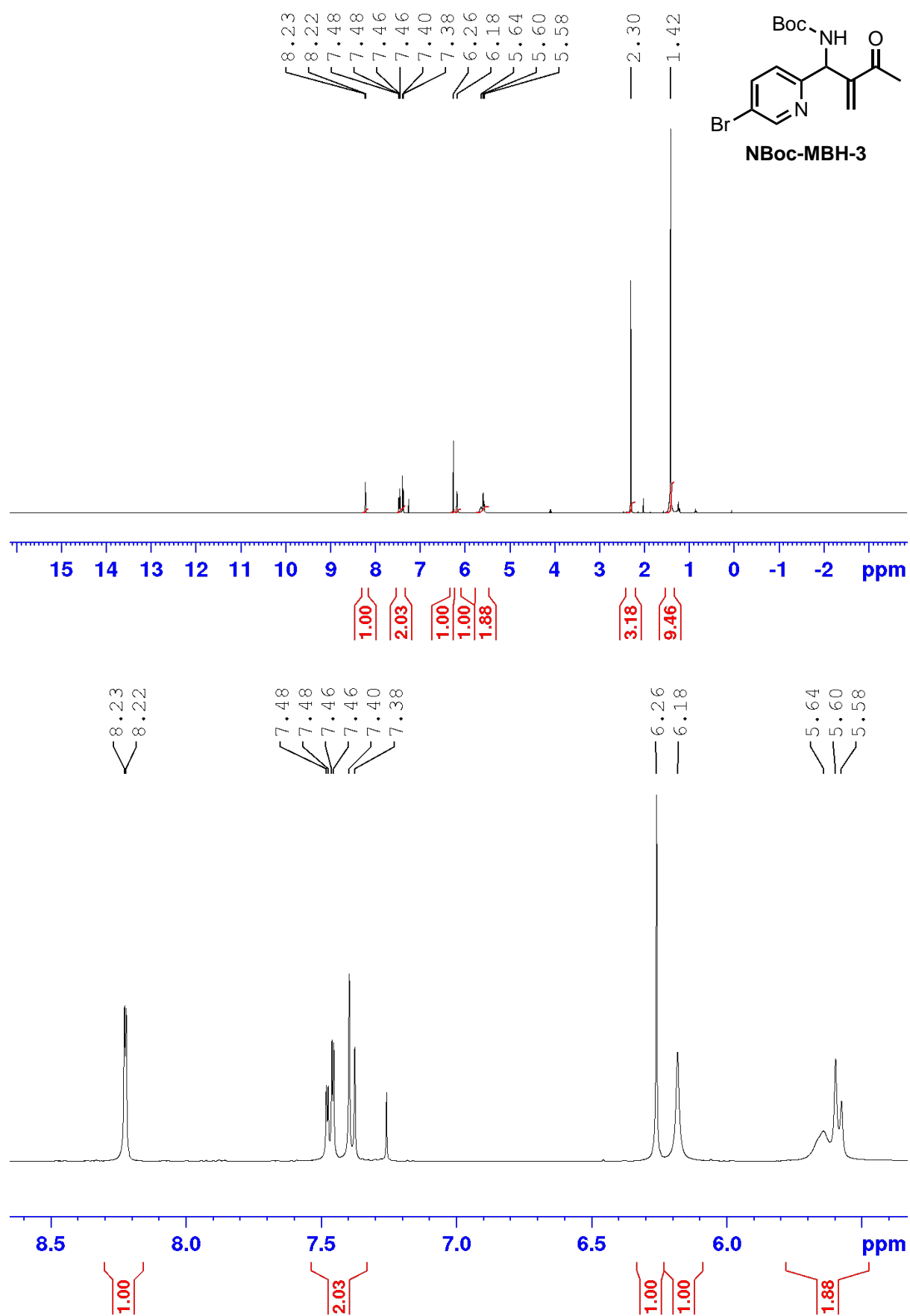
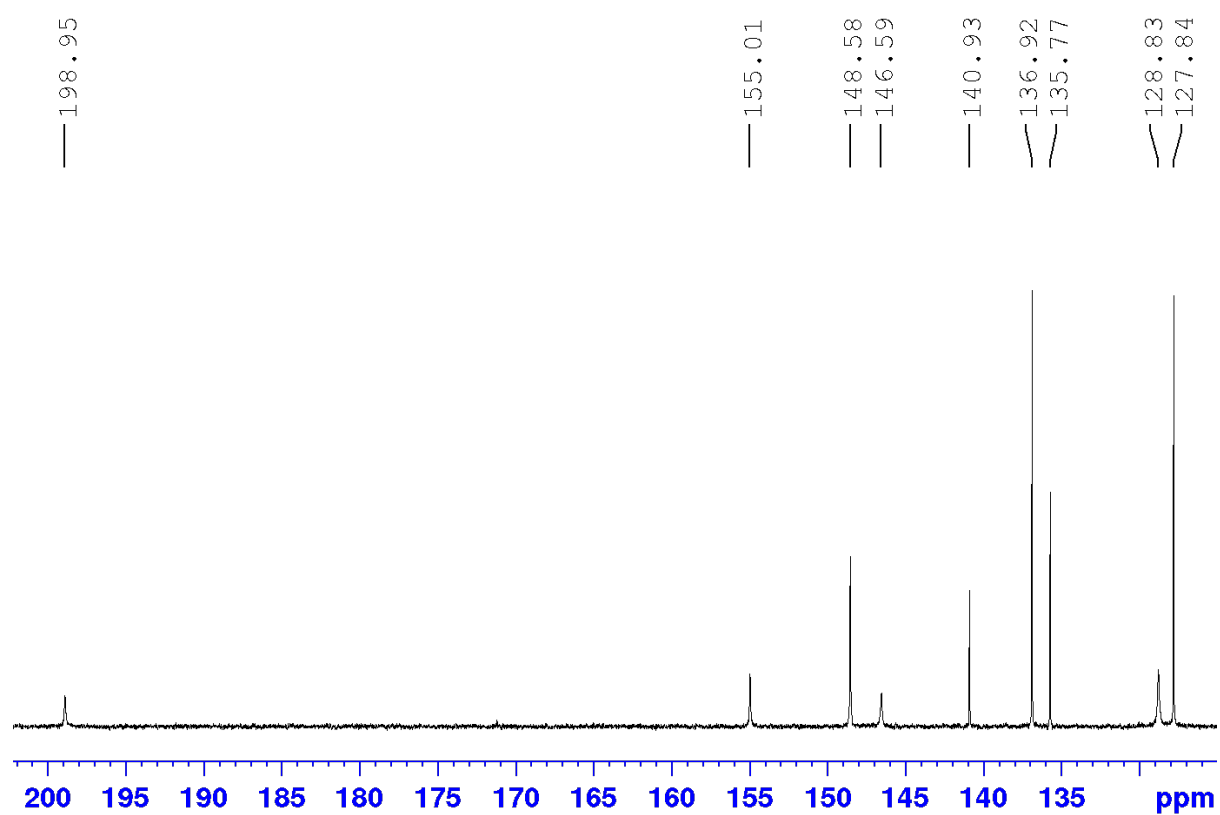
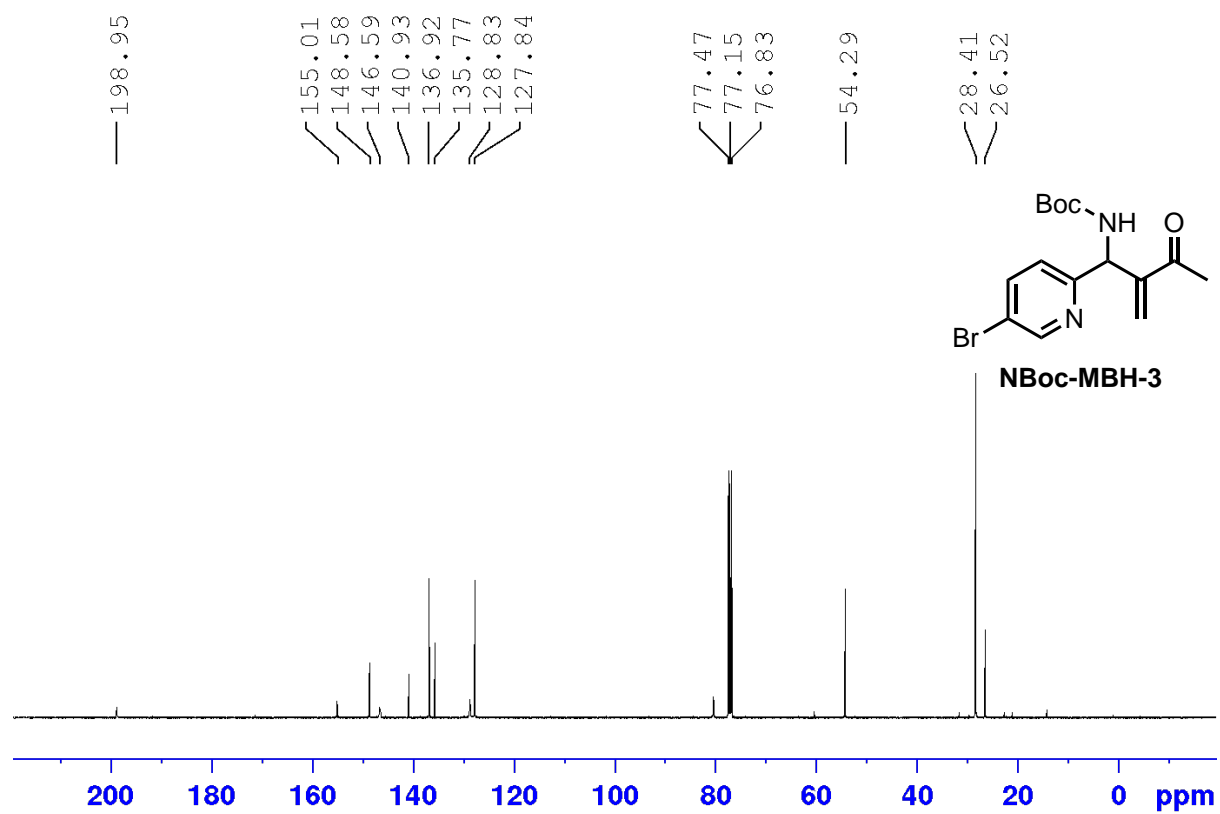
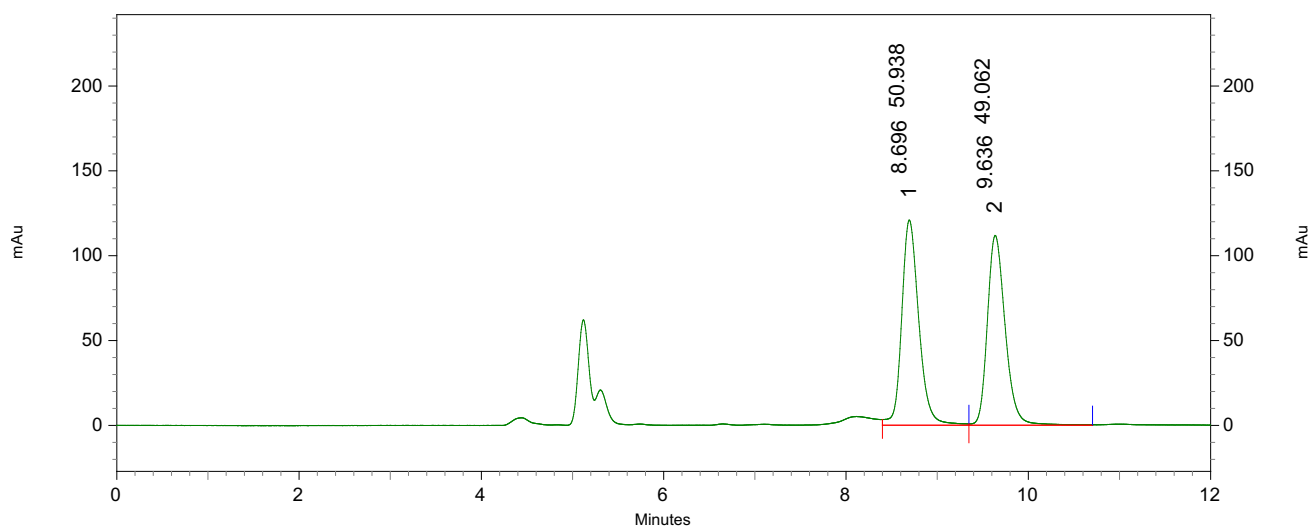


Figure A.77 <sup>1</sup>H NMR spectrum (400 MHz, CDCl<sub>3</sub>) for NBoc-MBH-3



**Figure A.78** <sup>13</sup>C NMR spectrum (100 MHz, CDCl<sub>3</sub>) for NBoc-MBH-3

### Racemic HPLC Trace

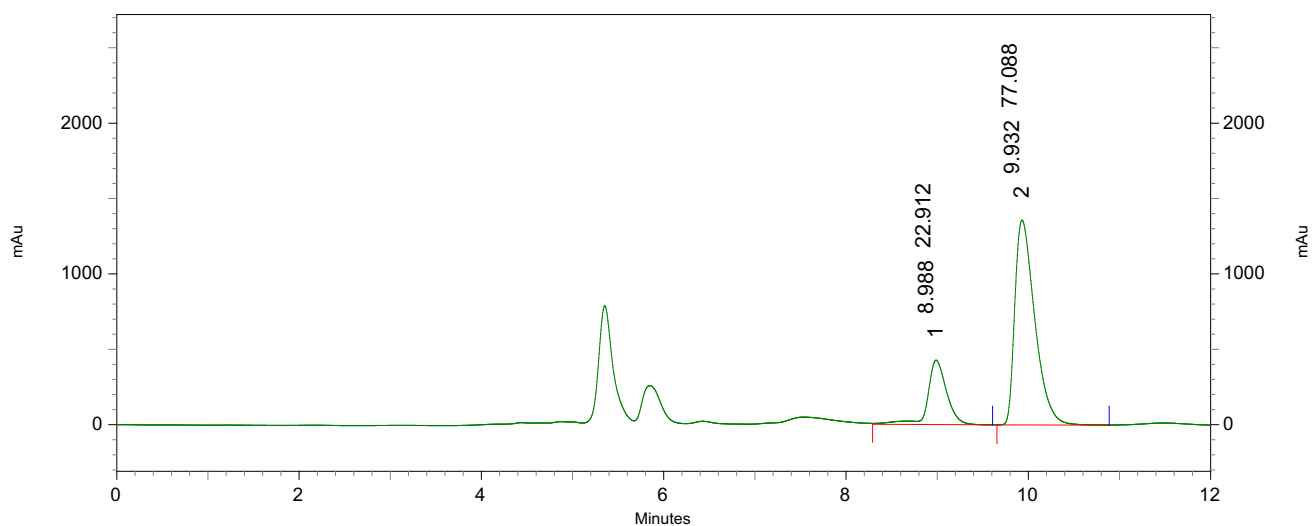


### 4: 220 nm, 4 nm Results

| Pk # | Retention Time | Area    | Area % |
|------|----------------|---------|--------|
| 1    | 8.696          | 1576766 | 50.94  |
| 2    | 9.636          | 1518696 | 49.06  |

|        |  |         |        |
|--------|--|---------|--------|
| Totals |  | 3095462 | 100.00 |
|--------|--|---------|--------|

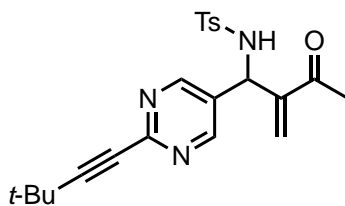
### Chiral HPLC Trace



### 4: 220 nm, 4 nm Results

| Pk # | Retention Time | Area     | Area % |
|------|----------------|----------|--------|
| 1    | 8.988          | 6141103  | 22.91  |
| 2    | 9.932          | 20662121 | 77.09  |

|        |  |          |        |
|--------|--|----------|--------|
| Totals |  | 26803224 | 100.00 |
|--------|--|----------|--------|



5.48

***N*-(1-(2-(3,3-dimethylbut-1-yn-1-yl)pyrimidin-5-yl)-2-methylene-3-oxobutyl)-4-methylbenzenesulfonamide (5.48)**

**<sup>1</sup>H NMR** (400 MHz, CDCl<sub>3</sub>, δ): 8.41 (s, 2H), 7.63 (d, *J* = 8.3, 2H), 7.24 (d, *J* = 8.3 Hz, 2H), 6.16 (s, 1H), 6.13 (s, 1H), 5.82 (d, *J* = 9.5 Hz, 1H), 5.23 (d, *J* = 9.5 Hz, 1H), 2.42 (s, 3H), 2.18 (s, 3H), 1.35 (s, 9H).

**<sup>13</sup>C NMR** (100 MHz, CDCl<sub>3</sub>, δ): 198.8, 155.5, 144.8, 144.2, 137.3, 130.4, 130.1, 129.9, 127.3, 98.6, 56.2, 30.5, 28.0, 26.3, 21.7.

**MS (ESI):** 412 [M+ H]

**Chiral HPLC:** 60:40 Hex/*i*-PrOH (0.7 mL min<sup>-1</sup>), Whelk-01 Column, RT<sub>1</sub>: 21.4 min, RT<sub>2</sub>: 24.86 min

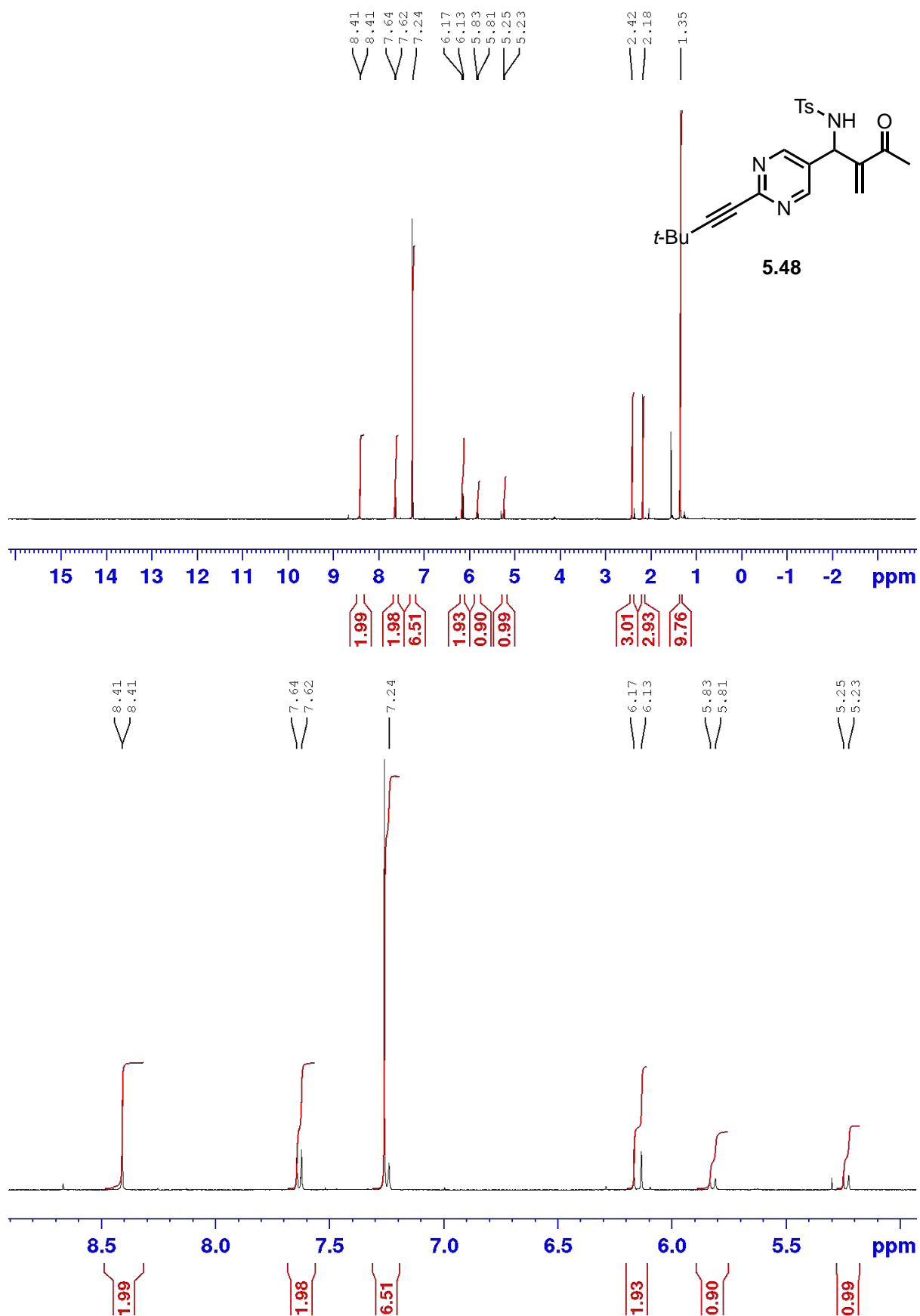


Figure A.79 <sup>1</sup>H NMR spectrum (400 MHz, CDCl<sub>3</sub>) for 5.49.

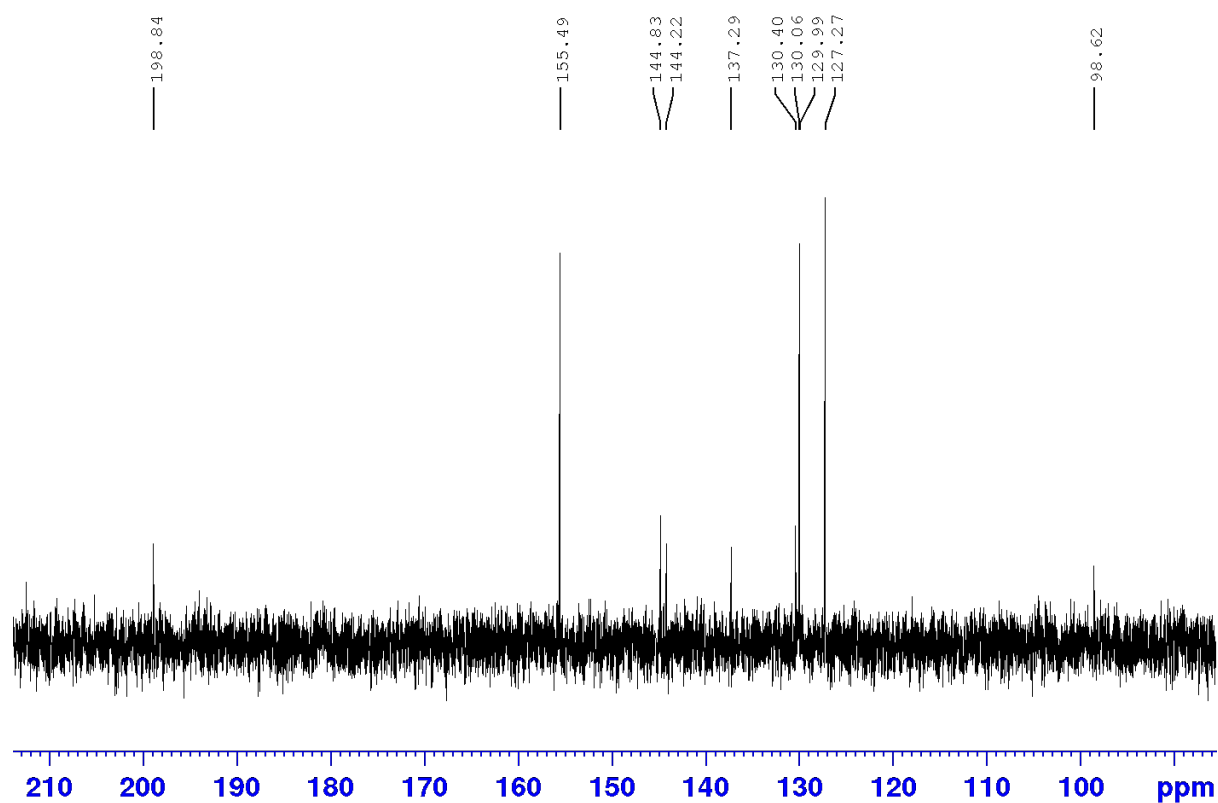
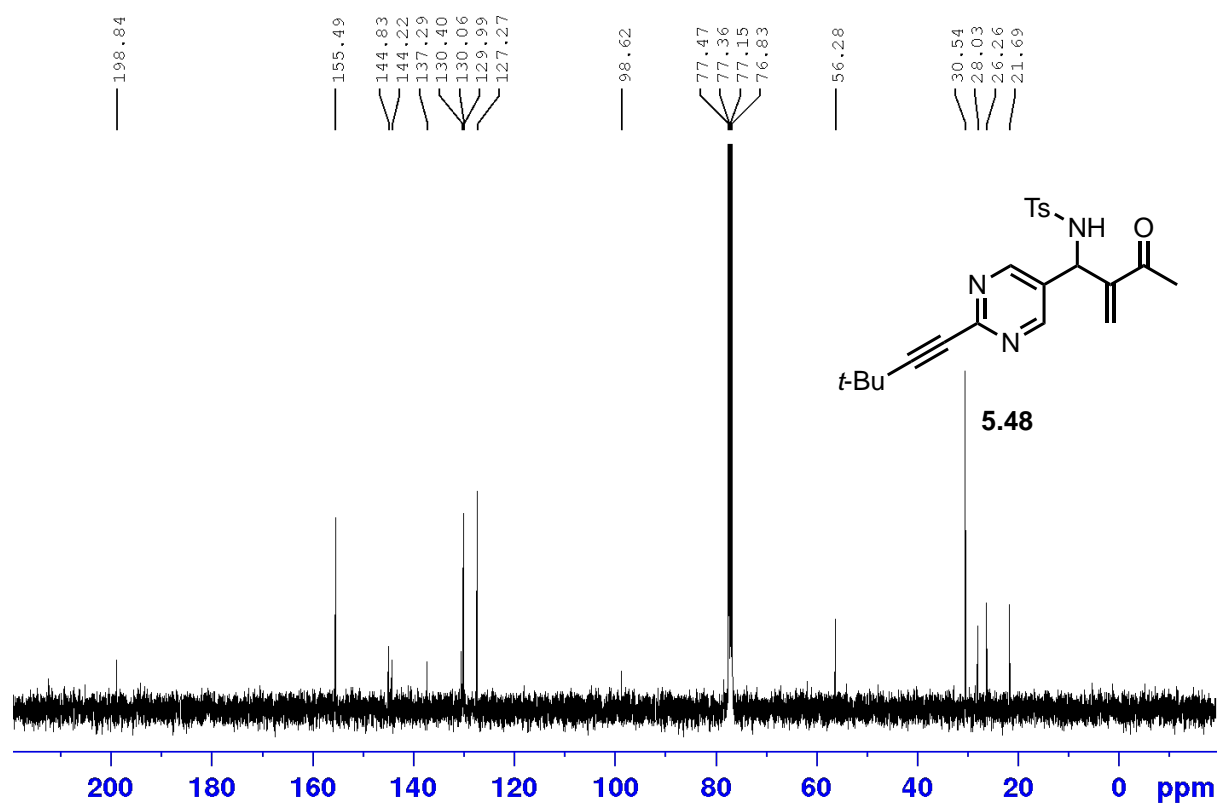
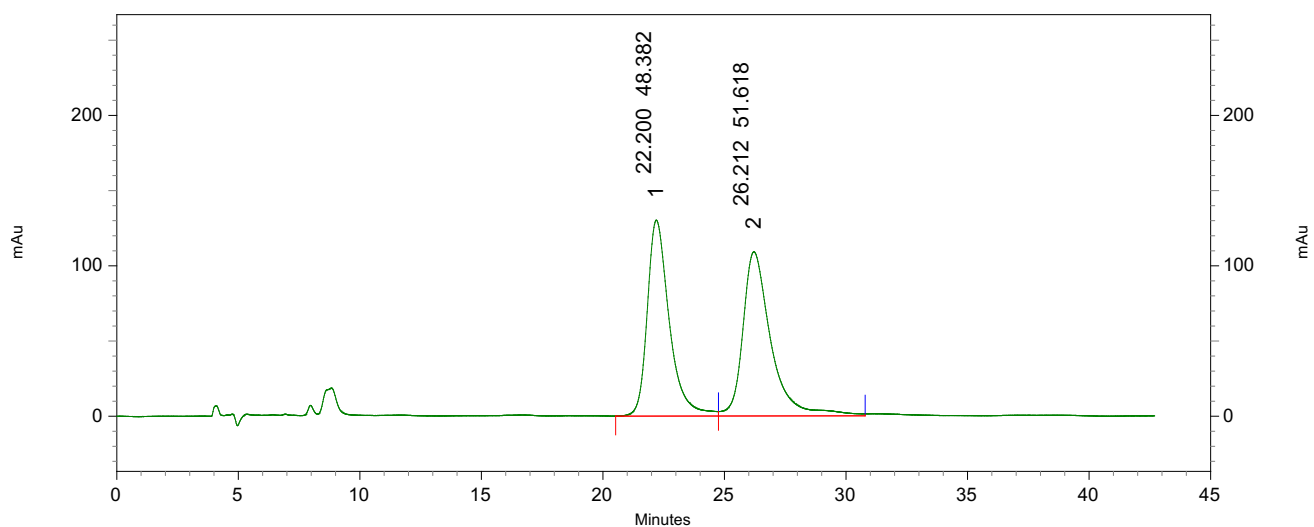


Figure A.80 <sup>13</sup>C NMR spectrum (100 MHz, CDCl<sub>3</sub>) for 5.49.

### Racemic HPLC Trace

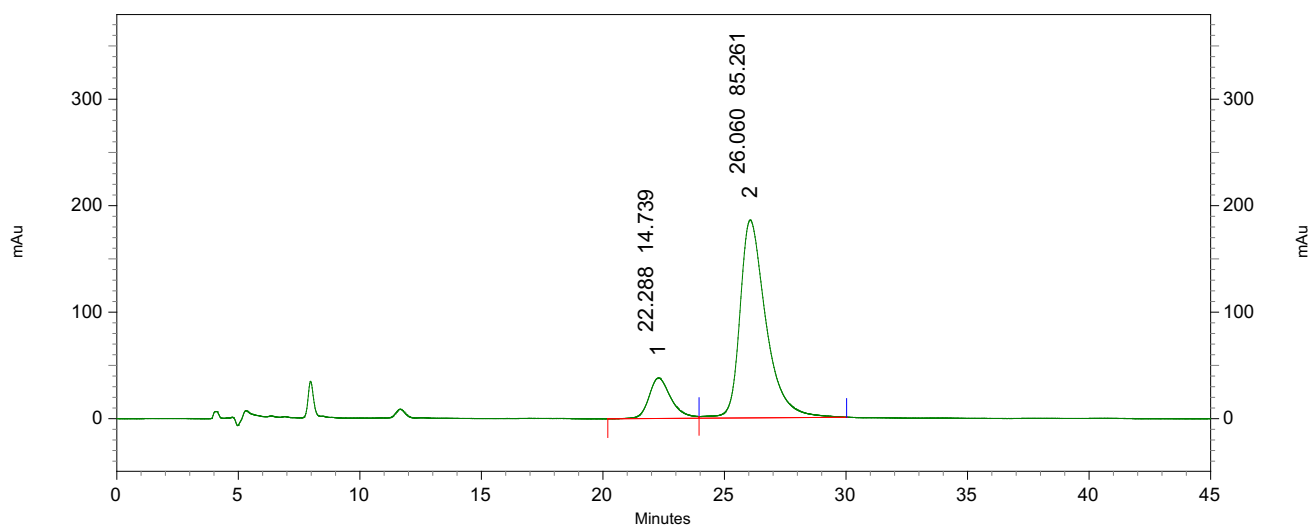


#### 4: 220 nm, 4 nm Results

| Pk # | Retention Time | Area    | Area % |
|------|----------------|---------|--------|
| 1    | 22.200         | 8230154 | 48.38  |
| 2    | 26.212         | 8780614 | 51.62  |

|        |  |          |        |
|--------|--|----------|--------|
| Totals |  | 17010768 | 100.00 |
|--------|--|----------|--------|

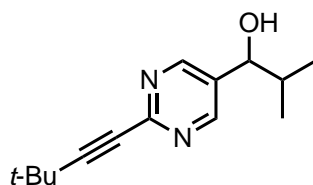
### Chiral HPLC Trace



#### 4: 220 nm, 4 nm Results

| Pk # | Retention Time | Area     | Area % |
|------|----------------|----------|--------|
| 1    | 22.288         | 2388511  | 14.74  |
| 2    | 26.060         | 13817378 | 85.26  |

|        |  |          |        |
|--------|--|----------|--------|
| Totals |  | 16205889 | 100.00 |
|--------|--|----------|--------|



5.2

**1-(2-(3,3-dimethylbut-1-yn-1-yl)pyrimidin-5-yl)-2-methylpropan-1-ol (5.2)**

**<sup>1</sup>H NMR** (400 MHz, CDCl<sub>3</sub>, δ): 8.62 (s, 2H), 4.51 (d, *J* = 6.1 Hz), 1.97 (m, 1H), 1.37 (s, 9H), 0.95 (d, *J* = 6.7 Hz, 3H), 0.87 (d, *J* = 6.7 Hz, 3H).

**<sup>13</sup>C NMR** (100 MHz, CDCl<sub>3</sub>, δ): 155.7, 153.3, 134.4, 97.9, 78.5, 75.3, 35.3, 30.5, 27.9, 18.5, 17.5.

**MS (ESI):** 187 [M+H-*i*-Pr]

**Chiral HPLC:** 95:5 Hex/*i*-PrOH (0.7 mL min<sup>-1</sup>), Chiralpal AD-H Column, RT<sub>1</sub>: 13.12 min, RT<sub>2</sub>: 14.63 min



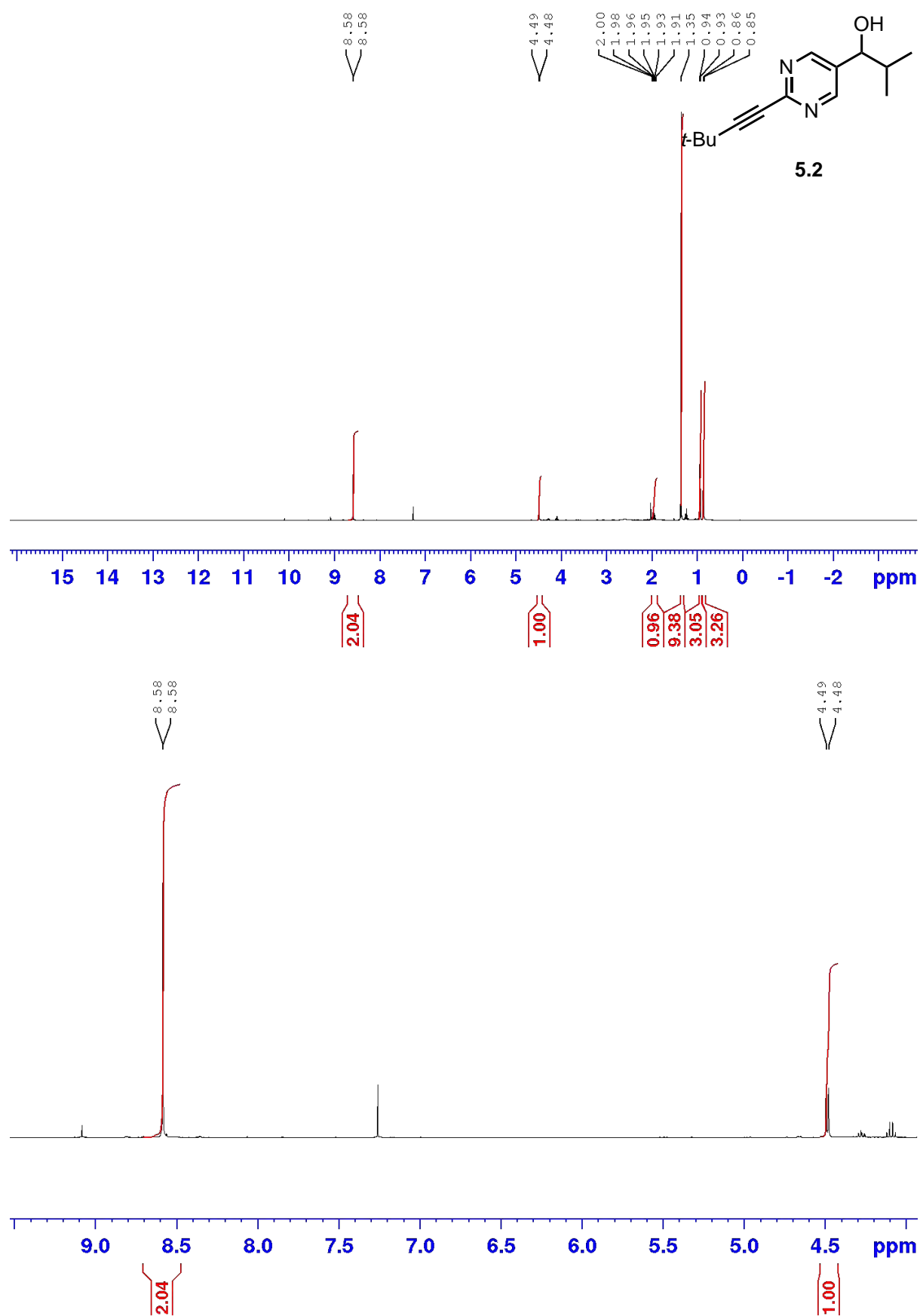


Figure A.81 <sup>1</sup>H NMR spectrum (400 MHz, CDCl<sub>3</sub>) for 5.2.

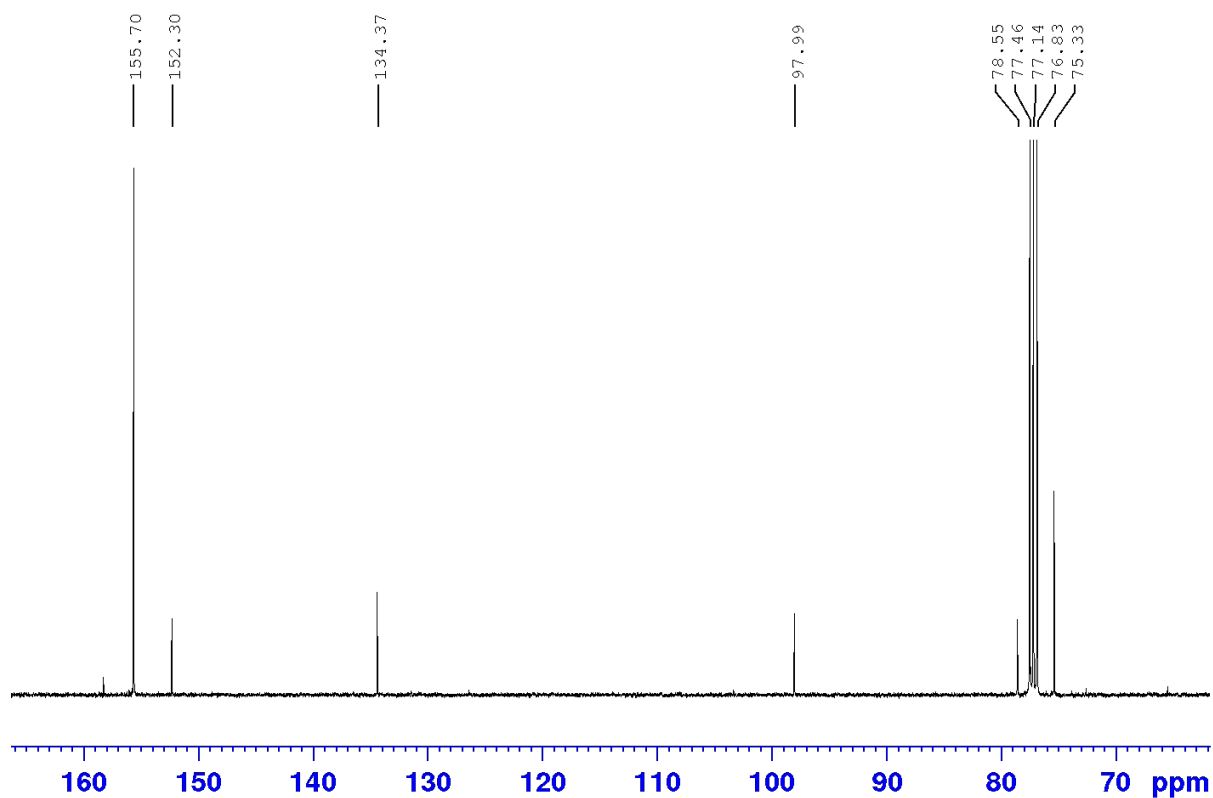
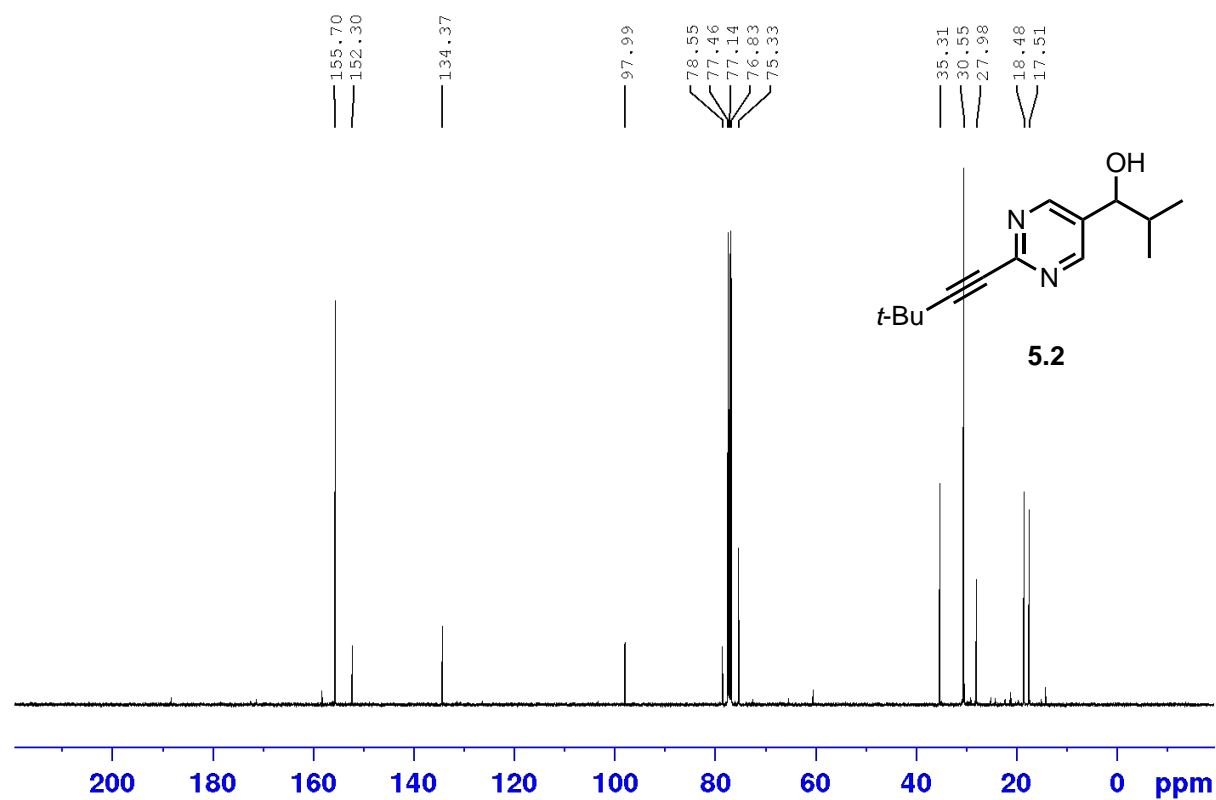
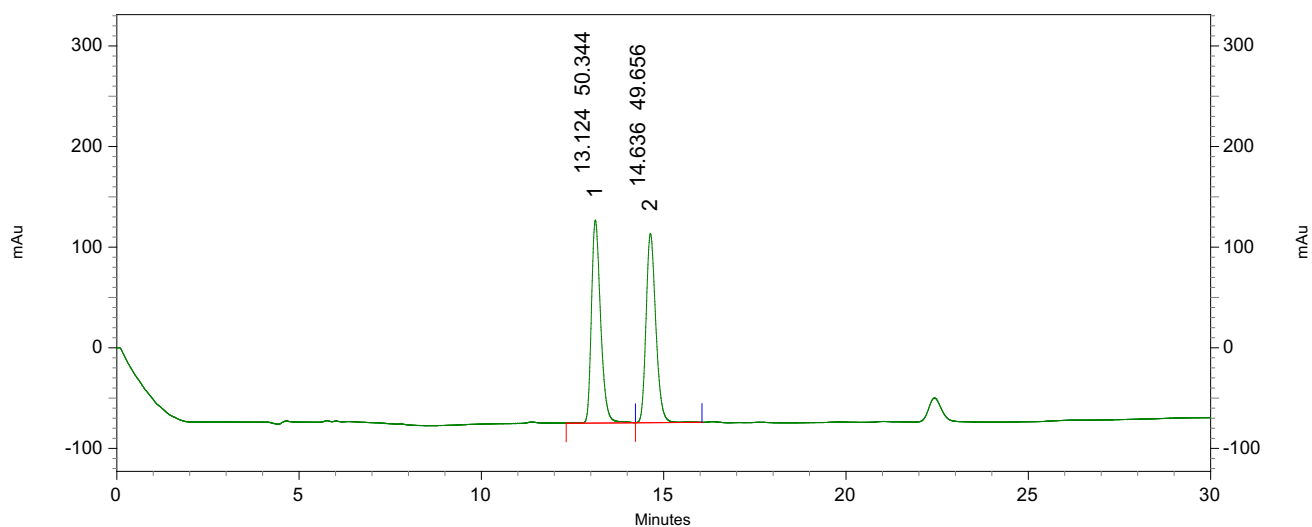


Figure A.82 <sup>13</sup>C NMR spectrum (100 MHz, CDCl<sub>3</sub>) for 5.2.

### Racemic HPLC Trace

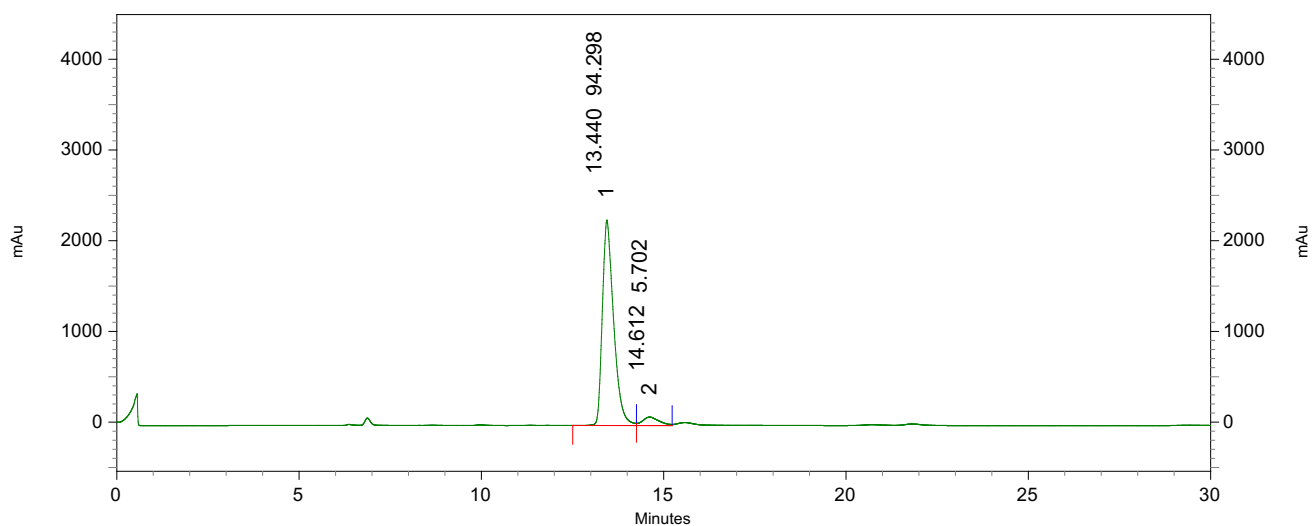


#### 4: 220 nm, 4 nm Results

| Pk # | Retention Time | Area    | Area % |
|------|----------------|---------|--------|
| 1    | 13.124         | 3538930 | 50.34  |
| 2    | 14.636         | 3490561 | 49.66  |

|        |  |         |        |
|--------|--|---------|--------|
| Totals |  | 7029491 | 100.00 |
|--------|--|---------|--------|

### Chiral HPLC Trace



#### 4: 220 nm, 4 nm Results

| Pk # | Retention Time | Area     | Area % |
|------|----------------|----------|--------|
| 1    | 13.440         | 48580656 | 94.30  |
| 2    | 14.612         | 2937481  | 5.70   |

|        |  |          |        |
|--------|--|----------|--------|
| Totals |  | 51518137 | 100.00 |
|--------|--|----------|--------|